#MeToo comes to Latin America p. 842

Lung-surfactant mimics give vaccines a boost pp. 852 & 869

Levitation gets really cool p. 892

Science

$15
21 FEBRUARY 2020
sciencemag.org

AAAS

GORDON RESEARCH CONFERENCES

Biology of winter, forensic DNA analysis, single-cell cancer biology, and more p. 922

CONTENTS

21 FEBRUARY 2020 • VOLUME 367 • ISSUE 6480

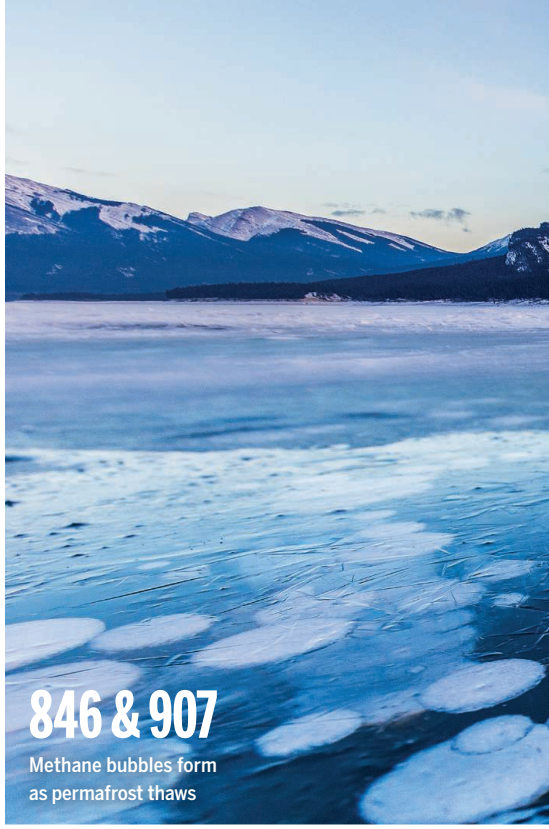

846 & 907
Methane bubbles form as permafrost thaws

NEWS

IN BRIEF

IN DEPTH

FEATURES

INSIGHTS

PERSPECTIVES

POLICY FORUM

BOOKS *ET AL.*

LETTERS

RESEARCH

IN BRIEF

REVIEW

RESEARCH ARTICLES

Published by AAAS

ON THE COVER

American witch hazel (*Hamamelis virginiana*) flowers encased in ice from a late winter storm. The effects of climate change on biological systems may be especially pronounced in winter. The Gordon Research Conference on the Biology of Winter will be held from 21 to 26 June 2020 in Waterville Valley, New Hampshire. See page 922 for the Gordon Research Conference schedule and preliminary programs. *Photo: Brent J. Sinclair*

SCIENCE (ISSN 0036-8075) is published weekly on Friday, except last week in December, by the American Association for the Advancement of Science, 1200 New York Avenue, NW, Washington, DC 20005. Periodicals mail postage (publication No. 484460) paid at Washington, DC, and additional mailing offices.

Domestic individual membership, including subscription (12 months): $165 ($74 allocated to subscription). Domestic institutional subscription (51 issues): $2148; Foreign postage extra: Air assist delivery: $98. First class, airmail, student, and emeritus rates on request. Canadian rates with GST available upon request, GST #125488122. Publications Mail Agreement Number 1069624. **Printed in the U.S.A.**
Change of address: Allow 4 weeks, giving old and new addresses and 8-digit account number. **Postmaster:** Send change of address to AAAS, P.O. Box 96178, Washington, DC 20090–6178. **Single-copy sales:** $15 each plus shipping and handling available from backissues.sciencemag.org; bulk rate on request. **Authorization to reproduce** material for internal or personal use under circumstances not falling within the fair use provisions of the Copyright Act can be obtained through the Copyright Clearance Center (CCC), www.copyright.com. The identification code for *Science* is 0036-8075. *Science* is indexed in the *Reader's Guide to Periodical Literature* and in several specialized indexes.

Published by AAAS

EDITORIAL

Smaller, greener, better

During my 15 years riding on the administrative Tilt-a-Whirl, I was a no-show at scientific conferences. Prior to that, during my faculty years, my go-to conferences were the national American Chemical Society meetings and Gordon Research Conferences—especially Metals in Biology, which is in January in Ventura, California. This past January, I went back to Ventura after a 15-year hiatus. A lot of things struck me about how things have changed—mostly for the better—and how some things have stayed the same. One thing that is increasingly on peoples' minds is the future of scientific meetings.

What has stayed the same is that a conference of that style, with 200 scientists from around the world, is a vital format for scientific exchange. The participants ranged from graduate students and postdocs to folks who created the field of bioinorganic chemistry 40 years ago. It was interesting to see how far a lot of the science has come, especially our understanding of how proteins control the second coordination sphere of metal sites to drive their reactivity. Some fields still have great mysteries: Even though we know a great deal more about the structures, we still don't know precisely how the N–N bond breaks during catalysis by nitrogenase or how the O–O bond forms in photosystem II.

One thing that has started to change for the better is the increasing number of women and people of color among conference speakers and participants. We are nowhere close to solving the equity problems in science or science meetings, but the change in the composition and atmosphere of meetings overall after 15 years is encouraging. This trend should continue, and more members of this diverse, emerging cohort should have prominent speaking roles to showcase their science. Such opportunities can help launch the careers of young scientists, and maybe small meetings could also require that a certain percentage of talks be given by postdocs and early career faculty.

"It's time to think creatively about how to reduce the carbon footprint of meetings while preserving—even improving—their value."

When it comes to big meetings, the interchange among scientists in person is still indispensable. But it's time for the scientific community to engage in frank talk about the impact of meetings on the climate. Some conferences have been supporting digital poster sessions to cut down on waste, but thousands of folks flying to these meetings is the real problem to focus on. It's time to think creatively about how to reduce the carbon footprint of meetings while preserving—even improving—their value.

What if we broke the large meetings into smaller, concurrent ones at regional sites where people could gather, sharing the drive or taking the train? Perhaps there could be a registration surcharge that is refunded if the participant doesn't fly. One thing that hasn't changed are the big sessions at national meetings; these are the big draw for most attendees. Unless you're in the front rows of the big ballrooms where these are held, you're watching the speaker on a screen from the back or even in an overflow room. Sitting with thousands of people in San Francisco watching a live talk on a jumbotron is no different from watching a streamed talk with thousands of people in New York—and vice versa. In a concurrent sites model, there would still be large enough audiences to make interchange with the speakers worthwhile. Major plenaries could be spread across different sites so that wherever one does take place, everyone at that particular location is in the room. This approach would push conferences to enhance technological capabilities. It also could lower the cost of attending conferences and thereby potentially increase the number and diversity of attendees. A group of graduate students piling into a van is much more democratic than having to decide who gets to fly.

Scientific conferences are vital to the collaboration that scientists rely on. Continuing to improve them in terms of equity for both the participants and the climate is something we can't stop striving to do.

I volunteer to drive the first van.

–H. Holden Thorp

H. Holden Thorp
Editor-in-Chief, *Science* journals.
hthorp@aaas.org;
@hholdenthorp

PHOTO: CAMERON DAVIDSON

10.1126/science.abb2790

> “The academic system is losing women at a higher rate at every stage of their careers.”
>
> From a study in the *Proceedings of the National Academy of Sciences* showing that women publish fewer scientific papers over their careers than men because of differences in career length, not annual output.

IN BRIEF

Edited by **Jeffrey Brainard**

The SARS-CoV-2 virus (purple) emerges from infected cells in this scanning electron microscope image.

PHOTO: NIAID-RML (DE WIT/FISCHER)

VIROLOGY

Coronavirus name splits scientists

What to call the pathogen paralyzing China and rattling the rest of the world? That question faces scientists after separate names emerged on 11 February for the virus and the disease it causes. Because the virus belongs to the same species as SARS-CoV—the coronavirus that caused the 2002–03 outbreak of severe acute respiratory syndrome—the International Committee for the Taxonomy of Viruses simply named it SARS-CoV-2. But that name creates “unnecessary fear,” the World Health Organization (WHO) says, especially in Asia, which was hit hardest by SARS. WHO has instead named the disease COVID-19, short for coronavirus disease 2019, and will use that term when talking about the virus as well. Scientists seem divided. Of 26 preprints published in the week ending 18 February that used COVID-19 to describe the disease, 11 also used that name for the virus; 11 others called the virus SARS-CoV-2 instead. (Four used the temporary moniker 2019-nCoV or did not name the virus.) The split is “unfortunate,” says Michael Osterholm, head of the Center for Infectious Disease Research and Policy at the University of Minnesota, Minneapolis, who’s hoping for “another effort to reconcile the two.”

NASA picks mission candidates

PLANETARY SCIENCE | NASA’s next $500 million planetary science missions will chart a return to Venus, the agency’s first visit since the early 1990s, or journey to exotic, geologically active moons of the outer planets, the agency announced last week. It chose four finalists for its Discovery line of lower-cost missions, two of which will be selected in 2021 after further study for flight later this decade. One of the Venus missions would use an orbiter and an armored spherical probe dropped from it to measure the planet’s atmosphere down to the surface. Another would deploy a radar-equipped mapper to reveal whether volcanoes or plate tectonics are active on the Venusian surface. A third candidate would study whether Io, a moon of Jupiter with spewing volcanoes, contains an internal magma ocean. A fourth finalist would inspect Triton, the icy moon of Neptune glimpsed by Voyager 2 in 1989.

Japan builds giant neutrino trap

ASTROPHYSICS | Japan’s legislature has begun funding Hyper-Kamiokande (Hyper-K), the world’s largest neutrino detector, managers announced last week. Construction of the 72 billion yen (about $660 million) project, in an underground hall in Hida City, is to begin in April and end by 2027. Hyper-K is 8.4 times larger than its predecessor, Super-Kamiokande, but works on the same principle. Its detector, a tank 74 meters wide and 60 meters tall, will hold 260,000 tons of water—enough to fill 100 Olympic swimming pools. Forty thousand photosensors lining its walls will watch for faint flashes of light that occur when a nearly massless neutrino interacts with a water molecule; the light yields clues to the neutrino’s type, energy, and direction of travel, allowing researchers to trace it back to its cosmic origin. Researchers will use Hyper-K to study neutrinos emanating from the Sun, distant stars, and supernovae. It will also analyze beams of neutrinos, fired at the detector from a particle accelerator 295 kilometers away, to look for differences between neutrinos and anti-neutrinos, which could help explain why the universe is made of matter and not anti-matter.

Published by AAAS

Former IPCC head dies

LEADERSHIP | Indian engineer Rajendra Pachauri, who led the Intergovernmental Panel on Climate Change (IPCC) for 13 years but resigned after accusations of sexual harassment emerged in 2015, died on 13 February at age 79. On Pachauri's watch, IPCC won a share of the 2007 Nobel Peace Prize, and he strengthened the role of peer review in the panel's assessments. But he generated controversy by defending a forecast, later reversed by the panel, that glaciers in the Himalayas would melt away by 2035. Later, a former colleague at the Energy and Resources Institute, a New Delhi think tank, alleged that Pachauri had grabbed her inappropriately and retaliated against her when she refused his advances; in 2018, a court ordered Pachauri to stand trial on criminal charges. The case was ongoing when he died. In 2016, Pachauri filed a defamation case against a second woman who accused him of harassment; that case was pending.

Satellite worries deepen

ASTRONOMY | The International Astronomical Union (IAU) last week raised new concerns about constellations of thousands of communications satellites in low-Earth orbit that create bright streaks in telescopes' fields of view. The union voiced alarm in June 2019 over the launch of the first of SpaceX's 1500 planned Starlink satellites, intended to provide worldwide internet access. "It was almost like they launched mirrors," says Patrick Seitzer, who studies orbital debris at the University of Michigan, Ann Arbor. Citing ongoing studies of the satellites' brightness, IAU now says they are unlikely to spoil the view of narrowly focused telescopes, but wide-field surveys will be "severely affected." A prime example is the Vera C. Rubin Observatory, which is set to start surveying the sky in 2022. SpaceX says it is working with astronomers to reduce the impact of its Starlink satellites. But other companies are also planning constellations, and the total number of satellites could reach the tens of thousands.

Facebook frees up political data

SOCIAL SCIENCE | Researchers finally have access to a trove of anonymized data on how Facebook users shared information—and misinformation—on recent political events around the world. Concerns over privacy had delayed its release for nearly 2 years. The data, released last week, contain 38 million URLs relating to civic discourse that were shared publicly on Facebook between January 2017 and July 2019. They provide such details as whether a linked site was considered to be fake news or hate speech, and whether a link was clicked on or liked. Information about the users, including their political affinities, is also available. The social media giant announced plans for such a release in April 2018 before it realized that existing systems to preserve the confidentiality of its users were inadequate. The new system applies a mathematically rigorous approach called differential privacy. Researchers can apply for access to the data through the nonprofit Social Science One (online at socialscience.one).

Engineers led job growth among U.S. Ph.D.s

Doctorates in engineering are gaining favor among employers, edging out computer science. The number of U.S. workers with doctoral degrees in engineering has risen since 2003, outpacing growth in all other scientific disciplines, according to a biennial compendium of statistics published in January by the National Science Foundation. These figures are compound annual growth rates in number of employed individuals from 2003–17.

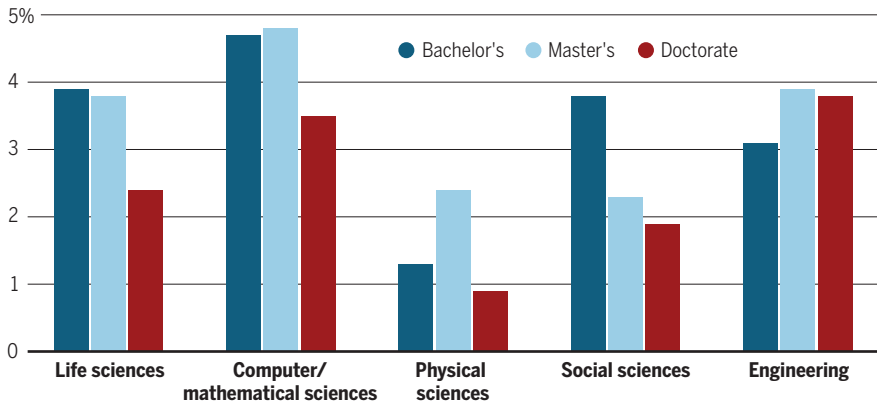

Early arrivals at an Iowa rally for a Democratic presidential candidate this month check their phones.

Databases can impair reviews

PUBLISHING | Scientists who conduct systematic reviews—rigorously designed surveys of the research literature on a topic—and meta-analyses of data from the papers they select use databases such as Google Scholar to locate all pertinent journal articles. But half of the 28 most widely used databases fall short for this job, a study accepted for publication in *Research Synthesis Methods* says, because of design limitations. Some databases, such as Google Scholar, do not produce consistently reproducible results and others do not allow Boolean searches, which allow search strings to be parsed with "and" and "or" to yield fine-grained results. Some search tools, such as CiteSeerX, automatically expand queries to retrieve more documents, which can also limit precision. The analysis is one of several in recent years documenting that individual search engines vary in how well they retrieve scholarly literature.

Bezos offers billions for climate

PHILANTHROPY | Jeff Bezos, founder and CEO of Amazon, promised this week to donate $10 billion for research on climate change and projects to address its effects. The world's richest man, with a stake in Amazon worth more than

CREDITS: (GRAPHIC) J. BRAINARD/*SCIENCE*; (DATA) SCIENCE & ENGINEERING INDICATORS 2020/U.S. NATIONAL SCIENCE FOUNDATION (PHOTO) REUTERS/JONATHAN ERNST

$100 billion, Bezos did not release details in his announcement, which was posted on Instagram. In 2019, he pledged to shift all of Amazon's energy use to renewable sources by 2030 and make the company net carbon neutral by 2040, the first major corporation to announce such a goal, in part by shifting to electric delivery vehicles. But Amazon employees have criticized the company for not moving fast enough to reduce its substantial carbon footprint. Amazon reported emitting 44.4 million metric tons of carbon dioxide in 2018, as much as some countries.

Agency restores animal records

ANIMAL RESEARCH | The U.S. Department of Agriculture (USDA) on 18 February announced it has restored to its website reports of inspections of animal research laboratories and other animal-holding facilities governed by the Animal Welfare Act (AWA). In February 2017, the department's Animal and Plant Health Inspection Service (APHIS) removed tens of thousands of inspection reports and records of enforcement actions for AWA violations. It later restored some, but they were heavily redacted to protect what it called private information. But an appropriations law enacted in December 2019 gave APHIS 60 days to restore the reports, which animal rights groups and journalists had regularly used to publicize AWA violations. APHIS says the restoration includes reports that were public in January 2017 and others created since, but "confidential business information" will still be redacted. People for the Ethical Treatment of Animals, which sued USDA after the removals, said it will check "that all the data have been properly restored to a fully functional database."

2020 AAAS MEETING

A spotlight on the brain

More than 6700 researchers and students converged on Seattle last week for the annual meeting of AAAS, which publishes *Science*. The meeting's theme was "Envisioning Tomorrow's Earth." Some highlights from the realms of neuroscience and criminal justice are below.

Body composting promises a more sustainable way of death

Death is not environmentally friendly. Cemeteries take up land, embalming the dead uses toxic chemicals, and cremation burns natural gas. So, Lynne Carpenter-Boggs, a soil scientist at Washington State University, Pullman, is advising a company that aims to do with bodies what many consumers do with leftover food: recycle it into compost. In May 2019, Washington became the first state to legalize natural organic reduction, or body composting. With oversight from her university, Carpenter-Boggs conducted a pilot study with six donated bodies to test the process, and she described some key measures. Decomposition is enhanced by a high (25:1) carbon-to-nitrogen ratio, achieved by mixing the body with plant material, for example. Also important are a steady warm temperature, aeration, and moisture control.

Dancing a Ph.D. on brain development

Antoina Groneberg's innovative portrayal of zebrafish brain development last week netted *Science*'s annual "Dance Your Ph.D." prize. Groneberg taught dance as a side job while pursuing her doctorate in neuroscience at Champalimaud Research in Lisbon, Portugal. Her doctoral thesis explored how the motions of groups of zebrafish larvae affected individual animals' brain development and behavior, teasing out the impact by raising some larvae in isolation. A version of her video, showing former dance students and kids, went viral last year, says Groneberg, now a postdoc at Charité University Hospital in Berlin—"You don't see too many dance videos about fish larvae." Her dance topped the social science category and won the $1000 overall prize, beating out the biology, physics, and chemistry winners, including one with a rap in Finnish on analyzing forests with radar. All the winning videos were shown at a AAAS meeting session.

The winning dance was chosen from 30 submissions on artistic and scientific merits.

PHOTO: TIAGO ALMEIDA

Donating brain tissue: not just for the dead anymore

Brains donated to science aren't delivered until after the donor dies. Now, more patients are giving researchers pieces of their living brains, opening new avenues for exploring how brains work, explained scientists from the Allen Institute for Brain Science. The sugar-cube–size tissue samples come from patients receiving neurosurgery to treat epilepsy or remove deep tumors. Ed Lein—a neuroscientist at the institute—and his team get about 50 brain samples a year. He says the living tissue supports findings not possible from studies of human cell cultures or cells from human cadavers or rodents. For example, serotonin receptors in living human neurons behave very differently than those from animal models.

Many psychological tests used by U.S. courts are flawed

Only 40% of psychological assessment tools used in U.S. courts have drawn favorable ratings in psychology reference books, and many lack a solid research basis, researchers report. The finding builds on previous findings that some judges admit evidence from methodologically flawed studies and that courts struggle to evaluate scientific evidence. The scientists, from several U.S. universities, assembled a list of 364 assessment instruments used in federal and state courts from 2016 to 2018 by psychologists serving as forensic experts. Courts employed the tools to help assess parents in child custody cases and determine whether criminal offenders should go to prison, for example. The findings, described at an AAAS meeting session, were published in the December 2019 issue of *Psychological Science in the Public Interest*. The scientists also found that lawyers challenge the admission of assessment evidence in only about 5% of cases. And only one-third of those challenges succeed.

INFECTIOUS DISEASES

Coronavirus epidemic snarls science worldwide

Experiments are halted as China remains locked down; many conferences are canceled

By **Robert F. Service**

The coronavirus epidemic now racing across China is forcing Jeffrey Erlich, a Canadian neuroscientist at New York University Shanghai, to weigh his science against concern for his staff. Erlich performs animal experiments at a neighboring university; as part of efforts to control the illness, known as COVID-19, officials there have asked him to halt the studies and use as few staff as possible to take care of his animals. But he is training mice and other species on very complex tasks; the interruption could set him back 6 to 9 months. "It's really hard balancing the research productivity of the lab and the safety and comfort of my staff," he says. "When you've invested years of work into experiments, where do you draw the line about what's considered essential?"

Erlich is just one of thousands of scientists in China whose work is suffering. Universities across the country have been closed since the Lunar New Year, 25 January. Access to labs is restricted, and projects have been mothballed, fieldwork interrupted, and travel severely curtailed. Scientists elsewhere in the world are feeling the impact as well, as collaborations with China are on pause and many scientific meetings, some as far away as June, have been canceled or postponed.

The damage to research pales compared with the human suffering wrought by the virus. As *Science* went to press, the total number of cases had risen to 73,332, almost 99% of them in China, and 1873 deaths had been counted; the specter of a pandemic is still very real. Still, for individual researchers the losses can be serious—and stressful. "Basically, everything has completely stopped," says John Speakman, who runs an animal behavior lab at the Chinese Academy of Sciences (CAS) in Beijing. "The disruption is enormous. The stress on the staff is really high." But Speakman says he understands why the Chinese government closed universities and institutes. "It's annoying, but I completely support what they have done," he says.

Disruptions are particularly acute in Wuhan and other cities in Hubei province, the epicenter of the outbreak, which are almost completely cut off from the outside world. "I'm working more now than ever before the epidemic," says Sara Platto, a professor of animal behavior at Jianghan University in Wuhan. But she faces major obstacles: Faculty and students living on campus are confined to their apartments, and Platto, who lives off-campus, can venture outside only once every 3 days. She is working with colleagues in Beijing who are studying the relationship of the novel virus to another coronavirus isolated from a pangolin. But a paper she is writing has been delayed because her notes are in her office and she can't get back on campus.

The situation is not much better in other cities. "Unfortunately, the virus is very annoying with regards to work," says Jingmai O'Connor, a paleontologist at CAS's Institute for Vertebrate Paleontology in Beijing. "There is no one working the collection, no one to sign paperwork so things can't get done, overseas travel is canceled. … No samples can be analyzed, all we can do is work on pre-existing data on our computers," O'Connor says. "It sucks!"

Some researchers in China have switched from lab work to writing papers and grant applications. The National Science Foundation of China has postponed grant application deadlines by several weeks, giving researchers time to catch up. Online classes, which many universities and institutes have ramped up to keep students on schedule, are also keeping scientists busy. Poo Muming, a neuroscientist at CAS's Center for Excellence in Brain Science and Intelligence Technology, says he is teaching daily 2-hour neurobiology lectures: "Surprisingly, there are thousands of people tuning in each day."

China's lockdown is felt even half a world away. Daniel Kammen, a renewable energy researcher at the University of California, Berkeley, says it is impeding his lab's efforts to help set up green transportation projects, including the roll-out of electric taxis, throughout China.

But labs working on the fight against COVID-19 are in overdrive. At Tsinghua University in Beijing, Zhang Linqi has switched from HIV to the novel coronavirus; his lab members even decided to forgo the Lunar New Year celebrations last month. "[We] decided we would celebrate it by conducting research," Zhang says. The team synthesized and characterized the "spike" on the coronavirus's surface, a protein that helps it enter

PHOTO: STRINGER/GETTY IMAGES

Like most universities in China, the campus of Huazhong University of Science and Technology in Wuhan is deserted.

PHOTO: ©GULF NEWS, DUBAI

human cells; Zhang's lab has joined industrial partners to develop a vaccine targeting the spike. Countless infectious disease labs in the rest of the world have put their regular work on hold as well. "The main effect has been the need to triage work, to push other projects to the back burner while we help our Chinese colleagues analyze the vast amount of new COVID-19 data," says Christopher Dye of the University of Oxford.

The spread of the virus has upended plans for numerous scientific conferences. So far, more than a dozen have been canceled or postponed—not just in China but elsewhere in Asia and Europe as well. Among the casualties are the International Society for Stem Cell Research's international symposium, which was scheduled for March in Shanghai, and the 2nd Singapore ECS Symposium on Energy Materials in early April. Organizers of the International Congress on Infectious Diseases, planned for 20-24 February in Kuala Lumpur, Malaysia, postponed their meeting, saying the priority for its registrants is to fight the coronavirus outbreak in their home countries.

Concern is also rising that the epidemic could disrupt the global medicine supply. China and India produce an estimated 80% of all active pharmaceutical ingredients, the raw materials for antibiotics and drugs for cancer, heart disease, and diabetes. With many Chinese factories shuttered, stockpiles could run short. "This is a very acute issue now," says Michael Osterholm, the head the Center for Infectious Disease Research and Policy at the University of Minnesota, Minneapolis, which studies drug availability.

But Mariângela Simão, assistant director general for access to medicines and health products at the World Health Organization, says the agency sees no "immediate risk" of COVID-19 affecting supplies of essential medicines. Simão's team is in daily contact with international pharmaceutical associations, which track shipping disruptions from their member companies. Many companies stockpiled 2 to 4 months of their products prior to the Lunar New Year celebrations, she says. And while Hubei is home to some pharmaceutical companies, far more are in Shanghai and other parts of China that are less affected. But the picture could change if the virus isn't brought under control, Simão notes. "It will all depend on how the situations evolve with the outbreak." ■

With reporting by Dennis Normile, Gretchen Vogel, Jon Cohen, and freelance journalist Rebecca Kanthor in Shanghai.

SCIENTIFIC COMMUNITY

Microbiome researcher accused of sexual misconduct

Questions arise about the work of researcher Jeff Leach, known for studies of Hadza hunter-gatherers in Tanzania

By **Gretchen Vogel**

A researcher famed for his work on the microbiomes of hunter-gatherers has been accused by several women of sexual assault, according to U.S. court documents. Jeff Leach, a resident of Terlingua, Texas, co-founded a major open-source, crowdfunded project on the microbiome and is the co-author of multiple papers on gut microbes, including one in *Science*. In the publicity resulting from the allegations, other questions have emerged about Leach's academic qualifications and his behavior in the field.

The sexual assault accusations came to light as a result of a defamation suit Leach filed in September 2019. In July 2019, Katy Schwartz, who worked at the Terlingua tourist lodge that Leach runs, filed a police report alleging that he had sexually assaulted her. Schwartz did not press charges, but asserts in court documents that she wanted her experience documented because she feared Leach could be a danger to others.

Microbiome researcher Jeff Leach

In the wake of the lawsuit against Schwartz, three other local women filed affidavits. One alleged that Leach had assaulted her, putting his hand up her shorts "without any warning." A second alleged that he raped her in a "violent assault" for which "there was no consent." A third affidavit alleged that Leach sexually assaulted a woman, became violent during an argument, and threatened her with litigation.

Leach and his lawyer, Rae Leifeste, told *Science* that all the charges are unfounded and are a coordinated attack motivated by jealousy and disagreements over money. In an affidavit and in an email to *Science*, Leach says any sexual contact was consensual and claims that, after the alleged attacks, all of his accusers were friendly toward him in text messages and in other encounters.

On 6 February, Presiding Judge Stephen Ables ruled in favor of Schwartz's motion to dismiss the defamation lawsuit, based on "anti-SLAPP" (strategic lawsuits against public participation) laws that protect free speech. Leifeste is preparing an appeal.

Leach has collaborated with researchers at King's College London (KCL), the University of California, San Diego (UCSD), and Stanford University, among others, to study the bacteria that live in the gut and on the skin. He is known for gathering microbiome samples from hunter-gatherers to explore the idea that their microbiomes are healthier than those of people in industrialized societies.

In 2014, Leach gave himself a fecal transplant from a member of the Hadza group of Tanzania, an event widely covered by the media and billed as an effort to boost his health. A few months earlier, he was profiled in *Science* (17 January 2014, p. 241).

Media accounts have described Leach as an anthropologist, but he told *Science* last week that he does not have a Ph.D. On various papers he lists affiliations with the University of Leicester and the London School of Hygiene & Tropical Medicine. KCL officials say he was a visiting research scholar there from August 2016 until July 2018 but is no longer associated with the university. Leach says he is now pursuing a Ph.D. at the University of York, which officials there confirmed. Leach did not answer queries from *Science* about whether he has an undergraduate degree.

Some researchers who have worked with Leach distanced themselves from him in comments to *Science*. In 2012, UCSD microbiome researchers Jack Gilbert and Rob Knight founded the American Gut Project with Leach. The project invites members of the public to submit a skin swab or samples of feces or saliva and pay $99 to have their microbes catalogued. Gilbert says he never met Leach in person, however. "That project

is now completely outside of his activities, and is being administered by the Microsetta Initiative at UCSD with Rob Knight," Gilbert told *Science*. Knight says he no longer collaborates with Leach, and the project's website no longer mentions him.

Another project removed Leach's name from its website last week, after its leaders learned of the lawsuit. Until 5 February, the website of the Microbiota Vault, an international project to collect human microbiome samples, said Leach would "work to secure samples" from remote populations in Tanzania and Namibia. Maria Gloria Dominguez-Bello, a microbiome researcher at Rutgers University and a coordinator of the project, told *Science* she was surprised by the accusations and called the news "very disturbing and sad."

She does not, however, doubt the quality of the samples and data that Leach collected. She notes they are stored in the labs of Knight and microbiome researcher Justin Sonnenburg at Stanford, both of whom have co-authored papers with Leach. Sonnenburg, who is the corresponding author on three papers with Leach, including one in *Science* (25 August 2017, p. 802), said he has never met Leach in person and received the samples via Dominguez-Bello; he declined any further comment.

Research on the Hadza takes "training in ethnographic data collection and, ideally, bioethics.."

Alyssa Crittenden, University of Nevada, Las Vegas

The *Science* paper reported seasonal variation in the Hadza gut microbes, based on samples Leach collected. "It was neat, it was orderly, and the metadata all checked out: Poop was poop, and skin samples were from skin. And when you analyze the samples, they cluster by season," says Dominguez-Bello, a co-author. The paper concludes that the gut flora varies because of seasonal shifts in diet.

Some anthropologists who have worked extensively with the Hadza are skeptical of the paper. Alyssa Crittenden, an anthropologist at the University of Nevada, Las Vegas, says the *Science* paper's generalizations about seasonal foods are "inconsistent with nearly 60 years of data on Hadza diet." In a critique posted on bioRxiv in 2018, she and colleagues reported that they couldn't replicate the paper's results from the authors' open source data.

Dominguez-Bello says, "The discussion [of diet] could be all wrong, but that doesn't invalidate the paper. ...[It] is claiming there are seasonal variations, that's all."

Crittenden says researchers who work with vulnerable groups such as the Hadza need "training in ethnographic data collection and, ideally, bioethics." As part of the case, Schwartz's lawyers submitted an affidavit by a Terlingua man who accompanied Leach to Tanzania in 2014. In it, he states that Leach smoked marijuana with study subjects in exchange for access to samples. In court filings, Leach's lawyers objected to the affidavit, saying the information it contains is not relevant to the defamation case. Leach wrote on his Human Food Project blog that "the Hadza are big pot smokers (they trade honey and meat for weed with the local Datoga)."

Tanzania's National Institute of Medical Research ethics board confirmed that it reviewed Leach's research proposal in 2011 or 2012, but could not say whether he currently has permits to work in the country. A member of the Hadza who is familiar with Leach but requested anonymity told *Science* that Leach's "work seems to be popular in the U.S., but my people don't really understand what it is for."

Daudi Peterson, co-founder of Dorobo Safaris in Tanzania, who works with the Hadza and has helped facilitate Leach's research, says Leach hasn't collected samples from the Hadza for more than a year, in part because he is waiting for permits. Peterson says Leach's relationships with the Hadza are "very good," and that Leach visited twice last year to connect with them. "Even today his name comes up," Peterson says. "He's fondly nicknamed the Hadza word for shit."

Epidemiologist Tim Spector of KCL, who went with Leach to Tanzania in 2017, says he saw no ethical issues with Leach's work. "I don't think he was doing anything others weren't doing."

Leach has had a colorful career. As part of the case, Schwartz's lawyers cited a 2003 civil case in Texas in which Leach was found to have violated laws against deceptive trade practices. The Texas attorney general alleged that Leach had sold subscriptions to magazines that had stopped publishing and had accepted more than $100,000 in payments for a tour in Egypt that was to feature the actor Omar Sharif, but was never organized. Leach failed to contest the claims and the court found them admitted and proven. Leifeste notes Leach has not admitted wrongdoing in this case and says it is not relevant to the lawsuit. Leach also co-launched a pizza chain and helped mount a search for Amelia Earhart's plane using a robotic submarine.

Leach says he plans to do his Ph.D. thesis on the Hadza. In 2018, he told a podcast he wanted to study the microbiome of Hadza children from birth, including collecting breast milk samples from mothers. ■

HUMAN EVOLUTION

Strange bedfellows for human ancestors

Homo erectus and other "super-archaics" may have interbred with ancient humans

By **Ann Gibbons**

The story of human evolution is full of ancient trysts. Genes from fossils have shown that the ancestors of many living people mated with Neanderthals and with Denisovans, a mysterious group of extinct humans who lived in Asia. Now, a flurry of papers suggests the ancestors of all three groups mixed at least twice with even older "ghost" lineages of unknown extinct hominins. One candidate partner: *Homo erectus*, an early human who left Africa by 1.8 million years ago, spread around the world, and could have mated with later waves of human ancestors.

The new genomic studies rely on complex models of inheritance and population mixing, and they have many uncertainties, not least the precise identities of our ancestors' strange bedfellows and when and where the encounters took place. But, taken together, they build a strong case that even before modern humans left Africa, it was not uncommon for different human ancestors to meet and mate. "It's now clear that interbreeding between different groups of humans goes all the way back," says computational biologist Murray Cox of Massey University of New Zealand, Turitea, who was not involved in the new studies.

The gold standard for detecting interbreeding with archaic humans is to sequence ancient DNA from fossils of the archaic group, then look for traces of it in modern genomes. Researchers have done just that with Neanderthal and Denisovan genomes up to 200,000 years old from Eurasia. But no one has been able to extract full genomes from more ancient human ancestors. So population geneticists have developed statistical tools to find unusually ancient DNA in genomes of living people. After almost a

decade of tantalizing but unproven sightings, several teams now seem to be converging on at least two distinct episodes of very ancient interbreeding.

In *Science Advances* this week, Alan Rogers, a population geneticist at the University of Utah, Salt Lake City, and his team identified variations at matching sites in the genomes of different human populations, including Europeans, Asians, Neanderthals, and Denisovans. The team tested eight scenarios of how genes are distributed before and after mixing with another group, to see which scenario best simulated the observed patterns. They conclude that the ancestors of Neanderthals and Denisovans—whom they call Neandersovans—interbred with a "super-archaic" population that separated from other humans about 2 million years ago. Likely candidates include early members of our genus, such as *H. erectus* or one of its contemporaries. The mixing likely happened outside of Africa, because that's where both Neanderthals and Denisovans emerged, and it could have taken place at least 600,000 years ago.

"I think the super-archaics were in the first wave of hominids who left Africa," Rogers says. "They stayed in Eurasia, largely isolated from Africans, until 700,000 years ago when Neandersovans left Africa and interbred with them."

Occurring much earlier than encounters of modern humans with Neanderthals and Denisovans, the episode was "the earliest known interbreeding between ancient human populations and an expansion out of Africa," Rogers says. Other studies have hinted at such ancient mixing, Cox says, but Rogers's analysis is "particularly convincing."

Others, though, say Rogers's bold claim needs testing. One challenge is reconciling it with new results from other researchers that show modern human ancestors mixed with super-archaic groups more recently, in Africa. Just last week, for example, population geneticist Sriram Sankararaman and his student Arun Durvasula at the University of California (UC), Los Angeles, identified signs of a separate, more recent episode of mixing. The researchers analyzed the genomes of 405 people from four subpopulations in West Africa that were included in the 1000 Genomes Project, a catalog of genomes from around the world. They found numerous gene variants not seen in Neanderthals or Denisovans and concluded that the best explanation was that the variants came from an archaic, extinct human.

This ghost species may have been late *H. erectus*, *H. heidelbergensis,* or a close relative. One or more late-surviving members of this ancient group met and mated with the ancestors of living Africans sometime in the past 124,000 years, the modern genomes suggest.

Another paper last month reported Neanderthal DNA in living Africans, likely from migrations back to Africa by early Europeans who bore Neanderthal DNA (*Science*, 31 January, p. 497). Sankararaman thinks some of the archaic DNA he detects in Africans may be from Neanderthals, but most is from the older ghost species. "I think the true picture is a combination of both an archaic population unrelated to Neanderthals as well as Neanderthal-related ancestry," he says.

In December 2019, yet another study found hints of an extinct ghost population in living Africans, although it was silent on the identity of the ghosts and when they bred with our ancestors. Population geneticist Jeff Wall at UC San Francisco and colleagues analyzed 1667 genomes from diverse populations in the GenomeAsia 100K consortium. They reported the strongest ghost signal in the Khoisan people and in Central African hunter-gatherers formerly known as pygmies.

But Wall and others warn their methods cannot rule out that the "ghosts" could be one or several groups of modern humans in Africa that were separated from other moderns for so long that their genes looked "archaic" when the groups finally came together again and mixed. "Our understanding of African population history in particular, is so far behind," says Joshua Akey of Princeton University.

Even if they differ on particulars, the studies emphasize that long after new lineages of humans emerge, they still can mix with others quite different from themselves. Other species, such as cave bears and mammoths, show the same pattern of divergence and later mixing, says population geneticist Pontus Skoglund of the Francis Crick Institute in London. "We are losing the idea that separation between populations is simple with instant isolation." Such mating between long isolated groups may quickly introduce valuable new genes (*Science*, 18 November 2016, p. 818). For example, some of the archaic alleles Sankararaman spotted in Africans were in genes that suppress tumors and regulate hormones.

Today, *H. sapiens* doesn't have the possibility of quickly grabbing a load of diversity by mating with another group: For perhaps the first time in our history, we're the only humans on the planet. It's another reason to miss our extinct cousins, says population geneticist Carina Schlebusch of Uppsala University. "To have such a large densely spread species with … so little genetic diversity … is a dangerous situation," she says. ■

Human ancestors mated with "super-archaics," perhaps like this 700,000-year-old *Homo erectus* from Java.

Ghosts in the family tree

At least two super-archaic "ghost" hominins interbred with the ancestors of Neanderthals, Denisovans, and modern humans (red lines). Later, those three groups also met and mingled (blue lines), leaving complex traces in each other's genomes. (Split times are rough estimates; timeline is not drawn to scale).

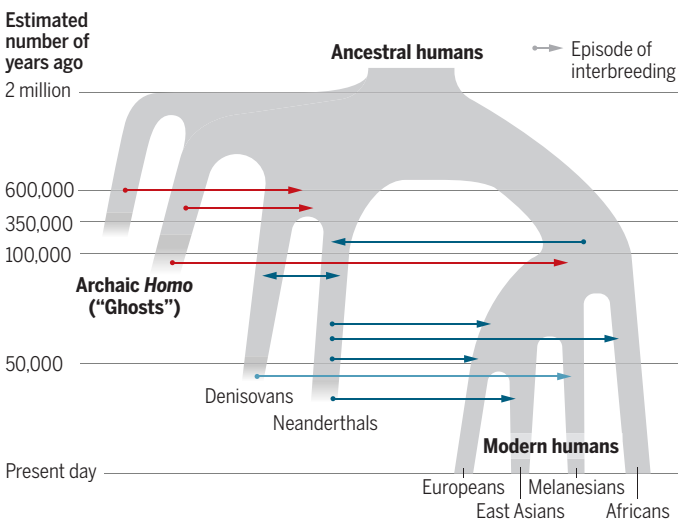

CREDITS: (PHOTO) NATURAL HISTORY MUSEUM, LONDON/SCIENCE SOURCE; (GRAPHIC) VERNOT *ET AL*./*SCIENCE*; ADAPTED BY V. ALTOUNIN/*SCIENCE*. (DATA) A. ROGERS AND S. SANKARARAMAN

MICROBIOLOGY

Tough microbe's DNA could be a lasting archive

Artist and DNA storage pioneer says microbes could preserve a record of humanity

By **Steve Nadis**

Joe Davis is looking for the ultimate time capsule. He wants to preserve a record of humanity that could survive for eons, to be read by successors to *Homo sapiens* on Earth or by sapient extraterrestrials. He has now found the right medium, he thinks: the DNA of an odd microbe that lives in deposits of rock salt. He believes this archive—protected by salt and renewed by the microbe—could possibly survive for hundreds of millions of years.

It's a visionary idea, owing as much to art as science. Davis, an artist affiliated with a Harvard University biology lab, bridges both worlds. His project took a step forward last week with a study posted on bioRxiv, a preprint repository. In the study, Davis and his colleagues show they can encode information in the DNA of *Halobacterium salinarum* (*Hsal*)—a hard-to-kill, salt-tolerant microbe that has, on average, 25 backup copies of each of its chromosomes.

Other researchers have explored the storage potential of DNA, which packs the equivalent of about 300 megabytes of data into the nucleus of a human cell. But Davis is combining that capacity with the resilience of an extraordinarily hardy organism. "If you want to keep data for a long, long time, the best way to do that may be to hold it inside cells and utilize the cellular machinery for DNA self-repair," he says. "They can conveniently and economically reproduce themselves with little or no intervention."

Jeff Nivala, a biological engineer at the University of Washington, Seattle, who studies halophiles and DNA storage, agrees. "For archival storage over millions of years, this might be a great application," he says. "If all other life is destroyed on Earth, and this is the only thing left, maybe that information could propagate on its own."

Davis has no formal training in biology, save for a single course at a Mississippi junior college in the 1960s. But he has a record of turning biology into performance art that sometimes leads back to science. In 1987, for an artistic venture called Microvenus, he encoded a depiction of the female form into the DNA of living *Escherichia coli* bacteria—a feat that is widely cited as the first experimental demonstration of DNA data storage.

Now, Davis is working with a tougher microbe than *E. coli*. *Hsal* can withstand desiccation, thermal extremes, prolonged vacuum, and intense radiation. Davis has even exposed it to ethylene oxide, a poisonous gas used to sterilize laboratory equipment, with no discernible effects. *Hsal* does have a kryptonite: Immersion in freshwater bursts its cells. But when entombed in briny pockets within salt crystals, Davis muses, *Hsal* could be "the thing that couldn't die."

Information was encoded in the DNA of a strain of salt-tolerant *Halobacterium salinarum*.

PHOTO: JOE DAVIS

For commercial DNA storage, in vitro techniques—encapsulating synthetic DNA in glass or stainless steel—are more advanced than in vivo approaches, says Emily Leproust, an organic chemist and CEO of Twist Bioscience. But living things could preserve DNA far longer, says Davis, who has revived hibernating *Hsal* cells from salt deposits hundreds of millions of years old. His collaborator, Harvard geneticist George Church, considers it "totally plausible" that the cells found deep within stable crystals survived all this time in a dormant state. The cells stop growing, and their DNA remains unchanged except for gradual degradation, he says. "But they can also replicate quickly when they need to," he adds, repairing damage and generating lots of copies for researchers to work with. "So *Hsal* appears to be a good choice."

Jocelyne DiRuggiero, a Johns Hopkins University biologist and *Hsal* expert, regards the plan as "a cool idea." Besides enduring environmental stresses, she says, *Hsal* is good at removing reactive oxygen species that harm DNA. With minimal nutrients, an *Hsal* colony could hibernate in salt for hundreds of thousands of years or more, she says. The microbes would not grow or reproduce, she says, and would only use energy to make repairs and counteract threats, such as DNA damage from cosmic rays.

The first step in the new work was to encode data in *Hsal*'s DNA. Davis chose the coordinates for a 3D picture of a needle and egg—objects in a Russian folktale about a wizard who hid his soul in the tip of a needle concealed inside an egg. After Davis synthesized the DNA, Alexandre Bisson, a biologist at Brandeis University, attached it to a site in the *Hsal* genome that wouldn't affect the microbe or produce anything in the cell. Bisson encouraged the modified halobacteria to replicate and sequenced their DNA to ensure the new code was unaltered.

To learn more about the microbes' potential as time capsules, Bisson is studying how they behave in salt crystals, which "is largely a mystery." Over the course of 10 years or more, he plans to compare *Hsal* strains encased in salt with "parent" or control strains kept in a freezer to see whether any mutations occur in the presumably more active salt strains. That data will help fill a void, though extrapolating it to millions of years "would be a stretch," he says. Bisson also plans to use fluorescent proteins to find out whether the organisms stay trapped within the briny pockets that sustain them or if they move around.

Davis hasn't lost sight of the project's primary motivation. "What kind of legacy should humans leave behind as a species?" he asks. Davis doesn't claim to know; he plans to gather input from scientists, historians, artists, poets, and philosophers. But he wants to safeguard more than just information. "I want to preserve the meaning," he says. ■

Steve Nadis is a journalist in Cambridge, Massachusetts.

SYNTHETIC BIOLOGY

In 'living materials,' microbes are makers

Cells enable materials to reproduce or manufacture medicines

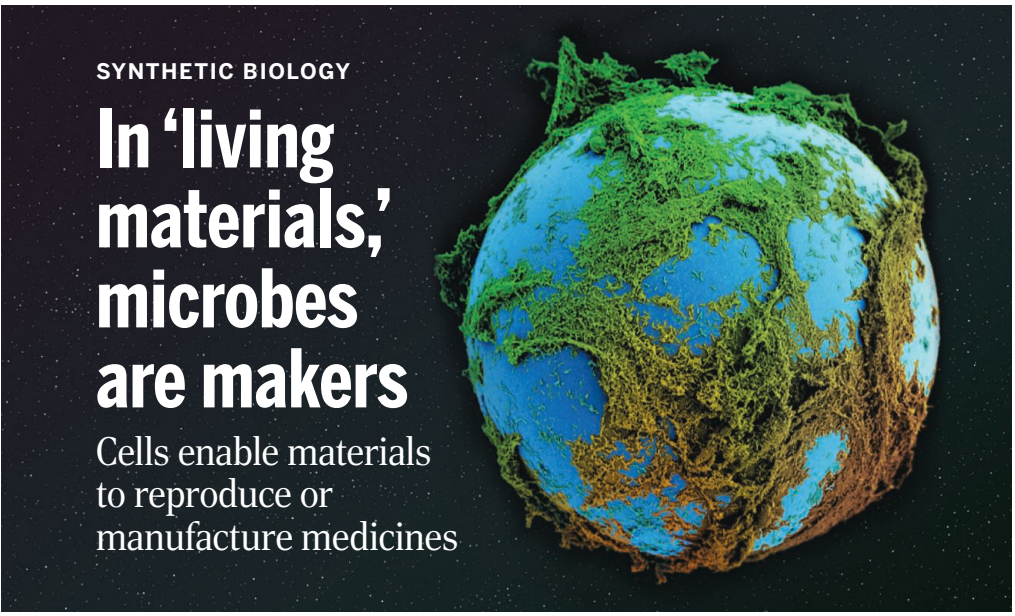

Engineered microbes tailormade this biofilm (green), shown on a glass bead.

PHOTO: NEEL JOSHI

By **Robert F. Service**

The bricks in Wil Srubar's lab at the University of Colorado, Boulder, aren't just alive, they're reproducing. They are churned out by bacteria that convert sand, nutrients, and other feedstocks into a form of biocement, much the way corals synthesize reefs. Split one brick, and in a matter of hours you will have two.

Engineered living materials (ELM) are designed to blur boundaries. They use cells, mostly microbes, to build inert structural substances such as hardened cement or woodlike replacements for everything from construction materials to furniture. Some, like Srubar's bricks, even incorporate living cells into the final mix. The result is materials with striking new capabilities, as the innovations on view last week at the Living Materials 2020 conference in Saarbrüken, Germany, showed: airport runways that build themselves and living bandages that grow within the body. "Cells are amazing fabrication plants," says Neel Joshi, an ELM expert at Northeastern University. "We're trying to use them to construct things we want."

Humanity has long harvested chemicals from microbes, such as alcohol and medicines. But ELM researchers are enlisting microbes to build things. Take bricks, normally made from clay, sand, lime, and water, which are mixed, molded, and fired to more than 1000°C. That takes lots of energy and generates hundreds of millions of tons of carbon emissions annually. A Raleigh, North Carolina, company called bioMASON was among the first to explore using bacteria instead of heat, relying on the microbes to convert nutrients into calcium carbonate, which hardens sand into a sturdy construction material at room temperature.

Now, several groups are taking the idea further. "Could you grow a temporary runway somewhere by seeding bacteria in sand and gelatin?" asks Sarah Glaven, a microbiologist and ELM expert at the U.S. Naval Research Laboratory. In June 2019, researchers at Wright-Patterson Air Force Base in Ohio did just that to create a 232-square-meter runway prototype. The hope, says Blake Bextine, who runs an ELM program for the U.S. Defense Advanced Research Projects Agency, is that rather than ferrying tons of materials to set up expeditionary air fields, military engineers could simply use local sand, gravel, and water, and apply a few drums of cementmaking bacteria to create new runways in days.

The bricks and runway cement don't retain living cells in the final structure. But Srubar's team is taking that next step. In their self-reproducing bricks, researchers mix a nutrient-based gel with sand and inoculate it with bacteria that form calcium carbonate. They then control the temperature and humidity to keep the bacteria viable. The researchers could split their original brick in half, add extra sand, hydro-gel, and nutrients, and watch as bacteria grew two full-size bricks in 6 hours. After three generations, they wound up with eight bricks, they reported in the 15 January issue of *Matter*. (Once the bacteria are done growing new bricks, the team can turn off the temperature and humidity controls.) Srubar calls it "exponential material manufacturing."

ELM makers are also harnessing microbes to make biomaterials for use in the human body. Microbes naturally exude proteins that bind to one another to form a physical scaffold. More bacteria can adhere to it, forming communal microbial mats known as biofilms, found on surfaces from teeth to ship hulls. Joshi's team is developing biofilms that could protect the gut lining, which erodes in people with inflammatory bowel disease, creating painful ulcers. In the 6 December 2019 issue of *Nature Communications*, they report that an engineered *Escherichia coli* in the guts of mice produced proteins that formed a protective matrix, which shielded the tissue from chemicals that normally induce ulcers. If the approach works in people, physicians could inoculate patients with an engineered form of a microbe that normally makes its home in the gut.

In another medical use, bacteria could turn conventional materials into drug factories. In the 2 December 2019 issue of *Nature Chemical Biology*, for example, Christopher Voigt of the Massachusetts Institute of Technology and his colleagues describe seeding a plastic with bacterial spores that continuously generate bacteria. The microbes synthesize an antibacterial compound effective against *Staphylococcus aureus*, a dangerous infectious bacterium.

A team of researchers led by Chao Zhong of ShanghaiTech University engineered biofilms for a different purpose: detoxifying the environment. They started with the bacterium *Bacillus subtilis*, which secretes a matrix-forming protein called TasA. Other researchers had shown that TasA was easy to genetically engineer to bind to other proteins. The team tweaked TasA to get it to bind an enzyme that degrades a toxic industrial compound called mono (2-hydroxyethyl terephthalic acid), or MHET. The researchers then showed that biofilms created by the engineered bacterium could break down MHET—and that biofilms made by a mix of two engineered strains of *B. subtilis* could carry out a two-step degradation of an organophosphate pesticide called paraoxon. The results, which the team reported in the January 2019 issue of *Nature Chemical Biology*, raise the prospect of living walls that purify the air.

Regulatory issues could slow progress, however. Many of the bacteria that ELM researchers have harnessed occur in nature and should not trigger regulatory scrutiny. But genetically engineered organisms will—and the prospect of engineered microbes embedded in, say, living walls might unsettle regulators. Still, Voigt predicts, "I think in 10 years, we're going to find living cells in a whole range of living products." ■

#METOO MOVES SOUTH

The fight against harassment in Latin American science gains strength

By **Lindzi Wessel** *and* **Rodrigo Pérez Ortega**

For decades, from his base at the University of Los Andes (Uniandes) in Bogotá, Colombia, biologist Adolfo Amézquita Torres made his name studying the diverse, jewel-like poisonous frogs of the Andes and the Amazon. But on campus, he compiled a darker record, former and current students have alleged in dozens of complaints. They say he mistreated women, including by favoring and emotionally abusing female students he was dating and retaliating against those who rejected his advances or complained about his behavior. Earlier this month, university officials concluded he was guilty of sexual harassment and misconduct and fired him in a watershed moment for the university—and for a growing effort to fight sexual misconduct on campuses across Latin America.

Amézquita Torres, who until recently was head of Uniandes's biology department, tells *Science* he did have consensual relationships with students, but claims that such dating was long considered acceptable and that he didn't knowingly violate any university rules. He denies harassing, favoring, or retaliating against anyone, and says he will challenge the 6 February verdict, claiming the process was flawed and unfair. He vows to "use all available legal tools to recover as much as I can of my dignity."

The firing marked a dramatic turn in a twisting, nearly 15-month-long controversy, which deeply divided one of Latin America's most prestigious private universities and was closely watched by Colombia's media and women's rights groups. Many applauded the university's decision. "This is going to send a huge message … I think instructors are going to be much more careful," says ecologist Ximena Bernal, a native of Colombia who earned her undergraduate degree at Uniandes and now works at Purdue University.

But she and others complain that the Uniandes investigation was marred by bureaucratic bungling and a lack of transparency. They say those missteps, which included reversing an earlier decision to fire Amézquita Torres, highlight how universities across Latin America are struggling to protect women within cultures that have long tolerated, and even celebrated, male privilege and a set of attitudes known as machismo.

"There is a lot of variation from university to university, but some places exhibit rampant and almost institutionalized ma-

PHOTO: MARCELO HERNANDEZ/GETTY IMAGES

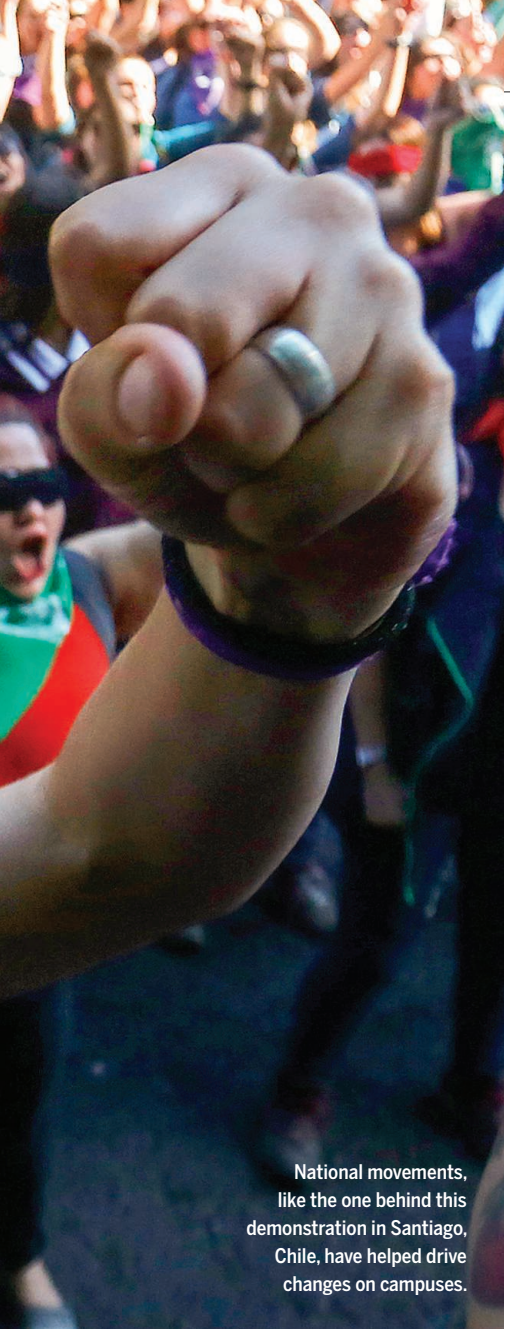

National movements, like the one behind this demonstration in Santiago, Chile, have helped drive changes on campuses.

chismo," says Juan Manuel Guayasamin Ernest, a herpetologist at San Francisco University of Quito in Ecuador. And although women have gained ground in employment and status at Latin American universities in recent years, most research institutions are still "dominated by men surrounded by more men," he says.

Such masculine demography has helped promote a sometimes toxic atmosphere for women in academia—including faculty and students in the sciences—according to dozens of researchers from across Latin America who spoke with *Science*. Machismo can actively deter women from pursuing a career in scientific research, Bernal says. "We have lost a lot of scientists because of this."

Many universities in the region lack formal policies for reporting, investigating, or punishing abuse or sexual misconduct, or don't rigorously enforce the policies they do have. And campus administrators have long winked at potentially problematic behaviors, such as male faculty members dating their female students. Women who speak out about such issues can face retaliation and public vilification. "It's very common to hear … 'Oh yeah, those feminazis, they're just crazy people,'" says Jennifer Stynoski, a herpetologist from the United States who works at the University of Costa Rica, San José.

Now, the tide might be turning. At Uniandes and elsewhere, administrators are promising to adopt stronger policies and enforce them. In some countries, legislators and agencies are moving to enact new, nationwide standards for reporting sexual harassment at campuses and research institutes. In 2019, more than 250 researchers signed a letter, published in *Science*, urging "scientists and institutions across Latin America to be aware of the damage that machismo, and its denial, inflicts on women and the enterprise of science as a whole," and to take stronger action to deter misbehavior. And an emerging constellation of advocacy groups has been ratcheting up the pressure for reform through social media campaigns, legal challenges, and other tactics—including marches and even the takeover of university buildings.

"In Latin American countries in the last 5 years or so, we've had this movement against gender-based violence and harassment," says Mario Pecheny, a political science researcher at the University of Buenos Aires. "It's raised a huge mobilization of women."

"Some places exhibit rampant and almost institutionalized machismo."

Juan Manuel Guayasamin Ernest, San Francisco University of Quito

NATIONS IN LATIN AMERICA have some of the world's highest reported rates of violence against women, according to a 2017 United Nations report. University campuses are no exception. The National University of Colombia, Bogotá, surveyed 1602 of its female students and found that more than half reported experiencing some kind of sexual violence while on campus or during university-related activities. (The survey was first reported by Vice Colombia.) Verbal harassment and discrimination are at least as prevalent.

But when victims go to university officials to report harassment or an assault, they often meet with indifference or confusion. In part, that's because many administrators have no guidebook. In 2019, journalists Ketzalli Rosas, Jordy Meléndez Yúdico, and a team of 35 reporters at Distintas Latitudes, a digital news platform that covers Latin America, surveyed 100 universities in 16 Latin American nations and found that 60% lacked policies for handling sexual harassment complaints.

Janneke Noorlag, a Dutch immigrant to Chile, got a firsthand look at the consequences of such gaps when she was a master's student studying environmental sustainability at the Pontifical Catholic University of Chile (PUC), Santiago. In 2015, Noorlag's husband and a faculty member, acting on her behalf, filed a sexual assault complaint against one of Noorlag's classmates and a second man. PUC declined to investigate because it "lacked the competence and technical means to investigate properly," according to a letter it sent to Noorlag's husband. The university acknowledges that, at the time, it had no "specific protocols on sexual violence."

Instead, university officials told Noorlag to pursue the matter with local law enforcement. (She did; they declined to pursue charges.) Noorlag says she ultimately dropped out of PUC because of the university's lapses, including allowing one of her alleged attackers to continue to attend classes and serve as a teaching assistant. (A university spokesperson says it did ultimately suspend the alleged attacker from teaching, adding that PUC now has a policy against allowing complainants and alleged perpetrators to attend the same classes.) Now, Noorlag says, "I really have no trust in university authorities."

Even a formal policy "doesn't guarantee anything," says Meléndez Yúdico, who is director of Distintas Latitudes. Some policies can be difficult to implement because they lack important details, he says, such as a clear deadline for filing complaints, definitions of ambiguous terms, and procedures for protecting an accuser's identity. And the existence of a policy "doesn't mean the will is there to use it," Meléndez Yúdico says. Universities have let cases drag on indefinitely, without communicating a timeline for resolution, says Isadora Fragoso, an undergraduate student at the National Autonomous University of Mexico (UNAM), Mexico City, and a member of the feminist student movement Rosas Rojas (Red Roses). "Although women go to the appropriate authorities to make complaints … they simply remain archived," she says. "They never proceed."

When universities do take action against alleged harassers, the punishment can seem mild. In 2017, Austral University of Chile scrambled to develop a sexual misconduct policy for professors after multiple allegations emerged against a prominent

faculty member, biochemist Alejandro Yáñez Cárcamo. Complainants alleged he had harassed a female administrator working under him, assaulted a female student, and made inappropriate comments toward women. (Yáñez Cárcamo did not respond to requests for comment.) In April 2018, after an investigation, the university suspended him from teaching for 2 years, but allowed him to continue his research at a field station.

Protests by those who felt the school's actions weren't strong enough erupted throughout Chile. At Austral, faculty and students took over a building and went on strike. The university then moved to fire Yáñez Cárcamo, but a court reinstated him, ruling he could not be punished twice for the same misbehavior. In September 2018, the case received renewed attention when Yáñez Cárcamo attended a campus event—defying a request from the university's president to stay away—and was confronted by ecologist Olga Barbosa, then a professor at the university, who respectfully asked him to leave. A photograph of the confrontation went viral, and the incident made Barbosa, now the southern regional secretary for Chile's Ministry of Science, Technology, Knowledge and Innovation, an icon for antiharassment activists. (Yáñez Cárcamo remains on the faculty and was allowed back on campus last year.)

In an image that went viral, ecologist Olga Barbosa confronts alleged harasser Alejandro Yáñez Cárcamo on a Chilean campus.

AT UNIANDES, the contentious case of Amézquita Torres put the challenges facing Latin American universities in the #MeToo era on very public display. Administrators at the university, which enrolls nearly 25,000 undergraduate and graduate students and is considered one of Latin America's top 10 training institutions, first began to examine the allegations against the herpetologist in November 2018, according to documents obtained by *Science*. That was just 2 years after Uniandes became one of the first universities in Colombia to adopt rules on reporting and investigating allegations of abusive behavior and sexual misconduct. By then, Amézquita Torres, who arrived at Uniandes as an undergraduate in 1985, had established an active international research program and become head of the biology department.

As word of the complaints against Amézquita Torres spread, some students and faculty rallied to his defense, praising him as a skilled mentor and researcher and arguing he was being attacked for behavior—particularly dating students—long considered acceptable. Others took a decidedly different view. Female and male complainants, as well as more than 20 people familiar with the case interviewed by *Science*, paint Amézquita Torres as a charismatic but mercurial personality who fostered divisiveness. "You go from being on his good side to being on his bad side, and then you kind of have this verbal abuse wrath," says one man, a former Uniandes student who worked with Amézquita Torres and asked not to be named for fear of retaliation. "He'll start not reading your manuscripts, he'll start neglecting you."

Mónica Pinzón, a former student of Amézquita Torres who is now a filmmaker, wrote to the university last year to describe how he targeted her for retribution. In 2003, he made sexually charged remarks and subjected her to "unmeasured rage" after she camped in an unapproved site during a field trip, she wrote. After that, "His treatment was horrible. … He wouldn't read my thesis. … He made the rest of my time in the lab very bitter," she says. Pinzón was also distressed by what she describes as controlling and manipulative behavior by Amézquita Torres toward his then-girlfriend, who was a student. The experience led Pinzón to leave academia. "The only thing I regret," she says, "is not speaking up when these things were happening."

In interviews with *Science* and in lengthy statements sent to the university, Amézquita Torres flatly denied many of the specific allegations against him, including that he retaliated against students. "I don't do that … I am not aggressive to the students," he told *Science* prior to the university's announcement that it was firing him. Many of the accusations, he said, were the result of a "witch hunt" led by one person who had a conflict with him over "politics and money." "Having relationships with the students," he said, "makes you vulnerable to people with evil intentions."

Such defenses ultimately did not sway university officials, but the process that produced their verdict was chaotic. In early 2019, after an initial investigation, the university fired Amézquita Torres for failing to disclose his sexual relationships with students, ruling that such ties constituted conflicts of interest. But he won reinstatement after arguing the university hadn't followed proper procedures. The university then removed him as head of the biology department and barred him from teaching, but allowed him to continue his research, while a special faculty panel conducted a new investigation.

In March 2019, fearing that the university was burying the case, the complainants and their allies used public demonstrations and other tactics to press their demands for more information and action. On social media, users widely shared a video of a student reading aloud from a statement written by a woman who claimed that Amézquita Torres had harassed her. Nearly 300 alumni of the biology department signed a letter to university officials, urging them to clarify where the investigation stood. Allies of Amézquita Torres responded by condemning the pressure campaign, and the researcher himself went to court in a bid to silence media outlets covering the case and students sharing the video on social media. He failed.

Amid the escalating public battle, Uniandes got a new president: economist Alejandro Gaviria Uribe, a former minister of health in Colombia. When he arrived in July 2019, Gaviria Uribe recalls promising to bring the case to "a fair and quick" resolution. "Unfortunately, the process [took] longer than I expected," he told *Science* earlier this month.

Now, students and faculty on all sides are digesting the verdict. "Before, [such behavior] was normalized," says a member of the university's faculty who asked not to be named for fear of retaliation. "But now, with the #MeToo movement and the various other movements of female students, it has stopped being normal. The spark has ignited so that this case would finally explode."

"This isn't just about him. … It's an action against bad behavior in science," adds one of the complainants, who asked to remain anonymous because of fears of

SCREENSHOT: TWITTER

In Santiago, Chile, women demonstrate against impunity for aggressors in a public performance piece that has since been replicated in many other nations.

PHOTO: JAVIER TORRES/AFP/GETTY IMAGES

retaliation. "It took us literally years, but something finally happened."

Gaviria Uribe has vowed to fix the bureaucratic problems exposed by the case. Although the sexual misconduct policy Uniandes adopted in 2016 "has no precedents in Colombia and only a few in Latin America … we still have much to learn," he says. The university plans to offer legal resources to complainants, he says, and add courses on gender issues. Officials will also need to define what constitutes appropriate relationships between students and professors, Gaviria Uribe notes.

Many hope the campus can now start to heal. Uniandes officials will be moving students who had been studying with Amézquita Torres to new supervisors. But biologist Catalina Palacios, a Uniandes doctoral student who aided some of the complainants, says, "We expect rough days ahead in terms of trying to rebuild the community here."

THE UNIANDES CASE underscores how far universities in Latin America have yet to go in addressing sexual harassment issues. One needed step, Bernal says, is for universities to step up training and awareness. She recalls that it wasn't until she left Colombia for the United States in 2001 that she realized behaviors long tolerated at Latin American universities weren't OK. Recently, she spoke to a group of female Ecuadorian students who characterized their university as free of harassment—until Bernal started to ask specific questions about whether their professors dated their students and made sexist remarks. "They were like, 'Oh yeah, well, guys are guys,'" she says. "When you think this is the norm, you don't realize there's a problem."

In 2018, such experiences led Bernal to circulate the letter eventually published in *Science* (22 February 2019, p. 825) that called for obliterating that norm. "Latin American women scientists … are immersed in a society where culturally ingrained masculine pride ('machismo') is normalized and deeply intertwined with the scientific endeavor," Bernal and her cosigners wrote. "Machismo promotes sexist attitudes that often pass unnoticed," they added. They urged scientists in the region to become "proactive about recognizing, confronting, and penalizing inappropriate behaviors."

Bernal and others see signs of progress, including a recent uptick in the number of universities adopting policies on sexual misconduct. UNAM, which adopted its policy in 2016, says it has now fielded more than 1200 complaints and ousted about 100 alleged perpetrators—albeit sometimes after student protests that included building takeovers. Mexican academics campaigning against harassment have even adopted a popular hashtag: #MeTooAcademicos (#MeTooAcademics). And across Latin America, students have taken to social media under the hashtag #MePasóEnLaU (It happened to me in the university).

The campus-based movements echo broader campaigns against gender violence. Brazil has #NãoéNão (No is No), Argentina #NiUnaMenos (Not One Less), and Chile Educación No Sexista (Nonsexist Education). In many countries, activists have replicated a Chilean mass protest anthem and performance, called "Un Violador En Tu Camino" ("A Rapist In Your Path"), which includes women donning blindfolds and chanting against impunity for aggressors.

Science groups and governments are also moving to address sexual misconduct in research. In recent years, major conferences held in the region—including those sponsored by the Latin American Conference of Herpetology and the Colombian National Conference of Zoology—have added symposiums on the issue. In August 2019, the Chilean Senate approved a bill requiring all government-sponsored institutions to develop detailed sexual harassment policies; the bill now awaits action in its House of Representatives. And the country's science ministry recently announced a gender equality policy. Argentina's National Scientific and Technical Research Council is working to establish similar policies at its research centers.

In many Latin American nations, inaction remains the norm. Yet Barbosa is encouraged by what she is seeing. The rising challenge to machismo, she says, has helped her realize that she's "not crazy" for envisioning a better future for female researchers in Latin America. Those who commit harassment and abuse are beginning to face consequences, she says, which is what is needed "to make sure that this will not happen to anyone else." ■

Lindzi Wessel is a journalist in Santiago, Chile.
Rodrigo Pérez Ortega is *Science*'s news intern.

CLIMATE

Old methane and modern climate change

Old methane is less important for our immediate future than contemporary sources

By **Joshua F. Dean**

Carbon is stored over thousands of years in many natural reservoirs in land and ocean ecosystems. This is vital for regulating global climate. These old carbon stores are vulnerable to climate change, which can cause this carbon to be released in the form of greenhouse gases such as methane. If these gases reach the atmosphere, they can drive further warming, which has implications for all life on Earth (see the figure) (*1*). But such positive feedback loops are a major uncertainty when predicting future climate change (*2*). On page 907 of this issue, Dyonisius *et al.* (*3*) describe their search for signals of old methane released to the atmosphere during the last deglaciation about 18,000 to 8000 years ago. This was when Earth last showed warming similar to what is predicted for our immediate future. They found that methane emissions from old carbon sources during this time were small, suggesting that substantial emissions of old methane may not be triggered in response to current and near-future climate change.

School of Environmental Sciences, University of Liverpool, Liverpool, UK. Email: joshua.dean@liverpool.ac.uk

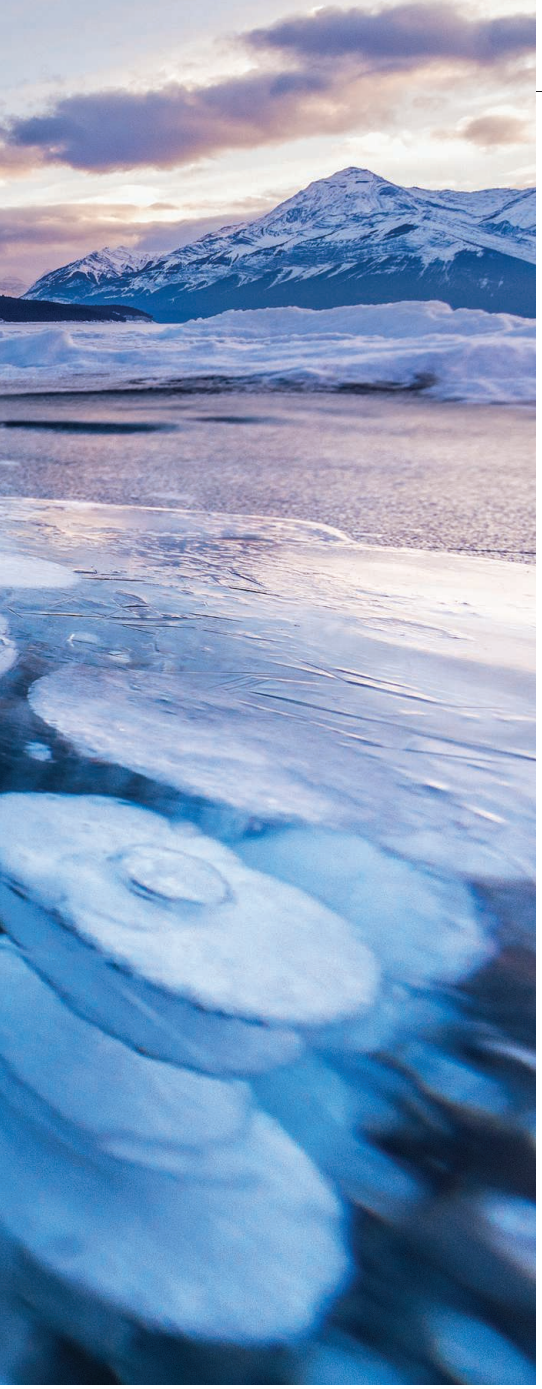

Methane gas bubbles released from lakes in permafrost regions can be generated from thawing reservoirs of old carbon.

Methane is about 86 times mores powerful as a greenhouse gas than carbon dioxide over a 20-year time period—the time scale in which global action is needed to reduce carbon emissions from human activities and limit catastrophic climate change. The two main sources of potential methane release to the atmosphere from destabilization of old carbon stores are methane hydrates and permafrost regions of the Arctic, taiga forests, and Tibetan Plateau (*4*). During the last deglaciation period, Earth shed much of its vast glacial ice sheets as the global climate warmed by around 4°C. If old methane was an important driver of that period of warming, it will likely be important in modern climate change.

Dyonisius *et al.* extracted methane from ice cores collected in Antarctica for radiocarbon (carbon-14) dating in the same way an archaeologist radiocarbon dates cultural artifacts. Contemporary methane will have a radiocarbon age close to the year of its release. By contrast, old methane will be so old that it will have no radiocarbon in it at all, a state known as "radiocarbon dead." Ice core records trap bubbles of air during formation, and these bubbles represent an archive of atmospheric composition that spans up to a million years. However, large amounts of ice on the order of 1000 kg are needed for a single radiocarbon date of this methane. The study of Dyonisius *et al.* presents an impressive 11 such dates spanning 15,000 to 8000 years ago.

Dyonisius *et al.* found no evidence for substantial releases of methane from old carbon sources. The methane they found was overwhelmingly contemporary relative to the time period that each sample represented, indicating that the vast majority of methane in the atmosphere during the period under study was derived from the decomposition of recently formed organic carbon, such as plants and soil, and not from the destabilization of old carbon stores. Given the substantial size of these old carbon reservoirs and their theorized sensitivity to climate change, why don't we see evidence for their release as methane?

Most old methane is oxidized before it can reach the atmosphere

Whether released from melting methane hydrates or produced from thawing permafrost, to reach the atmosphere, old methane must avoid being oxidized to carbon dioxide by microorganisms.

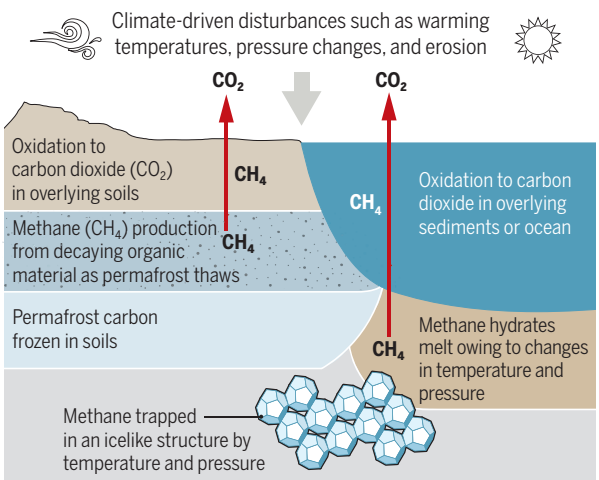

Methane hydrates contain between 500 and 4000 giga–metric tons of old carbon, roughly one to five times the amount of carbon currently in the atmosphere (including carbon dioxide). This old carbon is mostly biologically produced methane that has been trapped in a crystalline water (icelike) structure as the result of low temperatures and high pressures. Methane hydrates are found deep in the ocean and also trapped under permafrost and glacial ice sheets. Regions of permanently frozen ground, or permafrost, contain around 1300 giga–metric tons of carbon in frozen soils, almost a quarter of which is at least as old as the last glacial maximum (*5*). Both methane hydrates and permafrost are carbon reservoirs that are vulnerable to climate warming because their storage capabilities are temperature controlled. Methane hydrates are also vulnerable to pressure changes owing to sea level fluctuations and disappearing permafrost and ice sheets.

However, old methane release occurs much slower than the pace of modern climate change. This is because methane is a rich source of energy within ecosystem food webs, particularly for microorganisms that consume this methane and release carbon dioxide. Thus, old methane is often rapidly consumed by microorganisms living in sediments, soils, and water, which convert it to carbon dioxide before it can be released to the atmosphere (*6*, *7*). Some methane will escape this process and, along with the carbon dioxide produced from these microorganisms, will still have the potential to influence global climate (*8*).

How important will old methane be to modern climate change? Old methane release may have been important in the geological past because of the long time scales involved (*9*). Hundreds or even thousands of years of warming may be required to generate sustained methane release from old carbon stores that can then outpace methane consumption (*4*, *8*). Old methane release therefore does not occur fast enough nor at magnitudes that will be important in the immediate future when compared with methane release from contemporary sources such as wetlands and human activity, which release a third

GRAPHIC: N. CARY/SCIENCE

and half of all methane currently in the atmosphere, respectively (*2*, *10*, *11*). And despite the potency of methane as a greenhouse gas, it is still second in importance to carbon dioxide, which is a much more abundant climate pollutant from human industrial activity and a product of natural ecosystem carbon cycling.

Slowing modern climate change is important to decrease the chance of old methane adding substantially to an already overloaded atmospheric carbon pool (*11*). Reduction of methane as a product of human activity, such as agriculture and the fossil-fuel industry, remains an important component of climate change mitigation efforts (*2*, *12*). Although methane hydrates and permafrost carbon are unlikely to be major sources of methane to the atmosphere in the immediate future, unrestrained climate change over the coming century could lead to their destabilization. This could drive sustained emissions of old methane to the atmosphere over the following centuries, causing further warming.

How much methane would be released, at what rates, and for how long are important unanswered questions. In the geological past before the time span of ice cores, the full importance of methane to global climate fluctuations is a mystery. To better explore this geological time span, the development of a useful proxy for past atmospheric methane concentrations, parallel to what is used as a proxy for carbon dioxide (*13*), remains an elusive goal (*14*). It will also be important to search for evidence of old methane release as an indicator of destabilization of current old carbon reservoirs and to serve as a baseline for the future. Methane hydrates and permafrost regions are large potential sources of old methane to the atmosphere in the long term but are less important for our immediate future than contemporary sources. ■

REFERENCES AND NOTES

1. C. D. Elder *et al.*, *Nat. Clim. Chang.* **8**, 166 (2018).
2. E. G. Nisbet *et al.*, *Global Biogeochem. Cycles* **33**, 318 (2019).
3. M. N. Dyonisius *et al.*, *Science* **367**, 907 (2020).
4. J. F. Dean *et al.*, *Rev. Geophys.* **56**, 207 (2018).
5. J. Strauss *et al.*, *Earth Sci. Rev.* **172**, 75 (2017).
6. J. W. Pohlman *et al.*, *Proc. Natl. Acad. Sci. U.S.A.* **114**, 5355 (2017).
7. M. D. A. Cooper *et al.*, *Nat. Clim. Chang.* **7**, 507 (2017).
8. B. Ferré *et al.*, *Nat. Geosci.* **13**, 144 (2020).
9. J. Frieling *et al.*, *Proc. Natl. Acad. Sci. U.S.A.* **113**, 12059 (2016).
10. M. Saunois *et al.*, *Earth Syst. Sci. Data* **8**, 697 (2016).
11. S. E. Mikaloff Fletcher, H. Schaefer, *Science* **364**, 932 (2019).
12. R. B. Jackson, E. I. Solomon, J. G. Canadell, M. Cargnello, C. B. Field, *Nat. Sustain.* **2**, 436 (2019).
13. C. R. Witkowski, J. W. H. Weijers, B. Blais, S. Schouten, J. S. Sinninghe Damsté, *Sci. Adv.* **4**, eaat4556 (2018).
14. G. N. Inglis, B. D. A. Naafs, Y. Zheng, J. Schellekens, R. D. Pancost, *Geochim. Cosmochim. Acta* **260**, 244 (2019).

10.1126/science.aba8518

TOPOLOGICAL MATTER

Two paths to intrinsic quantization

A pair of materials demonstrate new and different routes to an exotic quantum behavior

By **Joshua P. Wakefield** *and* **Joseph G. Checkelsky**

Topological states of quantum matter hold promise as platforms for the next generation of electronics. They are characterized by the entanglement of their electron wave functions and properties inherently robust against disorder, but often only occur at low temperature, high magnetic field, or both. Combining magnetism with topology in a two-dimensional (2D) material opens the possibility of achieving an exotic phase known as the quantum anomalous Hall (QAH) insulator. Conceptually, QAH insulators could be stable at ambient conditions, but experimentally their observation has been limited to a single class of disordered systems at extremely low temperature. On pages 895 and 900 of this issue, Deng *et al.* (*1*) and Serlin *et al.* (*2*), respectively, report the discovery of the QAH effect in two materials that are driven by "intrinsic" magnetism. Not only do these effectively triple the number of QAH material platforms, but their dissimilarity also strongly suggests that there may be a multitude of material realizations beyond those presently known.

The QAH phase is insulating in its interior with chiral electrical currents running along its physical edge (see the figure). The circulation is dictated by the direction of spontaneous magnetization. This state is a close cousin of the integer quantum Hall insulator found in 2D systems subjected to large external magnetic fields. Stabilizing this type of phase instead with spontaneous magnetic order removes the need for the large external field sources. Additionally, the high-temperature stability of many magnetic materials raises hopes for bringing exotic quantum behavior to conditions acceptable for use in devices.

In 1988, F. D. M. Haldane first theorized that the quantum Hall effect could occur without an external magnetic field by placing magnetic moments at the center of each hexagon of the honeycomb lattice (*3*). This celebrated "toy model" was the first for a QAH insulator, and it inspired further developments in topology of electronic materials (*4*). In a QAH insulator, each edge current channel is topologically quantized to identically contribute e^2/h to the transverse (known as Hall) conductivity of the system (e is the charge of an electron and h is the Planck constant). As a result, dissipationless quantum modes carry the currents, which cannot backscatter into the insulating bulk or be otherwise altered.

Several proposals were put forward to realize a QAH insulator. In 2010, combining topology and magnetism was suggested by doping a magnetic element, Cr, into the topological insulator Bi_2Se_3 (a nonmagnetic analog of Haldane's model) (*5*). Four years later, the QAH phase was demonstrated, following this blueprint, through the growth of epitaxial thin films of $Cr_x(Bi,Sb)_{2-x}Te_3$ (*6*). A large technical challenge for this experiment was that, because of the randomly distributed Cr atoms, very low temperatures, below 0.05 K, were required to observe the QAH behavior. Although subsequent structural refinements increased the "operation temperature" of the QAH effect to above 1 K (*7*), the question remained whether any other system, especially one with intrinsic magnetism, could support the QAH phase.

Deng *et al.* and Serlin *et al.* both answer that question, but their pathways to the answer are remarkably different. Deng *et al.*, studied manganese bismuth telluride ($MnBi_2Te_4$), a system recently confirmed to be an antiferromagnetic topological insulator (*8*). Although similar to the original QAH platform material in that it combines the local magnetism of a transition element (Mn) with a topological insulator (Bi_2Te_3), $MnBi_2Te_4$ is an ordered crystal composed of pure MnTe blocks inserted into Bi_2Te_3 layers. The Mn atoms form ferromagnetic layers, but when stacked within $MnBi_2Te_4$, these layers couple between each other antiferromagnetically. This reveals a difference between the prototypical QAH insulator and $MnBi_2Te_4$; $MnBi_2Te_4$ has layers with alternating magnetic order instead of having a net magnetization that determines the edge current circulation. Deng *et al.* circumvented

Department of Physics, Massachusetts Institute of Technology, Cambridge, MA, USA. Email: checkelsky@mit.edu

Two routes to a QAH insulator

Two different materials with intrinsic magnetism were shown to host a quantum anomalous Hall (QAH) insulator state. In $MnBi_2Te_4$ (left, 1), the local spin magnetic moments of Mn align within a plane, but anti-align between adjacent planes. This allows for a QAH state in a five-layer device. Twisted bilayer graphene between hexagonal boron nitride (hBN) (right, 2) instead shows orbital ferromagnetism where the rotational motions of the electrons align. The close lattice alignment between the top hBN and graphene layers leads to the QAH behavior.

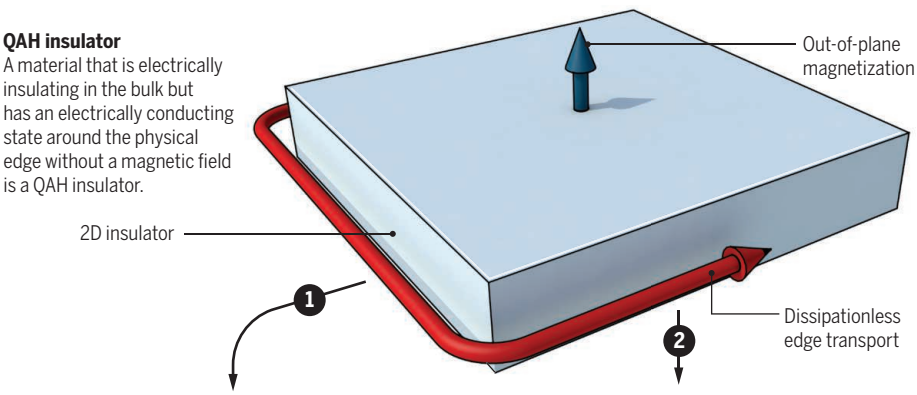

Five-layer device
$MnBi_2Te_4$ is naturally occurring and has an intrinsic magnetic moment if the material has an odd number of layers.

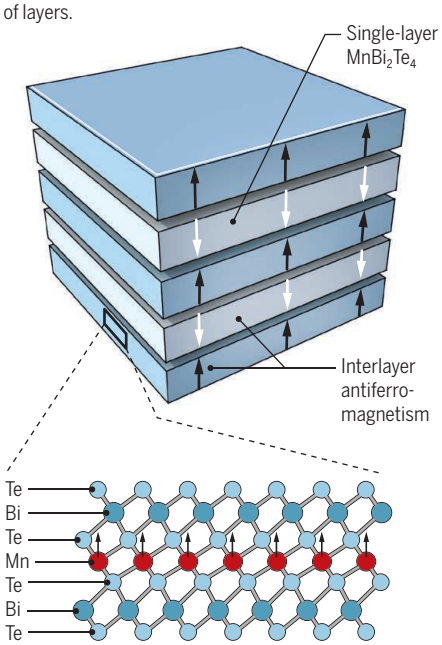

Atomic layering of $MnBi_2Te_4$
A close-up look at the magnetization for one layer of the material is shown.

Twisted bilayer graphene
Stacking bilayer graphene with hBN produces an intrinsic magnetic moment.

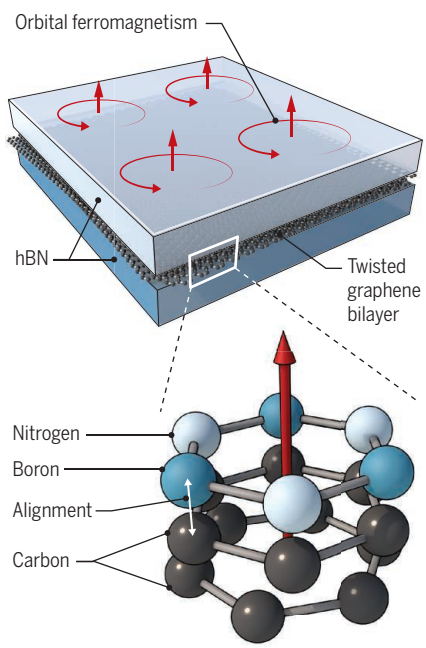

Origin of orbital ferromagnetism
The combination of layers creates the magnetic properties at the atomic scale.

GRAPHIC: C. BICKEL/*SCIENCE*

this by mechanically exfoliating their crystals down to a small, odd number of atomic layers, effectively removing the symmetric balance of magnetic layers. This enabled the detection of the QAH effect above 1 K.

Serlin *et al.* used modern techniques of 2D layer-by-layer assembly to construct a bilayer of graphene (BLG) sandwiched between layers of hexagonal boron nitride (hBN). The topological electronic structure was generated by a special "magic-angle" twist between the orientations of the two sheets of graphene (*9*), and magnetism arises from the orbital motion of the electron wave functions, driven by the effect of electron-electron interactions (*10*). However, akin to the symmetry of the antiferromagnetic order in $MnBi_2Te_4$, the BLG component of this structure has a crystallographic symmetry that needs to be broken to realize the QAH phase.

Serlin *et al.* overcame this limitation by using a device in which the lattice orientation of the top layer of graphene is precisely aligned with the hBN above it. Hexagonal boron nitride breaks the symmetry, as a 180° rotation exchanges the locations of boron and nitrogen atoms. When closely aligned, the coupling between the graphene and hBN also breaks the rotational symmetry for the BLG system, allowing ferromagnetism and the QAH effect to emerge above 1 K. Additionally, they found that the magnetism in this system could be permanently reversed by applying pulses of current as low as 1 nA, much lower than in other systems. This distinctive behavior could represent a new direction for the field of spintronics.

Deng *et al.* and Serlin *et al.* together provide an elegant experimental demonstration of the essential role of topology in condensed-matter science. Deng *et al.* studied a crystal formed by nature in a thermodynamic reaction, whereas Serlin *et al.* assembled an artificial one by hand in an extreme out-of-equilibrium process. For the former, local magnetism of a transition element is the driving factor, whereas for the latter, it is itinerant orbital magnetism. Despite these and other seemingly fundamental distinctions, one could not tell the two apart if shown only the main experimental results, which is equivalent to measuring the topological class of Haldane's toy model.

Research in this area is rapidly evolving, with the potential to further increase the QAH temperature for both these materials. Closely related materials are proving to be important platforms for this as well as other new exotic topological states. A recent report shows that devices made from an even number of $MnBi_2Te_4$ layers have the potential to host an elusive axion insulator state (*11*); other assemblies of graphene and boron nitride multilayers have exhibited features suggestive of a QAH state with two chiral edge channels instead of one (*12*). These observations suggest that a simpler, more prototypical high-temperature ferromagnetic material with the topology of QAH states may be on the horizon. Ultimately, the discovery of two ordered QAH systems paves the way for discovering many more such materials and reinforces hopes to someday realize such behavior at room temperature. ■

REFERENCES AND NOTES

1. Y. Deng *et al.*, *Science* **367**, 895 (2020).
2. M. Serlin *et al.*, *Science* **367**, 900 (2020).
3. F. D. M. Haldane, *Phys. Rev. Lett.* **61**, 2015 (1988).
4. C. L. Kane, E. J. Mele, *Phys. Rev. Lett.* **95**, 226801 (2005).
5. R. Yu *et al.*, *Science* **329**, 61 (2010).
6. C.-Z. Chang *et al.*, *Science* **340**, 167 (2013).
7. M. Mogi *et al.*, *Appl. Phys. Lett.* **107**, 182401 (2015).
8. M. M. Otrokov *et al.*, *Nature* **576**, 416 (2019).
9. Y. Cao *et al.*, *Nature* **556**, 80 (2018).
10. A. L. Sharpe *et al.*, *Science* **365**, 605 (2019).
11. C. Liu *et al.*, *Nat. Mater.* (2020); https://doi.org/10.1038/s41563-019-0573-3.
12. G. Chen *et al.*, arXiv [cond-mat.mes-hall] (2019); https://arxiv.org/abs/1905.06535.

10.1126/science.aba5313

NEUROBIOLOGY

Cross-modal sensory transfer: Bumble bees do it

Stored sensory input permits two sensory channels to exchange and compare information

By **Gerhard von der Emde**[1] *and* **Theresa Burt de Perera**[2]

Animal sensory systems acquire information about the physical world by transforming external stimuli into signals that can be read and interpreted by the nervous system. Animals possess several senses that provide separate streams of information based on different physical stimuli. However, objects and environments contain inherently multimodal information. Thus, neurobiologists have sought to define the mechanisms by which information is processed when it is received by different senses (*1*). Cross-modal recognition—the ability to transfer information across senses, irrespective of the sense that first accessed that information—is a highly complex cognitive capacity that was thought to be limited to vertebrates. Now, on page 910 of this issue, Solvi *et al.* (*2*) show that bumble bees are capable of performing the same task.

Humans execute spontaneous cross-modal recognition fairly easily (*3*). For example, people often rummage blindly through pockets to find, by touch, a set of keys that they first encountered visually. Cross-modal recognition is also useful for increasing the flexibility of object-recognition systems. The finding by Solvi *et al.* illustrates that tiny invertebrates, with brain structures that differ greatly from those of vertebrates, also can experience an object with one sensory modality and later recognize that same object with a different sensory modality.

Simple forms of cross-modal information transfer, which are based on direct associations between two specific stimuli, have been observed in various animal groups, including insects (*4*, *5*). However, cross-modal object recognition requires additional and more complex conditions—in particular, that the two senses provide information that is matched in content. This means that both senses provide information about the same characteristic of an object, such as its shape or surface structure. In addition, the sensory inputs must be encoded in a way that allows temporally disjointed information from two senses to be identified as identical, even though these senses rely on different physical stimuli. Thus, characteristic object features are stored in a neuronal representation that can be accessed by multiple senses. Up to now, spontaneous cross-modal object recognition has been described only in mammalian species (humans, apes, monkeys, dolphins, and rats) (*6*–*8*) and in one aquatic creature, the weakly electric elephantnose fish (*9*).

Solvi *et al.* trained bumble bees to discriminate two differently shaped objects (cubes and spheres) using only touch (in darkness) or only vision (in light, but where they could not touch the objects). After training, the bees discriminated between the same objects using only the information from the other sensory modality. This observation suggests that the brain encoded the sensory input in a way that allowed the two sensory channels to exchange information and to compare and match object-related inputs.

The mechanisms by which bees accomplish this task have yet to be elucidated. Perhaps the bee's brain stores a representation of the object in a way that allows it to be accessed and understood across different sensory systems. The sensory information would need to be integrated to form a representation that is independent of the sensory modality through which the information was introduced (that is, both senses use a matched encoding format). This would enable bees to recognize objects cross-modally without any previous experience, and cross-modal object recognition would not require training. Alternatively, information that originates from multiple senses might initially be unmatched in format, and cross-modal object recognition could depend on sensory experience and learning. In this case, bees might have learned to associate visual and tactile inputs of basic features common in other environmental objects when exposed to these features in the past. For example, a bee might have learned to associate a visual and a tactile image of a curved edge or a corner. Subsequently, these associations would generalize to new objects and new situations.

Whatever the mechanism, cross-modal object recognition requires storage (in the brain) of a representation of the object's features that can be accessed by different senses. This implies that an object can be recognized with a sense through which it had never before been experienced. Solvi *et al.* show that this capability exists in an insect brain, which contains a small fraction of the numbers of neurons in vertebrate brains (*10*).

How the organization of sensory systems achieves cross-modal object recognition remains unanswered. Sense organs respond to the physical stimuli of the outside world and

General scheme of cross-modal transfer

In both vertebrates and invertebrates, sense organs respond to physical stimuli and transfer information to specific monomodal sensory nuclei in the brain (dark yellow, vision; light yellow, touch). These nuclei then communicate, in a reciprocal manner, with multimodal sensory nuclei in higher brain centers. In principle, cross-modal sensory transfer can occur at any stage after the first monomodal sensory nuclei.

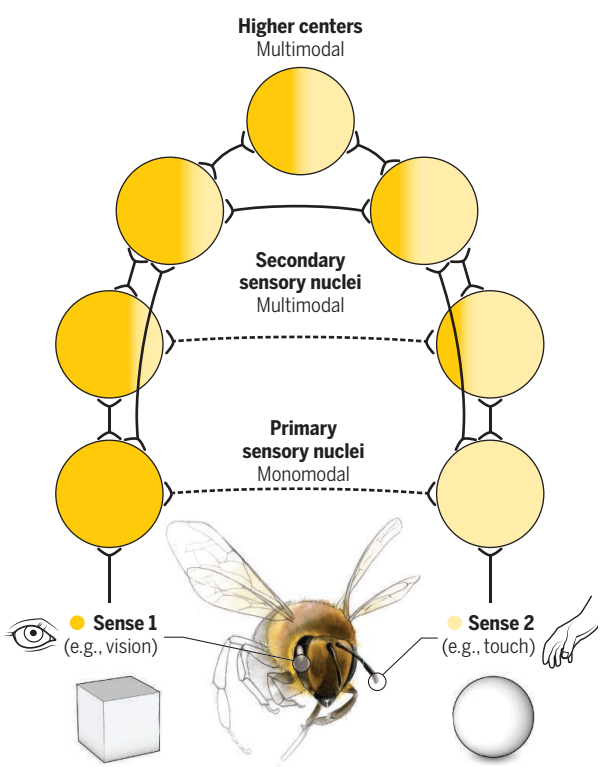

GRAPHIC: V. ALTOUNIAN/*SCIENCE*

[1]Institute of Zoology, University of Bonn, Bonn, Germany. [2]Department of Zoology, University of Oxford, Oxford, UK.
Email: vonderemde@uni-bonn.de; theresa.burt@sjc.ox.ac.uk

transduce them into action potentials encoding the specific stimulus parameters. Connections are then made with nerve cells in dedicated sensory nuclei in the brain, which in turn project to sensory nuclei in higher brain centers for further processing. These nuclei also project back to lower processing centers, forming reciprocal circuits and adding to the complexity (see the figure).

For multisensory integration and cross-modal transfer to occur, information from the different sensory modalities that encode characteristics of the same object must come together, eventually forming a multisensory representation of the object. In most cases, scientists still do not know exactly where in the sensory pathway this occurs, particularly in bees and fish, which do not possess specialized cortical structures. One possibility is that higher brain structures, such as the cortex in mammals or the mushroom bodies and central complex in bees, form the anatomical substrate for multisensory representations (*6*, *11*). Alternatively, because cross-talk between the senses also occurs at lower levels (e.g., in the midbrain and diencephalon) (*1*, *12*, *13*) and because sensory nuclei on different levels are connected in a reciprocal manner, a distributed representation of object properties might occur in several interconnected multisensory nuclei.

The fact that bees can achieve cross-modal object recognition might have implications for how we think about cognition in general. In humans, scientists assume that this ability involves mental imagery (*14*) based on internal representations in higher brain centers. Thus, some researchers have argued that this task relies on awareness. Whether that is also the case in bumble bees is a matter of debate, as simpler explanations are possible. Whatever the underlying mechanism, the newly found ability of bumble bees to perform cross-modal recognition shows that, like humans, they possess a sensory integration system that allows them to form a complex representation of their world. ■

REFERENCES AND NOTES

1. B. E. Stein *et al.*, *J. Neurosci.* **40**, 3 (2020).
2. C. Solvi, S. Gutierrez Al-Khudhairy, L. Chittka, *Science* **367**, 910 (2020).
3. M. O. Ernst, M. S. Banks, *Nature* **415**, 429 (2002).
4. J. Guo, A. Guo, *Science* **309**, 307 (2005).
5. L. Proops *et al.*, *Proc. Natl. Acad. Sci. U.S.A.* **106**, 947 (2009).
6. B. D. Winters, J. M. Reid, *J. Neurosci.* **30**, 6253 (2010).
7. L. M. Herman *et al.*, *J. Comp. Psychol.* **112**, 292 (1998).
8. A. Cowey, L. Weiskrantz, *Neuropsychologia* **13**, 117 (1975).
9. S. Schumacher *et al.*, *Proc. Natl. Acad. Sci. U.S.A.* **113**, 7638 (2016).
10. M. Giurfa, *Trends Neurosci.* **36**, 285 (2013).
11. F. Peng, L. Chittka, *Curr. Biol.* **27**, 224 (2017).
12. M. Zeymer *et al.*, *Front. Neuroanat.* **12**, 79 (2018).
13. H. F. Sperdin *et al.*, *Front. Neurosci.* **4**, 9 (2010).
14. B. Nanay, *Cortex* **105**, 125 (2018).

10.1126/science.aba8519

PHOTO: HU *ET AL.* (2)

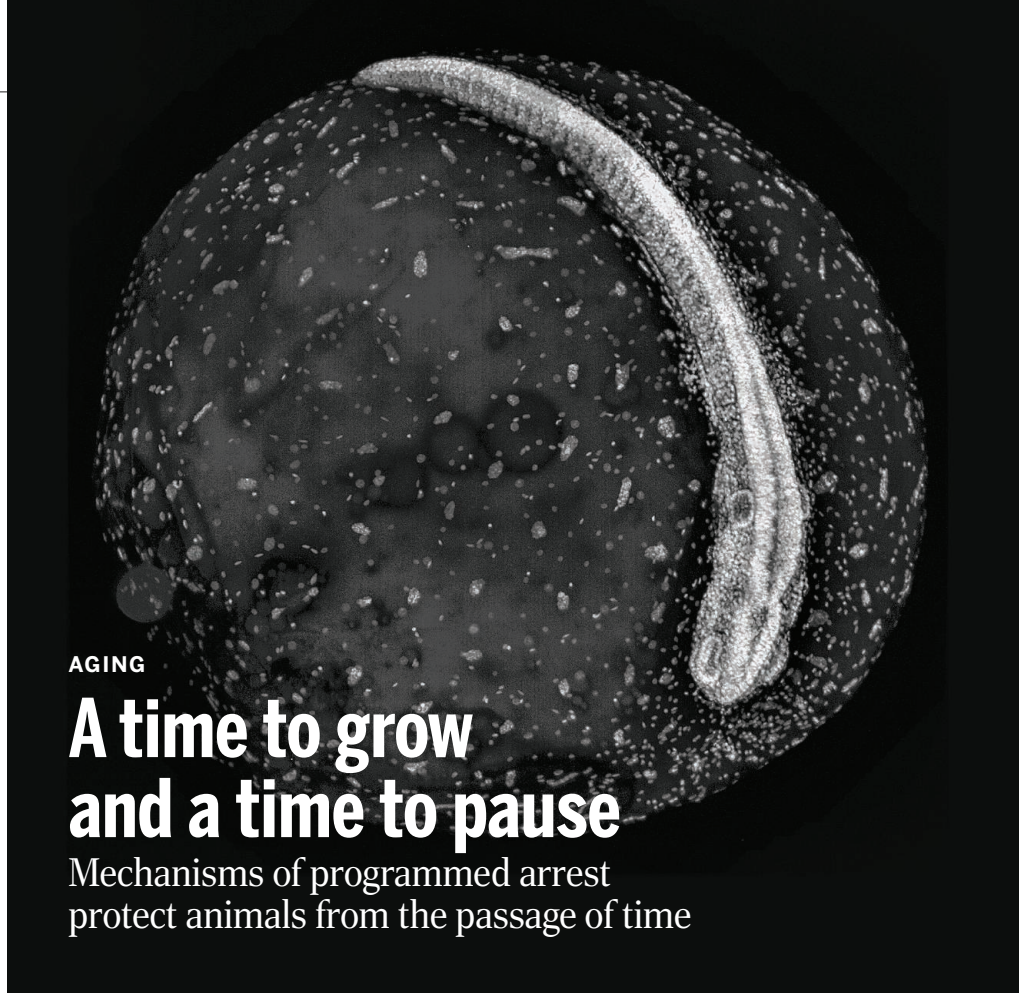

AGING

A time to grow and a time to pause

Mechanisms of programmed arrest protect animals from the passage of time

By **Marc Van Gilst**

An African turquoise killifish embryo developmentally suspended in the state of diapause. This vertebrate model could improve the understanding of aging.

Seasonal or environmental pressures are sometimes best dealt with by putting growth and reproduction on hold. Many animals have evolved mechanisms for reversibly arresting development at discrete developmental stages, so that the arrested embryo or larva can wait for more favorable conditions in which to resume development, grow, and reproduce. One common form of developmental arrest is diapause, which generally constitutes a genetically programmed arrest at a discrete point in development, most often in an embryonic, larval, or pupal stage (*1*). Diapause also involves physiological changes that protect the arrested animal from aging. On page 870 of this issue, Hu *et al.* (*2*) identify some of the mechanisms that maintain embryonic diapause in an emerging model of vertebrate aging, the African turquoise killifish. These findings might provide insight into the mysteries of aging and longevity.

Examples of diapause are found throughout the animal kingdom and have been well characterized in insects, fish, and mammals (*1*). Diapause may take the form of a facultative diapause, which is induced in response to environmental challenges such as starvation or dehydration, or an obligate diapause, which is generally brought about by seasonal pressures such as a harsh winter (*3*). Although diapause involves an arrest of development, the arrested state is not static. Indeed, diapause usually involves considerable physiological changes that help to prepare the animal to survive the forthcoming environmental challenges (*4*). These physiological changes also protect arrested animals, allowing them to be preserved for long periods of time until conditions are more favorable for development and reproduction.

In the simplest sense, aging is considered the inevitable wear and tear brought on by the passage of time. The basic idea is that the more time passes, the more an animal ages and the more it progresses toward its ultimate demise. This simplistic perspective is somewhat fatalistic and defines time as the ultimate enemy of youth. However, it has been established in many animals that aging is also heavily influenced by genetic and physiological programs, such that aging may not necessarily be an inevitable consequence

Department of Anesthesiology and Pain Medicine, University of Washington, Seattle, WA, USA. Email: vangilst@uw.edu

of time (*5*). One of the hallmarks of diapause is that animals can spend exceptionally long periods, sometimes multiple lifetimes, in an arrested state without substantially affecting the longevity or fertility of the animal once it resumes development. That is, the time spent in diapause does not "count" toward the overall aging of the animal.

Perhaps the most notable and well-studied example of the aging-resistant nature of diapause is the free-living nematode worm *Caenorhabditis elegans*. When grown under standard laboratory conditions, the normal lifespan of a *C. elegans* adult is 15 to 20 days. However, if *C. elegans* larvae are challenged with food deprivation and crowding, they often arrest as larvae in what is called the dauer diapause (*6*). Animals can remain in this state for 6 months or more, but no matter how long they remain in diapause, when they exit diapause they live a normal ~15- to 20-day lifespan as adults. In this way, the dauer diapause can extend the total lifespan of a worm by a factor of 10 to 20. That physiological mechanisms exist for resisting the negative consequences of the passage of time is one of the most interesting aspects of diapause. Further studies in *C. elegans* have shown that genetic manipulation of the genes involved in inducing and maintaining the larval diapause can also markedly extend the longevity of fully grown adults, and therefore that the anti-aging mechanisms of larval diapause may be transferable to adult animals (*7*, *8*).

However, many factors that influence aging or are influenced by aging, such as an adaptive immune system or a complex nervous system, are not present in nematodes or other invertebrate models. Therefore, establishing models of diapause in vertebrates is essential for furthering our understanding of anti-aging mechanisms and potentially translating them to human aging. Indeed, embryonic diapause is quite common in vertebrates such as fish and mammals (*1*, *3*). The African turquoise killifish has recently been developed as a model to study vertebrate aging because killifish share many vertebrate-specific features that play important roles in longevity, such as complex immune, cardiovascular, and nervous systems. Moreover, killifish are susceptible to some of the same aging-associated diseases that affect vertebrates, including humans (*9*–*11*). Among vertebrate models, killifish is a favorite because of its highly compressed lifespan of only 4 to 6 months, considerably shorter than more common vertebrate research models such as mice (2 years) and zebrafish (up to 4 years). Thus, aging studies can be conducted more quickly and in a more high-throughput fashion (*9*–*11*).

Hu *et al.* demonstrate that African turquoise killifish embryos can spend an additional lifetime or more in diapause without consequences for the total lifespan and fertility of the adults. Therefore, like *C. elegans* diapause, African turquoise killifish embryos are protected from the wear and tear of time, meaning that the killifish diapause possesses vertebrate anti-aging mechanisms potentially of considerable relevance to human aging.

Hu *et al.* demonstrate that diapause is a highly active state with considerable changes in gene expression during both induction and maintenance of diapause. The expression of genes involved in cell proliferation and organ development is down-regulated throughout diapause, whereas the expression of genes involved in muscle development and function is induced in early diapause, suggesting an important role for muscle maintenance during diapause. Among the genes whose expression is most strongly induced are regulators of chromatin, specifically the Polycomb group of transcriptional repressors. The expression of one of these Polycomb group family members, the chromobox 7 (*CBX7*) gene, is highly up-regulated throughout diapause. Disruption of *CBX7* expression revealed that CBX7 directly or indirectly represses genes involved in metabolism while stimulating the expression of genes involved in muscle maintenance and neurotransmission processes. Of note, the authors show that muscle tissue is not properly maintained during diapause in African turquoise killifish lacking *CBX7* expression.

Further study is required to more completely map the anti-aging mechanisms of diapause. But when there is a more complete understanding of diapause, the next step in the search for the fountain of youth will be to determine whether, similar to observations in nematodes, activation of CBX7 or other anti-aging mechanisms of diapause in adults can prevent aging and aging-associated disease later in life. ■

REFERENCES AND NOTES

1. S. C. Hand, D. L. Denlinger, J. E. Podrabsky, R. Roy, *Am. J. Physiol. Regul. Integr. Comp. Physiol.* **310**, R1193 (2016).
2. C.-K. Hu, X. Liu, J. Wang, *Science* **367**, 870 (2020).
3. L. Deng *et al.*, *Anim. Reprod. Sci.* **198**, 1 (2018).
4. L. Schiesari, M. B. O'Connor, *Curr. Top. Dev. Biol.* **105**, 213 (2013).
5. C. J. Kenyon, *Nature* **464**, 504 (2010).
6. J. R. Cypser, P. Tedesco, T. E. Johnson, *Exp. Gerontol.* **41**, 935 (2006).
7. C. Kenyon, J. Chang, E. Gensch, A. Rudner, R. Tabtiang, *Nature* **366**, 461 (1993).
8. H. A. Tissenbaum, G. Ruvkun, *Genetics* **148**, 703 (1998).
9. C. K. Hu, A. Brunet, *Aging Cell* **17**, e12757 (2018).
10. K. L. M. Martin, J. E. Podrabsky, *Dev. Dyn.* **246**, 858 (2017).
11. J. E. Podrabsky, S. C. Hand, *J. Exp. Biol.* **218**, 1897 (2015).

10.1126/science.aba8064

INFECTIOUS DISEASE

Toward a universal flu vaccine

A vaccine adjuvant elicits broad protection against influenza in animals

By **Susanne Herold**[1,2] and **Leif-Erik Sander**[3,4]

Influenza virus infections pose a major public health threat, accounting for 3.5 million severe infections and more than 400,000 deaths globally each year (*1*). Most seasonal vaccines consist of inactivated influenza virus components, which induce antibody responses against immunodominant epitopes in the viral hemagglutinin (HA) and neuraminidase (NA) proteins. The genes that encode HA and NA undergo continuous changes (antigenic drift), which necessitates annual reformulation and revaccination, leading to reduced vaccine coverage. Vaccine effectiveness thus varies depending on the accuracy of preseasonal predictions, and inactivated seasonal influenza vaccines generally provide insufficient protection against pandemic viruses (*2*). On page 869 of this issue, Wang *et al.* (*3*) explore an unconventional strategy to overcome these shortcomings by complementing inactivated influenza virus vaccines with an adjuvant that triggers mucosal immune responses to elicit rapid protection against a variety of influenza virus strains in mice and ferrets.

Current strategies for the development of such universal flu vaccines mainly focus on the generation of broadly protective antibodies directed against conserved but immunosubdominant viral surface epitopes that are accessible to antibody binding, such as the stalk region of HA and, recently, the active site of NA (*4*, *5*). In contrast to antibody responses (which are produced by B cells), virus-specific $CD8^+$ T cells generated in response to natural influenza virus infection may provide broad protection against infections with numerous virus subtypes (heterosubtypic protection) (*6*).

2′,3′-cyclic guanosine monophosphate–adenosine monophosphate (cGAMP) is a second messenger produced in response to viral infections and a potent activator of the innate immune sensor stimulator of interferon genes (STING) (*7*). To mimic natural influenza in-

fection and to elicit CD8⁺ T cell–mediated immunity, Wang *et al.* used cGAMP as an adjuvant to an inactivated influenza virus vaccine. Pulmonary surfactant (PS) is a phospholipoprotein complex produced by alveolar epithelial cells (AECs) to reduce surface tension and prevent alveolar collapse. Because PS is recognized by lung-resident alveolar macrophages, the authors used lipid components of PS to encapsulate cGAMP. They found that intranasally administered PS-GAMP nanoparticles were readily taken up by alveolar macrophages in mice. cGAMP was transferred from alveolar macrophages to AECs, where STING was subsequently activated.

Intranasal application of PS-GAMP nanoparticles together with an inactivated H1N1 influenza virus vaccine provided robust heterosubtypic protection—including against seasonally circulating H3N2, influenza B virus (IVB), and highly human-pathogenic avian H5N1 and H7N9—in mice and ferrets. Protection was observed as early as 2 days after vaccination and was maintained for up to 6 months. The PS-GAMP adjuvant vaccine elicited robust virus-specific CD8⁺ T cell responses days after immunization, and high-antibody titers were detected 2 weeks after vaccination.

Heterosubtypic protection after live viral infection has been linked to the presence of cross-reactive T cells (*8*, *9*). Recent studies have uncovered broad cross-reactivity among human influenza virus–specific CD8⁺ T cells (*10*, *11*), and cross-reactive CD8⁺ T cells have been associated with protection against heterosubtypic symptomatic influenza in humans (*12*), thus making T cells an appealing target for universal influenza vaccines. Animal studies have indicated that local immunity—in particular, tissue-resident memory T cells (T_{RM} cells) in the lung—are critical determinants of protection against heterosubtypic influenza virus infection (*13*, *14*). Hence, successful T cell–based universal vaccine strategies will likely require the generation of cross-reactive T_{RM} cells in the respiratory mucosa.

Strengthening influenza virus vaccination

Nasal delivery of inactivated H1N1 influenza virus and the adjuvant PS-GAMP leads to uptake by alveolar macrophages. cGAMP is transferred to AECs, where it activates STING. This stimulates DC differentiation and maturation, increases antibody production, and leads to a robust effector CD8⁺ T cell response and T_{RM} cells. Together, this provides strong heterosubtypic immunity in mice and ferrets.

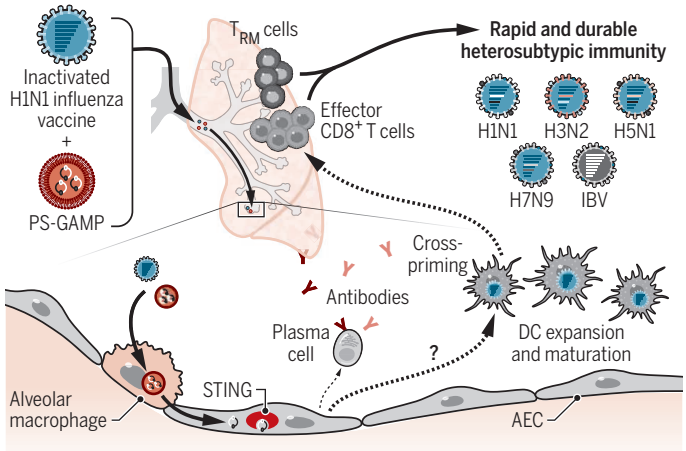

AECs, alveolar epithelial cells; cGAMP, 2′,3′-cyclic guanosine monophosphate–adenosine monophosphate; DC, dendritic cell; IBV, influenza B virus; PS-GAMP, pulmonary surfactant–cGAMP; STING, stimulator of interferon genes; T_{RM} cell, tissue-resident memory T cell.

The only live attenuated influenza vaccine (LAIV) licensed for use in humans is administered as a nasal spray. It induces cross-reactive T cells and generates CD8⁺ T_{RM} cells in respiratory tissues in mice, which is generally not observed with commonly used inactivated influenza vaccines given by intramuscular or subcutaneous injection (*14*). Both mucosal delivery and viability of LAIV were required for the generation of protective T_{RM} cells in mice. Wang *et al.* found that intranasal application of inactivated H1N1 with PS-GAMP led to an early increase in natural killer cells (which have antiviral functions) and pulmonary dendritic cells (which bridge innate and adaptive immunity by presenting antigens to T cells), followed by an accumulation of CD8⁺ T cells with a typical T_{RM} phenotype in the lungs of vaccinated mice. Further experiments in mice revealed that STING activation in AECs orchestrated dendritic cell recruitment and subsequent CD8⁺ T_{RM} cell generation (see the figure).

These results point to a central role of the alveolar epithelium in this protective multicellular cross-talk. AEC secretion of the cytokine granulocyte-macrophage colony-stimulating factor (GM-CSF) has been found to enhance the antigen-presenting capacity of lung dendritic cells, resulting in accelerated CD8⁺ T cell–mediated clearance of influenza viruses (*15*). Intranasal PS-GAMP administration also transiently increased GM-CSF and the cytokine interferon-β (IFN-β) in the lung, but the exact mechanisms by which cGAMP-STING–activated AECs expand lung dendritic cells and promote CD8⁺ T cell responses remain to be explored.

Promising advances toward universal influenza vaccines have been made in recent years, and several candidates are currently undergoing clinical testing (*4*, *5*). Recent strategies for universal influenza vaccines have centered on the generation of broadly protective antibodies, whereas the approach of Wang *et al.* elicited T cell–mediated heterosubtypic immunity. However, heterosubtypic protection induced by intranasal LAIV or previous influenza virus infection in humans is generally less effective compared with experimental mouse models (*5*, *14*). This discrepancy may be caused by interspecies variations and general differences between controlled experimental models and clinical reality. Although STING ligands have recently attracted attention as potential immunotherapeutics in cancer, their role in human T cell and vaccine responses remains to be investigated. It will therefore be critical to evaluate the efficacy of cGAMP as an adjuvant for mucosal influenza vaccines and their effect on cross-protective T cells in humans and other natural hosts for influenza viruses, such as pigs. Ultimately, effective adjuvants and targeted delivery systems combined with broadly protective vaccine antigens to elicit both cross-reactive CD8⁺ T cells and cross-protective antibodies may represent the most effective approach for urgently needed universal influenza vaccines. ■

[1]Department of Internal Medicine II for Pulmonary and Critical Care Medicine and Infectious Diseases, Universities of Giessen and Marburg Lung Center (UGMLC), [2]German Center for Lung Research (DZL), Giessen, Germany. [3]Department of Infectious Diseases and Pulmonary Medicine, Charité-Universitätsmedizin Berlin, Freie Universität Berlin, Humboldt-Universität zu Berlin, Berlin Institute of Health, Berlin, Germany. [4]DZL, Berlin, Germany. Email: susanne.herold@innere.med.uni-giessen.de

GRAPHIC: A. KITTERMAN/*SCIENCE*

REFERENCES AND NOTES

1. A. D. Iuliano *et al.*, *Lancet* **391**, 1285 (2018).
2. S. Yamayoshi, Y. Kawaoka, *Nat. Med.* **25**, 212 (2019).
3. J. Wang *et al.*, *Science* **367**, eaau0810 (2020).
4. D. Stadlbauer *et al.*, *Science* **366**, 499 (2019).
5. D. S. Rajão, D. R. Pérez, *Front. Microbiol.* **9**, 123 (2018).
6. S. Sridhar, *Front. Immunol.* **7**, 195 (2016).
7. J. Wu *et al.*, *Science* **339**, 826 (2013).
8. J. L. Schulman, E. D. Kilbourne, *J. Bacteriol.* **89**, 170 (1965).
9. S. H. Seo, M. Peiris, R. G. Webster, *J. Virol.* **76**, 4886 (2002).
10. M. Koutsakos *et al.*, *Nat. Immunol.* **20**, 613 (2019).
11. S. Sridhar *et al.*, *Nat. Med.* **19**, 1305 (2013).
12. A. C. Hayward *et al.*, *Am. J. Respir. Crit. Care Med.* **191**, 1422 (2015).
13. S. R. McMaster, J. J. Wilson, H. Wang, J. E. Kohlmeier, *J. Immunol.* **195**, 203 (2015).
14. K. D. Zens, J. K. Chen, D. L. Farber, *JCI Insight* **1**, e85832 (2016).
15. B. Unkel *et al.*, *J. Clin. Invest.* **122**, 3652 (2012).

ACKNOWLEDGMENTS

The authors are supported by the German Research Foundation [DFG; SFB1021 197785619 (S.H.), SFB-TR84 405350772 (S.H. and L.-E.S.), KFO 309 284237345 (S.H.), GRK 2290 313717432 (L.-E.S.), and Excellence Cluster Cardio-Pulmonary Institute EXC2026 390649896 (S.H.)].

10.1126/science.aba2754

CELL THERAPY

Stem cells and the heart—the road ahead

After 20 years of research, pluripotent stem cells move to the fore to treat heart disease

By **Charles E. Murry**[1,2] *and* **W. Robb MacLellan**[1]

Heart disease is the primary cause of death worldwide, principally because the heart has minimal ability to regenerate muscle tissue. Myocardial infarction (heart attack) caused by coronary artery disease leads to heart muscle loss and replacement with scar tissue, and the heart's pumping ability is permanently reduced. Breakthroughs in stem cell biology in the 1990s and 2000s led to the hypothesis that heart muscle cells (cardiomyocytes) could be regenerated by transplanting stem cells or their derivatives. It has been ~18 years since the first clinical trials of stem cell therapy for heart repair were initiated (*1*), mostly using adult cells. Although cell therapy is feasible and largely safe, randomized, controlled trials in patients show little consistent benefit from any of the treatments with adult-derived cells (*2*). In the meantime, pluripotent stem cells have produced bona fide heart muscle regeneration in animal studies and are emerging as leading candidates for human heart regeneration.

In retrospect, the lack of efficacy in these adult cell trials might have been predicted. The most common cell type delivered has been bone marrow mononuclear cells, but other transplanted cell types include bone marrow mesenchymal stromal cells and skeletal muscle myoblasts, and a few studies have used putative progenitors isolated from the adult heart itself. Although each of these adult cell types was originally postulated to differentiate directly into cardiomyocytes, none of them actually do. Indeed, with the exception of skeletal muscle myoblasts, none of these cell types survive more than a few days in the injured heart (see the figure). Unfortunately, the studies using bone marrow and adult resident cardiac progenitor cells were based on a large body of fraudulent work (*3*), which has led to the retraction of >30 publications. This has left clinical investigators wondering whether their trials should continue, given the lack of scientific foundation and the low but measurable risk of bleeding, stroke, and infection.

Additionally, investigators have struggled to explain the beneficial effects of adult cell therapy in preclinical animal models. Because none of these injected cell types survive and engraft in meaningful numbers or directly generate new myocardium, the mechanism has always been somewhat mysterious. Most research has focused on paracrine-mediated activation of endogenous repair mechanisms or preventing additional death of cardiomyocytes. Multiple protein factors, exosomes (small extracellular vesicles), and microRNAs have been proposed as the paracrine effectors, and an acute immunomodulatory effect has recently been suggested to underlie the benefits of adult cell therapy (*4*). Regardless, if cell engraftment or survival is not required, the durability of the therapy and need for actual cells versus their paracrine effectors is unclear.

Of particular importance to clinical translation is whether cell therapy is additive to optimal medical therapy. This remains unclear because almost all preclinical studies do not use standard medical treatment for myocardial infarction. Given the uncertainties about efficacy and concerns over the veracity of much of the underlying data, whether agencies should continue funding clinical trials using adult cells to treat heart disease should be assessed. Perhaps it is time for proponents of adult cardiac cell therapy to reconsider the approach.

Pluripotent stem cells (PSCs) include embryonic stem cells (ESCs) and their reprogrammed cousins, induced pluripotent stem cells (iPSCs). In contrast to adult cells, PSCs can divide indefinitely and differentiate into virtually every cell type in the human body, including cardiomyocytes. These remarkable attributes also make ESCs and iPSCs more challenging to control. Through painstaking development, cell expansion and differentiation protocols have advanced such that batches of 1 billion to 10 billion pharmaceutical-grade cardiomyocytes, at >90% purity, can be generated.

Preclinical studies indicate that PSC-cardiomyocytes can remuscularize infarcted regions of the heart (see the figure). The new myocardium persists for at least 3 months (the longest time studied), and physiological studies indicate that it beats in synchrony with host myocardium. The new myocardium results in substantial improvement in cardiac function in multiple animal models, including nonhuman primates (*5*). Although the mechanism of action is still under study, there is evidence that these cells directly support the heart's pumping function, in addition to providing paracrine factors. These findings are in line with the original hope for stem cell therapy—to regenerate lost tissue and restore organ function. Additional effects, such as mechanically buttressing the injured heart wall, may also contribute.

Breakthroughs in cancer immunotherapy have led to the adoption of cell therapies using patient-derived (autologous) T cells that are genetically modified to express chimeric antigen receptors (CARs) that recognize cancer cell antigens. CAR T cells are the first U.S. Food and Drug Administration (FDA)–approved, gene-modified cellular pharmaceutical (*6*). The clinical and commercial success of autologous CAR T cell transplant to treat B cell malignancies has opened doors for other complex cell therapies, including PSC derivatives. There is now a regulatory path to the clinic, private-sector funding is attracted to this field, and clinical investigators in other areas are encouraged to embrace this technology. Indeed, the first transplants of human ESC-derived cardiac progenitors, surgically delivered as a patch onto the heart's surface, have been carried out (*7*). In the coming years, multiple attempts to use PSC-derived cardiomyocytes to repair the human heart are likely.

What might the first human trials look like? These studies will probably employ an allogeneic (non-self), off-the-shelf, cryopreserved cell product. Although the discovery of iPSCs raised hopes for widespread use of autologous stem cell therapies, the current technology and regulatory requirements likely make this approach too costly for something as common as heart disease, although this could change as technology and regulations evolve. Given that it would take at least 6 months to generate a therapeutic dose of iPSC-derived cardiomyocytes, such cells could only be applied to patients whose infarcts are in the chronic phase where scarring (fibrosis) and ventricular remodeling are complete. Preclinical data indicate that chronic infarcts benefit less from cardiomyocyte transplantation than do those with active wound-healing processes.

[1]Center for Cardiovascular Biology and Institute for Stem Cell and Regenerative Medicine, University of Washington, Seattle, WA 98109, USA. [2]Sana Biotechnology, Seattle, WA 98102, USA. Email: murry@uw.edu; wrmaclellan@cardiology.washington.edu

The need for allogeneic cells raises the question of how to prevent immune rejection, both from innate immune responses in the acute phase of transplantation or from adaptive immune responses that develop more slowly through the detection of non-self antigens presented by major histocompatibility complexes (MHCs). A current strategy is the collection of iPSCs from patients who have homozygous MHC loci, which results in exponentially more MHC matches with the general population. However, studies in macaque monkeys suggest that MHC matching will be insufficient. In a macaque model of brain injury, immunosuppression was required to prevent rejection of MHC-matched iPSC-derived neurons (*8*). Similarly, MHC matching reduced the immunogenicity of iPSC-derived cardiomyocytes transplanted subcutaneously or into the hearts of rhesus macaques, but immunosuppressive drugs were still required to prevent rejection (*9*).

Numerous immune gene editing approaches have been proposed to circumvent rejection, including preventing MHC class I and II molecule expression, overexpressing immunomodulatory cell-surface factors, such CD47 and human leukocyte antigen E (HLA-E) and HLA-G (two human MHC molecules that promote maternal-fetal immune tolerance), or engineering cells to produce immunosuppressants such as programmed cell death ligand 1 (PDL1) and cytotoxic T lymphocyte–associated antigen 4 (CTLA4) (*10*). These approaches singly or in combination seem to reduce adaptive immune responses in vitro and in mouse models. Overexpressing HLA-G or CD47 also blunts the innate natural killer cell–mediated response that results from deleting MHC class I genes (*11*). However, these manipulations are not without theoretical risks. It could be difficult to clear viral infections from an immunostealthy "patch" of tissue, and possible tumors resulting from engraftment of PSCs might be difficult to clear immunologically.

Ventricular arrhythmias have emerged as the major toxicity of cardiomyocyte cell therapy. Initial studies in small animals showed no arrhythmic complications (probably because their heart rates are too fast), but in large animals with human-like heart rates, arrhythmias were consistently observed (*5*, *12*). Stereotypically, these arrhythmias arise a few days after transplantation, peak within a few weeks, and subside after 4 to 6 weeks. The arrhythmias were well tolerated in macaques (*5*) but were lethal in a subset of pigs (*12*). Electrophysiological studies indicate that these arrhythmias originate in graft regions from a source that behaves like an ectopic pacemaker. Understanding the mechanism of these arrhythmias and developing solutions are major areas of research. There is particular interest in the hypothesis that the immaturity of PSC-cardiomyocytes contributes to these arrhythmias, and that their maturation in situ caused arrhythmias to subside.

A successful therapy for heart regeneration also requires understanding the host side of the equation. PSC-derived cardiomyocytes engraft despite transplantation into injured myocardium that is ischemic with poor blood flow. Although vessels eventually grow in from the host tissue, normal perfusion is not restored. Achieving a robust arterial input will be key to restoring function, which may require cotransplanting other cell populations or tissue engineering approaches (*13*, *14*). Most PSC-mediated cardiac cell therapy studies have been performed in the subacute window, equivalent to 2 to 4 weeks after myocardial infarction in humans. At this point, there has been insufficient time for a substantial fibrotic response. Fibrosis has multiple deleterious features, including mechanically stiffening the tissue and creating zones of electrical insulation that can cause arrhythmias. Extending this therapy to other clinical situations, such as chronic heart failure, will require additional approaches that address the preexisting fibrosis. Cell therapy may again provide an answer because CAR T cells targeted to cardiac fibroblasts reduced fibrosis (*15*).

Developing a human cardiomyocyte therapy for heart regeneration will push the limits of cell manufacturing. Each patient will likely require a dose of 1 billion to 10 billion cells. Given the widespread nature of ischemic heart disease, 10^5 to 10^6 patients a year are likely to need treatment, which translates to 10^{14} to 10^{16} cardiomyocytes per year. Growing cells at this scale will require introduction of next generation bioreactors, development of lower-cost media, construction of large-scale cryopreservation and banking systems, and establishment of a robust supply chain compatible with clinical-grade manufacturing practices.

Beyond PSC-cardiomyocytes, other promising approaches include reactivating cardiomyocyte division and reprogramming fibroblasts to form new cardiomyocytes. However, these approaches are at an earlier stage of development, and currently, PSC-derived cardiomyocyte therapy is the only approach that results in large and lasting new muscle grafts. The hurdles to this treatment are known, and likely addressable, thus multiple clinical trials are anticipated. ■

Cardiac stem cell therapy

Adult cells from bone marrow or the adult heart secrete beneficial paracrine factors but do not engraft in the infarcted heart. Pluripotent stem cells give rise to cardiomyocytes that engraft long term in animal models, beat in synchrony with the heart, and secrete beneficial paracrine factors. Long-term cardiomyocyte engraftment partially regenerates injured heart, which is hypothesized to bring clinical benefits.

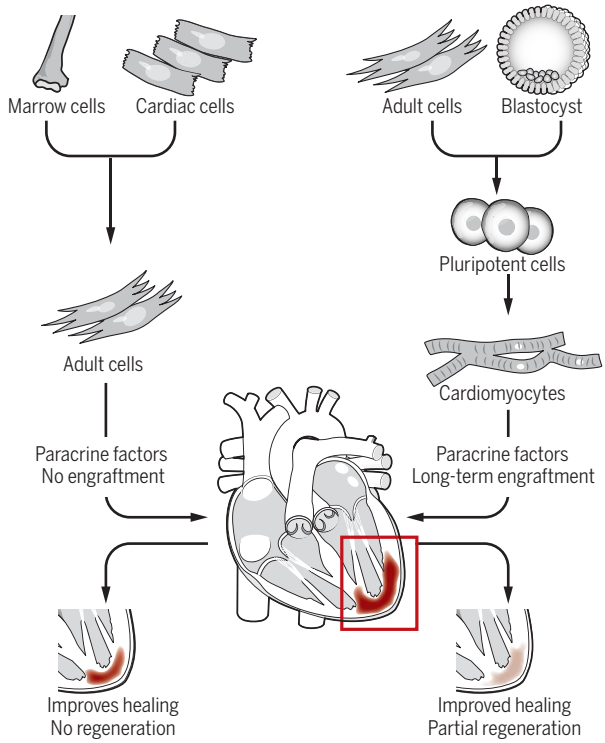

GRAPHIC: N. DESAI/*SCIENCE*

REFERENCES AND NOTES

1. P. Menasché, *Nat. Rev. Cardiol.* **15**, 659 (2018).
2. K. Nakamura, C. E. Murry, *Circ. J.* **83**, 2399 (2019).
3. K. R. Chien *et al.*, *Nat. Biotechnol.* **37**, 232 (2019).
4. R. J. Vagnozzi *et al.*, *Nature* **577**, 405 (2020).
5. Y. W. Liu *et al.*, *Nat. Biotechnol.* **36**, 597 (2018).
6. M. M. Boyiadzis *et al.*, *J. Immunother. Cancer* **6**, 137 (2018).
7. P. Menasché *et al.*, *Eur. Heart J.* **36**, 2011 (2015).
8. R. Aron Badin *et al.*, *Nat. Commun.* **10**, 4357 (2019).
9. T. Kawamura *et al.*, *Stem Cell Reports* **6**, 312 (2016).
10. R. Lanza *et al.*, *Nat. Rev. Immunol.* **19**, 723 (2019).
11. T. Deuse *et al.*, *Nat. Biotechnol.* **37**, 252 (2019).
12. R. Romagnuolo *et al.*, *Stem Cell Reports* **12**, 967 (2019).
13. J. Bargehr *et al.*, *Nat. Biotechnol.* **37**, 895 (2019).
14. M. A. Redd *et al.*, *Nat. Commun.* **10**, 584 (2019).
15. H. Aghajanian *et al.*, *Nature* **573**, 430 (2019).

ACKNOWLEDGMENTS

C.E.M. and W.R.M. are scientific founders of and equity holders in Sana Biotechnology. C.E.M. is an employee of Sana Biotechnology. W.R.M. is a consultant for Sana Biotechnology. C.E.M. and W.R.M. hold issued and pending patents in the field of stem cell and regenerative biology.

10.1126/science.aaz3650

A biosecurity credential will create a well-trained, responsible workforce with a core set of skills necessary to secure the life sciences of the future.

BIOSECURITY

Promoting biosecurity by professionalizing biosecurity

A credential system could improve policy and practice

By **Rebecca L. Moritz [1], Kavita M. Berger[2], Barbara R. Owen[3], David R. Gillum[4]**

New biotechnologies have the power to transform medicine, provide new sources of energy, and fill an expanding need for renewable, biologically derived products (the "bioeconomy"). But many of these powerful technologies and their products have the potential to be exploited for malevolent purposes or subverted to cause harm. Although many natural, accidental, and deliberate biological threats are governed by laws, agency- and national-level strategies, international instruments, guidance documents, and best risk management practices (*1*, *2*), these policies and practices are often based on a defined list of pathogens and toxins (*1*, *3*, *4*), do not necessarily mitigate the risks of the hazards, are not flexible to address new discoveries, may be political in nature, and may not keep pace with technological and workforce advances (*5*, *6*). We suggest that such limitations and variability in biosecurity policy and practice internationally could be addressed in part by enhancing and growing a workforce able to identify, assess, mitigate, and communicate security risks and solutions. We outline core competencies that such professionals should demonstrate and key steps needed to grow the profession by establishing a biosecurity credential.

Biosecurity is a multidisciplinary concept focused on keeping the researcher, public, and environment secure from the malicious exploitation of biological knowledge technologies and products (*7*). Biosecurity is distinct from securing other materials and technologies because biological organisms are found in nature, replicate, and can evolve through mutation, and much of the science and technology advances are developed in academia and industry throughout the world. Although biosecurity traditionally has focused on prevention, deterrence, and dissuasion of the development, production, and malicious use of microbes and toxins as weapons, it has expanded to include preventing the exploitation of knowledge, skills, technologies, and equipment to harm animals, plants, humans, and the environment. Life sciences researchers in academic and government institutions and bio-related industries are facing unprecedented security risks, including pathogens and toxins known to be harmful to public health and safety; unauthorized access to infectious materials in use, storage, and during transfer; culturing of pathogens from ancient reservoirs; synthesis of pathogens from published sequence data; and theft of data from and disruption of operations at biological facilities from cyber attacks. Adding to these concerns is the rapid progress of synthetic biology (for example, gene drives, synthesis of extinct viruses, creation of new pathogenic viruses, and production of chemicals in microbial systems), which presents new challenges to promote advancement while preventing malicious use.

Several positions at research, industry, health, law enforcement, security, and emergency response organizations are being asked to address different issues related to biosecurity. Yet although an individual may be delegated as the "responsible official" on paper, often requirements for a baseline level of biosecurity expertise do not exist. At the same time, many diverse professionals within an organization may have biosecurity as a component of their job yet may not be clearly designated as go-to biosecurity experts. Moreover, work in biosecurity has become, whether they fully realize it, the responsibility of every scientist and engineer working in the life sciences and with biological materials and/or data; every businessperson, entrepreneur, and venture capitalist working with life science products and information; and every life science explorer—including those in do-it-yourself biology (DIYBio) laboratories (*8*).

In our experience, we see a need for greater clarity and consistency in how to deal with biosecurity issues at many institutions (such as who to call, what to do, and what is considered dual use) and in different countries. For example, private and public institutions have documented incidents involving biosecurity breaches and/or lack

[1]University of Wisconsin–Madison, Madison, WI, USA. [2]Gryphon Scientific, Takoma Park, MD, USA. [3]Merck & Co., Inc., Kenilworth, NJ, USA. [4]Arizona State University, Tempe, AZ, USA. Email: rebecca.moritz@wisc.edu

PHOTO: ANNA SCHROLL/FOTOGLORIA/NEWSCOM

of internal biosecurity controls that have resulted in use of pathogenic bacteria to deliberately harm co-workers; unauthorized importation of viral samples; and theft of scientific data, results, and technologies. We suggest that many policy efforts suffer from being too focused on mere compliance with policies ("checking the box") rather than on an enterprise- or system-wide approach to addressing biosecurity risks and threats. Biosecurity needs to become integral in many different professions and countries, highlighting the need for consistent and common understanding of capabilities for the prevention of such risks and threats.

Layered on top of this is a catch-22: Risk and threat management measures must recognize that our best defense to counter the malicious application of life science research relies in part on continued research, knowledge gain, and scientific and technology advancement. The solution can become the problem and the problem can become the solution—for example, the fundamental research to understand mechanisms behind transmission of influenza and coronavirus. Efforts to prevent malicious application of life science knowledge, skills, and technologies thus must be developed in a manner that does not unduly impede scientific progress to advance health, defense, agriculture, environmental health, science, and energy (*1*). Having individuals who are well versed in biosecurity and collaborate directly with researchers on a regular basis is critical.

PATHWAY TO PROFESSIONALIZATION

We suggest that a biosecurity credential based on core competencies could help ensure that professionals can address biosecurity gaps regardless of their home institution and collaborate with the life science community to mediate biosecurity risks in a manner that ensures continued advancement of life sciences research for the benefit of all. Such a credential must go beyond the governance of microbes and toxins and must consider the risks associated with the malicious use of synthetic biology, genome editing, genomics and health care data, neuroscience, and other enabling biotechnologies. Risks associated with digitization of biological information and networked systems also is included within the broader scope of biosecurity.

As the scope of biosecurity expands, the creation of a biosecurity credential would allow individuals from different disciplines, professions, backgrounds, and countries to be recognized by scientists, administrators, funders, and policy-makers as go-to resources for knowledge and expertise in the reduction of deliberate biological risks.

Establishing a biosecurity credential could provide individuals who are responsible for implementation and oversight of biosecurity practices at institutions with baseline knowledge about how to assess and address existing and new risks in their facilities, which promotes consistency in countering global biosecurity issues. A biosecurity credential should include, at a minimum, competencies that focus on biosafety, program management, physical security, personal security, personnel suitability, material control and accountability, transport security, cyber security, and information security (see the box) (*9*). These core competencies were identified by an exploratory task force led by the American Biological Safety Association (ABSA) International to cultivate a well-prepared biosecurity workforce. The task force had representation from academia, agriculture, government, private industry, public health, and security sectors. These core competencies were formulated on the basis of biosecurity lessons learned and shared experiences from this cross-functional task force.

Individuals who obtain a biosecurity credential may be subject-matter experts in one or more of these core competencies (some of which, such as biosafety and cyber security, have credentialing programs of their own). Obtaining a biosecurity credential would not require that an individual achieve expertise equivalent to a separate credential in each of the individual core competencies, but a credential would mean that an individual has substantial knowledge in all of the core competencies to be able to identify and remediate risks and to know whom to engage for deeper disciplinary expertise.

For a credential to be successful, the diverse international biosecurity community involved in biothreat reduction in high-, middle-, and low-income countries must be engaged to help identify specific areas relevant to their scientific, policy, infrastructure, and threat environments. Developing an assessment of core biosecurity competencies based on skills and knowledge that is not specific to one country is necessary for a successful and meaningful credential. Implementation may be as comprehensive as offering degrees from accredited institutions or as light as incorporating common norms and industry standards. For example, the implementation of the credential could be modeled after work being done within the DIYbio community, which involves obtaining widespread adoption of safety practices among distributed communities from around the world (*10*). This is an example of what can be achieved through engagement, communication, and partnership.

One possible first step could be to document current approaches for addressing each of the competencies at various institutions internationally. To the best of our knowledge, this has not been done systematically, and even within the United States there is a lack of clear and rigorous processes by which an individual develops knowledge and skills for practicing biosecurity. This step is critical for understanding current comprehension of each area, challenges in implementing long-term solutions, and lessons learned from past efforts. Together, this information helps to identify misconceptions about the core competencies, which would need to be addressed during development of the biosecurity credential. For example, the biosafety and biosecurity action package of the Global Health Security Agenda—an international effort to help countries develop capabilities for prevention of, detection of, and response to infectious disease threats such as Ebola virus and new coronavirus 2019 outbreaks—could provide an opportunity to compile a list of biosecurity practices that countries are developing and or implementing (*11*).

Another key step would be for stakeholders from different sectors, disciplines, and industries to come together to identify their needs and interest level for a biosecurity credential and to gain buy-in for assistance with the development and long-term implementation of the credential. There are multiple opportunities for international engagement. For example, the cooperative threat-reduction programs, international scientific organizations, and the Biological and Toxin Weapons Convention could support multisectoral discussions on the development of an international biosecurity credential and associated core competencies. This step is important for including that representatives from a variety of stakeholders are engaged, which ensures that the credential does not meet the needs of a subset of stakeholders at the expense (or even exclusion) of others. This step also promotes better understanding of biosecurity needs and resources among institutions, sectors, and countries, which is critical for sustainability and durability of the credential.

Documentation of risks and threats presented by different biological science and technology sectors and fields could help to ensure that the core competencies are relevant and applicable to past, current, and future risks and threats. For example, funding agencies, scientific journals, and the scientific and security communities could interact with governments of all countries to compile anonymized biosecurity lessons learned.

The concept of biosecurity has been a focus of several global initiatives, and many countries have supported efforts to build institutional, national, and regional capacity for biosafety and biosecurity and, to some

Biosecurity credential core competencies and examples of necessary knowledge and skills

Cyber security
Knowledge of protecting unauthorized access to computer networks involved in facility operation; equipment uses; and data generation, analysis, and storage

- Frameworks, methods, and technologies for protecting computers and facility control systems from cyber attacks and espionage
- Methods for encrypting documents for protecting information
- Methods for detecting, quarantining, and addressing malicious code
- Cybersecurity Framework of the U.S. National Institute of Standards and Technology

Information security
Knowledge about the methods to protect data and information associated with biological materials from unauthorized or accidental disclosure

- Different means of protecting data
- Identification and mitigation of vulnerabilities associated with data in transit and storage, including through access to software and cloud computing and storage

Program management
Ability to oversee the implementation of a comprehensive biosecurity program

- Risk assessment and risk management
- Knowledge of how to write and implement a biosecurity plan that addresses personnel management, physical security, material control and accountability, transport controls (such as locks, key card access, and/or biometric features), and cyber and data security

Personnel suitability
Knowledge regarding the actions and behaviors that lead to unauthorized access to materials and information resulting in theft, use, or release

- Best practices in personnel security
- Institutional and community entities involved in initial and ongoing vetting and evaluation of personnel for reliability and trustworthiness
- Awareness of elicitation techniques used to collect information without raising suspicion that certain facts are being sought
- Protections and processes for reporting insider incidents

Biosafety
Knowledge regarding containment principles and practices implemented to prevent accidental exposures and releases of biological materials

- Perform risk assessments, assign risk groups and containment levels, and design facilities to ensure safe work with biological materials

Physical security
Knowledge regarding the physical measures designed to prevent unauthorized access to facilities and equipment and theft of biological materials

- Various means of securing facilities and equipment
- Defining security zones with increasingly strict controls as you move toward an area where a high-risk agent is handled
- Using physical structures or barriers such as a gated property or access controls (such as locks, key card access, and/or biometric features)

Personal security
Knowledge regarding the risks to people with access to biological materials or associated information

- Guidance on how to train individuals on understanding their vulnerabilities to coercion or elicitation
- Knowledge of how to train individuals to be aware of threats to themselves, co-workers, workplace, and/or their families
- Processes and authorities to contact if an incident or suspected incident occurs
- Methods for protecting one's personal information and policies governing personally identifiable information or personal health information

Material control and accountability
Knowledge regarding the methods for inventorying and tracking high-consequence biological agents and toxins

- Various inventory and tracking systems
- Awareness of what materials exist, where they are located, and who is accountable for them
- Laboratory notebook accountability and archive programs, signature logs, inventories, and chain of custody policies

Transport security
Knowledge regarding systems in place to reduce the risk of theft during the transportation of materials from one area to another, between facilities within the same country, or from one country to another

- Chain of custody forms, package tracking, shipping regulations, permitting requirements, and surveillance options

extent, cyber and data security for biological facilities and information systems. We now see a credential system as a potential way to help strengthen and standardize ongoing international initiatives in biosecurity and incorporate emerging risks and cultivate a well-trained cadre of biosecurity professionals in a dynamic biotechnology landscape. ■

REFERENCES AND NOTES

1. D. DiEuliis, V. Rao, E. A. Billings, C. B. Meyer, K. Berger, *Health Secur.* **17**, 83 (2019).
2. World Health Organization (WHO), *International Health Regulations* (WHO, ed. 3, 2005).
3. The Biological Weapons and Toxins Convention includes microbes produced with genetic engineering or synthetic biology approaches, which broadens the scope of biological threats slightly.
4. K. M. Berger, *Science* **354**, 1237 (2016).
5. National Academies of Sciences, Engineering, Medicine, *Biodefense in the Age of Synthetic Biology* (National Academies Press, 2018).
6. J. B. Tucker, Innovation, *Dual Use, and Security. Managing the Risks of Emerging Biological and Chemical Technologies* (MIT Press, 2012).
7. In defense spheres, biosecurity refers to measures to prevent, deter, and dissuade efforts to develop, produce, stockpile, and use biological agents (pathogens and toxins) as weapons. The broader application of biosecurity includes prevention, deterrence, and dissuasion of usage of nonmicrobial or toxin-based biological material, biologically derived chemicals and small molecules, and data to harm others deliberately.
8. T. Kuiken, *Nature* **531**, 167 (2016).
9. R. Salerno, J. Gaudioso, *Laboratory Biosecurity Handbook* (CRC Press, 2007).
10. Baltimore Under Ground Science Space (BUGGS), a nonprofit public laboratory to safely and affordably investigate the living world; www.bugssonline.org/diybio-biosafety
11. Global Health Security Agenda (GHSA), https://ghsagenda.org

ACKNOWLEDGMENTS

D.R.G, R.L.M, and B.R.O. were members of the ABSA International exploratory biosecurity credentialing task force. D.R.G. is the 2020 president of ABSA International. B.R.O. and R.L.M. are former council members of ABSA International. K.M.B. serves as a deputy chair of the Global Health Security Consortium.

10.1126/science.aba0376

Noninvasive electrodes can detect some brain waves when secured to a subject's scalp.

PHOTO: ULRICHW/PIXABAY/CC 4.0

NEUROSCIENCE

Recording waves, reading minds

A neuroscientist confronts the history and future of our quest to understand electricity's role in brain function

By **Cyan James**

Imagine that you are living in Rome in the year 44 CE and that you are suffering from an appalling migraine and have gone to see a doctor. The doctor approaches you, hoisting a shining torpedo fish toward your pounding skull. The goal? The fish will shock you until your head feels numb and your migraine abates. Luckily for modern migraine sufferers, such practices are far behind us, but contemporary physicians and researchers are still working to understand the myriad ways electricity comes into play in the brain. In his new book, *Electric Brain*, neuroscientist R. Douglas Fields delves into the complicated relationships between neurobiology, electricity, capability, and impairment.

Our brains, each of which thrums with enough electrical energy to power a low-wattage light bulb, can now be measured and explored much better than ever before—a boon for doctors seeking better medical treatments and a thrill for inventors crossing neuroscience thresholds, but a warning, too, as our personalities and thoughts become less private and potentially more exploitable. *Electric Brain* details scientists' quest to understand brain waves throughout history, covering a good deal of unsettling material in the process and touching on today's emerging technology and most pressing ethical questions.

Where, Fields inquires, are the boundaries of electricity's effects in the brain? To what extent can precisely directed electrical impulses measure our minds and change our behaviors? Specific kinds of brain stimulation, he explains, can make your muscles move involuntarily, induce sexual arousal, or prompt attacks of rage. Modern scientists can now also interpret the brain's electrical activity with much greater accuracy, classifying patterns associated with certain images and letters, for example. With training and the right interface, a paralyzed person can operate a motorized wheelchair, a competitor can race a toy car, and a writer can type out a paragraph using just the electricity that underlies thought.

Fields adopts a "writer as adventurer" approach to the book's narrative. To gain insight into how mountaineers risk brain swelling at high altitudes, he subjects himself to a magnetic resonance imaging scan after climbing Mount Rainier. To learn about emerging ways to heal brain damage and boost productivity, he struggles through multiple sessions of neurofeedback.

Fields returns repeatedly to a tension inherent in brain wave studies, comparing scientific research conducted in good faith with research that veers more into ethically questionable or methodologically compromised territory. Here, he highlights the work of Hans Berger, a tight-lipped German physician working in the early 1900s who conducted invasive experiments on patients for nontherapeutic purposes. Although his methods were blunt and exploratory, he was among the first to record human brain waves.

Even today, it can be difficult to separate legitimate brain science from studies that may prove cringe-worthy in the future. Comparatively crude brain wave–measuring tools, misleading hypotheses, and our own ignorance have dogged the field since the beginning and continue to challenge modern researchers.

Fields ranges widely, pointing out how modern brain wave research is entangled with contemporary geopolitical concerns. War, he argues, both accelerates and interrupts certain kinds of research, while cultural concerns can determine which avenues of research are pursued and which lie dormant. He relates the story of neuroscientist José Delgado, a medical corpsman and concentration camp survivor during the Spanish Civil War, who believed that electrodes implanted in the brain could "psychocivilize" humans. However, the vividness of Delgado's experimental work—he once used an electrical implant to halt a charging bull on command, for example—elicited concerns about mind control and dampened research on electrical stimulation, research that has only recently been revived.

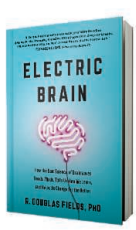

Electric Brain
R. Douglas Fields
BenBella Books, 2020.
480 pp.

As our scientific capabilities expand, so do related ethical concerns, Fields reminds readers. Some of the book's most sobering passages deal with possible future advances, including the ability to "hack" the brain, the weaponization of brain control, and the capacity for brain imaging to be used to identify troubling character traits or aspects of performance.

We may soon inhabit a world in which our thoughts are not entirely private. As we proceed, we must be sure to temper our excitement for these emerging technologies with wisdom and respect. ■

The reviewer is a freelance science writer based in Seattle, WA, USA. Email: cyanj@uw.edu

10.1126/science.aba5496

Iron, copper, and mercury are represented as Roman gods and goddesses (Mars, Venus, and Mercury, respectively) in these 17th-century illustrations.

CHEMISTRY

Etymology of the elements

Charming anecdotes and historical diversions come to life in tales of how the chemical elements were named

By **Nicola Pohl**

Beryllium would taste as sweet by any other name. Indeed, the element was once also known as glucinum or glucinium, derived from the Ancient Greek word for "sweet." However, clarity is key when the substance in question is also poisonous.

The need to establish clear chemical nomenclature originated with alchemists centuries ago and continues today as an ongoing international mission now led jointly by the International Union of Pure and Applied Chemistry and the International Union of Pure and Applied Physics. But, as Peter Wothers reveals in his new book, *Antimony, Gold, and Jupiter's Wolf*, this sort of work is not always straightforward.

Wothers, a teaching fellow at the University of Cambridge, is interested in the names of elements whose origins are murky. And while a simple web search can provide the etymologies of element names (*1*), his book provides tales about how those names came to be. Included as well are dozens of renderings of woodcuts depicting old chemical procedures and instruments and other images that enliven his stories.

Antimony, Gold, and Jupiter's Wolf unfolds as a series of more-or-less separate and chronological stories. Without an overarching narrative, this makes it easy for a reader to easily dip in at any point.

Humans have been using chemicals for thousands of years to produce everything from soap to glass. However, the development of a shared vocabulary around these processes has not always been straightforward. Symbols and code names were sometimes used to keep an artisan's methods secret. In other cases, independent discoveries and naming traditions led to confusion.

Lavoisier's chemical revolution of the late 1700s marked a turning point in our understanding of chemical reactions, and a reproduction of one of the tables from his key work, *Traité élémentaire de chimie*, helpfully translates ancient nomenclature into new names, many of which a modern scientist would recognize. But the periodic table was still rather small in the late 18th century.

New methods accelerated element discovery in the 1800s and drove some competition that makes for interesting stories. Wothers writes, for example, about Humphry Davy, who, in 1807, isolated pure potassium from a solution of lye. Davy's own report of the discovery was staid, but—as Wothers reveals—his young assistant reported that Davy was bouncing ecstatically around the room after completing the experiment.

Wothers shares how the limits of historical knowledge come into play in element names, revealing, for example, that "[t]he name 'cobalt' may derive from the word '*cobathia*,' which was what the ancient Greeks called the poisonous smoke of white arsenic oxide formed when arsenic ores are roasted in air." Meanwhile, bismuth, we learn, was first used as a cosmetic face powder, although sulfur-containing spring water turns the white powder black, thereby outing its surreptitious wearers.

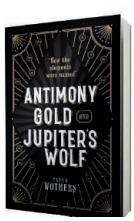

Antimony, Gold, and Jupiter's Wolf: How the Elements Were Named
Peter Wothers
Oxford University Press, 2020. 304 pp.

The many names given to a single substance by different discoverers have, at times, constrained later researchers. Davy, for example, originally named one of his discoveries "magnium," knowing that his preferred name had already been claimed for the metallic form of manganese. We now call his metal magnesium (his original choice).

The book concludes on the question of whether unstable elements should be named at all. (Ultimately, scientists decided that, yes, these new elements—however transient—deserve names too.) The story of the creation and naming has been told recently in another book (*2*) that would make a perfect reading companion for this lively volume. ■

The reviewer is at the Department of Chemistry, Indiana University, Bloomington, IN 47405, USA. Email: npohl@indiana.edu

REFERENCES AND NOTES

1. https://elements.vanderkrogt.net/index.php.
2. K. Chapman, *Superheavy: Making and Breaking the Periodic Table* (Bloomsbury Sigma, 2019).

10.1126/science.aba3488

Mourners lower the coffin of conservationist Homero Gómez González into a grave in Michoacán state, Mexico.

PHOTO: AP PHOTO/REBECCA BLACKWELL

Edited by **Jennifer Sills**

Conservationists deserve protection

The global conservation community is shocked and deeply concerned about the deaths of two butterfly conservationists in Mexico. On 29 January, environmentalist Homero Gómez González was found dead in Michoacán state, near the El Rosario Monarch Butterfly Preserve he managed (*1*, *2*). On 1 February, the body of a second butterfly activist, Raúl Hernández Romero, was also found (*3*, *4*). Although official investigations are ongoing, both deaths are presumed to be related to retaliation by criminal groups of illegal loggers (*1*–*4*). Environmental defenders around the world are increasingly exposed to threats and violence (*5*)—sometimes, as in the recent tragic events in Mexico, at the risk of their lives. Any threat or attack experienced by nonviolent environmental defenders is unacceptable.

Many countries, by signing international biodiversity agreements, have agreed implicitly to protect conservationists and environmental human rights defenders. For example, 89 states—including Mexico—are members of the International Union for Conservation of Nature and are thus signatories to resolutions that call for support for environmental defenders (*6*). Another example, the Escazú Agreement, is currently undergoing ratification by Latin American countries (*7*).

Crimes committed against environmental defenders cannot go unpunished, and justice must be prompt. Those who would attack the people who try to protect nature do so at their own peril. Humans depend on plants, animals, and fungi for survival, and those working to achieve global targets to halt biodiversity loss deserve nothing but support. To recognize the importance of conservation work and the risks it too often entails, countries should make explicit their commitment to protecting conservationists.

Later this year, at the 15th Conference of the Parties to the Convention on Biological Diversity in Kunming, China, new biodiversity targets will be set to guide future conservation action. It is paramount that at this pivotal time the biodiversity crisis is taken seriously by governments through direct action that protects not just biodiversity but also those working tirelessly to preserve it. It is our duty to pursue the legacy of conservationists like Homero and Raúl.

Monika Böhm[1]*, Sergio Henriques[1,2], Axel Hochkirch[3], Jon Paul Rodríguez[4,5,6]
[1]Institute of Zoology, Zoological Society of London, Regent's Park, London NW1 4RY, UK. [2]Department of Genetics, Evolution and Environment, Centre for Biodiversity & Environment Research, University College London, Gower Street, London, WC1E 6BT, London, UK. [3]Department of Biogeography, Trier University, D-54286 Trier, Germany. [4]IUCN Species Survival Commission (SSC), Calle La Joya, Edificio Unidad Técnica del Este, Chacao, Caracas 1060, Venezuela. [5]Provita, Calle La Joya, Edificio Unidad Técnica del Este, Chacao, Caracas 1060, Venezuela.
[6]Venezuelan Institute for Scientific Investigation (IVIC), Caracas 1020-A, Venezuela.
*Corresponding author.
Email: monika.bohm@ioz.ac.uk

REFERENCES AND NOTES

1. K. Semple, P. Villegas, "Mexican butterfly conservationist is found dead, two weeks after vanishing," *The New York Times* (2020).
2. D. Agren, "Mexico: Defender of monarch butterflies found dead two weeks after he vanished," *The Guardian* (2020).
3. A. Ortega, "At famed Mexican butterfly reserve, second worker found dead," *Reuters* (2020).
4. "Second Mexico monarch butterfly activist found dead," *BBC* (2020).
5. Global Witness, "Enemies of the state? How governments and business silence land and environmental defenders" (2019).
6. Resolution 2.37 of the 2000 IUCN World Conservation Congress (2000); www.iucn.org/sites/dev/files/import/downloads/wcc_amman_res_2_37.pdf.
7. United Nations, "Regional agreement on access to information, public participation and justice in environmental matters in Latin America and the Caribbean" (2018); www.cepal.org/en/escazuagreement.

COMPETING INTERESTS

M.B. chairs the IUCN Species Survival Commission (SSC) Butterfly Specialist Group. S.H. chairs the IUCN SSC Spider and Scorpion Specialist Group. A.H. chairs the IUCN SSC Invertebrate Conservation Committee.

10.1126/science.abb1514

Public health scientists in the crosshairs

In his Editorial "Stick to science" (10 January, p. 125), *Science* Editor-in-Chief H. Holden Thorp urges scientists to resist

politically motivated calls to "stay in our lane" and instead speak up about the importance of evidence-based decision-making. We agree that science advocacy is particularly important when populist movements and "post-truth politics" (*1*) ignore, distort, or undermine scientific evidence. However, we must acknowledge that scientists are sometimes threatened with the loss of their freedom and civil rights for doing this work. For example, Bülent Şık, a food engineer in Turkey, received a 15-month jail sentence in September, 2019, for publishing his results on toxic pollution in food and water sources in Western Turkey (*2*). To ensure that scientists can make their voices heard, we must guarantee their safety.

These risks feel particularly personal to public health scientists, who cannot stay out of politics (and legislation) given the potential for populist policies—or any policy put in place uninformed by evidence—to negatively affect health. Women suffer from limited access to abortion and contraception (*3*). Immigrants face restricted access to health care (*1*). Entire health infrastructures have been destroyed by human-made armed conflict (*4*). We are all threatened by climate change denial and withdrawals from international agreements (*5*).

Public health scientists must follow Thorp's advice to speak up in defense of scientific evidence when questionable policies are proposed, and their autonomy and freedom must not be threatened when they do so. We urge all governments to guarantee academic freedom and to preserve the integrity of public health science and all scientific disciplines worldwide as directed by the U.N. Educational, Scientific and Cultural Organization (UNESCO) (*6*, *7*) and international human rights law (*8*, *9*). In the meantime, independent professional organizations must advocate for scientific autonomy, and education and human rights organizations, such as the Scholars at Risk network and Scholar Rescue Fund, will need to protect scientists.

Lisa Wandschneider*, Yudit Namer, Oliver Razum
Department of Epidemiology and International Public Health, School of Public Health, Bielefeld University, D-33501 Bielefeld, North Rhine Westphalia, Germany.
*Corresponding author.
Email: lisa.wandschneider@uni-bielefeld.de

REFERENCES AND NOTES

1. E. Speed, R. Mannion, *Int. J. Health Pol. Manag.* **6**, 249 (2017).
2. K. McTighe, "Turkish scientist gets 15-month sentence for publishing environmental study," *Science* 10.1126/science.aaz6627 (2019).
3. M. Murray, *N. Engl. J. Med.* **376**, 301 (2017).
4. R. I. Donaldson, Y. W. Hung, P. Shanovich, T. Hasoon, G. Evans, *J. Trauma Acute Care Surg.* **69**, 1379 (2010).
5. N. Watts *et al.*, *Lancet* **391**, 581 (2018).
6. UNESCO, "Recommendation concerning the status of higher-education teaching personnel" (29 C/12, 1997); http://portal.unesco.org/en/ev.php-URL_ID=13144&URL_DO=DO_TOPIC&URL_SECTION=201.html.
7. UNESCO, "Revision of the Recommendation on the Status of Scientific Researchers (1974)" (SHS/BIO/SSR/2017/1, 2017); https://unesdoc.unesco.org/ark:/48223/pf0000248910.
8. U.N. General Assembly, "International covenant on economic, social and cultural rights" (Treaty Series, United Nations, 1999), vol. 993; www.ohchr.org/en/professionalinterest/pages/cescr.aspx.
9. Committee on Economic, Social, and Cultural Rights, "Implementation of the international covenant on economic, social, and cultural rights: General Comment No. 13: The right to education (article 13 of the Covenant)" (1999); www.right-to-education.org/sites/right-to-education.org/files/resource-attachments/CESCR_General_Comment_13_en.pdf.

COMPETING INTERESTS

O.R. is member of the Executive Board of the Association of Schools of Public Health in the European Region. Y.N. receives nonfinancial support from Scholars at Risk.

10.1126/science.abb1787

Illegal poachers turn to helmeted hornbills

The helmeted hornbill (*Rhinoplax vigil*)—a charismatic bird that lives only in intact tropical forests in southeast Asia—has faced unprecedented levels of poaching in recent years to satisfy the high demand of its casque, known as "red ivory" in the illegal trade (*1*–*3*). The hornbill's decline has been so precipitous that the International Union for Conservation of Nature recently recategorized its conservation status as Critically Endangered, from Near Threatened in 2012 (*2*, *4*).

The popularity of "red ivory" products made from the hornbill's casque, including beads, pendants, and intricate works of art, has triggered a boom in poaching since 2012 (*2*, *5*). The products sell for three to five times the price of elephant ivory (*6*, *7*). Between March 2012 and August 2014, Indonesian and Chinese enforcement yielded the seizure of at least 2170 casques (*8*). According to a collaborative investigation by the Environmental Investigation Agency and TRAFFIC, seizures and market observations between 2010 and 2017 account for at least 2878 helmeted hornbills, but this is only a fraction of the number killed for trade each year (*2*, *3*). In 2013, at least 500 adult helmeted hornbills were estimated to have been killed each month in Indonesia's West Kalimantan (*9*). In recent years, poachers in West Kalimantan were hunting an estimated

1200 to 27,000 hornbills annually (*8*). Forest habitat loss and fragmentation caused by widespread logging and land conversion serve as additional threats to wild hornbill populations (*6*–*8*).

The helmeted hornbill plays a vital ecological role in southeast Asia's forests, dispersing seeds for abundant plant species (*7*). Although the species was listed on Appendix I of the Convention on International Trade in Endangered Species of Wild Fauna and Flora (CITES) (*10*), protection remains weak and illegal trade persists (*11*). To better preserve the hornbill, Asian governments must strengthen regional collaborations and step up protection efforts such as implementing scientific conservation policies, eliminating illegal poaching and trade, and investing in the expansion of nature reserves. Researchers and international conservation groups should take multinational protection actions to monitor remaining hornbill populations, strengthen enforcement and engagement with communities, and raise public awareness to reduce "red ivory" consumption. The increased poaching pressure on the helmeted hornbill has come in recent years as the world has condemned and forbidden other illegal trade, including elephant ivory and rhino horn. Only by shifting the culture of pursuing rare species and curbing the demand for them can we prevent Asia's helmeted hornbill from following in the path of the now functionally extinct northern white rhinoceros (*Ceratotherium cottoni*) (*12*).

Wei Li[1]* and Wei Huang[2]
[1]School of Business Administration, Hunan University, Changsha 410082, China. [2]College of Environmental Science and Engineering, Hunan University, Changsha 410082, China.
*Corresponding author.
Email: liweimiss@hnu.edu.cn

REFERENCES AND NOTES

1. BirdLife International, "Saving the Helmeted Hornbill" (2018); www.birdlife.org/worldwide/news/saving-helmeted-hornbill.
2. Environmental Investigation Agency (EIA), "Illegal trade seizures: Helmeted hornbills" (2017); http://eia-international.org/wildlife/wildlife-trade-maps/illegal-trade-seizures-helmeted-hornbills/.
3. TRAFFIC, "Traffic Bulletin Volume 29, No 2: Helping the hornbill keep its head" (2017); www.traffic.org/site/assets/files/3018/traffic_pub_bulletin_29_2.pdf.
4. BirdLife International, "Helmeted hornbill: *Rhinoplax vigil*," The IUCN Red List of Threatened Species (2019); www.iucnredlist.org/species/22682464/155467793.
5. R. Bale, "Poached for its horn, this rare bird struggles to survive," *National Geographic* (2018); www.nationalgeographic.com/magazine/2018/09/helmeted-hornbill-bird-ivory-illegal-wildlife-trade/.
6. N. J. Collar, *BirdingASIA* **24**, 12 (2015).
7. Global Conservation, "Fighting in Asia's national parks to save the helmeted hornbill" (2019); http://globalconservation.org/news/fighting-asias-national-parks-save-helmeted-hornbill/.
8. C. Beastall *et al.*, *Bird Conserv. Int.* **26**, 137 (2016).
9. S. Furnival, "Traders of 'red ivory' from rare birds are arrested in Indonesia," *MONGABAY* (2015); http://news.mongabay.com/2015/08/traders-of-red-ivory-from-rare-birds-are-arrested-in-indonesia/.
10. CITES, "*Rhinoplax vigil*," Appendix I of CITES (2019); http://cites.org/eng/app/appendices.php.
11. Chinanews, "China Guangdong coast guard seized 138 smuggled helmeted hornbill casques" (2017); www.chinanews.com/shipin/2017/03-09/news698272.shtml [in Chinese].
12. Fauna & Flora International, "Northern white rhino *Ceratotherium cottoni*" (www.fauna-flora.org/species/northern-white-rhino).

10.1126/science.abb1832

ERRATA

Erratum for the Research Article: "Loci associated with skin pigmentation identified in African populations" by Nicholas G. Crawford *et al.*, *Science* **367**, eaba7178 (2020). Published online 17 January 2020; 10.1126/science.aba7178

Erratum for the Report: "Treadmilling by FtsZ filaments drives peptidoglycan synthesis and bacterial cell division" by A. W. Bisson-Filho *et al.*, *Science* **367**, eaba6311 (2020). Published online 17 January 2020; 10.1126/science.aba6311

RESEARCH

Nucleosome recognition by a chromatin remodeling complex

He et al., *p. 875*

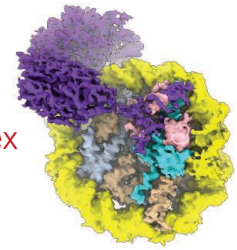

IN *SCIENCE* JOURNALS

Edited by **Michael Funk**

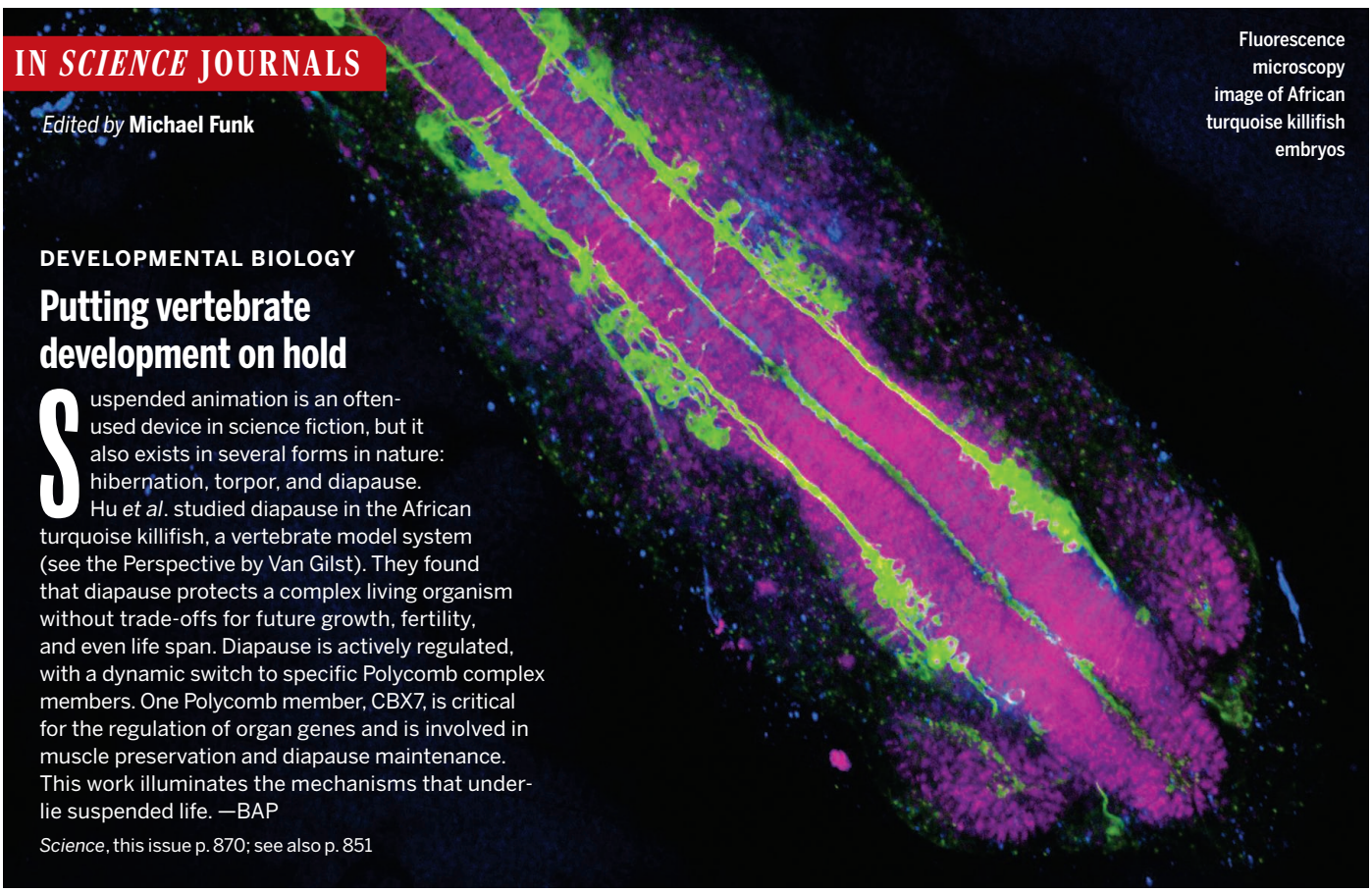

Fluorescence microscopy image of African turquoise killifish embryos

DEVELOPMENTAL BIOLOGY

Putting vertebrate development on hold

Suspended animation is an often-used device in science fiction, but it also exists in several forms in nature: hibernation, torpor, and diapause. Hu *et al*. studied diapause in the African turquoise killifish, a vertebrate model system (see the Perspective by Van Gilst). They found that diapause protects a complex living organism without trade-offs for future growth, fertility, and even life span. Diapause is actively regulated, with a dynamic switch to specific Polycomb complex members. One Polycomb member, CBX7, is critical for the regulation of organ genes and is involved in muscle preservation and diapause maintenance. This work illuminates the mechanisms that underlie suspended life. —BAP

Science, this issue p. 870; see also p. 851

OPTOMECHANICS

A nanoparticle trapped and cooled

Cooling massive particles to the quantum ground state allows fundamental tests of quantum mechanics to be made; it would provide an experimental probe of the boundary between the classical and quantum worlds. Delić *et al*. laser-cooled an optically trapped solid-state object (a ~150-nanometer-diameter silica nanoparticle) into its quantum ground state of motion starting from room temperature. Because the object is levitated using optical forces, the experimental configuration can be switched to free fall, thereby providing a test bed for several macroscopic quantum experiments. —ISO

Science, this issue p. 892

NANOMATERIALS

Larger monolayers with gold tapes

Although the exfoliation of monolayers of materials such as transition metal dichalcogenides produces high-quality electronic materials with low defect densities, the size of the monolayers is limited to the micrometer scale. Liu *et al*. modified this method by creating atomically flat gold layers on polymer supports. The strong van der Waals adhesion of the gold layer allowed monolayers to be exfoliated on the centimeter scale. Multilayers could be reassembled to artificial structures, such as a $MoSe_2$/WSe_2 single-crystal bilayer with a twist angle chosen to quench intralayer exciton formation. —PDS

Science, this issue p. 903

ANIMAL COGNITION

These bees have "seen" that before

Humans excel at mental imagery, and we can transfer those images across senses. For example, an object out of view, but for which we have a mental image, can still be recognized by touch. Such cross-modal recognition is highly adaptive and has been recently identified in other mammals, but whether it is widespread has been debated. Solvi *et al*. tested for this behavior in bumble bees, which are increasingly recognized as having some relatively advanced cognitive skills (see the Perspective by von der Emde and Burt de Perera). They found that the bees could identify objects by shape in the dark if they had seen, but not touched, them in the light, and vice versa, demonstrating a clear ability to transmit recognition across senses. —SNV

Science, this issue p. 910; see also p. 850

CREDIT (TOP TO BOTTOM): HE *ET AL*.; CHI-KUO HU

IN OTHER JOURNALS

Edited by **Caroline Ash** *and* **Jesse Smith**

ATMOSPHERIC SCIENCE

Air contaminants act differently indoors

Indoor air quality strongly affects human health, and features of the indoor environment influence exposure to contaminants. Wang *et al*. found that many molecules that are volatile in typical outdoor air conditions are more abundant indoors, exhibit semivolatile behaviors on surface reservoirs, and participate in dynamic surface-gas partitioning. This model may provide a better understanding of how chemicals respond to different indoor surface reservoirs and how to mitigate exposure to indoor pollutants. —KVH

Sci. Adv. 10.1126/sciadv.aay8973 (2020).

CARDIOLOGY

Prosthetics provide room to grow

Children with congenital heart disease who require heart valve replacement often must undergo multiple high-risk surgeries because the replacement valve cannot grow as their heart grows. Inspired by this problem, Hofferberth *et al*. developed a prosthetic valve that mimics the geometry of the human venous valve, which maintains function despite large fluctuations in blood volume. The prosthesis, composed of polymeric leaflets attached to a stainless-steel stent, can be mechanically expanded using transcatheter balloon dilation to adapt to larger fluid volumes. Size-adaptable valves maintained function when implanted into growing lambs and could be mechanically expanded over 10 weeks. —CC

Sci. Transl. Med. **12**, eaay4006 (2020).

STRUCTURAL BIOLOGY

Choosing the drug to fit the protein

Many approved drugs bind to G protein–coupled receptors (GPCRs). A challenge in targeting GPCRs is that different ligands preferentially activate different signaling pathways. Two papers show how biased signaling arises for the angiotensin II type 1 receptor that couples to two signaling partners (G proteins and arrestins). Suomivuori *et al*. used large-scale atomistic simulations to show that coupling to the two pathways is through two distinct GPCR conformations and that extracellular ligands favor one or the other conformation. Wingler *et al*. present crystal structures of the same receptor bound to ligands with different bias profiles. These structures show conformational changes in and around the binding pocket that match those observed in simulations. This work could provide a framework for the rational design of drugs that are more effective and have fewer side effects. —VV

Science, this issue p. 881, p. 888

TOPOLOGICAL MATTER

Quantum anomalous Hall goes intrinsic

Quantum anomalous Hall effect—the appearance of quantized Hall conductance at zero magnetic field—has been observed in thin films of the topological insulator Bi_2Se_3 doped with magnetic atoms. The doping, however, introduces inhomogeneity, reducing the temperature at which the effect occurs. Two groups have now observed quantum anomalous Hall effect in intrinsically magnetic materials (see the Perspective by Wakefield and Checkelsky). Serlin *et al*. did so in twisted bilayer graphene aligned to hexagonal boron nitride, where the effect enabled the switching of magnetization with tiny currents. In a complementary work, Deng *et al*. observed quantum anomalous Hall effect in the antiferromagnetic layered topological insulator $MnBi_2Te_4$. —JS

Science, this issue p. 900, p. 895; see also p. 848

Nicotiana benthamiana plants, which are related to tobacco, are a model organism used in the production of proteins, including antibodies.

PHOTO: SEAN GALLUP/GETTY IMAGES

PLANT SCIENCE

Fixing the Fc of plantibodies

Plants offer a cost-effective means to produce therapeutically useful monoclonal antibodies. However, antibodies produced in plants differ from those produced in mammalian cells. Notably, the glycan composition of plant antibodies can affect their binding activity. Stelter *et al.* generated variants of a broadly neutralizing HIV monoclonal antibody in the plant *Nicotiana benthamiana* that differed by glycosylation. Plant-generated antibodies with typical plant glycosylation patterns were less able to engage with the cell-surface receptors required for immune activation. However, cell-binding affinity was successfully improved by targeted glycoengineering. The plant-produced antibodies were also more susceptible to oxidation of methionine residues in the Fc region. Oxidation reduced the affinity of the antibodies for the protective neonatal Fc receptor, which in turn reduced their half-life and therapeutic window. This phenomenon requires a solution before plant-produced antibodies can fulfill their therapeutic promise. —PJH

Plant Biotechnol. J. **18**, 402 (2020).

HEART DISEASE

Targeting the core of atherosclerosis

A major villain in heart attacks and stroke is the inflamed necrotic core of atherosclerotic plaque. When the plaque ruptures, debris from this necrotic core, which largely consists of dead and dying cells, is released into the bloodstream, where it can cause blood clots and arterial blockage. Flores *et al*. designed and tested a nanoparticle-based therapy aimed at inducing certain immune cells to clear away the dead cells. They loaded single-walled carbon nanotubes with a drug that stimulated macrophages localized within atherosclerotic plaque to engulf and destroy dead and dying cells by a process called efferocytosis. Administration of the nanoparticles to mice predisposed to develop atherosclerosis reduced plaque burden without detectable damage to healthy tissue. —PAK

Nat. Nanotechnol. **15**, 154 (2020).

A fatty plaque inside a coronary artery, visualized by false-color scanning electron microscopy

IMMUNOMETABOLISM

Lipid restriction enhances suppression

Regulatory T cells (T_{regs}) suppress immune responses to maintain tolerance and limit autoimmunity. Because lipid metabolism is crucial for the activity of T_{regs}, Field *et al*. explored the role of the lipid chaperone fatty-acid binding protein 5 (FABP5) in mouse and human T_{reg} function. Targeting FABP5 through either genetic or pharmacological means caused mitochondrial dysfunction, which depressed oxidative phosphorylation and promoted a switch to glycolysis. FABP5 inhibition enhanced the suppressive activity of T_{regs} through a mechanism involving mitochondrial DNA release and subsequent cGAS-STING–dependent type I interferon signaling. The researchers found that the lipid-restrictive nature of the tumor microenvironment influenced *Fabp5* gene expression and facilitated T_{reg} suppressor function. —PNK

Cell Metab. **31**, 422 (2019).

ORGANIC SYNTHESIS

Advancing C–H functionalization

The ability to selectively functionalize C–H bonds of complex molecules is one of the long-standing challenges for the organic synthesis community. Huang *et al*. demonstrate a practically useful method for highly regioselective C–H functionalization of ethers by using trisaminocyclopropenium as the electrophotocatalyst in the presence of a mild electrochemical potential and visible-light irradiation. The method was successfully applied to couple ethers with alkenes, alkynes, isoquinolines, and other azoles with no need of an external oxidizing agent. The electrophotocatalytic cycle involves hydrogen atom transfer from the substrate to the photoexcited catalyst radical dication. High regioselectivities for the less-hindered α position are achieved thanks to the steric effects of the catalyst structure. —YS

J. Am. Chem. Soc. **142**, 1698 (2020).

HUMAN GENETICS

Alternative polygenic associations

To predict traits and/or disease from genomic information, we must understand the genetics of the associations between genotype and phenotype. Polygenic risk scores are increasingly used to make predictions of phenotype on the basis of all the loci that correlate with a specific trait identified in genome-wide association studies (GWASs). However, population-level genetics and variable environmental effects can affect GWAS results. To determine the extent of any skewed GWAS results, Mostafavi *et al*. examined the accuracy of GWASs in a relatively homogeneous population: individuals of European-British descent within the UK Biobank. They found that sex, age, and socioeconomic status can affect GWAS signals. The authors suggest that using data from families within GWASs should help pull out direct and indirect effects, such as shared environmental factors and assortative mating to increase the accuracy of polygenic risk score prediction. —LMZ

eLife **9**, e48376 (2020).

VISA POLICY

Quotas, delays... no thanks, bye

Allocating permanent residency visas on the basis of per-country quotas rather than demand for skilled workers caused delays that led many Chinese and Indian STEM Ph.Ds to give up and take their talents home instead of staying in the United States. Kahn and MacGarvie show that delays in processing EB-2 visas disproportionately affected retention in fields that have driven economic growth and in which U.S.-born talent cannot satisfy industry demand, such as electrical and computer engineering. They also show that improvements in the quality of scientific enterprise in the individuals' home countries influenced decisions to leave the United States. —BW

Res. Policy 10.1016/j.respol.2019.103879 (2019).

2D MATERIALS

Straining free-standing graphene

Graphene is known, at least theoretically, to have a very high stiffness, which has been difficult to measure experimentally. Part of the challenge is being able to stretch and monitor a free-standing single-crystal monolayer of graphene instead of one that is supported. Cao *et al*. developed a new protocol for transferring, shaping, and straining graphene inside the scanning electron microscope. The authors found that free-standing graphene, even with edge defects, has mechanical properties close to the theoretical estimates and mechanical robustness attractive for many applications. —BG

Nat. Commun. **11**, 284 (2020).

CREDIT: PROF. P.M. MOTTA, G. MACCHIARELLI, S.A. NOTTOLA/SCIENCE SOURCE

ALSO IN *SCIENCE* JOURNALS

Edited by **Michael Funk**

REGENERATIVE MEDICINE

Next steps in heart disease cell therapy

Almost 20 years ago, the first trials that implanted stem cells into the heart were carried out. The aim of those trials, and many since, has been to regenerate lost heart muscle to recover function after a heart attack. However, numerous cell therapy strategies using adult stem cells have not shown efficacy in patients, despite positive preclinical experiments in animal models. In a Perspective, Murry and MacLellan discuss the reasons underlying this lack of success in the clinic, including lack of stem cell engraftment and survival. An emerging strategy to overcome these problems is the use of pluripotent stem cells, which have demonstrated long-term engraftment and regeneration in preclinical studies. The authors discuss the future hurdles that need to be overcome to successfully develop this cell therapy. —GKA

Science, this issue p. 854

PLANT ECOLOGY

The pervasive power of mycorrhizas

Associations between plants and symbiotic fungi—mycorrhizas—are ubiquitous in plant communities. Tedersoo *et al*. review recent developments in mycorrhizal research, revealing the complex and pervasive nature of this largely invisible interaction. Complex networks of mycorrhizal hyphae connect the root systems of individual plants, regulating nutrient flow and competitive interactions between and within plant species, controlling seedling establishment, and ultimately influencing all aspects of plant community ecology and coexistence. —AMS

Science, this issue p. 867

IMMUNOGENOMICS

Thymus development, cell by cell

The human thymus is the organ responsible for the maturation of many types of T cells, which are immune cells that protect us from infection. However, it is not well known how these cells develop with a full immune complement that contains the necessary variation to protect us from a variety of pathogens. By performing single-cell RNA sequencing on more than 250,000 cells, Park *et al*. examined the changes that occur in the thymus over the course of a human life. They found that development occurs in a coordinated manner among immune cells and with their developmental microenvironment. These data allowed for the creation of models of how T cells with different specific immune functions develop in humans. —LMZ

Science, this issue p. 868

VACCINES

Pitching cGAMP as a vaccine strategy

One strategy to address the variable effectiveness of many influenza vaccines is to induce antiviral resident memory T cells, which can mediate cross-protection against multiple substrains (heterosubtypic immunity). Unfortunately, such vaccines typically use attenuated active viruses, which may be unsafe for certain populations. Wang *et al*. report a vaccine using an inactivated virus that effectively induced heterosubtypic immunity in both mice and ferrets (see the Perspective by Herold and Sander). They coadministered the virus with 2′,3′-cyclic guanosine monophosphate–adenosine monophosphate (cGAMP), a potent activator of the innate immune system, encapsulated in pulmonary surfactant–biomimetic liposomes. This adjuvant was taken up by alveolar epithelial cells, whose activation resulted in effective antiviral T cell and humoral immune responses without accompanying immunopathology. —STS

Science, this issue p. 869; see also p. 852

STRUCTURAL BIOLOGY

Architecture of human BAF complex

The SWI/SNF family chromatin remodelers regulate chromatin and transcription. The protein complexes BAF and PBAF are mammalian SWI/SNF remodelers that play essential functions in diverse developmental and physiological processes. He *et al*. determined the structure of the human BAF complex, which contains three modules that bind the nucleosome on the top, bottom, and side, making this nucleosome-recognition pattern distinct from other chromatin remodelers. Mutations in BAF that are frequently associated with human cancer cluster into a nucleosome-interacting region. This structure provides a framework for understanding the BAF-mediated chromatin remodeling mechanism and its dysregulation in cancer. —SYM

Science, this issue p. 875

ATMOSPHERIC METHANE

Small burden from old sources

Methane is a potent greenhouse gas with large natural sources, reservoirs, and sinks. Dyonisius *et al*. found that methane emissions from old, cold-region carbon reservoirs like permafrost and methane hydrates were minor during the last deglaciation (see the Perspective by Dean). They analyzed the carbon isotopic composition of atmospheric methane trapped in bubbles in Antarctic ice and found that methane emissions from those old carbon sources during the warming interval were small. They argue that this finding suggests that methane emissions in response to future warming likely will not be as large as some have suggested. —HJS

Science, this issue p. 907; see also p. 846

ENZYME REGULATION

Evolution of a kinase allosteric site

Enzyme activity is often regulated by conformational changes coupled to binding of an effector at an allosteric site, a feature especially important for enzymes involved in signaling cascades. Hadzipasic *et al*. studied the origins of allosteric regulation of Aurora A, a kinase involved in progression of the eukaryotic cell cycle. Aurora A is allosterically regulated through the binding of an effector protein named TPX2, which also targets the kinase to spindle microtubules. By reconstructing ancestor kinase sequences, they found that TPX2 bound to an early Aurora A but had very weak activation that was gradually strengthened by evolution of an allosteric network within the kinase. An evolutionary advantage from localizing the active protein at the mitotic spindle may have driven the development of this regulatory mechanism. —MAF

Science, this issue p. 912

CANCER

Treatments from the dark kinome

Ovarian cancer is frequently fatal because it is difficult to detect and challenging to treat. Using cell lines and patient tumors, Kurimchak *et al*. analyzed the functional kinome of high-grade serous ovarian carcinoma (HGSOC) and identified a kinase called MRCKA as being important for HGSOC cell survival and tumor growth. Decreasing

abundance of this kinase or inhibiting its activity killed HGSOC cells but led to activation of other survival-promoting kinases in the remaining cells, which could be targeted by cotreating cells with a different kinase inhibitor or platinum-based chemotherapy. —LKF

Sci. Signal. **13**, eaax8238 (2020).

BIOCATALYSIS

Enzymes lock in planar chirality

Molecules with very large rings—macrocycles—are often conformationally constrained, and some exhibit planar chirality when substituents of the ring cannot rotate freely. Restricted rotation is generally valued in macrocycles because it can hold the molecule in functional conformations. Using a well-established lipase enzyme, Gagnon *et al*. developed a synthesis of planar chiral macrocycles with handles that can be easily functionalized. Computational docking suggests how using an enzyme as the catalyst for sequential acylation reactions can impart the observed stereochemistry. —MAF

Science, this issue p. 917

REVIEW SUMMARY

PLANT ECOLOGY

How mycorrhizal associations drive plant population and community biology

Leho Tedersoo*, Mohammad Bahram, Martin Zobel

BACKGROUND: All vascular plants associate with fungi and bacteria—the microbiome. Root associations with mycorrhizal fungi benefit most plants by enhancing their nutrient access and stress tolerance. Mycorrhizal fungi also mediate plant interactions with other soil microbes, including pathogens and mycorrhizosphere mutualists that produce vitamins and protect against antagonists. Through these functions, mycorrhizal root symbionts influence the belowground traits of plants, regulate plant-plant interactions, and alter ecosystem processes. Extensive mycorrhizal networks physically connect conspecific and heterospecific plant individuals belowground, mediating nutrient transfer and transmission of phytochemical signals. Arbuscular mycorrhiza (AM), ectomycorrhiza (EcM), ericoid mycorrhiza (ErM), and orchid mycorrhiza (OM) have a distinct evolutionary history, anatomy, and ecology, thereby differently affecting plant protection, nutrient acquisition, and belowground C and nutrient cycling.

ADVANCES: Mycorrhizal fungi are commonly the key determinants of plant population and community dynamics, with several principal differences among mycorrhizal types. We synthesize current knowledge about mycorrhizal effects on plant-plant interactions and ecological specialization. We conclude that mycorrhizal associations per se and fungal diversity and mycorrhizal types directly or indirectly affect plant dispersal and competition that shape plant populations and communities, and regulate plant coexistence and diversity at a local scale. Among AM plants, which represent nearly 80% of plant species globally, mycorrhizal associations and belowground hyphal networks tend to intensify intraspecific competition and alleviate interspecific competition by promoting the performance of inferior competitors. In AM systems, fungal diversity enhances plant diversity and vice versa, by providing species-specific benefits and suppressing superior competitors. Compared with other mycorrhizal types, EcM fungi provide substantial protection against soil-borne pathogens by ensheathing feeder roots and acidifying soil. Pathogen suppression leads to positive plant-soil feedback that promotes seedling establishment near adult trees, which can result in monodominant plant communities with a low diversity of various organism groups. Orchids produce millions of dust seeds with high dispersal potential to encounter compatible OM fungal partners, which nourish plants, at least in the seedling stage. Species of Ericaceae achieve competitive advantage and large population densities by shedding allelopathic litter and establishing ErM root symbiosis with selected groups of ubiquitous humus saprotrophs that have evolved efficient enzymes to access nutrients in recalcitrant organic compounds in strongly acidic environments.

OUTLOOK: Increasing evidence suggests that mycorrhizal fungi drive plant population biology and community ecology by affecting dispersal and establishment and regulating plant coexistence. Plant-fungal mycorrhizal associations per se and interlinking hyphal networks synergistically determine the functional traits and hence autecology of host plants, which is best reflected in the specialized nutrition and dispersal of orchids. Habitat patches dominated by either positive plant-soil feedback near EcM plants or negative conspecific feedback near AM plants may generate distinct regeneration patches for different plant species. Furthermore, niche differentiation both within and among mycorrhizal types enhances coexistence by leveraging interspecific competition through different rooting depths, foraging strategies, and soil nutrient partitioning. We still lack critical information about the mechanistic basis of several processes, such as interplant nutrient transfer through mycelial networks and the principles of carbon-to-nutrient exchange and trading in the mycorrhizal interface, as well as kin recognition and promotion. Understanding these processes will enable us to improve predictions about the impacts of global change and pollution on vegetation and soil processes and to elaborate technologies to improve yields in agriculture and forestry. ■

ON OUR WEBSITE

Read the full article at http://dx.doi.org/10.1126/science.aba1223

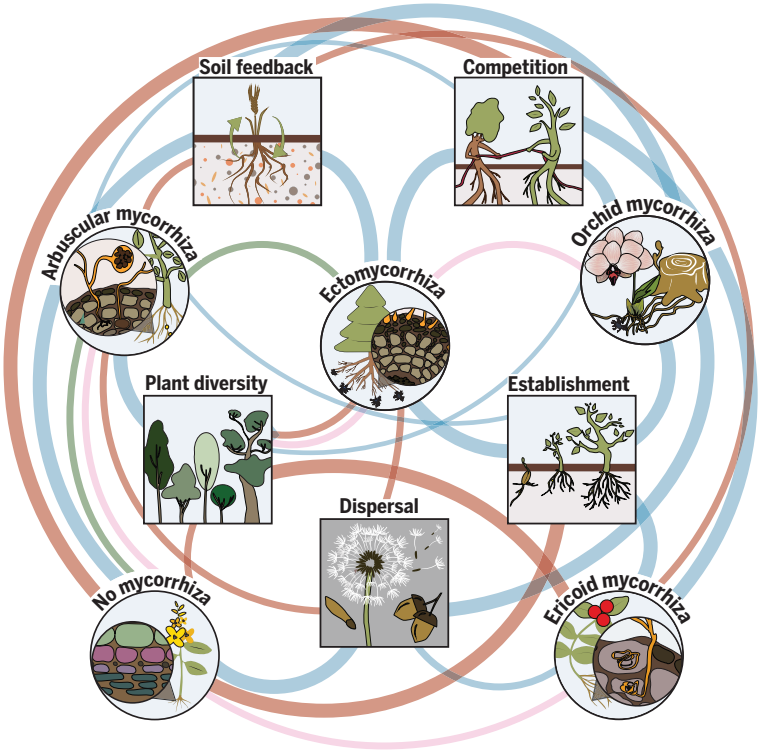

ILLUSTRATION: SIIRI JÜRIS

Scheme indicating how mycorrhizal types (circles) differ in their effects on plant population- and community-level processes (squares). Blue lines, positive effects; red lines, negative effects; green lines, overlap of plant taxa among mycorrhizal types; pink lines, overlap of fungal taxa among mycorrhizal types. Line breadth indicates relative effect strength.

The list of author affiliations is available in the full article online.
*Corresponding author. Email: leho.tedersoo@ut.ee
Cite this article as L. Tedersoo *et al.*, *Science* **367**, eaba1223 (2020). DOI: 10.1126/science.aba1223

REVIEW

PLANT ECOLOGY

How mycorrhizal associations drive plant population and community biology

Leho Tedersoo[1]*, Mohammad Bahram[2], Martin Zobel[3]

Mycorrhizal fungi provide plants with a range of benefits, including mineral nutrients and protection from stress and pathogens. Here we synthesize current information about how the presence and type of mycorrhizal association affect plant communities. We argue that mycorrhizal fungi regulate seedling establishment and species coexistence through stabilizing and equalizing mechanisms such as soil nutrient partitioning, feedback to soil antagonists, differential mycorrhizal benefits, and nutrient trade. Mycorrhizal fungi have strong effects on plant population and community biology, with mycorrhizal type–specific effects on seed dispersal, seedling establishment, and soil niche differentiation, as well as interspecific and intraspecific competition and hence plant diversity.

Plant ecology has traditionally focused on community responses to abiotic variables, competitive interactions among plant individuals, and aboveground herbivory (*1*). However, in recent decades, it has become clear that dispersal, speciation (*2*), and particularly symbiotic associations (*3*) also play important roles in plant population and community biology. Therefore, belowground interactions have been increasingly incorporated into species coexistence models (*4*). Herbivores, microbial antagonists, and mutualists differentially affect the fitness of individual plants and mediate intraspecific and interspecific competition and hence coexistence (*3*–*5*). Whereas the detrimental effects of parasites and pathogens can be relatively easily observed, the benefits of mutualistic microorganisms such as mycorrhizal fungi are not as immediately apparent in natural conditions (*5*), and consequently their effects on plant populations and communities are less well understood.

Mycorrhizal associations benefit most terrestrial plants by providing enhanced nutrient access and tolerance to abiotic and biotic stress (*6*, *7*). Mycorrhizal fungi mediate plant interactions with the soil microbiome, including pathogens and mycorrhizosphere mutualists that fix atmospheric nitrogen, take up phosphorus, produce vitamins, and/or protect against antagonists (*8*). Through these functions, mycorrhizal root symbionts drive the belowground traits of plants (*9*), regulate plant-plant interactions (*5*), and alter ecosystem processes (*10*) along with other biotic and abiotic drivers. Extensive common mycorrhizal networks (CMNs) physically connect conspecific and heterospecific plant individuals in soil, governing nutrient transfer into plants and transmitting phytochemical signals (*11*). There are four principal types of mycorrhiza—arbuscular mycorrhiza (AM), ectomycorrhiza (EcM), ericoid mycorrhiza (ErM) and orchid mycorrhiza (OM)—which differ in their anatomy and evolutionary ecology (Table 1) (*6*, *12*). Recent studies have revealed substantial differences among mycorrhizal types in plant nutrient acquisition, soil C and nutrient cycling, and the capacity to protect against soil-borne pathogens (*10*, *13*) These differences have global-scale consequences for soil C sequestration and for mitigating N pollution and climate warming (*14*, *15*).

Several authors have reviewed the effect of mycorrhizas on plant community ecology, with a strong emphasis on AM in grassland ecosystems or OM (*5*, *16*). However, recently published controlled ecological experiments and comparative studies in ecophysiology, nutrient cycling, and plant-soil feedback (*17*–*20*) extend the mechanisms of mycorrhizal impact and suggest several key differences among mycorrhizal types.

Here we integrate results from experimental and observational studies from several disciplines and demonstrate that various stabilizing and equalizing mechanisms related to mycorrhizal associations regulate plant coexistence and diversity at local plant community and landscape levels (Fig. 1). We aim to answer two major questions: (i) What are the principal mechanisms by which mycorrhizal associations affect plant population and community ecology? and (ii) how do the mechanisms differ between mycorrhizal types? Finally, we provide a synthesis of mycorrhizal and mycorrhizal-type effects on plant biology.

Dispersal and establishment

To establish in a given community, viable diaspores first need to reach the target habitat. Plant distribution is often dispersal-limited; that is, not all potential community members reach suitable habitats (*21*). For many mutualistic associations, and in particular those involving plant taxa with negligible photosynthetic capacity, a plant individual has to encounter a fungal symbiont during the seedling establishment phase (*16*, *22*). Limitation of suitable partners may occur with higher probability when the host specificity of associations is high, which is relatively more common among OM and EcM associations than among other mycorrhizal types (*23*). For example, generalist EcM host plants were more efficient postglacial dispersers than specialists, perhaps owing to the better access to appropriate symbionts in new habitats (*24*).

Plant mycorrhizal types differ somewhat in their primary dispersal vectors: Nearly all ErM plants are animal- or wind-dispersed, and OM plants are wind-dispersed, but EcM and AM plants exhibit multiple dispersal strategies (*25*). Certain angiosperms such as orchids (all known species) produce dust seeds, which can disperse over long distances. At the same time, dust seeds lack energy reserves, and therefore seedlings rely strongly on symbiotic fungi during the early growth stages (*22*, *26*). Similarly, the dust-sized spores of pteridophytes disperse efficiently, and the gametophytes of some species may be mycoheterotrophic (receive much of the C from fungi), requiring a specific fungal partner (*22*). Among such groups, the presence of suitable fungi at a target site or codispersal of partners becomes a prerequisite for the maintenance and establishment of plant populations.

Although fungi produce microscopic diaspores, they may also be dispersal-limited (*27*). For example, dispersal limitation of EcM fungi and plants hampers their establishment in vegetation matrices dominated by AM or ErM species (*27*, *28*). Most species of EcM fungi have limited distribution ranges that are commonly shaped by those of their hosts (*29*). Conversely, the saprotrophic ErM fungal species exhibit cross-continental distributions, and their inoculum is present nearly everywhere (*30*). Similarly, many AM fungal taxa display nearly global distributions despite their relatively large propagule size—spores or root fragments colonized by hyphae—indicating efficient long-distance dispersal (*31*). Unlike the sexual spores of most other fungi, AM fungal glomerospores can tolerate seawater for >1 week (*32*).

To conclude, dispersal limitation is a common ecological phenomenon in both mycorrhizal plants and fungi, which may to a relatively greater extent affect establishment of plants with obligately mycorrhizal associations. Mycorrhiza-dependent dispersal limitation tends to be relatively more important in determining the establishment success and population dynamics of OM and EcM plants because of their generally high partner specificity.

[1]Natural History Museum of Estonia, Tallinn, Estonia. [2]Department of Ecology, Swedish University of Agricultural Sciences, Uppsala, Sweden. [3]Institute of Ecology and Earth Sciences, University of Tartu, Tartu, Estonia.
*Corresponding author. Email: leho.tedersoo@ut.ee

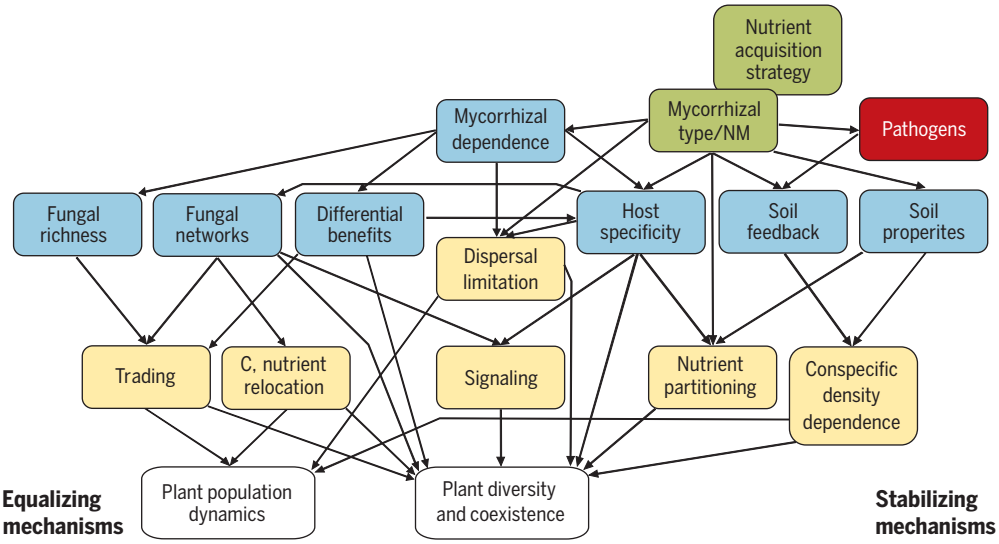

Fig. 1. Overview of stabilizing and equalizing mechanisms by which mycorrhizal associations promote plant coexistence and diversity and plant population dynamics. Mechanisms in the center have both stabilizing and equalizing aspects. Green, red, blue, and yellow boxes represent plants, various pathogens, direct mycorrhiza-related mechanisms, and mycorrhiza-associated processes, respectively. NM, nonmycorrhizal.

Belowground fungal linkages

The common mycelial network (CMN)

Genetic individuals of mycorrhizal fungi form CMNs in soil, connecting the root systems of conspecific and heterospecific plants of various ontogenetic stages (*11*). CMNs among plant species are strongly compartmentalized by mycorrhizal type (*33*) and to a lesser extent by association specificity (*23*). CMNs may redistribute carbon and nutrients among plants, enhance belowground signaling by plants, and regulate competition (*11*, *34*).

The mycelium of mycorrhizal fungi transports plant-derived carbon into soil in the form of sugars, amino acids, and polyols to sustain the mycorrhizosphere microbiome (*8*, *34*). The largest plant individuals with greatest net photosynthesis probably contribute most to the maintenance of mycorrhizal networks in AM and EcM symbioses. Besides maintaining the C demand of many nonphotosynthetic plants, the interconnecting mycelia transport C and macronutrients between photosynthesizing plants, representing 0 to 10% of net C movement (*11*). Using stable isotope labeling of carbon dioxide (CO_2) in a field experiment, Klein *et al.* (*35*) estimated that 40% of fine root carbon and 4% of total carbon originated from other trees.

Even if the rate of interplant C transfer is relatively low, it may be biologically important if it sustains the growth of shaded understory plants, especially seedlings at the stage of initial establishment. In EcM plants, Pickles *et al.* (*36*) demonstrated that relatively more C is transferred to kin than non-kin seedlings of *Pseudotsuga menziesii* by mycorrhizal networks. Although the mechanisms controlling carbon flow remain poorly understood, these results suggest that plants may be able to selectively provide their offspring with a competitive advantage in a way similar to promoting growth of root suckers in clonal plants. Enhancing kin seedlings relative to other conspecific seedlings may reduce genetic heterogeneity in plant populations, especially at fine scales.

Macro- and micronutrients also move between plants (*37*, *38*). N transfer may be biologically relevant in communities that comprise plants with large differences in N nutrition and N content, such as those containing actinorhizal and rhizobial plants. However, the net positive N transfer recorded from *Eucalyptus* sp. to the actinorhizal *Casuarina cunninghamiana* (*37*) runs counter to the hypothesis of nutrient movement from nitrogen-fixing plants to other plants and suggests that the mechanisms determining actual N transfer rates are not fully understood. Several other experiments demonstrated N or P flow via host-specific EcM fungi from a nonhost to a host plant (*38*, *39*). However, compared with mycorrhizal transportation, indirect nutrient transfer pathways, by root and leaf litter decomposition or uptake of root exudates, are estimated to be more important (*38*). Thus, it appears that AM and EcM fungi generally play a minor role in mutualistic interplant nutrient transfer.

Mycorrhizal fungi communicate with plants using organic acids, volatile organic compounds (VOCs), and phytohormones to initiate formation of the symbiosis (*40*) and to communicate warnings (*41*). AM and EcM CMNs are known to mediate plant-to-plant belowground signaling (*42*); and the same processes may, in theory, also occur through ErM, OM, and endophytic interactions. AM fungi deliver warning signals from pathogen- or herbivore-attacked plants to healthy individuals, inducing expression of defense-related genes and production of stress-related molecules (*42*–*44*), which lead to signal transfer via jasmonic acid and salicylic acid pathways (*44*). These warning systems may operate within species or at higher taxonomic levels (*43*). Besides providing warnings, AM and EcM fungi mediate plant kin recognition (and potentially self-recognition) in soil (*36*, *45*), which is probably communicated via root exudates (*46*). Efficient signal transmission may be under positive selection in both plants and fungi to maintain a stable environment and nutrient supply (*42*).

Taken together, signaling and nutrient transfer among plants are strongest between kin, which allows us to hypothesize that adult plants may support their direct offspring relative to other seedlings establishing in the rooting zone (Fig. 2). Conspecific non-kin and heterospecific plants from the same mycorrhizal type probably experience weaker communication and more variable costs and benefits from CMNs. Plants belonging to different mycorrhizal types are generally not connected by belowground signaling pathways and nutrient transfer, apart from occasional C or nutrient loss by means of parasitism.

Nutrient trade

Mycorrhiza can shape plant communities through its differential effects on plant species. Large plant individuals that contribute more C to mycorrhizal symbionts gain relatively more benefits from nutrient uptake by mycobionts (*47*), implying nutrient trading. Indeed, AM plants manipulate C flow to symbionts to promote root colonization by those fungi supplying most mineral P or N (*48*). Recently, the C-to-N trading model was extended to EcM symbiosis (*49*). For plants, the benefits of trading and partner selection are greater in conditions of nutrient limitation and high carbon availability (*48*).

Modeling studies indicate that both plants and fungi benefit from multiple trading partners that have no direct access to the resources limiting their performance (*50*). This leads to selection for more nutrition-specialist partners and thereby explains the rapid evolutionary loss of soil C acquisition capacity in mycorrhizal

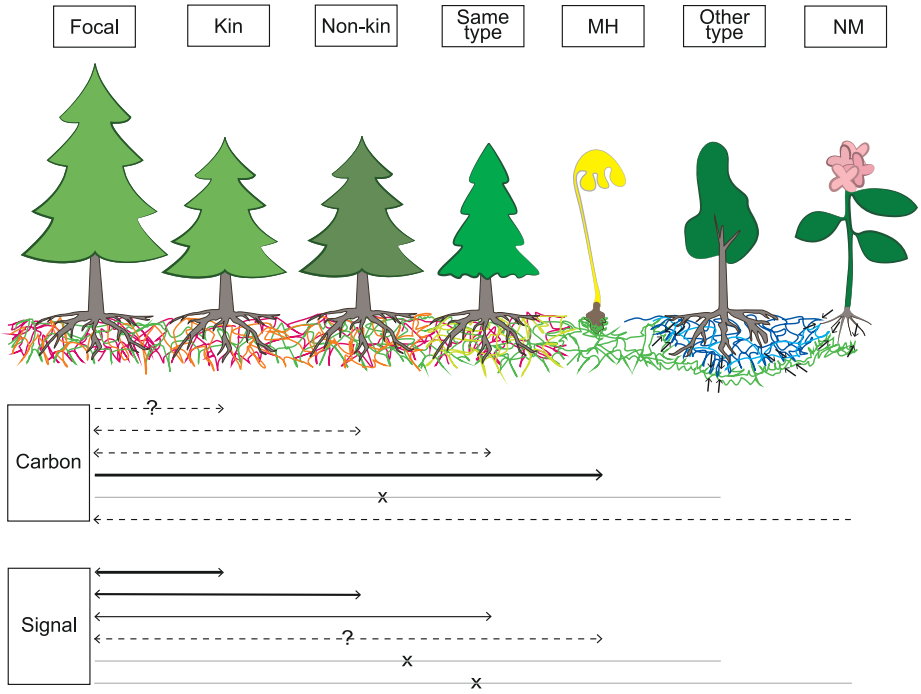

Fig. 2. Mycorrhizal network effects on carbon and signal transfer among plants. From left to right: focal (donor) plant; conspecific kin, conspecific non-kin, heterospecific but same mycorrhizal type, mycoheterotroph (MH; overlapping symbionts), heterospecific but other mycorrhizal type, and non-mycorrhizal (NM) plant. Colored lines indicate mycorrhizal fungal networks of different species or different mycorrhizal type (blue). Arrowheads depict potential antagonism among mycorrhizal fungi and plants of another mycorrhizal type or NM habit. Arrows indicate the direction of carbon and signal transfer; line width depicts the relative strength of transfer; dashed lines indicate weak and potentially biologically unimportant associations; gray, crossed-out lines indicate no association. Lines with question marks represent hypothetical flows that have not been studied.

fungi (*51*) and dominance of mycorrhizal plants in most terrestrial ecosystems (*12*). With an increasing number of fungal traders, nutrients become "cheaper" to plants (*52*). The presence of multiple trading partners also favors more cooperative symbionts and secures greater stability in the symbiosis (*48*, *50*).

Stabilizing mechanisms of plant coexistence

Stabilizing mechanisms of coexistence enhance negative intraspecific interactions relative to interspecific interactions. These mechanisms include resource partitioning among species, which results in relaxing interspecific competition, and frequency-dependent herbivory, resulting in greater losses of common species (*53*). Fluctuations in population densities and environmental factors in space and time may also contribute to resource partitioning and thus to species coexistence (*53*). However, classical coexistence theory does not address mutualistic relationships such as mycorrhiza. Here we outline how mycorrhizal associations contribute to stabilizing mechanisms.

Negative microbial feedback

Negative density dependence may arise not only from intraspecific competition but also from species-specific pathogens under their preferred hosts (*5*, *54*, *55*). In natural and experimental conditions, NM and AM plants experience more negative feedback from their soil biota compared with EcM plants, suggesting that EcM fungi protect plant root systems relatively more efficiently, compared with other mycorrhizal guilds (*13*, *17*, *18*). Indeed, AM plants accumulate relatively more pathogenic fungi in their mycorrhizosphere (*55*). Furthermore, in temperate and subtropical forests, EcM saplings and adult trees tend to exhibit positive density dependence, whereas AM trees show neutral density dependence (*55*–*57*). A combination of positive density dependence and differences in soil nutrition may lead to clustering of EcM tree seedlings around adult EcM trees and a lack of AM tree saplings around conspecific adult AM trees (*19*, *57*). Over time, aggregation of individuals belonging to a single species can lead to monodominance (>60% of basal area or stems belong to a single species), which is a particularly common phenomenon in EcM plant communities (*58*).

The magnitude of negative feedback may also differ within mycorrhizal types, depending on the level of root colonization. Plant species with potentially high growth rates and competitive ability tend to exhibit low AM root colonization and suffer most from negative soil feedback, compared with slow-growing species, which tend to experience high AM colonization and suffer less from negative feedback (*59*).

Exclusive partners

Potentially suitable partners represent a biotic niche space for plants and fungi that form mycorrhiza. Biotic niche differentiation is expected to reduce interspecific competition relative to intraspecific competition and hence enhance coexistence. Partner exclusivity (host specificity) is most common in mycoheterotrophic associations, where the EcM ("monotropoid" subtype) Ericaceae and OM Orchidaceae are highly dependent on specific, exploited fungal partners (*22*). In EcM systems, a few *Scleroderma* spp. are exclusive partners of the gymnosperm *Gnetum* spp. Conversely, EcM plant species of *Pinus*, *Alnus*, and *Pisonia* host multiple highly specific fungal species (*60*). The facultative nature of symbiosis for ErM fungi may disfavor specificity in ErM associations. In AM fungi, host specificity may be lacking because of asexuality and the presence of multiple heterogeneous nuclei in hyphae, which presents an obstacle to the synchronized evolution of specificity. Although there is currently no direct evidence for partner specificity favoring coexistence in mycorrhizal systems [but see (*61*)], specialization enhances coexistence in the plant-pollinator mutualistic system (*62*). Besides providing a stabilizing mechanism through biotic niche differentiation, specialist partners may enhance coexistence via enhanced benefits (see equalizing mechanisms).

Equalizing mechanisms of plant coexistence

Equalizing mechanisms reduce fitness differences between species and render interspecific plant competition more balanced (*63*). From this perspective, signaling and nutrient trading can be viewed partly as equalizing mechanisms in cases where inferior competitors linked to mycorrhizal networks are beneficiaries. Coexistence is enhanced if mycorrhiza benefits the competitively inferior species relatively more than fast-growing dominant species.

Mutualistic mycorrhizal types

Equalizing effects of mycorrhizal colonization have been demonstrated in multiple experimental systems with AM (*63*) and EcM (*64*) plants. However, there are also conflicting examples from studies of native and invasive plants, where mycorrhiza enhances dominant species and thus impedes coexistence (*65*).

Mycorrhizal dependency—the relative growth benefit of mycorrhizal association—differs among genotypes and species of plants belonging to all mycorrhizal types (*59*). In AM plants, early successional species and facultatively

mycorrhizal taxa exhibit lower growth responses than late successional taxa (*65*). These differences are usually enhanced in species mixtures compared with monocultures, resulting in enhancement of competitively inferior plant species (if these species are more mycorrhizal dependent) and thus promoting coexistence (*59*).

In nonspecific mycorrhizal associations, genotypes and species of mycorrhizal fungi benefit the growth of plant species differentially (*65*–*67*). Natural mycorrhizal fungal communities also differ in their effects on plant species (*66*, *67*). This renders observed mycorrhizal colonization effects on plant performance variable and

Table 1. Evolutionary and functional differences among plant mycorrhizal types. Ma, millions of years ago; NA, not applicable.

	Arbuscular mycorrhiza	Ectomycorrhiza	Ericoid mycorrhiza	Orchid mycorrhiza	Nonmycorrhizal
Plant symbionts (percent of plant species) (*12*)	Most vascular plants (78%)	30 lineages of angiosperms and gymnosperms; mostly trees (2%)	Ericaceae, Diaspensiaceae (1.4%)	Orchidaceae (10%)	Several angiosperm groups (Brassicaceae, Proteaceae; 8%)
Typical habitat (*15*, *97*)	Ubiquitous, particularly grasslands, croplands, temperate and tropical biomes	N-poor soils, mostly temperate and boreal forests, Mediterranean biomes, patchily in lowland rainforests	Highly acidic soils with mostly high organic content, usually cold tundra, boreal forests, and montane habitats	Ubiquitous but never dominant, including epiphytic habitats	Extreme: disturbed, early successional, nutrient-rich, P-starved, cold, aquatic habitats
Fungal symbionts (percent of described fungal species; our estimates)	Glomeromycota, Endogonomycetes (Mucoromycota); obligate mutualists (<0.5%)	>80 lineages of Basidiomycota, Ascomycota, and some Endogonomycetes; obligate mutualists (~15%)	Multiple lineages of Ascomycota and some Basidiomycota; free-living saprotrophs and root endophytes (<0.1%)	Ceratobasidiaceae, Serendipitaceae, Tulasnellaceae (all Basidiomycota), sometimes EcM fungi; free-living saprotrophs (<1%)	None, sometimes loose associations and nutritional benefits from free-living fungi
Anatomy (*12*)	Intracellular "arbuscules"	Intercellular "Hartig net," sheathing "mantle"	Intracellular "coils"	Intracellular "pelotons," their digestion	No specialized structures, sometimes AM hyphae
Extraradical hyphae (*6*)	Aseptate-multinucleate; few to abundant	Septate; few to abundant; may form rhizomorphs and high biomass	Septate; abundant	Septate; few to abundant	NA
Evolutionary history (*12*)	>450 Ma	150 to 180 Ma and onward	~100 Ma	~110 Ma	~110 Ma and onward
Nutrient acquisition (*6*, *10*, *51*)	Mostly P; low C biodegradation capacity	N and P; moderate C biodegradation capacity	N and P; strong C biodegradation capacity	N and P, some C; strong C biodegradation capacity	N and P; no C biodegradation capacity
Plant dispersal (*25*)	Variable	Variable	Zoochory, anemochory; efficient	Anemochory; dust seeds; highly efficient	Mostly anemochory; efficient
Seedling establishment	Seldom limited by mutualist availability	Often limited by mutualist availability; kin promotion (*36*)	Mutualists obtained from soil and roots of other plants (*30*)	Critically limited by specific mutualist availability (*22*)	Prefers mycorrhiza-free soil (*12*)
Plant soil feedback (*13*, *17*, *18*)	Negative or neutral	Positive or neutral	Not addressed	Positive (*22*)	Negative
Allelochemical production (*79*, *82*)	Uncommon	Common	Very common	Not addressed	Variable (substantial in Brassicaceae)
Fungal diversity effects	Positive on plant diversity and productivity (*78*)	None or weakly positive (*78*)	Not addressed	Biotic niche to species (*61*)	Not addressed
Mycorrhizal means of altering plant co-occurrence and diversity (see text)	Differential benefits, hyphal networks, trading	None intraguild; suppresses overall plant diversity	None intraguild; suppresses overall plant diversity	Not addressed	Suppression via resource competition and parasitism

strongly dependent on the selection of experimental organisms (66). From an ecological perspective, species- or strain-specific benefits promote C for nutrient trading and partner selection. Hence, the availability of more fungal genotypes and species with complementary benefits may promote plant species coexistence and improve community productivity (68).

In mycorrhizal associations, specialist symbionts may provide enhanced benefits to their partners. If these partners are superior competitors, such as most large trees from the Pinaceae and Fagaceae families, their specialist fungi may promote interspecific competition. Conversely, inferior competitors, such as *Alnus* and *Salix* species, may potentially gain a competitive advantage. However, there is, as yet, no evidence that host-specific and nonspecific EcM fungi provide differential benefits. From an evolutionary perspective, host-specific mycorrhizal partners can be viewed as trapped, because they can only efficiently interact with a limited number of congeneric hosts and are therefore forced to be highly cooperative to survive. Although direct evidence is lacking, specific partners may have evolved more efficient communication and nutrient transfer mechanisms than their generalist competitors, which may somewhat relax the cost of cooperation. Laboratory experiments reveal that specialist fungi may deliver resources from nonhosts to hosts (39), but the occurrence and biological importance of this phenomenon require verification in natural conditions.

Mycoheterotrophs

Mycorrhizal networks play a fundamental role in equalizing interspecific plant competition in communities where mycoheterotrophs are found. A strategy of theft rather than fair trading has evolved among mycoheterotrophs, in which specialization reflects a host-parasite arms race, where the plant aims to gain greater control over a particular fungal "victim" (22). Fully or partly mycoheterotrophic plants tap into EcM or AM fungal networks and acquire some or all of their energy via mycorrhizal fungi from dominant plant individuals (22). All mycoheterotrophs are small and slow-growing, and most occur at low abundance; hence, drawing resources from overstory species allows them to coexist with more competitive species. Even when they occur at high abundance (e.g., Pyroleae), and despite sometimes displaying very high rates of transpiration, there is currently no evidence that mycoheterotrophs drain C in sufficiently large amounts to damage nurse trees (69).

Most mycoheterotrophs specialize on a particular fungal species, narrow group of species, or genus during the early germination and adult stages (22). Although there is evidence for coevolution between plants and fungi in some orchid genera, abrupt partner shifts are common in the mycoheterotrophic Orchidaceae and Ericaceae (70). Because of relatively specific symbiotic associations, mycoheterotrophs, including orchids, present a relatively high number of reproductively isolated sympatric races and low hybridization rates. Shifting fungal or pollinator partners in populations of orchid species may characterize these most common forms of specialization and underlie the hyperdiversity and ultrahigh diversification rates observed in Orchidaceae (22, 70). Biotic niche partitioning through association with different fungal symbionts promotes the coexistence of multiple orchid species (16). However, mycoheterotrophs have historically very high rates of extinction due to the evolution of multiple nonviable partner shifts and extinctions of intimate partners (70). Both mycoheterotrophic and autotrophic specialist plant and fungal species would themselves be extremely threatened by the extinction of their sole partner.

Initially, mutualistic fungal nursing of seedlings in small-seeded plants triggered the loss of photosynthesis, further seed size reduction, and autogamy in mycoheterotrophs to secure efficient dispersal (26). Increasing specialization toward fungal and pollinator partners has led to high ecological specificity and increased diversification rates at population and species levels, which underlie the high richness and sometimes strong contribution to local-scale plant diversity observed among orchids.

Partial mycoheterotrophy has long been considered an uncommon feature characteristic of certain orchids and EcM-associated ericaceous plants. However, recent stable isotopic evidence in natural plant communities suggests that this phenomenon may be widespread (>10% of plant species) among shade-tolerant AM herbs that develop hyphal coils rather than typical arbuscules in root cells (71). As these herbs are slow-growing, supplementary C from dominant AM trees and grasses received via

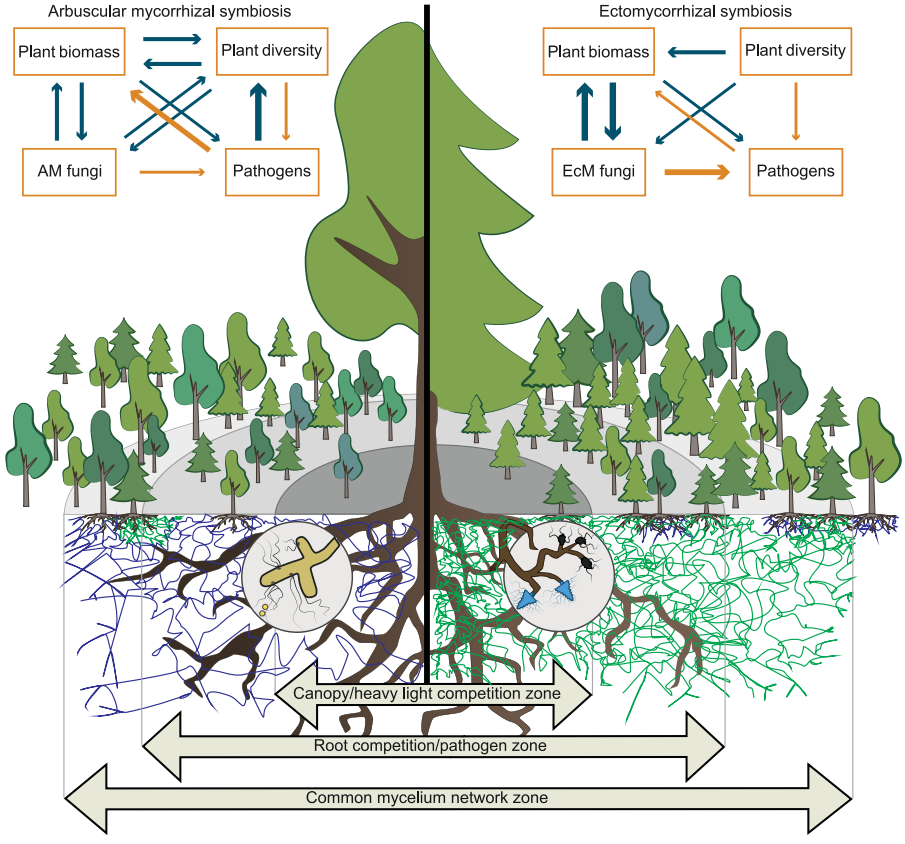

Fig. 3. Relative arbuscular mycorrhizal (left pane) and ectomycorrhizal (right pane) regeneration niches and the principal differences among mycorrhizal types in plant-mutualist-pathogen relationships (insets). The regeneration niche incorporates spatial heterogeneity in light competition (shade), root competition, the extent of common mycelial networks, conspecific versus heterospecific nurse plants and the same versus different mycorrhizal types. Symbol shapes indicate different mycorrhizal types ("spruce," ectomycorrhizal; "maple," arbuscular mycorrhizal); symbol colors indicate different species. Double-sized symbols indicate flourishing seedlings escaping from root competition and pathogens, and benefiting from common mycelial networks. In the insets, blue and orange arrows indicate positive and negative effects, respectively; arrow width depicts the relative importance of the effect; plant-to-plant diversity association is considered here as a productivity-to-diversity relationship.

CMNs may account for a previously unrecognized equalizing mechanism promoting plant coexistence.

Mycorrhizal fungi mediate competition

Mycorrhizal fungi regulate plant coexistence either by amplifying or equalizing plant competition. Classical plant ecology views competition either as direct interference between plant individuals or an indirect impact through resource depletion (*72*), but actual competitive interactions are much more complex owing to the involvement of antagonists and mutualists, including different mycorrhizal guilds.

Competitive effects of mycorrhizal fungi on plants

The availability of mineral nutrients may limit the growth of both plants and fungi in nutrient-poor ecosystems. In EcM ecosystems, nutrients are immobilized in fungal biomass to maintain mycelial structures and maximize reproductive effort. This may lead to a loss of nutrient-demanding AM plant species and reduced primary production (*73*).

Competitive interactions between plant individuals may be shaped by interactions with symbiotic fungi. For instance, EcM fungi reduce mycorrhizal root colonization of neighboring AM herbs (*74*) and enhance the competitive dominance of EcM trees over AM trees (*75*) by promoting litter accumulation and limiting access to nutrients (Fig. 3). Similarly, AM fungi were found to exacerbate iron deficiency in *Eucalyptus* seedlings and inhibit their establishment in Australian AM-dominated rainforest (*76*).

EcM and ErM fungi may reduce germination and growth of nonhost plants through direct interactions or allelochemicals (*77*). As yet there is no evidence for allelopathy in AM fungi (*78*). Nonetheless, in both laboratory and field experiments, AM fungi sometimes distort the root tissues of non-AM plants, hampering root development and functioning (*78*). Controlled experiments show that incompatible mycorrhizal interactions trigger defense mechanisms in nonhost plants and sometimes result in C loss to interacting fungi (*39*).

Competitive effects of plants on mycorrhizal fungi

Plant individuals can affect other plants by influencing the mycorrhizal fungi associating with their neighbors. By producing allelochemicals and VOCs, plants may inhibit the mycorrhizal fungi that associate with other plants. Ericaceae species are well known for producing phenolics-rich leaf litter that retards the growth of both AM and EcM fungi (*18*, *79*, *80*). By releasing allelopathic compounds or altering soil chemistry, AM shrubs reduce root length, root fungal colonization, and fungal richness of EcM plants (*81*). Conversely, EcM trees can suppress AM colonization of herbs via allelopathic litter or nutrient competition (*74*). The relative importance of allelochemicals in suppressing root colonization of other mycorrhizal types remains poorly understood owing to the design of experiments, which typically lack intraguild controls (i.e., testing the impact of allelochemicals on conspecific individuals or on other species from the same mycorrhizal type) in most experiments (*79*).

Much information on the effects of allelopathy comes from studies of aggressive invasive plants from the Brassicaceae and Chenopodiaceae families (*82*). These groups may have evolved the NM habit along with a high content of allelochemicals in their roots to suppress AM and EcM fungi and hence, indirectly, their mycorrhizal hosts (*79*). For example, the highly invasive NM herb *Alliaria petiolata* produces allelochemicals that severely reduce the local abundance of EcM and AM fungi and the degree to which they colonize other herbaceous plants and trees (*79*).

Competitive effects of plants on plants mediated by mycorrhizal fungi

Competition among plants may be related to plant mycorrhizal type and mycorrhizal dependence (the relative fungal benefits to plant species). For instance, ErM plants shed allelopathic and slowly decomposing litter, which hampers the development of other plants. ErM fungi with strong saprotrophic capacity render ericaceous plants highly competitive in acidic, nutrient-poor soils (*30*). Both AM and EcM fungi can protect their host plants from the detrimental effects of certain allelochemicals or extend their impact beyond the rhizosphere (*82*). In particular, AM fungi transport herbicides and allelochemicals to competing plants, hampering their growth up to 15 to 20 cm distant from roots (*83*). Such synergistic effects of plants and mycorrhizal fungi in alleviating and redistributing allelochemicals may well occur in other mycorrhizal types as well. Under certain conditions, NM plants may also have a competitive advantage. NM plants have evolved several strategies to avoid direct nutrient competition, such as nutrient acquisition from ultrapoor soils or early colonization of pioneer habitats where mycorrhizal competitors perform poorly, as well as allelopathic suppression of potential competitors (*84*).

Plant diversity and mycorrhiza

Experiments with AM plants and fungi have shown that simultaneous colonization and network formation by a diverse set of fungi can synergistically promote coexistence and diversity of plant species, compared to a system with a low diversity of fungi (*85*). Field studies in various natural ecosystems also suggest that mycorrhizal fungal and plant diversity are positively related (*86*, *87*). Besides increasing resource use complementarity (*88*), high fungal diversity may enhance nutrient trading (*50*), improve overall nutrient acquisition by plants, and promote primary productivity (*85*). In contrast to AM systems, experiments with EcM plants have revealed no fungal diversity effect on host performance or ecosystem services (*64*), despite some evidence for partitioning of organic P sources (*89*) and high functional complementarity among EcM fungal species (*10*, *51*). However, the lack of such effects may be related to studying seedlings over a short time.

Across geographic scales, EcM-dominated plant communities tend to be less diverse than AM-dominated communities (*90*, *91*). The above-described mechanisms related to altered nutrient availability (*10*) and accumulation of organic material and allelopathic compounds in EcM systems (*79*) provide plausible explanations. Alternatively, differences in plant diversity between EcM- and AM-dominated habitats may be related to plant-soil feedback. Because AM plants are relatively vulnerable to soil-borne pathogen attack and accumulate soil-borne pathogens, density-dependent accumulation of taxon-specific pathogens in the rhizosphere may suppress the abundance of prevalent AM plant species and hence contribute to the high plant diversity in AM-dominated communities (*5*, *73*, *92*). We suggest that these four mechanisms—access to organic nutrients, accumulation of organic material and allelopathic compounds, and positive plant soil feedback—act synergistically in EcM-dominated plant communities to maintain community monodominance over multiple generations.

Different mycorrhizal types

In many terrestrial ecosystems, three or more mycorrhizal types coexist, which may reflect different biological mechanisms. Fungi from all mycorrhizal types compete for mineral nutrients, but their differential capacity for organic nutrition enables a certain level of resource partitioning. In boreal and temperate forests, there is evidence for vertical niche partitioning among fungi belonging to different mycorrhizal types (*93*, *94*). For example, AM and ErM fungi specialize in uptake of different forms of P (*95*), whereas AM and EcM fungi partition sources of N (*96*). AM fungi can only access a subset of P forms available to EcM fungi (*20*), although this may be compensated by a lower C cost to AM fungi. Fine-scale disturbance and spatial heterogeneity of soil nutrients may further promote coexistence of plants associating with different groups of fungi (*6*, *97*). Such niche differentiation among plant mycorrhizal types potentially increases competition within mycorrhizal types, while enhancing coexistence of plants belonging to different mycorrhizal types.

Plant coexistence from a mycorrhizal perspective: Synthesis

Plant nutrient acquisition strategies and resistance to soil-borne pathogens strongly depend on mycorrhizal associations. Fungal partners belonging to different mycorrhizal types modify local soil conditions and generate habitat patches of differential quality, which affects offspring establishment of both host and nonhost plant species (*19*, *55*). EcM and ErM associations acidify soil by producing recalcitrant litter, deplete available nutrients, and produce allelochemicals (*10*, *82*, *97*), whereas AM systems accumulate relatively more soil-borne pathogens (*13*, *55*). Therefore, the size and distinctness of such habitat patches are a function of plant traits related to mycorrhizal associations, root and foliar chemistry, and competition. The resulting local abiotic and biotic heterogeneity creates specific regeneration niches for plants with different functional traits, including mycorrhizal type (*75*, *98*, *99*). Although most plants preferentially establish outside the zone of direct root competition and shade, establishment of EcM plants seems to depend most on the availability of preestablished CMNs (*19*, *100*). Orchids and most mycoheterotrophic groups require the presence of specific fungal species for germination and growth. Establishment of AM plants tends to fail under conspecific AM trees (*19*, *55*) and under EcM vegetation (*13*), their main regeneration niche being under heterospecific AM plants (Fig. 3).

To conclude, local-scale coexistence of plant species from *different* mycorrhizal types is enhanced by mycorrhiza-mediated resource partitioning. In EcM systems, positive soil feedback, build-up of recalcitrant organic material in topsoil, and access to nutrients in these organic layers enhance dominance and lead to lower diversity compared to AM systems. Conversely, negative soil feedback and differential mycorrhizal effects favor coexistence of AM plants, leading to high diversity of plants, soil microbes, and fauna.

Research needs

Despite insights from experimental mycorrhizal research conducted during more than a century, relatively little is known about the roles of mycorrhizal fungi in shaping plant communities. We identify three major unresolved issues and propose ways of addressing them.

Balanced incorporation of different mycorrhizal types in experimental research

The relative ease of manipulating herbaceous plants has favored use of AM symbiosis as a model mycorrhizal association in plant ecology (*78*), although difficulties in handling uncultured fungal taxa limit the range of possible experiments. We identified substantial functional differences among plants and fungi belonging to different mycorrhizal types, which invalidate generalization from AM-based models to other types of mycorrhiza. In particular, knowledge about the function and ecology of ErM associations needs to be improved. To disentangle the actual role of mycorrhiza in structuring plant communities, ecologists should address systems in which different mycorrhizal types are represented, such as temperate deciduous forests, Mediterranean shrublands, and tropical montane forests.

Mycorrhizal response to global change

Changes in climate, water, and nutrient availability, as well as invasions of plants and antagonists, trigger major shifts in vegetation and its associated microbiome (*15*). Changing abiotic and biotic environments may alter the costs and benefits of mycorrhizal associations and shift the competitive balance among mycorrhizal types and related ecosystem services. Information about the dispersal capacities and climatic tolerances of symbiotic fungi, and potential shifts in mycorrhizal functionality, would notably inform predictions about global change effects on agriculture, forestry, and conservation (*27*, *101*).

Role of the common mycelial network

CMNs represent one of the most fascinating features of mycorrhizal associations. Multiple studies have addressed C and nutrient redistribution among plants via CMNs and revealed the vital role of CMNs in the mycoheterotrophic lifestyle; yet the ecological importance of CMNs for autotrophic plants remains heavily debated (*11*, *35*, *78*). Novel tools such as -omics techniques; stable isotopes of O, K, and Ca; or nanoparticles offer real promise to trace the fate of resources in greater detail and in natural conditions (*102*–*104*). It has only recently been recognized that CMNs can transfer allelochemicals and transmit plant signals. Theoretically, hyphal networks could also represent pathways for virus transmission, given that several phytoviruses can infect fungi (*105*). If this were true, it would represent a new stabilizing mechanism promoting plant species co-occurrence and diversity, when abundant and fast-growing plant species, which usually invest little to defense systems, are affected most.

Conclusions

We posit that plant-fungal mycorrhizal associations per se and interlinking hyphal networks synergistically affect plant communities and ecosystem services through the altered functional traits and autecology of host plants. This is perhaps most clearly apparent in the specialized C nutrition of orchids and mycoheterotrophs. ErM plants but also some NM plants have evolved specific means of mineral nutrition in extremely nutrient-poor or otherwise extreme environmental conditions. Both high hyphal biomass and physical ensheathing of plant feeder roots may underlie the relatively strong protective benefits of EcM fungi to their host plants, which results in positive plant-soil feedback and high population densities and may, in the long term, lead to the development of low-diversity, potentially monodominant, ecosystems. The ways in which mycorrhizal plants and fungi modify the environment produce spatially distinct regeneration niches that favor establishment of plant species with different functional traits.

We recognize three ways in which different types of mycorrhiza influence plant population and community ecology: by affecting plant dispersal, establishment, and coexistence (the latter through stabilizing and equalizing mechanisms). Dispersal limitation of one or both symbiotic partners restricts the distribution of OM and EcM plants more than AM, ErM, and NM plants. Failure of either partner to arrive or establish in a given habitat may alter the diversity, as well as the taxonomic and mycorrhizal type composition, of plant communities. Stabilizing mechanisms via negative soil feedback are best understood in the context of AM systems. Niche differentiation both within and among mycorrhizal types enhances coexistence by leveraging interspecific competition via different rooting depths, foraging strategies, and soil nutrient partitioning. Equalizing mechanisms, which enhance weaker competitors, may operate through differential mycorrhizal benefits that elicit relatively stronger positive growth responses or enhancement of seedling establishment via CMNs. Although CMNs are important in AM, OM, and EcM associations, evidence that they enhance coexistence and diversity is so far limited to AM and OM systems. Species-specific benefits and resource trading may represent key mechanisms by which diversity begets diversity in plant-mycorrhizal fungi mutualistic systems.

REFERENCES AND NOTES

1. D. Tilman, *Resource Competition and Community Structure* (Princeton Univ. Press, 1982).
2. L. Götzenberger *et al*., Ecological assembly rules in plant communities—Approaches, patterns and prospects. *Biol. Rev. Camb. Philos. Soc.* **87**, 111–127 (2012). doi: 10.1111/j.1469-185X.2011.00187.x; pmid: 21692965
3. D. A. Wardle *et al*., Ecological linkages between aboveground and belowground biota. *Science* **304**, 1629–1633 (2004). doi: 10.1126/science.1094875; pmid: 15192218
4. J. D. Bever, Dynamics within mutualism and the maintenance of diversity: Inference from a model of interguild frequency dependence. *Ecol. Lett.* **2**, 52–61 (1999). doi: 10.1046/j.1461-0248.1999.21050.x
5. J. D. Bever *et al*., Rooting theories of plant community ecology in microbial interactions. *Trends Ecol. Evol.* **25**, 468–478 (2010). doi: 10.1016/j.tree.2010.05.004; pmid: 20557974
6. S. E. Smith, D. J. Read, *Mycorrhizal Symbiosis* (Academic Press, ed. 3, 2008).
7. S. Rasmann, A. Bennett, A. Biere, A. Karley, E. Guerrieri, Root symbionts: Powerful drivers of plant above- and belowground indirect defenses. *Insect Sci.* **24**, 947–960 (2017). doi: 10.1111/1744-7917.12464; pmid: 28374534

8. M. Buée, W. De Boer, F. Martin, L. van Overbeek, E. Jurkevitch, The rhizosphere zoo: An overview of plant-associated communities of microorganisms, including phages, bacteria, archaea, and fungi, and some of their structuring factors. *Plant Soil* **321**, 189–212 (2009). doi: 10.1007/s11104-009-9991-3
9. M. L. McCormack *et al*., Building a better foundation: Improving root-trait measurements to understand and model plant and ecosystem processes. *New Phytol.* **215**, 27–37 (2017). doi: 10.1111/nph.14459; pmid: 28295373
10. L. Tedersoo, M. Bahram, Mycorrhizal types differ in ecophysiology and alter plant nutrition and soil processes. *Biol. Rev.* **94**, 1857–1880 (2019). doi: 10.1111/brv.12538; pmid: 31270944
11. S. W. Simard *et al*., Mycorrhizal networks: Mechanisms, ecology and modelling. *Fungal Biol. Rev.* **26**, 39–60 (2012). doi: 10.1016/j.fbr.2012.01.001
12. M. C. Brundrett, L. Tedersoo, Evolutionary history of mycorrhizal symbioses and global host plant diversity. *New Phytol.* **220**, 1108–1115 (2018). doi: 10.1111/nph.14976; pmid: 29355963
13. K. Kadowaki *et al*., Mycorrhizal fungi mediate the direction and strength of plant-soil feedbacks differently between arbuscular mycorrhizal and ectomycorrhizal communities. *Commun. Biol.* **1**, 196 (2018). doi: 10.1038/s42003-018-0201-9; pmid: 30480098
14. C. Terrer, S. Vicca, B. A. Hungate, R. P. Phillips, I. C. Prentice, Mycorrhizal association as a primary control of the CO_2 fertilization effect. *Science* **353**, 72–74 (2016). doi: 10.1126/science.aaf4610; pmid: 27365447
15. N. A. Soudzilovskaia *et al*., Global mycorrhizal plant distribution linked to terrestrial carbon stocks. *Nat. Commun.* **10**, 5077 (2019). doi: 10.1038/s41467-019-13019-2
16. M. K. McCormick, D. F. Whigham, A. Canchani-Viruet, Mycorrhizal fungi affect orchid distribution and population dynamics. *New Phytol.* **219**, 1207–1215 (2018). doi: 10.1111/nph.15223; pmid: 29790578
17. J. A. Bennett *et al*., Plant-soil feedbacks and mycorrhizal type influence temperate forest population dynamics. *Science* **355**, 181–184 (2017). doi: 10.1126/science.aai8212; pmid: 28082590
18. F. P. Teste *et al*., Plant-soil feedback and the maintenance of diversity in Mediterranean-climate shrublands. *Science* **355**, 173–176 (2017). doi: 10.1126/science.aai8291; pmid: 28082588
19. D. J. Johnson, K. Clay, R. P. Phillips, Mycorrhizal associations and the spatial structure of an old-growth forest community. *Oecologia* **186**, 195–204 (2018). doi: 10.1007/s00442-017-3987-0; pmid: 29086005
20. X. Liu *et al*., Partitioning of soil phosphorus among arbuscular and ectomycorrhizal trees in tropical and subtropical forests. *Ecol. Lett.* **21**, 713–723 (2018). doi: 10.1111/ele.12939; pmid: 29536604
21. J. A. Myers, K. E. Harms, Seed arrival, ecological filters, and plant species richness: A meta-analysis. *Ecol. Lett.* **12**, 1250–1260 (2009). doi: 10.1111/j.1461-0248.2009.01373.x; pmid: 19723285
22. V. Merckx, *Mycoheterotrophy: The Biology of Plants Living on Fungi* (Springer, 2013).
23. S. Põlme *et al*., Host preference and network properties in biotrophic plant-fungal associations. *New Phytol.* **217**, 1230–1239 (2018). doi: 10.1111/nph.14895; pmid: 29165806
24. J. Pither, B. J. Pickles, S. W. Simard, A. Ordonez, J. W. Williams, Below-ground biotic interactions moderated the postglacial range dynamics of trees. *New Phytol.* **220**, 1148–1160 (2018). doi: 10.1111/nph.15203; pmid: 29770964
25. M. Correia, R. Heleno, P. Vargas, S. Rodríguez-Echeverría, Should I stay or should I go? Mycorrhizal plants are more likely to invest in long-distance seed dispersal than non-mycorrhizal plants. *Ecol. Lett.* **21**, 683–691 (2018). doi: 10.1111/ele.12936; pmid: 29536599
26. O. Eriksson, K. Kainulainen, The evolutionary ecology of dust seeds. *Perspect. Plant Ecol. Evol. Syst.* **13**, 73–87 (2011). doi: 10.1016/j.ppees.2011.02.002
27. T. R. Horton, Spore dispersal in ectomycorrhizal fungi at fine and regional scales. *Ecol. Stud.* **230**, 61–78 (2017). doi: 10.1007/978-3-319-56363-3_3
28. K. G. Peay, M. Garbelotto, T. D. Bruns, Evidence of dispersal limitation in soil microorganisms: Isolation reduces species richness on mycorrhizal tree islands. *Ecology* **91**, 3631–3640 (2010). doi: 10.1890/09-2237.1; pmid: 21302834
29. H. Sato, R. Tsujino, K. Kurita, K. Yokoyama, K. Agata, Modelling the global distribution of fungal species: New insights into microbial cosmopolitanism. *Mol. Ecol.* **21**, 5599–5612 (2012). doi: 10.1111/mec.12053; pmid: 23062148
30. P. Kohout, Biogeography of ericoid mycorrhiza. *Ecol. Stud.* **230**, 179–193 (2017). doi: 10.1007/978-3-319-56363-3_9
31. J. Davison *et al*., Microbial island biogeography: Isolation shapes the life history characteristics but not diversity of root-symbiotic fungal communities. *ISME J.* **12**, 2211–2224 (2018). doi: 10.1038/s41396-018-0196-8; pmid: 29884829
32. R. E. Koske, J. N. Gemma, VA Mycorrhizae in strand vegetation of Hawaii: Evidence for long-distance codispersal of plants and fungi. *Am. J. Bot.* **77**, 466–474 (1990). doi: 10.1002/j.1537-2197.1990.tb13577.x; pmid: 30139163
33. H. Toju, P. R. Guimarães, J. M. Olesen, J. N. Thompson, Assembly of complex plant-fungus networks. *Nat. Commun.* **5**, 5273 (2014). doi: 10.1038/ncomms6273; pmid: 25327887
34. J. Leake *et al*., Networks of power and influence: The role of mycorrhizal mycelium in controlling plant communities and agroecosystem functioning. *Can. J. Bot.* **82**, 1016–1045 (2004). doi: 10.1139/b04-060
35. T. Klein, R. T. L. Siegwolf, C. Körner, Belowground carbon trade among tall trees in a temperate forest. *Science* **352**, 342–344 (2016). doi: 10.1126/science.aad6188; pmid: 27081070
36. B. J. Pickles *et al*., Transfer of ^{13}C between paired Douglas-fir seedlings reveals plant kinship effects and uptake of exudates by ectomycorrhizas. *New Phytol.* **214**, 400–411 (2017). doi: 10.1111/nph.14325; pmid: 27870059
37. X. He, C. Critchley, C. S. Bledsoe, Nitrogen transfer within and between plants through common mycorrhizal networks (CMNs). *Crit. Rev. Plant Sci.* **22**, 531–567 (2003). doi: 10.1080/713608315
38. J. W. Munroe, M. E. Isaac, N_2-fixing trees and the transfer of fixed-N for sustainable agroforestry: A review. *Agron. Sustain. Dev.* **34**, 417–427 (2014). doi: 10.1007/s13593-013-0190-5
39. R. D. Finlay, Functional aspects of incompatible ectomycorrhizal associations. *Agric. Ecosyst. Environ.* **28**, 127–131 (1990). doi: 10.1016/0167-8809(90)90027-B
40. F. Martin, *Molecular Mycorrhizal Symbiosis* (Wiley-Blackwell, 2017).
41. S. Werner, A. Polle, N. Brinkmann, Belowground communication: Impacts of volatile organic compounds (VOCs) from soil fungi on other soil-inhabiting organisms. *Appl. Microbiol. Biotechnol.* **100**, 8651–8665 (2016). doi: 10.1007/s00253-016-7792-1; pmid: 27638017
42. M. A. Gorzelak, A. K. Asay, B. J. Pickles, S. W. Simard, Inter-plant communication through mycorrhizal networks mediates complex adaptive behaviour in plant communities. *AoB Plants* **7**, plv050 (2015). doi: 10.1093/aobpla/plv050; pmid: 25979966
43. Y. Y. Song, S. W. Simard, A. Carroll, W. W. Mohn, R. S. Zeng, Defoliation of interior Douglas-fir elicits carbon transfer and stress signalling to ponderosa pine neighbors through ectomycorrhizal networks. *Sci. Rep.* **5**, 8495 (2015). doi: 10.1038/srep08495; pmid: 25683155
44. D. Johnson, L. Gilbert, Interplant signalling through hyphal networks. *New Phytol.* **205**, 1448–1453 (2015). doi: 10.1111/nph.13115; pmid: 25421970
45. A. L. File, J. Klironomos, H. Maherali, S. A. Dudley, Plant kin recognition enhances abundance of symbiotic microbial partner. *PLOS ONE* **7**, e45648 (2012). doi: 10.1371/journal.pone.0045648; pmid: 23029158
46. M. Semchenko, S. Saar, A. Lepik, Plant root exudates mediate neighbour recognition and trigger complex behavioural changes. *New Phytol.* **204**, 631–637 (2014). doi: 10.1111/nph.12930; pmid: 25039372
47. H. Ek, S. Andersson, B. Söderström, Carbon and nitrogen flow in silver birch and Norway spruce connected by a common mycorrhizal mycelium. *Mycorrhiza* **6**, 465–467 (1997). doi: 10.1007/s005720050148
48. J. D. Bever, Preferential allocation, physio-evolutionary feedbacks, and the stability and environmental patterns of mutualism between plants and their root symbionts. *New Phytol.* **205**, 1503–1514 (2015). doi: 10.1111/nph.13239; pmid: 25561086
49. S. Hortal *et al*., Role of plant-fungal nutrient trading and host control in determining the competitive success of ectomycorrhizal fungi. *ISME J.* **11**, 2666–2676 (2017). doi: 10.1038/ismej.2017.116; pmid: 28731478
50. G. A. K. Wyatt, E. T. Kiers, A. Gardner, S. A. West, A biological market analysis of the plant-mycorrhizal symbiosis. *Evolution* **68**, 2603–2618 (2014). doi: 10.1111/evo.12466; pmid: 24909843
51. A. Kohler *et al*., Convergent losses of decay mechanisms and rapid turnover of symbiosis genes in mycorrhizal mutualists. *Nat. Genet.* **47**, 410–415 (2015). doi: 10.1038/ng.3223; pmid: 25706625
52. A. Argüello *et al*., Options of partners improve carbon for phosphorus trade in the arbuscular mycorrhizal mutualism. *Ecol. Lett.* **19**, 648–656 (2016). doi: 10.1111/ele.12601; pmid: 27074533
53. P. Chesson, Updates on mechanisms of maintenance of species diversity. *J. Ecol.* **106**, 1773–1794 (2018). doi: 10.1111/1365-2745.13035
54. A. Packer, K. Clay, Soil pathogens and spatial patterns of seedling mortality in a temperate tree. *Nature* **404**, 278–281 (2000). doi: 10.1038/35005072; pmid: 10749209
55. L. Chen *et al*., Differential soil fungus accumulation and density dependence of trees in a subtropical forest. *Science* **366**, 124–128 (2019). doi: 10.1126/science.aau1361; pmid: 31604314
56. I. A. Dickie, N. Koele, J. D. Blum, J. D. Gleason, M. S. McGlone , Mycorrhizas in changing ecosystems. *Botany* **92**, 149–160 (2014). doi: 10.1139/cjb-2013-0091
57. T. Sasaki *et al*., Role of mycorrhizal associations in tree spatial distribution patterns based on size class in an old-growth forest. *Oecologia* **189**, 971–980 (2019). doi: 10.1007/s00442-019-04376-2; pmid: 30919108
58. K. S. Peh, S. L. Lewis, J. Lloyd, Mechanisms of monodominance in diverse tropical tree-dominated systems. *J. Ecol.* **99**, 891–898 (2011). doi: 10.1111/j.1365-2745.2011.01827.x
59. M. Moora, M. Zobel, Arbuscular mycorrhizae and plant-plant interactions, in *Positive Plant Interactions and Community Biology*, F. Pugnaire, Ed. (CRC Press, 2010), pp. 79–98.
60. P. G. Kennedy, J. K. M. Walker, L. M. Bogar, Interspecific mycorrhizal networks and non-networking hosts: Exploring the ecology of host genus *Alnus*. *Ecol. Stud.* **224**, 227–254 (2015). doi: 10.1007/978-94-017-7395-9_8
61. M. W. Waud, P. Busschaert, B. Lievens, H. Jacquemyn, Specificity and localised distribution of mycorrhizal fungi in the soil may contribute to co-existence of orchid species. *Fungal Ecol.* **20**, 155–165 (2016). doi: 10.1016/j.funeco.2015.12.008
62. A. Pauw, Can pollination niches facilitate plant coexistence? *Trends Ecol. Evol.* **28**, 30–37 (2013). doi: 10.1016/j.tree.2012.07.019; pmid: 22951227
63. S. Stanescu, H. Maherali, Arbuscular mycorrhizal fungi alter the competitive hierarchy among old-field plant species. *Oecologia* **183**, 479–491 (2017). doi: 10.1007/s00442-016-3771-6; pmid: 27848080
64. D. A. Perry *et al*., Mycorrhizal fungi in mixed-species forests and other tales of positive feedback, redundancy and stability, in *The Ecology of Mixed-Species Stands of Trees*, M. G. Cannell *et al*., Eds. (Blackwell, London, 1992), pp. 151–179.
65. D. C. Hartnett, G. W. T. Wilson, Mycorrhizae influence plant community structure and diversity in tallgrass prairie. *Ecology* **80**, 1187–1195 (1999). doi: 10.1890/0012-9658(1999)080[1187:MIPCSA]2.0.CO;2
66. J. D. Hoeksema *et al*., Evolutionary history of plant hosts and fungal symbionts predicts the strength of mycorrhizal mutualism. *Commun. Biol.* **1**, 116 (2018). doi: 10.1038/s42003-018-0120-9; pmid: 30271996
67. C. Hazard, L. Kruitbos, H. Davidson, A. F. S. Taylor, D. Johnson, Contrasting effects of intra- and interspecific identity and richness of ectomycorrhizal fungi on host plants, nutrient retention and multifunctionality. *New Phytol.* **213**, 852–863 (2017). doi: 10.1111/nph.14184; pmid: 27636558
68. B. Bachelot, M. Uriarte, K. L. McGuire, J. Thompson, J. Zimmerman, Arbuscular mycorrhizal fungal diversity and natural enemies promote coexistence of tropical tree species. *Ecology* **98**, 712–720 (2017). doi: 10.1002/ecy.1683; pmid: 27984646
69. L. Tedersoo, P. Pellet, U. Kõljalg, M.-A. Selosse, Parallel evolutionary paths to mycoheterotrophy in understorey Ericaceae and Orchidaceae: Ecological evidence for mixotrophy in Pyroleae. *Oecologia* **151**, 206–217 (2007). doi: 10.1007/s00442-006-0581-2; pmid: 17089139
70. D. L. Taylor *et al*., Progress and prospects for the ecological genetics of mycoheterotrophs, in *Mycoheterotrophy*, V. Merckx, Ed. (Springer, 2013), pp. 245–266.
71. P. Giesemann, H. N. Rasmussen, H. T. Liebel, G. Gebauer, Discreet heterotrophs: Green plants that receive fungal

carbon through *Paris*-type arbuscular mycorrhiza. *New Phytol.* nph.16367 (2019). doi: 10.1111/nph.16367; pmid: 31837155
72. E. T. Aschehoug, R. Brooker, D. Z. Atwater, J. L. Maron, R. M. Callaway, The mechanisms and consequences of interspecific competition among plants. *Annu. Rev. Ecol. Evol. Syst.* **47**, 263–281 (2016). doi: 10.1146/annurev-ecolsys-121415-032123
73. O. Franklin, T. Näsholm, P. Högberg, M. N. Högberg, Forests trapped in nitrogen limitation—An ecological market perspective on ectomycorrhizal symbiosis. *New Phytol.* **203**, 657–666 (2014). doi: 10.1111/nph.12840; pmid: 24824576
74. K. M. Becklin, M. L. Pallo, C. Galen, Willows indirectly reduce arbuscular mycorrhizal fungal colonization in understorey communities. *J. Ecol.* **100**, 343–351 (2012). doi: 10.1111/j.1365-2745.2011.01903.x
75. M. G. Booth, J. D. Hoeksema, Mycorrhizal networks counteract competitive effects of canopy trees on seedling survival. *Ecology* **91**, 2294–2302 (2010). doi: 10.1890/09-1139.1; pmid: 20836451
76. D. P. Janos, J. Scott, C. Aristizábal, D. M. J. S. Bowman, Arbuscular-mycorrhizal networks inhibit *Eucalyptus tetrodonta* seedlings in rain forest soil microcosms. *PLOS ONE* **8**, e57716 (2013). doi: 10.1371/journal.pone.0057716; pmid: 23460899
77. V. Rinaudo, P. Bàrberi, M. Giovannetti, M. G. A. van der Heijden, Mycorrhizal fungi suppress aggressive agricultural weeds. *Plant Soil* **333**, 7–20 (2010). doi: 10.1007/s11104-009-0202-z
78. C. Wagg, R. Veiga, M. G. A. van der Heijden, Facilitation and antagonism in mycorrhizal networks. *Ecol. Stud.* **224**, 203–226 (2015). doi: 10.1007/978-94-017-7395-9_7
79. A. Javaid, Allelopathic interactions in mycorrhizal associations. *Allelopathy J.* **20**, 29–42 (2007).
80. P. Kohout *et al*., Ericaceous dwarf shrubs affect ectomycorrhizal fungal community of the invasive *Pinus strobus* and native *Pinus sylvestris* in a pot experiment. *Mycorrhiza* **21**, 403–412 (2011). doi: 10.1007/s00572-010-0350-2; pmid: 21161550
81. K. A. Meinhardt, C. A. Gehring, Disrupting mycorrhizal mutualisms: A potential mechanism by which exotic tamarisk outcompetes native cottonwoods. *Ecol. Appl.* **22**, 532–549 (2012). doi: 10.1890/11-1247.1; pmid: 22611852
82. D. Cipollini, C. M. Rigsby, E. K. Barto, Microbes as targets and mediators of allelopathy in plants. *J. Chem. Ecol.* **38**, 714–727 (2012). doi: 10.1007/s10886-012-0133-7; pmid: 22585095
83. E. K. Barto *et al*., The fungal fast lane: Common mycorrhizal networks extend bioactive zones of allelochemicals in soils. *PLOS ONE* **6**, e27195 (2011). doi: 10.1371/journal.pone.0027195; pmid: 22110615
84. M. C. Brundrett, Global diversity and importance of mycorrhizal and nonmycorrhizal plants. *Ecol. Stud.* **230**, 533–556 (2017). doi: 10.1007/978-3-319-56363-3_21
85. M. G. A. van der Heijden *et al*., Mycorrhizal fungal diversity determines plant biodiversity, ecosystem variability and productivity. *Nature* **396**, 69–72 (1998). doi: 10.1038/23932
86. I. Hiiesalu *et al*., Species richness of arbuscular mycorrhizal fungi: Associations with grassland plant richness and biomass. *New Phytol.* **203**, 233–244 (2014). doi: 10.1111/nph.12765; pmid: 24641509
87. L. Tedersoo *et al*., Tree diversity and species identity effects on soil fungi, protists and animals are context dependent. *ISME J.* **10**, 346–362 (2016). doi: 10.1038/ismej.2015.116; pmid: 26172210
88. H. Maherali, J. N. Klironomos, Influence of phylogeny on fungal community assembly and ecosystem functioning. *Science* **316**, 1746–1748 (2007). doi: 10.1126/science.1143082; pmid: 17588930
89. J. Köhler *et al*., Ectomycorrhizal fungal diversity increases phosphorus uptake efficiency of European beech. *New Phytol.* **220**, 1200–1210 (2018). doi: 10.1111/nph.15208; pmid: 29770963
90. E. B. Allen *et al*., Patterns and regulation of mycorrhizal plant and fungal diversity. *Plant Soil* **170**, 47–62 (1995). doi: 10.1007/BF02183054
91. M. Gerz, C. G. Bueno, M. Zobel, M. Moora, Plant community mycorrhization in temperate forests and grasslands: Relations with edaphic properties and plant diversity. *J. Veg. Sci.* **27**, 89–99 (2016). doi: 10.1111/jvs.12338
92. R. Bagchi *et al*., Pathogens and insect herbivores drive rainforest plant diversity and composition. *Nature* **506**, 85–88 (2014). doi: 10.1038/nature12911; pmid: 24463522
93. B. D. Lindahl *et al*., Spatial separation of litter decomposition and mycorrhizal nitrogen uptake in a boreal forest. *New Phytol.* **173**, 611–620 (2007). doi: 10.1111/j.1469-8137.2006.01936.x; pmid: 17244056
94. H. Toju, O. Kishida, N. Katayama, K. Takagi, Networks depicting the fine-scale co-occurrences of fungi in soil horizons. *PLOS ONE* **11**, e0165987 (2016). doi: 10.1371/journal.pone.0165987; pmid: 27861486
95. M. F. Ahmad-Ramli, T. Cornulier, D. Johnson, Partitioning of soil phosphorus regulates competition between *Vaccinium vitis-idaea* and *Deschampsia cespitosa*. *Ecol. Evol.* **3**, 4243–4252 (2013). doi: 10.1002/ece3.771; pmid: 24324874
96. S. Luo, B. Schmid, G. B. De Deyn, S. Yu, Soil microbes promote complementarity effects among co-existing trees through soil nitrogen partitioning. *Funct. Ecol.* **32**, 1879–1889 (2018). doi: 10.1111/1365-2435.13109
97. D. J. Read, Mycorrhizas in ecosystems. *Experientia* **47**, 376–391 (1991). doi: 10.1007/BF01972080
98. L. Gómez-Aparicio *et al*., Spatial patterns of soil pathogens in declining Mediterranean forests: Implications for tree species regeneration. *New Phytol.* **194**, 1014–1024 (2012). doi: 10.1111/j.1469-8137.2012.04108.x; pmid: 22428751
99. E. Laliberté, H. Lambers, T. I. Burgess, S. J. Wright, Phosphorus limitation, soil-borne pathogens and the coexistence of plant species in hyperdiverse forests and shrublands. *New Phytol.* **206**, 507–521 (2015). doi: 10.1111/nph.13203; pmid: 25494682
100. I. A. Dickie, S. A. Schnitzer, P. B. Reich, S. E. Hobbie, Spatially disjunct effects of co-occurring competition and facilitation. *Ecol. Lett.* **8**, 1191–1200 (2005). doi: 10.1111/j.1461-0248.2005.00822.x; pmid: 21352443
101. W. H. van der Putten *et al*., Plant-soil feedbacks: The past, the present and future challenges. *J. Ecol.* **101**, 265–276 (2013). doi: 10.1111/1365-2745.12054
102. R. H. Nilsson *et al*., Mycobiome diversity: High-throughput sequencing and identification of fungi. *Nat. Rev. Microbiol.* **17**, 95–109 (2019). doi: 10.1038/s41579-018-0116-y; pmid: 30442909
103. F. Z. Teng, N. Dauphas, J. M. Watkins, Non-traditional stable isotopes: Retrospective and prospective. *Rev. Mineral. Geochem.* **82**, 1–26 (2017). doi: 10.2138/rmg.2017.82.1
104. M. D. Whiteside *et al*., Mycorrhizal fungi respond to resource inequality by moving phosphorus from rich to poor patches across networks. *Curr. Biol.* **29**, 2043–2050.e8 (2019). doi: 10.1016/j.cub.2019.04.061; pmid: 31178314
105. M. J. Roossinck, Evolutionary and ecological links between plant and fungal viruses. *New Phytol.* **221**, 86–92 (2019). doi: 10.1111/nph.15364; pmid: 30084143

ACKNOWLEDGMENTS

We thank S. Jüris for preparing figures. We thank J. Davison and R.H. Nilsson for constructive comments on earlier versions of this manuscript. **Funding:** This work was supported by the Estonian Research Council PUT1399, PRG632, MOBERC13, EMP442, University of Tartu PLTOM20903, the Swedish Research Council Vetenskapsrådet (2017-05019), and by the European Regional Development Fund (Centre of Excellence EcolChange). **Author contributions:** L.T., M.B., and M.Z. contributed to design, interpretation, and writing. **Competing interests:** The authors declare no competing interests.

10.1126/science.aba1223

RESEARCH ARTICLE SUMMARY

IMMUNOGENOMICS

A cell atlas of human thymic development defines T cell repertoire formation

Jong-Eun Park, Rachel A. Botting, Cecilia Domínguez Conde, Dorin-Mirel Popescu, Marieke Lavaert, Daniel J. Kunz, Issac Goh, Emily Stephenson, Roberta Ragazzini, Elizabeth Tuck, Anna Wilbrey-Clark, Kenny Roberts, Veronika R. Kedlian, John R. Ferdinand, Xiaoling He, Simone Webb, Daniel Maunder, Niels Vandamme, Krishnaa T. Mahbubani, Krzysztof Polanski, Lira Mamanova, Liam Bolt, David Crossland, Fabrizio de Rita, Andrew Fuller, Andrew Filby, Gary Reynolds, David Dixon, Kourosh Saeb-Parsy, Steven Lisgo, Deborah Henderson, Roser Vento-Tormo, Omer A. Bayraktar, Roger A. Barker, Kerstin B. Meyer, Yvan Saeys, Paola Bonfanti, Sam Behjati, Menna R. Clatworthy, Tom Taghon*, Muzlifah Haniffa*, Sarah A. Teichmann*

INTRODUCTION: The thymus is the critical organ for T cell development and T cell receptor (TCR) repertoire formation, which shapes the landscape of adaptive immunity. T cell development in the thymus is spatially coordinated, and this process is orchestrated by diverse cell types constituting the thymic microenvironment. Although the thymus has been extensively studied using diverse animal models, human immunity cannot be understood without a detailed atlas of the human thymus.

RATIONALE: To provide a comprehensive atlas of thymic cells across human life, we performed single-cell RNA sequencing (scRNA-seq) using dissociated cells from human thymus during development, childhood, and adult life. We sampled 15 embryonic and fetal thymi spanning thymic developmental stages between 7 and 17 post-conception weeks, as well as nine postnatal thymi from pediatric and adult individuals. Diverse sorting schemes were applied to increase the coverage on underrepresented cell populations. Using the marker genes obtained from single-cell transcriptomes, we spatially localized cell states by single-molecule fluorescence in situ hybridization (smFISH). To provide a systematic comparison between human and mouse, we also generated single-cell data on postnatal mouse thymi and combined this with preexisting mouse datasets. Finally, to investigate the bias in the recombination and selection of human TCR repertoires, we enriched the TCR sequences for single-cell library generation.

RESULTS: We identified more than 50 different cell states in the human thymus. Human thymus cell states dynamically change in abundance and gene expression profiles across development and during pediatric and adult life. We identified novel subpopulations of human thymic fibroblasts and epithelial cells and located them in situ. We computationally predicted the trajectory of human T cell development from early progenitors in the hematopoietic fetal liver into diverse mature T cell types. Using this trajectory, we constructed a framework of putative transcription factors driving T cell fate determination. Among thymic unconventional T cells, we noted a distinct subset of CD8$\alpha\alpha^+$ T cells, which is marked by *GNG4* expression and located in the perimedullary region of the thymus. This subset expressed high levels of *XCL1* and colocalized with XCR1$^+$ dendritic cells. Comparison of human and mouse thymic cells revealed divergent gene expression profiles of these unconventional T cell types. Finally, we identified a strong bias in human VDJ usage shaped by recombination and multiple rounds of selection, including a TCRα V-J bias for CD8$^+$ T cells.

ON OUR WEBSITE

Read the full article at http://dx.doi.org/10.1126/science.aay3224

CONCLUSION: Our single-cell transcriptome profile of the thymus across the human lifetime and across species provides a high-resolution census of T cell development within the native tissue microenvironment. Systematic comparison between the human and mouse thymus highlights human-specific cell states and gene expression signatures. Our detailed cellular network of the thymic niche for T cell development will aid the establishment of in vitro organoid culture models that faithfully recapitulate human in vivo thymic tissue. ■

The list of author affiliations is available in the full article online.
*Corresponding author. Email: m.a.haniffa@newcastle.ac.uk (M.H.); tom.taghon@ugent.be (T.T.); st9@sanger.ac.uk (S.A.T.)
Cite this article as J.-E. Park *et al.*, *Science* **367**, eaay3224 (2020). DOI: 10.1126/science.aay3224

Constructing the human thymus cell atlas. We analyzed human thymic cells across development and postnatal life using scRNA-seq and spatial methods to delineate the diversity of thymic-derived T cells and the localization of cells constituting the thymus microenvironment. With T cell development trajectory reconstituted at single-cell resolution combined with TCR sequence, we investigated the bias in the VDJ recombination and selection of human TCR repertoires. Finally, we provide a systematic comparison between human and mouse thymic cell atlases.

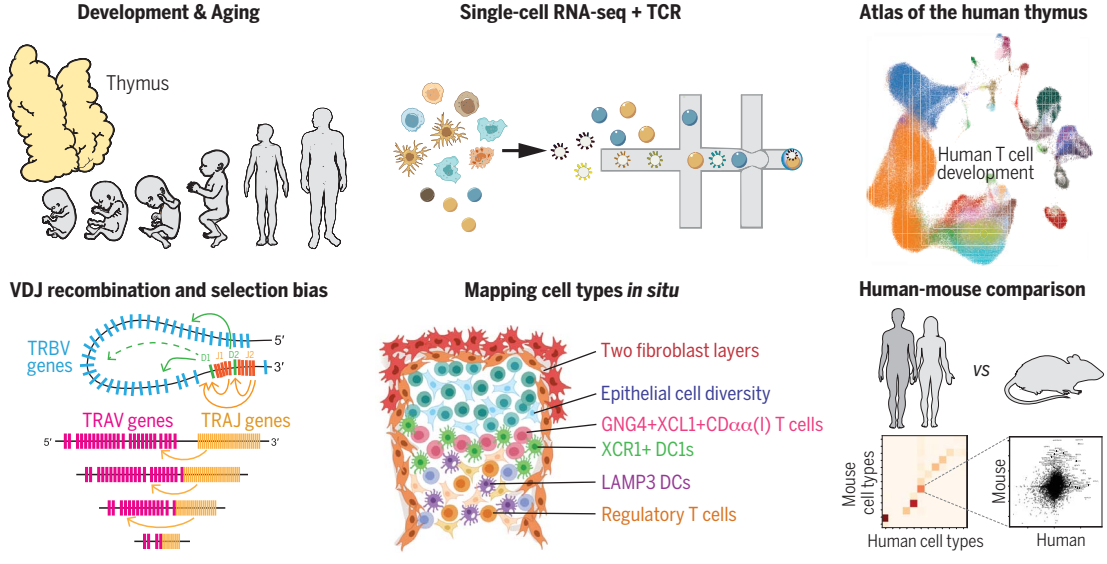

RESEARCH ARTICLE

IMMUNOGENOMICS

A cell atlas of human thymic development defines T cell repertoire formation

Jong-Eun Park[1], Rachel A. Botting[2], Cecilia Domínguez Conde[1], Dorin-Mirel Popescu[2], Marieke Lavaert[3,4], Daniel J. Kunz[1,5,6], Issac Goh[2], Emily Stephenson[2], Roberta Ragazzini[7,8], Elizabeth Tuck[1], Anna Wilbrey-Clark[1], Kenny Roberts[1], Veronika R. Kedlian[1], John R. Ferdinand[9], Xiaoling He[10], Simone Webb[2], Daniel Maunder[2], Niels Vandamme[11,12], Krishnaa T. Mahbubani[13], Krzysztof Polanski[1], Lira Mamanova[1], Liam Bolt[1], David Crossland[2,14], Fabrizio de Rita[14], Andrew Fuller[2], Andrew Filby[2], Gary Reynolds[2], David Dixon[2], Kourosh Saeb-Parsy[13], Steven Lisgo[2], Deborah Henderson[2], Roser Vento-Tormo[1], Omer A. Bayraktar[1], Roger A. Barker[10,15], Kerstin B. Meyer[1], Yvan Saeys[11,12], Paola Bonfanti[7,8,16], Sam Behjati[1,17], Menna R. Clatworthy[1,9,18], Tom Taghon[3,4]*, Muzlifah Haniffa[1,2,19]*, Sarah A. Teichmann[1,5]*

The thymus provides a nurturing environment for the differentiation and selection of T cells, a process orchestrated by their interaction with multiple thymic cell types. We used single-cell RNA sequencing to create a cell census of the human thymus across the life span and to reconstruct T cell differentiation trajectories and T cell receptor (TCR) recombination kinetics. Using this approach, we identified and located in situ CD8αα$^+$ T cell populations, thymic fibroblast subtypes, and activated dendritic cell states. In addition, we reveal a bias in TCR recombination and selection, which is attributed to genomic position and the kinetics of lineage commitment. Taken together, our data provide a comprehensive atlas of the human thymus across the life span with new insights into human T cell development.

The thymus plays an essential role in the establishment of adaptive immunity and central tolerance as it mediates the maturation and selection of T cells. This organ degenerates early during life, and the resulting reduction in T cell output has been linked to age-related incidence of cancer, infection, and autoimmunity (*1*, *2*). T cell precursors from fetal liver or bone marrow migrate into the thymus, where they differentiate into diverse types of mature T cells (*3*, *4*). The thymic microenvironment cooperatively supports T cell differentiation (*5*, *6*). Although thymic epithelial cells (TECs) provide critical cues to promote T cell fate (*7*), other cell types are also involved in this process, such as dendritic cells (DCs), which undertake antigen presentation, and mesenchymal cells, which support TEC differentiation and maintenance (*8*–*11*). Seminal experiments in animal models have provided major insights into the function and cellular composition of the thymus (*12*, *13*). More recently, single-cell RNA sequencing (scRNA-seq) has revealed new aspects of thymus organogenesis and new types of TECs in mouse (*14*–*16*). However, the human organ matures in a mode and tempo that is unique to our species (*17*–*19*), calling for a comprehensive genome-wide study for human thymus.

T cell development involves a parallel process of staged T cell lymphocyte differentiation accompanied by acquisition of a diverse TCR repertoire for antigen recognition (*20*). This is achieved by the genomic recombination process that selects variable (V), joining (J), and, in some cases, diversity (D) gene segments from the multiple genomic copies. This V(D)J gene recombination can preferentially include certain gene segments, leading to the skewing of the repertoire (*21*–*23*). To date, most of our knowledge of VDJ recombination and repertoire biases has come from animal models and human peripheral blood analysis, with little comprehensive data on the human thymic TCR repertoire (*22*, *24*, *25*).

Here, we applied scRNA-seq to generate a comprehensive transcriptomic profile of the diverse cell populations present in embryonic, fetal, pediatric, and adult stages of the human thymus, and we combined this with detailed TCR repertoire analysis to reconstruct the T cell differentiation process.

Cellular composition of the human thymus across life

We performed scRNA-seq on 15 prenatal thymi ranging from 7 PCW (post-conception weeks), when the thymic rudiment can be dissected, to 17 PCW, when thymic development is complete (Fig. 1, A and B). We also analyzed nine postnatal samples covering the entire period of active thymic function. Isolated single cells were sorted on the basis of CD45, CD3, or epithelial cell adhesion molecule (EpCAM) expression to sample thymocytes and enrich for non-thymocytes, prior to single-cell transcriptomic analysis coupled with TCRαβ profiling. After quality control including doublet removal, we obtained a total of 138,397 cells from developing thymus and 117,504 cells from postnatal thymus (table S1). If available, other relevant organs were collected from the same donor. We performed batch correction using the BBKNN algorithm combined with linear regression (fig. S1) (*26*).

We annotated cell clusters into more than 40 different cell types or cell states (Fig. 1, C and D, and tables S2 and S3), which can be clearly identified by the expression of specific marker genes (fig. S2 and table S4). Differentiating T cells are well represented in the dataset, including double negative (DN), double positive (DP), CD4$^+$ single positive (CD4$^+$), CD8$^+$ single positive (CD8$^+$), FOXP3$^+$ regulatory (T_{reg}), CD8αα$^+$, and γδ T cells. We also identified other immune cells including B cells, natural killer (NK) cells, innate lymphoid cells (ILCs), macrophages, monocytes, and DCs. DCs can be further classified into myeloid/conventional DC1 and DC2 and plasmacytoid DC (pDC).

Our dataset also featured the diverse non-immune cell types that constitute the thymic microenvironment. We further classified them into subtypes including TECs, fibroblasts, vascular smooth muscle cells (VSMCs), endothelial cells, and lymphatic endothelial cells (Fig. 1E). Thymic fibroblasts were further divided

[1]Wellcome Sanger Institute, Wellcome Genome Campus, Hinxton, Cambridge CB10 1SA, UK. [2]Biosciences Institute, Faculty of Medical Sciences, Newcastle University, Newcastle upon Tyne NE2 4HH, UK. [3]Faculty of Medicine and Health Sciences, Department of Diagnostic Sciences, Ghent University, 9000 Ghent, Belgium. [4]Cancer Research Institute Ghent (CRIG), Ghent University, Ghent, Belgium. [5]Theory of Condensed Matter Group, Cavendish Laboratory/Department of Physics, University of Cambridge, Cambridge CB3 0HE, UK. [6]Wellcome Trust/Cancer Research UK Gurdon Institute, University of Cambridge, Cambridge, UK. [7]Epithelial Stem Cell Biology and Regenerative Medicine Laboratory, Francis Crick Institute, London NW1 1AT, UK. [8]Great Ormond Street Institute of Child Health, University College London, London, UK. [9]Molecular Immunity Unit, Department of Medicine, University of Cambridge, MRC Laboratory of Molecular Biology, Cambridge CB2 0QQ, UK. [10]John van Geest Centre for Brain Repair, University of Cambridge, Cambridge CB2 0PY, UK. [11]Data Mining and Modeling for Biomedicine, VIB Center for Inflammation Research, Ghent, Belgium. [12]Department of Applied Mathematics, Computer Science and Statistics, Ghent University, Ghent, Belgium. [13]Department of Surgery, University of Cambridge and NIHR Cambridge Biomedical Research Centre, Cambridge CB2 0QQ, UK. [14]Department of Adult Congenital Heart Disease and Paediatric Cardiology/Cardiothoracic Surgery, Freeman Hospital, Newcastle Hospitals NHS Foundation Trust, Newcastle upon Tyne NE2 4LP, UK. [15]WT-MRC Cambridge Stem Cell Institute, Jeffrey Cheah Biomedical Centre Cambridge Biomedical Campus, Cambridge CB2 0AW, UK. [16]Institute of Immunity and Transplantation, University College London, London, UK. [17]Department of Paediatrics, University of Cambridge, Cambridge CB2 0SP, UK. [18]Cambridge University Hospitals NHS Foundation Trust, Cambridge CB2 0QQ, UK. [19]Department of Dermatology and NIHR Newcastle Biomedical Research Centre, Newcastle Hospitals NHS Foundation Trust, Newcastle upon Tyne NE2 4LP, UK.
*Corresponding author. Email: m.a.haniffa@newcastle.ac.uk (M.H.); tom.taghon@ugent.be (T.T.); st9@sanger.ac.uk (S.A.T.)

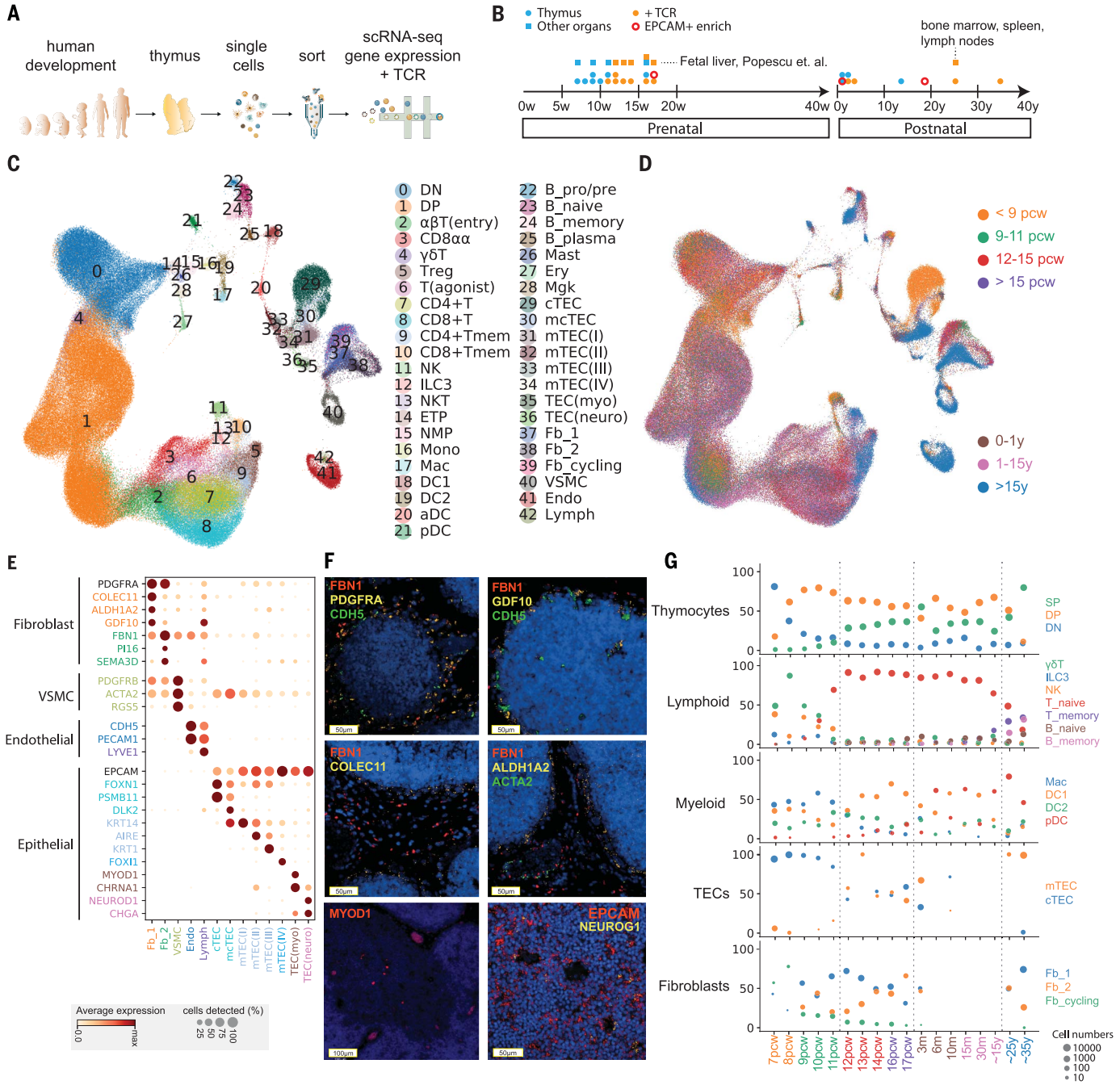

Fig. 1. Cellular composition of the developing human thymus. (**A**) Schematic of single-cell transcriptome profiling of the developing human thymus. (**B**) Summary of gestational stage/age of samples, organs (circles denote thymus; rectangles denote fetal liver or adult bone marrow, adult spleen, and lymph nodes), and 10x Genomics chemistry (colors). (**C**) UMAP visualization of the cellular composition of the human thymus colored by cell type (DN, double-negative T cells; DP, double-positive T cells; ETP, early thymic progenitor; aDC, activated dendritic cells; pDC, plasmacytoid dendritic cells; Mono, monocyte; Mac, macrophage; Mgk, megakaryocyte; Endo, endothelial cells; VSMC, vascular smooth muscle cells; Fb, fibroblasts; Ery, erythrocytes). (**D**) Same UMAP plot colored by age groups, indicated by post-conception weeks (PCW) or postnatal years (y). (**E**) Dot plot for expression of marker genes in thymic stromal cell types. Here and in later figures, color represents maximum-normalized mean expression of marker genes in each cell group, and size indicates the proportion of cells expressing marker genes. (**F**) RNA smFISH in human fetal thymus slides with probes targeting stromal cell populations. Top left: Fb2 population marker *FBN1* and general fibroblast markers *PDGFRA* and *CDH5*. Top right: Fb1 marker *GDF10*, *FBN1*, and *CDH5*. Middle left: Fb1 marker *COLEC11* and *FBN1*. Middle right: Fb1 marker *ALDH1A2*, VSMC marker *ACTA2*, and *FBN1*. Bottom left: TEC(myo) marker *MYOD1*. Bottom right: Epithelial cell marker *EPCAM* and TEC(neuro) marker *NEUROG1*. Data are representative of two experiments. (**G**) Relative proportion of cell types throughout different age groups. Dot size is proportional to absolute cell numbers detected in the dataset. Statistical testing for population dynamics was performed by *t* tests using proportions between stage groups. The *x* axis shows age of samples, which are colored in the same scheme as (D).

into two subtypes, neither of which has been previously described: fibroblast type 1 (Fb1) cells (*COLEC11*, *C7*, *GDF10*) and fibroblast type 2 (Fb2) cells (*PI16*, *FN1*, *FBN1*) (Fig. 1E). Fb1 cells uniquely express *COLEC11*, which plays an important role in innate immunity (*27*), and *ALDH1A2*, an enzyme responsible for the production of retinoic acid, which regulates epithelial growth (*28*). In contrast, extracellular matrix (ECM) genes and semaphorins, which regulate vascular development (*29*), are specifically detected in Fb2 (fig. S3A). To explore the localization pattern of these fibroblast subtypes, we performed in situ single-molecule fluorescence in situ hybridization (smFISH) targeting Fb1 and Fb2 markers (*COLEC11* and *FBN1*) together with general fibroblast (*PDGFRA*), endothelial (*CDH5*), and VSMC (*ACTA2*) markers (Fig. 1F). The results show that Fb1 cells were perilobular, whereas Fb2 cells were interlobular and were often associated with large blood vessels lined with VSMCs, consistent with their transcriptomic profile of genes regulating vascular development. We confirmed the expression of *GDF10* and *ALDH1A2* localized in the perilobular area (Fig. 1F).

In addition to fibroblasts, we also identified subpopulations of human TECs (Fig. 1E and fig. S4), such as medullary and cortical TECs (mTECs and cTECs). To maximize the coverage of epithelial cells, we enriched for EpCAM-positive cells across several time points (Fig. 1B). To annotate human TECs, we compared our human dataset to the published mouse TEC dataset (*15*) (figs. S5 to S7). We were able to identify conserved TEC populations across species, including *PSMB11*-positive cTECs, *KRT14*-positive mTEC(I)s, *AIRE*-expressing mTEC(II)s, and *KRT1*-expressing mTEC(III)s (Fig. 1E and fig. S4). Interestingly, cTECs were more abundant during early development (7 to 8 PCW), and an intermediate population (mcTECs), marked by expression of *DLK2*, was evident in late fetal and pediatric human thymi (fig. S4B). We identified a very rare population of mTEC(IV)s in humans, which are similar to tuft-like mTEC(IV)s described in the mouse thymus. However, *DCLK1* or *POU2F3*, the markers used to define mTEC(IV)s in mouse (*15*, *16*), were enriched but not specific to this population in human (figs. S4B, S5, and S6). We noted two EpCAM$^+$ cell types that are specific to human: (i) *MYOD1*- and *MYOG*-expressing myoid cells [TEC(myo)s] and (ii) *NEUROD1*-, *NEUROG1*-, and *CHGA*-expressing TEC(neuro)s, which resemble neuroendocrine cells (Fig. 1E and figs. S6 and S7). Notably, *CHRNA1*, which has been associated with the autoimmune disease myasthenia gravis (*30*), was specifically expressed by both of these cell types in addition to mTEC(II)s (Fig. 1E), expanding the pool of candidate cell types that may be involved in tolerance induction in myasthenia gravis (*31*, *32*). In support of this possibility, we detected *MYOD1*- and *NEUROG1*-expressing cells preferentially located in thymic medulla (Fig. 1F).

Lastly, we analyzed the expression pattern of genes known to cause congenital T cell immunodeficiencies to provide insight into when and where these rare disease genes may play a role during thymic development (fig. S8).

Coordinated development of thymic stroma and T cells

Next, we investigated the dynamics of the different thymic cell types across development (Fig. 1G). In the early fetal samples (7 to 8 PCW), the lymphoid compartment contained NK cells, γδ T cells, and ILC3s, with very few differentiating αβT cells. Differentiating T cells were mostly found at DN stage in 7 PCW samples; they gradually progressed through DP to SP stages thereafter, reaching equilibrium around 12 PCW. Conversely, the proportion of innate lymphocytes decreased.

Of note, the adult sample showed morphological evidence of thymic degeneration (fig. S9). Comparison with spleen and lymph nodes taken from the same donor showed the presence of terminally differentiated T cells in the thymus, suggesting reentry into thymus or contamination with circulating cells (Fig. 1G and fig. S10). Notably, cytotoxic CD4$^+$ T lymphocytes (CD4$^+$ CTLs) expressing *IL10*, perforin, and granzymes were enriched in the degenerated thymus sample (*33*) (fig. S10C). The trend of increased memory T cells and B cells was also confirmed in other samples (Fig. 1G; $P = 9.3 \times 10^{-6}$ for memory T cells, $P = 0.0096$ for memory B cells).

The trend in T cell development was mirrored by corresponding changes in thymic stromal cells. We observed temporal changes in TEC populations starting from enriched cTECs toward the balanced representation of cTECs and mTECs (Fig. 1G; $P = 0.0054$), aligned with the onset of T cell maturation. This supports the notion of "thymic cross-talk" in which epithelial cells and mature T cells interact synergistically to support their mutual differentiation (*34*).

Moreover, fibroblast composition also changed during development. The Fb1 population mentioned above dominated early development, with similar numbers of Fb1 and Fb2 cells observed at later developmental time points ($P = 0.014$) and a reduction in the number of cycling cells (Fig. 1G). This was also confirmed by thymic fibroblast explant cultures, which showed an increase in the Fb2 cell marker PI16 by fluorescence-activated cell sorter (FACS) analysis (fig. S3, B and C).

Finally, other immune cells also change dynamically over gestation and in postnatal life. Macrophages were abundant during early gestation, whereas DCs increased throughout development (Fig. 1G). DC1 was dominant after 12 PCW, and pDCs increased in frequency in postnatal life ($P = 2.7 \times 10^{-8}$ for macrophage, $P = 1.05 \times 10^{-3}$ for DC1, $P = 4.86 \times 10^{-5}$ for DC2).

To further investigate the factors mediating the coordinated development of thymic stroma and T cells, we systematically investigated cellular interactions using our public database CellPhoneDB.org (*35*) to predict the ligand-receptor pairs specifically expressed across them (table S5). Among the predicted interactions, we checked the expression pattern of signaling factors known to be involved in thymic development across different cell types and developmental stages (fig. S11) (*36*–*41*). Lymphotoxin signaling (*LTB*:*LTBR*) comes from diverse immune cells and is received by most of the stromal cell states. In contrast, RANKL-RANK (*TNFRSF11*:*TNFRSF11A*) signaling is confined between ILC3 and mTEC(II)s/lymphatic endothelial cells. FGF signaling (*FGF7*:*FGFR2*) comes from fibroblasts signaling to TECs, with decreasing expression of *FGFR2* in adult thymus. For Notch signaling, *NOTCH1* is the main receptor expressed in early thymic progenitors (ETPs), and diverse Notch ligands are expressed by different cell types: cTECs and endothelial cells express both *JAG2* and *DLL4*, and other TECs broadly express *JAG1* (*42*, *43*).

Conventional T cell differentiation trajectory

Because fetal liver is the main hematopoietic organ and source of hematopoietic stem cells and multipotent progenitors (HSCs/MPPs) when the thymic rudiment develops, we analyzed paired thymus and liver samples from the same fetus (*44*), similar to what has been described for early hematopoietic organs (*45*). We merged the thymus and liver data, and selected clusters including liver HSCs/MPPs, thymic ETPs, and DN thymocytes for data analysis and visualization (Fig. 2, A and B, and fig. S12). This positioned thymic ETPs at the isthmus between fetal liver HSCs/MPPs and pre/pro-B cells. We integrated our liver/thymic hematopoietic progenitor subset with the single-cell transcriptomes of human hematopoietic progenitors sorted from bone marrow using defined markers (*46*) (fig. S13). This analysis positions the ETPs next to the multilymphoid progenitor (MLP) from bone marrow and early lymphoid progenitor in fetal liver.

To investigate the downstream T cell differentiation trajectory, we selected the T cell populations and projected them using UMAP and force-directed graph analysis (Fig. 2C, fig. S14A, and data S1), which showed a continuous trajectory of differentiating T cells. To confirm the validity of this trajectory, we overlaid hallmark genes of T cell differentiation: CD4/CD8A/CD8B genes (Fig. 2D), cell cycle (*CDK1*) and recombination (*RAG1*) genes (Fig. 2E), and fully recombined TCRαs/TCRβs (Fig. 2F) (*47*).

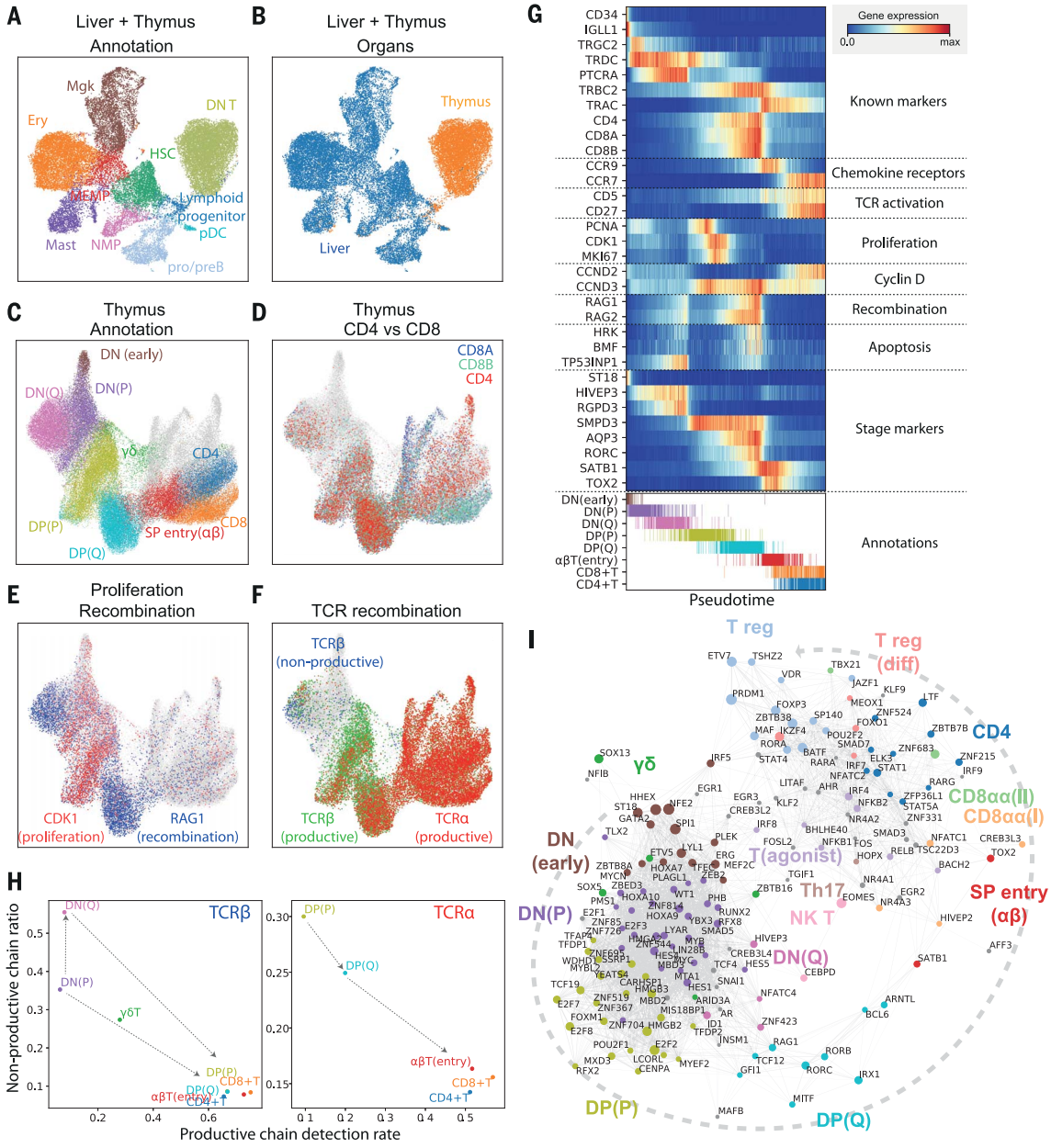

Fig. 2. Thymic seeding of early thymic progenitors (ETPs) and T cell differentiation trajectory. (**A**) UMAP visualization of ETP and fetal liver hematopoietic stem cells (HSCs) and early progenitors. NMP, neutrophil-myeloid progenitor; MEMP, megakaryocyte/erythrocyte/mast cell progenitor. (**B**) The same UMAP colored by organ (liver in blue, thymus in yellow/red). (**C**) UMAP visualization of developing thymocytes after batch correction. DN, double-negative T cells; DP, double-positive T cells; SP, single-positive T cells; P, proliferating; Q, quiescent). The data contain cells from all sampled developmental stages. Cells from abundant clusters are downsampled for better visualization. The reproducibility of structure is confirmed across individual samples. Unconventional T cells are in gray. (**D** to **F**) The same UMAP plot showing *CD4*, *CD8A*, and *CD8B* gene expression (D), *CDK1* cell cycle and *RAG1* recombination gene expression (E), and TCRα, productive TCRβ, and nonproductive TCRβ VDJ genes (F). (**G**) Heat map showing differentially expressed genes across T cell differentiation pseudotime. Top: The *x* axis represents pseudo-temporal ordering. Gene expression levels across the pseudotime axis are maximum-normalized and smoothed. Genes are grouped by their functional categories and expression patterns. Bottom: Cell type annotation of cells aligned along the pseudotime axis. Colors are as in (C). (**H**) Scatterplot showing the rate of productive chain detection within cells in specific cell types (*x* axis) and the ratio of nonproductive/productive TCR chains detected in specific cell types (*y* axis). Left: TCRβ; right, TCRα. (**I**) Graph showing correlation-based network of transcription factors expressed by thymocytes. Nodes represent transcription factors; edge widths are proportional to the correlation coefficient between two transcription factors. Transcription factors with significant association to specific cell types are depicted in color. Node size is proportional to the significance of association to specific cell types.

The trajectory started from $CD4^{-}CD8^{-}$ DN cells, which gradually express CD4 and CD8 to become $CD4^{+}CD8^{+}$ DP cells, and then transitioned through a $CCR9^{high}$ Tαβ(entry) stage to diverge into mature $CD4^{+}$ or $CD8^{+}$ SP cells (Fig. 2D). We also noted a separate lineage of cells diverging from the DN-DP junction corresponding to γδ T cell differentiation. Additional T cell lineages identified in this analysis are discussed below (Fig. 2C, gray). DN and DP cells were separated into two phases by the expression of cell cycle genes (Fig. 2E). We designated the early population with strong cell cycle signature as proliferating (P) and the later population as quiescent (Q) (Fig. 2C). Expression of VDJ recombination genes (*RAG1* and *RAG2*) increased from the late proliferative phase and peaked at the quiescent phases. This pattern reflects the proliferation of T cells that precedes each round of recombination (*48*, *49*).

Next, we aligned the TCR recombination data to this trajectory (Fig. 2F). In the DN stage, recombined TCRβ sequences were detected from the late P phase, which coincides with an increase in recombination signature and the expression of pre-TCRα (*PTCRA*) (Fig. 2G and fig. S15). The ratio of nonproductive to productive recombination events (nonproductivity score) for TCRβ was relatively higher in DN stages and dropped to a basal level as

cells entered DP stages, demonstrating the impact of beta selection (Fig. 2H). Notably, the nonproductivity score for TCRβ was highest in the DN(Q) stage, which suggests that cells failing to secure a productive TCRβ recombination for the first allele undergo recombination of the other allele. In the DP stage, recombined TCRα chains were detected from P stage onward. In contrast to TCRβ, nonproductive TCRα chains were not enriched in the DP(Q) cells, but rather were depleted (Fig. 2H).

To match the transcriptome-based clustering from this study to a published protein marker–based sorting strategy, we compared our data with repository data from FACS-sorted thymocytes analyzed by microarray (*50*) (fig. S16). On the basis of cell cycle gene signature and marker gene expression, DN(P), DN(Q), and DP(P) stages are closely matched to CD34$^+$CD1A$^+$, ISP CD4$^+$, and DP CD3$^-$ populations, respectively. Both our DP(Q)-stage and Tαβ(entry)-stage cell signatures are enriched in the bulk transcriptome data from the DP CD3$^+$ FACS-sorted cells. The enrichment of pre–beta selection cells in DN(Q) cells matches well with the characteristics of ISP CD4$^+$ serving as a checkpoint for beta selection (Fig. 2F and fig. S15).

To model the development of conventional αβT cells in more detail, we performed pseudotime analysis, which resulted in an ordering of cells highly consistent with known marker genes and transcription factors (Fig. 2G). In addition, we identified T cell developmental markers, including *ST18* for early DN, *AQP3* for DP, and *TOX2* for DP-to-SP transition. To derive further insights into transcription factors that specify T cell stages and lineages, we created a correlation-based transcription factor network, after imputing gene expression (see materials and methods), which demonstrated modules of transcription factors specific for lineage commitment (Fig. 2I).

Development of T_{regs} and unconventional T cells

In addition to conventional CD4$^+$ or CD8$^+$ T cells, which constitute the majority of T cells in the developing thymus, our data identified multiple unconventional T cell types, which were grouped by the expression of signature marker genes (Fig. 2I and Fig. 3, A and B). Unconventional T cells have been suggested to require agonist selection for development (*3*). In support of this, we observed a lower ratio of nonproductive TCR chains for these cells, implying that they reside longer in the thymus than do conventional T cells (Fig. 3C).

Next, we investigated whether development of these unconventional T cells is dependent on the thymus. We reasoned that if a population is thymus-dependent, it would accumulate after thymic maturation (~10 PCW) and would be enriched in the thymus relative to other hematopoietic organs. Consistent with this idea, we found that all unconventional T cells were enriched in the thymus, particularly after thymic maturation, which suggests that they are thymus-derived (Fig. 3D).

T_{regs} were the most abundant unconventional T cells in the thymus. There was a clear differentiation trajectory connecting αβT cells and T_{regs}. We defined the connecting population as differentiating T_{regs} ($T_{reg(diff)}$) (Fig. 3A). Relative to canonical T_{regs}, $T_{reg(diff)}$ cells displayed lower expression of *FOXP3* and *CTLA4* and higher expression of *IKZF4*, *GNG8*, and *PTGIR* (Fig. 3B). These genes have been associated with autoimmunity and T_{reg} differentiation (*51*).

We also noted another population that shares expression modules with $T_{reg(diff)}$ cells, but not with terminally differentiated T_{reg} cells. We named this population—defined by the expression of a noncoding RNA, *MIR155HG*—as $T_{(agonist)}$ (Fig. 3, A and B). Interestingly, this population expressed IL2RA but has low *FOXP3* mRNA. These features are similar to those of a previously described mouse CD25$^+$FOXP3$^-$ T_{reg} progenitor (*52*) (fig. S17). Further analysis showed that the signature of two T_{reg} progenitors (CD25$^+$ and FOXP3^{lo} T_{reg} progenitors) defined in previous studies are expressed at a higher level in $T_{(agonist)}$ and $T_{reg(diff)}$ populations, respectively (fig. S17B). The UMAP and force-directed graph showed that both of these populations are linked to mature T_{regs} (fig. S17A), suggesting the possibility of two T_{reg} progenitors in the human thymus.

Other unconventional T cell populations included CD8αα$^+$ T cells, NKT-like cells, and T_H17-like cells (Fig. 3B). There were three distinct populations of CD8αα$^+$ T cells: GNG4$^+$ CD8αα$^+$ T(I) cells, ZNF683$^+$ CD8αα$^+$ T(II) cells, and a CD8αα$^+$ NKT-like population marked by *EOMES* (Fig. 3E). GNG4$^+$CD8αα$^+$ T(I) cells and ZNF683$^+$ CD8αα$^+$ T(II) cells shared *PDCD1* expression at an early stage, which decreased in their terminally differentiated state (fig. S14B). Whereas GNG4$^+$ CD8αα$^+$ T(I) cells display a clear trajectory diverging from late DP stage (αβT SP entry cells), ZNF683$^+$CD8αα$^+$ T(II) cells have a mixed αβ and γδ T cell signatures, and sit next to both GNG4$^+$CD8αα$^+$ T(I) cells and γδ T cells (Fig. 3A and fig. S14B).

EOMES$^+$ NKT-like cells have a shared gene expression profile with NK cells (*NKG7*, *IFNG*, *TBX21*) and are enriched in γδ T cells; that is, their TCRs are γδ rather than αβ (Fig. 3B and fig. S14B). Interestingly, previously described gene sets from bulk RNA sequencing of human thymic or cord blood CD8αα$^+$ T cells can now be deconvoluted into our three CD8αα$^+$ T cell populations using signature genes. These results suggest that our three CD8αα$^+$ T cell populations are present in these previously published thymic and cord blood samples at different frequencies, as shown in fig. S18 (*53*).

Finally, we found another fetal-specific cell cluster that we named "T_H17-like cells" based on *CD4*, *CD40LG*, *RORC*, and *CCR6* expression (Fig. 3B). T_H17-like cells and NKT-like cells expressed *KLRB1* and *ZBTB16*, which are hallmarks of innate lymphocytes (*54*, *55*) (Fig. 3F).

As described above, many cell clusters contained a mixed signature of αβ and γδ T cells, meaning that a single cluster contained some cells with αβ TCR expression and others with γδ TCR expression. To classify cells into αβ and γδ T cells, we analyzed the TCRα/δ loci, where recombination of TCRα excises TCRδ, making the two mutually exclusive (Fig. 3G). This clearly showed that γδ T cells diverging between the DN and DP populations are pure γδ T cells. In contrast, CD8αα$^+$ T(II), NKT-like, and T_H17-like cells included both αβ and γδ T cell populations, suggesting transcriptomic convergence of some αβ and γδ T cells.

Interestingly, *TRDV1* and *TRDV2*, the two most frequently used TCRδ V genes in human, displayed clear usage bias: *TRDV2* was used at an earlier stage (DN), whereas *TRDV1* was used exclusively in later T cell development [DP(Q) and αβT entry] (Fig. 3H). On the basis of this pattern, we can attribute the stage of origin of γδ T cell populations, which suggests that CD8αα$^+$ T(II) cells are derived from the late DP stage, whereas NKT-like/T_H17-like cells arise from earlier stages (Fig. 3H).

Discovery and characterization of *GNG4*$^+$ CD8αα T cells in the thymic medulla

Having identified unconventional T cells and their trajectory of origin within thymic T cell development, we focused on our newly identified GNG4$^+$CD8αα$^+$ T(I) cells, as they have a unique gene expression profile (*GNG4*, *CREB3L3*, and *CD72*). This is in contrast to CD8αα$^+$ T(II) cells, which express known markers of CD8αα$^+$ T cells such as *ZNF683* and *MME* (*53*). Moreover, the expression level of *KLF2*, a regulator of thymic emigration, was extremely low in CD8αα$^+$ T(I) cells, which suggests that they may be thymic-resident (Fig. 3B). To locate and validate CD8αα$^+$ T(I) cells in situ, we performed RNA smFISH targeting *GNG4* in fetal thymus tissue sections. The *GNG4* RNA probe identified a distinct group of cells enriched in the thymic medulla, and colocalized with *CD8A* RNA (Fig. 3I). *TNFRSF9* (CD137) is a marker shared between CD8αα$^+$ T(I) cells and T_{regs}. When tested in situ, GNG4$^+$ cells were a subset of TNFRSF9$^+$ cells, further confirming the validity of the localization pattern.

Because CD137 is a surface marker of both CD8αα$^+$ T(I) cells and T_{regs}, we enriched these cells using this marker (fig. S19). Further refinement using CD3$^+$CD137$^+$CD4$^-$ FACS sorting allowed us to specifically enrich for CD8αα$^+$ T(I)

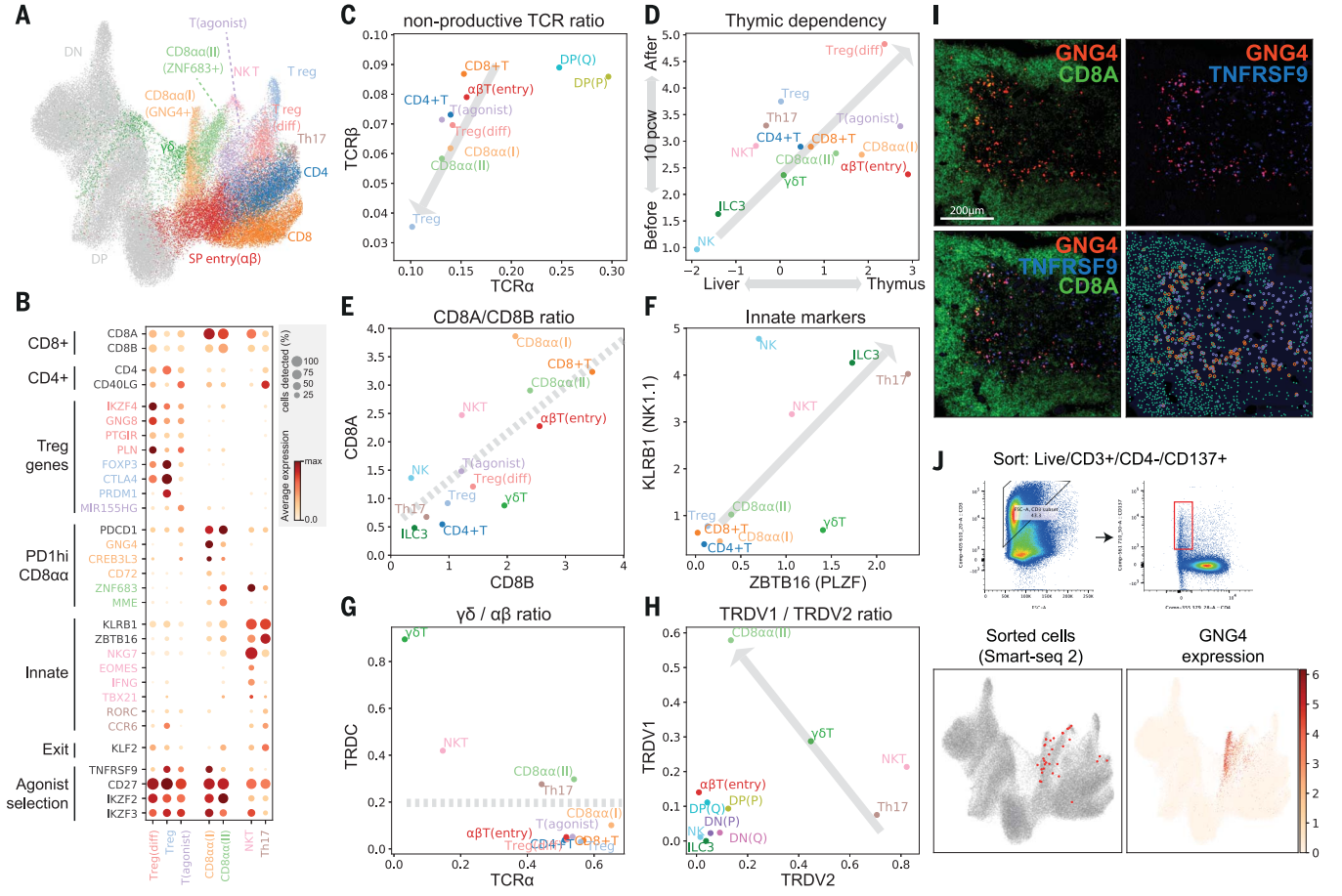

Fig. 3. Identification of GNG4$^+$ CD8αα T cells in the thymic medulla. (**A**) UMAP visualization of mature T cell populations in the thymus. Axes and coordinates are as in Fig. 2C. (The cell annotation color scheme used here is maintained throughout this figure.) (**B**) Dot plot showing marker gene expression for the mature T cell types. Genes are stratified according to associated cell types or functional relationship. (**C**) Scatterplot showing the ratio of nonproductive/productive TCR chains detected in specific cell types in TCRα chain (*x* axis) and TCRβ chain (*y* axis). The gray arrow indicates a trendline for decreasing nonproductive TCR chain ratio in unconventional versus conventional T cells. (**D**) Scatterplot showing the relative abundance of each cell type between fetal liver and thymus (*x* axis) and before and after thymic maturation (delimited at 10 PCW) (*y* axis). Gray arrow indicates trendline for increasing thymic dependency. (**E** to **H**) Scatterplots comparing the characteristics of unconventional T cells based on *CD8A* versus *CD8B* expression levels (E), *KLRB1* versus *ZBTB16* expression levels (F), TCRα productive chain versus *TRDC* detection ratio (G), and *TRDV1* versus *TRDV2* expression levels (H). Gray arrows or lines are used to set boundaries between groups [(E), (G), (H)] or to indicate the trend of innate marker gene expression (F). (**I**) RNA smFISH showing *GNG4*, *TNFRSF9*, and *CD8A* in a 15 PCW thymus. Lower right panel shows detected spots from the image on top of the tissue structure based on 4′,6-diamidino-2-phenylindole (DAPI) signal. Color scheme for spots is the same as in the image. (**J**) FACS gating strategy to isolate CD8αα(I) cells (live/CD3$^+$/CD4$^-$/CD137$^+$) and Smart-seq2 validation of FACS-isolated cells projected to the UMAP presentation of total mature T cells from the discovery dataset (lower left). *GNG4* expression pattern is overlaid onto the same UMAP plot (lower right).

cells and confirm their identity by Smart-seq2 scRNA sequencing, thereby providing additional transcriptomic phenotyping of these cells (Fig. 3J).

To compare our findings in human thymus to mouse thymus, we generated a comprehensive mouse thymus single-cell atlas of postnatal murine samples (4, 8, or 24 weeks old) and combined these data with a published prenatal mouse thymus scRNA-seq dataset (*14*) (fig. S20). Integrative analysis of mature T cells from human and mouse showed that cell states are well mixed across species (fig. S21). This analysis showed that GNG4$^+$ CD8αα$^+$ T(I) cells in humans are most similar to the mouse intraepithelial lymphocyte precursor type A (IELpA) cells (*56*) (fig. S21), sharing expression of *HIVEP3*, *NR4A3*, *PDCD1*, and *TNFRSF9* (fig. S22). However, there were also highly differentially expressed genes between them, including *GNG4* and *XCL1* in human and *ZEB2* and *CLDN10* in mouse, suggesting a potential difference in function (fig. S23). Moreover, human CD8αα$^+$ T(I) cells fully mature into a CD8A^{high}/CD8B^{low} phenotype, whereas mouse IELpA cells become triple negative (CD8A^{low} CD8B^{low}CD4^{low}) cells (fig. S23). This shows that human and mouse TNFRSF9^{high} agonist–selected cells in the thymus take on distinct transcriptional characteristics.

Recruitment and activation of DCs for thymocyte selection

Selection of T cells is coordinated by specialized TECs and DCs. We identified three previously well-characterized thymic DC subtypes: DC1 (XCR1$^+$CLEC9A$^+$), DC2 (SIRPA$^+$CLEC10A$^+$), and pDC (IL3RA$^+$CLEC4C$^+$) (*6*, *57*, *58*). We also identified a population that was previously incompletely described, which we call "activated DCs" (aDCs), characterized by *LAMP3* and *CCR7* expression (Fig. 4, A and B) (*59*, *60*). aDCs expressed a high level of chemokines and costimulatory molecules, together with transcription factors such as *AIRE* and *FOXD4*, which we validated in situ (Fig. 4B and fig. S24);

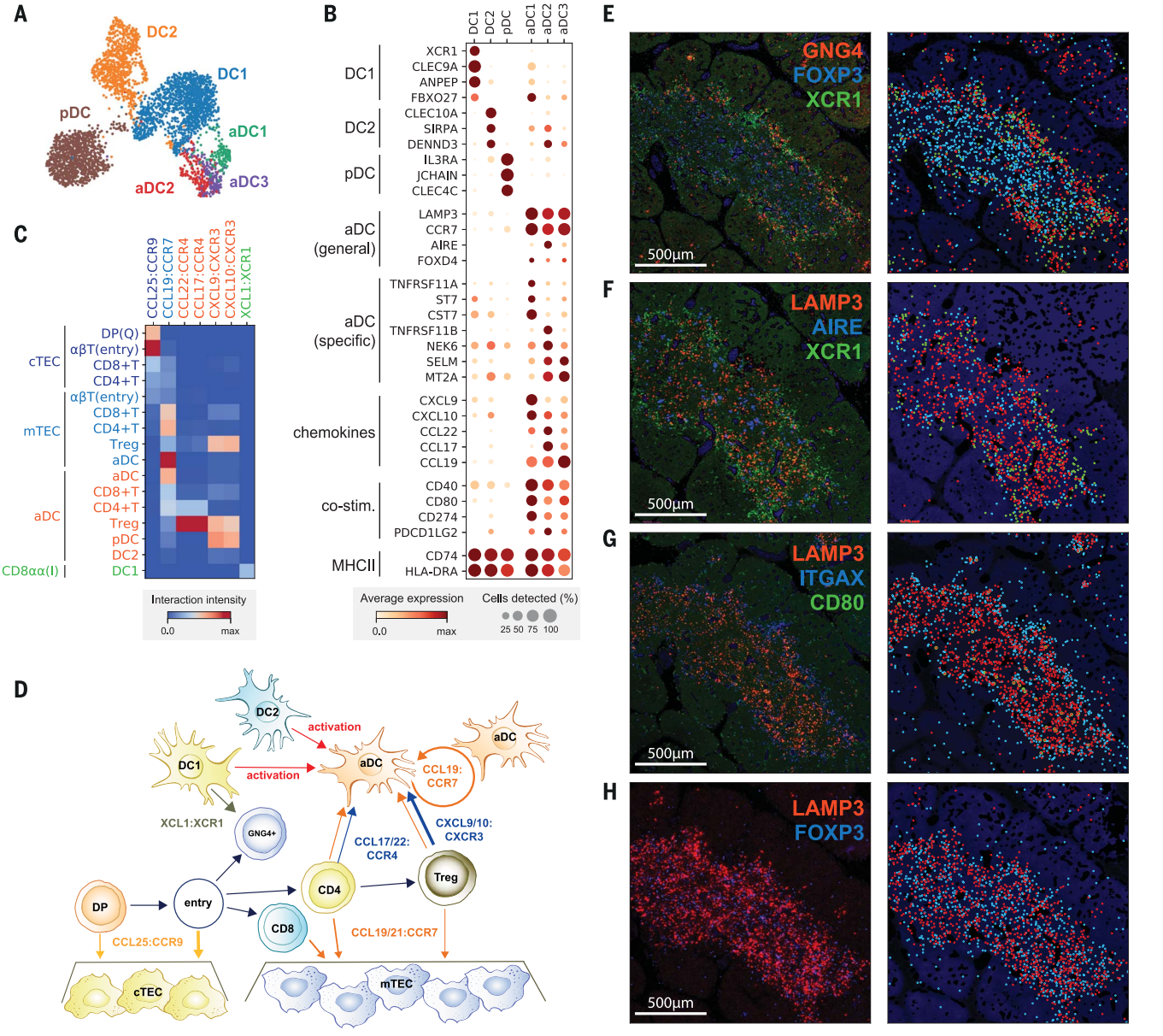

Fig. 4. Recruitment and activation of dendritic cells for thymocyte selection. (**A** and **B**) UMAP visualization of thymic DC populations (A) and dot plot of their marker genes (B). (**C**) Heat map of chemokine interactions among T cells, DCs, and TECs, where the chemokine is expressed by the outside cell type and the cognate receptor by the inside cell type. (**D**) Schematic model summarizing the interactions of TECs, DCs, and T cells. The ligand is secreted by the cell at the beginning of an arrow, and the receptor is expressed by the cell at the end of that arrow. (**E**) Left: RNA smFISH detection of *GNG4*, *XCR1*, and *FOXP3* in 15 PCW thymus. Right: Computationally detected spots are shown as solid circles over the tissue structure based on DAPI signal. Color schemes for circles are the same as in the image. (**F** to **H**) Sequential slide sections from the same sample are stained for the detection of *LAMP3*, *AIRE*, and *XCR1* (F), *LAMP3*, *ITGAX*, and *CD80* (G), and *LAMP3* and *FOXP3* (H). Spot detection and representation are as in (E). Data are representative of two experiments.

these findings suggest that they may correspond to the previously described AIRE^{+}CCR7^{+} DCs in human tonsils and thymus (*61*).

Interestingly, our single-cell data revealed three subsets within the aDC group, identified by distinct gene expression profiles: aDC1, aDC2, and aDC3 (Fig. 4, A and B). aDC1 and aDC2 subtypes shared several marker genes with DC1 and DC2, respectively. To systematically compare aDC subtypes to canonical DCs, we calculated an identity score for each DC population by summarizing marker gene expression. This demonstrated a clear relationship between aDC1-DC1 and aDC2-DC2 pairs, which suggests that each aDC subtype derives from a distinct DC population (fig S25). Interestingly, aDC1 and aDC2 displayed distinct patterns of chemokine expression, suggesting functional diversification of these aDCs (Fig. 4B). Moreover, aDC3 cells had decreased major histocompatibility complex (MHC) class II and costimulatory molecule expression relative to other aDC subsets, which may reflect a post-activation DC state.

Having identified two canonical TECs and a variety of DC subsets, we used CellPhoneDB analysis to identify specific interactions between these antigen-presenting cells and differentiating T cells (*35*). We focused on interactions mediated by chemokines, which enable cell migration and anatomical colocalization (Fig. 4C). This demonstrated the relay of differentiating T cells from the cortex to the

medulla, which is orchestrated by *CCL25*:*CCR9* and *CCL19/21*:*CCR7* interactions between cTEC/mTEC and DP/SP T cells, respectively (*62*). Interestingly, aDCs expressed *CCR7*, together with *CCL19*, enabling attraction to and recruitment of T cells into the thymic medulla. Moreover, they strongly expressed the chemokines *CCL17* and *CCL22*, whose receptor *CCR4* was enriched in $CD4^+$ T cells and particularly T_{regs}. aDCs also potentially recruit other DCs and mature T_{regs} via *CXCL9/10*:*CXCR3* interactions and are able to provide a strong costimulatory signal, which suggests a role in T_{reg} generation. We also noted that $GNG4^+CD8\alpha\alpha^+$ T(I) cells expressed XCL1, which may be involved in the recruitment of XCR1-expressing DC1 cells (*63*). Our analysis shows that XCL1 is expressed most highly by $CD8\alpha\alpha^+$ T(I) cells and at a lower level by NK cells (fig. S26). The location of $CD8\alpha\alpha^+$ T(I) cells in the perimedullary region suggests a potential relay of signals from $CD8\alpha\alpha^+$ T(I) cells to recruit $XCR1^+$ DC1 cells into the medulla, where these cells are activated and up-regulate CCR7 (Fig. 4D).

To confirm our in silico predictions, we performed smFISH to identify the anatomical location of $CD8\alpha\alpha^+$ T(I) cells (*GNG4*), DC1s (*XCR1*), aDCs (*LAMP3*, *CD80*), and T_{regs} (*FOXP3*). A generic marker of nonactivated DCs (*ITGAX*) and mTECs (*AIRE*) was also used to provide a reference for the organ structure. Imaging of consecutive sections of fetal thymus (15 PCW) revealed the zonation of $CD8\alpha\alpha^+$ T(I) cells, DC1s, and nonactivated DCs located in the perimedullary region, and aDCs and T_{regs} enriched in the center of the medulla (Fig. 4, E to H). All localization patterns are supportive of our in silico model, demonstrating the power of single-cell transcriptomics coupled with CellPhoneDB predictions.

Bias in human TCR repertoire formation and selection

Because our data featured detailed T cell trajectories combined with single-cell resolution TCR sequences, it provided an opportunity to investigate the kinetics of TCR recombination. TCR chains detected from the TCR-enriched 5′ sequencing libraries were filtered for full-length recombinants and were associated with our cell type annotation. This allowed us to analyze patterns in TCR repertoire formation and selection (Fig. 5, A and B).

For TCRβ, we observed a strong bias in VDJ gene usage that persisted from the initiation of recombination (DN cells) to the mature T cell stage (Fig. 5A). This bias is not explained by recombination signal sequence (RSS) score (fig. S27). The bias does correlate well with genomic position (fig. S27), and this is consistent with a looping structure of the locus, which has been observed in the mouse (Fig. 5C) (*64*). However, the V gene usage bias that we observe in human is not found in mouse (*25*). We also observed a preferential association of D2 genes with J2 genes, whereas D1 genes can recombine with J1 and J2 genes with similar frequency (fig. S28). There was no clear association between TCRβ V-D or V-J pairs (fig. S28A).

Although the initial recombination pattern largely shapes the repertoire, selection also contributes to the preference in TCRβ repertoire. We observed that several TRBV genes were depleted or enriched after beta selection (DP cells) relative to before beta selection (DN cells). This suggests that there are germline-encoded differences between the different Vβ genes' ability to respond to peptide-MHC (pMHC) stimulation (fig. S29A). This result is in line with the molecular finding that Vβ makes the most contacts with pMHC molecule versus DJ (and also Vα) (*65*).

For the TCRα locus, we found a clear association between developmental timing and V-J pairing, as previously described (*66*): Proximal pairs were recombined first, followed by recombination of distal pairs (Fig. 5B), which in turn restricted the pairing between V and J genes (fig. S28B). This provides direct evidence for progressive recombination of the TCRα locus (Fig. 5D). Notably, proximal pairs were depleted in mature T cells relative to DP cells, showing a further bias in the positive selection step (fig. S28B).

To investigate whether differential TCR repertoire bias exists between cell types, we compared the TCR repertoire of different cell types by running a principal components analysis (Fig. 5E). Notably, we observed a clear separation of $CD8^+$ T cells and other cell types. The trend was consistent in all individual donor samples. Statistical testing of the difference in odds ratios identified several TCR genes responsible for this phenomenon (fig. S29B). The observed trend was largely similar to that seen in naïve $CD4^+/CD8^+$ T cells isolated from peripheral blood (*22*, *23*). Notably, relative to other cell types, the TRAV-TRAJ repertoire of $CD8^+$ T cells was biased toward distal V-J pairs (Fig. 5F). Considering that distal repertoires are generated at a later stage of progressive TCRα recombination, this might be due to slower or less efficient commitment toward the $CD8^+$ T lineage (Fig. 5D). There was also a slight bias toward proximal V-J pairs for $CD8\alpha\alpha^+$ T(I) cells that was much more evident in the postnatal thymic sample compared to fetal samples (fig. S29C) (*53*).

Discussion

We reconstructed the trajectory of human conventional and unconventional T cell differentiation combined with TCR repertoire information, which revealed a bias in the TCR repertoire of mature conventional T cells. Because TCR repertoire bias predisposes our reactivity to diverse pMHC combinations, this may have profound implications for how we respond to antigenic challenges.

Our analysis of the thymic microenvironment revealed the complexity of cell types constituting the thymus, as well as the breadth of interactions between stromal cells and innate immune cells to coordinate thymic development to support T cell differentiation. The intercellular communication network that we describe between thymocytes and supporting cells can be used to enhance in vitro culture systems to generate T cells, and will influence future T cell therapeutic engineering strategies.

Materials and methods

Tissue acquisition and processing

All tissue samples used for this study were obtained with written informed consent from all participants in accordance with the guidelines in the Declaration of Helsinki 2000 from multiple centers. All tissues were processed immediately after isolation using consistent protocols with variation in enzymatic digestion strength. Tissue was transferred to a sterile 10-mm^2 tissue culture dish and cut into segments (<1 mm^3) before being transferred to a 50-ml conical tube. For mild digestion, tissues were digested with collagenase type IV (1.6 mg/ml, Worthington) in RPMI (Sigma-Aldrich) supplemented with 10% (v/v) heat-inactivated fetal bovine serum (FBS; Gibco), penicillin (100 U/ml, Sigma-Aldrich), streptomycin (0.1 mg/ml, Sigma-Aldrich), and 2 mM L-glutamine (Sigma-Aldrich) for 30 min at 37°C with intermittent shaking. For stringent digestion, tissue was digested with Liberase (0.2 mg/ml, Roche)/0.125 KU DNase1 (Sigma-Aldrich)/10 mM HEPES in RPMI for 30 min at 37°C with intermittent shaking. The dissociated cells were separated and remaining undigested tissue were digested again with fresh media. This procedure was repeated until the tissue was completely dissociated. Digested tissue was passed through a 100-μm filter, and cells collected by centrifugation (500*g* for 5 min at 4°C). Cells were treated with 1× red blood cell [RBC lysis buffer (eBioscience)] for 5 min at room temperature and washed once with flow buffer [PBS containing 5% (v/v) FBS and 2 mM EDTA] prior to cell counting.

Single-cell RNA sequencing experiment

For FACS sorting of isolated thymus cells, dissociated cells were stained with a panel of antibodies prior to sorting based on CD45 or CD3 expression gate. Enrichment of EpCAM-positive cells was performed using CD326 (EpCAM) microbeads (Miltenyi Biotec, 130-061-101) according to manufacturer's protocol. CD45 depleted cells were obtained using CD45 microbeads (Miltenyi Biotec, 130-045-801) according to manufacturer's protocol. Cell number and viability were checked

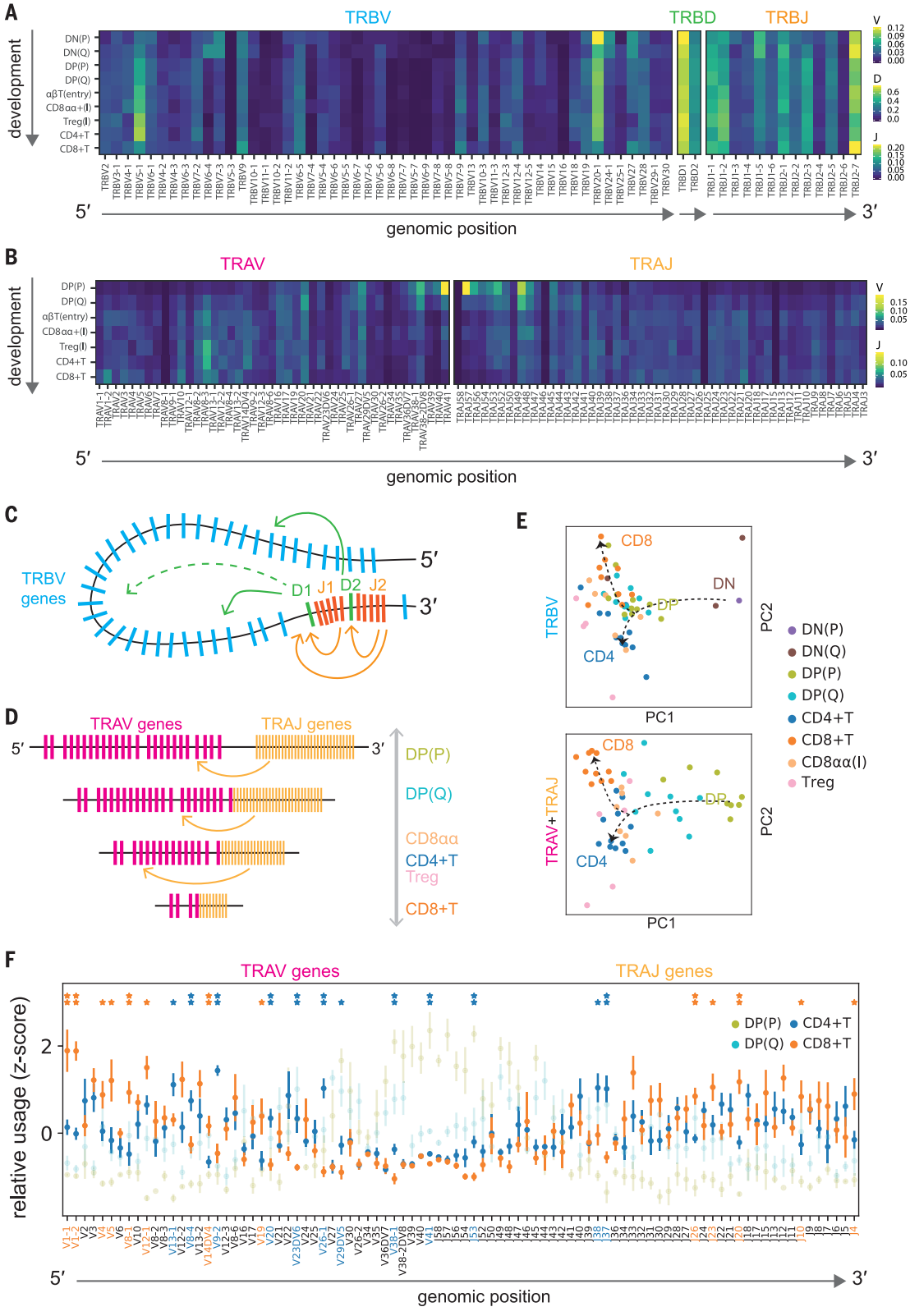

Fig. 5. Intrinsic bias in human TCR repertoire formation and selection. (**A**) Heat map showing the proportion of each TCRβ V, D, and J gene segment present at progressive stages of T cell development. Gene segments are positioned according to genomic location. (**B**) Same scheme as in (A) applied to TCRα V and J gene segments. Although there is a usage bias of segments at the beginning of development, segments are evenly used by the late developmental stages, indicating progressive recombination leading to even usage of segments. (**C** and **D**) Schematics illustrating a hypothetical chromatin loop that may explain genomic location bias in recombination of TCRβ locus (C) and the mechanism of progressive recombination of TCRα locus leading to even usage of segments (D). (**E**) Principal components analysis plots showing TRBV or TRAV and TRAJ gene usage pattern in different T cell types. Arrows depict T cell developmental order. For TRBV, there is a strong effect from beta selection, after which point the $CD4^+$ and $CD8^+$ repertoires diverge. The development for TRAV+TRAJ is more progressive, with stepwise divergence into the $CD4^+$ and $CD8^+$ repertoires. (**F**) Relative usage of TCRα V and J gene segments according to cell type. The z-score for each segment is calculated from the distribution of normalized proportions stratified by the cell type and sample. *P* value is calculated by comparing z-scores in $CD4^+$ T and $CD8^+$ T cells using *t* test, and false discovery rate (FDR) is calculated using Benjamini-Hochberg correction: $*P < 0.05$, **FDR < 10%. Gene names and asterisks are colored by significant enrichment in $CD4^+$ T cells (blue) or $CD8^+$ T cells (orange).

after the enrichment to ensure that no significant cell death has been caused by the process.

For the droplet-encapsulation scRNA-seq experiments, 8000 live, single, $CD45^+$ or $CD45^-$ FACS-isolated cells or MACS-enriched cells were loaded on to each of the Chromium Controller (10x Genomics). Single-cell cDNA synthesis, amplification, and sequencing libraries were generated using the Single Cell 3′ and 5′ Reagent Kit following the manufacturer's instructions. The libraries from up to eight loaded channels were multiplexed together and sequenced on an Illumina HiSeq 4000. The libraries were distributed over eight lanes per

flow cell and sequenced using the following parameters: Read1: 26 cycles, i7: 8 cycles, i5: 0 cycles; Read2: 98 cycles to generate 75-bp paired-end reads. For the plate-based scRNA-seq experiments, a slightly modified Smart-Seq2 protocol was used. After cDNA generation, libraries were prepared (384 cells per library) using the Illumina Nextera XT kit. Index v2 sets A, B, C, and D were used per library to barcode each cell for multiplexing. Each library was sequenced (384 cells) per lane at a sequencing depth of 1 to 2 million reads per cell on HiSeq 4000 using v4 SBS chemistry to create 75-bp paired-end reads.

Single-cell RNA sequencing data analysis

Droplet-based sequencing data were aligned and quantified using the Cell Ranger Single-Cell Software Suite (version 2.0.2 for 3′ chemistry and version 2.1.0 for 5′ chemistry, 10x Genomics Inc.) using the GRCh38 human reference genome (official Cell Ranger reference, version 1.2.0). Cells with fewer than 2000 UMI counts and 500 detected genes were considered as empty droplets and removed from the dataset. Cells with more than 7000 detected genes were considered as potential doublets and removed from the dataset.

Smart-seq2 sequencing data were aligned with *STAR* (version 2.5.1b), using the STAR index and annotation from the same reference as the 10x data. Gene-specific read counts were calculated using htseq-count (version 0.10.0). Scanpy (version 1.3.4) python package was used to load the cell-gene count matrix and perform downstream analysis. Doublet detection, clustering, annotation, batch alignment, trajectory analysis, cell-cell interaction, and repertoire analysis is performed using the tools in Scanpy package complemented with some custom codes.

RNA smFISH

Samples were fixed in 10% NBF, dehydrated through an ethanol series, and embedded in paraffin wax. Samples (5 μm) were cut, baked at 60°C for 1 hour, and processed using standard pre-treatment conditions, as per the RNAscope multiplex fluorescent reagent kit version 2 assay protocol (manual) or the RNAscope 2.5 LS fluorescent multiplex assay (automated). TSA-plus fluorescein, Cy3, and Cy5 fluorophores were used at 1:1500 dilution for the manual assay, or 1:300 dilution for the automated assay. Slides were imaged on different microscopes: Hamamatsu Nanozoomer S60 or 3DHistech Pannoramic MIDI. Stained sections were also imaged with a Perkin Elmer Opera Phenix High-Content Screening System, in confocal mode with 1 μm z-step size, using 20× (NA 0.16, 0.299 μm/pixel) and 40× (NA 1.1, 0.149 μm/pixel) water-immersion objectives.

REFERENCES AND NOTES

1. S. Palmer, L. Albergante, C. C. Blackburn, T. J. Newman, Thymic involution and rising disease incidence with age. *Proc. Natl. Acad. Sci. U.S.A.* **115**, 1883–1888 (2018). doi: 10.1073/pnas.1714478115; pmid: 29432166
2. H. E. Lynch *et al*., Thymic involution and immune reconstitution. *Trends Immunol.* **30**, 366–373 (2009). doi: 10.1016/j.it.2009.04.003; pmid: 19540807
3. G. L. Stritesky, S. C. Jameson, K. A. Hogquist, Selection of self-reactive T cells in the thymus. *Annu. Rev. Immunol.* **30**, 95–114 (2012). doi: 10.1146/annurev-immunol-020711-075035; pmid: 22149933
4. M. J. Sánchez *et al*., Putative prethymic T cell precursors within the early human embryonic liver: A molecular and functional analysis. *J. Exp. Med.* **177**, 19–33 (1993). doi: 10.1084/jem.177.1.19; pmid: 8418199
5. L. Sun *et al*., FSP1(+) fibroblast subpopulation is essential for the maintenance and regeneration of medullary thymic epithelial cells. *Sci. Rep.* **5**, 14871 (2015). doi: 10.1038/srep14871; pmid: 26445893
6. L. Wu, K. Shortman, Heterogeneity of thymic dendritic cells. *Semin. Immunol.* **17**, 304–312 (2005). doi: 10.1016/j.smim.2005.05.001; pmid: 15946853
7. G. Anderson, Y. Takahama, Thymic epithelial cells: Working class heroes for T cell development and repertoire selection. *Trends Immunol.* **33**, 256–263 (2012). doi: 10.1016/j.it.2012.03.005; pmid: 22591984
8. Y.-J. Liu, A unified theory of central tolerance in the thymus. *Trends Immunol.* **27**, 215–221 (2006). doi: 10.1016/j.it.2006.03.004; pmid: 16580260
9. J. Gameiro, P. Nagib, L. Verinaud, The thymus microenvironment in regulating thymocyte differentiation. *Cell Adhes. Migr.* **4**, 382–390 (2010). doi: 10.4161/cam.4.3.11789; pmid: 20418658
10. W. E. Jenkinson, S. W. Rossi, S. M. Parnell, E. J. Jenkinson, G. Anderson, PDGFRα-expressing mesenchyme regulates thymus growth and the availability of intrathymic niches. *Blood* **109**, 954–960 (2007). doi: 10.1182/blood-2006-05-023143; pmid: 17008543
11. S. Inglesfield, E. J. Cosway, W. E. Jenkinson, G. Anderson, Rethinking Thymic Tolerance: Lessons from Mice. *Trends Immunol.* **40**, 279–291 (2019). doi: 10.1016/j.it.2019.01.011; pmid: 30803714
12. J. F. A. P. Miller, The golden anniversary of the thymus. *Nat. Rev. Immunol.* **11**, 489–495 (2011). doi: 10.1038/nri2993; pmid: 21617694
13. J. Gordon, N. R. Manley, Mechanisms of thymus organogenesis and morphogenesis. *Development* **138**, 3865–3878 (2011). doi: 10.1242/dev.059998; pmid: 21862553
14. E. M. Kernfeld *et al*., A Single-Cell Transcriptomic Atlas of Thymus Organogenesis Resolves Cell Types and Developmental Maturation. *Immunity* **48**, 1258–1270.e6 (2018). doi: 10.1016/j.immuni.2018.04.015; pmid: 29884461
15. C. Bornstein *et al*., Single-cell mapping of the thymic stroma identifies IL-25-producing tuft epithelial cells. *Nature* **559**, 622–626 (2018). doi: 10.1038/s41586-018-0346-1; pmid: 30022162
16. C. N. Miller *et al*., Thymic tuft cells promote an IL-4-enriched medulla and shape thymocyte development. *Nature* **559**, 627–631 (2018). doi: 10.1038/s41586-018-0345-2; pmid: 30022164
17. J. Mestas, C. C. W. Hughes, Of mice and not men: Differences between mouse and human immunology. *J. Immunol.* **172**, 2731–2738 (2004). doi: 10.4049/jimmunol.172.5.2731; pmid: 14978070
18. A. M. Farley *et al*., Dynamics of thymus organogenesis and colonization in early human development. *Development* **140**, 2015–2026 (2013). doi: 10.1242/dev.087320; pmid: 23571219
19. B. V. Kumar, T. J. Connors, D. L. Farber, Human T Cell Development, Localization, and Function throughout Life. *Immunity* **48**, 202–213 (2018). doi: 10.1016/j.immuni.2018.01.007; pmid: 29466753
20. J. Nikolich-Žugich, M. K. Slifka, I. Messaoudi, The many important facets of T cell repertoire diversity. *Nat. Rev. Immunol.* **4**, 123–132 (2004). doi: 10.1038/nri1292; pmid: 15040585
21. R. Jores, T. Meo, Few V gene segments dominate the T cell receptor β-chain repertoire of the human thymus. *J. Immunol.* **151**, 6110–6122 (1993). pmid: 8245454
22. J. A. Carter *et al*., T cell receptor αβ chain pairing is associated with CD4+ and CD8+ lineage specification. bioRxiv 293852 [preprint]. 3 April 2018.
23. P. L. Klarenbeek *et al*., Somatic Variation of T cell Receptor Genes Strongly Associate with HLA Class Restriction. *PLOS ONE* **10**, e0140815 (2015). doi: 10.1371/journal.pone.0140815; pmid: 26517366
24. R. L. Warren *et al*., Exhaustive T cell repertoire sequencing of human peripheral blood samples reveals signatures of antigen selection and a directly measured repertoire size of at least 1 million clonotypes. *Genome Res.* **21**, 790–797 (2011). doi: 10.1101/gr.115428.110; pmid: 21349924
25. S. Gopalakrishnan *et al*., Unifying model for molecular determinants of the preselection Vβ repertoire. *Proc. Natl. Acad. Sci. U.S.A.* **110**, E3206–E3215 (2013). doi: 10.1073/pnas.1304048110; pmid: 23918392
26. K. Polański *et al*., BBKNN: Fast Batch Alignment of Single Cell Transcriptomes. *Bioinformatics* btz625 (2019). doi: 10.1093/bioinformatics/btz625; pmid: 31400197
27. S. Hansen *et al*., Collectin 11 (CL-11, CL-K1) is a MASP-1/3-associated plasma collectin with microbial-binding activity. *J. Immunol.* **185**, 6096–6104 (2010). doi: 10.4049/jimmunol.1002185; pmid: 20956340
28. K. M. Sitnik *et al*., Mesenchymal cells regulate retinoic acid receptor-dependent cortical thymic epithelial cell homeostasis. *J. Immunol.* **188**, 4801–4809 (2012). doi: 10.4049/jimmunol.1200358; pmid: 22504647
29. C. Gu, E. Giraudo, The role of semaphorins and their receptors in vascular development and cancer. *Exp. Cell Res.* **319**, 1306–1316 (2013). doi: 10.1016/j.yexcr.2013.02.003; pmid: 23422037
30. H. J. Garchon, F. Djabiri, J. P. Viard, P. Gajdos, J. F. Bach, Involvement of human muscle acetylcholine receptor α-subunit gene (CHRNA) in susceptibility to myasthenia gravis. *Proc. Natl. Acad. Sci. U.S.A.* **91**, 4668–4672 (1994). doi: 10.1073/pnas.91.11.4668; pmid: 7910962
31. L. Mesnard-Rouiller, J. Bismuth, A. Wakkach, S. Poëa-Guyon, S. Berrih-Aknin, Thymic myoid cells express high levels of muscle genes. *J. Neuroimmunol.* **148**, 97–105 (2004). doi: 10.1016/j.jneuroim.2003.11.013; pmid: 14975590
32. A. Zóttowska *et al*., Myoid cells and neuroendocrine markers in myasthenic thymuses. *Arch. Immunol. Ther. Exp.* **46**, 253–257 (1998). pmid: 9779292
33. V. S. Patil *et al*., Precursors of human CD4+ cytotoxic T lymphocytes identified by single-cell transcriptome analysis. *Sci. Immunol.* **3**, eaan8664 (2018). doi: 10.1126/sciimmunol.aan8664; pmid: 29352091
34. N. Lopes, A. Sergé, P. Ferrier, M. Irla, Thymic Crosstalk Coordinates Medulla Organization and T cell Tolerance Induction. *Front. Immunol.* **6**, 365 (2015). doi: 10.3389/fimmu.2015.00365; pmid: 26257733
35. R. Vento-Tormo *et al*., Single-cell reconstruction of the early maternal-fetal interface in humans. *Nature* **563**, 347–353 (2018). doi: 10.1038/s41586-018-0698-6; pmid: 30429548
36. D. Elewaut, C. F. Ware, The unconventional role of LTαβ in T cell differentiation. *Trends Immunol.* **28**, 169–175 (2007). doi: 10.1016/j.it.2007.02.005; pmid: 17336158
37. S. W. Rossi *et al*., RANK signals from CD4+3- inducer cells regulate development of Aire-expressing epithelial cells in the thymic medulla. *J. Exp. Med.* **204**, 1267–1272 (2007). doi: 10.1084/jem.20062497; pmid: 17502664
38. J. M. Revest, R. K. Suniara, K. Kerr, J. J. Owen, C. Dickson, Development of the thymus requires signaling through the fibroblast growth factor receptor R2-IIIb. *J. Immunol.* **167**, 1954–1961 (2001). doi: 10.4049/jimmunol.167.4.1954; pmid: 11489975
39. M. J. García-León, P. Fuentes, J. L. de la Pompa, M. L. Toribio, Dynamic regulation of NOTCH1 activation and Notch ligand expression in human thymus development. *Development* **145**, dev165597 (2018). doi: 10.1242/dev.165597; pmid: 30042180
40. G. E. Desanti *et al*., Developmentally regulated availability of RANKL and CD40 ligand reveals distinct mechanisms of fetal and adult cross-talk in the thymus medulla. *J. Immunol.* **189**, 5519–5526 (2012). doi: 10.4049/jimmunol.1201815; pmid: 23152561
41. E. J. Cosway *et al*., Redefining thymus medulla specialization for central tolerance. *J. Exp. Med.* **214**, 3183–3195 (2017). doi: 10.1084/jem.20171000; pmid: 28830910
42. I. Van de Walle *et al*., Jagged2 acts as a Delta-like Notch ligand during early hematopoietic cell fate decisions. *Blood* **117**, 4449–4459 (2011). doi: 10.1182/blood-2010-06-290049; pmid: 21372153
43. I. Van de Walle *et al*., Specific Notch receptor-ligand interactions control human TCR-αβ/γδ development by

inducing differential Notch signal strength. *J. Exp. Med.* **210**, 683–697 (2013). doi: 10.1084/jem.20121798; pmid: 23530123
44. D.-M. Popescu *et al*., Decoding human fetal liver haematopoiesis. *Nature* **574**, 365–371 (2019). doi: 10.1038/s41586-019-1652-y; pmid: 31597962
45. Y. Zeng *et al*., Single-Cell RNA Sequencing Resolves Spatiotemporal Development of Pre-thymic Lymphoid Progenitors and Thymus Organogenesis in Human Embryos. *Immunity* **51**, 930–948.e6 (2019). doi: 10.1016/j.immuni.2019.09.008; pmid: 31604687
46. D. Pellin *et al*., A comprehensive single cell transcriptional landscape of human hematopoietic progenitors. *Nat. Commun.* **10**, 2395 (2019). doi: 10.1038/s41467-019-10291-0; pmid: 31160568
47. D. K. Shah, J. C. Zúñiga-Pflücker, An overview of the intrathymic intricacies of T cell development. *J. Immunol.* **192**, 4017–4023 (2014). doi: 10.4049/jimmunol.1302259; pmid: 24748636
48. H. T. Petrie, M. Tourigny, D. B. Burtrum, F. Livak, Precursor thymocyte proliferation and differentiation are controlled by signals unrelated to the pre-TCR. *J. Immunol.* **165**, 3094–3098 (2000). doi: 10.4049/jimmunol.165.6.3094; pmid: 10975821
49. M. R. Tourigny, S. Mazel, D. B. Burtrum, H. T. Petrie, T cell receptor (TCR)-β gene recombination: Dissociation from cell cycle regulation and developmental progression during T cell ontogeny. *J. Exp. Med.* **185**, 1549–1556 (1997). doi: 10.1084/jem.185.9.1549; pmid: 9151892
50. W. A. Dik *et al*., New insights on human T cell development by quantitative T cell receptor gene rearrangement studies and gene expression profiling. *J. Exp. Med.* **201**, 1715–1723 (2005). doi: 10.1084/jem.20042524; pmid: 15928199
51. B. J. Schmiedel *et al*., Impact of Genetic Polymorphisms on Human Immune Cell Gene Expression. *Cell* **175**, 1701–1715.e16 (2018). doi: 10.1016/j.cell.2018.10.022; pmid: 30449622
52. D. L. Owen *et al*., Thymic regulatory T cells arise via two distinct developmental programs. *Nat. Immunol.* **20**, 195–205 (2019). doi: 10.1038/s41590-018-0289-6; pmid: 30643267
53. G. Verstichel *et al*., The checkpoint for agonist selection precedes conventional selection in human thymus. *Sci. Immunol.* **2**, eaah4232 (2017). doi: 10.1126/sciimmunol.aah4232; pmid: 28783686
54. J. R. Fergusson, V. M. Fleming, P. Klenerman, CD161-expressing human T cells. *Front. Immunol.* **2**, 36 (2011). doi: 10.3389/fimmu.2011.00036; pmid: 22566826
55. E. S. Alonzo, D. B. Sant'Angelo, Development of PLZF-expressing innate T cells. *Curr. Opin. Immunol.* **23**, 220–227 (2011). doi: 10.1016/j.coi.2010.12.016; pmid: 21257299
56. R. Ruscher, R. L. Kummer, Y. J. Lee, S. C. Jameson, K. A. Hogquist, CD8αα intraepithelial lymphocytes arise from two main thymic precursors. *Nat. Immunol.* **18**, 771–779 (2017). doi: 10.1038/ni.3751; pmid: 28530714
57. J. Oh, J.-S. Shin, The Role of Dendritic Cells in Central Tolerance. *Immune Netw.* **15**, 111–120 (2015). doi: 10.4110/in.2015.15.3.111; pmid: 26140042
58. A.-C. Villani *et al*., Single-cell RNA-seq reveals new types of human blood dendritic cells, monocytes, and progenitors. *Science* **356**, eaah4573 (2017). doi: 10.1126/science.aah4573; pmid: 28428369
59. N. Watanabe *et al*., Hassall's corpuscles instruct dendritic cells to induce $CD4^+CD25^+$ regulatory T cells in human thymus. *Nature* **436**, 1181–1185 (2005). doi: 10.1038/nature03886; pmid: 16121185
60. P. J. Fairchild, J. M. Austyn, Thymic dendritic cells: Phenotype and function. *Int. Rev. Immunol.* **6**, 187–196 (1990). doi: 10.3109/08830189009056629; pmid: 2152502
61. J. R. Fergusson *et al*., Maturing Human $CD127^+$ $CCR7^+$ $PDL1^+$ Dendritic Cells Express AIRE in the Absence of Tissue Restricted Antigens. *Front. Immunol.* **9**, 2902 (2019). doi: 10.3389/fimmu.2018.02902; pmid: 30692988
62. Z. Hu, J. N. Lancaster, L. I. R. Ehrlich, The Contribution of Chemokines and Migration to the Induction of Central Tolerance in the Thymus. *Front. Immunol.* **6**, 398 (2015). doi: 10.3389/fimmu.2015.00398; pmid: 26300884
63. Y. Lei *et al*., Aire-dependent production of XCL1 mediates medullary accumulation of thymic dendritic cells and contributes to regulatory T cell development. *J. Exp. Med.* **208**, 383–394 (2011). doi: 10.1084/jem.20102327; pmid: 21300913
64. J. A. Skok *et al*., Reversible contraction by looping of the Tcra and Tcrb loci in rearranging thymocytes. *Nat. Immunol.* **8**, 378–387 (2007). doi: 10.1038/ni1448; pmid: 17334367
65. R. J. Mallis *et al*., Pre-TCR ligand binding impacts thymocyte development before αβTCR expression. *Proc. Natl. Acad. Sci. U.S.A.* **112**, 8373–8378 (2015). doi: 10.1073/pnas.1504971112; pmid: 26056289
66. Z. M. Carico, K. Roy Choudhury, B. Zhang, Y. Zhuang, M. S. Krangel, Tcrd Rearrangement Redirects a Processive Tcra Recombination Program to Expand the Tcra Repertoire. *Cell Rep.* **19**, 2157–2173 (2017). doi: 10.1016/j.celrep.2017.05.045; pmid: 28591585

ACKNOWLEDGMENTS

We gratefully acknowledge the Sanger Flow Cytometry Facility, Newcastle University Flow Cytometry Core Facility, Sanger Cellular Generation and Phenotyping (CGaP) Core Facility, and Sanger Core Sequencing pipeline for support with sample processing and sequencing library preparation. We thank the MRC/Engineering and Physical Sciences Research Council Newcastle Molecular Pathology Node for support on paraffin embedding fetal tissues; J. Eliasova for graphical images, J. Choi for helpful discussions, and S. Aldridge for editing the manuscript. The human embryonic and fetal material was provided by the Joint MRC/Wellcome (MR/R006237/1) Human Developmental Biology Resource (www.hdbr.org). The material from the deceased organ donor was provided by the Cambridge Biorepository for Translational Medicine. Pediatric thymus material was provided by Ghent University Hospital. We are grateful to the donors and donor families for granting access to the tissue samples. This publication is part of the Human Cell Atlas: www.humancellatlas.org/publications. **Funding:** Supported by Wellcome Human Cell Atlas Strategic Science Support (WT211276/Z/18/Z) and the Chan Zuckerberg Initiative (CZF2019-002445); Wellcome (WT206194), ERC Consolidator (no. 646794), and EU MRG-Grammar awards (S.A.T.); Wellcome (WT107931/Z/15/Z), the Lister Institute for Preventive Medicine and NIHR and Newcastle-Biomedical Research Centre (M.H.); Research Foundation Flanders (FWO grant G053816N) and Ghent University Special Research Fund (BOF18-GOA-024) (T.T.); an EMBO Long-Term Fellowship (J.-E.P.); the Wellcome Trust under grants 203828/Z/16/A and 203828/Z/16/Z (D.J.K.); and the European Research Council (ERC-Stg 639429), the Rosetrees Trust (M362; M362-F1), the UCL Therapeutic Acceleration Support Fund, and the GOSH BRC (P.B.). R.A.B. is an NIHR Senior Investigator and is also supported by NIHR funding of the Cambridge Biomedical Research Centre. Cambridge fetal tissue was collected in part from funding from the WT MRC Cambridge Stem Cell Institute. **Author contributions:** J.-E.P., S.A.T., M.H., and T.T. designed the experiments; J.-E.P., R.A.B., D.-M.P., E.S., M.L., C.D.C., J.R.F., N.V., K.T.M., I.G., L.B., D.C., F.D., and X.H. performed sampling and library prep with help from S.W., D.M., A.Fu., A.Fi., L.M., G.R., D.D., S.L., D.H., K.S.-P., and R.V.-T.; J.-E.P., D.J.K., K.P., M.L., C.D.C., and V.R.K. analyzed the data; J.-E.P., C.D.C., E.T., O.B., K.R., A.W.-C., R.A.B., and R.R. performed validation experiments; J.-E.P., C.D.C., S.A.T., M.H., and T.T. wrote the manuscript with contributions from R.A.B., K.B.M., Y.S., M.R.C., P.B., S.B., R.V.-T., K.S.-P., and D.J.K. All authors read and approved the manuscript. **Competing interests:** J.-E.P. and S.A.T. are inventors on a patent application (GB1918902.6) submitted by Genome Research Limited that covers a defined set of transcription factors. **Data and materials availability:** All sequencing data have been deposited to ArrayExpress (accession number E-MTAB-8581) and can be accessed online through a web portal (https://developmentcellatlas.ncl.ac.uk). All codes used for data analysis are available from Zenodo repository (DOI: 10.5281/zenodo.3572422).

SUPPLEMENTARY MATERIALS

science.sciencemag.org/content/367/6480/eaay3224/suppl/DC1
Materials and Methods
Supplementary Text
Figs. S1 to S29
Tables S1 to S8
Data S1
References (*67*–*72*)

View/request a protocol for this paper from *Bio-protocol*.

8 June 2019; accepted 16 January 2020
10.1126/science.aay3224

RESEARCH ARTICLE SUMMARY

VACCINES

Pulmonary surfactant–biomimetic nanoparticles potentiate heterosubtypic influenza immunity

Ji Wang*, Peiyu Li*, Yang Yu*, Yuhong Fu, Hongye Jiang, Min Lu, Zhiping Sun, Shibo Jiang, Lu Lu†, Mei X. Wu†

INTRODUCTION: Current influenza vaccines must be refreshed annually to address constant mutations of viral hemagglutinin (HA) and neuraminidase (NA) genes because the vaccines induce primarily neutralizing antibodies against these surface antigens. Even with annual updates, there have been years in which influenza vaccines were ineffective because of mismatched HA and/or NA antigenicity between the vaccine viral strains and strains in circulation. Thus, resources have been poured into developing "universal" influenza vaccines that can protect the population from divergent influenza viruses. However, none of these have passed human clinical trials thus far. Broad immunity can be evoked by natural viral infections or live vector–engineered and attenuated influenza vaccines, which all induce lung resident memory T cells (T_{RM} cells) apart from humoral immunity. However, a delicate balance must be struck between safety and immunogenicity of these "replicating" vaccines. Moreover, these vaccines are suitable for only some populations. Thus, safe and potent mucosal adjuvants are urgently needed as part of nonreplicating vaccines in order to stimulate lung T_{RM} cells and engender strong heterosubtypic immunity.

RATIONALE: Type I interferons (IFN-Is) are the chief immune mediators for protective immunity against viral infections and can be vigorously induced by influenza viral infection of alveolar epithelial cells (AECs) as well as immune cells. Thus, the activation of stimulator of interferon genes (STING) in these two cell types may recapitulate the immune responses provoked by viral infection or replicating vaccines. However, delivery of STING agonists into the cytosol of AECs without breaching the integrity of the pulmonary surfactant (PS) layer remains a substantial challenge because the PS layer forms a strong barrier to prevent nanoparticles and hydrophilic molecules from accessing them. To address this challenge, we encapsulated 2′,3′-cyclic guanosine monophosphate–adenosine monophosphate (cGAMP), a natural and potent STING agonist, with PS-biomimetic liposomes (PS-GAMP) in an attempt to increase the breadth of nonreplicating influenza vaccines toward universality.

RESULTS: In mice, PS-GAMP entered alveolar macrophages (AMs) in concert with lung-specific surfactant protein–A (SP-A) and SP-D because of its resemblance to PS. Its cargo was released into the cytosol followed by a flux from AMs into AECs through gap junctions. Disguised as "self," PS-GAMP escaped immune surveillance after intranasal immunization, activating the STING pathway in both AMs and AECs without breaching PS and alveolar epithelial barriers. Through this mechanism, PS-GAMP averted viral infection–provoked immunopathology while robustly augmenting the recruitment and differentiation of $CD11b^+$ dendritic cells (DCs) and $CD8^+$ T cell and humoral responses of influenza vaccines such as those induced by viral infection in terms of both timing and magnitude. The adjuvant in conjunction with inactivated H1N1 vaccine generated wide-spectrum cross-protection against distant H1N1 and heterosubtypic H3N2, H5N1, and H7N9 viruses as early as 2 days after a single immunization. This cross-protection lasted for at least 6 months, concurrent with durable lung $CD8^+$ T_{RM} cells in mice. The effectiveness of this vaccine approach was also demonstrated in a U.S. Food and Drug Administration–approved ferret model. PS-GAMP–mediated adjuvanticity was abrogated in vivo when AECs were deficient in *Sting* or when mice were administered gap junction inhibitors.

ON OUR WEBSITE

Read the full article at http://dx.doi.org/10.1126/science.aau0810

CONCLUSION: Nonreplicating influenza vaccines or conventional adjuvants primarily activate immune cells, but this approach appears to be inadequate to induce lung T_{RM} cells, a key element of heterosubtypic immunity. By contrast, PS-GAMP activated immune cells as well as AECs without breaching PS and AEC barriers, effectively averting exaggerated inflammation in the lung. STING activation in both immune cells and AECs resulted in a broad spectrum of immune protection against heterosubtypic influenza viruses. The study sheds light on the pivotal role AECs play in generating broad cross-protection against various influenza viruses. Thus, PS-GAMP is a promising mucosal adjuvant for "universal" influenza vaccines. ■

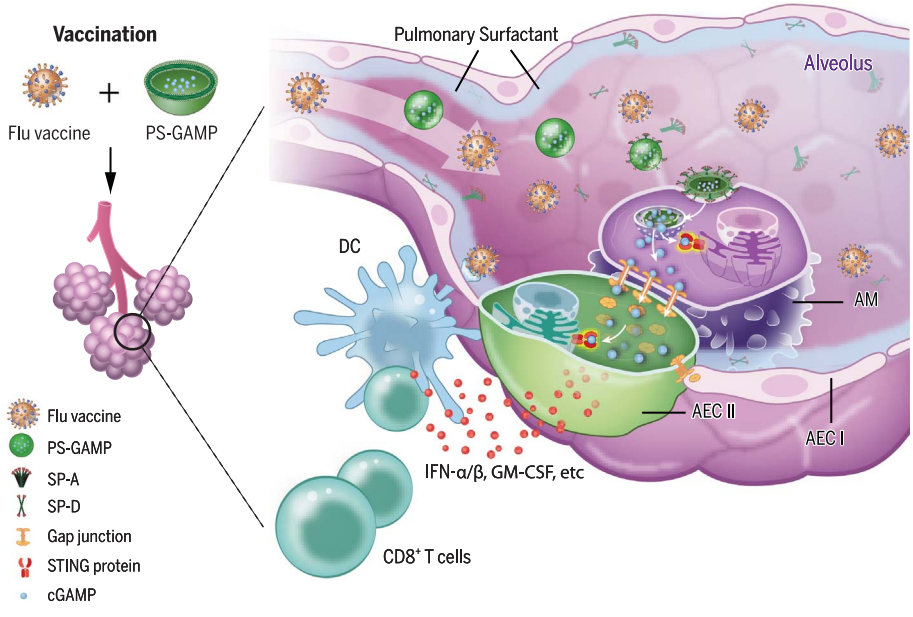

PS-GAMP–mediated adjuvanticity. In alveoli, PS-GAMP associates with SP-A or SP-D before entering AMs by means of SP-A– or SP-D–mediated endocytosis. cGAMP is subsequently released into the cytosol and fluxes into AECs by way of gap junctions. It then activates STING in these cells, resulting in the vigorous production of type 1 immune mediators. These mediators facilitate the recruitment and differentiation of $CD11b^+$ DCs, which in turn direct robust antiviral $CD8^+$ T cell and humoral immune responses.

The list of author affiliations is available in the full article online.
*These authors contributed equally to this work.
†Corresponding author. Email: mwu5@mgh.harvard.edu (M.X.W.); lul@fudan.edu.cn (L.L.)
Cite this article as J. Wang *et al.*, *Science* 367, eaau0810 (2020). DOI: 10.1126/science.aau0810

RESEARCH ARTICLE

VACCINES

Pulmonary surfactant–biomimetic nanoparticles potentiate heterosubtypic influenza immunity

Ji Wang[1,2]*, Peiyu Li[1,3]*, Yang Yu[1]*, Yuhong Fu[3], Hongye Jiang[1], Min Lu[1], Zhiping Sun[3], Shibo Jiang[3], Lu Lu[3]†, Mei X. Wu[1]†

Current influenza vaccines only confer protection against homologous viruses. We synthesized pulmonary surfactant (PS)–biomimetic liposomes encapsulating 2′,3′-cyclic guanosine monophosphate–adenosine monophosphate (cGAMP), an agonist of the interferon gene inducer STING (stimulator of interferon genes). The adjuvant (PS-GAMP) vigorously augmented influenza vaccine–induced humoral and $CD8^+$ T cell immune responses in mice by simulating the early phase of viral infection without concomitant excess inflammation. Two days after intranasal immunization with PS-GAMP–adjuvanted H1N1 vaccine, strong cross-protection was elicited against distant H1N1 and heterosubtypic H3N2, H5N1, and H7N9 viruses for at least 6 months while maintaining lung-resident memory $CD8^+$ T cells. Adjuvanticity was then validated in ferrets. When alveolar epithelial cells (AECs) lacked *Sting* or gap junctions were blocked, PS-GAMP–mediated adjuvanticity was substantially abrogated in vivo. Thus, AECs play a pivotal role in configuring heterosubtypic immunity.

Current influenza vaccines protect against viral infections primarily by inducing neutralizing antibodies specific for viral surface hemagglutinin (HA) and neuraminidase (NA). However, these surface proteins undergo constant antigenic drift or shift, greatly limiting the efficacy of these vaccines (*1*). Studies demonstrating the essential role of lung $CD8^+$ resident memory T cells (T_{RM} cells) in heterosubtypic immunity may provide an explanation to this limitation (*2*, *3*). Induced sufficiently by natural viral infections, these cells not only recognize highly conserved internal proteins that are shared among heterosubtypic influenza viruses but are also capable of clearing viruses at the site of viral entrance when their numbers are low (*4*–*6*). Similarly, live vector–engineered and attenuated influenza vaccines can induce lung $CD8^+$ T_{RM} cells (*7*, *8*), but a delicate balance must be struck between their safety and immunogenicity. Moreover, these replicating vaccines are often compromised by preexisting immunity and consequently are suitable in only some populations (*9*). By contrast, nonreplicating influenza vaccines induce poor T cell immunity in the respiratory tract and require potent mucosal adjuvants to overcome the immunoregulatory mechanisms of the respiratory mucosa. However, there continues to be a dearth of effective mucosal adjuvants despite decades of investigation.

2′,3′-cyclic guanosine monophosphate–adenosine monophosphate (cGAMP), a natural agonist of the stimulator of interferon genes (STING), is a secondary messenger generated in response to DNA viral infections or tissue damage (*10*, *11*). It stimulates the production of type I interferons (IFN-Is), which help determine the magnitude of type 1 immune responses, particularly those of $CD8^+$ T cells (*12*, *13*). STING agonists are potent adjuvants capable of eliciting robust antitumor immunity after intratumoral administration and augmenting intradermal influenza vaccines (*13*, *14*). Using these small, water-soluble agonists as mucosal adjuvants, however, is a challenge. They must be delivered into the cytosol of antigen (Ag)–presenting cells (APCs) and/or alveolar epithelial cells (AECs) without breaching the integrity of the pulmonary surfactant (PS) layer, a mixture of lipids and proteins secreted by type II AECs. This PS layer forms a strong barrier, which separates exterior air from internal alveolar epithelium in alveoli and prevents nanoparticles and hydrophilic molecules from accessing AECs (*15*, *16*).

cGAMP-containing liposomes are fabricated with PS constituents

We synthesized a series of liposomes, based on PS constituents (*17*), to encapsulate cGAMP (fig. S1A). The negatively charged nano4 was closest to PS in terms of lipid composition and charge. It was the only liposome that, when intranasally administered with whole inactivated A/Vietnam/1203/2004(VN04) H5N1 vaccine, vigorously stimulated the production of serum immunoglobulin G (IgG) and bronchoalveolar lavage fluid (BALF) IgA, concomitant with no body weight loss over vaccine-alone controls (fig. S1, B to E). By contrast, liposomes that were neutral (such as nano1), replaced anionic phosphatidylglycerol (DPPG) with cationic 1,2-dipalmitoyl-3-trimethylammonium-propane (DPTAP) (such as nano3 or naon5), or lacked polyethylene glycol, molecular weight 2000 (PEG-2000) (such as nano2 and nano3) showed substantially less adjuvanticity while causing significant loss in body weight (fig. S1, A to E). This was despite the similar size and encapsulation rate of these preparations to nano4 (fig. S1, F to G). Thus, negative charge and PEG-2000 appear to play an important role in the function and safety of the liposomes. Unexpectedly, bone marrow (BM)–derived dendritic cells (BMDCs) stimulated in vitro with cGAMP encapsulated in positively charged liposomes (nano3 or nano5) expressed higher levels of *Ifnb1* than when stimulated with negatively charged liposomes (nano2 and nano4) (fig. S1H). An analogous pattern emerged for BM-derived macrophages (BMMs) when similarly stimulated (fig. S1I). We next added trehalose to the liposome suspension before lyophilization to increase nano4 stability (fig. S1A). The resultant nano6 liposome, which we termed PS-GAMP, was stable at −20°C for at least 6 months and exhibited similar ζ potential, size, function, and safety as those of freshly prepared nano4 (fig. S1, A, B to E, F, and J). Moreover, high Ag-specific IgG titers induced by PS-GAMP–adjuvanted influenza vaccine in wild-type (WT) but not in *Sting*-deficient mice confirmed that cGAMP, rather than any other constituents, was responsible for PS-GAMP adjuvanticity (fig. S1K).

PS-GAMP uptake by alveolar macrophages requires surfactant proteins A and D

We next studied cellular targets of nano4 and its cargo by labeling nano4 and nano5 membranes with DiD, a fluorescent lipophilic carbocyanine, and packaging another fluorescent dye with a molecular mass and net negative charge comparable with that of cGAMP [sulforhodamine B (SRB)] within the liposomes (Fig. 1A). The nasal tissue, brains, mediastinal lymph nodes (MLNs), and lungs of mice were analyzed by means of flow cytometry at various time points after intranasal administration of these liposomes. The lung was the only tissue in which SRB^+ signals were higher than that in controls (Fig. 1B and fig. S2A). There, alveolar macrophages (AMs), recognized as $CD11b^-CD11c^+CD24^-$, were SRB^+DiD^+, whereas $CD11b^-CD11c^-EpCAM^+MHC\ II^+$ AECs were SRB^+ but DiD^-(Fig. 1, B to D, and fig. S4A) (*18*). This suggests that only the former took up nano4 directly (Fig. 1E). SRB^+AMs represented

[1]Wellman Center for Photomedicine, Massachusetts General Hospital, Department of Dermatology, Harvard Medical School, Boston, MA 02114, USA. [2]Precision Medicine Institute, The First Affiliated Hospital of Sun Yat-Sen University, Sun Yat-Sen University, Guangzhou 510080, China. [3]Key Laboratory of Medical Molecular Virology (MOE/NHC/CAMS), School of Basic Medical Sciences and Shanghai Public Health Clinical Center, Biosafety Level 3 Laboratory, Fudan University, Shanghai 200032, China.
*These authors contributed equally to this work.
†Corresponding author. Email: mwu5@mgh.harvard.edu (M.X.W.); lul@fudan.edu.cn (L.L.)

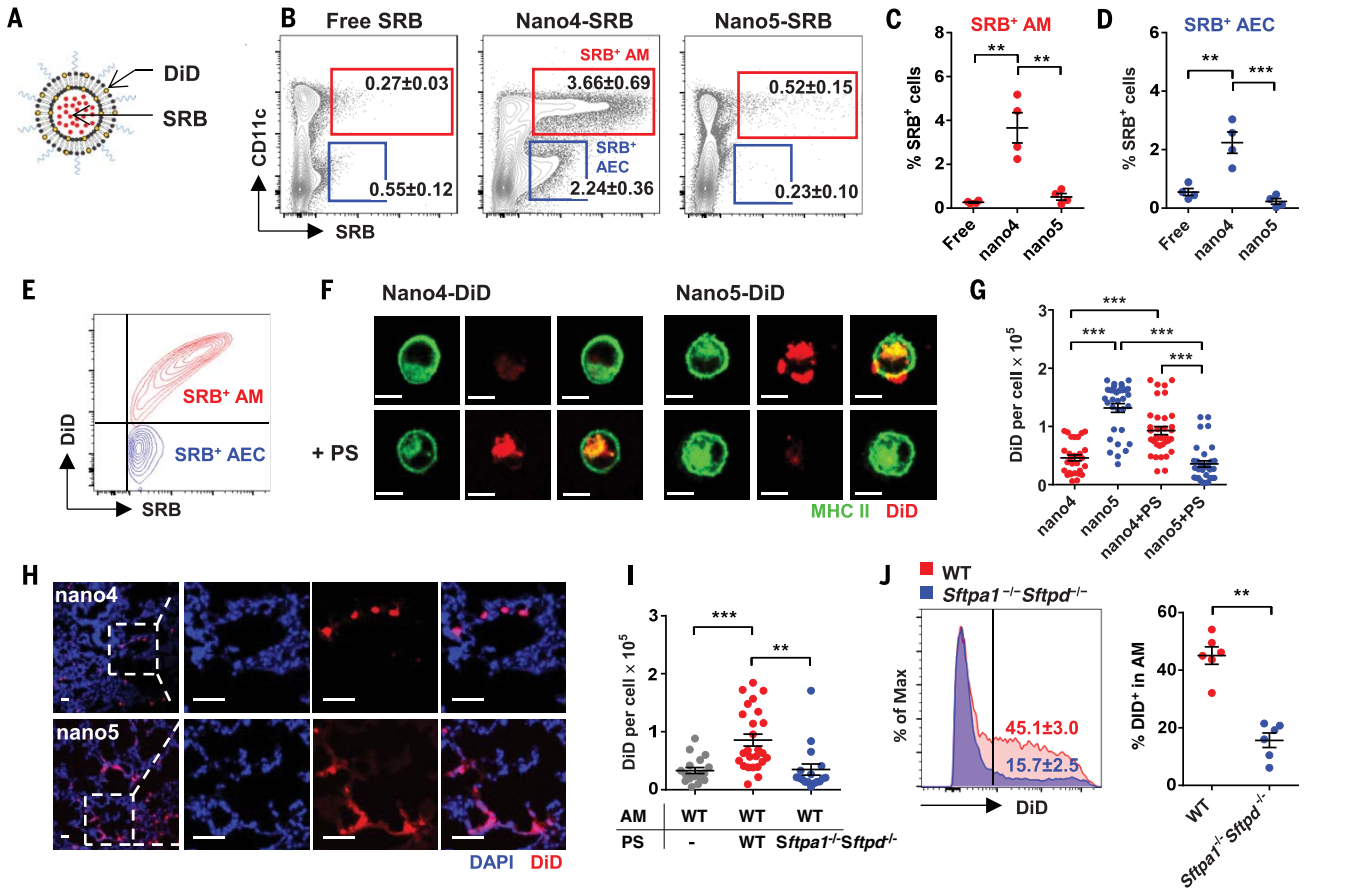

Fig. 1. PS-GAMP uptake by AMs requires SP-A and SP-D. (**A**) A schematic diagram of PS-liposomes labeled with SRB and DiD. (**B** to **E**) Free SRB (20 μg) or SRB-DiD-nano4 or SRB-DiD-nano5 (20 μg SRB) was intranasally administered to mice, followed 12 hours later by flow cytometry analysis of SRB^+ and/or DiD^+ pulmonary cells. The percentages of SRB^+ cells that were also $CD11c^+$ AMs (red) or $CD11c^-$ AECs (blue) were analyzed (B) and quantitated [(C) and (D)] (n = 4 mice). (E) A representative overlay flow cytometry plot of AM and AEC staining for DiD and SRB. (**F**) AMs were isolated from MHC II–GFP mice and incubated with DiD-nano4 or DiD-nano5 for 4 hours after preincubation with (bottom) or without (top) PS for 30 min. Scale bar, 10 μm. (I) Alternatively, AMs were isolated from wild-type (WT) mice and incubated for 4 hours with DiD-nano4 that was pretreated with WT or $Sftpa1^{-/-}Sftpd^{-/-}$ PS for 30 min. (**G** and **I**) The cells were imaged by means of fluorescent microscopy and quantified for DiD fluorescence intensity in individual cells with Image J; n = 18 to 36 cells. (**H**) Lungs were visualized by means of fluorescent microscopy 12 hours after receiving DiD-nano4 or DiD-nano5. Scale bar, 50 μm. (**J**) DiD-nano4 was intranasally administered to WT or $Sftpa1^{-/-}Sftpd^{-/-}$ mice. $CD11c^+CD11b^-CD24^-$ AMs were analyzed 12 hours later for DiD^+; n = 6 mice. Each symbol represents individual mice in (C), (D), and (J) or cells in (G) and (I). The results were presented as means ± SEM. Statistical analysis, one-way ANOVA for (C), (D), (G), and (I) and Student's t test for (J). $^{**}P < 0.01$ and $^{***}P < 0.001$ between indicated groups. All experiments were repeated three times with similar results.

>95% of $CD11c^+SRB^+$ cells (fig. S4A, middle) or 44% of total AMs in the lung (fig. S4B, left). The proportions of SRB^+ AMs and SRB^+ AECs peaked in the lung at 12 hours and 18 hours, respectively, returning to basal levels within 36 hours (fig. S2B). In marked contrast, very few pulmonary $CD103^+$ dendritic cells (DCs) (<2%) and $CD11b^+$ DCs (<2%) were DiD^+ and SRB^+, which ruled out the direct uptake of the liposomes by these cells (fig. S4B). The ability of PS-GAMP to deliver cGAMP into AMs was functionally verified through CD40 up-regulation in DiD^+ AMs after intranasal inoculation with DiD-labeled and cGAMP-encapsulated nano4 (DiD-PS-GAMP). The same nanoparticle lacking cGAMP (DiD-PS) had no effect on CD40 expression (fig. S5, A and B) (*19*). In contrast with nano4, nano5 did not significantly associate with either AMs or AECs when compared with free SRB (Fig. 1, B to D, and fig. S2C). Thus, AM activation appears to result directly from PS-GAMP uptake rather than through a bystander effect (fig. S5C).

Surprisingly, AMs isolated from lung lavage did not efficiently ingest nano4 ex vivo. AMs took up more nano5 than nano4, as evidenced by higher DiD fluorescence (Fig. 1, F and G), which complemented our earlier observation that nano5 induced higher *Ifnb1* expression in BMDCs and BMMs (fig. S1, H and I). Differences between in vivo and ex vivo uptake of these liposomes may have been due to the lack of PS in ex vivo cultures. We therefore purified PS from BALF and incubated the PS with nanoparticles for 30 min before adding them to AMs. Nano4 uptake increased substantially, whereas nano5 uptake was diminished (Fig. 1, F and G). Positively charged nano5 aggregated on the negatively charged PS, explaining its poor entry into AMs (fig. S6). No such aggregates were formed when PS was incubated with nano4 under similar conditions (fig. S6). Similar results were obtained when AMs and PS were isolated from nonhuman primates (fig. S7). Thus, PS may play an evolutionarily conserved role in PS-GAMP endocytosis.

Consistent with these ex vivo observations, DiD-nano4 localized within individual cells positive for Siglec F, a biomarker for AMs, after intranasal administration (Fig. 1H and fig. S8). By contrast, positively charged nano5 electrostatically interacted and fused with negatively charged PS, exhibiting diffuse staining

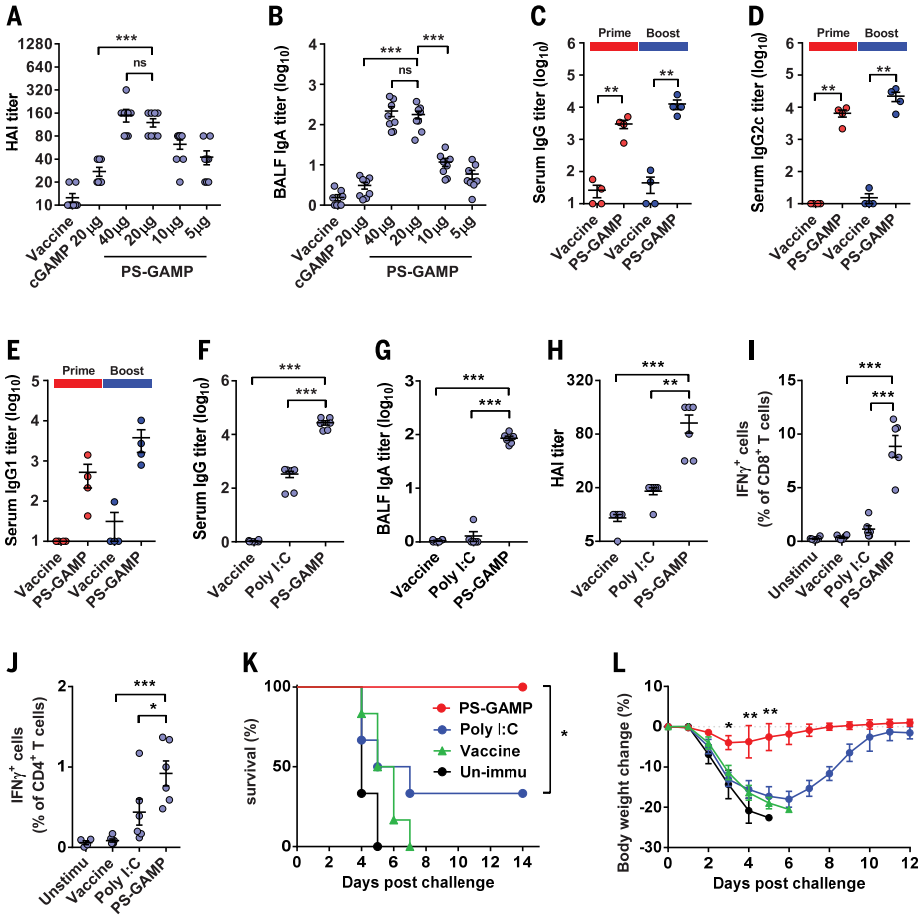

Fig. 2. Adjuvanticity of PS-GAMP. (**A** and **B**) Swiss Webster mice were intranasally immunized with VN04 H5N1 vaccine plus 20 μg of free cGAMP or PS-GAMP containing an indicated amount of cGAMP. Ag-specific serum HAI (A) and BALF IgA (B) titers were measured 2 weeks later; n = 8 mice. (**C** to **E**) C57BL/6 mice were intranasally immunized with VN04 H5N1 vaccine in presence or absence of PS-GAMP (20 μg cGAMP) on day 0 and boosted on day 14. Sera were collected on day 14 (Prime) or 21 (Boost) and measured for Ag-specific IgG (C), IgG2c (D), and IgG1 (E) titers; n = 4 mice. (**F** to **L**) C57BL/6 mice were intranasally immunized with CA09 H1N1 vaccine with or without 20 μg of PS-GAMP or poly(I:C). Serum IgG (F), BALF IgA (G), and serum HAI (H) titers were measured 2 weeks later. [(I) to (J)] Splenocytes were isolated 7 days after immunization and stimulated with the CA09 H1N1 vaccine. $CD8^+$ (I) and $CD4^+$ (J) T cells producing IFN-γ after viral Ag stimulation were determined by means of flow cytometry. [(K) and (L)] Survival curves (K) and changes in body weight (L) of unimmunized mice (black) or mice receiving a single immunization of vaccine alone (green), the vaccine combined with poly(I:C) (blue), or PS-GAMP (red), which were challenged 28 days later with 10 × LD_{50} CA09 H1N1 virus; n = 6 mice. The results are presented as means ± SEM. Each symbol represents individual mice in (A) to (J). Statistical analysis, one-way ANOVA for (A) to (J), two-way ANOVA for (L), and log-rank test for (K). *P < 0.05, **P < 0.01, and ***P < 0.001 in the presence or absence of PS-GAMP. ns, no significance. All experiments were repeated twice with similar results.

along the alveolar surface (Fig. 1H). Distinct localizations of nano4 and nano5 were corroborated by means of transmission electron microscopy (TEM) using nanogold-labeled nano5 and nano4 (fig. S9). In vitro validation of effective uptake of nano4 only in the presence of PS hinted that surfactant protein A (SP-A) and SP-D (termed "collectins") played a role in this uptake. In support, PS isolated from *Sftpa1*$^{-/-}$ *Sftpd*$^{-/-}$ mice failed to enhance nano4 uptake by WT AMs in vitro over controls, in marked contrast to PS isolated from WT mice (Fig. 1I). Moreover, nano4 uptake was severely impeded in *Sftpa1*$^{-/-}$*Sftpd*$^{-/-}$ mice (Fig. 1J), which was not due to any defect of *Sftpa1*$^{-/-}$*Sftpd*$^{-/-}$ AMs because *Sftpa1*$^{-/-}$*Sftpd*$^{-/-}$ AMs took up comparable amounts of nano4 as did WT AMs after preincubation in vitro with WT PS (fig. S10).

PS-GAMP transiently activates innate immunity in the lung

Reliance on SP-A and SP-D in nano4 uptake suggested that a natural and molecule-specific mechanism of particle clearance in the lung was involved, which would be the best approach to sustain the integrity of PS and alveolar epithelial barriers (*20*). Two days after PS-GAMP, whole inactivated VN04H5N1 vaccine, or a combination of both was intranasally administered, mouse lungs, nasal tissue, and brains were indistinguishable, by means of histology, from phosphate-buffered saline (PBS) controls (fig. S11, A and B). There was no cell death, damage to the epithelial barrier, or overt infiltration of inflammatory cells in these tissues (fig. S11). Only modest and transient infiltration of monocytes was found in the lung on day 3, which was markedly less severe than the monocyte response to viral infection (fig. S12E). We also did not observe any significant cytokine production in the brain over controls (fig. S11C). By contrast, administration of a VN04 H5N1 vaccine formulated with cholera toxin (CT) resulted in substantial inflammatory cell infiltration of the lung and measurable cytokine mRNA expression in the brains of some mice (fig. S11).

Although there was a lack of overt lung inflammation over time observed with histology (fig. S13A), PS-GAMP rapidly and robustly, but only transiently, activated innate immunity. *Ifnb1*, *Gmcsf*, and *Tnf* as well as *Ccl2*, *Ccl3*, *Ccl5*, and *Cxcl10* expression peaked 12 hours after stimulation and resolved within 48 hours (fig. S14). By contrast, a low-dose infection with CA09 H1N1 influenza virus induced substantially higher levels of these mediators (fig. S14), giving rise to overt lung inflammation that worsened over the course of viral infection, despite robust *Il10* expression (figs. S13, B and C, and S14). Transient IFN-β protein was also found in BALF, but tumor necrosis factor–α (TNF-α) and interleukin-10 (IL-10) levels were below the limit of detection (fig. S15). Substantially higher levels of these cytokines were produced on days 2 to 6 as infection proceeded (fig. S15). The transient activation of innate immunity was confined to the lung; serum IFN-β, IFN-γ, IL-6, IL-10, and TNF-α levels did not differ from those of controls (fig. S16, C to G). This accorded with the lack of adjuvant side effects on mouse body weight and temperature (fig. S16, A and B).

PS-GAMP is a potent adjuvant for both humoral and cellular immune responses

Although PS-GAMP only transiently activated innate immunity, it was sufficient to augment both humoral and cellular immune responses, which is consistent with our previous findings that prolonged activation of innate immunity was not necessary for strong adaptive immunity (*13*, *21*, *22*). PS-GAMP elevated serum hemagglutination inhibitory (HAI) antibody

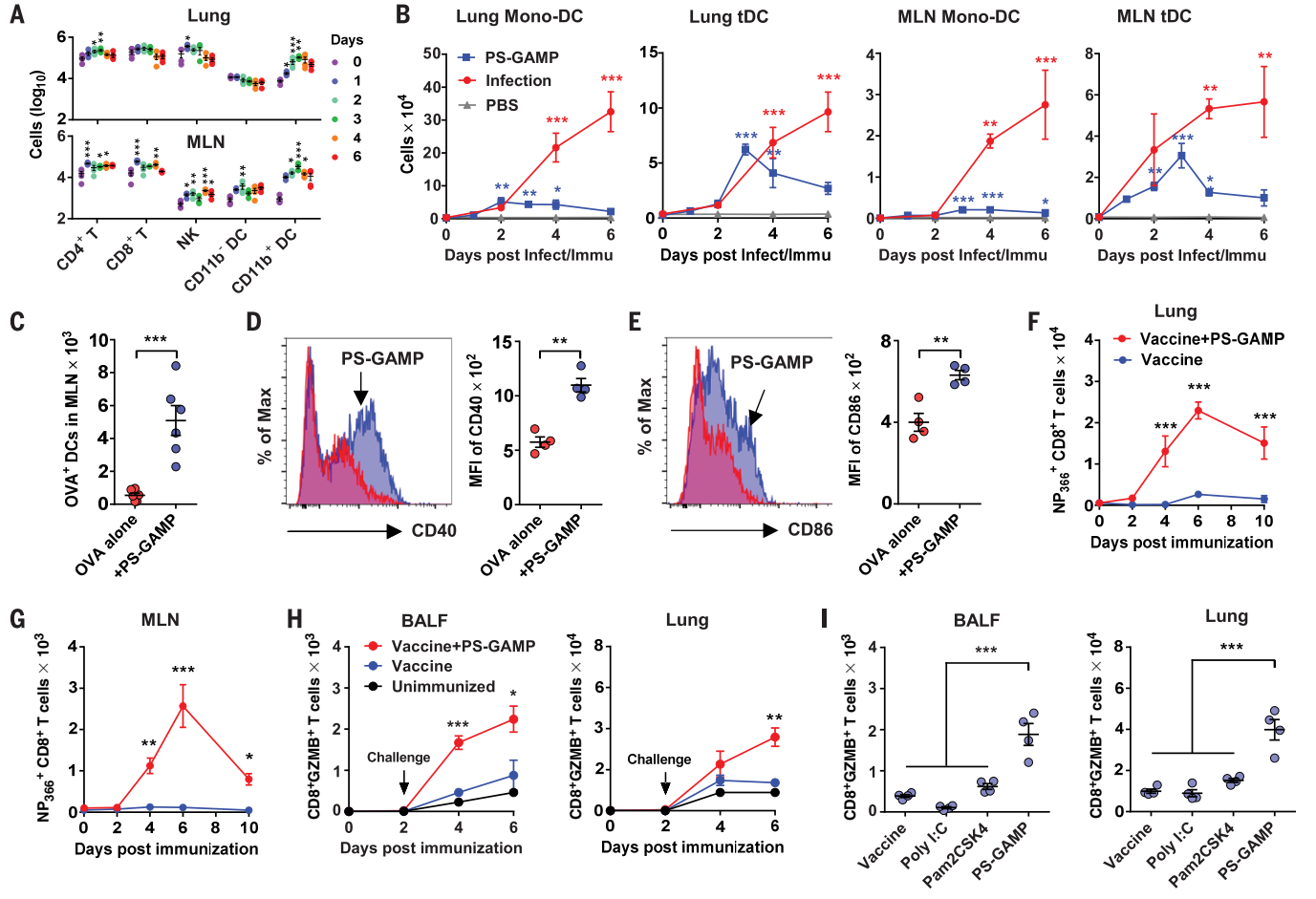

Fig. 3. CD8$^+$ T cell responses are induced by PS-GAMP. (**A**) Numbers of CD4$^+$ and CD8$^+$ T cells, NK cells, and CD11b$^+$ and CD11b$^-$ DCs in the lung (top) and MLN (bottom) were analyzed by means of flow cytometry at an indicated day after mice were intranasally administered with PS-GAMP; n = 4 mice. (**B**) CD11b$^+$ mono-DCs and CD11b$^+$ tDC were quantified by means of flow cytometry in the lung and MLN at an indicated day after mice were intranasally immunized with PS-GAMP or infected with 1 × LD_{50} CA09 H1N1 virus; n = 4 mice. (**C** to **E**) Mice were intranasally vaccinated with OVA-AF647 with or without PS-GAMP. (C) DCs capturing OVA were enumerated in the MLN 36 hours after immunization; n = 6 mice. The mean fluorescence intensity (MFI) of CD40 (D) or CD86 (E) on these DCs was quantified by means of flow cytometry; n = 4 mice. (**F** and **G**) Mice were intranasally immunized with CA09 H1N1 vaccine with or without PS-GAMP or PBS alone as unimmunized controls. CD8$^+$ T cells in the lung and MLN were analyzed on the indicated day after immunization for their Ag-specificity by staining with $NP_{366\text{-}374}$ tetramer; n = 4 to 8 mice. Representative flow cytometry plots are shown in fig. S20A. (**H**) Mice were immunized as described in (F) and (G) and challenged 2 days later with 10 × LD_{50} CA09 H1N1 virus. BALF and lung cells were enumerated for GZMB$^+$CD8$^+$ T cells at indicated days after immunization; n = 4 mice. (**I**) Mice were similarly immunized and challenged as in (H), except that 20 μg of poly(I:C) or Pam2CSK4 was used in place of PS-GAMP for immunization. GZMB$^+$CD8$^+$ T cells were counted 4 days after challenge as in (H); n = 4 mice. Each symbol represents individual mice in (A), (C) to (E), and (I). The results were presented as means ± SEM. Statistical analysis, one-way ANOVA for (A), (B), and (I); two-way ANOVA for (F) to (H); and Student's t test for (C) to (E). *P < 0.05; **P < 0.01, and ***P < 0.001 compared with day 0 [(A) and (B)], influenza vaccine alone [(F) to (H)], or between indicated groups. All experiments were repeated twice with similar results.

and BALF IgA titers in a dose-dependent manner (Fig. 2, A and B). The adjuvant had potent effects on both primary and booster immune responses, raising Ag-specific IgG1 10-fold, IgG more than 100-fold, and IgG2c ~1000-fold over VN04 H5N1 vaccine alone in the serum (Fig. 2, C to E). In addition to the whole inactivated VN04 H5N1 vaccine, PS-GAMP also exhibited strong adjuvanticity when combined with split virion (SV) vaccines such as the A/California/7/2009 (CA09) H1N1 vaccine. The adjuvant augmented HAI titers 10-fold, BALF IgA 60-fold, and IgG 10,000-fold over the SV vaccine alone (Fig. 2, F to H). Under similar conditions, polyinosinic: polycytidylic acid [poly(I:C)] showed substantially less efficacy in augmenting HAI titers, BALF IgA, and serum IgG production (Fig. 2, F to H). PS-GAMP not only augmented humoral immune responses but also profoundly enhanced cellular immune responses. PS-GAMP–adjuvanted CA09 H1N1 vaccine increased IFN-γ$^+$CD8$^+$ T cells 24-fold compared with vaccine alone or eightfold over the vaccine formulated with poly(I:C) (Fig. 2I and fig. S20A). This combination also induced the highest proportion of IFN-γ$^+$CD4$^+$ T cells among all vaccination groups (Fig. 2J and fig. S20A). These robust immune responses translated into full protection against 10× the median lethal dose (LD_{50}) CA09 H1N1 viral challenge, concurrent with only mild to no body weight loss (Fig. 2, K and L). By contrast, poly(I:C)–adjuvanted CA09H1N1 vaccine conferred only partial (33%) protection against the viral challenge, with severe body weight loss.

PS-GAMP elicits robust CD8$^+$ T cell responses

After intranasal administration of PS-GAMP, CD11b$^+$ DCs but not CD11b$^-$ DCs were elevated 14-fold and 36-fold on day 3 relative to day 0 in the lung (Fig. 3A, top) and MLN

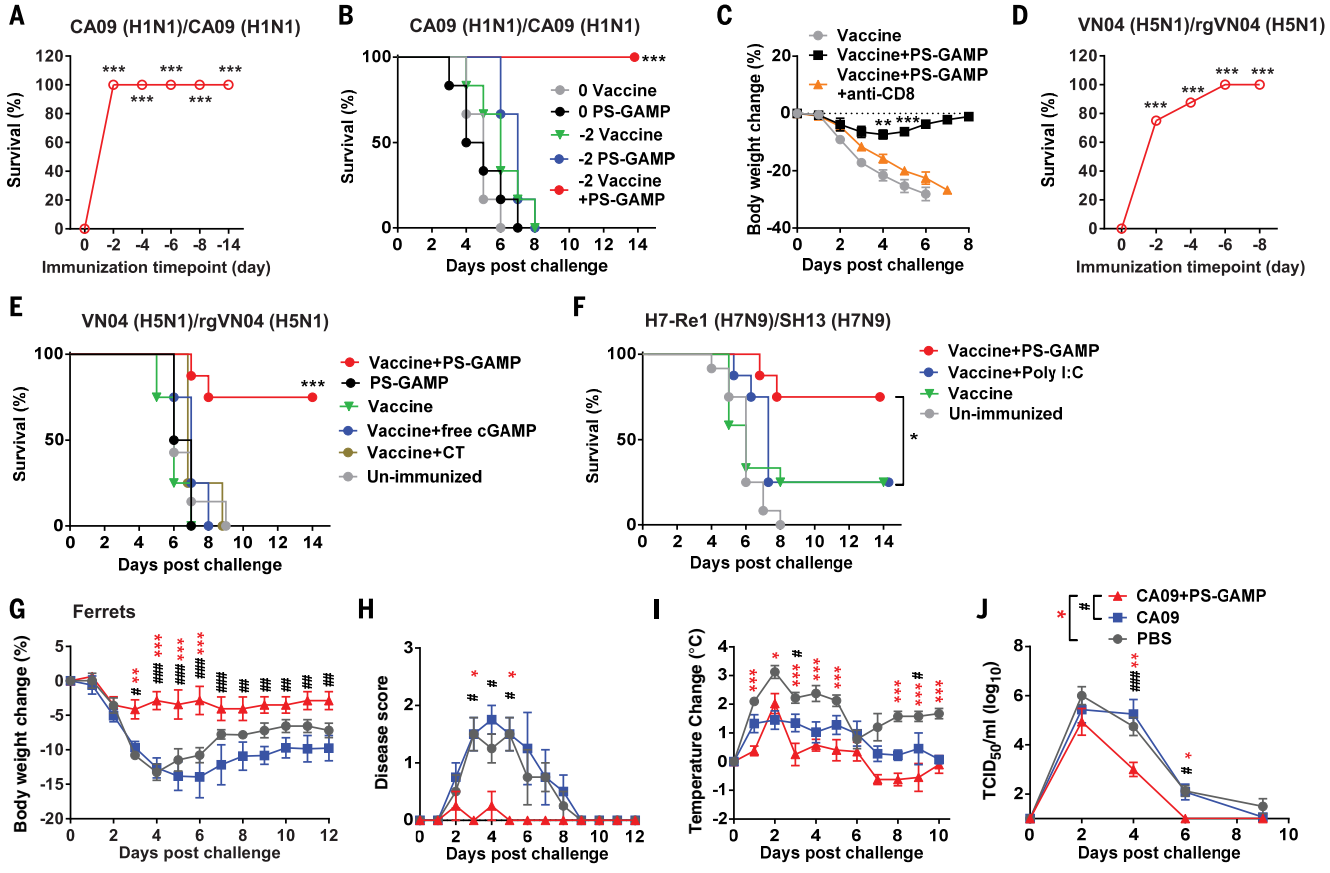

Fig. 4. PS-GAMP mediates early protection. (**A** and **B**) Survival rates of immunized C57BL/6 mice after 10 × LD_{50} CA09 H1N1 viral challenge. (A) The mice were intranasally immunized with CA09 H1N1 vaccine (0.5 μg HA) and PS-GAMP (20 μg cGAMP) on day 2, 4, 6, 8, or 14 before viral challenging (fig. S22A); *n* = 6 to 11 mice. (B) Mice were immunized and challenged either on the same day (0) or 2 days (−2) after immunization; *n* = 6 mice. (**C**) Mice were immunized and challenged 2 days later as in (A). $CD8^+$ T cells were depleted in some mice through injections of antibody to CD8 2 days before and 0, 2, and 4 days after vaccination; *n* = 4 mice. (**D**) Survival rates of mice immunized with VN04 H5N1 vaccine plus PS-GAMP at indicated day before challenge on day 0 with 10 × LD_{50} rgVN04 H5N1 virus (fig. S22A); *n* = 4 to 8 mice. (**E**) Survival rates of mice immunized with VN04 H5N1 vaccine, PS-GAMP, or the vaccine plus free cGAMP, CT, or PS-GAMP, followed with rgVN04 H5N1 viral challenge 2 days later; *n* = 4 to 8 mice. (**F**) Mice were intranasally immunized with H7-Re1 H7N9 vaccine and 20 μg of PS-GAMP or poly(I:C) and challenged 2 days later with a clinically isolated SH13 H7N9 virus at 40 × LD_{50}; *n* = 8 to 12 mice. (**G** to **J**) Ferrets were intranasally immunized with CA09 H1N1 vaccine (9 μg) with or without 200 μg of PS-GAMP and challenged with 10^6 $TCID_{50}$ CA09 H1N1 virus 2 days later. Body weight (G), disease score (H), temperature (I), and nasal wash viral titers (J) were monitored for 12 days; *n* = 4 ferrets. The results were presented as means ± SEM. **P* < 0.05, ***P* < 0.01, and ****P* < 0.001 compared with day 0 [(A) and (D)], vaccine alone [(B), (E), and (F)], or in the presence or absence of antibody to CD8 (C). Mouse experiments were repeated twice with similar results. For ferrets, asterisks indicate significance between PBS and vaccine+PS-GAMP, and pound signs (#) indicate significance between vaccine and vaccine+PS-GAMP. *,#*P* < 0.05; **,##*P* < 0.01; and ***,###*P* < 0.001. Statistical analysis, two-way ANOVA for (C), (G), (I), and (J); Kruskal–Wallis test for (H); and the log-rank test for (A), (B), and (D) to (F).

(Fig. 3A, bottom), respectively. Among $CD11b^+$ DCs, monocyte-derived $CD11b^+$ DCs (Mono-DCs), and tissue-resident $CD11b^+$ DCs (tDCs) were distinguished through major histocompatibility complex II (MHC II) and Ly6C expression (fig. S3B) (*23*, *24*). MHC $II^{hi}CD11b^+$ tDCs are the main lung DC population that cross-presents to $CD8^+$ T cells during influenza viral infection (*23*). After PS-GAMP administration, tDCs expanded to levels matching those seen during the first 3 days of viral infection. By contrast, pro-inflammatory mono-DCs increased only slightly during the same experimental period (Fig. 3B). $CD11b^+$ tDCs declined thereafter in the lung and MLN, in marked contrast to the continued increase of these cells in both the lung and MLN during the 6 days of infection (Fig. 3B). Various other immune cell populations were characterized in the lungs, MLNs, nasal tissue, and brains after immunization or infection (fig. S12). In addition to DCs, only natural killer (NK) cell and $CD4^+$ T cell numbers were briefly elevated for 1 or 2 days in the lung (Fig. 3A).

These $CD11b^+$ DCs appeared to efficiently cross-prime CD8 T cells and induce robust proliferation. When fluorescently labeled ovalbumin (OVA) was intranasally administered, very few lung $CD11b^+$ DCs (0.3%) showed OVA uptake. The proportion of these DCs ingesting OVA, however, rose substantially from 3% at 12 hours to 26% at 36 hours after immunization in the presence of PS-GAMP (fig. S17A). This translated into a 10-fold increase in MLN OVA^+ (mostly $CD11b^+$) DCs compared with that in mice receiving OVA alone (Fig. 3C and fig. S17B). These DCs had matured and were activated, as suggested by CD40 and CD86 up-regulation (Fig. 3, D and E). This effect was presumably secondary to AEC and AM activation because most MLN DCs were PS-GAMP–negative (fig. S17, C and D). The increase in Ag-specific $CD11b^+$ DCs did not result from altered Ag processing or uptake because OVA uptake or its proteolytic cleavage was unaffected by PS-GAMP (fig. S18, D and E). Thus, the enhanced proliferation of transferred OVA-specific OT-I cells in the

presence of PS-GAMP was likely due to the augmented differentiation and maturation of $CD11b^+$ DCs. These cells, in turn, gave rise to a greater than sixfold increase in highly proliferating OT-I cells in both the lungs and MLNs (fig. S19, A to D).

A large number of nucleoprotein $(NP)_{366-374}$–specific $CD8^+$ T cells were observed in the lung and, to a lesser extent, in the MLN, as early as 4 days after immunization with PS-GAMP–adjuvanted influenza vaccine (Fig. 3, F and G, and fig. S20B). $NP_{366-374}$ was the dominant $CD8^+$ T cell epitope, and $CD8^+$ T cells specific for other epitopes, such as $PA_{224-233}$ or $PB1_{703-711}$, were undetectable in these animals, probably because of a low copy number of these proteins in inactivated influenza vaccine (fig. S20C) (*25*). These virus-specific $CD8^+$ T cells expressed the early activation biomarker, granzyme B (GZMB), upon viral challenge (fig. S21A) (*26*). The proportion of $GZMB^+CD8^+$ T cells rose significantly 4 days in BALF and 6 days in the lung after receiving PS-GAMP–adjuvanted CA09 H1N1 vaccine (Fig. 3H). More than 65% of these $GZMB^+CD8^+$ T cells were also positive for $NP_{366-374}$, whereas only ~3% of the cells were positive for $PA_{224-233}$ or $PB1_{703-711}$ (fig. S21B). Under similar conditions, vaccine alone failed to expand $GZMB^+CD8^+$ T cells significantly (Fig. 3H). The $CD8^+$ T cell response evoked by PS-GAMP was superior to poly(I:C) or Toll-like receptor 2 (TLR2) agonist Pam2CSK4 (Fig. 3I) (*27*, *28*). Although T cell immune responses were induced soon after immunization, Ag-specific BALF IgA and IgM were undetectable on day 6 after immunization (fig. S21C). Thus, PS-GAMP mimics crucial events of viral infection such as $CD8^+$ T cell induction without provoking excessive lung inflammation or immunopathology (figs. S11 to S16).

PS-GAMP offers robust protection as early as 2 days after immunization

The rapid induction of $CD8^+$ T cells prompted us to determine how quickly protection could be achieved with PS-GAMP. To this end, mice were challenged on day 0, 2, 4, 6, 8, or 14 after immunization (fig. S22A). Inclusion of PS-GAMP in the vaccination fully protected mice from homologous viral challenges as early as 2 days after immunization (Fig. 4A). At all early challenge time points (days −2, −4, and −6), mice experienced only minor reductions in body weight (<10%) (fig. S22B), and all mice survived (Fig. 4A). When challenged 8 days after immunization, mice showed no body weight loss, with 100% survival (Fig. 4A and fig. S22B). This early protection did not result directly from innate immunity because PS-GAMP alone given on day 0 or 2 prior did not confer any protection (Fig. 4B and fig. S22C). To determine whether $CD8^+$ T cells were responsible for the early protection, $CD8^+$ T cells were depleted by intraperitoneal injections of antibodies to CD8 every other day starting 2 days before and ending 4 days after immunization. Depletion of $CD8^+$ T cells abolished the early protection, as evidenced by a precipitous body weight loss and 100% mortality similar to those of mice receiving vaccine alone (Fig. 4C and fig. S22D). To ensure that this early protection was not specific to the CA09 H1N1 vaccine, we administered the H5N1 vaccine, which is an immunogenically weak vaccine by comparison. PS-GAMP conferred 75 to 100% protection against rgVN04 H5N1 viral challenge for mice immunized 2 to 8 days prior in an adaptive-immune–dependent manner (Fig. 4D and fig. S22E) because no protection was attained with PS-GAMP alone (Fig. 4E and fig. S22F). Under similar conditions, the vaccine combined with CT provided no early protection (Fig. 4E and fig. S22F), arguing persuasively that the heightened inflammation is not necessarily required for strong adaptive immune responses (fig. S11). Mice were also significantly or fully protected from a lethal challenge of a clinical isolate of prepandemic A/Shanghai/4664T/2013 (SH13) H7N9 virus 2 or 14 days after immunization with PS-GAMP–adjuvanted inactivated H7N9 vaccine (H7-Re1) (Fig. 4F and fig. S22, G to I). Vaccine adjuvanted by poly(I:C) provided no benefit over vaccine alone under similar conditions (Fig. 4F and fig. S22I).

The ability of PS-GAMP to quickly establish protection was then validated in a U.S. Food and Drug Administration–approved ferret model. Ferrets receiving PS-GAMP–adjuvanted CA09 H1N1 vaccine 2 days prior experienced <5% body weight loss when infected with homologous CA09H1N1 virus, which is concomitant with mild to no clinical symptoms and only a brief and limited spike in body temperature on day 2 after viral challenges (Fig. 4, G to I). Viral shedding was significantly blunted from day 4 onward (Fig. 4J). By contrast, CA09H1N1 vaccine alone failed to prevent substantial weight loss after a similar viral challenge and did not improve clinical symptoms or reduce viral shedding over controls, despite showing milder increases in body temperature compared with that of controls (Fig. 4, G to J).

AECs are indispensable for PS-GAMP–mediated adjuvanticity

cGAMP can be readily transferred by way of gap junctions presented between AMs and AECs (*29*, *30*). A dynamic flux from AMs to AECs was marked by the gradual loss of SRB in AMs, concurrent with the continuous gain of SRB in AECs from 12 to 18 hours after intranasal administration of SRB-nano4 (fig. S23A). The loss of SRB in AMs could not be ascribed to a loss of the liposomes because the number of DiD^+ cells was unaltered up to 18 hours later (fig. S23B). The entry of SRB into AECs was blocked by carbenoxolone (CBX) (Fig. 5, A and C), a gap-junction blocker (*29*), which did not affect SRB uptake by AMs (Fig. 5, A and B). In AMs and AECs sorted from lungs receiving PS-GAMP, CBX greatly diminished the transcription of *Ifnb1* and *Gmcsf* in AECs while increasing *Ifnb1* transcription in AMs (fig. S24, B and C). This was most likely a consequence of elevated cGAMP levels in the cells. Thus, there is a gap junction–mediated flux of cGAMP to AECs from AMs. By contrast, poly(I:C) remained primarily within AMs (>97%) after intranasal immunization (fig. S25A). Only 0.4% of total AECs and 4% of total DCs took up poly(I:C) in the lung (fig. S25, B and C). MLN and nasal tissue DCs as well as nasal epithelial cells rarely internalized poly(I:C) (fig. S25, D and E).

PS-GAMP induced 100-fold–higher IgG2c titers than did poly(I:C) (Fig. 5D). However, the adjuvanticity was blunted substantially when mice were treated with CBX or two other gap junction inhibitors, tonabersat and meclofenamate, before and during immunization (Fig. 5D) (*31*, *32*). By contrast, these inhibitors had few effects on poly(I:C)–mediated adjuvanticity (Fig. 5D), which is consistent with the inability of poly(I:C), a large molecule, to enter the neighbor cells by way of gap junctions (fig. S25A). The blockade on the entry of cGAMP into AECs reduced recruitment of $CD11b^+$ DCs by 50% (Fig. 5E) and exhibited more profound effects on the early $CD8^+$ T cell responses in both the BALF and lung (Fig. 5, F and G). Moreover, chimeric mice (ST→WT) comprising *Sting*-deficient ($Sting^{-/-}$ or ST) BM cells and WT AECs had similar BALF and lung $CD8^+$ T cell numbers as those of WT→WT mice (Fig. 5, H to J, and fig. S26) (*33*). By contrast, significantly lower numbers of Ag-specific $CD8^+$ T cells were recovered from the BALF and lungs of chimeras with *Sting*-deficient AECs and a WT hematopoietic compartment (WT→ST mice) (Fig. 5, I and J). WT→ST mice showed poor protection by PS-GAMP–adjuvanted CA09 H1N1 vaccine, as suggested by body weight loss and high lung viral titers, in contrast to the similarly observed protection between ST→WT and WT→WT mice (Fig. 5, K and L). There was an inverse correlation between viral titers and the number of $GZMB^+CD8^+$ T cells in the BALF and lung, supporting the notion that $GZMB^+CD8^+$ T cells play a pivotal role in the control of viral infections (Fig. 5, M and N). Thus, AECs rather than AMs appear to be essential for determining the potency of PS-GAMP, which is consistent with their critical role in orchestrating innate and adaptive immune responses in the respiratory system during viral infection (*24*, *34*–*36*).

PS-GAMP broadens protection against heterosubtypic influenza viruses

Mice that received CA09H1N1 vaccine (Fig. 6, A to F) or A/Shanghai/37T/2009 (SH09) H1N1

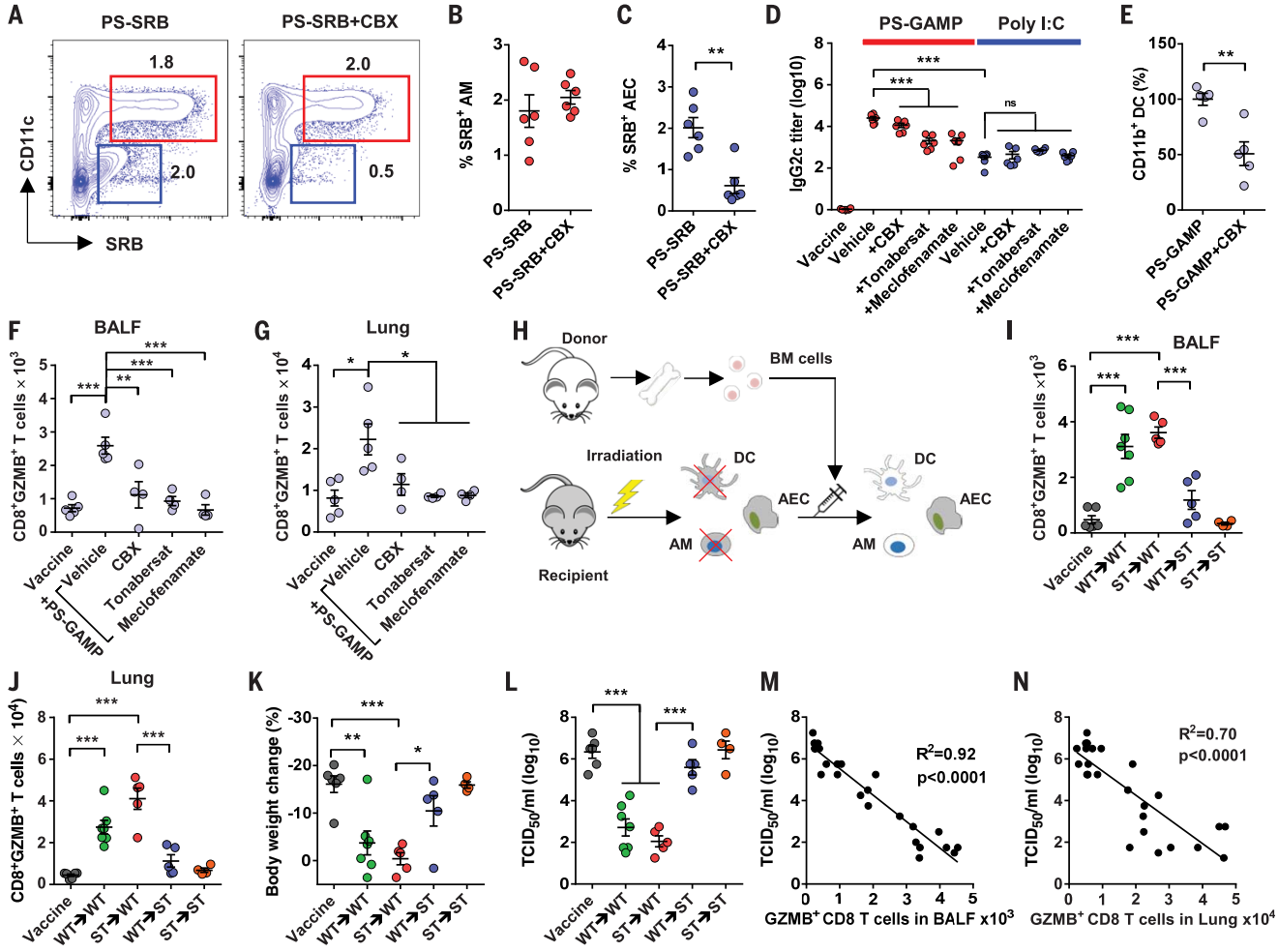

Fig. 5. AECs make an indispensable contribution to PS-GAMP adjuvanticity. (**A**) Mice were intraperitoneally administered CBX once a day for 3 consecutive days, after which SRB-nano4 was intranasally administered to the mice. (**B** and **C**) Percentages of SRB$^+$ AMs (red) and AECs (blue) that were analyzed 12 hours after (A); *n* = 6 mice. (**D**) Mice were intraperitoneally administered CBX, tonabersat, or meclofenamate and intranasally immunized with CA09 H1N1 vaccine with or without 20 μg of poly(I:C) or PS-GAMP. Sera were collected 14 days later and analyzed for IgG2c; *n* = 6 mice. (**E**) Mice were immunized with CA09 H1N1 vaccine and PS-GAMP in the presence or absence of CBX as in (D). Lung CD11b$^+$ DCs were counted 24 hours later; *n* = 4 mice. (**F** and **G**) Mice receiving an indicated gap junction inhibitor were immunized as in (D) and challenged with 10 × LD_{50} CA09 H1N1 virus 2 days later. GZMB$^+$CD8$^+$ T cells in BALF (F) and the lung (G) were analyzed by means of flow cytometry; *n* = 4 mice. (**H**) A schematic diagram of generating chimeric mice. Mice were administered lethal irradiation before BM cell transfer. Chimeras were confirmed after 3 months (fig. S26), immunized, and challenged as in (F). (**I** and **J**) Four days after challenge, GZMB$^+$CD8$^+$ T cells were enumerated by means of flow cytometry in BALF (I) and lung (J). (**K** and **L**) Changes in body weight relative to day 0 (K) and lung viral titers (L) were also measured; *n* = 4 to 7 mice. (**M** and **N**) A correlation between the number of GZMB$^+$CD8$^+$ T cells and viral titers was determined by means of regression analysis. The results were presented as means ± SEM. Each symbol represents individual mice. Statistical analysis, one-way ANOVA for (D), (F), (G), and (I) to (L); Student's *t* test for (B), (C), and (E). **P* < 0.05, ***P* < 0.01, and ****P* < 0.001. All experiments were repeated twice with similar results.

vaccine (Fig. 6, G and H), together with PS-GAMP, were highly protected from lethal challenges with distinct PR8 H1N1 virus and heterosubtypic A/Aichi/2/1968 (Aichi) H3N2, rgVN04 H5N1, or the highly pathogenic SH13 H7N9 virus, irrespective of whether the animals were infected at either 2 days (Fig. 6, A, C, E, and G) or 14 days (Fig. 6, B, D, F, and H) after immunization (fig. S27, A to H). This vaccination strategy also protected mice from an oseltamivir-resistant A/North Carolina/39/2009 H1N1 virus with an H275Y mutation (NC09) [in which histidine (H) at position 275 was replaced with tyrosine (Y)] (Fig. 6I and fig. S27I), which emerged during 2009 H1N1 pandemic and H7N9 epidemic (*37*, *38*). The resistance of this virus to oseltamivir was verified by the ability of oseltamivir to effectively control CA09H1N1, but not NC09, viral infection (Fig. 6I). Under similar conditions, H1N1 vaccines alone provided little to no protection against challenges with these heterosubtypic variants (Fig. 6, A to I, and fig. S27, A to I). In contrast to PS-GAMP, poly(I:C)–adjuvanted SH09 H1N1 vaccine failed to generate significant heterosubtypic protection against H7N9 virus (Fig. 6, G and H, and fig. S27, G and H). In addition to monovalent vaccines, PS-GAMP enhanced the breadth of immune responses induced by trivalent 2018–2019 seasonal influenza vaccines (SIV18-19) against mismatched reassortant A/Guizhou/54/1989 H3N2 (rgGZ89) virus (Fig. 6J and fig. S27J) or Florida/4/2006 influenza B virus from Yamagata-lineage (fig. S28). Thus, PS-GAMP appears to be similarly effective for both influenza A and B viral vaccines.

Long-lived Ag-specific memory CD8$^+$ T cells capable of rapid recall upon viral infection are

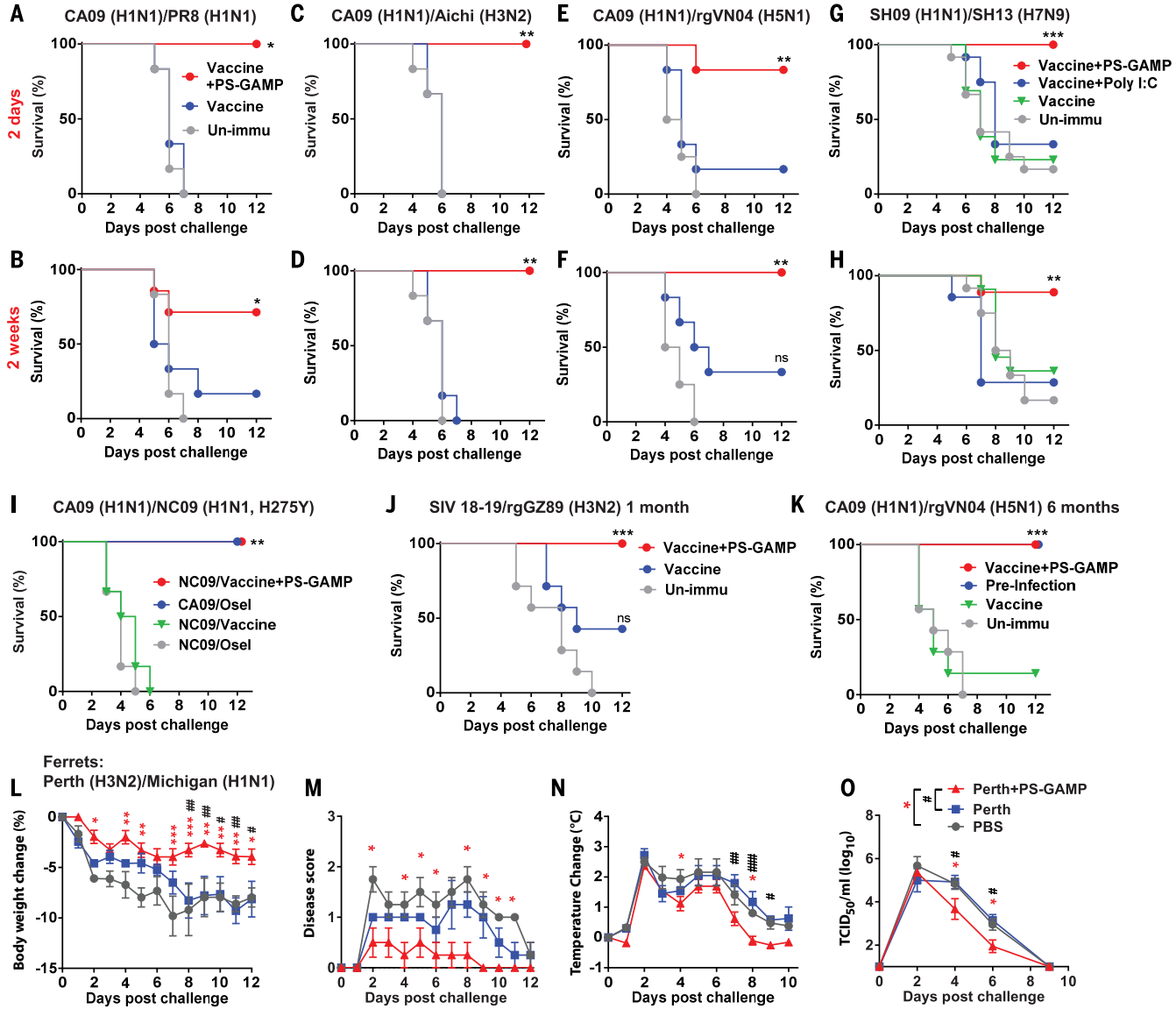

Fig. 6. PS-GAMP broadens cross-protection against heterosubtypic influenza A viruses. (**A** to **H**) Mice were intranasally immunized with CA09 H1N1 vaccine except for SH09 H1N1 vaccine in (G) and (H) or the vaccine plus PS-GAMP and challenged 2 days (top row) or 2 weeks (bottom row) later with 5 × LD_{50} distant PR8 H1N1 virus [(A) and (B)] and heterosubtypic Aichi H3N2 [(C) and (D)], rgVN04 H5N1 [(E) and (F)], or SH13 H7N9 virus [(G) and (H)]; n = 6 to 7 mice for (A) to (F) and n = 8 to 13 mice for (G) and (H). (**I**) Mice were immunized as in (A) and challenged 2 days later with 10 × LD_{50} oseltamivir-resistant NC09 H1N1 virus. Unimmunized mice were treated with oseltamivir (20 mg/kg/day) 6 hours before challenge and then daily after viral challenge until the end of the study. The treated mice were challenged with either 10 × LD_{50} CA09 H1N1 or NC09 H1N1 virus; n = 6 mice. (**J**) Mice were immunized with 2018–2019 trivalent seasonal influenza vaccine (SIV18-19) alone or alongside PS-GAMP and challenged 1 month later with 5 × LD_{50} mismatched GZ89 H3N2 virus; n = 6 to 12 mice. (**K**) Mice were immunized with CA09 H1N1 vaccine alone or together with PS-GAMP and challenged 6 months later with 5 × LD_{50} heterosubtypic rgVN04 H5N1 virus. Alternatively, mice were infected with 1 × LD_{50} PR8 H1N1 virus, and the mice that survived the infection were challenged again 6 months later with 5 × LD_{50} rgVN04 H5N1 virus for comparison (preinfection); n = 6 to 7 mice. (**L** to **O**) Ferrets were intranasally immunized with inactivated Perth H3N2 vaccine (15 μg) with or without PS-GAMP (200 μg). Thirty days after immunization, ferrets were challenged with 10^6 $TCID_{50}$ heterosubtypic Michigan15 H1N1 virus. Body weight (L), disease score (M), temperature (N), and nasal wash viral titers (O) were monitored for 12 days; n = 4 ferrets. The results were presented as means ± SEM. Mice, $^*P < 0.05$, $^{**}P < 0.01$, and $^{***}P < 0.001$ compared with unimmunized mice. Experiments with mice were repeated twice with similar results. For ferrets, asterisks indicate significance between PBS and Vaccine+PS-GAMP, and pound signs (#) indicate significance between Vaccine and Vaccine+PS-GAMP. *,#$P < 0.05$; **,##$P < 0.01$, and ***,###$P < 0.001$. Statistical analysis, two-way ANOVA for (L), (N), and (O); Kruskal–Wallis test for (M); and the log-rank test for (A) to (K).

critical for the control of viral replication in the lung (*2*, *3*). In mice that received OT-I cells, the number of lung $CD8^+CD103^+CD49a^+CD69^+$ T_{RM} cells rose 20-fold after immunization with OVA combined with PS-GAMP relative to OVA alone (fig. S29, A to C). Moreover, PS-GAMP–adjuvanted CA09 H1N1 vaccine fully protected mice from heterosubtypic rgVN04 H5N1 viral challenge 6 months after a single immunization (Fig. 6K and fig. S27K). This long-term cross-protection concurred with durable influenza-specific $CD8^+$ T_{RM} cells in the lung, which could also be readily detected 6 months after immunization (fig. S29, D and E). These $CD8^+$ T_{RM} cells, rather than

circulating memory $CD8^+$ T cells, contributed to the long-term protection observed because their function was not compromised by T cell egress inhibitor FTY720 (fig. S30) (*3*).

Heterosubtypic immunity was further corroborated in ferrets by means of immunization with PS-GAMP alongside inactivated rgPerthH3N2 vaccine. The body weight and temperature of these animals did not differ from those receiving PBS or the vaccine alone, demonstrating a good safety profile for PS-GAMP in ferrets (fig. S31, A and B). The immunization induced 40-fold higher serum IgG titers and fivefold higher HAI titers against homologous Perth H3N2 virus than vaccine alone did 28 days after immunization (fig. S31, C and D), but no HAI antibody was detected against heterosubtypic A/Michigan/45/2015 H1N1 (Michigan H1N1) virus, as anticipated (fig. S31E). Ferrets receiving the vaccine and PS-GAMP, when challenged with Michigan H1N1 virus, showed significantly less body weight loss and milder clinical symptoms, especially in the late phase (>7 days) of the infection, and normalized their temperature more quickly compared with animals that received PBS or vaccine alone (Fig. 6, L to N). PS-GAMP–treated ferrets also shed significantly lower amounts of virus 2 days after infection (Fig. 6O). Thus, the ability to induce heterosubtyptic immunity in ferrets by PS-GAMP–adjuvanted inactivated influenza vaccines suggests the potential for PS-GAMP use in humans.

Discussion

The development of a universal influenza vaccine that confers protection against not only intrasubtypic variants but other subtypes of influenza viruses as well would be highly desirable. However, despite decades of extensive investigation, whether such universal influenza vaccines are achievable remains unclear. It has been long recognized in both humans and animal models that viral infection can stimulate heterosubtypic immunity primarily mediated by $CD8^+$ T cells (*2*, *3*, *6*). In this work, a single immunization with inactivated H1N1 vaccine adjuvanted with PS-GAMP confers protection against lethal challenges with H1N1, H3N2, H5N1, or H7N9 viruses as early as 2 days after immunization. This cross-protection was sustained for at least 6 months, concurrent with durable virus-specific $CD8^+$ T_{RM} cells in the lung. This was largely due to the fact that PS-GAMP–adjuvant influenza vaccine simulated viral infection–induced immunity, characterized by AEC activation, rapid $CD11b^+$ DC recruitment and differentiation, and robust $CD8^+$ T cell responses in the respiratory system. PS-GAMP is a standalone adjuvant, compatible with not only inactivated influenza viral vaccines but also vaccines comprising cocktails of multiple B and T cell epitopes or influenza vaccine subunits. The ability of PS-GAMP to potentiate nonreplicating influenza vaccines for strong heterosubtypic immunity makes it a promising adjuvant for "universal" influenza vaccines if its efficacy can be shown in humans. As such, it would offer a substantial advantage over "replicating" vaccines.

Distinct from conventional vaccine adjuvants that target primarily APCs, PS-GAMP activated both AMs and AECs, with activation of the latter appearing to be crucial for its adjuvanticity. Pharmacological inhibition of gap junctions and *Sting* deficiency in AECs both diminished the adjuvanticity of this preparation considerably. By contrast, *Sting* deficiency in myeloid cells did not. The pivotal role played by AECs over AMs in orchestrating innate and adaptive immune responses is in agreement with what has been described during the early phase of influenza viral infection (*24*). The ability of cGAMP to enter AECs without breaching the PS layer was ascribed to SP-A/D-receptor–mediated endocytosis after incorporation of SP-A and SP-D into PS-biomimetic liposomes, which is not feasible in any non–PS-biomimetic liposomes (*39*–*41*). Additionally, this adjuvant could induce robust protection within just 2 days after immunization, which is in sharp contrast to current influenza vaccines, which require at least 10 to 14 days to be effective. Early cross-protection is extremely important to protect first responders and high-risk individuals, especially when antiviral drug-resistant viruses or highly pathogenic viruses such as H5N1 and H7N9 viruses emerge to become pandemics. Because viral spreading can accelerate exponentially after a transition from an epidemic to pandemic, early protection would be the most effective means to confine viral spreading during an epidemic phase and prevent pandemics, potentially saving millions of lives (*42*).

Materials and methods

PS-GAMP synthesis

All lipids were purchased from Avanti Polar Lipids, including 1,2-dipalmitoyl-sn-glycero-3-phosphocholine (DPPC), 1,2-dipalmitoyl-sn-glycero-3-phospho-(1'-rac-glycerol) (DPPG), 1,2-dipalmitoyl-3-trimethylammonium-propane (DPTAP), and 1,2-dipalmitoyl-sn-glycero-3-phosphoethanolamine-N-[methoxy(polyethylene glycol)-2000] (DPPE-PEG2000). Cholesterol was obtained from Sigma Aldrich. The mass ratio of nano4 and nano6 was DPPC/DPPG/DPPE-PEG/Chol at 10:1:1:1. The lipids were dissolved in 3 ml of chloroform and mixed with 1 ml cGAMP solution (200 μg cGAMP, 13.7 mM NaCl, 0.27 mM KCl, 0.43 mM Na_2HPO4, and 0.147 mM KH_2PO4). Alternatively, cGAMP was replaced with SRB (Sigma Aldrich) and/or 0.5 μmol DiD dye (Life Technologies) was added to the lipid mixture to label cargo or liposome membrane, respectively. The liposomes were synthesized by reverse-phase evaporation (*43*). In brief, the mixture of lipids and cGAMP was sonicated to achieve a water-in-oil emulsion under N_2 for 30 min at 50°C, followed by gentle removal of the solvent via rotary evaporation at a speed of 220 rpm. An excess amount of buffer was added to the mixture and continuously rotated for another 5 min at 50°C. Resultant liposomes were extruded through 400- and 200-nm membranes (Avanti Polar Lipids) at 50°C. The size and zeta potential of liposomes were measured by Zetasizer (Malvern). Encapsulation efficiency was determined by UV absorption of cGAMP at 260 nm in Nanodrop (Life Technologies) and confirmed by liquid chromatography-mass spectrometry (LC-MS) (Agilent). Free cGAMP was removed by a size-exclusion column G-50 (GE Healthcare). To stabilize the liposomes, trehalose was added to the liposome suspension at a final concentration of 2.5%. The resultant suspension was frozen in dry ice/ethanol bath and then lyophilized at −45°C under vacuum by Freezone 4.5 (Labconco). The lyophilized liposome (PS-GAMP) was stored at −20°C until use and used in all in vivo studies unless otherwise specified.

Animals

C57BL/6J and BALB/c mice were purchased from Jackson Laboratories or Shanghai SLAC Laboratory Animal Co. *Sting*-deficient mice (C57BL/6J-Tmem173 gt/J), *Sftpa1*$^{-/-}$*Sftpd*$^{-/-}$ mice (B6.Cg-Sftpa1tm2Haw Sftpdtm2Haw/J), C57BL/6 CD45.1 mice (B6.SJL-Ptprca Pepcb/BoyJ), and Swiss Webster mice were attained from Jackson Laboratories or Charles River Laboratories. MHC II-EGFP mice expressing MHC class II molecule infused into enhanced green fluorescent protein (EGFP) was a kind gift of H. Ploegh, Massachusetts Institute of Technology. Influenza-free 4-month-old female ferrets were purchased from Marshall BioResources. Healthy naïve 6-year-old male rhesus macaques were obtained from Beijing Institute of Xieerxin Biology Resource, China. The animals were housed in the pathogen-free animal facilities of Massachusetts General Hospital (MGH) or Fudan University in compliance with institutional, hospital, and NIH guidelines. The studies were reviewed and approved by the MGH or Fudan University Institutional Animal Care and Use Committee.

Influenza viruses and vaccines

SH13 H7N9 virus (A/Shanghai/4664T/2013), SH09 H1N1 virus (A/Shanghai/37T/2009), and reverse-genetically (rg) modified GZ89 H3N2 (rgGZ89 H3N2) virus consisting of H3 and N2 of A/Guizhou/54/1989 H3N2 virus and A/Puerto Rico/8/1934 (PR8) viral backbone were obtained from Fudan University. Pandemic CA09 H1N1 virus was requested from the American Type

Culture Collection (ATCC, #FR-201). PR8 (NR-348), A/Aichi/2/68 H3N2 (Aichi, NR-3177), rgPerth H3N2 (NR-41803), and B/Florida/4/2006 (Florida06, NR-9696) viral strains were obtained from BEI Resources, NIAID. rgVN04 H5N1 virus was a kind gift of R. Webby, St. Jude Children's Research Hospital, which comprised H5 and N1 genes from A/Vietnam/1203/2004 H5N1 virus and a PR8 viral backbone. A/Michigan/45/2015 H1N1 (Michigan15, FR-1483) and antiviral drug-resistant A/North Carolina/39/2009 H1N1 viruses (NC09, FR-488) were acquired from International Reagent Resources, CDC. Viruses were expanded in 10-day-old embryonated chicken eggs (Charles River Laboratories) at 35°C for 3 d, harvested, purified by sucrose gradient ultracentrifugation, and frozen at −80°C. To challenge mice, the virus was adapted in mice for three cycles of intranasal instillation–lung homogenate preparation, and their infectivity in mice was assayed by the LD_{50} following a standard protocol.

Monovalent CA09 H1N1 vaccine (NR-20347, Sanofi Pasteur) and whole inactivated H5N1 vaccine (NR-12148, Baxter AG) were obtained from BEI Resources, NIAID. H7-Re1 H7N9 whole inactivated vaccine was a kind gift from Harbin Veterinary Research Institute, Chinese Academy of Agricultural Sciences. Trivalent seasonal influenza vaccine 2018-2019 (SIV 18-19) was attained from Hualan Biological Bacterin Co., China. SH09 H1N1 and Perth H3N2 inactivated vaccines were made by inactivation of the viruses with 0.02% formalin for 24 hours at 37°C and purified as above. Ag concentration was quantified by the BCA protein assay and SDS–polyacrylamide gel electrophoresis based on HA content.

Mouse immunizations and challenges

Mice were sedated with ketamine/xylazine and intranasally inoculated with 30 μl (15 μl per nostril) of an indicated influenza vaccine or a mixture of the vaccine and an adjuvant. VN04 H5N1, SIV 18-19, and CA09 H1N1 SV vaccines were employed at a corresponding dose of 1 μg (HA content), 1 μg, or 0.5 μg per mouse, respectively, whereas H7-Re1 and SH09 H1N1 vaccines each were administered at 0.25 μg or 3 μg per dose, respectively. Poly(I:C) (Invivogen), Pam2CSK4 (Invivogen), and cholera toxin (Sigma) each were administered at 20, 20, or 10 μg per mouse, respectively. To block gap junctions, CBX, tonabersat, and meclofenamate were obtained from Sigma Aldrich and intraperitoneally injected into individual mice for 4 consecutive days (from 2 days prior to 1 day after immunization) at corresponding dosages of 25, 10, or 20 mg/kg/day, respectively (*31*, *32*). To deplete $CD8^+$ T cells during vaccination and challenge, mice were administered anti-CD8α (53-6.7, BioLegend) antibody 2 days prior and in 0, 2, and 4 days after immunization at a dose of 200 μg/day. C57BL/6 mice were used for the challenge studies, except for Aichi H3N2, Florida06 influenza B, and GZ89 viruses which challenged Swiss Webster mice or BALB/c mice instead unless otherwise indicated, because C57BL/6 mice were relatively less susceptible to these viruses. To verify antiviral drug resistance of the NC09 virus, unimmunized mice were treated with oseltamivir (20 mg/kg/day) at 6 hours before the challenge and then daily until the end of the study. Immunized and control mice were challenged with intranasal instillation of 10 × LD_{50} mouse-adapted homologous virus at an indicated day after immunization, except for H7N9 virus at 40 × LD_{50}. However, heterologous viruses each at 5 × LD_{50} were utilized for challenges except for Florida06 influenza B virus at a dose of 4×10^5 median tissue culture infectious dose ($TCID_{50}$) as this virus is not lethal to mice. Body weight and survival were monitored daily for 12 days after the challenge.

Ferret immunizations and challenges

Four-month-old female ferrets negative to anti-influenza virus antibody were anesthetized by ketamine/xylazine/atropine and intranasally immunized with a vehicle, an influenza vaccine, or a mixture of the vaccine and PS-GAMP. To assay early protection, each ferret receiving 9 μg of CA09 H1N1 vaccine alone or alongside 200 μg of PS-GAMP was challenged with 10^6 $TCID_{50}$ CA09 H1N1 viruses 2 days post-immunization. To evaluate cross-protection, each ferret was intranasally immunized with 15 μg of PerthH3N2 vaccine in the presence or absence of 200 μg of PS-GAMP and challenged with 10^6 $TCID_{50}$ heterosubtypic Michigan15 H1N1 viruses 30 days after immunization. Body temperature was monitored by two microchips implanted in each animal (BioMedic Data Systems) and clinical symptoms were scored according to a published protocol (table S1) (*44*). Animals were euthanized humanely 2 weeks after viral challenge by sedation and injection of 0.5 ml of Euthanasia-III into the heart.

Tissue processing and flow cytometry

Lungs, nasal tissues, MLNs, and spleens were dissected from indicated mice and processed into single-cell suspensions for analysis by flow cytometry. Specifically, the lung and nasal tissues were minced into 1-mm^2 pieces, digested with 1 ml of collagenase D (2 mg/ml)/DNase I (5 mg/ml), both from Roche, at 37°C for 60 min, and then passed through 40-μm cell strainers (*18*). To collect BALF, mice were first perfused thoroughly with ice-cold PBS followed by intratracheal lavage with 0.5% BSA in PBS. Single-cell suspensions of the spleen and MLN were prepared by passing the tissues through 40-μm cell strainers directly. After removal of red blood cells in ACK buffer, the remaining cells were washed, blocked by anti-CD16/CD32 antibody (clone 93,10 μg/ml, BioLegend) for 20 min, and stained with fluorescently conjugated antibodies for 30 min on ice or $NP_{366-374}$, $PA_{224-233}$, $PB1_{703-711}$ MHC I tetramers for 1 hour on ice. Activated T cells were fixed and permeabilized after surface staining, followed by intracellular staining with anti-granzyme B antibody at 4°C overnight. Stained cells were acquired on a FACSAria II (BD) and analyzed using FlowJo software (Tree Star). Cell populations and subsets in the mouse respiratory system were gated and analyzed as described (*18*). The information of various antibodies is provided in table S2.

Cytokine and chemokine measurements

C57BL/6 mice were intranasally administered 20 μg of PS-GAMP or infected with 1 × LD_{50} CA09 H1N1 virus. Lungs were harvested at indicated times and prepared for total RNA extraction with an RNA purification kit (Roche). To measure cytokines in brains, mice were intranasally administered VN04 H5N1 vaccine (1 μg HA) alone or together with PS-GAMP (20 μg) or CT (10 μg) and sacrificed 48 hours later to collect the brain tissue for RNA extraction as above. The RNA was reverse-transcribed (Life technologies) and amplified by real-time PCR using an SYBR Green PCR kit (Roche). Glyceraldehyde 3-phosphate dehydrogenase (GAPDH) served as an internal control. All primers used are listed in table S3. Mouse GM-CSF (eBioscience), IFN-β (Invivogen), TNF-α (BioLegend), IFN-γ (eBioscience), IL-6 (eBioscience), and IL-10 (BioLegend) levels in BALF and serum were measured by specific ELISA kits.

Histology

Swiss Webster mice were intranasally administered PBS, PS-GAMP (20 μg), H5N1 vaccine (1 μg HA), or the vaccine plus PS-GAMP or CT (5 μg). Some mice were infected by CA09 H1N1 virus (250 PFU) as positive controls. Lungs, nasal tissue, and brains were dissected at indicated days after immunization or infection, fixed, and stained using a standard H&E procedure. The slides were scanned and analyzed using a NanoZoomer (Hamamatsu).

Confocal microscopy

To track DiD-labeled liposomes in the lung, C57BL/6 mice were intranasally administered an equal amount of DiD-nano4 or DiD-nano5. Lungs were excised after 12 hours, embedded in an optimal cutting temperature (OCT) compound (Sakura Finetek), and cut into 5-μm frozen sections. The slides were mounted with a ProLong Antifade Mountant containing DAPI (Life Technologies) and imaged by confocal microscopy (Olympus FV1000, UPLSAPO 60XW). To visualize AM uptake of nanoparticles ex vivo, mouse lungs were lavaged six times with 1 ml of PBS containing 0.5% BSA and 5 mM EDTA. The lung lavage was pooled and centrifuged at 220 × *g*. The cells were collected, washed

thoroughly by PBS, and cultured in RPMI 1640 medium for 45 min, followed by removal of nonadherent cells. The adherent cells were collected as AMs, suspended at 2×10^5 cells/ml in medium, and added to 96-well-plates at 200 μl/well. To purify PS, lung lavage was prepared by washing the lung for six times with 1 ml of PBS and centrifuged at $220 \times g$ for 10 min to remove cell debris and then at $100{,}000 \times g$ for 1 hour to pellet PS. The supernatant (6 ml) was concentrated to 200 μl by 3-kDa Amicon Ultra Centrifugal Filter Units (Merk Millipore) and mixed with PS pellet prepared above. The resultant PS (100 μg total protein) was then mixed with DiD-nano4 or DiD-nano5 (12 μg lipid content in nanoparticles) for 30 min before added to AM cell culture with 4×10^4 cells in 200 μl of medium. After 4 hours incubation under 5% CO_2 at 37°C, cells were stained with a vital dye Calcein-AM (Life Technologies). Uptake of liposomes was quantified by confocal microscopy (Olympus FV1000, UPLSAPO 60XW) followed by ImageJ software analysis.

Statistical analysis

A two-tailed Student's *t* test was used to analyze differences between two groups. analysis of variance (ANOVA) or Kruskal–Wallis test was used to analyze differences among multiple groups by PRISM software (GraphPad). A P value of <0.05 was considered statistically significant. Sample sizes were determined on the basis of preliminary experiments to give a statistical power of 0.8. Most experiments were repeated at least twice with similar results. The investigators were not blinded to the experiments which were carried out under highly standardized and predefined conditions, except for microscopy images and H&E slide examinations, which were evaluated in an investigator-blind manner.

REFERENCES AND NOTES

1. C. I. Paules, S. G. Sullivan, K. Subbarao, A. S. Fauci, Chasing seasonal influenza—The need for a universal influenza vaccine. *N. Engl. J. Med.* **378**, 7–9 (2018). doi: 10.1056/NEJMp1714916; pmid: 29185857
2. A. Pizzolla *et al*., Influenza-specific lung-resident memory T cells are proliferative and polyfunctional and maintain diverse TCR profiles. *J. Clin. Invest.* **128**, 721–733 (2018). doi: 10.1172/JCI96957; pmid: 29309047
3. K. D. Zens, J. K. Chen, D. L. Farber, Vaccine-generated lung tissue-resident memory T cells provide heterosubtypic protection to influenza infection. *JCI Insight* **1**, 85832 (2016). doi: 10.1172/jci.insight.85832; pmid: 27468427
4. S. Sridhar *et al*., Cellular immune correlates of protection against symptomatic pandemic influenza. *Nat. Med.* **19**, 1305–1312 (2013). doi: 10.1038/nm.3350; pmid: 24056771
5. J. T. Weinfurter *et al*., Cross-reactive T cells are involved in rapid clearance of 2009 pandemic H1N1 influenza virus in nonhuman primates. *PLOS Pathog.* **7**, e1002381 (2011). doi: 10.1371/journal.ppat.1002381; pmid: 22102819
6. M. Koutsakos *et al*., Human $CD8^+$ T cell cross-reactivity across influenza A, B and C viruses. *Nat. Immunol.* **20**, 613–625 (2019). doi: 10.1038/s41590-019-0320-6; pmid: 30778243
7. L. Si *et al*., Generation of influenza A viruses as live but replication-incompetent virus vaccines. *Science* **354**, 1170–1173 (2016). doi: 10.1126/science.aah5869; pmid: 27934767
8. L. Wang *et al*., Generation of a live attenuated influenza vaccine that elicits broad protection in mice and ferrets. *Cell Host Microbe* **21**, 334–343 (2017). doi: 10.1016/j.chom.2017.02.007; pmid: 28279345
9. D. F. Hoft *et al*., Live and inactivated influenza vaccines induce similar humoral responses, but only live vaccines induce diverse T-cell responses in young children. *J. Infect. Dis.* **204**, 845–853 (2011). doi: 10.1093/infdis/jir436; pmid: 21846636
10. A. Ablasser *et al*., cGAS produces a 2′-5′-linked cyclic dinucleotide second messenger that activates STING. *Nature* **498**, 380–384 (2013). doi: 10.1038/nature12306; pmid: 23722158
11. J. Wu *et al*., Cyclic GMP-AMP is an endogenous second messenger in innate immune signaling by cytosolic DNA. *Science* **339**, 826–830 (2013). doi: 10.1126/science.1229963; pmid: 23258412
12. X. D. Li *et al*., Pivotal roles of cGAS-cGAMP signaling in antiviral defense and immune adjuvant effects. *Science* **341**, 1390–1394 (2013). doi: 10.1126/science.1244040; pmid: 23989956
13. J. Wang, P. Li, M. X. Wu, Natural STING Agonist as an "Ideal" adjuvant for cutaneous vaccination. *J. Invest. Dermatol.* **136**, 2183–2191 (2016). doi: 10.1016/j.jid.2016.05.105; pmid: 27287182
14. L. Corrales *et al*., Direct activation of STING in the tumor microenvironment leads to potent and systemic tumor regression and immunity. *Cell Reports* **11**, 1018–1030 (2015). doi: 10.1016/j.celrep.2015.04.031; pmid: 25959818
15. J. A. Whitsett, S. E. Wert, T. E. Weaver, Alveolar surfactant homeostasis and the pathogenesis of pulmonary disease. *Annu. Rev. Med.* **61**, 105–119 (2010). doi: 10.1146/annurev.med.60.041807.123500; pmid: 19824815
16. K. A. Woodrow, K. M. Bennett, D. D. Lo, Mucosal vaccine design and delivery. *Annu. Rev. Biomed. Eng.* **14**, 17–46 (2012). doi: 10.1146/annurev-bioeng-071811-150054; pmid: 22524387
17. E. Parra, J. Pérez-Gil, Composition, structure and mechanical properties define performance of pulmonary surfactant membranes and films. *Chem. Phys. Lipids* **185**, 153–175 (2015). doi: 10.1016/j.chemphyslip.2014.09.002; pmid: 25260665
18. A. V. Misharin, L. Morales-Nebreda, G. M. Mutlu, G. R. Budinger, H. Perlman, Flow cytometric analysis of macrophages and dendritic cell subsets in the mouse lung. *Am. J. Respir. Cell Mol. Biol.* **49**, 503–510 (2013). doi: 10.1165/rcmb.2013-0086MA; pmid: 23672262
19. H. Qin, C. A. Wilson, S. J. Lee, X. Zhao, E. N. Benveniste, LPS induces CD40 gene expression through the activation of NF-κB and STAT-1α in macrophages and microglia. *Blood* **106**, 3114–3122 (2005). doi: 10.1182/blood-2005-02-0759; pmid: 16020513
20. A. Haczku, Protective role of the lung collectins surfactant protein A and surfactant protein D in airway inflammation. *J. Allergy Clin. Immunol.* **122**, 861–881 (2008). doi: 10.1016/j.jaci.2008.10.014; pmid: 19000577
21. J. Wang, B. Li, M. X. Wu, Effective and lesion-free cutaneous influenza vaccination. *Proc. Natl. Acad. Sci. U.S.A.* **112**, 5005–5010 (2015). doi: 10.1073/pnas.1500408112; pmid: 25848020
22. J. Wang, D. Shah, X. Chen, R. R. Anderson, M. X. Wu, A microsterile inflammation array as an adjuvant for influenza vaccines. *Nat. Commun.* **5**, 4447 (2014). doi: 10.1038/ncomms5447; pmid: 25033973
23. A. Ballesteros-Tato, B. León, F. E. Lund, T. D. Randall, Temporal changes in dendritic cell subsets, cross-priming and costimulation via CD70 control $CD8^+$ T cell responses to influenza. *Nat. Immunol.* **11**, 216–224 (2010). doi: 10.1038/ni.1838; pmid: 20098442
24. B. Unkel *et al*., Alveolar epithelial cells orchestrate DC function in murine viral pneumonia. *J. Clin. Invest.* **122**, 3652–3664 (2012). doi: 10.1172/JCI62139; pmid: 22996662
25. J. S. Sullivan *et al*., Heterosubtypic anti-avian H5N1 influenza antibodies in intravenous immunoglobulins from globally separate populations protect against H5N1 infection in cell culture. *J. Mol. Genet. Med.* **3**, 217–224 (2009). pmid: 20076794
26. C. W. Lawrence, R. M. Ream, T. J. Braciale, Frequency, specificity, and sites of expansion of $CD8^+$ T cells during primary pulmonary influenza virus infection. *J. Immunol.* **174**, 5332–5340 (2005). doi: 10.4049/jimmunol.174.9.5332; pmid: 15843530
27. T. Ichinohe *et al*., Synthetic double-stranded RNA poly(I:C) combined with mucosal vaccine protects against influenza virus infection. *J. Virol.* **79**, 2910–2919 (2005). doi: 10.1128/JVI.79.5.2910-2919.2005; pmid: 15709010
28. J. Y. Kang *et al*., Recognition of lipopeptide patterns by Toll-like receptor 2-Toll-like receptor 6 heterodimer. *Immunity* **31**, 873–884 (2009). doi: 10.1016/j.immuni.2009.09.018; pmid: 19931471
29. A. Ablasser *et al*., Cell intrinsic immunity spreads to bystander cells via the intercellular transfer of cGAMP. *Nature* **503**, 530–534 (2013). doi: 10.1038/nature12640; pmid: 24077100
30. K. Westphalen *et al*., Sessile alveolar macrophages communicate with alveolar epithelium to modulate immunity. *Nature* **506**, 503–506 (2014). doi: 10.1038/nature12902; pmid: 24463523
31. P. W. Furlow *et al*., Mechanosensitive pannexin-1 channels mediate microvascular metastatic cell survival. *Nat. Cell Biol.* **17**, 943–952 (2015). doi: 10.1038/ncb3194; pmid: 26098574
32. Q. Chen *et al*., Carcinoma-astrocyte gap junctions promote brain metastasis by cGAMP transfer. *Nature* **533**, 493–498 (2016). doi: 10.1038/nature18268; pmid: 27225120
33. H. Ramsey *et al*., Stress-induced hematopoietic failure in the absence of immediate early response gene X-1 (IEX-1, IER3). *Haematologica* **99**, 282–291 (2014). doi: 10.3324/haematol.2013.092452; pmid: 24056813
34. J. H. Fritz, L. Le Bourhis, J. G. Magalhaes, D. J. Philpott, Innate immune recognition at the epithelial barrier drives adaptive immunity: APCs take the back seat. *Trends Immunol.* **29**, 41–49 (2008). doi: 10.1016/j.it.2007.10.002; pmid: 18054284
35. S. A. Saenz, B. C. Taylor, D. Artis, Welcome to the neighborhood: Epithelial cell-derived cytokines license innate and adaptive immune responses at mucosal sites. *Immunol. Rev.* **226**, 172–190 (2008). doi: 10.1111/j.1600-065X.2008.00713.x; pmid: 19161424
36. J. A. Whitsett, T. Alenghat, Respiratory epithelial cells orchestrate pulmonary innate immunity. *Nat. Immunol.* **16**, 27–35 (2015). doi: 10.1038/ni.3045; pmid: 25521682
37. R. Hai *et al*., Influenza A(H7N9) virus gains neuraminidase inhibitor resistance without loss of in vivo virulence or transmissibility. *Nat. Commun.* **4**, 2854 (2013). doi: 10.1038/ncomms3854; pmid: 24326875
38. C. Moore *et al*., Evidence of person-to-person transmission of oseltamivir-resistant pandemic influenza A(H1N1) 2009 virus in a hematology unit. *J. Infect. Dis.* **203**, 18–24 (2011). doi: 10.1093/infdis/jiq007; pmid: 21148492
39. A. Hidalgo, A. Cruz, J. Pérez-Gil, Barrier or carrier? Pulmonary surfactant and drug delivery. *Eur. J. Pharm. Biopharm.* **95** (Pt A), 117–127 (2015). doi: 10.1016/j.ejpb.2015.02.014; pmid: 25709061
40. B. Olsson *et al*., in *Controlled Pulmonary Drug Delivery*, A. J. H. Hugh D.C. Smyth, Ed. (Springer-Verlag, 2011), pp. 21–50.
41. J. C. Sung, B. L. Pulliam, D. A. Edwards, Nanoparticles for drug delivery to the lungs. *Trends Biotechnol.* **25**, 563–570 (2007). doi: 10.1016/j.tibtech.2007.09.005; pmid: 17997181
42. I. J. Bakken *et al*., Febrile seizures after 2009 influenza A (H1N1) vaccination and infection: A nationwide registry-based study. *BMC Infect. Dis.* **15**, 506 (2015). doi: 10.1186/s12879-015-1263-7; pmid: 26553258
43. F. Szoka Jr., D. Papahadjopoulos, Procedure for preparation of liposomes with large internal aqueous space and high capture by reverse-phase evaporation. *Proc. Natl. Acad. Sci. U.S.A.* **75**, 4194–4198 (1978). doi: 10.1073/pnas.75.9.4194; pmid: 279908
44. Y. Matsuoka, E. W. Lamirande, K. Subbarao, The ferret model for influenza. *Curr. Protoc. Microbiol.* **13**, 15G.2.1–15G.2.29 (2009).

ACKNOWLEDGMENTS

We thank R. J. Webby at St. Jude Children's Research Hospital for rgVN04 H5N1 virus and D. J. Irvine at MIT for consultation of liposome preparation; M. Hogan and S. Andrea at MGH CCM for their assistance in ferret study; Q. Wang at FDU SHMC for technical support; J. H. Wu, M. Ishii, and L. Leanse for editing; and staff in Wellman photopathology core for histology and flow cytometry. We are grateful to BEI Resources, NIH, and International Reagent Resources, CDC, for their generous support in providing various influenza viruses and vaccines. **Funding:** This work is supported by NIH grants AI089779, AI070785, and AI097696; MGH ECOR 230002; and a department fund to M.X.W.; by China National Megaprojects for Major Infectious Diseases 2018ZX10301403 and National Natural Science Foundation 81822045 to L.L.; and by Hundred-Talents program of Sun Yat-sen University to J.W. **Author contributions:** Conceptualization and supervision, M.X.W., J.W., and L.L. Investigation and data analysis, J.W., P.L., Y.Y., Y.F., H.J., M.L., and Z.S. Writing, M.X.W., J.W., L.L., and S.J. **Competing interests:** M.X.W. has filed a provisional patent application entitled

"Pulmonary surfactant-mimetic liposomes for safe delivery of small molecules for therapeutics and prophylaxis of respiratory diseases or infections." The authors declare that they have no other competing interests. S.J. is affiliated with Lindsley F. Kimball Research Institute, New York Blood Center, New York, NY 10065, USA, and P.L. is affiliated with the Key Laboratory of Endogenous Infection, Shenzhen Nanshan People's Hospital, Guangdong Medical University, Shenzhen 518052, China. **Data and material availability:** All data are available in the main text or the supplementary materials.

SUPPLEMENTARY MATERIALS

science.sciencemag.org/content/367/6480/eaau0810/suppl/DC1
Materials and Methods
Figs. S1 to S31
Tables S1 to S3
References (*45*–*49*)

View/request a protocol for this paper from *Bio-protocol*.

3 July 2018; resubmitted 3 May 2019
Accepted 23 December 2019
10.1126/science.aau0810

RESEARCH ARTICLE

DEVELOPMENTAL BIOLOGY

Vertebrate diapause preserves organisms long term through Polycomb complex members

Chi-Kuo Hu[1], Wei Wang[2,3]*, Julie Brind'Amour[4]*, Param Priya Singh[1], G. Adam Reeves[1,5], Matthew C. Lorincz[4], Alejandro Sánchez Alvarado[2,3], Anne Brunet[1,6]†

Diapause is a state of suspended development that helps organisms survive extreme environments. How diapause protects living organisms is largely unknown. Using the African turquoise killifish (*Nothobranchius furzeri*), we show that diapause preserves complex organisms for extremely long periods of time without trade-offs for subsequent adult growth, fertility, and life span. Transcriptome analyses indicate that diapause is an active state, with dynamic regulation of metabolism and organ development genes. The most up-regulated genes in diapause include Polycomb complex members. The chromatin mark regulated by Polycomb, H3K27me3, is maintained at key developmental genes in diapause, and the Polycomb member CBX7 mediates repression of metabolism and muscle genes in diapause. CBX7 is functionally required for muscle preservation and diapause maintenance. Thus, vertebrate diapause is a state of suspended life that is actively maintained by specific chromatin regulators, and this has implications for long-term organism preservation.

To survive extreme conditions, many species have evolved specific states of suspended life in the form of hibernation, torpor, and diapause. Diapause suspends embryonic development when environmental conditions are harsh, enabling birth in favorable conditions. The African turquoise killifish (*Nothobranchius furzeri*) has been proposed as a vertebrate model to study embryonic diapause (*1*, *2*). This killifish lives in transient ponds that are only present during the rainy season and entirely desiccate during the dry season (*3*–*6*). To survive the long drought and enable perpetuation of the species, African killifish embryos enter diapause (*1*, *2*) (Fig. 1A). Although features of diapause have been described in killifish species (*6*, *7*), the mechanisms by which diapause protects organisms remain unknown.

Diapause protects complex organs with no trade-offs for future life

We characterized African killifish diapause and investigated whether diapause comes with trade-offs for subsequent life. More than 70% of African killifish embryos enter diapause and they stay in this state for 5 to 6 months before naturally exiting (Fig. 1B and fig. S1). Some embryos remain in diapause for >10 months and occasionally 2 years (Fig. 1B, inset, and table S1). Hence, diapause is longer than the adult life of African killifish and may reflect a programmed adaptation to survive the annual drought while also protecting against unpredictable weather. Diapause embryos have muscles, a heart, primordial germ cells, a brain comprising stem and differentiated cells, as well as complex systems such as neuromuscular junctions (Fig. 1, C and D, and fig. S2). Staying in diapause for 5 months (a period equivalent to their adult life span) did not negatively affect subsequent adult growth, fertility, or subsequent life span of these killifish (Fig. 2, A to C, and fig. S3). Thus, the time spent in diapause does not come with observed trade-offs for future life, and diapause confers protective mechanisms to complex organs against damage caused by the passage of time.

Diapause is an active state with dynamic gene regulation

To understand how diapause preserves a complex organism, we first performed a transcriptomic time course in diapause. Using the change in heartbeat pattern as an early diapause hallmark, we collected synchronized populations of killifish embryos for RNA sequencing (RNA-seq): embryos in diapause for 3 days, 6 days, and 1 month, and embryos in development right before and after the time corresponding to diapause onset (Fig. 3A, figs. S4 and S5A, and table S2). Diapause time points were easily separated by principal component analysis and clustering (Fig. 3B, fig. S5B, and table S3). The transcriptome was substantially reprogrammed in diapause: >33% of the transcripts changed more than twofold in diapause (fig. S5C) and had dynamic expression patterns (fig. S5D). Genes involved in cell proliferation and organ development were down-regulated throughout or late in diapause, respectively (Fig. 3C and fig. S5E). One notable exception was muscle. Genes implicated in muscle development and function were up-regulated early and down-regulated late in diapause (Fig. 3D and table S4), suggesting that muscle might be maintained in a different manner in diapause. Finally, genes involved in autophagy and metabolic pathways (e.g., nucleotides and amino acids) were up-regulated throughout diapause (Fig. 3D, fig. S5E, and table S4). Thus, diapause is an active state, with up-regulation of metabolic genes and dynamic regulation of organ development genes.

Switch to specific Polycomb complex members in diapause

To identify candidate regulators of organ maintenance in diapause, we focused on the most up-regulated genes in diapause. Although several of them relate to amino acid metabolism, three of the 10 most up-regulated genes are implicated in chromatin regulation: *EZH1*, *CBX7(1of2)* (hereafter *CBX7*), and *PCGF5* (Fig. 3E and table S4). EZH1 is a core Polycomb complex enzyme that trimethylates lysine 27 in histone H3 (H3K27me3), whereas CBX7 binds to H3K27me3 and mediates specific transcriptional repression (*8*–*12*) (Fig. 4A). Overall, diapause was accompanied by a switch to members of the canonical Polycomb repressive complex 1 (PRC1) (Fig. 3F and fig. S6), suggesting that a specialized Polycomb complex may be important for the diapause state.

H3K27me3, a mark regulated by Polycomb complex members, is maintained at key organ genes in diapause

Polycomb complex members are critical for stem cell identity, development, and cancer, and they act by depositing or binding to histone marks, notably H3K27me3 (*10*–*12*) (Fig. 4A). We first assessed the global H3K27me3 landscape in diapause by performing H3K27me3 chromatin immunoprecipitation sequencing (ChIP-seq) in diapause or developing (without diapause) embryos (fig. S7). Despite the substantial transcriptomic changes in diapause, the H3K27me3 landscape was very similar in diapause compared with development (Fig. 4B). Genes with maintained H3K27me3 (~7000 genes) were mostly involved in organ development, whereas genes that were not marked (~14,000 genes) were involved in cellular processes (e.g., autophagy) (Fig. 4B and fig. S7G), suggesting maintenance of developmental identity in diapause. Overall, H3K27me3 did not correlate with gene repression in diapause (fig. S7D). However, genes with maintained H3K27me3 (e.g., organ

[1]Department of Genetics, Stanford University, Stanford, CA 94305, USA. [2]Stowers Institute for Medical Research, Kansas City, MO 64110, USA. [3]Howard Hughes Medical Institute, Stowers Institute for Medical Research, Kansas City, MO 64110, USA. [4]Department of Medical Genetics, Life Sciences Institute, The University of British Columbia, Vancouver, British Columbia V6T 1Z3, Canada. [5]Graduate Program of Genetics, Department of Genetics, Stanford University, Stanford, CA 94305, USA. [6]Glenn Laboratories for the Biology of Aging, Stanford University, Stanford, CA 94305, USA.
*These authors contributed equally to this work.
†Corresponding author. Email: abrunet1@stanford.edu

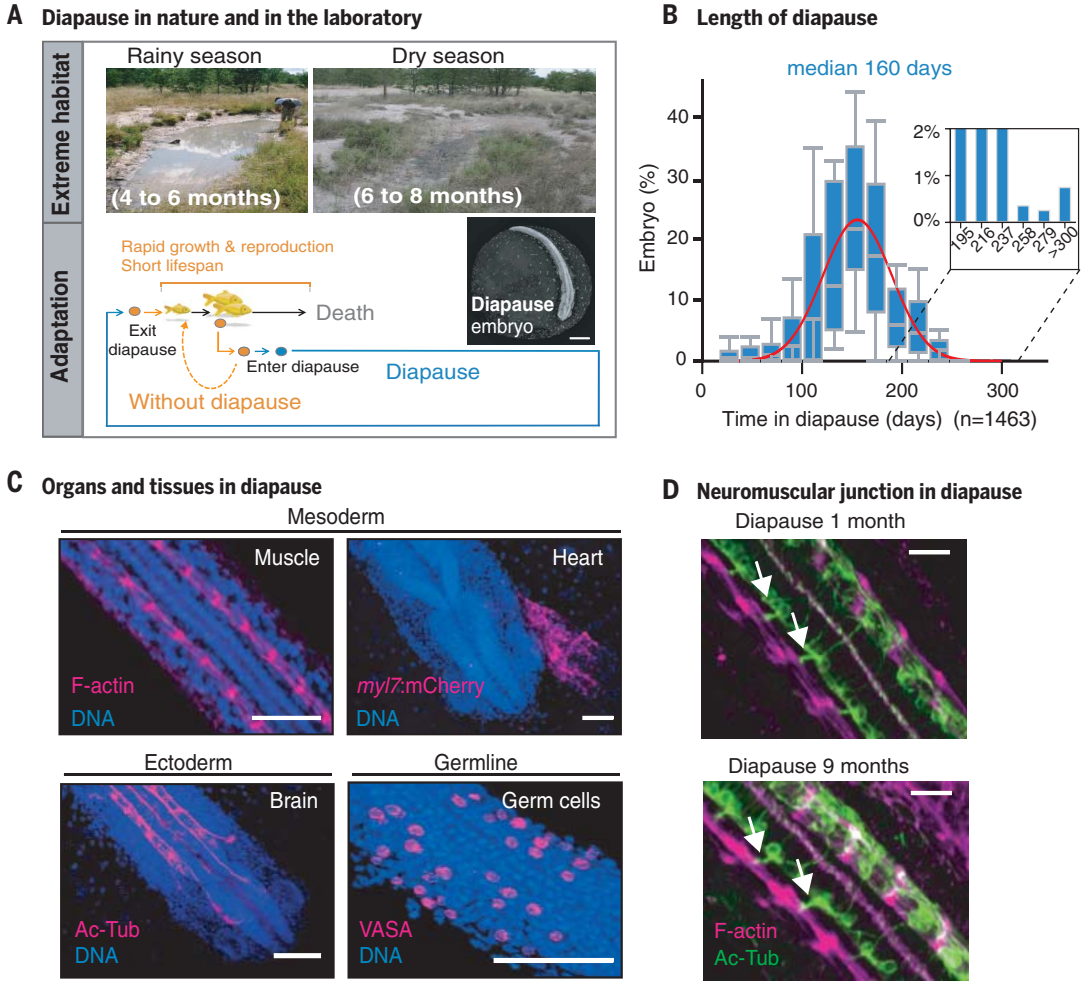

Fig. 1. Diapause lasts for long periods of time and diapause embryos have complex organs. (**A**) African killifish life cycle. [Natural habitat images: copyright 2015 from *The Evolutionary Ecology of African Annual Fishes* by M. Reichard.] Scale bar in embryo image, 200 μm. (**B**) Percentage of embryos that stayed in diapause for the indicated length of time (1463 embryos). Boxes show the median and interquartile ranges. Whiskers indicate maximum 1.5 interquartile range. Red indicates the Gaussian curve fitted to the distribution. About 1% of embryos stayed in diapause for >300 days (inset) (table S1). (**C** and **D**) Killifish embryos in diapause have muscle, heart, brain, germ cells, and neuromuscular junctions. Muscle: Alexa Fluor-647–labeled phalloidin. Heart: Transgenic line expressing cardiac-specific mCherry. Brain: Antibodies to SOX2, GFAP, and acetylated tubulin (Ac-Tub). Germ cells: Antibodies to VASA. Scale bars, 50 μm. Arrows indicate neuromuscular junctions.

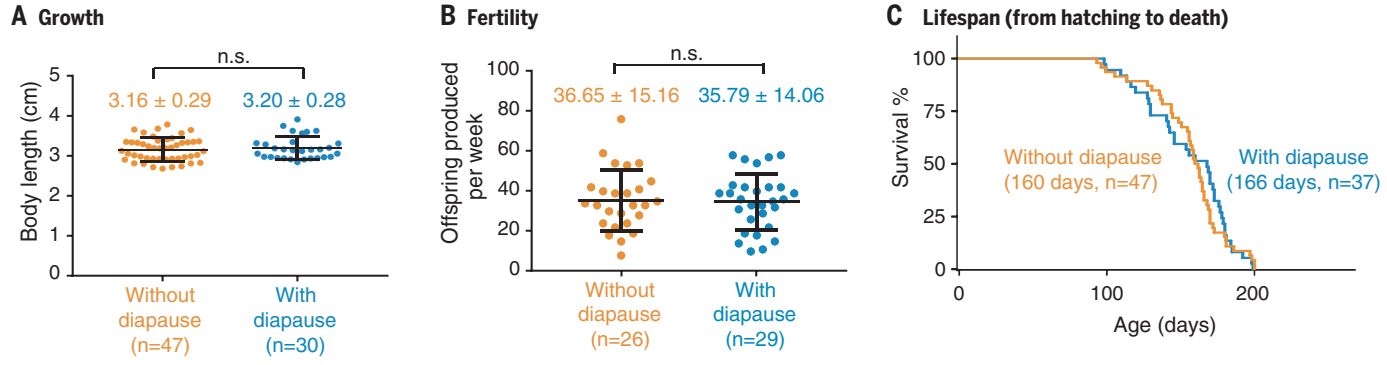

Fig. 2. Diapause protects complex organisms with no trade-offs for future life. (**A**) Mean ± SD of body length of adult male fish originating from 47 embryos that developed directly (without diapause; orange) or 30 embryos that stayed in diapause for 5 months (with diapause; blue). Each dot represents an individual fish. $P = 0.73$, Mann–Whitney unpaired nonparametric test. n.s., nonsignificant (see table S1). (**B**) Mean ± SD of offspring number from 3 breeding pairs originating from embryos without diapause (orange) or in diapause for 5 months (blue). Each dot represents a weekly collection of offspring. $P = 0.95$, Mann–Whitney unpaired nonparametric test (table S1). (**C**) Kaplan–Meier survival curves of 47 adults originating from embryos without diapause (one censored) and 37 adults from embryos that stayed 5 months in diapause. Log-rank (Mantel–Cox) test, $P = 0.84$. Median life spans are shown in parentheses (table S1).

development genes, including muscle genes) tended to be down-regulated late in diapause (Fig. 4, C and D; fig. S7, E and F; and table S5), and a few genes with H3K27me3 loss were up-regulated in diapause (e.g., *CDKN1B*) (fig. S7, H and I). Thus, the switch to specific Polycomb complex members may serve to maintain H3K27me3 at genes involved in organ development and may mediate their repression late in diapause.

Polycomb complex member CBX7 mediates repression of lipid metabolism and muscle genes

Because H3K27me3 is maintained in diapause, we next investigated whether Polycomb members that act downstream of H3K27me3 could

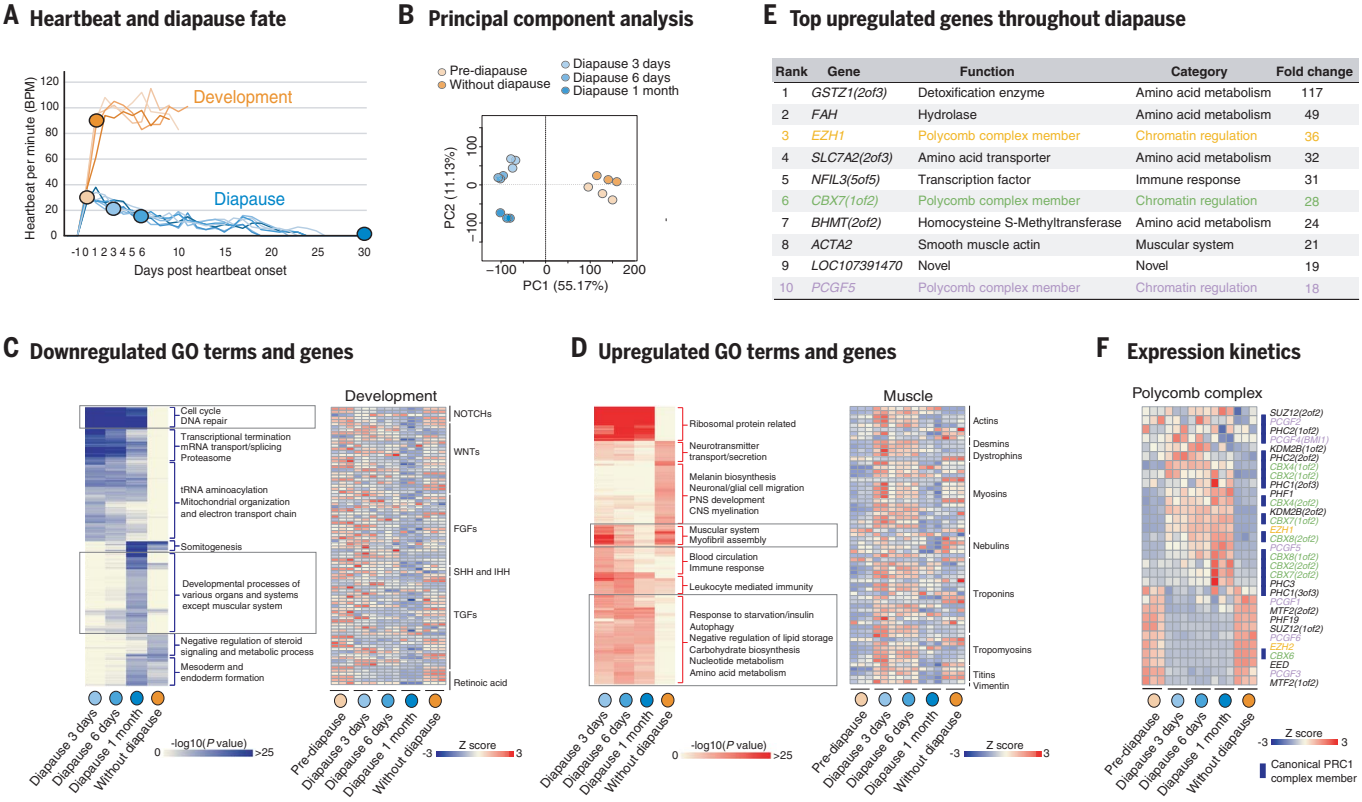

Rank	Gene	Function	Category	Fold change
1	*GSTZ1(2of3)*	Detoxification enzyme	Amino acid metabolism	117
2	*FAH*	Hydrolase	Amino acid metabolism	49
3	*EZH1*	Polycomb complex member	Chromatin regulation	36
4	*SLC7A2(2of3)*	Amino acid transporter	Amino acid metabolism	32
5	*NFIL3(5of5)*	Transcription factor	Immune response	31
6	*CBX7(1of2)*	Polycomb complex member	Chromatin regulation	28
7	*BHMT(2of2)*	Homocysteine S-Methyltransferase	Amino acid metabolism	24
8	*ACTA2*	Smooth muscle actin	Muscular system	21
9	*LOC107391470*	Novel	Novel	19
10	*PCGF5*	Polycomb complex member	Chromatin regulation	18

Fig. 3. Dynamic gene regulation in diapause and switch to specific Polycomb complex members. (**A**) Heartbeat patterns of embryos developing without diapause (orange) or entering diapause (blue) (see also fig. S4, A and B). Each colored circle represents a time point for RNA-seq selected on the basis of heartbeat onset and pattern. (**B**) Principal component analysis on log2-transformed transcripts per million (TPM) of all genes. Each dot represents the transcriptome from pooled embryos. (**C** and **D**) Left: Heat map of gene ontology (GO) terms enriched by differentially expressed genes with false discovery rate (FDR) < 0.01 in at least one of the time points (table S4 and data S1). Enriched GO terms are clustered based on *P* values (blue, down-regulated; red, up-regulated). Right: Heat maps of key gene families of development or muscle. *Z*-scores are based on the normalized expression value of each gene (TPM). (**E**) Genes most up-regulated in diapause (fold change > 2, FDR < 0.01, TPM > 25 in all 3 diapause conditions) but not during development (without diapause) (fold change < 2) (table S4). (**F**) Heat map showing the expression profile of select Polycomb complex members (see also fig. S6, A and B). *Z*-scores are based on the normalized expression value of each gene (TPM). Paralog numbers are shown in parentheses.

mediate the repression of specific genes. We focused on CBX7 because it binds H3K27me3 (*8*, *9*, *13*–*16*) and is highly up-regulated throughout diapause. Using CRISPR-Cas9 genome editing (*17*), we generated two independent *CBX7* killifish mutants predicted to give rise to premature stop codons (Fig. 5A and fig. S8). RNA-seq analysis of wild-type (WT) and *CBX7* mutant embryos in diapause revealed that up-regulated (i.e., derepressed) genes in *CBX7* mutant embryos were enriched for metabolism and cytokine and hormone regulation processes, whereas down-regulated genes were enriched for muscle and neurotransmission processes (Fig. 5B; fig. S9, A to C; and table S7). Of the derepressed genes in *CBX7* mutant embryos, 142 also exhibited H3K27me3 maintenance in diapause and could therefore represent direct targets of CBX7. These targets are implicated in lipid metabolism (e.g., *PLTP*) and organ development (e.g., *SOX9*), and one of them, *UBE2H*, is involved in muscle atrophy (*18*, *19*) (Fig. 5, C and D, and fig. S9, D and E). The other gene expression changes in *CBX7* mutants, down-regulation of muscle assembly genes (e.g., *NEBL*), could be indirect consequences or reflect phenotypic differences in *CBX7* mutants (Fig. 5, C and D, and fig. S9C). Thus, CBX7 could mediate the repressive effect of H3K27me3 on specific lipid metabolism and muscle genes.

CBX7 is required for muscle preservation and diapause maintenance

We next tested the functional importance of CBX7 in diapause. *CBX7* mutant embryos entered diapause normally and initially were similar to their WT counterparts. However, *CBX7* mutant embryos from both lines exhibited deterioration in their muscles after a month in diapause (Fig. 6, A and B). This is consistent with the up-regulation of the muscle atrophy gene *UBE2H* and the down-regulation of several muscle assembly genes in *CBX7* mutants. Muscle defects in *CBX7* mutant embryos were specific to diapause (Fig. 6, B and C), consistent with the selective expression of *CBX7* in diapause (fig. S6B). *CBX7* mutants did not exhibit overt defects in neurons or neuromuscular junctions (Fig. 6, D and E, and fig. S10, A and B). But these CBX7 mutants could not stay in the diapause state as long as their WT counterparts did, although they were viable afterward (Fig. 6F and fig. S10C). Thus, CBX7 is required for long-term preservation of muscles in diapause and for the maintenance of this state.

Our results show that killifish diapause preserves organs, complex systems such as neuromuscular junctions, and various cell types for long periods of time without trade-offs for future life. Diapause is an active and dynamic state, with genes involved in organ development being down-regulated late. We identify specific members of the Polycomb complex, notably CBX7, as functional regulators of long-term organ preservation in diapause. CBX7 may maintain muscles by directly and indirectly regulating specific genes involved in muscle function and metabolism (fig. S10D). It will be interesting to determine how *CBX7* deficiency in diapause affects subsequent adult life. The role of CBX7 and other specialized Polycomb

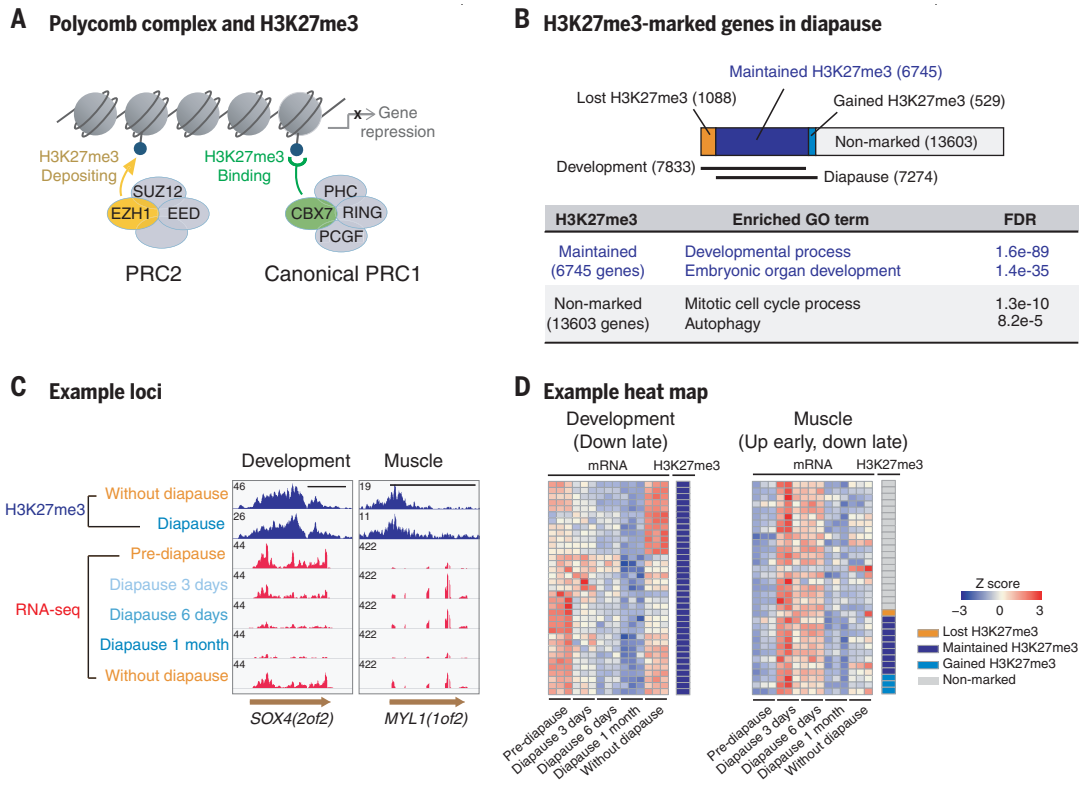

H3K27me3	Enriched GO term	FDR
Maintained (6745 genes)	Developmental process	1.6e-89
	Embryonic organ development	1.4e-35
Non-marked (13603 genes)	Mitotic cell cycle process	1.3e-10
	Autophagy	8.2e-5

Fig. 4. H3K27me3 is maintained at key organ genes in diapause. (**A**) Selected members of the Polycomb complex and their interaction with H3K27me3. (**B**) Number of genes marked by H3K27me3 that are maintained, lost, or gained in diapause or not marked in either state. GO terms associated with maintained H3K27me3 or unmarked genes in embryos in diapause (table S6; see also fig. S7G). (**C**) Example loci with H3K27me3 ChIP-seq and RNA-seq peaks in development (without diapause) or diapause. The data range of H3K27me3 tracks was individually autoscaled. Scale bars, 5 kb. (**D**) Heat maps showing genes with dynamic transcriptomic trajectories in diapause and H3K27me3 marking. *Z*-scores are based on the normalized expression value of each gene (TPM).

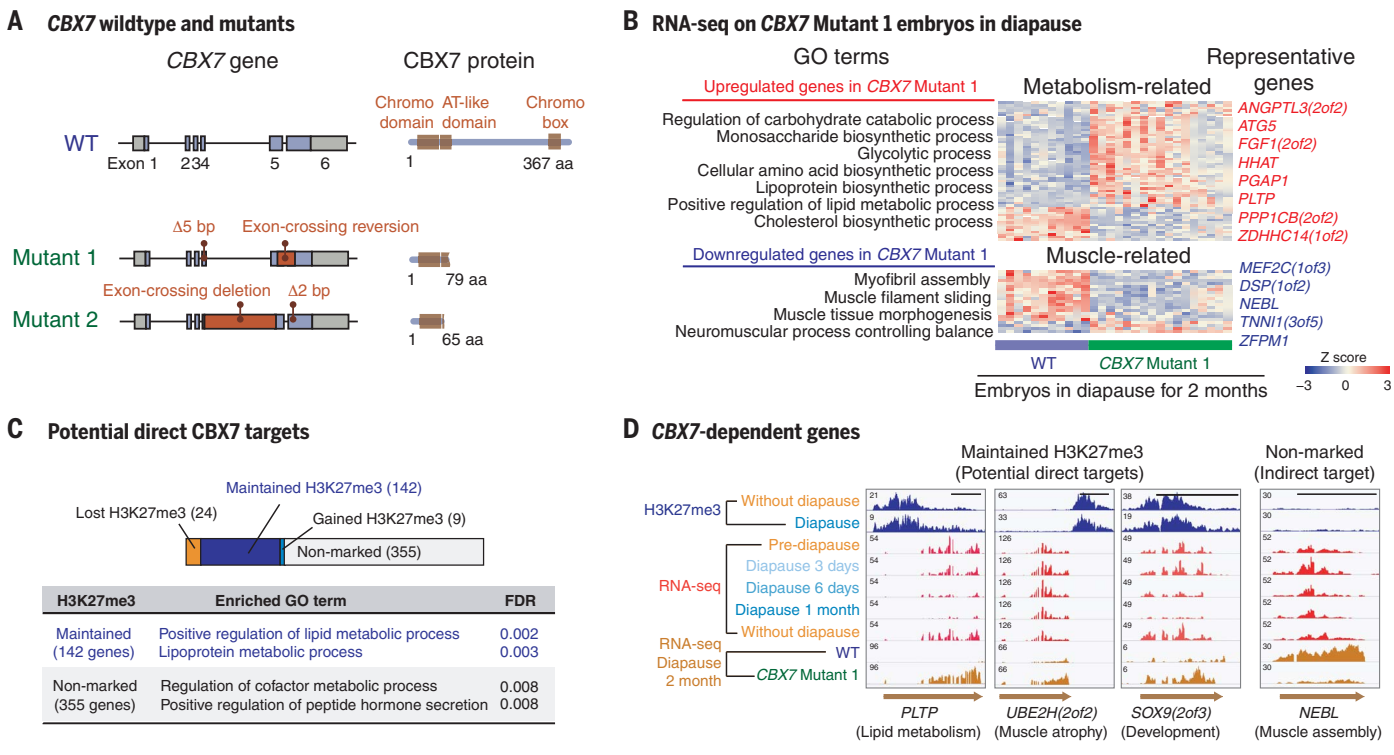

H3K27me3	Enriched GO term	FDR
Maintained (142 genes)	Positive regulation of lipid metabolic process	0.002
	Lipoprotein metabolic process	0.003
Non-marked (355 genes)	Regulation of cofactor metabolic process	0.008
	Positive regulation of peptide hormone secretion	0.008

Fig. 5. The Polycomb complex member CBX7 mediates repression of a subset of lipid metabolism and muscle genes. (**A**) Two independent *CBX7* mutant lines were generated by CRISPR-Cas9 genome editing. (**B**) GO terms (FDR < 0.01) enriched by differentially expressed genes (fold change > 1.5, FDR < 0.01) of *CBX7* Mutant 1 embryos in diapause for 2 months. Relevant genes were clustered into heat maps on the basis of expression level (TPMs) across 11 WT and 17 *CBX7* Mutant 1 embryos. Representative genes are shown on the right (red, up-regulated; blue, down-regulated; see also fig. S9C). (**C**) Number of genes up-regulated in *CBX7* Mutant 1 embryos and marked by H3K27me3 (potential direct targets) and their associated GO terms. (**D**) Example loci (as in Fig. 4C). Scale bars, 2 kb.

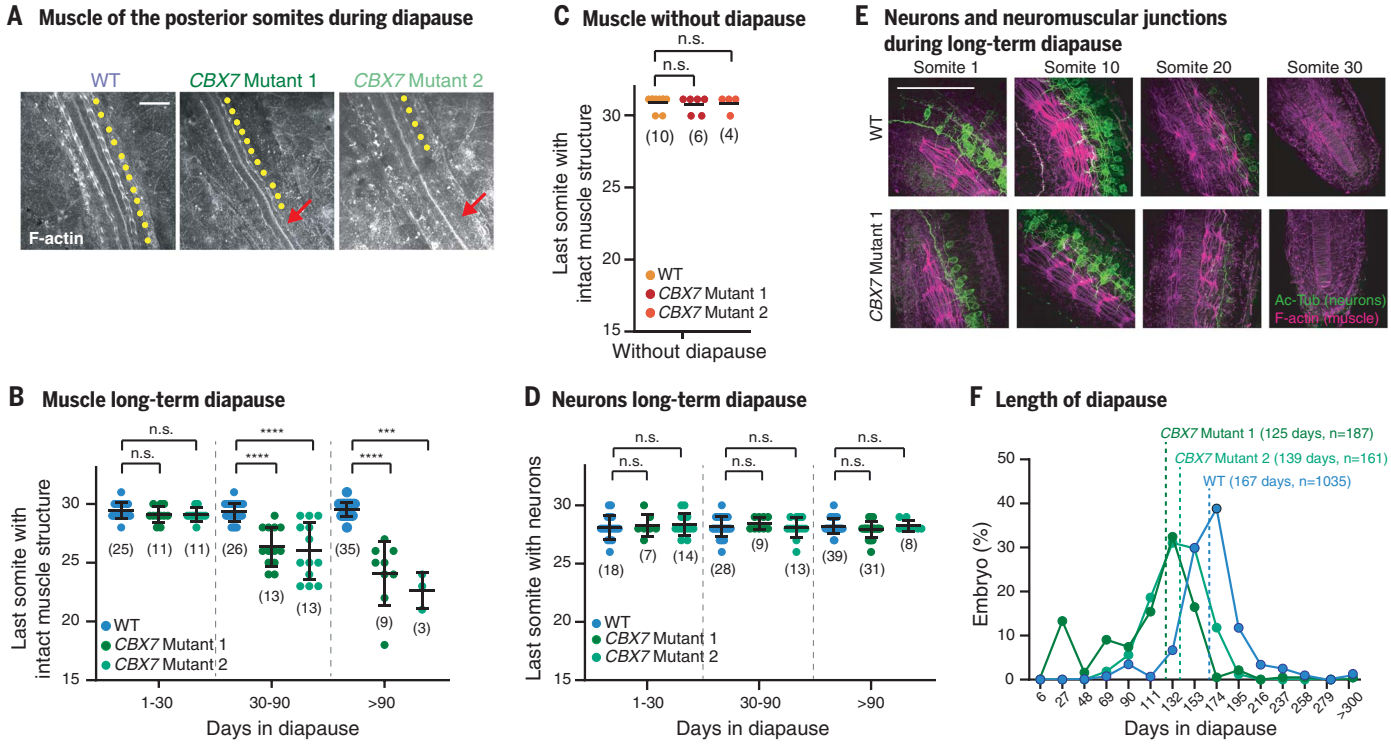

Fig. 6. The Polycomb complex member CBX7 is required for muscle preservation and diapause maintenance. (**A**) Example of muscle deterioration in *CBX7* mutant embryos in diapause for 5 months. Muscle: Alexa Fluor-647–labeled phalloidin. Red arrows: posterior somites lacking muscle fiber bundles. Yellow dots: somites with muscle fiber bundles. Scale bar, 50 μm. (**B** and **C**) Mean ± SD of the number of the last somite with intact muscle in WT and *CBX7* mutant embryos at different times in diapause (B) or without diapause (C). Each dot represents an embryo. Embryo numbers are shown in parentheses. ***$P < 0.001$, ****$P < 0.0001$, Mann–Whitney unpaired nonparametric test (table S1). (**D**) Mean ± SD of the number of the last somite with neurons in WT and *CBX7* mutant embryos in diapause [as in (B)]. (**E**) Neurons and neuromuscular junctions in the somites of WT and *CBX7* Mutant 1 embryos in diapause for 4 months. Muscle: Alexa Fluor-647–labeled phalloidin. Neurons: Antibodies to Ac-Tub (see also fig. S10A). Scale bar, 50 μm. (**F**) Percentage of WT *CBX7* mutant embryos that stayed in diapause for the indicated length of time. Median diapause length and embryo numbers are shown in parentheses.

complex members could extend to other organisms and forms of long-term preservation (*20*–*22*) or to longevity (*23*, *24*). Indeed, Polycomb complex genes are involved in insect diapause and seasonal responses in plants (*20*–*22*). Finally, because the metabolic pathways up-regulated during diapause in killifish are similar to those up-regulated in *Caenorhabditis elegans* Dauer (*25*), longevity mutants (*26*, *27*), and mammalian hibernation (*28*, *29*), a switch in metabolic and chromatin states could coordinate longevity and suspended life. Our study has important implications for long-term organism preservation and resistance to extreme environments.

REFERENCES AND NOTES

1. M. Platzer, C. Englert, *Trends Genet.* **32**, 543–552 (2016).
2. C. K. Hu, A. Brunet, *Aging Cell* **17**, e12757 (2018).
3. E. Terzibasi, D. R. Valenzano, A. Cellerino, *Exp. Gerontol.* **42**, 81–89 (2007).
4. M. Reichard, M. Polačik, *eLife* **8**, e41548 (2019).
5. D. R. Valenzano *et al.*, *Cell* **163**, 1539–1554 (2015).
6. K. Reichwald *et al.*, *Cell* **163**, 1527–1538 (2015).
7. A. L. T. Romney, E. M. Davis, M. M. Corona, J. T. Wagner, J. E. Podrabsky, *Proc. Natl. Acad. Sci. U.S.A.* **115**, 12763–12768 (2018).
8. L. Morey *et al.*, *Cell Stem Cell* **10**, 47–62 (2012).
9. K. Klauke *et al.*, *Nat. Cell Biol.* **15**, 353–362 (2013).
10. B. Schuettengruber, H. M. Bourbon, L. Di Croce, G. Cavalli, *Cell* **171**, 34–57 (2017).
11. J. R. Yu, C. H. Lee, O. Oksuz, J. M. Stafford, D. Reinberg, *Genes Dev.* **33**, 903–935 (2019).
12. M. B. Ardehali *et al.*, *Mol. Cell* **68**, 872–884.e6 (2017).
13. Z. Gao *et al.*, *Mol. Cell* **45**, 344–356 (2012).
14. F. Forzati *et al.*, *Biol. Open* **3**, 871–879 (2014).
15. L. Morey, L. Aloia, L. Cozzuto, S. A. Benitah, L. Di Croce, *Cell Rep.* **3**, 60–69 (2013).
16. N. A. Fursova *et al.*, *Mol. Cell* **74**, 1020–1036.e8 (2019).
17. I. Harel *et al.*, *Cell* **160**, 1013–1026 (2015).
18. J. S. Yi *et al.*, *Nat. Commun.* **4**, 2354 (2013).
19. I. A. Johnston, N. I. Bower, D. J. Macqueen, *J. Exp. Biol.* **214**, 1617–1628 (2011).
20. H. Yang *et al.*, *Science* **357**, 1142–1145 (2017).
21. A. Angel, J. Song, C. Dean, M. Howard, *Nature* **476**, 105–108 (2011).
22. Y. X. Lu, D. L. Denlinger, W. H. Xu, *J. Biol. Chem.* **288**, 23554–23564 (2013).
23. M. Baumgart *et al.*, *Aging Cell* **13**, 965–974 (2014).
24. C. Cencioni *et al.*, *Cells* **8**, 1169 (2019).
25. J. J. McElwee, E. Schuster, E. Blanc, J. H. Thomas, D. Gems, *J. Biol. Chem.* **279**, 44533–44543 (2004).
26. S. S. Lee, S. Kennedy, A. C. Tolonen, G. Ruvkun, *Science* **300**, 644–647 (2003).
27. C. T. Murphy *et al.*, *Nature* **424**, 277–283 (2003).
28. M. Hampton, R. G. Melvin, M. T. Andrews, *PLOS ONE* **8**, e85157 (2013).
29. I. Seim *et al.*, *Nat. Commun.* **4**, 2212 (2013).

ACKNOWLEDGMENTS

We thank Brunet laboratory members and P. Abitua, B. Demmitt, A. McKay, J. Miklas, P. Navarro, K. Papsdorf, T. Ruetz, and X. Zhao for helpful discussion and reading of the manuscript; M. Buckley, A. McKay, and R. Yeo for code checking; B. Machado and S. Murphy for killifish help; K. Gotting and S. Robb for bioinformatic help; and the Stanford Genomics Facility and the Molecular Biology Core Facility of the Stowers Institute for Medical Research. **Funding:** This work was supported by NIH DP1AG044848 and the Glenn Laboratories for the Biology of Aging (A.B.), NIH T32 CA 930235 and the Life Science Research Foundation (C-K.H.), Stanford CEHG (P.P.S), NIH T32 GM 00779040 (G.A.R.), and CIHR PJT-153049 (M.C.L). A.S.A. is an investigator for the Stowers Institute for Medical Research and Howard Hughes Medical Institute. **Author contributions:** C.-K.H. designed the project with the help of A.B. C.-K.H. performed and analyzed all experiments unless otherwise indicated. W.W. generated the *ubb*:GFP transgenic line and analyzed ChIP-seq data under A.S.A.'s supervision. J.B.'A. generated ChIP-seq data and helped with analysis under M.C.L.'s supervision. P.P.S. developed the pathway enrichment pipeline for RNA-seq. G.A.R. helped with RNA-seq dynamic analyses. P.P.S. and G.A.R. helped with code checking. C.-K.H., P.P.S., and W.W. generated an updated version of killifish gene models. All authors provided intellectual input. C.-K.H. wrote the manuscript with the help of A.B., and it was reviewed by all authors. **Competing interests:** The authors declare no competing interests. **Data and materials availability:** Sequencing data have been deposited to the Sequence Read Archive (SRA) under BioProject number PRJNA503701. Original data from Stowers in this manuscript can be accessed from the Stowers Original Data Repository at www.stowers.org/research/publications/libpb-1498. All code used for the RNA-seq and ChIP-seq analyses is deposited in GitHub (https://github.com/oplz/African_Killifish_Diapause).

SUPPLEMENTARY MATERIALS

science.sciencemag.org/content/367/6480/870/suppl/DC1
Materials and Methods
Tables S1 to S8
Figs. S1 to S10
Data S1
References (*30*–*48*)

View/request a protocol for this paper from *Bio-protocol*.

11 December 2018; resubmitted 26 November 2019
Accepted 23 December 2019
10.1126/science.aaw2601

STRUCTURAL BIOLOGY

Structure of nucleosome-bound human BAF complex

Shuang He[1,2]*, Zihan Wu[1,2]*, Yuan Tian[1,2]*, Zishuo Yu[1,2], Jiali Yu[1,2], Xinxin Wang[1,2], Jie Li[1], Bijun Liu[1], Yanhui Xu[1,2,3,4]†

Mammalian SWI/SNF family chromatin remodelers, BRG1/BRM-associated factor (BAF) and polybromo-associated BAF (PBAF), regulate chromatin structure and transcription, and their mutations are linked to cancers. The 3.7-angstrom-resolution cryo–electron microscopy structure of human BAF bound to the nucleosome reveals that the nucleosome is sandwiched by the base and the adenosine triphosphatase (ATPase) modules, which are bridged by the actin-related protein (ARP) module. The ATPase motor is positioned proximal to nucleosomal DNA and, upon ATP hydrolysis, engages with and pumps DNA along the nucleosome. The C-terminal α helix of SMARCB1, enriched in positively charged residues frequently mutated in cancers, mediates interactions with an acidic patch of the nucleosome. AT-rich interactive domain-containing protein 1A (ARID1A) and the SWI/SNF complex subunit SMARCC serve as a structural core and scaffold in the base module organization, respectively. Our study provides structural insights into subunit organization and nucleosome recognition of human BAF complex.

The adenosine triphosphate (ATP)–dependent chromatin remodeling complexes (also known as chromatin remodelers) regulate the chromatin packing state by sliding, ejecting, and restructuring the nucleosome to enable dynamic regulation of chromatin structure (*1*, *2*). As prototype chromatin remodelers, the SWI/SNF complexes demonstrate nucleosome sliding activity and distinctive ejection activity, by which they create nucleosome-depleted regions (NDRs) that are essential for transcriptional regulation (*3*–*10*). Mammalian SWI/SNF (mSWI/SNF) complexes, BRG1/BRM-associated factor (BAF) and polybromo-associated BAF (PBAF), consist of up to 15 subunits encoded by more than 29 genes, generating more than 1400 possible complexes (*6*, *7*, *11*, *12*). Up to 20% of malignancies contain mutations of BAF and/or PBAF subunits, making these complexes among the most frequently dysregulated targets in human cancer (*4*, *7*, *13*).

Although the compositions and subunit functions of SWI/SNF complexes have been extensively studied (*8*, *11*, *14*–*19*), the structural studies of SWI/SNF complexes have been limited to the low-resolution electron microscopy (EM) structures of yeast SWI/SNF complexes (*20*–*23*) and structures of isolated domains (*15*, *24*–*27*). A recent study reported an ~7-Å-resolution structure of RSC (yeast homolog of PBAF) bound to the nucleosome with the substrate recruitment module refined to 3.4-Å resolution (*28*). However, the molecular mechanisms of subunit organization and nucleosome recognition of mammalian BAF complex remain largely unknown.

[1]Fudan University Shanghai Cancer Center, Institutes of Biomedical Sciences, State Key Laboratory of Genetic Engineering, and Shanghai Key Laboratory of Medical Epigenetics, Shanghai Medical College of Fudan University, Shanghai 200032, China. [2]The International Co-laboratory of Medical Epigenetics and Metabolism, Ministry of Science and Technology, China, Department of Systems Biology for Medicine, School of Basic Medical Sciences, Shanghai Medical College of Fudan University, Shanghai 200032, China. [3]Human Phenome Institute, Collaborative Innovation Center of Genetics and Development, School of Life Sciences, Fudan University, Shanghai 200433, China. [4]CAS Center for Excellence in Molecular Cell Science, Chinese Academy of Sciences, Shanghai 200031, China.
*These authors contributed equally to this work.
†Corresponding author. Email: xuyh@fudan.edu.cn

Structure determination

We reconstituted human BAF complex consisting of the catalytic subunit SMARCA4 (BRG1) and nine auxiliary subunits (Fig. 1A, figs. S1 and S2, and table S1). The purified BAF complexes exhibited nucleosome sliding activities (fig. S1, D and H to J) and were complexed with nucleosome core particle (NCP) in the absence of ATP and adenosine diphosphate (ADP) (fig. S1D). The cryo-EM structure of the BAF-NCP complex (~1.2 MDa) was determined at an overall resolution of 3.7 Å, with the map of the base module locally refined to 3.0-Å resolution (Figs. 1, B to F, and 2A; figs. S3 and S4; table S2; and movies S1 to S5). The structural models were built by fitting available structures into the cryo-EM maps (*15*, *24*, *26*, *27*, *29*) followed by manual model building aided by cross-linking mass spectrometry (XL-MS) (fig. S2, A and B, and data S1 and S2). The 3.7-Å-resolution map and corresponding model were used hereafter unless otherwise specified.

BAF sandwiches the nucleosome

The human BAF complex sandwiches the nucleosome, and its nucleosome-binding manner is distinct from that of other representative chromatin remodelers, including Chd1, SWR1, and INO80 (*30*–*32*) (Fig. 1, B to D, and fig. S5). These remodelers primarily bind nucleosomal DNA and/or histone tails but have fewer contacts with core histones. The sandwiched nucleosome binding of BAF may provide a structural basis to support nucleosome ejection activity (discussed below). The nucleosomal DNA tends to be detached or disordered at both entry and exit sites (Fig. 1, E and F, and movie S5), which may allow the DNA translocation to occur more efficiently owing to fewer restraints.

The BAF complex consists of three modules: the adenosine triphosphatase (ATPase) module, the actin-related protein (ARP) module, and the base module (Fig. 1A). A large portion of the catalytic subunit SMARCA4 (residues 521 to 1647) forms the ATPase module, which grasps the nucleosome with the ATPase motor partially wrapping around the nucleosomal DNA (Fig. 1, B to D). Within the ARP module, the helicase-SANT–associated region (HSA; residues 446 to 520) of SMARCA4 binds the heterodimer formed by ACTL6A (BAF53A) and ACTB (β-actin) (Fig. 1, A and B). The pre-HSA (residues 350 to 445) of SMARCA4 is anchored into the base module, in which the SMARCB1 (BAF47, hSNF5, or INI1) packs against the bottom surface of the nucleosome (Fig. 1, A and B).

The ARP module bridges the ATPase and base modules

The ARP module is formed by the ACTL6A-ACTB heterodimer and the long α helix of the HSA of SMARCA4 (Fig. 1G), revealing a fold similar to the yeast HSA^{Snf2}-arp7-arp9-Rtt102 structure (*27*). The ARP module has no direct contact with the nucleosome, but it associates with and bridges the ATPase and base modules (Fig. 1, B, C, and G). A cryo-EM map reveals considerable contacts between lobe 1 of the SMARCA4 ATPase domain and subdomain 4 (residues 266 to 305) of ACTL6A (Fig. 1, B and G). Moreover, the pre-HSA in the base module and post-HSA in the ATPase module are directly connected by the HSA helix. Thus, the ARP module maintains a rigid conformation of the HSA helix and likely couples the motions of the ATPase and base modules during chromatin remodeling. This observation is consistent with the essential role of the ARP module both in "coupling" the DNA translocation and ATP hydrolysis and in the assembly of functional SWI/SNF complexes (*8*, *18*, *27*).

The ATPase motor engages with nucleosomal DNA

The cryo-EM density of the ATPase motor is relatively weak and reveals a tilted and open conformation (angle of ~90° between the two ATPase lobes), indicating that the structure represents a pre-engaged conformation (fig. S6), which is consistent with the lack of ATP and ADP in the BAF-NCP structure. The ATPase motor is positioned at nucleosomal DNA near superhelical location (SHL) 2.5, and the positioning is likely guided by the HSA-associated ARP module and ATPase-associated Snf2 ATP coupling (SnAC) domain. We observed weak cryo-EM density stretching across the top

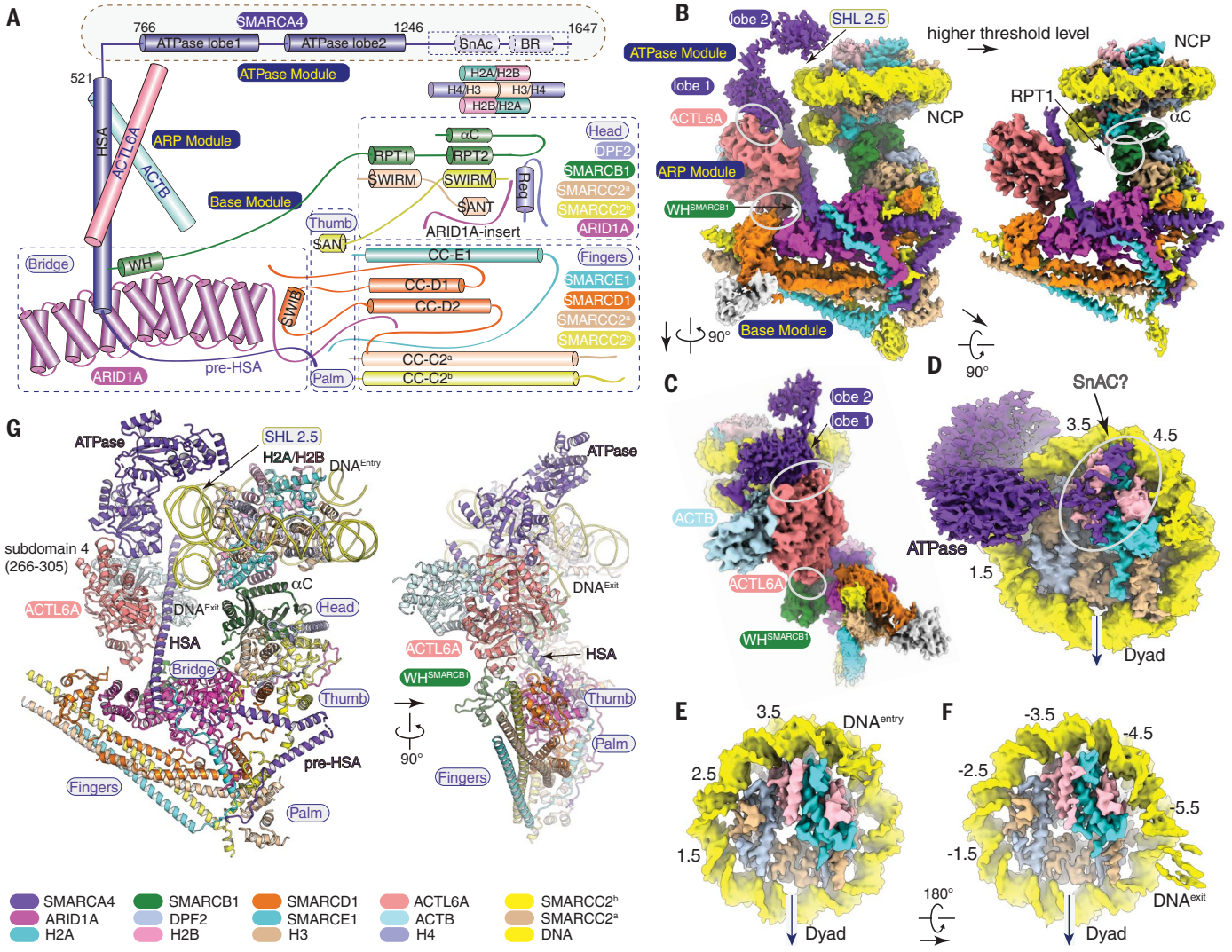

Fig. 1. Cryo-EM structure of human BAF bound to NCP. (**A**) Schematic architecture of BAF complex organization and domain structure of BAF subunits. Color scheme for BAF subunits is indicated in (G) and used throughout all figures. (**B** to **D**) The 3.7-Å-resolution cryo-EM map of BAF-NCP in the absence of ADP in three different views. The map at a higher threshold level [(B), right panel] reveals more details, with the ATPase module fading out. The map at lower threshold level [(B), left panel] reveals density (likely derived from SnAC) packing across the top surface of nucleosome. The intermodular contacts and BAF-NCP contacts are indicated with white circles. (**E** and **F**) Two different views of the cryo-EM map of the nucleosome showing detached and disordered DNA at entry (E) and exit (F) sites. The positions of nucleosomal DNA are labeled with SHL numbers. (**G**) Cartoon model of BAF-NCP structure shown in two different views. RPT, repeat domain; Req, Requiem domain; SWIRM, SWI3, RSC8, and MOIRA; SANT, Swi3, Ada2, N-Cor, and TFIIIB; ARM, armadillo repeats; CC, coiled coil; HSA, helicase-SANT–associated; ARP, actin-related protein; BR, bromodomain; WH, winged helix; SWIB, SWI/SNF complex B/MDM2.

surface of the nucleosome (Fig. 1D and fig. S6A). This region is likely derived from the SnAC and/or bromodomain, which have been shown to bind DNA and/or histone (*25*, *33*, *34*).

The structure of BAF-NCP in the presence of ADP was refined to 10.3-Å resolution, showing that the ATPase motor adopts a relatively closed conformation (~70°) and has tight contacts to nucleosomal DNA around SHL 2 (fig. S6B and movie S6). Thus, ATP or ADP would promote conformational transition of the BAF complex from a pre-engaged to an engaged state, with the ATPase engaging with nucleosomal DNA and, upon ATP hydrolysis, pumping DNA toward the nucleosome dyad and generating DNA translocation.

The organization of the base module

The pre-HSA of SMARCA4 is anchored into the base module, which consists of seven additional auxiliary subunits: two BAF-specific subunits, ARID1A (BAF250A) and DPF2 (BAF45D); and five BAF/PBAF-shared subunits, SMARCB1, SMARCD1 (BAF60A), SMARCE1 (BAF57), and two copies of SMARCC (*8*, *11*, *15*–*19*) (Figs. 1 and 2). These auxiliary subunits exist exclusively in the base module and account for ~80% of the total molecular mass of the BAF complex (fig. S4).

The base module reveals a compact fold and can be divided into five closely associated submodules: the head, thumb, palm, bridge, and fingers (Fig. 2). The head and bridge bind the nucleosome and the ARP module, respectively, generating intermodular contacts (Fig. 1G). The thumb is formed by a SANT domain of SMARCC, the pre-HSA of SMARCA4, and the C-terminal helices of SMARCD1 (Fig. 2). The fingers submodule reveals a characteristic Y-shaped five-helix bundle formed by coiled-coil (CC) domains of SMARCD1, SMARCE1,

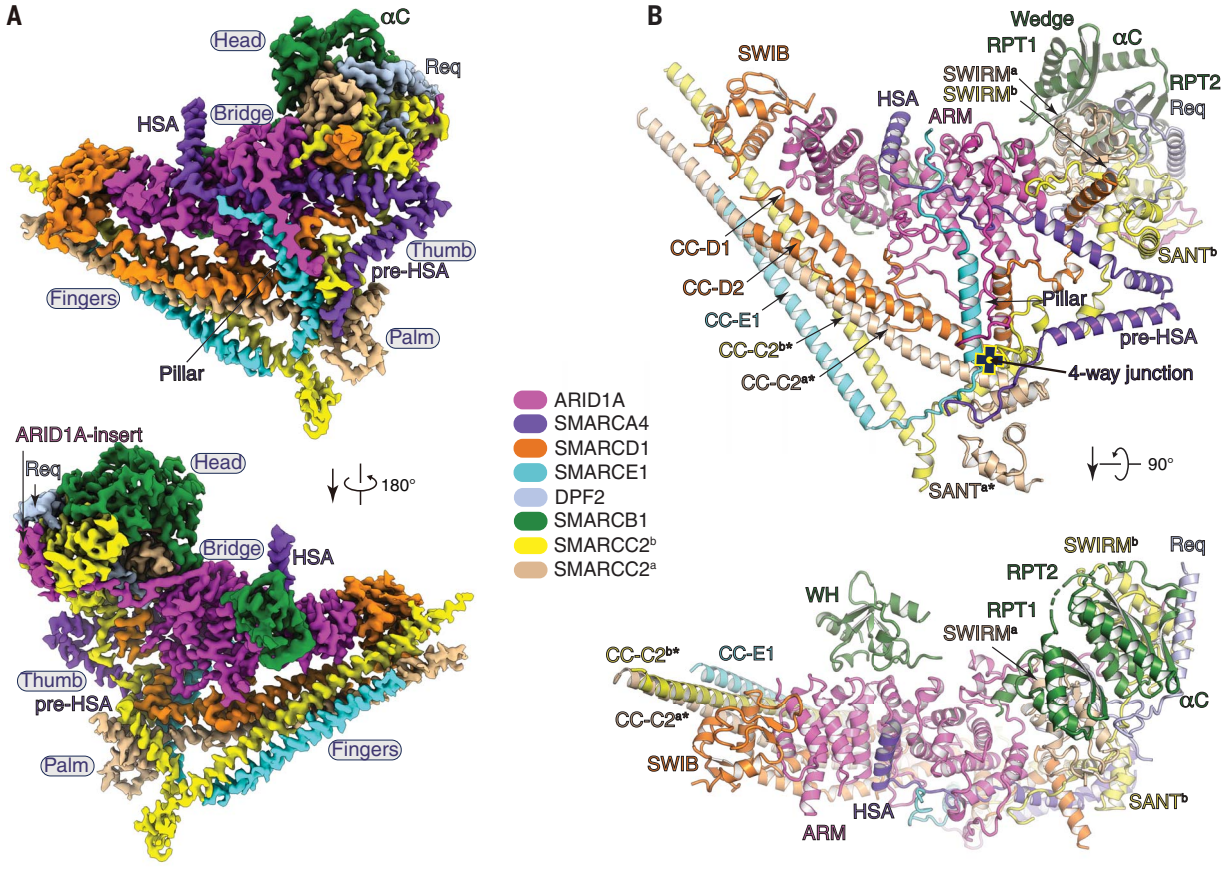

Fig. 2. Structure of the base module. (**A**) The cryo-EM map of the base module locally refined to 3.0-Å resolution. The submodules and elements involved in complex assembly are indicated. (**B**) Cartoon model of the base module in two different views. Regions that are involved in nucleosome recognition and complex formation are indicated. CC-C2^{a*} and CC-C2^{b*} represent the possibility of two CCs of SMARCC2 because of a disconnected cryo-EM map.

and two SMARCC subunits. The palm connects pre-HSA, SMARCD1, SMARCE1, and SMARCC, which merge at a four-way junction.

Nucleosome recognition by SMARCB1 in the head submodule

The head directly binds the histone octamer on the bottom (Fig. 1, B and C, and fig. S7A). It consists of two repeat (RPT) domains and a C-terminal α (αC) helix of SMARCB1, the requiem (Req) domain of DPF2, two SWIRM domains of SMARCCs, and an insert derived from ARID1A (ARID1A-insert) (Fig. 3A and fig. S7B). The two SWIRM domains bind the RPT1 and RPT2 domains, respectively. The two RPT-SWIRM complexes adopt a similar fold and asymmetrically bind each other, with the intermolecular interactions buttressed by the ARID1A-insert (residues 1802 to 1862) and Req domain (residues 13 to 82) of DPF2 (Fig. 3, A and B). The head merges with the bridge and thumb at a three-way junction, and the interactions are mediated by the interwoven loops from DPF2, ARID1A, and two SMARCCs (Fig. 3A). The Req domain of DPF2 is almost identical to that of DPF1 and DPF3 in primary sequence, indicating a similar role of DPF1, DPF2, and DPF3 in BAF complex organization (fig. S2D).

SMARCB1 is required for structural integrity and function of the SWI/SNF complex (*16*, *17*, *35*), and inactivation of SMARCB1 was reported in almost all malignant rhabdoid tumors (*14*, *36*–*38*). The αC helix, which is enriched in residues that are frequently mutated in human cancers, packs against the bottom H2A-H2B heterodimer and serves as a hinge to connect the base module and nucleosome (Fig. 3C and fig. S7A). The four most frequently mutated arginine residues (R370, R373, R374, and R377) together form a positively charged cluster and pack against an acidic patch on the bottom of the nucleosome (Fig. 3D). The four arginine residues are invariant across species, from yeast to humans (Fig. 3E), and were clearly visualized in the cryo-EM map (Fig. 3F). This observation highlights the importance of the αC helix of SMARCB1 in binding of the nucleosome and is consistent with recent studies (*14*, *28*). Although the αC helix of Sfh1 (yeast homolog of SMARCB1) is disordered in the yeast RSC-NCP complex structure, the deletion of this helix impairs nucleosome ejection activity (*28*).

The RPT1 domain of SMARCB1 is in close proximity to the α2 helix of histone H2A and likely causes steric clash between the histone octamer and DNA (Figs. 1, B and G, and 3C; and fig. S5A), suggesting that RPT1 serves as a "wedge" that favors DNA detachment around the exit site. The N-terminal winged helix (WH) domain of SMARCB1 binds the ARM domain of ARID1A and is located more than 40 Å away from nucleosomal DNA (Fig. 1, C and G), suggesting a role independent of its previously reported DNA binding ability (*26*). The WH domain is in close proximity to the ARP module, suggesting a role in regulating ARP–base intermodular interactions (Fig. 1, B and C).

ARID1A serves as a rigid core to stabilize the base module

ARID1A is the largest subunit of the BAF complex. A large portion of ARID1A, including the characteristic AT-rich interacting domain (ARID), was invisible in the complex structure, possibly owing to intrinsic flexibility

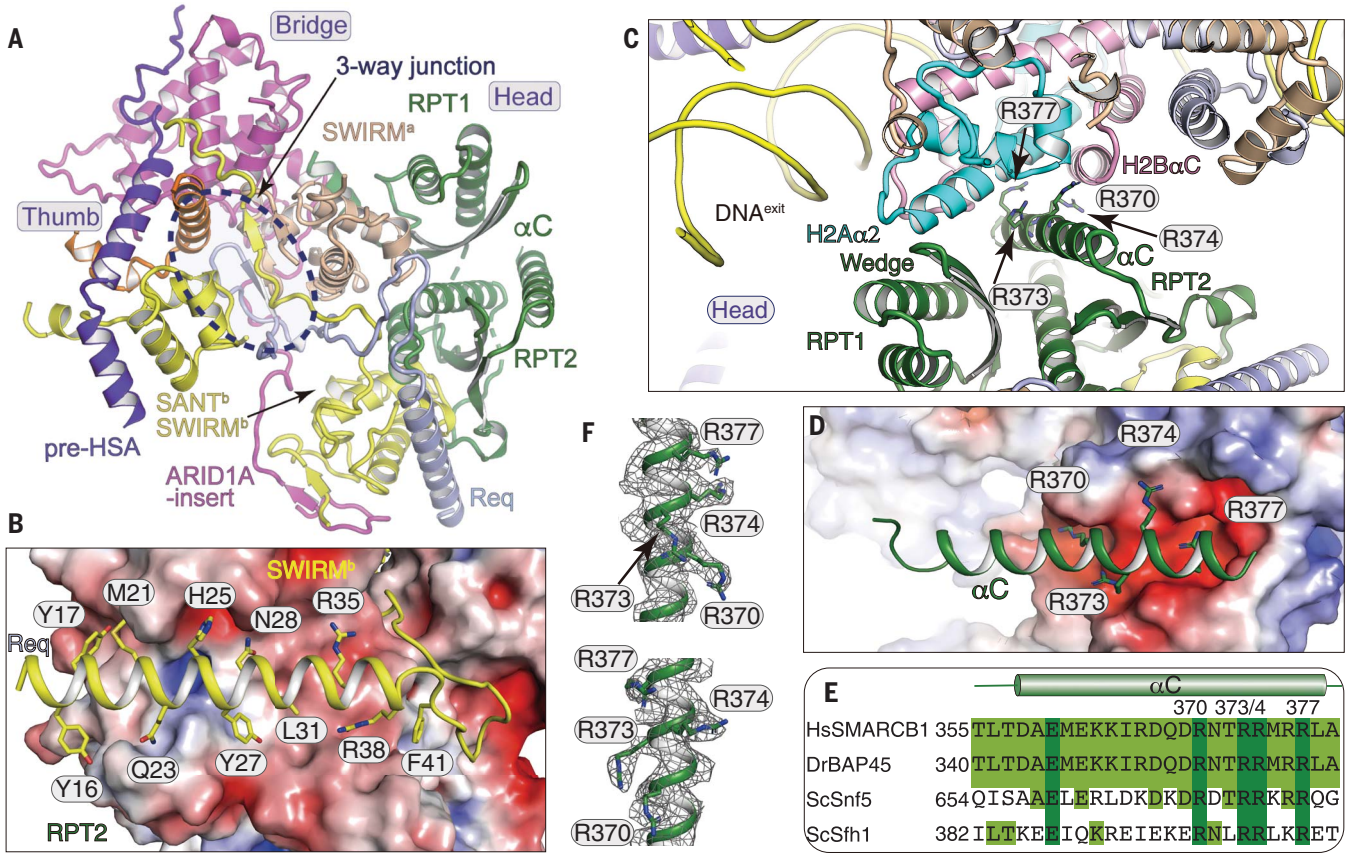

Fig. 3. Structure of the head submodule and role of SMARCB1 in nucleosome recognition. (**A**) Close-up view of the head submodule and its interactions with the bridge and thumb submodules. The sandwiched loops located in a three-way junction are indicated with a dashed blue circle. (**B**) Close-up view of interactions between the Req domain of DPF2 shown in cartoon and RTP2-SWIRM^{b} shown in surface representation (red, negative charge; blue, positive charge). (**C**) Close-up view of the contacts between SMARCB1 and the bottom surface of the nucleosome. Four histone-contacting arginine residues on the αC helix are shown in stick representation. Single-letter abbreviations for the amino acid residues are as follows: A, Ala; C, Cys; D, Asp; E, Glu; F, Phe; G, Gly; H, His; I, Ile; K, Lys; L, Leu; M, Met; N, Asn; P, Pro; Q, Gln; R, Arg; S, Ser; T, Thr; V, Val; W, Trp; and Y, Tyr. (**D**) Basic residues of the αC helix pack against the acidic surface of the histone octamer. The positively charged residues are shown as sticks. (**E**) Conservation of the αC helix of SMARCB1. The invariant and highly conserved residues are highlighted with dark-green and green backgrounds, respectively. (**F**) The cryo-EM map around the αC helix is shown in mesh in two views. The side chains of the abovementioned residues are well covered by the map.

(fig. S2D). The modeled C-terminal ARM domain consists of seven ARM repeats arranged in a superhelical conformation and serves as a rigid core to bind SMARCA4 and all other base subunits (Fig. 4A). A zinc finger is formed with a zinc atom coordinated with residues H2019 and H2021 on ARM3 and residues H2090 and C2094 on ARM4 (Fig. 4B). The zinc finger stabilizes two ARM repeats and the associated loop regions. The ARM domain is located in the center of the base module, with the bottom associating with the fingers, one end joining with the head and thumb, and the other end capped by the SWIB domain of SMARCD1. The N-terminal helical turns of HSA and the preceding loop pack against the concave surface of the ARM domain. The surface residues of ARM contacting SMARCA4 and SMARCD1 are highly conserved, suggesting evolutionarily conserved functions in stabilizing the base module.

We found that, in a manner consistent with the central role of the ARM domain in base module organization, ARID1A bound to other base subunits and the purified base subcomplex (fig. S8, A to C). ARID1A is one of the most frequently mutated mSWI/SNF subunits in human cancer, and frameshift mutations occur near the C terminus (*11*, *39*), supporting the importance of the C-terminal ARM domain in BAF structure and function. The structure showed that the overall fold of the BAF complex would not be properly maintained in the absence of ARID1A (Fig. 4C), although other BAF subunits would remain associated with SMARCC1 and SMARCC2 because the BAF$^{\Delta ARID1A}$ complex survived ion-exchange chromatography (fig. S1C). The sliding activity of BAF$^{\Delta ARID1A}$ was considerably enhanced by the addition of larger amounts of purified ARID1A (Fig. 4D and fig. S8D), indicating that ARID1A is required for efficient nucleosome sliding activity.

ARID1A and ARID1B share highly similar primary sequences and are mutually exclusive in the BAF complex, suggesting that ARID1B-containing BAF is assembled in a similar manner (fig. S2D). As a PBAF-specific subunit, ARID2 is not a paralog of ARID1A or ARID1B and shows a distinct domain architecture. However, the N-terminal helical region (residues 150 to 470) of ARID2 is predicted to form a seven-repeat ARM domain (*40*). Thus, the N-terminal ARM domain of ARID2 and the C-terminal ARM domain of ARID1A may play a similar role in organizing PABF and BAF, respectively.

SMARCCs compose base module scaffold, and SMARCD1 and SMARCE1 facilitate organization

As the scaffold of the base module, the two SMARCC subunits bind all other base subunits and thread through the head, thumb, palm, and fingers submodules (Fig. 4C). The

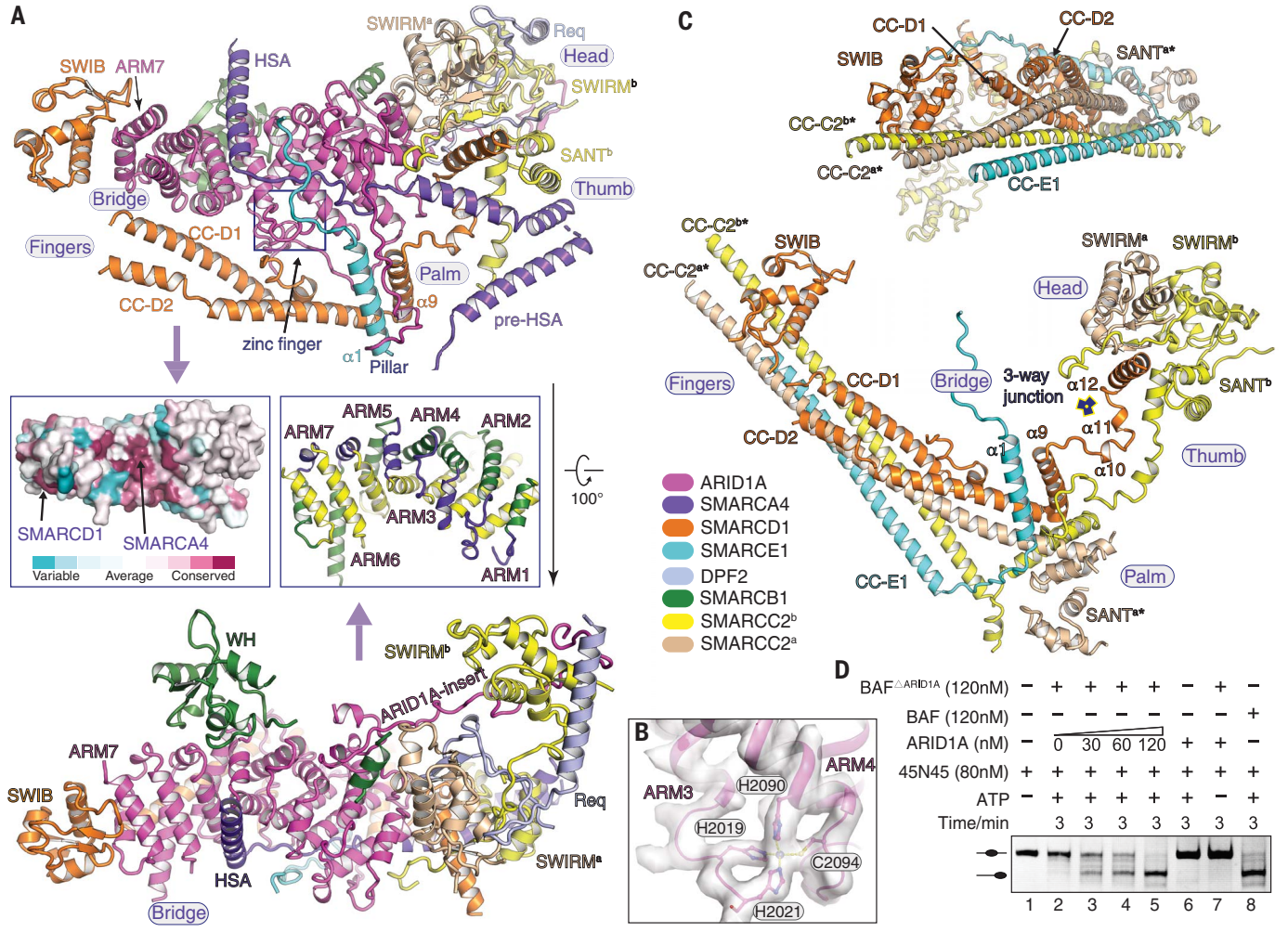

Fig. 4. Subunit organization in the base module. (**A**) Cartoon model of interactions between ARID1A and other subunits is shown in two views. (Left middle panel) The surface of the ARM domain is shown and colored according to the conservation scores. (Right middle panel) Seven ARM repeats are shown, with front helices colored in yellow, back helices colored in green, and ridge helices and loops colored in blue. (**B**) Close-up view of the zinc finger connecting ARM3 and ARM4, with zinc-coordinating residues shown in sticks and zinc atom shown as a gray ball. The location of the zinc finger is indicated with a blue rectangle in the upper panel of (A). (**C**) Cartoon of the base module with ARID1A and SMARCA4 omitted. The lack of ARID1A would lead to a clash of the base module, although other subunits remain associated by the scaffold subunits, SMARCC1 and SMARCC2. The three-pronged yellow and blue shape indicates a three-way junction of the head, thumb, and bridge. (**D**) In vitro nucleosome sliding assay performed using purified BAF$^{\Delta ARID1A}$ complex and increasing amounts of purified ARID1A. Note that BAF$^{\Delta ARID1A}$ demonstrates nucleosome sliding activity in higher protein concentration (fig. S8D). 45N45, a center-positioned nucleosome with two 45–base pair flanking DNA fragments.

BAF complexes containing SMARCC1 and SMARCC2 (BAF-CC1/CC2) and two SMARCC2 subunits (BAF-CC2/CC2) generated almost identical cryo-EM maps (fig. S3). SMARCC1 and SMARCC2 behave similarly in binding other BAF subunits and subcomplexes (fig. S9, D to I, and supplementary text). This observation is consistent with a previous study showing that SMARCC1 and SMARCC2 are functionally similar and play critical roles in the early stage of mSWI/SNF complex assembly (*11*).

SMARCD1 adopts an elongated conformation and runs alongside the two SMARCC subunits (Fig. 4C). The SWIB domain adopts a compact globular fold and binds the ARM7 of ARID1A and the CC of SMARCC (Fig. 4A). The α9 helix of SMARCD1 packs against the α1 helix of SMARCE1 and a loop of ARID1A, generating a "pillar" that connects to the bridge (Figs. 2 and 4A). The α10, α11, and α12 helices of SMARCD1 interact with the SANT^{b} domain and pre-HSA with the α12 helix protruding out of the intersection of the head, bridge, and thumb (Fig. 4, A and C). Thus, SMARCD1 and SMARCE1 assist SMARCC1 and SMARCC2 in organizing the base module.

Comparison of BAF-NCP and RSC-NCP complex structures

The yeast RSC complex is the homolog of the mammalian PBAF complex, consisting of ARID2 (instead of ARID1A and ARID1B) and a PBAF-specific subunit, polybromo-1 (PBRM1, or BAF180). Comparison of our BAF-NCP structure and a recently published yeast RSC-NPC structure (*28*) revealed a similar nucleosome-binding mode (fig. S10). Unexpectedly, the nucleosome is mainly bound by the ATPase domain, and the αC helix of Sfh1 is invisible in the RSC-NCP structure (*28*). In contrast, the nucleosome is sandwiched by BAF with H2A-H2B dimer stably associated with the αC helix of SMARCB1. The two complexes may represent different conformational states, or this difference might result from different experimental conditions. Structural comparison also revealed considerable differences in the base module organization. ARID1A, SMARCC1, SMARCC2, SMARCD1, and SMARCE1 exhibit conformations distinct from their counterparts in the RSC complex. The comparison

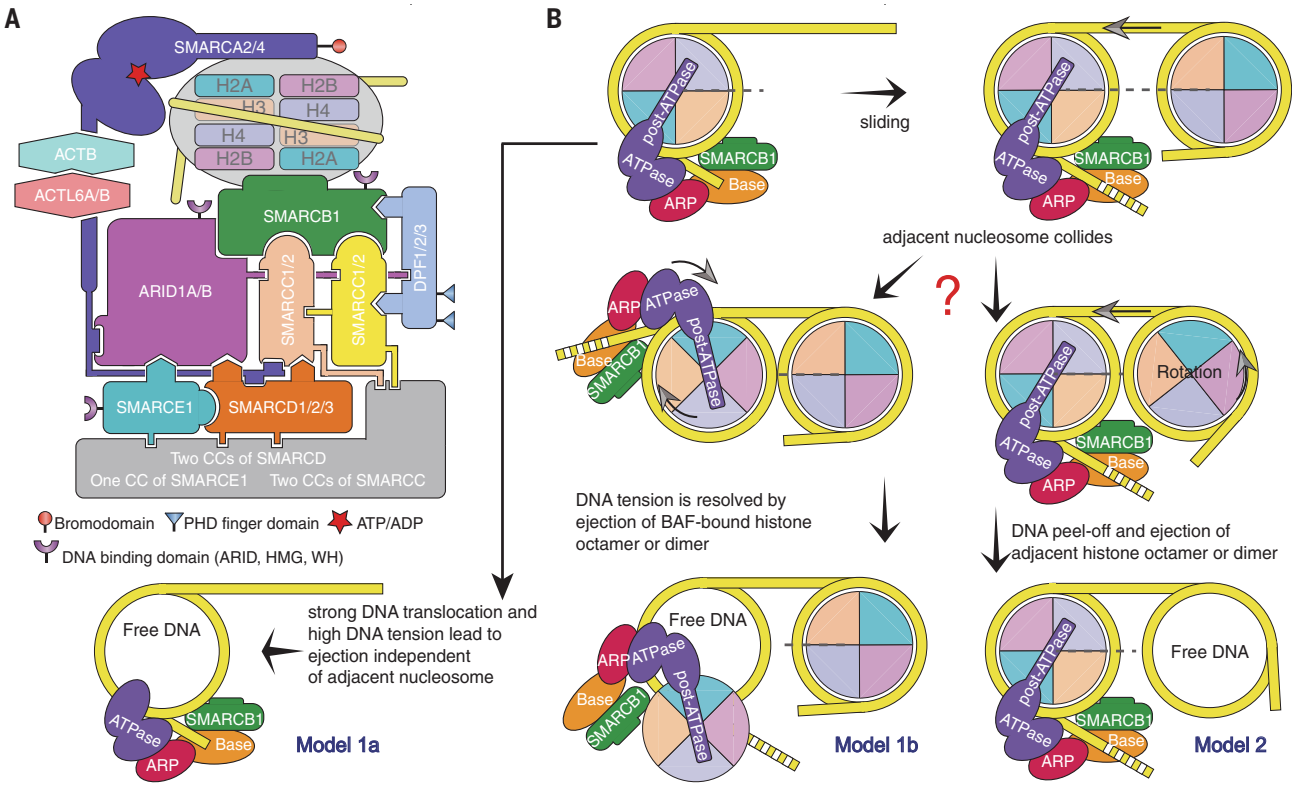

Fig. 5. Models of chromatin remodeling of the BAF complex. (**A**) BAF subunits are shown in cartoon model. The indicated paralogs of BAF subunits are mutually exclusive in the BAF complex. The nucleosome is sandwiched by SMARCA2/4 and SMARCB1. The ATPase of SMARCA2/4 grasps nucleosomal DNA and generates DNA translocation in an ATP-dependent manner. PHD, plant homeodomain; HMG, high-mobility group. (**B**) The BAF-NCP structure could fit two nonexclusive models of nucleosome ejection. The histone octamer or dimer could be ejected from BAF-bound nucleosome (model 1) or the adjacent nucleosome (model 2). The ejection could occur independent of (model 1a) or dependent upon (model 1b) the adjacent nucleosome.

also suggested that Rsc7 and Htl1 in RSC are equivalents of DPF2 and SMARCE1 of BAF, respectively. BAF has no histone tail–binding lobe, which may exist exclusively in RSC and PBAF complexes. Homologs of yeast DNA interaction subunits, RSC3 and RSC30, do not exist in mammals, suggesting that PBAF is also structurally different from RSC.

Model of chromatin remodeling of the BAF complex

Our structural and biochemical analyses illustrated the mechanisms of organization and nucleosome recognition of the human BAF complex, the prototype mSWI/SNF remodeler (Fig. 5A). BAF ejects the nucleosome and creates and maintains NDRs that are essential for transcription. Two non–mutually exclusive models of nucleosome ejection have been proposed (*2*). The BAF-NCP structure could fit both models (Fig. 5B). In the first model, the BAF-bound histone octamer, and more possibly the H2A-H2B dimer, could be evicted because of DNA tension resulting from either strong DNA translocation (Fig. 5B, model 1a; independent of the adjacent nucleosome) or collision with the adjacent nucleosome (Fig. 5B, model 1b). In the second model, BAF sandwiches the nucleosome to ensure that the ATPase domain stably engages with DNA and "peels" the DNA off of the adjacent nucleosome. In both cases, the two nucleosome-sandwiching regions, the SnAC domain of SMARCA4 and the αC helix of SMARCB1, likely play important roles in nucleosome ejection, which has been experimentally demonstrated (*14*, *16*, *28*, *33*). The DNA detachment may facilitate efficient DNA translocation of the BAF-associated nucleosome because of fewer DNA–histone contacts. The chromatin ejection may also be promoted by the DNA-interacting ARID domain of ARID1A and/or acetylated histone tail–binding bromodomain of SMARCA4, which were not observed in the cryo-EM map, owing to flexibility.

REFERENCES AND NOTES

1. C. Y. Zhou, S. L. Johnson, N. I. Gamarra, G. J. Narlikar, *Annu. Rev. Biophys.* **45**, 153–181 (2016).
2. C. R. Clapier, J. Iwasa, B. R. Cairns, C. L. Peterson, *Nat. Rev. Mol. Cell Biol.* **18**, 407–422 (2017).
3. L. K. Elfring, R. Deuring, C. M. McCallum, C. L. Peterson, J. W. Tamkun, *Mol. Cell. Biol.* **14**, 2225–2234 (1994).
4. J. Masliah-Planchon, I. Bièche, J. M. Guinebretière, F. Bourdeaut, O. Delattre, *Annu. Rev. Pathol.* **10**, 145–171 (2015).
5. L. Neigeborn, M. Carlson, *Genetics* **108**, 845–858 (1984).
6. W. Wang *et al.*, *EMBO J.* **15**, 5370–5382 (1996).
7. C. Kadoch, G. R. Crabtree, *Sci. Adv.* **1**, e1500447 (2015).
8. C. R. Clapier *et al.*, *Mol. Cell* **62**, 453–461 (2016).
9. M. L. Dechassa *et al.*, *Mol. Cell* **38**, 590–602 (2010).
10. H. Boeger, J. Griesenbeck, J. S. Strattan, R. D. Kornberg, *Mol. Cell* **14**, 667–673 (2004).
11. N. Mashtalir *et al.*, *Cell* **175**, 1272–1288.e20 (2018).
12. L. Ho, G. R. Crabtree, *Nature* **463**, 474–484 (2010).
13. C. Kadoch *et al.*, *Nat. Genet.* **45**, 592–601 (2013).
14. A. M. Valencia *et al.*, *Cell* **179**, 1342–1356.e23 (2019).
15. L. Yan, S. Xie, Y. Du, C. Qian, *J. Mol. Biol.* **429**, 1650–1660 (2017).
16. P. Sen *et al.*, *Cell Rep.* **18**, 2135–2147 (2017).
17. X. Wang *et al.*, *Nat. Genet.* **49**, 289–295 (2017).
18. H. Szerlong *et al.*, *Nat. Struct. Mol. Biol.* **15**, 469–476 (2008).
19. M. L. Phelan, S. Sif, G. J. Narlikar, R. E. Kingston, *Mol. Cell* **3**, 247–253 (1999).
20. M. L. Dechassa *et al.*, *Mol. Cell. Biol.* **28**, 6010–6021 (2008).
21. Y. Chaban *et al.*, *Nat. Struct. Mol. Biol.* **15**, 1272–1277 (2008).
22. C. L. Smith, R. Horowitz-Scherer, J. F. Flanagan, C. L. Woodcock, C. L. Peterson, *Nat. Struct. Biol.* **10**, 141–145 (2003).
23. F. J. Asturias, W. H. Chung, R. D. Kornberg, Y. Lorch, *Proc. Natl. Acad. Sci. U.S.A.* **99**, 13477–13480 (2002).
24. M. Li *et al.*, *Nature* **567**, 409–413 (2019).
25. E. A. Morrison *et al.*, *Nat. Commun.* **8**, 16080 (2017).
26. M. D. Allen, S. M. Freund, G. Zinzalla, M. Bycroft, *Structure* **23**, 1344–1349 (2015).
27. H. L. Schubert *et al.*, *Proc. Natl. Acad. Sci. U.S.A.* **110**, 3345–3350 (2013).
28. Y. Ye *et al.*, *Science* **366**, 838–843 (2019).
29. K. Luger, A. W. Mäder, R. K. Richmond, D. F. Sargent, T. J. Richmond, *Nature* **389**, 251–260 (1997).
30. L. Farnung, S. M. Vos, C. Wigge, P. Cramer, *Nature* **550**, 539–542 (2017).
31. O. Willhoft *et al.*, *Science* **362**, eaat7716 (2018).
32. R. Ayala *et al.*, *Nature* **556**, 391–395 (2018).

33. P. Sen *et al*., *Mol. Cell. Biol.* **33**, 360–370 (2013).
34. W. Shen *et al*., *Biochemistry* **46**, 2100–2110 (2007).
35. R. T. Nakayama *et al*., *Nat. Genet.* **49**, 1613–1623 (2017).
36. I. Versteege *et al*., *Nature* **394**, 203–206 (1998).
37. C. Kadoch, G. R. Crabtree, *Cell* **153**, 71–85 (2013).
38. M. J. McBride *et al*., *Cancer Cell* **33**, 1128–1141.e7 (2018).
39. R. Mathur *et al*., *Nat. Genet.* **49**, 296–302 (2017).
40. L. A. Kelley, S. Mezulis, C. M. Yates, M. N. Wass, M. J. Sternberg, *Nat. Protoc.* **10**, 845–858 (2015).

ACKNOWLEDGMENTS

We thank the Center of Cryo-Electron Microscopy, Fudan University; the Center of Cryo-Electron Microscopy, ShanghaiTech University; the Center for Biological Imaging of Institute of Biophysics (IBP) of Chinese Academy of Sciences (CAS); and the National Center for Protein Science Shanghai (NCPSS) for supporting cryo-EM data collection and data analyses. We also thank the Biomedical Core Facility, Fudan University, for supporting mass spectrometry analyses. **Funding:** This work was supported by grants from the National Key R&D Program of China (2016YFA0500700), the National Natural Science Foundation of China (31830107, 31821002, and 31425008), the National Ten-Thousand Talent Program (Y.X.), the National Program for Support of Top-Notch Young Professionals (Y.X.), the Shanghai Municipal Science and Technology Major Project (2017SHZDZX01), and the Strategic Priority Research Program of the Chinese Academy of Sciences (XDB08000000). **Author contributions:** S.H. prepared the samples for structural and biochemical analyses with help from J.Y., J.L., X.W., and B.L. Z.W. and Y.T. performed EM analyses and model building with help from Z.Y. Y.X. and S.H. wrote the manuscript. Y.X. supervised the project. **Competing interests:** The authors declare no competing interests. **Data and materials availability:** Cryo-EM maps have been deposited in the Electron Microscopy Data Bank (EMDB) under accession numbers EMD-0968 (base module), EMD-0969 (ARP module), EMD-0970 (ATPase-NCP with αC of SMARCB1), EMD-0972 (ATPase-NCP with detached DNA), EMD-0974 (BAF-NCP, 3.7 Å), EMD-0971 (BAF-NCP, 6.6 Å), and EMD-0973 (BAF^{ADP}-NCP). Atomic coordinates for the base module and BAF-NCP have been deposited in the Protein Data Bank under IDs 6LTH and 6LTJ, respectively.

SUPPLEMENTARY MATERIALS

science.sciencemag.org/content/367/6480/875/suppl/DC1
Materials and Methods
Supplementary Text
Figs. S1 to S10
Tables S1 and S2
References (*41*–*61*)
Movies S1 to S6
Data S1 and S2

View/request a protocol for this paper from *Bio-protocol*.

24 October 2019; resubmitted 10 January 2020
Accepted 22 January 2020
Published online 30 January 2020
10.1126/science.aaz9761

STRUCTURAL BIOLOGY

Molecular mechanism of biased signaling in a prototypical G protein–coupled receptor

Carl-Mikael Suomivuori[1,2,3,4]*, Naomi R. Latorraca[1,2,3,4,5]*†, Laura M. Wingler[6,7], Stephan Eismann[1,2,3,4,8], Matthew C. King[1,2,3,4], Alissa L. W. Kleinhenz[6,7,9], Meredith A. Skiba[10], Dean P. Staus[6,7], Andrew C. Kruse[10], Robert J. Lefkowitz[6,7,11], Ron O. Dror[1,2,3,4,5]‡

Biased signaling, in which different ligands that bind to the same G protein–coupled receptor preferentially trigger distinct signaling pathways, holds great promise for the design of safer and more effective drugs. Its structural mechanism remains unclear, however, hampering efforts to design drugs with desired signaling profiles. Here, we use extensive atomic-level molecular dynamics simulations to determine how arrestin bias and G protein bias arise at the angiotensin II type 1 receptor. The receptor adopts two major signaling conformations, one of which couples almost exclusively to arrestin, whereas the other also couples effectively to a G protein. A long-range allosteric network allows ligands in the extracellular binding pocket to favor either of the two intracellular conformations. Guided by this computationally determined mechanism, we designed ligands with desired signaling profiles.

Binding of an extracellular agonist to a G protein–coupled receptor (GPCR) generally stimulates multiple intracellular signaling pathways by causing the GPCR to couple to both G proteins and arrestins. GPCRs represent the targets of roughly one-third of all drugs (*1*), and, in many cases, the desired effects of a drug stem from arrestin signaling and the undesired ones from G protein signaling, or vice versa. Intriguingly, certain GPCR ligands preferentially stimulate either arrestin or G protein signaling, a phenomenon known as biased signaling (*2*).

The molecular mechanism of biased signaling remains unknown, hindering the discovery and optimization of biased ligands that are more effective and have fewer side effects than conventional drugs. Biophysical studies indicate that ligands with distinct bias profiles stabilize distinct receptor conformations (*3*, *4*), but these studies do not identify what these conformations are or how ligands induce them. The receptor adopts similar conformations in experimental structures of GPCR–G protein (*5*–*9*) and GPCR-arrestin (*10*–*12*) complexes, leaving unclear what intracellular conformations are responsible for biased signaling and how ligands in the extracellular binding pocket select among the relevant signaling conformations.

The angiotensin II (AngII) type 1 receptor (AT_1R) is a model system for studies of biased signaling (*13*–*15*). It stimulates both G protein–mediated and arrestin-mediated signaling pathways upon binding of its native ligand, the octapeptide AngII. Small modifications to AngII can result in either arrestin-biased or G protein–biased ligands, which induce a higher or lower ratio of arrestin signaling to G protein signaling than AngII, respectively (*13*, *14*). AT_1R is also a major drug target, and there is interest in developing arrestin-biased AT_1R ligands as drugs for heart failure because such ligands can increase cardiac contractility without undesired hypertensive effects (*16*–*18*).

The companion manuscript (*19*) presents crystal structures of AT_1R bound to AngII and to arrestin-biased agonists. The intracellular conformations in these structures and in the previously published active-state structure (*20*) are essentially identical, most likely because they are all stabilized for crystallography by binding to the same high-affinity nanobody on the intracellular side. To determine how differences in intracellular conformation relate to the bias profile of the bound ligand, we performed extensive molecular dynamics (MD) simulations of AT_1R without the nanobody.

AT_1R transitions between two active intracellular conformations

Our simulations were initiated from the previously published active-state AT_1R structure (*20*), with the nanobody removed. In most of these simulations, the cocrystallized ligand was removed, and different ligands were modeled in its place, including AngII, four arrestin-biased ligands, and two G protein–biased ligands (fig. S1 and table S1). We also performed control simulations from the structures reported in the companion manuscript (*19*), and these simulations converged to the same behavior.

In simulations with the nanobody removed, agonist-bound AT_1R transitions between two intracellular conformations that differ primarily in transmembrane helix 7 (TM7) (Fig. 1 and fig. S2). One of these, the "canonical active" conformation, closely resembles previously determined structures of GPCRs in complex with G proteins (*5*–*9*) as well as the active-state structure of the AngII type 2 receptor (AT_2R) (*21*). The other—the "alternative" conformation—differs in several regards. Viewed from the extracellular side, TM7 is twisted counterclockwise above its proline kink, causing N1.50 (Asn^{46}) to switch its preferred hydrogen-bond acceptor from N7.46 (Asn^{295}) to C7.47 (Cys^{296}). [We use the Ballesteros-Weinstein numbering scheme, where the digit before the decimal point specifies the TM helix (*22*).] As a result of this twist, the intracellular portion of TM7 shifts toward TM3, causing the side chains of Y7.53 (Tyr^{302}) of the NPXXY motif (N, Asn; P, Pro; X, any residue; Y, Tyr) and R3.50 (Arg^{126}) of the DRY motif (D, Asp; R, Arg) to adopt "downward" rotamers pointing toward the intracellular side. Interestingly, the nanobody-bound AT_1R structures resemble the alternative intracellular conformation, except that Y7.53 adopts the upward rotamer of the canonical active conformation because its downward rotamer would clash with the nanobody. Both the alternative and canonical active conformations retain the TM6 conformation observed in the nanobody-bound AT_1R structures (*19*, *20*), which is characteristic of active-state GPCR structures in that it is shifted outward relative to inactive-state structures (*23*, *24*).

Unlike the canonical active conformation, the alternative conformation has not been observed in experimental GPCR structures. The alternative conformation of TM7 closely resembles several GPCR structures (fig. S2) (*25*–*30*), including the serotonin 2B receptor ($5\text{-}HT_{2B}R$) bound to arrestin-biased ligands. However, these structures exhibit more inactive-like positions of TM6, likely owing to the absence of intracellular binding partners. In previous simulations of the β_2-adrenergic receptor (β_2AR) transitioning from its canonical active to inactive conformation, we observed a rare intermediate in which both TM6 and TM7 match the alternative conformation, but we did not suggest a connection to biased signaling (*31*).

[1]Department of Computer Science, Stanford University, Stanford, CA 94305, USA. [2]Department of Molecular and Cellular Physiology, Stanford University School of Medicine, Stanford, CA 94305, USA. [3]Department of Structural Biology, Stanford University School of Medicine, Stanford, CA 94305, USA. [4]Institute for Computational and Mathematical Engineering, Stanford University, Stanford, CA 94305, USA. [5]Biophysics Program, Stanford University, Stanford, CA 94305, USA. [6]Howard Hughes Medical Institute, Duke University Medical Center, Durham, NC 27710, USA. [7]Department of Medicine, Duke University Medical Center, Durham, NC 27710, USA. [8]Department of Applied Physics, Stanford University, Stanford, CA 94305, USA. [9]School of Medicine, University of Michigan, Ann Arbor, MI 48109, USA. [10]Department of Biological Chemistry and Molecular Pharmacology, Blavatnik Institute, Harvard Medical School, Boston, MA 02115, USA.
*These authors contributed equally to this work.
†Present address: Department of Molecular and Cellular Biology, University of California, Berkeley, CA 94720, USA.
‡Corresponding author. Email: ron.dror@stanford.edu

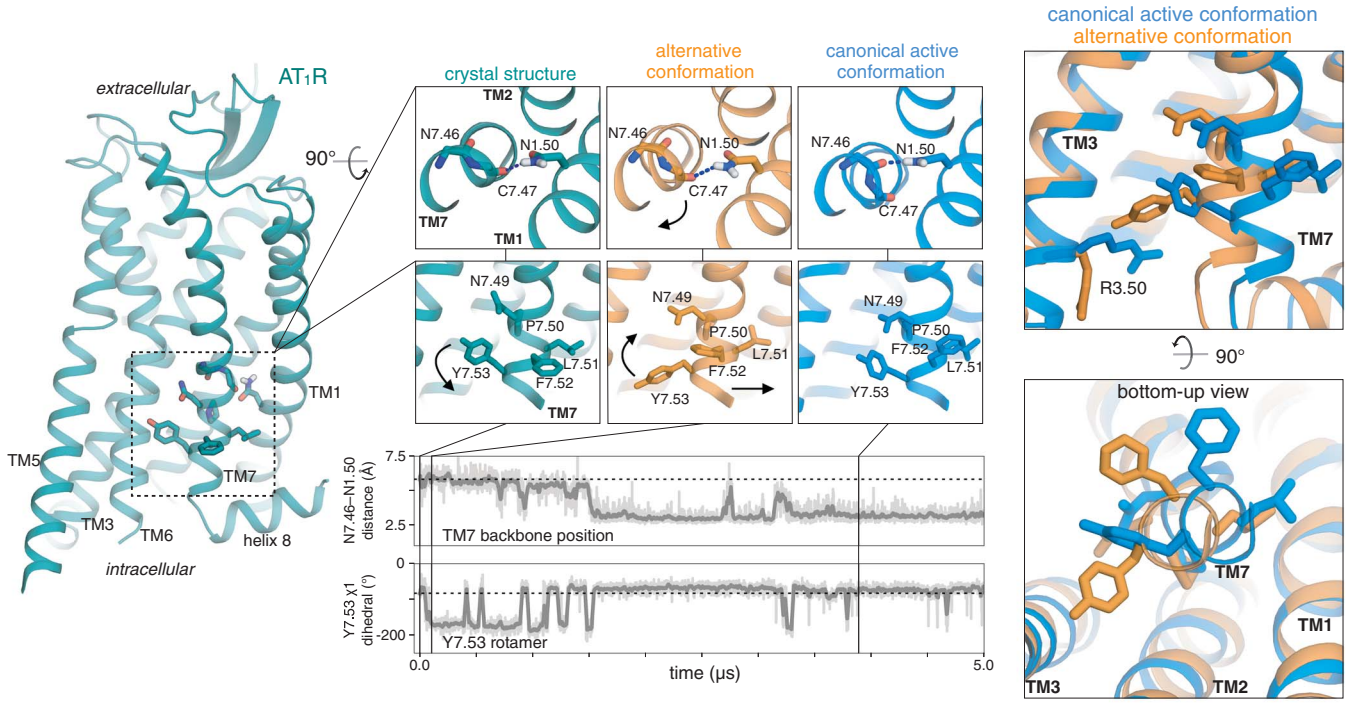

Fig. 1. In simulation, AT_1R adopts two major signaling conformations. In a representative simulation with the nanobody removed, AT_1R (left, with magnified views in the middle) first adopts the alternative conformation and then transitions to the canonical active conformation. During this transition, TM7 twists above its proline kink, leading the intracellular portion of TM7 to shift away from TM2 and TM3. The twisting motion causes N1.50 to switch its preferred hydrogen bond acceptor from C7.47 to N7.46 (top trace, distance between N1.50 side-chain nitrogen and N7.46 backbone oxygen). The conformational transition also leads to rearrangements of side chains, including those of Y7.53 and R3.50, which are oriented downward (toward the intracellular side) in the alternative conformation and more upward in the canonical active conformation (bottom trace; see also fig. S3). Thick traces represent moving averages, whereas thin traces represent original, unsmoothed values (see methods). Dashed horizontal lines indicate values for the nanobody-bound crystal structures. Superimposed views of the canonical active and alternative conformations are shown on the right.

The alternative conformation appears to accommodate β-arrestins but not Gq

To determine whether these two conformations couple differently to G proteins and arrestins, we prepared structural models of AT_1R in complex with its preferred partners, Gq and β-arrestins 1 and 2 (Fig. 2). These models suggest that, although the canonical active conformation couples well to both Gq and β-arrestins, the alternative conformation couples well to β-arrestins but not Gq. The alternative conformation stabilizes R3.50 in a downward rotamer, which clashes with the α5 helix of Gq. R3.50 shifts upward on transition to the canonical active conformation, accommodating insertion of the Gα subunit. Both the alternative and canonical active conformations appear to readily accommodate the β-arrestin finger loop.

In simulations of rhodopsin bound to visual arrestin, rhodopsin occasionally transitions spontaneously from the canonical active conformation to the alternative conformation, with both R3.50 and Y7.53 forming interactions with backbone atoms on the finger loop (fig. S4). This indicates that both canonical active and alternative conformations of rhodopsin couple to arrestin.

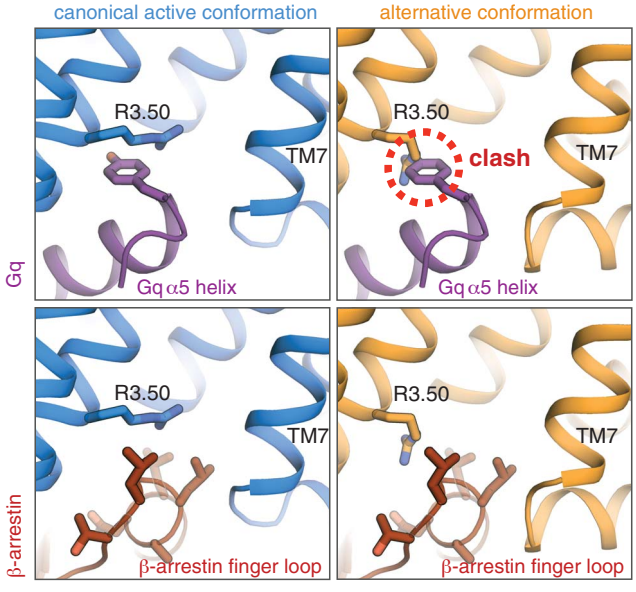

Fig. 2. Structural models suggest that the alternative conformation couples preferentially to β-arrestins, whereas the canonical active conformation couples well to both Gq and β-arrestins. In the alternative conformation, R3.50 adopts an orientation that clashes with a tyrosine on the α5 helix of Gq (top right). The bottom row shows models with β-arrestin 1; models with β-arrestin 2 yield essentially identical results (see methods).

Intracellular TM7 conformation is allosterically coupled to the ligand-binding pocket

In simulations that transition between the alternative and canonical active conformations, we observed rearrangements in several residues that form an allosteric network between the ligand-binding pocket and the intracellular side of the receptor (Fig. 3A and fig. S5). The intracellular TM7 conformation is closely coupled to the position of Y7.43

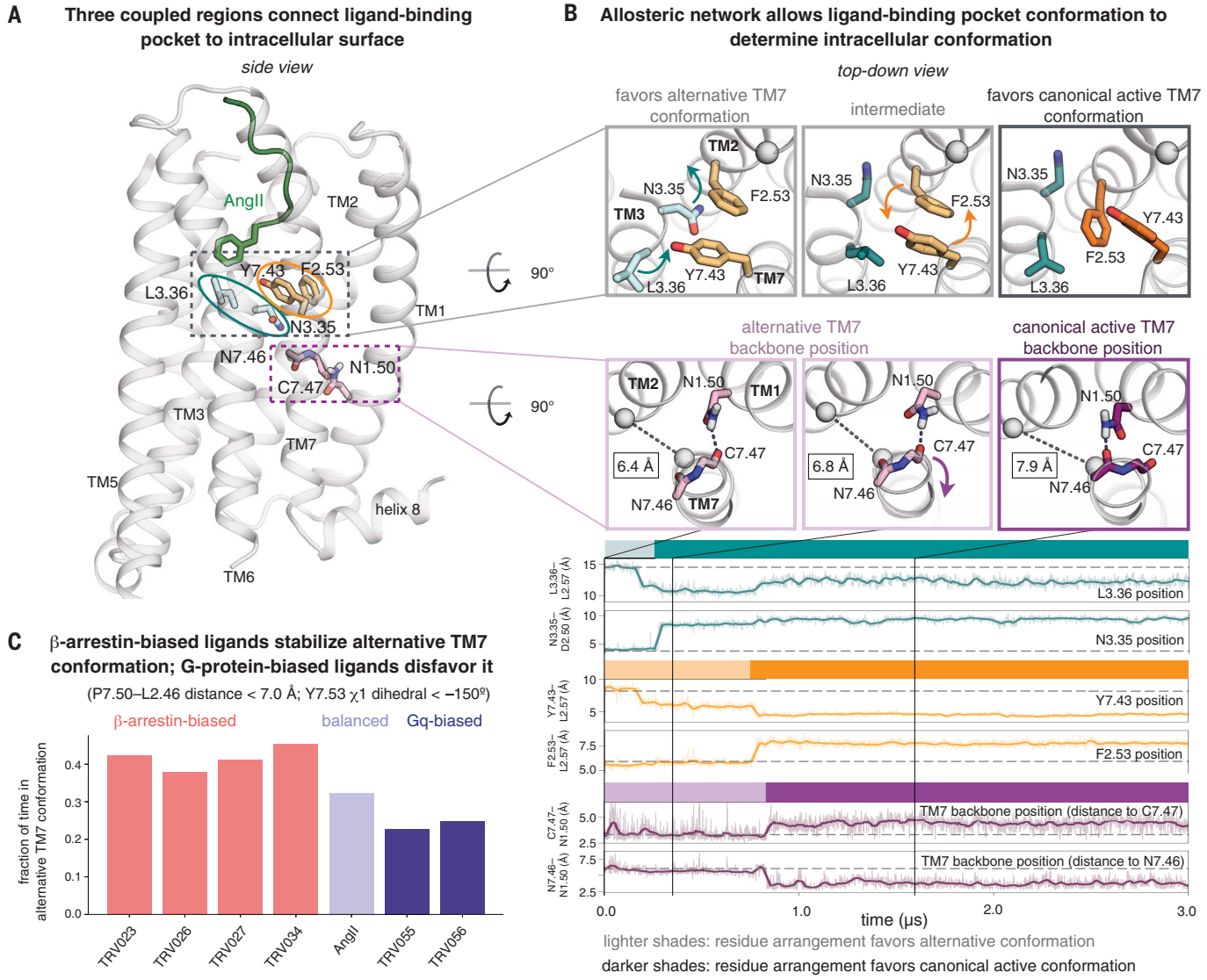

Fig. 3. Allosteric network allows ligands to favor either intracellular conformation. (**A**) Three coupled regions of AT_1R connect the ligand-binding pocket to the intracellular surface. Key residues for the three regions are shown in turquoise, orange, and purple. (**B**) Mechanism for coupling between the three regions. In simulations that transition from the alternative conformation to the canonical active conformation, a rotation of TM3 at the binding pocket triggers subsequent rearrangements in other regions of the protein (top row, left and middle). Such transitions typically begin when L3.36 moves closer to TM2 (top turquoise trace) and N3.35 flips outward from the helical bundle (bottom turquoise trace). The outward displacement of N3.35 creates space for F2.53 to switch positions with Y7.43 (orange traces) (top row, middle and right). The motion of Y7.43 leads TM7 to twist just above its proline kink (bottom row, left, middle, and right), such that N7.46 replaces C7.47 as the hydrogen bonding partner of N1.50 (purple traces). This TM7 twist also leads to an outward shift of TM7 on the intracellular side, as measured by increasing P7.50-to-L2.46 Cα-to-Cα distances; these distances are shown in black rectangles in the bottom row of molecular renderings. See also fig. S5. (**C**) In simulation, the fraction of time spent in the alternative TM7 conformation correlates with the ligand's bias profile. β-Arrestin–biased ligands favor this conformation much more than Gq-biased ligands (P = 0.0006, two-sided Welch's t test; see methods) and also more than the balanced ligand AngII (P = 0.007), which favors it more than Gq-biased ligands (P = 0.04). Reported values are based on REMD simulations of AT_1R bound to each ligand. We performed two REMD simulations for AngII (with very similar results of 0.32 and 0.33) and one for each other ligand shown. Each REMD simulation consists of 36 coupled MD simulations, each 3.6 μs in length (see methods).

(Tyr^{292}) higher on TM7. The alternative conformation is favored when Y7.43 points toward TM3, and the canonical active conformation is favored when Y7.43 points toward TM2 (Fig. 3B).

Y7.43 is coupled to the ligand via two adjacent residues on TM3, N3.35 (Asn^{111}) and L3.36 (Leu^{112}) (Fig. 3, A and B). When N3.35 points inward (toward the center of the helical bundle), Y7.43 nearly always points toward TM3. N3.35 must point outward for Y7.43 to point toward TM2, which requires that the side chains of Y7.43 and F2.53 (Phe^{77}) swap positions (Fig. 3B). L3.36, which is often in direct contact with ligands, influences the position of neighboring residue N3.35: TM5- and TM2-proximal positions of L3.36 favor the inward- and outward-pointing positions of N3.35, respectively. L3.36 and Y7.43 can also interact directly, so repositioning of L3.36 also has some direct effect on Y7.43 conformation.

Arrestin-biased ligands favor the alternative conformation, and Gq-biased ligands favor the canonical active conformation

In replica-exchange MD (REMD) simulations designed to sample efficiently the conformational ensemble of AT_1R bound to each ligand, we found that TM7 adopted the alternative conformation more frequently with arrestin-biased ligands bound than with AngII bound and more frequently with AngII bound than with Gq-biased ligands bound (Fig. 3C). Combined with our observation that the alternative conformation preferentially binds arrestin, this suggests that ligands achieve arrestin bias by favoring the alternative conformation and G protein bias by favoring the canonical active conformation.

Ligands select among the alternative and canonical active conformations through the allosteric network described above. In simulation, L3.36 of the ligand-binding pocket was shifted toward TM2 more frequently with AngII than with arrestin-biased ligands and even more frequently with Gq-biased ligands (Fig. 4B). The arrestin-biased ligands extend much less deeply into the binding pocket (Fig. 4A and fig. S1), so they cannot readily push L3.36 toward TM2. By contrast, AngII and the Gq-biased ligands possess a bulky phenylalanine at position 8 (F8) and thus tend to push L3.36 toward TM2.

Our simulations indicate that the F8 residue of AngII and the Gq-biased ligands adopts distinct orientations with distinct effects on L3.36 (Fig. 4B and figs. S6 and S7). When L3.36 is in the TM5-proximal position that favors the alternative conformation, F8 tends to be vertical (i.e., the ring plane is perpendicular to the membrane plane), packing tightly above L3.36 (Fig. 4B and fig. S6). When F8 instead adopts a horizontal orientation, it forces L3.36 toward TM2, which in turn favors the canonical active conformation as described above.

In simulation, Gq-biased ligands adopted the horizontal F8 orientation more frequently than AngII (fig. S7). This is likely because, at AngII and arrestin-biased ligands, a positively charged arginine at position 2 (R2) engages negatively charged binding pocket residues D6.58 (Asp^{263}) and D7.32 (Asp^{281}), pulling the extracellular end of TM6 inward. The Gq-biased ligands lack a positively charged residue at position 2, and as a result, the extracellular end of TM6 tends to move outward, creating more space within the binding pocket for F8 to adopt a horizontal orientation (Fig. 4C).

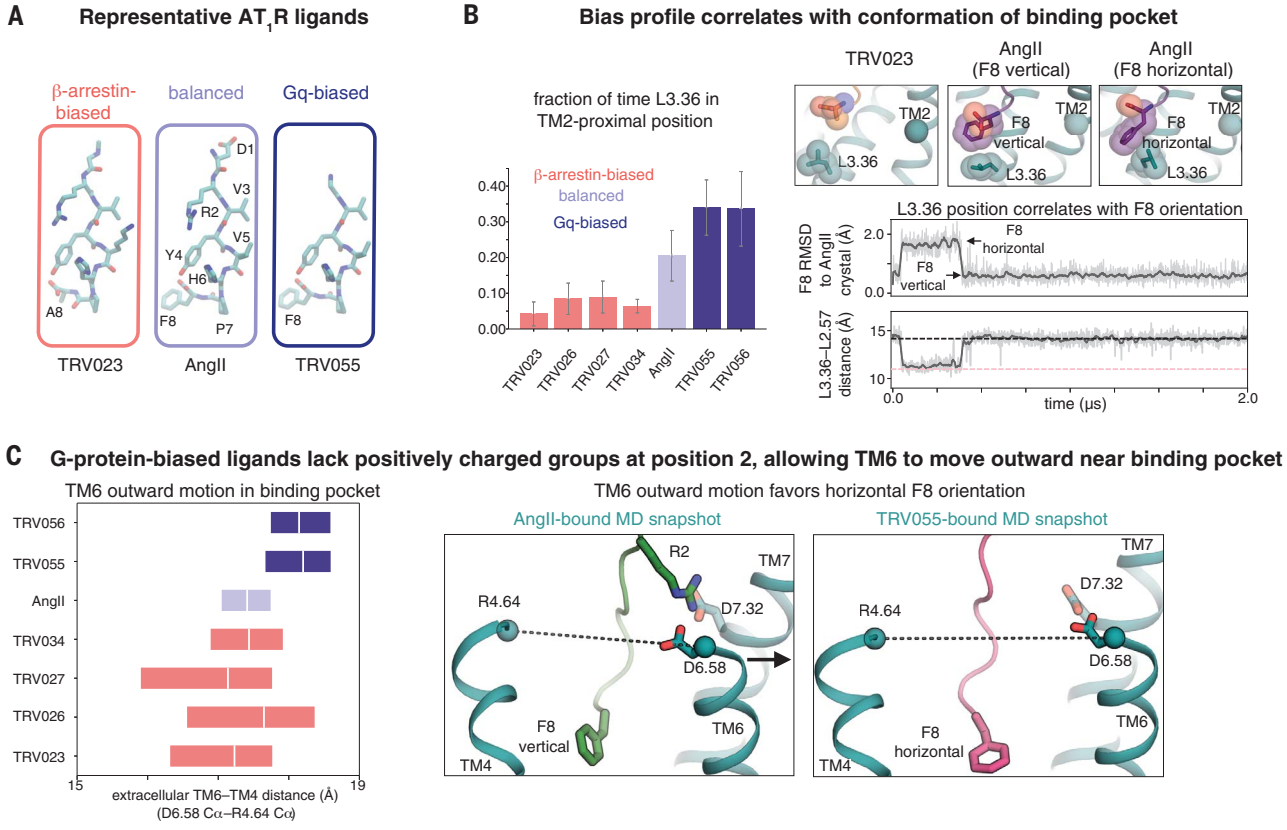

Fig. 4. Arrestin-biased, balanced, and G protein–biased ligands favor distinct binding-pocket conformations. (**A**) Structures of representative β-arrestin–biased, balanced, and Gq-biased AT_1R ligands. All ligands studied in this work are shown in fig. S1. A, Ala; F, Phe; H, His; V, Val. (**B**) In comparison to β-arrestin–biased ligands, AngII drives L3.36 of the binding pocket toward its TM2-proximal position, which favors the canonical active conformation, and Gq-biased ligands do so even more (P = 0.002 for β-arrestin–biased versus Gq-biased ligands, two-sided Welch's t test; see methods) (left; the bar plot shows means and standard errors across five independent 2-μs simulations per ligand). When the F8 residue of AngII and Gq-biased ligands adopts a horizontal orientation, it pushes L3.36 toward the TM2-proximal position (right; gray and pink dashed lines indicate values for TRV023- and AngII-bound structures, respectively; traces are for a simulation with AngII bound, and additional simulation traces are shown in fig. S6). RMSD is root-mean-square deviation (see methods). (**C**) AngII and β-arrestin–biased ligands stabilize more inward TM6 positions in the binding pocket compared with positions favored by Gq-biased ligands (P = 0.005 for Gq-biased ligands versus AngII; P = 0.001 for Gq-biased ligands versus β-arrestin–biased ligands), as shown by the box plot at left (boxes extend from the 25th to the 75th percentile of simulation frames), because the ligand R2 residue interacts with D6.58 and D7.32 (right; dashed lines correspond to distance plotted at left). The more outward position of the extracellular portion of TM6 observed for Gq-biased ligands allows their F8 residue to adopt a horizontal orientation more frequently than that of AngII (see also fig. S7).

The crystal structures in the companion manuscript (*19*) support this biased signaling mechanism, which we identified using simulations initiated from the previously published active-state structure (*20*). These crystal structures are locked into a single intracellular conformation, but in the structures with arrestin-biased ligands bound, residues near the binding pocket—N3.35, L3.36, and Y7.43—adopt positions that favor the alternative conformation in simulation. In the AngII-bound structure, on the other hand, N3.35 adopts a position (fig. S8) that favors the canonical active conformation in simulation. The density for L3.36 in this structure is weak, suggesting that this residue adopts multiple conformations, and Y7.43 is so mobile that it cannot be resolved at all.

In agreement with our computational results, our recent double electron-electron resonance (DEER) spectroscopy study of AT_1R (*4*) suggested that arrestin-biased, balanced, and G protein–biased ligands stabilize subtly different intracellular TM7 conformations. The DEER data also show differences in helix 8 position, which are likely due to these conformational changes in TM7. Differences in TM6 position might be due to adoption of the TM6-bent conformation discussed below. The DEER data suggest that the receptor undergoes additional ligand-dependent conformational changes on time scales longer than those of our simulations, although changes in other receptor regions may not be relevant to biased signaling. For example, although the various arrestin-biased ligands stabilize diverse conformations in DEER experiments, these ligands have very similar pharmacological bias profiles. Their pharmacological profiles are consistent with our simulations, which indicate that the various arrestin-biased ligands stabilize the alternative TM7 conformation to a similar degree.

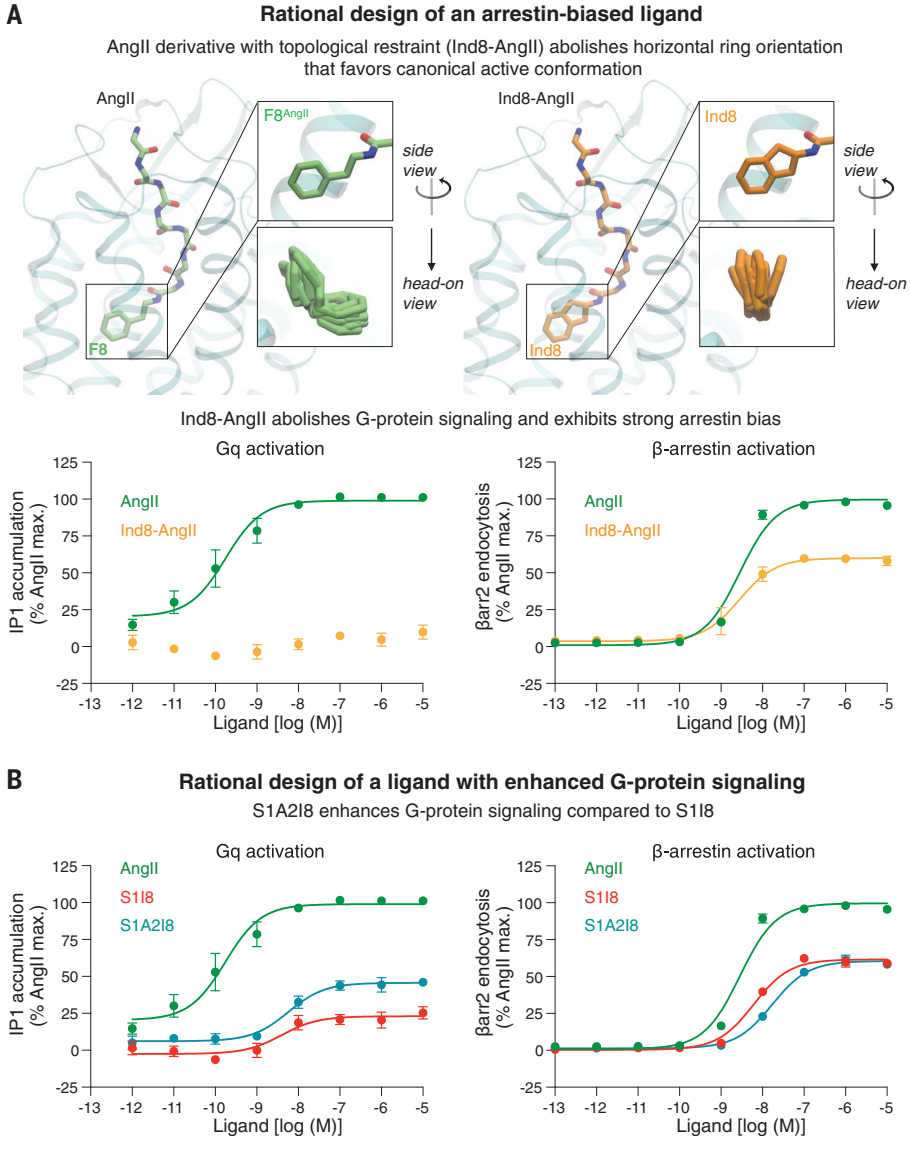

Fig. 5. Rational design of ligands with desired signaling profiles. (**A**) The addition of a single connecting methylene group to the phenyl moiety of AngII restrains the C-terminal ring to remain vertical, producing a strongly arrestin-biased ligand, Ind8-AngII, which barely couples to Gq. IP1, inositol monophosphate; βarr2, β-arrestin 2. (**B**) S1I8 has partial activity toward both the Gq-mediated and β-arrestin–mediated pathways. S1A2I8, which was designed to increase Gq signaling relative to S1I8 by favoring outward motion of TM6 in the binding pocket, shows increased Gq efficacy without any corresponding increase in β-arrestin efficacy. S1A2I8 is the R2A (Arg^2→Ala) mutant of S1I8. Error bars represent standard error from three to four independent experiments. See also table S2.

Computational design of ligands with desired biased signaling profiles

To further validate our computationally determined mechanism, we used it to design ligands with desired biased signaling profiles (Fig. 5), a long-standing challenge in GPCR drug discovery.

Decreasing the size of the C-terminal AngII residue is known to result in arrestin bias, but our simulations indicate that the conformation of the C-terminal peptide residue—not just its size—is a key determinant for bias. We predicted that a variant of AngII with the C-terminal aromatic ring constrained in a vertical orientation would favor the alternative intracellular conformation, leading to arrestin bias. We thus prepared an AngII analog with a 2-aminoindan-2-carboxylic acid substitution at F8 (Ind8-AngII, Fig. 5A). Ind8-AngII is structurally identical to AngII except that the C-terminal phenyl moiety is tied back to the Cα atom by the addition of a single connecting methylene group. Our simulations show that this modification restricts the phenyl ring to remain vertical. Indeed, experimental characterization of Ind8-AngII shows that it is strongly arrestin-biased despite having a C-terminal residue even larger than that of AngII and the Gq-biased ligands (Fig. 5A and table S2).

On the basis of our finding that outward motion of TM6 near the binding pocket is associated with the increased Gq signaling of Gq-biased ligands, we hypothesized that an alanine substitution at R2 would recover Gq activity for the partial agonist S1I8, which lacks a C-terminal phenylalanine but has another relatively large residue, isoleucine, at this position. Indeed, mutating R2 of S1I8 to alanine increases Gq activity without increasing β-arrestin activity (Fig. 5B and table S2).

Discussion

To what extent does the molecular mechanism of biased signaling that we have identified for AT_1R generalize to other GPCRs? Several lines

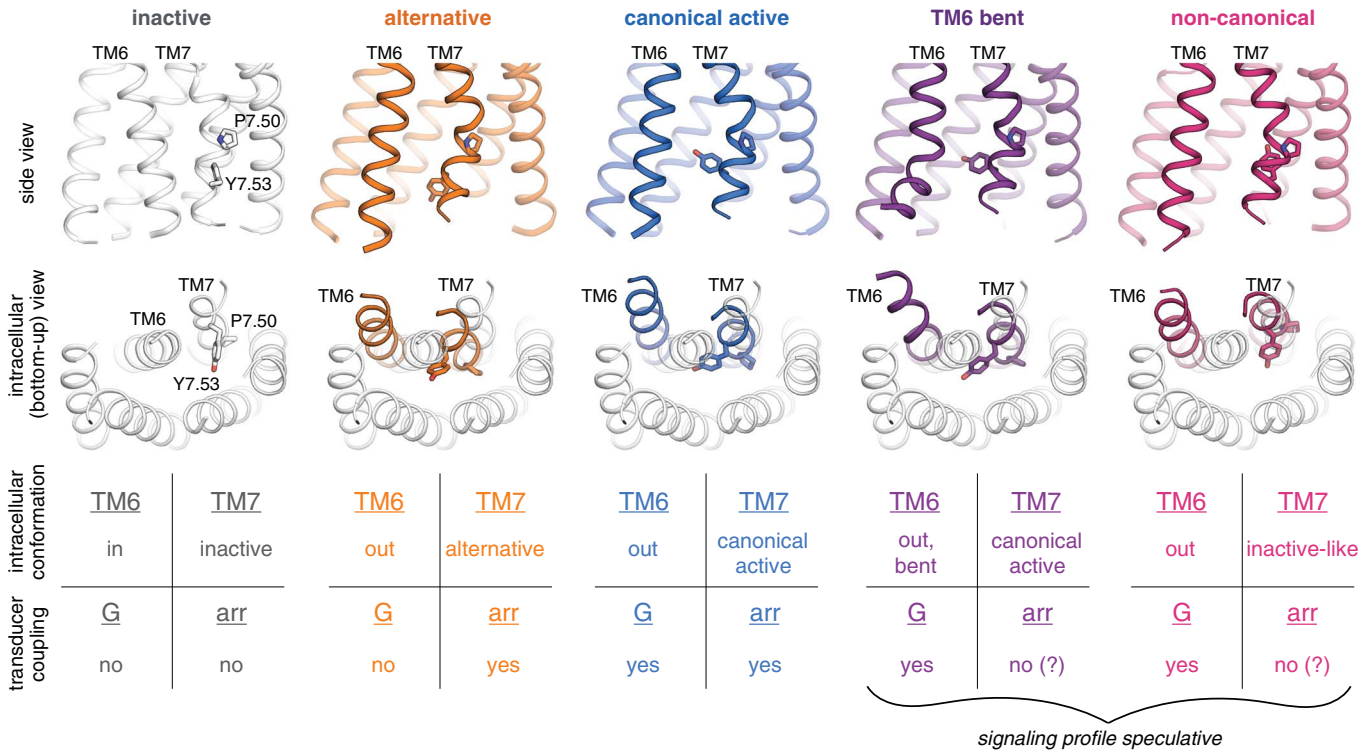

Fig. 6. Observed intracellular conformations of AT_1R. Simulations indicate that AT_1R adopts at least five distinct conformations that differ substantially in the intracellular positions of TM6 and TM7 and may have distinct cellular signaling profiles. In the inactive conformation [gray; illustrated by crystal structure (*24*)], TM6 occludes the transducer-binding pocket, hindering coupling to either G proteins or arrestins. The remaining four conformations all exhibit more outward positions of TM6 but differ substantially in the conformation of TM7, as illustrated by representative frames from our AT_1R simulations. In the middle row, we show TM6 and TM7 of these four conformations (colored) overlaid on all TMs of the inactive structure (gray). Our results suggest that in the alternative conformation (orange), the intracellular surface hinders coupling to G proteins but allows for arrestin coupling, whereas the canonical active conformation (blue) couples to both G proteins and arrestins. Two other conformations that AT_1R adopts in simulation—the TM6-bent and non-canonical conformations in purple and pink, respectively—have been observed in G protein–bound structures of other GPCRs but might hinder arrestin coupling by increasing the volume of the transducer-binding pocket, preventing the arrestin finger loop from packing tightly against this pocket.

of evidence suggest that similar intracellular conformations may be involved in biased signaling at other GPCRs. The key residues on the intracellular side of the receptor are highly conserved (*32*), with R3.50 found in 95% of class A GPCRs and Y7.53 in 89%. Studies of β_2AR and 5-HT_{2B}R (*3*, *26*, *29*, *33*) have suggested that arrestin-biased ligands modulate the conformation of TM7, albeit without capturing the specific signaling conformations leading to bias or identifying how ligands select among these conformations. The R3.50 and Y7.53 rotamers associated with the canonical active and alternative AT_1R conformations have been observed in experimental structures and simulations of other GPCRs (*25*–*30*, *34*–*36*). Residues near the binding pocket are much less conserved across GPCRs, however, suggesting that the specific interactions ligands form to stabilize different intracellular conformations will vary substantially among receptors.

Other intracellular conformations likely also play a role in biased signaling at certain GPCRs. The canonical active and alternative conformations, which both appear to allow arrestin coupling, are sufficient to explain how bias arises at AT_1R, where all known agonists substantially promote arrestin recruitment despite a great deal of variation in G protein stimulation. At GPCRs such as the μ-opioid receptor (μOR), however, ligands have been identified that essentially eliminate arrestin signaling while stimulating G protein signaling (*37*, *38*). This suggests the existence of one or more conformations that couple effectively to G proteins but not arrestins.

Our AT_1R simulations suggest two candidate conformations. First, we observed a conformation in which the intracellular end of TM6 moves even farther away (4 to 5 Å) from the center of the helical bundle while TM7 remains in its canonical active conformation, resulting in an intracellular conformation that closely resembles Gs-bound class A GPCR structures (*5*, *6*, *39*) (Fig. 6 and fig. S9). The larger intracellular cavity in this TM6-bent conformation might hinder efficient β-arrestin coupling by reducing the ability of the arrestin finger loop to pack favorably against the intracellular surface of the receptor (*40*). Second, TM7 sometimes adopts an inactive-like conformation, with the NPXXY motif shifted farther away from the helical bundle, while the intracellular end of TM6 remains in the outward position of the canonical active and alternative conformations (Fig. 6). This "non-canonical" intracellular conformation, which has been observed in a Gi-bound neurotensin receptor structure (*41*) and in β_2AR simulations (*31*), also has a larger intracellular cavity than the canonical active conformation and could thus hinder efficient β-arrestin coupling.

We note that a counterclockwise twist (seen from the extracellular side) of TM7 above its proline kink favors the alternative conformation, which couples preferentially to arrestins, whereas a clockwise twist favors the canonical active, TM6-bent, and non-canonical conformations, all of which couple effectively to

G proteins. Modulating the orientation of TM7 might thus represent a general strategy for developing biased ligands.

The intracellular conformations we have identified may also confer signaling bias by affecting coupling to GPCR kinases (GRKs) (*42*). In particular, each of these conformations might promote or hinder GRK-mediated receptor phosphorylation, thus favoring or disfavoring arrestin coupling, respectively.

At AT_1R, abolishing arrestin signaling while promoting G protein signaling has proven more difficult than abolishing G protein signaling while promoting arrestin signaling. Why is the reverse true at certain other GPCRs, such as μOR? First, sequence differences between GPCRs likely stabilize different signaling conformations. For example, as discussed in the companion manuscript (*19*), most class A GPCRs have a serine at position 7.46, which forms a key part of the sodium-binding site. In the same position, AT_1R has an asparagine (N7.46), which not only prevents sodium binding but also stabilizes the alternative conformation by forming polar contacts with TM3. Second, propensity to achieve particular signaling profiles may depend on the specific G proteins and arrestins to which a GPCR couples. For example, at the position on the α5 helix where Gq and Gs have a tyrosine that clashes with the downward R3.50 rotamer in AT_1R's alternative conformation, Gi and Go have a smaller cysteine residue. This cysteine could avoid severe clashes with the downward R3.50 rotamer in some (but not all) of the α5 helix orientations observed in GPCR-Gi and GPCR-Go complexes (fig. S10), so the alternative conformation would likely disfavor Gi and Go coupling less than Gq or Gs coupling. This may contribute to the difficulty of eliminating G protein signaling at μOR, whose cognate G protein is Gi. Indeed, a recent study indicates that, at AT_1R, arrestin-biased ligands reduce Gq coupling more than Gi coupling (*43*).

Our results provide a detailed mechanism for biased signaling at AT_1R, allowing the rational design of biased ligands. Our findings also suggest a general framework for achieving bias at other GPCRs, but further work will be necessary to elucidate detailed mechanisms of bias at these receptors.

REFERENCES AND NOTES

1. R. Santos *et al.*, *Nat. Rev. Drug Discov.* **16**, 19–34 (2017).
2. L. Tan, W. Yan, J. D. McCorvy, J. Cheng, *J. Med. Chem.* **61**, 9841–9878 (2018).
3. J. J. Liu, R. Horst, V. Katritch, R. C. Stevens, K. Wüthrich, *Science* **335**, 1106–1110 (2012).
4. L. M. Wingler *et al.*, *Cell* **176**, 468–478.e11 (2019).
5. S. G. Rasmussen *et al.*, *Nature* **477**, 549–555 (2011).
6. J. García-Nafría, Y. Lee, X. Bai, B. Carpenter, C. G. Tate, *eLife* **7**, e35946 (2018).
7. A. Koehl *et al.*, *Nature* **558**, 547–552 (2018).
8. A. Glukhova *et al.*, *ACS Pharmacol. Transl. Sci.* **1**, 73–83 (2018).
9. S. Maeda, Q. Qu, M. J. Robertson, G. Skiniotis, B. K. Kobilka, *Science* **364**, 552–557 (2019).
10. Y. Kang *et al.*, *Nature* **523**, 561–567 (2015).
11. X. E. Zhou *et al.*, *Cell* **170**, 457–469.e13 (2017).
12. W. Yin *et al.*, *Cell Res.* **29**, 971–983 (2019).
13. S. Rajagopal *et al.*, *Mol. Pharmacol.* **80**, 367–377 (2011).
14. R. T. Strachan *et al.*, *J. Biol. Chem.* **289**, 14211–14224 (2014).
15. J. Cabana *et al.*, *J. Biol. Chem.* **290**, 15835–15854 (2015).
16. J. D. Violin *et al.*, *J. Pharmacol. Exp. Ther.* **335**, 572–579 (2010).
17. S. M. DeWire, J. D. Violin, *Circ. Res.* **109**, 205–216 (2011).
18. D. M. Ryba *et al.*, *Circulation* **135**, 1056–1070 (2017).
19. L. M. Wingler *et al.*, **367**, 888–892 (2020).
20. L. M. Wingler, C. McMahon, D. P. Staus, R. J. Lefkowitz, A. C. Kruse, *Cell* **176**, 479–490.e12 (2019).
21. H. Asada *et al.*, *Nat. Struct. Mol. Biol.* **25**, 570–576 (2018).
22. J. A. Ballesteros, H. Weinstein, in *Receptor Molecular Biology*, vol. 25 of *Methods in Neurosciences*, S. C. Sealford, Ed. (Elsevier, 1995), chap. 19, pp. 366–428.
23. W. I. Weis, B. K. Kobilka, *Annu. Rev. Biochem.* **87**, 897–919 (2018).
24. H. Zhang *et al.*, *Cell* **161**, 833–844 (2015).
25. F. Xu *et al.*, *Science* **332**, 322–327 (2011).
26. D. Wacker *et al.*, *Science* **340**, 615–619 (2013).
27. W. Liu *et al.*, *Science* **342**, 1521–1524 (2013).
28. D. Wacker *et al.*, *Cell* **168**, 377–389.e12 (2017).
29. J. D. McCorvy *et al.*, *Nat. Struct. Mol. Biol.* **25**, 787–796 (2018).
30. G. Lebon *et al.*, *Nature* **474**, 521–525 (2011).
31. R. O. Dror *et al.*, *Proc. Natl. Acad. Sci. U.S.A.* **108**, 18684–18689 (2011).
32. A. J. Venkatakrishnan *et al.*, *Nature* **536**, 484–487 (2016).
33. N. R. Latorraca, A. J. Venkatakrishnan, R. O. Dror, *Chem. Rev.* **117**, 139–155 (2017).
34. S. Yuan, S. Filipek, K. Palczewski, H. Vogel, *Nat. Commun.* **5**, 4733 (2014).
35. B. C. Taylor, C. T. Lee, R. E. Amaro, *Proc. Natl. Acad. Sci. U.S.A.* **116**, 8131–8136 (2019).
36. R. Nygaard *et al.*, *Cell* **152**, 532–542 (2013).
37. A. Manglik *et al.*, *Nature* **537**, 185–190 (2016).
38. C. L. Schmid *et al.*, *Cell* **171**, 1165–1175.e13 (2017).
39. B. Carpenter, R. Nehmé, T. Warne, A. G. W. Leslie, C. G. Tate, *Nature* **536**, 104–107 (2016).
40. N. Saleh, G. Saladino, F. L. Gervasio, T. Clark, *Chem. Sci.* **8**, 4019–4026 (2017).
41. H. E. Kato *et al.*, *Nature* **572**, 80–85 (2019).
42. M. Choi *et al.*, *Sci. Signal.* **11**, eaar7084 (2018).
43. Y. Namkung *et al.*, *Sci. Signal.* **11**, eaat1631 (2018).
44. C.-M. Suomivuori *et al.*, Data for "Molecular mechanism of biased signaling in a prototypical G protein–coupled receptor", Zenodo (2020); https://doi.org/10.5281/zenodo.3629830.

ACKNOWLEDGMENTS

We thank B. Ha, J. Wang, J. Paggi, and all members of the Dror lab for assistance with MD simulations, and D. Arlow for insightful comments. **Funding:** Funding was provided by the Sigrid Jusélius Foundation (C.-M.S.), the Human Frontier Science Program (LT000916/2018-L) (C.-M.S.), a Stanford Bio-X Bowes Fellowship (S.E.), the Vallee Foundation (A.C.K.), the Smith Family Foundation (A.C.K.), and National Institutes of Health grants R01GM127359 (R.O.D.), R01HL16037 (R.J.L.), and 5DP5OD021345 (A.C.K.). A.L.W.K. is a Howard Hughes Medical Institute Medical Research Fellow. R.J.L. is an investigator with the Howard Hughes Medical Institute. This research used resources of the Oak Ridge Leadership Computing Facility, which is a U.S. Department of Energy Office of Science User Facility supported under contract DE-AC05-00OR22725. **Author contributions:** C.-M.S., N.R.L., and R.O.D. designed the research. C.-M.S., N.R.L., S.E., and M.C.K. performed and analyzed MD simulations with direction from R.O.D. L.M.W., A.L.W.K., and D.P.S. performed and analyzed functional experiments with direction from R.J.L. C.-M.S., N.R.L., M.A.S., and A.C.K. interpreted structural data. C.-M.S., N.R.L., and R.O.D. wrote the paper with input from all authors. **Competing interests:** R.J.L. is a founder and stockholder of Trevena and a director of Lexicon Pharmaceuticals. A.C.K. is an advisor for the Institute for Protein Innovation, a nonprofit research institute. **Data and materials availability:** Analysis code and data have been deposited at Zenodo (*44*).

SUPPLEMENTARY MATERIALS

science.sciencemag.org/content/367/6480/881/suppl/DC1
Materials and Methods
Figs. S1 to S10
Tables S1 and S2
References (*45–75*)
Representative Simulation Frames

View/request a protocol for this paper from *Bio-protocol*.

7 August 2019; accepted 23 January 2020
10.1126/science.aaz0326

REPORT

STRUCTURAL BIOLOGY

Angiotensin and biased analogs induce structurally distinct active conformations within a GPCR

Laura M. Wingler[1,2]*, Meredith A. Skiba[3]*, Conor McMahon[3], Dean P. Staus[1,2], Alissa L. W. Kleinhenz[1,2,4], Carl-Mikael Suomivuori[5,6,7], Naomi R. Latorraca[5,6,7,8]†, Ron O. Dror[5,6,7,8], Robert J. Lefkowitz[1,2,9]‡, Andrew C. Kruse[3]‡

Biased agonists of G protein–coupled receptors (GPCRs) preferentially activate a subset of downstream signaling pathways. In this work, we present crystal structures of angiotensin II type 1 receptor (AT1R) (2.7 to 2.9 angstroms) bound to three ligands with divergent bias profiles: the balanced endogenous agonist angiotensin II (AngII) and two strongly β-arrestin–biased analogs. Compared with other ligands, AngII promotes more-substantial rearrangements not only at the bottom of the ligand-binding pocket but also in a key polar network in the receptor core, which forms a sodium-binding site in most GPCRs. Divergences from the family consensus in this region, which appears to act as a biased signaling switch, may predispose the AT1R and certain other GPCRs (such as chemokine receptors) to adopt conformations that are capable of activating β-arrestin but not heterotrimeric G_q protein signaling.

Agonist binding to an extracellular-facing pocket of G protein–coupled receptors (GPCRs) initiates conformational changes that are propagated to the intracellular regions of the receptor. GPCR activation by agonists typically not only activates heterotrimeric G proteins but also promotes receptor phosphorylation by G protein–coupled receptor kinases (GRKs) and subsequent binding of β-arrestins (*1*). In addition to promoting GPCR desensitization and endocytosis, β-arrestins initiate additional signaling cascades (*2*). Although most agonists activate both G protein and β-arrestin pathways, it has been well established that many GPCR ligands show pronounced bias and can preferentially—or, in the limiting case, exclusively—activate particular downstream pathways (*3*).

The angiotensin II type 1 receptor (AT1R) is a particularly compelling model system for investigating biased agonism because small structural modifications to the angiotensin II (AngII) octapeptide agonist lead to strongly biased signaling. In particular, alteration of the C-terminal F8 of AngII profoundly attenuates G_q-mediated signaling but not β-arrestin coupling (*4*, *5*). For example, TRV026, which lacks an eighth residue, and TRV023, which has an F8→A (F8A) substitution, are deficient in G_q-dependent inositol phosphate generation; however, both of these β-arrestin–biased ligands robustly promote β-arrestin–dependent endocytosis (Fig. 1, A to C) (*6*, *7*). These β-arrestin–biased ligands are of interest for the treatment of heart failure, as they have the same antihypertensive effects as clinically used AT1R antagonists (angiotensin receptor blockers) but also improve cardiac function through β-arrestin–mediated pathways (*8*, *9*).

To date, the molecular mechanisms of biased agonist action remain unclear. Although several structures of GPCRs bound to ligands exhibiting varying degrees of bias have been reported (*10*, *11*), it has been challenging to trace how the conformational changes induced by biased agonists are transmitted from the extracellular ligand-binding site to the intracellular transducer-binding pocket. This question is best addressed through the use of several complementary techniques. Using double electron-electron resonance spectroscopy, we have previously demonstrated that AngII, TRV023, and TRV026 each promote distinct sets of intracellular conformations of the AT1R (*12*). Because this approach can only report on conformational changes in the intracellular regions that are accessible to chemical labeling, we turned to crystallography to delineate, at high resolution, the structural rearrangements induced by AngII and biased ligands elsewhere in the receptor. Molecular dynamics simulations, presented in a companion manuscript (*13*), capture the same structural rearrangements and relate them to distinct intracellular conformations that affect transducer binding.

We recently reported an active-state crystal structure of the AT1R bound to the high-affinity partial agonist S1I8 (Fig. 1A) in complex with an active state–stabilizing synthetic nanobody, AT110i1 (*14*). Compared with the strongly β-arrestin–biased ligands TRV026 and TRV023, S1I8 activates G_q signaling more potently and, thus, shows less bias toward β-arrestin pathways (Fig. 1, B and C). AT110i1 shows a positive allosteric interaction with AngII, TRV026, and TRV023, increasing their affinity for the AT1R, as assessed by radioligand binding (Fig. 1D and table S1), and stabilizing the receptor-ligand complex, as measured by thermal shift assays (fig. S1 and table S2). Likewise, AngII and the β-arrestin–biased ligands promote interaction of the AT1R with a lower-affinity variant of AT110i1 (Fig. 1E), which suggests that AT110i1 would be a suitable crystallographic chaperone for AT1R bound to all of these ligands. Consistent with these data, when the nanobody is removed from the AT1R-S1I8-AT110i1 structure in molecular dynamics simulations, the intracellular side of the AT1R relaxes to a conformation that is highly similar to that observed crystallographically, even when the ligand is replaced with AngII, TRV026, or TRV023 (*13*).

For crystallography efforts, we employed a previously described AT1R construct (*14*). The construct contains an insertion of thermostabilized apocytochrome b562RIL (BRIL) in the third intracellular loop and a C-terminal truncation, which is compatible with AT110i1 complex formation in the presence of AngII and β-arrestin–biased ligands (table S1). Diffraction-quality crystals of AT1R-AT110i1 with AngII (2.9 Å), TRV026 (2.7 Å), and TRV023 (2.8 Å) (table S3) were obtained in several distinct crystal forms by lipidic mesophase crystallization (*15*) under similar conditions to those used for AT1R-AT110i1-S1I8 (fig. S2). Globally, all three AT1R structures are similar to each other and to the S1I8 structure in their backbone conformations [0.39 Å root mean square deviation (RMSD) to AT1R-AngII for 271 Cα atoms in the seven transmembrane (TM) helices]. In the extracellular regions, we observe a marked contraction of the ligand-binding pocket relative to small molecule antagonist-bound AT1R structures (fig. S3) (*14*, *16*, *17*). AT110i1 binding to the transducer pocket stabilizes an intracellular conformation with features characteristic of GPCR activation, such as the outward displacement of TM6 (Fig. 2A). Extracellular and intracellular conformational changes are linked by the rearrangement of conformational locks in the receptor (Fig. 2A). Notably, as reported in our companion manuscript (*13*), the crystallographically observed conformation is almost identical to one of the two major

[1]Howard Hughes Medical Institute, Duke University Medical Center, Durham, NC 27710, USA. [2]Department of Medicine, Duke University Medical Center, Durham, NC 27710, USA. [3]Department of Biological Chemistry and Molecular Pharmacology, Blavatnik Institute, Harvard Medical School, Boston, MA 02115, USA. [4]School of Medicine, University of Michigan, Ann Arbor, MI 48109, USA. [5]Department of Computer Science, Stanford University, Stanford, CA 94305, USA. [6]Departments of Molecular and Cellular Physiology and Structural Biology, Stanford University School of Medicine, Stanford, CA 94305, USA. [7]Institute for Computational and Mathematical Engineering, Stanford University, Stanford, CA 94305, USA. [8]Biophysics Program, Stanford University, Stanford, CA 94305, USA. [9]Department of Biochemistry, Duke University Medical Center, Durham, NC 27710, USA.
*These authors contributed equally to this work. †Present address: Department of Molecular and Cellular Biology, University of California, Berkeley, CA 94720, USA.
‡Corresponding author. Email: lefko001@receptor-biol.duke.edu (R.J.L.); andrew_kruse@hms.harvard.edu (A.C.K.)

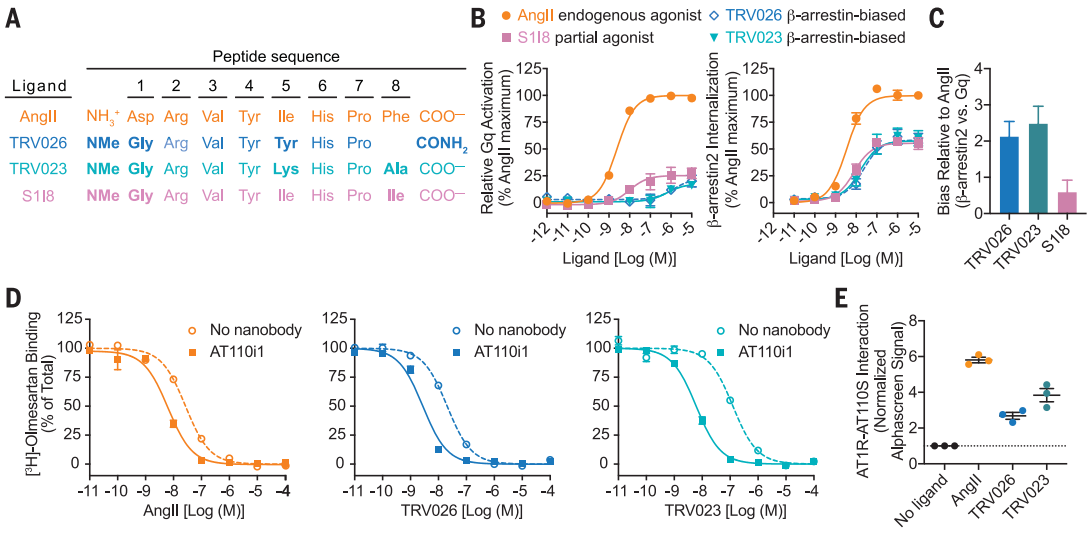

Fig. 1. Endogenous and biased AT1R ligands. (**A**) Peptide ligands crystallized with the AT1R. Bold residues indicate mutations relative to AngII, the endogenous agonist. NMe, N-methyl. (**B**) Ligand activation of G_q-mediated inositol monophosphate increases and β-arrestin2 endocytosis. M, Molar. (**C**) Bias factors of ligands relative to AngII, determined from the data shown in panel (B) as described in the materials and methods. A bias factor of 1 represents a 10-fold difference in the ligand's ability to activate the β-arrestin pathway compared with the G_q pathway. (**D**) Nanobody AT110i1 allosterically increases the binding of AngII, TRV026, and TRV023 to purified AT1R [K_i (inhibition constant) values are in table S1]. (**E**) AngII, TRV026, and TRV023 promote interaction of FLAG-AT1R and AT110S-His6, the lower-affinity, parental clone of AT110i1, by AlphaScreen. Data are normalized to signal without ligand. In (B), (D), and (E), the means ± SE from three independent experiments are shown. In (C), error bars represent the SE in bias factors derived from curve fit parameters from (B).

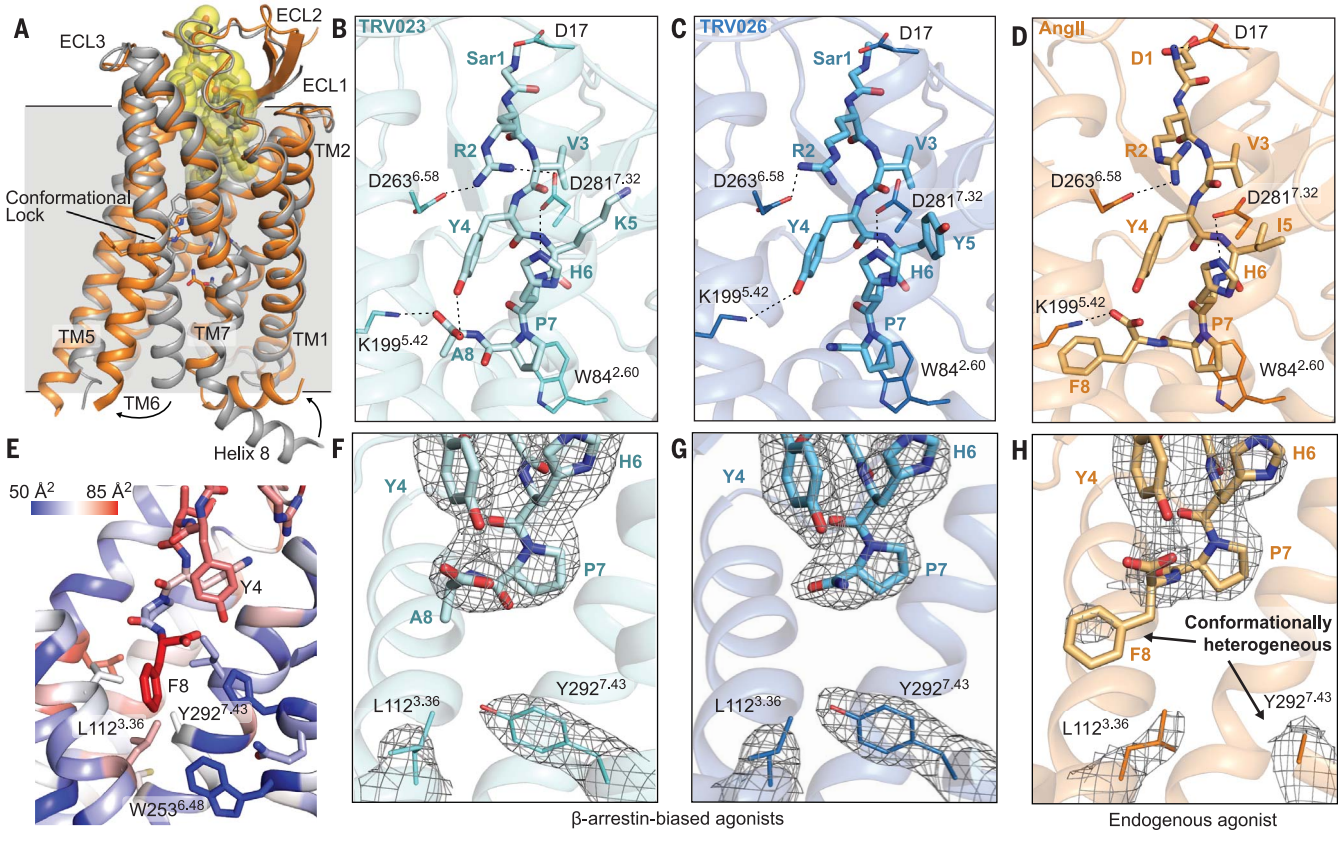

Fig. 2. Comparison of AngII- and β-arrestin–biased ligand-bound AT1R. (**A**) Activated AT1R (orange) bound to AngII (yellow) displays characteristic TM6 and TM7 movements stabilized by TM6 conformational locks (shown in stick representation). AT1R bound to TRV023 (0.43 Å RMSD for 264 Cα atoms) and TRV026 (0.42 Å RMSD for 264 Cα atoms) is nearly identical in overall conformation. ECL, extracellular loop. (**B** to **D**) Similar binding modes of TRV023 (B), TRV026 (C), and AngII (D). Dashed lines indicate hydrogen bonds. (**E**) AngII-AT1R ligand-binding pocket colored by Cα B-factors, highlighting the mobility of F8. (**F** to **H**) Electron density (gray mesh shows $2F_o$-F_c electron density map contoured at 1σ) of C-terminal regions of TRV023 (F), TRV026 (G), and AngII (H) and the surrounding AT1R residues. Weak density for AngII F8 and Y292 (H) indicates that the residues are structurally heterogeneous within the crystal lattice, likely because they are dynamic (*13*). Single-letter abbreviations for the amino acid residues are as follows: A, Ala; C, Cys; D, Asp; E, Glu; F, Phe; G, Gly; H, His; I, Ile; K, Lys; L, Leu; M, Met; N, Asn; P, Pro; Q, Gln; R, Arg; S, Ser; T, Thr; V, Val; W, Trp; and Y, Tyr.

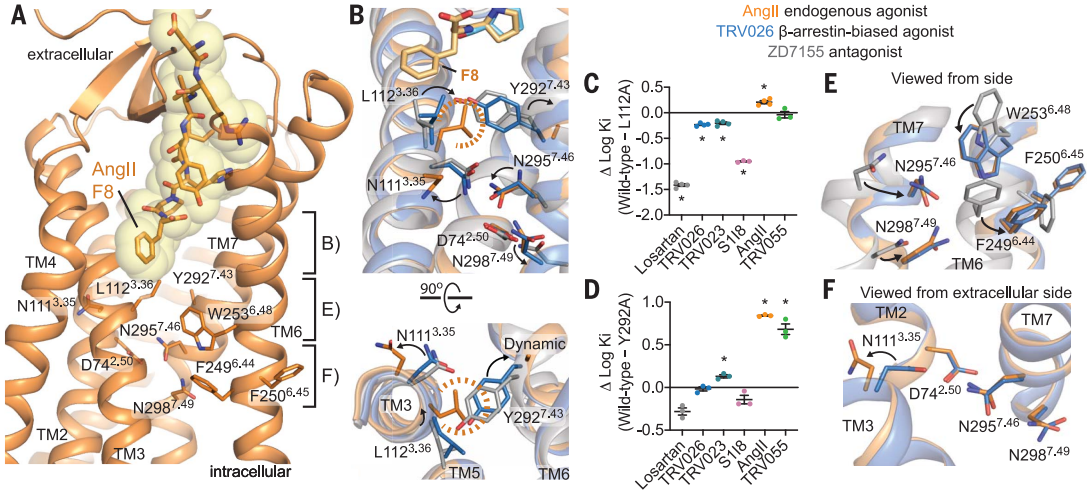

Fig. 3. AngII-AT1R exhibits distinct configurations of conformational locks. (**A**) View of AngII-AT1R, with key residues highlighted. (**B**) Movement of L112$^{3.36}$ accommodates the position of AngII F8. The concomitant rotation of TM3 repositions N111$^{3.35}$ outside the receptor core. TRV026 binding does not have this effect. (**C** and **D**) Change in affinity of AT1R ligands for AT1R L112A$^{3.36}$ (C) and Y292A$^{7.43}$ (D) versus wild-type AT1R. Losartan is a small-molecule antagonist; TRV055 is a G_q-biased agonist with a C-terminal phenylalanine (*7*). Error bars represent the SE of the difference in the log K_i values determined from three to four independent experiments. See also fig. S6 and table S4. For (C) and (D), the asterisk symbol indicates statistically significant difference (*P < 0.05) for mutant versus wild-type K_i values, as determined by a t test with Holm-Sidak correction for multiple comparisons. (**E**) Both AngII-bound and TRV026-bound structures exhibit the outward rotation of TM6 and inward rotation of TM7, rearranging the conformational locks. (**F**) AngII-induced rotation of N111$^{3.35}$ alters the polar network at the canonical sodium-binding site in the receptor core, involving D74$^{2.50}$, N295$^{7.46}$, and N298$^{7.49}$ (of the NPXXY motif).

conformations to which the AT1R relaxes when the nanobody is removed from the AT1R-AT110i1-S1I8 structure in molecular dynamics simulations. The conformation seen in the simulation differs only in the rotameric state of Y302$^{7.53}$ [superscripts indicate Ballesteros-Weinstein numbering for conserved GPCR residues (*18*)] at the intracellular end of TM7 and, notably, appears to be able to accommodate β-arrestin but not G_q binding in models of AT1R-transducer complexes (*13*). This suggests that although AT110i1 constrains the intracellular conformation of the receptor in our structure, the crystal structures reflect a conformation sampled by the agonist-bound receptor in the absence of the nanobody.

All of the peptide ligands assume a similar binding pose, with their N termini positioned at the extracellular face and C termini positioned at the base of the ligand-binding pocket (Fig. 2, B to D). Although residues 1 and 5 vary among the ligands, these substitutions do not substantially alter interactions with the receptor, which is consistent with data showing that these changes are not required to convert AngII into a biased ligand (*7*, *19*). In contrast to the other structures of GPCRs bound to agonists exhibiting varying degrees of bias that have been reported to date—which tend to differ in how ligands engage the extracellular receptor face (*10*, *11*, *20*)—pronounced differences between the AngII-bound and β-arrestin–biased ligand-bound structures occur only at the base of the ligand-binding pocket, around the C-terminal residues of the ligands (Fig. 2, E to H). Clear and continuous density is observed for each residue of TRV026 and TRV023 and the surrounding AT1R residues (Fig. 2, F and G, and fig. S4). However, AngII F8 is poorly resolved and displays markedly high B-factors for its side-chain and main-chain atoms—despite residing in the core of the receptor (Fig. 2, E and H, and fig. S4)—suggesting that it is conformationally heterogeneous. In support of this observation, simulations of the AngII-bound receptor show that the F8 side chain visits multiple distinct conformations that are consistent with the observed density (*13*). Weak electron density is also observed for the nearby L112$^{3.36}$ side chain, and no density is observed for the side chain of the nearby Y292$^{7.43}$ (Fig. 2H). In the AngII-bound structure, TM3 rotates on-axis, and L112$^{3.36}$ moves past W253$^{6.48}$ and into the position previously occupied by Y292$^{7.43}$ (Fig. 3, A and B). Despite containing a hydrophobic I residue at position 8, the partial agonist S1I8 does not induce rotation of TM3 (fig. S5).

Consistent with these crystallographic observations, an L112A$^{3.36}$ substitution, which is expected to better accommodate the presumed flexibility of AngII F8, increases AT1R affinity for AngII but decreases affinity for TRV026, TRV023, and S1I8 (Fig. 3C, fig. S6, and table S4). A Y292A$^{7.43}$ substitution designed to mimic the disordered side chain induced by AngII increases AT1R affinity for G_q-active ligands with a C-terminal F8, but it has relatively minor effects on TRV026, TRV023, and S1I8 affinity (Fig. 3D, fig. S6, and table S4). Despite having enhanced affinities for AngII, L112A$^{3.36}$ and Y292A$^{7.43}$ do not show increased efficacy or potency in activating AngII-dependent G_q signaling (fig. S7 and table S5). This supports the hypothesis that L112A$^{3.36}$ and Y292A$^{7.43}$ play a key role in coupling AngII binding to G_q activation. The L112A$^{3.36}$ variant reduces affinity but increases G_q efficacy for the partial agonist S1I8 (Fig. 3C, figs. S6 and S7, and tables S4 and S5). This suggests that the alanine substitution is sufficient to permit rotation of TM3 in the presence of I8 by reducing the hydrophobic interaction between L112$^{3.36}$ and W253$^{6.48}$.

In addition to showing differences in the ligand-binding pocket compared with structures with β-arrestin–biased ligands, AngII-AT1R displays more-substantial changes in conformational locks located deeper in the receptor core (Fig. 3, A, E, and F). In all of the active-state AT1R structures, the outward rotation of TM6 and associated inward rotation of TM7 (Fig. 2A and Fig. 3E) disrupt an inactive state–stabilizing interaction between N111$^{3.35}$ and N295$^{7.46}$ underneath the ligand-binding pocket (Fig. 3B and fig. S5). Rotation of N295$^{7.46}$ rearranges a central hydrogen bonding network of polar residues in the receptor core that also involves D74$^{2.50}$ and N298$^{7.49}$, the first residue of the NPXXY motif (where X denotes any residue), which is involved in stabilizing the active state of many GPCRs (Fig. 3F and fig. S5). In the S1I8 and β-arrestin–biased ligand structures, N111$^{3.35}$ remains in proximity to the reoriented N295$^{7.46}$ (Fig. 3, B and F, and fig. S5) and may restrict the orientations of TMs 3 and 7. However, the rotation of TM3 in the AngII-bound structure, which is associated with L112$^{3.36}$-repositioning in the ligand-binding pocket, is also accompanied by the side chain of N111$^{3.35}$ flipping outside the TM bundle (Fig. 3, B and F). This results in a configuration of the polar network in the core of the AngII-bound structure that is distinct from the configurations observed in both antagonist-bound and β-arrestin–biased ligand-bound AT1R (Fig. 3, B and F). Notably, coupled movements of L112$^{3.36}$ and N111$^{3.35}$ also occur in molecular dynamics simulations of AT1R—in the absence

of the stabilizing nanobody—and are frequently accompanied by changes in intracellular conformation (*13*).

Our structures suggest that the binding of partial or β-arrestin–biased peptide agonists triggers a shift of TM6, a hallmark of GPCR activation, and a conformational change in $N295^{7.46}$, whereas the binding of AngII induces the additional outward movement of $N111^{3.35}$. Based on the functional profiles of these ligands, the rearrangement of $N295^{7.46}$ is likely sufficient to promote the conformational changes that are needed for β-arrestin coupling, whereas the flipping of $N111^{3.35}$ is essential for G_q signaling. Consistent with this model, the balance of G_q and β-arrestin activation at the AT1R is acutely sensitive to mutagenesis of the polar network beneath the ligand-binding pocket. $N111G^{3.35}$, releasing the constraints on TM3, exhibits high levels of ligand-independent activity, particularly with respect to G_q signaling (*21*–*23*). Furthermore, the partial agonist S1I8 and the β-arrestin–biased agonist SII (sarcosine1, I4, I8-AngII) behave as full agonists toward G_q signaling at AT1R $N111G^{3.35}$ (*23*). An important role for $D74^{2.50}$ is supported by the fact that AT1R $D74N^{2.50}$ shows impaired G_q activity but still robustly activates β-arrestin pathways (*24*, *25*).

In most family A GPCRs, the corresponding conserved polar residues form a sodium-binding site, which allosterically stabilizes TMs 3 and 7 in the inactive conformation and collapses upon receptor activation (*26*) (Fig. 4, A and B). However, sodium has almost no effect on AngII affinity for the AT1R (Fig. 4C) (*16*), and there is no electron density for sodium in the inactive AT1R structures (*16*, *17*) (Fig. 4D). Substitution of the highly conserved $S^{7.46}$ with $N295^{7.46}$ in the AT1R (Fig. 4, A and D) disrupts the sodium coordination sphere and precludes sodium binding. Instead, a hydrogen bond between $N295^{7.46}$ and $N111^{3.35}$ replaces the need for sodium to stabilize the inactive state (Fig. 4D). This substitution appears to have helped create a bipartite activation mechanism that renders the AT1R particularly prone to biased signaling (Fig. 4, D and E). Deviations from the conserved sodium-binding motif are particularly enriched in peptide- and protein-binding family A GPCRs that are closely related to the AT1R (Fig. 4A). For example, only 3 out of 22 chemokine receptors possess all of the conserved residues typically required for tight sodium binding (*27*). Notably, the chemokine receptor family also contains a number of atypical receptors that do not signal through G proteins, some of which have been shown to activate β-arrestins (*28*), and endogenous chemokines function as biased ligands at many chemokine receptors (*29*, *30*). Furthermore, substitutions in and immediately surrounding the sodium-binding site of many GPCRs [e.g., δ-opioid receptor (*31*), CCR5 (*32*), and NK1 receptor (*33*)] can bias receptor signaling either

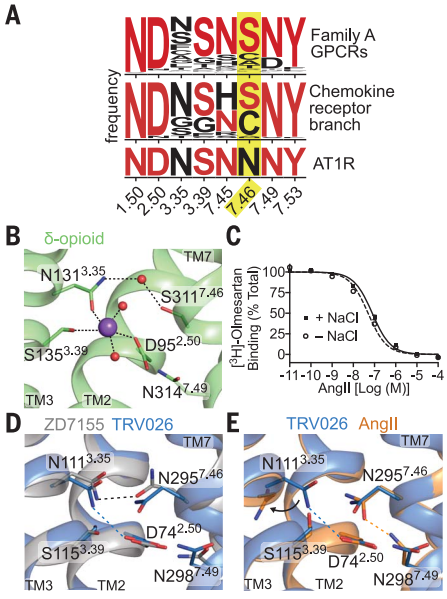

Fig. 4. Structural diversity in the polar core of GPCRs. (**A**) Conservation of sodium coordination residues (*26*), with family A GPCR consensus residues shown in red. Many chemokine receptors (*36*) deviate from the consensus sequence. (**B**) Sodium binding in the δ-opioid receptor. $N^{3.35}$ and $S^{7.46}$ are found in the sodium coordination sphere. (**C**) Effect of sodium on AngII binding to wild-type AT1R in membranes. Competition radioligand binding was performed in buffer containing 150 mM NaCl (log K_{iAngII} = −7.54 ± 0.06, K_i = 29 nM; $K_{d[3H]\text{-olmesartan}}$ = 1.2 ± 0.1 nM) or lacking sodium and containing 150 mM KCl (log K_{iAngII} = −7.73 ± 0.02, K_i = 19 nM; $K_{d[3H]\text{-olmesartan}}$ = 1.2 ± 0.3 nM). The means ± SE from three independent experiments are shown. (**D** and **E**) Residues associated with sodium binding make up the AT1R polar network. (D) The $N111^{3.35}$-$N295^{7.46}$ hydrogen bond stabilizes the inactive state in antagonist (ZD7155)–bound AT1R. Upon TRV026 binding, TM7 movement disrupts the hydrogen bond. (E) AngII binding rotates $N111^{3.35}$ away from the polar core, yielding a second active conformation.

toward G proteins or β-arrestins, which demonstrates that transducer coupling is exquisitely sensitive to manipulation of this region. A pathogenic mutation associated with cancer is located in the canonical sodium-binding region of CysLTR2 and yields a constitutively active G protein–biased receptor (*34*). We provide the first direct, experimental evidence that this critical polar network assumes at least three configurations—the inactive configuration and two distinct active conformations—which provides a molecular explanation for how it contributes to differential transducer activation.

Our structures of the AT1R define a mechanism for biased agonist action that undoubtedly has parallels in other GPCRs. AngII—but not β-arrestin–biased ligands—disrupts the receptor core, yielding a conformation that is structurally distinct from that induced by β-arrestin–biased ligands. Although allosteric effects of the intracellular nanobody required for crystallogenesis could mask additional ligand-specific changes, even beyond those observed in this study, the notable conformational differences that persist beyond the ligand-binding site attest to the loose allosteric coupling known to exist in GPCRs (*35*). Double electron-electron resonance spectroscopy experiments and molecular dynamics simulations confirm that the conformational differences initiated by AngII and β-arrestin–biased agonist binding are propagated all the way to the intracellular surface when the AT1R is structurally unconstrained (*12*, *13*). Consistent with our crystallographic observations of the ligand-binding site and the receptor core, these complementary methods demonstrate that AngII promotes a more fully activated receptor conformation than that promoted by β-arrestin–biased ligands. Given the similarity of conformations of GPCRs once they have fully engaged G proteins and β-arrestin, these mounting data suggest that the initial recognition of the AT1R by GRKs and β-arrestins could involve the conformations that are stabilized preferentially by β-arrestin–biased ligands. Our work provides a structural explanation for the complex signaling pharmacology of this family of drug targets.

REFERENCES AND NOTES

1. R. J. Lefkowitz, *Angew. Chem. Int. Ed.* **52**, 6366–6378 (2013).
2. Y. K. Peterson, L. M. Luttrell, *Pharmacol. Rev.* **69**, 256–297 (2017).
3. Z. Rankovic, T. F. Brust, L. M. Bohn, *Bioorg. Med. Chem. Lett.* **26**, 241–250 (2016).
4. A. C. Holloway *et al.*, *Mol. Pharmacol.* **61**, 768–777 (2002).
5. H. Wei *et al.*, *Proc. Natl. Acad. Sci. U.S.A.* **100**, 10782–10787 (2003).
6. S. Rajagopal *et al.*, *Mol. Pharmacol.* **80**, 367–377 (2011).
7. R. T. Strachan *et al.*, *J. Biol. Chem.* **289**, 14211–14224 (2014).
8. J. D. Violin *et al.*, *J. Pharmacol. Exp. Ther.* **335**, 572–579 (2010).
9. D. M. Ryba *et al.*, *Circulation* **135**, 1056–1070 (2017).
10. J. D. McCorvy *et al.*, *Nat. Struct. Mol. Biol.* **25**, 787–796 (2018).
11. D. Wacker *et al.*, *Science* **340**, 615–619 (2013).
12. L. M. Wingler *et al.*, *Cell* **176**, 468–478.e11 (2019).
13. C.-M. Suomivuori *et al.*, *Science* **367**, 881–887 (2020).
14. L. M. Wingler, C. McMahon, D. P. Staus, R. J. Lefkowitz, A. C. Kruse, *Cell* **176**, 479–490.e12 (2019).
15. M. Caffrey, *Annu. Rev. Biophys.* **38**, 29–51 (2009).
16. H. Zhang *et al.*, *J. Biol. Chem.* **290**, 29127–29139 (2015).
17. H. Zhang *et al.*, *Cell* **161**, 833–844 (2015).
18. J. A. Ballesteros, H. Weinstein, in *Receptor Molecular Biology*, vol. 25 of *Methods in Neurosciences*, S. C. Sealfon, Ed. (Academic Press, 1995), pp. 366–428.
19. B. Zimmerman *et al.*, *Sci. Signal.* **5**, ra33 (2012).
20. M. Bermudez, A. Bock, *Trends Pharmacol. Sci.* **40**, 236–239 (2019).
21. J. Cabana *et al.*, *J. Biol. Chem.* **290**, 15835–15854 (2015).
22. C. Lee *et al.*, *FEBS Lett.* **581**, 2517–2522 (2007).
23. K. Noda *et al.*, *Biochemistry* **35**, 16435–16442 (1996).
24. L. Hunyady, A. J. Baukal, T. Balla, K. J. Catt, *J. Biol. Chem.* **269**, 24798–24804 (1994).
25. M. M. Bonde *et al.*, *PLOS ONE* **5**, e14135 (2010).
26. V. Katritch *et al.*, *Trends Biochem. Sci.* **39**, 233–244 (2014).
27. B. Taddese *et al.*, *PLOS Comput. Biol.* **14**, e1006209 (2018).
28. S. Rajagopal *et al.*, *Proc. Natl. Acad. Sci. U.S.A.* **107**, 628–632 (2010).
29. S. Rajagopal *et al.*, *J. Biol. Chem.* **288**, 35039–35048 (2013).

30. T. A. Kohout *et al.*, *J. Biol. Chem.* **279**, 23214–23222 (2004).
31. G. Fenalti *et al.*, *Nature* **506**, 191–196 (2014).
32. A. Steen *et al.*, *J. Biol. Chem.* **288**, 12511–12521 (2013).
33. L. Valentin-Hansen, T. M. Frimurer, J. Mokrosinski, N. D. Holliday, T. W. Schwartz, *J. Biol. Chem.* **290**, 24495–24508 (2015).
34. E. Ceraudo *et al.*, Uveal melanoma oncogene CYSLTR2 encodes a constitutively active GPCR highly biased toward Gq signaling. bioRxiv 663153 [Preprint]. 6 June 2019.
35. A. Manglik *et al.*, *Cell* **161**, 1101–1111 (2015).
36. R. Fredriksson, M. C. Lagerström, L. G. Lundin, H. B. Schiöth, *Mol. Pharmacol.* **63**, 1256–1272 (2003).

ACKNOWLEDGMENTS

We thank V. Brennand, Q. Lennon, and J. Taylor for administrative assistance. We thank the staff at Advanced Photon Source GM/CA beamlines for technical assistance and support of data collection. GM/CA@APS is supported by the NIH National Institute of General Medical Sciences (AGM-12006) and the National Cancer Institute (ACB-12002). **Funding:** Funding was provided by the Sigrid Jusélius Foundation (C.-M.S.); the International Human Frontier Science Program Organization (LT000916/2018-L) (C.-M.S.); the Mandel Center for Hypertension and Atherosclerosis at Duke (R.J.L.); the Vallee Foundation (A.C.K.); the Smith Family Foundation (A.C.K.); and NIH grants R01GM127359 (R.O.D.), R01HL16037 (R.J.L.), and DP5OD021345 (A.C.K.). A.L.W.K. is a Howard Hughes Medical Institute Medical Research Fellow. R.J.L. is an investigator with the Howard Hughes Medical Institute. **Author contributions:** L.M.W., D.P.S., and A.L.W.K. performed signaling and functional characterization experiments. L.M.W. crystallized the complexes. L.M.W., C.M., and A.C.K. collected x-ray diffraction data. M.A.S., C.M., and A.C.K. performed x-ray data processing and refinement. C.-M.S., N.R.L., and R.O.D. proposed experiments on the basis of structural analysis. All authors interpreted data. R.J.L. and A.C.K. supervised the project. All authors wrote the manuscript. **Competing interests:** R.J.L. is a founder and stockholder of Trevena and is a director of Lexicon Pharmaceuticals. A.C.K. is an advisor for the Institute for Protein Innovation, a nonprofit research institute. **Data and materials availability:** Coordinates and structure factors for the AT1R-AT110i1 complexes with AngII, TRV023, and TRV026 ligands are deposited in the Protein Data Bank under accession codes 6OS0, 6OS1, and 6OS2, respectively.

SUPPLEMENTARY MATERIALS

science.sciencemag.org/content/367/6480/888/suppl/DC1
Materials and Methods
Figs. S1 to S7
Tables S1 to S5
References (*37*–*48*)

View/request a protocol for this paper from *Bio-protocol*.

2 August 2019; accepted 23 January 2020
10.1126/science.aay9813

OPTOMECHANICS

Cooling of a levitated nanoparticle to the motional quantum ground state

Uroš Delić[1,2]*, Manuel Reisenbauer[1], Kahan Dare[1,2], David Grass[1]†, Vladan Vuletić[3], Nikolai Kiesel[1], Markus Aspelmeyer[1,2]*

Quantum control of complex objects in the regime of large size and mass provides opportunities for sensing applications and tests of fundamental physics. The realization of such extreme quantum states of matter remains a major challenge. We demonstrate a quantum interface that combines optical trapping of solids with cavity-mediated light-matter interaction. Precise control over the frequency and position of the trap laser with respect to the optical cavity allowed us to laser-cool an optically trapped nanoparticle into its quantum ground state of motion from room temperature. The particle comprises 10^8 atoms, similar to current Bose-Einstein condensates, with the density of a solid object. Our cooling technique, in combination with optical trap manipulation, may enable otherwise unachievable superposition states involving large masses.

Optical levitation of dielectric particles works by using forces induced by laser light that are strong enough to overcome gravity. At its most fundamental level, an incoming laser polarizes the dielectric material, which in turn interacts with the radiation field of the laser. As a consequence, a particle in a tightly focused laser beam experiences a gradient force toward the intensity maximum of the beam, resulting in a three-dimensional confinement of the particle (*1*). Such "optical tweezers" have become a powerful tool to manipulate dielectric objects in isolation from other environments.

In the domain of quantum physics, optical trapping and cooling of atoms has enabled the study of individual atoms and quantum gases. It is also a fundamental technique for confining particles to optical lattice geometries for the study of many-body quantum phenomena. As such, laser cooling techniques should enable the preparation of a levitated solid-state particle in its quantum ground state of motion (*2*–*4*). The particle wave packet can then be expanded and modified by a sequence of free fall, coherent manipulations, and quantum measurement operations (*5*). This provides a promising platform for exploring macroscopic quantum phenomena. It entails the ability to manipulate the spatial profile of the trapping laser for implementing nonlinear potentials, and may open the possibility of creating nonclassical states of motion such as non-Gaussian states or large spatial superpositions. This is in stark contrast to experiments that prepare motional quantum states using solid-state harmonic oscillators, where coupling to external nonlinear systems or measurements provides the interaction for nonclassical state preparation (*6*–*8*). Unlike ultracold quantum gases, motional quantum states of trapped solids involve the collective motion of all atoms and hence provide a natural way toward spatial superpositions of large mass differences in so-called Schrödinger cat states, which is a fundamentally hard task for gaseous systems (*9*).

A key requirement for entering this new regime is to prepare the particle wave packet in a sufficiently pure quantum state—in this case, to cool its motion into the quantum ground state. One possibility is to monitor the particle motion with a sensitivity at or below the ground-state size of the wave packet and apply a feedback force to directly counteract the motion. Such feedback cooling to the quantum ground state has recently been demonstrated for harmonic modes of cryogenically cooled micromechanical membranes (*10*). In the context of levitated nanoparticles, feedback cooling was initially introduced to provide stable levitation in high vacuum. At present, feedback cooling is limited to approximately four motional quanta (phonons) (*11*). A different approach is derived from the laser cooling of atoms, where the absorption and reemission of Doppler-shifted laser photons provides a velocity-dependent scattering force. The presence of an optical cavity modifies the electromagnetic boundary conditions for the scattered light. We can use this to tailor the scattering rates and therefore cool particles without an accessible internal level structure, such as molecules or dielectric solids (*12*, *13*). These cavity-cooling schemes have been used in the past to achieve ground-state cooling of various systems ranging from individual atoms to cryogenically cooled modes of solid-state nano- and micromechanical oscillators in the context of cavity optomechanics (*14*). Previous attempts to apply cavity cooling to levitated solids have proven challenging, and cooling was limited to several hundred phonons (*15*–*18*), mainly as a result of co-trapping associated with high intracavity photon number and excessive laser phase noise heating at low motional frequencies (<1 MHz) (*17*, *18*). We apply a modified scheme—cavity cooling by coherent scattering (*19*–*21*)—that circumvents these shortcomings and enables direct ground-state cooling of a solid in a room-temperature environment.

In our experimental setup, we trap a spherical silica particle inside a vacuum chamber using an optical tweezer. A tightly focused laser beam (power in the focus $P_{tw} \approx 400$ mW, wavelength $\lambda = 1064$ nm, and frequency $\omega_{tw} = 2\pi c/\lambda$, where c is the speed of light in vacuum) creates a three-dimensional harmonic potential for the particle motion with motional frequencies $(\Omega_x, \Omega_y, \Omega_z)/2\pi \approx (305, 275, 80)$ kHz. We position the particle within an optical cavity (cavity finesse $\mathcal{F} \approx 73.000$; cavity linewidth $\kappa/2\pi = 193 \pm 4$ kHz; cavity frequency $\omega_{cav} = \omega_{tw} + \Delta$, where Δ is the laser detuning), which collects the tweezer light scattered off the nanoparticle under approximately a right angle (Fig. 1A). The particle has subwavelength dimension and hence resembles, to a good approximation, a dipole emitter. When driven by the optical tweezer, the particle coherently scatters dipole radiation predominantly orthogonal to the tweezer polarization axis. Motorized translation stages in the tweezer optics allow us to position the particle with an accuracy of a few nanometers with respect to the cavity axis (x-direction) such that the particle can be well localized within one period of the cavity standing wave field. To achieve optimal cooling along the cavity axis, the particle needs to be located at an intensity minimum of the cavity standing wave field (*19*, *20*). At that location the particle is "dark," and accordingly all dipole scattering into the cavity mode is inhibited because of destructive interference imposed by the cavity. The particle motion breaks this symmetry, and therefore only inelastically scattered Stokes- and anti-Stokes photons at sideband frequencies $\omega_{tw} \pm \Omega_x$ can propagate in the cavity.

Cavity cooling of the particle motion occurs because Stokes scattering processes along the cavity, which increase the kinetic energy of the particle by $\hbar\Omega_x$ per photon, are suppressed, while anti-Stokes scattering processes, which reduce the energy accordingly, are enhanced (*14*). This process is maximized at the optimal detuning $\Delta \approx \Omega_x$, where the anti-Stokes sideband becomes fully resonant with the cavity. A particle in its quantum ground state of motion cannot further reduce its energy, hence anti-Stokes scattering close to the ground state is fundamentally inhibited (Fig. 1, B and C). The

[1]Vienna Center for Quantum Science and Technology, Faculty of Physics, University of Vienna, A-1090 Vienna, Austria. [2]Institute for Quantum Optics and Quantum Information, Austrian Academy of Sciences, A-1090 Vienna, Austria. [3]Department of Physics and Research Laboratory of Electronics, Massachusetts Institute of Technology, Cambridge, MA 02139, USA.
*Corresponding author. Email: uros.delic@univie.ac.at (U.D.); markus.aspelmeyer@univie.ac.at (M.A.)
†Present address: Department of Chemistry, Duke University, Durham, NC 27708, USA.

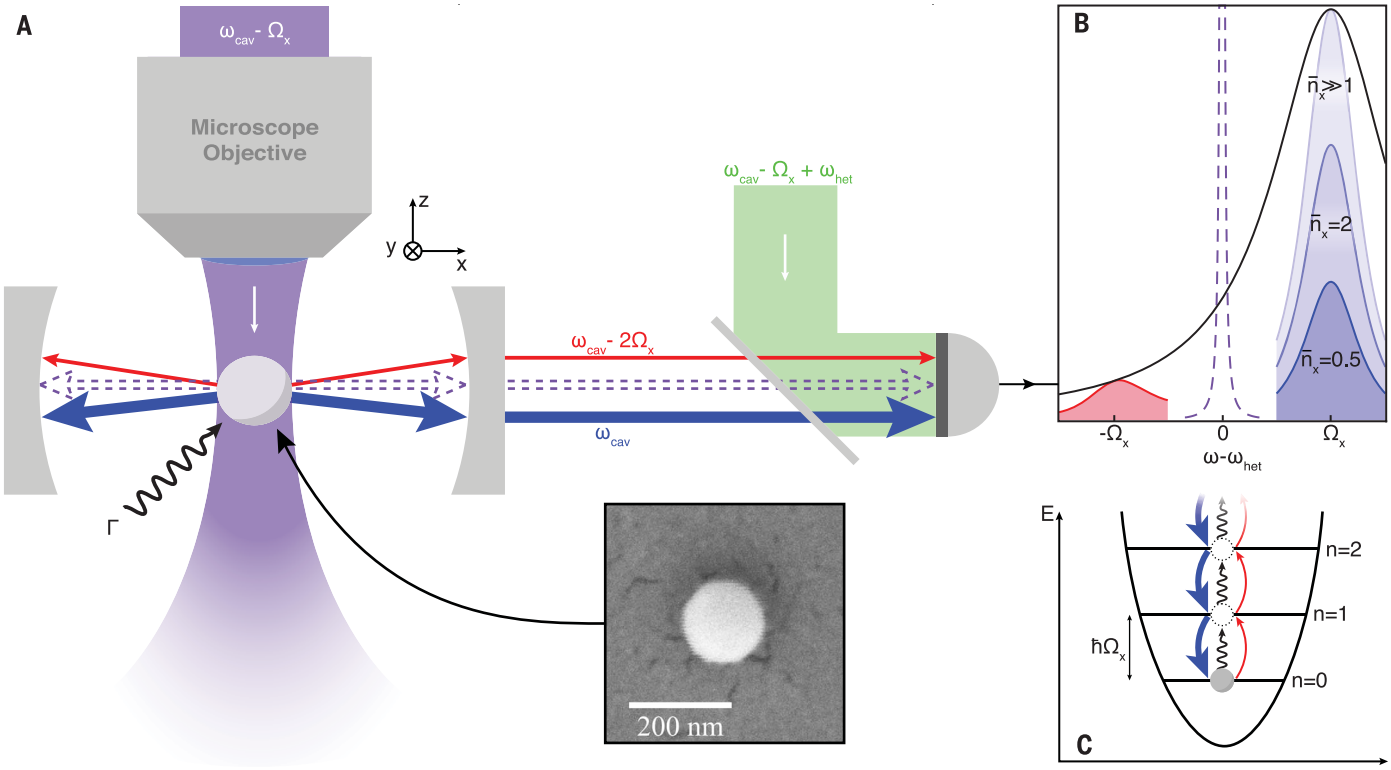

Fig. 1. Cavity cooling and sideband thermometry. (**A**) A silica nanoparticle of nominal diameter d = 143 ± 4 nm (SEM image) is trapped in an optical tweezer (purple). The frequency of the tweezer laser ω_{tw} is detuned from the initially empty cavity resonance ω_{cav} such that $\omega_{tw} = \omega_{cav} - \Omega_x$. Scattering of the tweezer light into the optical cavity is maximized via the tweezer polarization. The spatial mode overlap between the dipole emission pattern of the silica nanoparticle and the optical cavity mode results in a Purcell enhancement of the scattered radiation by a factor of 8 relative to a free-space configuration. When the particle is positioned at a cavity node, the elastic scattering of the tweezer light (dashed purple arrows) is suppressed, leaving only the inelastically scattered Stokes (red) and anti-Stokes (blue) sidebands at frequencies $\omega_{cav} - 2\Omega_x$ and ω_{cav}, respectively. Mixing the scattered sidebands with a strong local oscillator (green) at $\omega_{LO} = \omega_{tw} + \omega_{het}$ allows us to separately detect both sidebands in a heterodyne measurement at the cavity output port. The total heating rate from the environment is represented here as Γ. (**B**) Heterodyne measurement of the Stokes and anti-Stokes sidebands. The phonon occupation affects the overall scattering rates, which are initially modified by the cavity response (black). For large phonon occupations ($\bar{n}_x >> 1$), the relative amplitudes of the Stokes and anti-Stokes sidebands are completely described by the cavity transmission function. As the nanoparticle approaches the motional ground state, the sideband ratio is modified because the oscillator cannot undergo an anti-Stokes scattering process. This asymmetry allows for direct thermometry of the phonon occupation. The suppressed elastic scattering contribution is depicted in dashed purple for reference. (**C**) Depiction of the phonon energy levels close to the ground state. The heating rate from the environment and the Stokes scattering rate are balanced by the anti-Stokes scattering rate.

resulting sideband asymmetry in the scattering rates is a direct measure of the temperature of the harmonic particle motion, which does not require calibration to a reference bath (*22*). We observe these sidebands, which are modulated by the cavity envelope (*23*), using frequency-selective heterodyne detection of the cavity output, specifically by mixing it with a strong local oscillator field ($P_{LO} \approx 400$ μW) detuned from the tweezer laser by $\omega_{het}/2\pi$ = 10.2 MHz.

Independent measurements of the cavity linewidth κ and the laser detuning Δ allow us to correct the detected sideband ratios for the cavity envelope (*24*), and hence to extract the motional temperature of the particle via the fundamental sideband asymmetry (Fig. 2A). For this method to work reliably, it is important to exclude all relevant influences of noise contributions to the sideband asymmetry (*25*). We ensure this by confirming that the detection process is shot noise–limited and that both amplitude- and phase-noise contributions of the drive laser are negligible (*24*). Figure 2B shows the measured phonon number $\bar{n}_x$ along the cavity axis for different laser detunings Δ. For near-optimal detuning of $\Delta/2\pi$ = 315 kHz, we observe a final occupation as low as $\bar{n}_x$ = 0.43 ± 0.03, corresponding to a temperature of 12.2 ± 0.5 μK and a ground-state probability of 70 ± 2%. Note that in contrast to previous quantum experiments involving cryogenically cooled solid-state oscillators, ground-state cooling here is achieved in a room-temperature environment.

The final occupation $\bar{n}_{fin}$ along any direction is reached when the total heating rate Γ_x is balanced by the cooling rate $\bar{n}_{fin} \times \gamma$, where γ is the linewidth of the motional sidebands (*26*). For the resolved sideband regime ($\kappa < \Omega_x$) as studied here, and in the absence of any other heating mechanisms, Stokes scattering due to the finite cavity linewidth limits cooling with optimal parameters to a minimum phonon occupation of $\bar{n}_{min} = (\kappa/4\Omega_x)^2 \approx 0.025$. Note that in this case, detailed balance implies that the fundamental ground-state asymmetry exactly compensates the effect of the cavity envelope and therefore both sidebands have equal power. Additional sources of heating are balanced by larger anti-Stokes scattering, which results in the overall observed sideband imbalance. By independently measuring $\bar{n}_x$ and γ, we extract a total heating rate as low as $\Gamma_x/2\pi$ = 20.6 ± 2.3 kHz at a pressure of ~10^{-6} mbar. This is consistent with the separately measured heating rate due to background gas collisions (*18*), $\Gamma_{gas}/2\pi$ = 16.1 ± 1.2 kHz, and the expected heating contributions from photon recoil, $\Gamma_{rec}/2\pi \approx 6$ kHz, and from laser phase noise, $\Gamma_{phase}/2\pi < 200$ Hz (*24*).

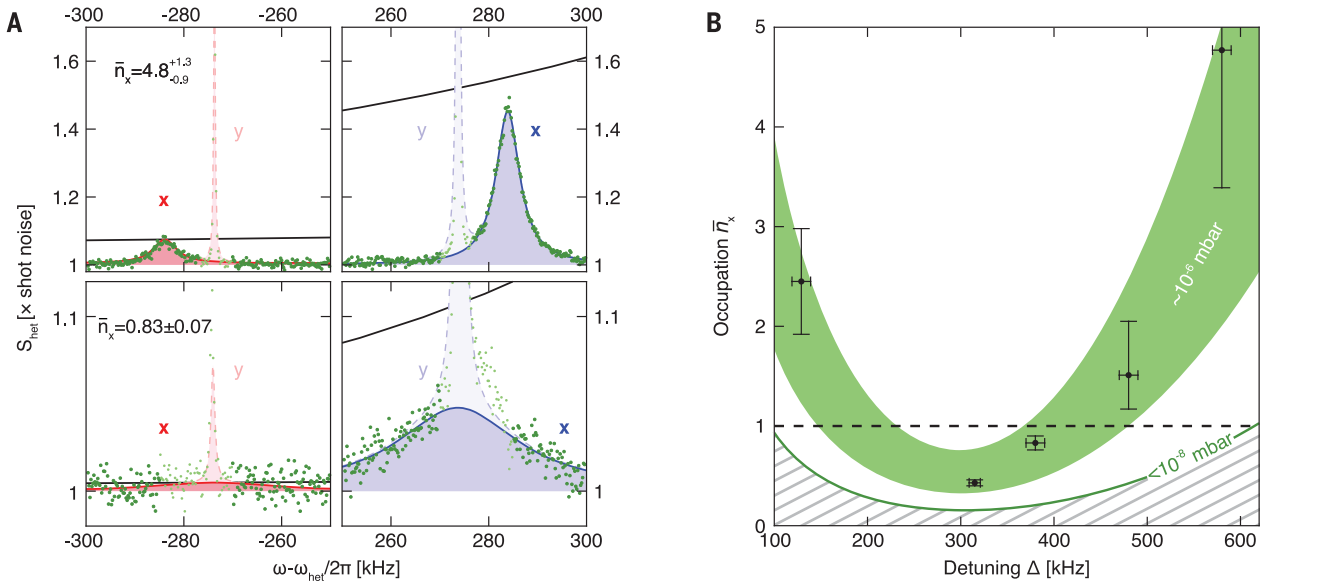

Fig. 2. Thermometry of the phonon occupation associated with the cavity axial motion. (**A**) Heterodyne spectra. Shown are the sideband power spectra for Stokes (left) and anti-Stokes (right) scattering for different detunings $\Delta/2\pi$ = 580 ± 10 kHz (top row) and $\Delta/2\pi$ = 380 ± 10 kHz (bottom row). Red and blue solid lines are fits to the data representing the *x* motion. Also shown are lighter red and blue dashed lines, which are part of the fitted spectrum corresponding to the *y* motion at $\Omega_y/2\pi$ = 275 ± 1 kHz. Black solid line indicates the cavity transmission function normalized to the Stokes sideband power. Smaller temperatures show a stronger deviation of the anti-Stokes scattered sideband power from the cavity envelope, as described in the text. The ratio of amplitudes together with the independently measured cavity transmission function yields the final occupation $\bar{n}_x$. (**B**) Occupation $\bar{n}_x$ as a function of tweezer laser detuning. The cooling rate is maximal when the optical tweezer is detuned from the cavity resonance by approximately the motional frequency $\Delta/2\pi \approx$ 315 kHz. At this maximal cooling point, we achieve a phonon occupation of $\bar{n}_x$ = 0.43 ± 0.03. Error bars take into account the experimental uncertainty of the laser detuning and the cavity decay rate in combination with the errors inherent to the fit. The wide green band is a theoretical model based on system parameters, which takes into account pressure drifts during the measurement. The lower dark green line corresponds to the expected occupation when the environment pressure is below 10^{-8} mbar, at which heating due to collisions with the background gas becomes negligible relative to recoil heating.

In future experiments, reduction of decoherence can be achieved mainly by lower background pressures, but potentially also by operating at lower temperatures and using smaller cavity mode volumes. At present, using the measured heating rates, we estimate a maximum coherence time of 7.6 ± 1 μs in the optical trap, corresponding to approximately 15 coherent oscillations before populating the ground state with one phonon (*2*, *27*). In a free-fall experiment, where the particle would be released from the optical trap, the dominant source for decoherence is the collision with background gas molecules. At the achieved pressure of 10^{-6} mbar, this limits the free-fall coherence time to 1.4 μs, which would allow for an expansion of the wave packet by approximately a factor of 3, from the ground state size of 3.1 pm to 10.2 pm (*24*, *28*). Larger wave packet sizes can be achieved by further decreasing this decoherence rate—for example, by operating at much lower pressures. Blackbody radiation will then become the dominant source of decoherence and will, for our room-temperature parameters, allow for wave packet expansions up to several nanometers. A wave packet size on the order of the particle radius could be achieved by combining ultrahigh vacuum (approximately 10^{-11} mbar) with cryogenic temperatures (below 130 K).

The combination of cavity optomechanical quantum control of levitated systems and free-fall experiments can open up a new regime of macro–quantum physics, with additional potential applications in quantum sensing (*29*) and other fields of fundamental physics (*30*). Most important, we believe that the quantum control of levitated systems is a viable route toward experiments in which quantum systems can act as gravitational source masses, as was originally suggested by Feynman (*31*) and recently revisited in the context of levitation (*32*, *33*).

REFERENCES AND NOTES

1. A. Ashkin, J. M. Dziedzic, J. E. Bjorkholm, S. Chu, *Opt. Lett.* **11**, 288 (1986).
2. D. E. Chang *et al.*, *Proc. Natl. Acad. Sci. U.S.A.* **107**, 1005–1010 (2010).
3. O. Romero-Isart, M. L. Juan, R. Quidant, J. I. Cirac, *New J. Phys.* **12**, 033015 (2010).
4. P. F. Barker, M. N. Shneider, *Phys. Rev. A* **81**, 023826 (2010).
5. O. Romero-Isart *et al.*, *Phys. Rev. Lett.* **107**, 020405 (2011).
6. A. D. O'Connell *et al.*, *Nature* **464**, 697–703 (2010).
7. Y. Chu *et al.*, *Nature* **563**, 666–670 (2018).
8. R. Riedinger *et al.*, *Nature* **530**, 313–316 (2016).
9. J. I. Cirac, M. Lewenstein, K. Mølmer, P. Zoller, *Phys. Rev. A* **57**, 1208–1218 (1998).
10. M. Rossi, D. Mason, J. Chen, Y. Tsaturyan, A. Schliesser, *Nature* **563**, 53–58 (2018).
11. F. Tebbenjohanns, M. Frimmer, V. Jain, D. Windey, L. Novotny, *Phys. Rev. Lett.* **124**, 013603 (2020).
12. P. Horak, G. Hechenblaikner, K. M. Gheri, H. Stecher, H. Ritsch, *Phys. Rev. Lett.* **79**, 4974–4977 (1997).
13. V. Vuletić, S. Chu, *Phys. Rev. Lett.* **84**, 3787–3790 (2000).
14. M. Aspelmeyer, T. J. Kippenberg, F. Marquardt, *Rev. Mod. Phys.* **86**, 1391–1452 (2014).
15. N. Kiesel *et al.*, *Proc. Natl. Acad. Sci. U.S.A.* **110**, 14180–14185 (2013).
16. J. Millen, P. Z. G. Fonseca, T. Mavrogordatos, T. S. Monteiro, P. F. Barker, *Phys. Rev. Lett.* **114**, 123602 (2015).
17. N. Meyer *et al.*, *Phys. Rev. Lett.* **123**, 153601 (2019).
18. U. Delić *et al.*, arXiv 1902.06605 [physics.optics] (18 February 2019).
19. U. Delić *et al.*, *Phys. Rev. Lett.* **122**, 123602 (2019).
20. D. Windey *et al.*, *Phys. Rev. Lett.* **122**, 123601 (2019).
21. S. Nimmrichter, K. Hammerer, P. Asenbaum, H. Ritsch, M. Arndt, *New J. Phys.* **12**, 083003 (2010).
22. A. H. Safavi-Naeini *et al.*, *Phys. Rev. Lett.* **108**, 033602 (2012).
23. R. W. Peterson *et al.*, *Phys. Rev. Lett.* **116**, 063601 (2016).
24. See supplementary materials.
25. V. Sudhir *et al.*, *Phys. Rev. X* **7**, 011001 (2017).
26. V. Jain *et al.*, *Phys. Rev. Lett.* **116**, 243601 (2016).
27. O. Romero-Isart *et al.*, *Phys. Rev. A* **83**, 013803 (2011).
28. O. Romero-Isart, *Phys. Rev. A* **84**, 052121 (2011).
29. A. A. Geraci, S. B. Papp, J. Kitching, *Phys. Rev. Lett.* **105**, 101101 (2010).
30. J. Bateman, I. McHardy, A. Merle, T. R. Morris, H. Ulbricht, *Sci. Rep.* **5**, 8058 (2015).
31. D. Rickles, C. M. DeWitt, *The Role of Gravitation in Physics: Report from the 1957 Chapel Hill Conference* (2011); https://edition-open-sources.org/media/sources/5/Sources5.pdf.
32. S. Bose *et al.*, *Phys. Rev. Lett.* **119**, 240401 (2017).
33. C. Marletto, V. Vedral, *Phys. Rev. Lett.* **119**, 240402 (2017).

ACKNOWLEDGMENTS

We thank O. Romero-Isart, L. Novotny, and T. Monteiro for insightful comments. U.D. and M.A. thank J. Ye for initially pointing out the relevance of coherent scattering to us. **Funding:** Supported by the European Research Council (ERC CoG QLev4G), the ERA-NET program QuantERA, QuaSeRT (project no. 11299191 via the EC, the Austrian ministries BMDW and BMBWF, and research promotion agency FFG), the Austrian Science Fund (FWF, project TheLO, Y 952-N36, START) and the doctoral school CoQuS (project W1210), and the research platform TURIS at the University of Vienna. **Author**

contributions: U.D., V.V., N.K., and M.A. conceived the experiment; U.D., M.R., and K.D. built the experiment (with initial contributions from D.G.) and performed the measurements; U.D. and D.G. performed the data analysis; and all authors were involved in writing and editing the paper. **Competing interests:** The authors declare no competing interests. **Data and materials availability:** All data needed to evaluate the conclusions in the paper are present in the paper or the supplementary materials.

SUPPLEMENTARY MATERIALS

science.sciencemag.org/content/367/6480/892/suppl/DC1
Supplementary Text
Figs. S1 to S7
References (*34*–*57*)

29 November 2019; accepted 21 January 2020
Published online 30 January 2020
10.1126/science.aba3993

TOPOLOGICAL MATTER

Quantum anomalous Hall effect in intrinsic magnetic topological insulator $MnBi_2Te_4$

Yujun Deng[1,2]*, Yijun Yu[1,2]*, Meng Zhu Shi[3]*, Zhongxun Guo[1,2], Zihan Xu[4], Jing Wang[1,2]†, Xian Hui Chen[3]†, Yuanbo Zhang[1,2]†

In a magnetic topological insulator, nontrivial band topology combines with magnetic order to produce exotic states of matter, such as quantum anomalous Hall (QAH) insulators and axion insulators. In this work, we probe quantum transport in $MnBi_2Te_4$ thin flakes—a topological insulator with intrinsic magnetic order. In this layered van der Waals crystal, the ferromagnetic layers couple antiparallel to each other; atomically thin $MnBi_2Te_4$, however, becomes ferromagnetic when the sample has an odd number of septuple layers. We observe a zero-field QAH effect in a five–septuple-layer specimen at 1.4 kelvin, and an external magnetic field further raises the quantization temperature to 6.5 kelvin by aligning all layers ferromagnetically. The results establish $MnBi_2Te_4$ as an ideal arena for further exploring various topological phenomena with a spontaneously broken time-reversal symmetry.

A distinct feature that is common to all topological materials is the presence of topologically protected quantum states that are robust against local perturbations (*1*–*4*). For example, in a topological insulator (TI) such as Bi_2Te_3, the bulk band topology guarantees the existence of two-dimensional (2D) surface states with gapless Dirac dispersion (*5*, *6*). Introducing magnetism into the initially time-reversal invariant TIs induces profound changes in their electronic structures. Specifically, the long-range magnetic order breaks the time-reversal symmetry and causes an exchange gap in the gapless Dirac dispersion of the surface states (*2*, *7*). The gap opening is accompanied by the emergence of a chiral edge mode that is predicted to give rise to a quantum anomalous Hall (QAH) effect when the Fermi level is situated inside of the exchange gap (*2*, *8*–*10*). The dissipationless QAH edge channel, combined with the spin-momentum locking that is inherent in topological materials, may lead to advances in device concepts for topological electronic applications (*11*).

The experimental observation of the QAH effect in chromium-doped $(Bi,Sb)_2Te_3$ (*10*, *12*–*14*) required precise control of the ratio of the multiple elements in this nonstoichiometric material. However, the fine-tuning needed to reconcile conflicting demands—i.e., large magnetization and low initial carrier doping—poses a challenge for material growth, and the randomly distributed magnetic dopants act as impurities that limit the quality of the magnetic TIs. As a result, the exact quantization of the anomalous Hall effect appears only at low temperatures, up to $T = 2$ K (in the penta-layer sandwich structure of topological insulators) (*15*), which is far below the Curie temperature (a few tens of kelvin) and the exchange gap (hundreds of kelvin) (*16*) in the material. Further exploration of rich topological phenomena and their potential applications calls for intrinsic magnetic TIs—stoichiometric TIs with an innate magnetic order—so that topological effects can be studied in pristine crystals.

In this work, we probe the quantum transport in atomically thin flakes of intrinsic magnetic TI $MnBi_2Te_4$. $MnBi_2Te_4$ is a layered ternary tetradymite compound that consists of Te-Bi-Te-Mn-Te-Bi-Te septuple layers (SLs, or "layers" hereafter), so the material can be viewed as layered TI Bi_2Te_3 with each of its Te-Bi-Te-Bi-Te quintuple layers intercalated by an additional Mn-Te bilayer (inset of Fig. 1C). The resultant $MnBi_2Te_4$ crystal remains a TI but now becomes intrinsically magnetic (*17*–*21*). The magnetism originates from the Mn^{2+} ions in the crystal, which have a high spin of $S = 5/2$ and a large magnetic moment of ~$5\mu_B$ (where μ_B is the Bohr magneton) (*17*, *18*, *20*, *22*). Below a Neel temperature of $T_N = 25$ K, the spins couple ferromagnetically in each SL with an out-of-plane easy axis, but adjacent SLs couple antiparallel to each other. Bulk $MnBi_2Te_4$ is, therefore, an antiferromagnet (AFM) (*18*, *20*). In this work, we study thin flakes of $MnBi_2Te_4$ to minimize the parallel bulk conduction, focusing on $MnBi_2Te_4$ flakes with an odd number of layers, N. Because the layer magnetization in these odd-layer flakes does not completely cancel, the flakes become ferromagnetic while remaining a TI for $N \geq 3$ (*18*, *19*). Because the SLs are separated by van der Waals gaps in bulk $MnBi_2Te_4$, the extensive arsenal of fabrication techniques developed for 2D materials enables us to obtain few-layer samples that preserve the high quality of the bulk crystals.

We start with high-quality $MnBi_2Te_4$ single crystals that are grown by flux methods (*20*, *23*), and we obtain atomically thin $MnBi_2Te_4$ using an Al_2O_3-assisted exfoliation technique described in (*24*). Specifically, we first thermally evaporate an Al_2O_3 thin film onto a freshly prepared surface of the bulk crystal. We then lift the Al_2O_3 thin film, along with $MnBi_2Te_4$ thin flakes cleaved from the bulk, using a thermal release tape. The Al_2O_3/$MnBi_2Te_4$ stack is subsequently released onto a piece of transparent polydimethylsiloxane (PDMS) and inspected under an optical microscope in transmission mode. Figure 1A displays the optical image of few-layer $MnBi_2Te_4$ flakes on the Al_2O_3 film attached to PDMS. The transmittance of various numbers of SLs follows the Beer-Lambert law (Fig. 1B), which enables us to precisely determine the layer number. The thin flakes are finally stamped onto a Si wafer covered with 285-nm-thick SiO_2, followed by deposition of Cr/Au contacts for transport measurements. The degenerately doped Si serves as a backgate, so a voltage bias (V_g) applied between Si and the sample can electrostatically dope electron or hole carriers into $MnBi_2Te_4$ flakes, depending on the polarity of V_g. The entire device-fabrication process is performed in an argon-filled glove box, where O_2 and H_2O content is kept below 0.5 parts per million to mitigate sample degradation. Figure 1C displays temperature-dependent longitudinal resistance, R_{xx}, of few-layer $MnBi_2Te_4$. The AFM transition manifests as a resistance peak at T_N (*25*). Compared with the bulk value of 25 K, T_N monotonically decreases as the samples become thinner ($T_N = 23$ K in the five-layer sample, 21 K in the four-layer sample, and 18 K in the three-layer sample). We ascribe the suppression of T_N to increased thermal fluctuations as the samples approach the 2D limit. The resistance rises again at the lowest temperatures, probably because of the localization of the carriers in the presence of disorder in the 2D samples.

Few-layer $MnBi_2Te_4$ flakes exhibit a rich set of magnetic states under a vertical magnetic field. The states manifest as steps in the Hall resistance, R_{yx}, as the magnetic field, $\mu_0 H$, is varied (Fig. 1D). There are three main points to notice in Fig. 1D. First, the three- and five-layer samples (samples 3a and 5a, respectively, as labeled in table S1) become ferromagnetic, whereas the four-layer sample (sample 4a) remains largely antiferromagnetic. The small, residual ferromagnetic response in R_{yx} may come from possible substrate-induced, top-bottom surface asymmetry or from disorders in the sample. Second, juxtaposing the

[1]State Key Laboratory of Surface Physics and Department of Physics, Fudan University, Shanghai 200438, China. [2]Institute for Nanoelectronic Devices and Quantum Computing, Fudan University, Shanghai 200433, China. [3]Hefei National Laboratory for Physical Science at Microscale and Department of Physics, University of Science and Technology of China, and Key Laboratory of Strongly-coupled Quantum Matter Physics, Chinese Academy of Sciences, Hefei, Anhui 230026, China. [4]SixCarbon Technology, Youmagang Industry Park, Shenzhen 518106, China.
*These authors contributed equally to this work.
†Corresponding author. Email: zhyb@fudan.edu.cn (Y.Z.); chenxh@ustc.edu.cn (X.H.C.); wjingphys@fudan.edu.cn (J.W.)

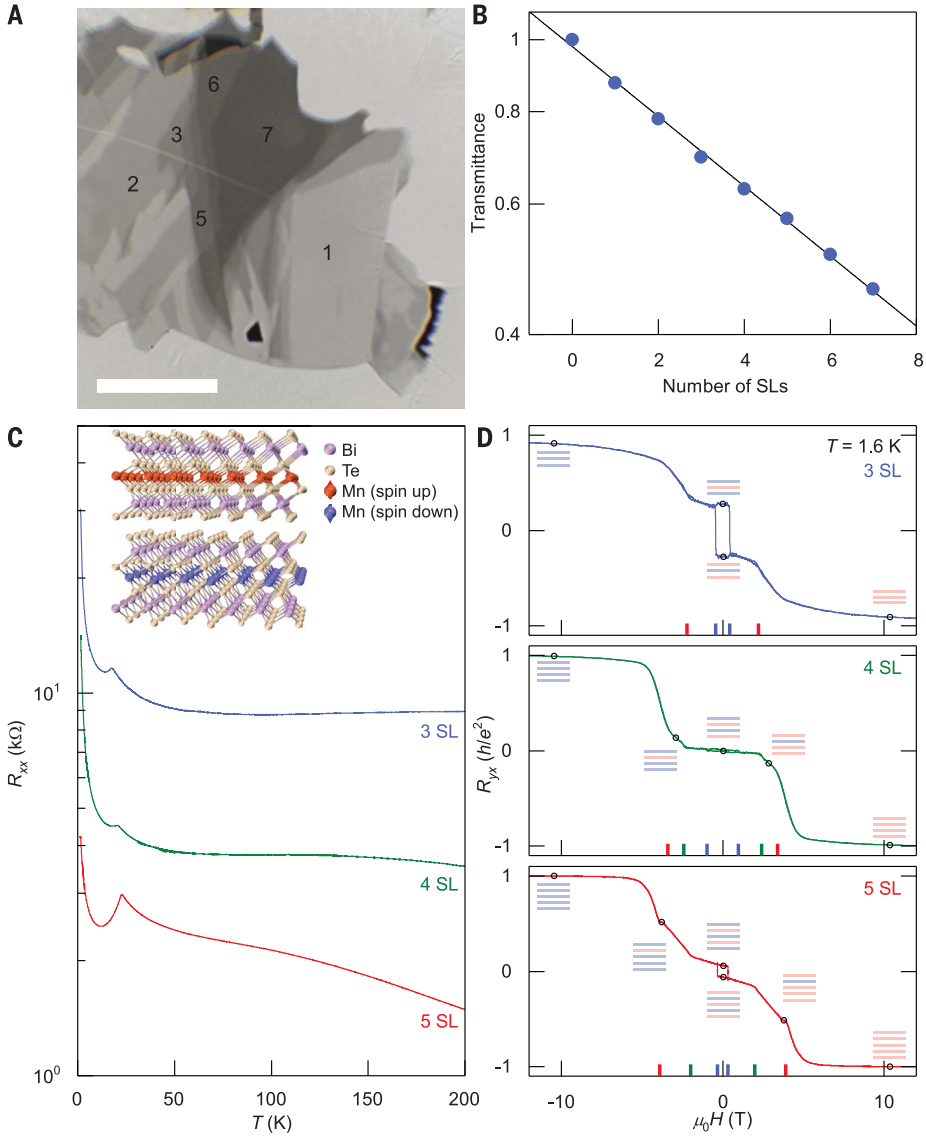

Fig. 1. Fabrication and characterization of few-layer $MnBi_2Te_4$ devices. (**A**) Optical image of few-layer flakes of $MnBi_2Te_4$ cleaved onto thermally evaporated Al_2O_3 thin film (thickness ~70 nm). The $MnBi_2Te_4/Al_2O_3$ stack is supported on a PDMS substrate. Image was taken in transmission mode. Number of SLs is labeled on selected flakes. Scale bar, 20 μm. (**B**) Transmittance as a function of the number of SLs. The transmittance (filled circles) follows the Beer-Lambert law (solid line). (**C**) Temperature-dependent sample resistance of few-layer $MnBi_2Te_4$. The antiferromagnetic transition manifests as a resistance peak in the three-, four-, and five-layer samples (samples 3a, 4a, and 5a, respectively; see table S1). Inset shows the layered crystal structure of $MnBi_2Te_4$ in the antiferromagnetic state. The spins of Mn^{2+} ions order ferromagnetically within a layer, whereas neighboring layers couple antiferromagnetically with an out-of-plane magnetocrystalline anisotropy. (**D**) R_{yx} of the same three-, four-, and five-layer $MnBi_2Te_4$ samples shown in (C) as a function of external magnetic field applied perpendicularly to the sample plane. Data were obtained at T = 1.6 K. All data sets were antisymmetrized to remove the R_{xx} component (*23*). The external magnetic field flips individual ferromagnetic SLs, one SL at a time, and eventually fully polarizes all SLs. The magnetic transitions manifest as jumps in R_{yx} that are marked by colored ticks on the horizontal axes. Cartoons illustrate the magnetic states at representative magnetic fields (marked by open circles). SLs with up or down magnetization are shown in red or blue, respectively. For simplicity, only one of the possible configurations is shown when there are degeneracies; we also ignore magnetic domains that may be present in some of the magnetic states.

$R_{yx}(\mu_0 H)$ of the three samples provides insight into those magnetic states. $R_{yx}(\mu_0 H)$ in the three-layer sample exhibits three plateaus that indicate three distinct magnetic states marked by empty circles, in contrast with five magnetic states indicated in the four-layer sample and six magnetic states in the five-layer sample. It is evident that the SLs are initially antiferromagnetically coupled, and an increasing external magnetic field flips individual ferromagnetic SLs, one SL at a time, eventually reaching a fully polarized magnetic state above $\mu_0 H$ ~ 6 T. These magnetic states are schematically illustrated by the insets in Fig. 1D. The transitions between the states can be described by the Stoner-Wohlfarth model with bipartite AFM (*23*). The model further points out that each layer flip takes place in two steps via a spin flop transition, where the layer magnetization is free to rotate in directions approximately perpendicular to the easy axis (*23*). Close examination of the transitions in $R_{yx}(\mu_0 H)$ reveal signs of such spin flop transitions in sample 5a (fig. S11).

Third, we observe that the anomalous Hall response quantizes to $R_{yx} = h/e^2$ once the external magnetic field fully aligns the magnetization in all SLs (here h/e^2 = 25.8 kilohm is the resistance quantum, h is the Planck constant, and e the charge of an electron). The quantization of anomalous R_{yx} is accompanied by a vanishing longitudinal resistance R_{xx} (fig. S3); both features are hallmarks of a QAH state with a dissipationless chiral edge channel. As a voltage, V_g, applied on backgate tunes the charge carrier in the five-layer sample (sample 5c; fig. S5) from the electron to the hole side, the QAH effect does not change sign, in distinct contrast to the carrier-type–dependent ordinary quantum Hall effect that is originated from Landau level (LL) quantization. Furthermore, the quantization is best developed as V_g is tuned to the charge neutrality point (CNP), V_g^{CNP}, where the Fermi level lies in the middle of the exchange gap (*23*). The large exchange gap in the fully polarized magnetic state leads to a robust QAH effect at elevated temperatures (fig. S4A). In particular, the anomalous Hall effect in sample 5a remains well quantized ($|R_{xx}|$ stays above $0.97h/e^2$ and R_{xx} below $0.017h/e^2$), under a magnetic field of $\mu_0 H$ = 12 T, at temperatures up to T = 4.5 K (fig. S4, C and D). Finally, we note that the zero-field anomalous Hall response in typical few-layer samples reaches a substantial fraction of the quantum resistance h/e^2 (up to 27% in sample 3a and 23% in sample 5c) but does not quantize, probably owing to disorder in the samples.

A well-developed QAH effect emerges at zero magnetic field in $MnBi_2Te_4$ with much-improved sample quality. Figure 2, A and B, displays the R_{yx} and R_{xx} of a high-quality five-layer sample (sample 5b), recorded as a function of a magnetic field at T = 1.4 K. The measurements are performed when the backgate is biased at V_g =

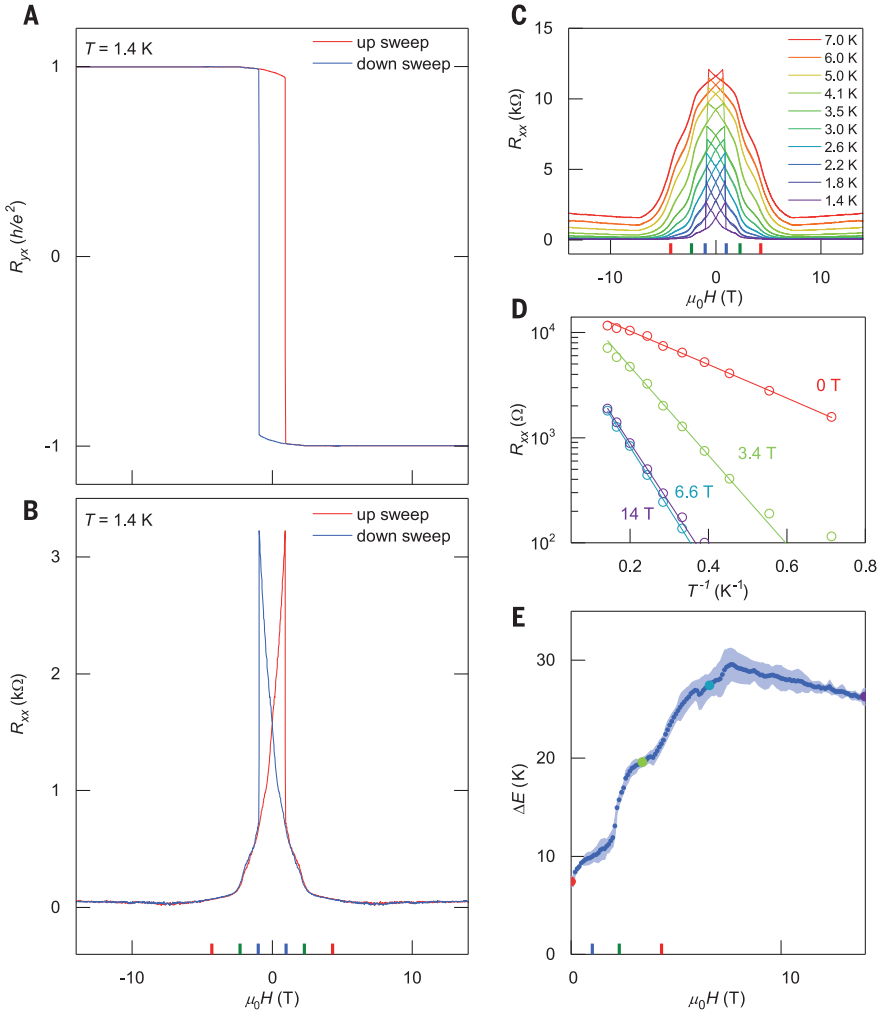

Fig. 2. QAH effect in a five-layer $MnBi_2Te_4$ flake. (**A** and **B**) Magnetic-field–dependent R_{yx} (A) and R_{xx} (B) acquired in the five-layer sample 5b at T = 1.4 K. R_{yx} and R_{xx} data shown here are antisymmetrized and symmetrized, respectively, to remove the mixing of the two components (*23*). Up and down sweeps of the magnetic field are shown in red and blue, respectively. R_{yx} reaches $0.97h/e^2$, concomitant with a R_{xx} of $0.061h/e^2$ at $\mu_0 H$ = 0 T. These features are unambiguous evidence of zero-field QAH effect. The external magnetic field polarizes the ferromagnetic SLs individually and further improves the QAH quantization; R_{yx} quantizes to $0.998h/e^2$ under magnetic fields above $\mu_0 H$ ~ 2.5 T. (**C**) R_{xx} of sample 5b as a function of magnetic field acquired at various temperatures. Data are symmetrized to remove the R_{yx} component. (**D**) Arrhenius plot of R_{xx} as a function of $1/T$ under representative magnetic fields. Solid lines are line fits, the slopes of which yield the energy gap of the thermally activated charge transport. (**E**) Energy gap as a function of magnetic field extracted from fitting the Arrhenius plots exemplified in (D). The shaded region represents the error bound of the energy gap from the line fits. Solid circles highlight the representative gap values obtained from the fittings shown in (D). Colored ticks on the horizontal axes in (B), (C), and (E) mark the locations of magnetic transitions. All data were obtained under a backgate bias of V_g = −200 V.

−200 V, close to the CNP. The zero-field remnant anomalous Hall response $R_{yx}\,|_{\mu_0 H\,=\,0\ \mathrm{T}}$ reaches $0.97h/e^2$, whereas $R_{xx}\,|_{\mu_0 H\,=\,0\ \mathrm{T}}$ drops to $0.061h/e^2$ at the same time—both are unambiguous evidence of a zero-field QAH effect. The QAH quantization is comparable to that in best magnetically doped TI thin films—R_{yx} ~ $0.97h/e^2$ and R_{xx} ~ $0.2h/e^2$, obtained in Cr modulation-doped $(Bi_{1-y}Sb_y)_2Te_3$ at T = 2 K (*15*). We adopt the same R_{yx} ~ $0.97h/e^2$ quantization criterion as in (*15*) throughout this work. An external magnetic field further enhances the quantization by aligning the ferromagnetic SLs (such magnetic transitions are visible in R_{xx} as a function of magnetic field as shown in Fig. 2C) and R_{yx} plateaus at $0.998h/e^2$, under magnetic fields above $\mu_0 H$ ~ 2.5 T. The ferromagnetic alignment of the SLs also improves the robustness of the QAH effect against thermal fluctuations. We observe that $|R_{yx}|$ stays within 3% of the resistance quantum at temperatures up to T = 6.5 K, under a magnetic field of $\mu_0 H$ = 7.6 T (fig. S6G).

Temperature-dependent measurements of R_{xx} further reveal the energetics of the QAH effect in the five-layer flake. Specifically, R_{xx} at V_g = −200 V exhibits a thermally activated behavior, $R_{xx} \sim \exp(-\Delta E/2k_B T)$, at elevated temperatures (where k_B is the Boltzmann constant and ΔE the energy gap; Fig. 2C). Line fits to the Arrhenius plots of $\ln R_{xx}$ as a function of $1/T$ yield the energy gap ΔE under various magnetic fields, as shown in Fig. 2, D and E. At zero magnetic field, we obtain an energy gap of ΔE = 0.64 meV, or 7.4 K, which reflects the energy scale of the zero-field QAH effect in sample 5b (Fig. 2D, red line). Such an energy gap is larger than the value found in magnetically doped TI thin films (*14*), but the energy gap is still much smaller than the exchange gap, E_{ex}, expected in $MnBi_2Te_4$ (*19*, *20*, *23*, *25*). We emphasize, however, that ΔE does not directly measure the bandgap E_g of the surface states [$E_g = E_{ex}$ in a pristine five-layer $MnBi_2Te_4$; see (*23*)], but rather characterizes the minimum energy required to excite an electron from the valence to the conduction band. The large difference between ΔE and predicted E_{ex} implies marked surface-band broadening that may be caused by various disorders in the sample. The Fermi energy, E_F, may not be situated exactly in the middle of the top and bottom surface gap at V_g = −200 V. This deviation will also contribute to the difference between the two gap values (*23*). The broadening may be responsible for the lack of direct observation of the exchange gap in spectroscopy measurements (*26*–*29*); there is much room for further increasing the energy scale of the QAH effect in pristine, high-quality $MnBi_2Te_4$.

As an external magnetic field is applied, we observe that ΔE increases in three steps and peaks at 30 ± 2 K when the sample is fully polarized under $\mu_0 H$ = 7.6 T. These steps coincide with the magnetic transitions (Fig. 2E). We attribute the stepwise increase in ΔE to the enhanced E_{ex} as the magnetic field aligns the magnetization of the SLs, one layer at a time (*23*). After the magnetic field fully polarizes the five-layer sample, ΔE diminishes with increasing magnetic field above $\mu_0 H$ = 7.6 T (Fig. 2E). The suppression of ΔE stems from the fact that the exchange field (that produces E_{ex}) in $MnBi_2Te_4$ is opposite to the external magnetic field (*30*). The linear $\Delta E(\mu_0 H)$ in the fully polarized magnetic state exhibits a slope

of −0.74, whereas an effective model of the surface bands yields an estimate of the *g*-factor of −2.6 (*23*). The mismatch between the two values may again come from the possibility that E_F is not situated in the middle of the top and bottom surface gap under a backgate bias of V_g = −200 V (*23*). Finally, we note that the energy gap stays open from $\mu_0 H$ = 0 to 14 T. This provides evidence that the high-field QAH state is adiabatically connected to the zero-field QAH state and that they are, topologically, the same state.

The QAH states gradually evolve into metallic ones as the backgate voltage shifts away from the CNP. The evolution provides a glimpse into the electronic structure of the surface bands outside of the bandgap. Figure 3A presents R_{yx} of sample 5b as a function of magnetic field under various gate voltages. The four magnetic states on each side of the field sweep are clearly separated by magnetic transitions that

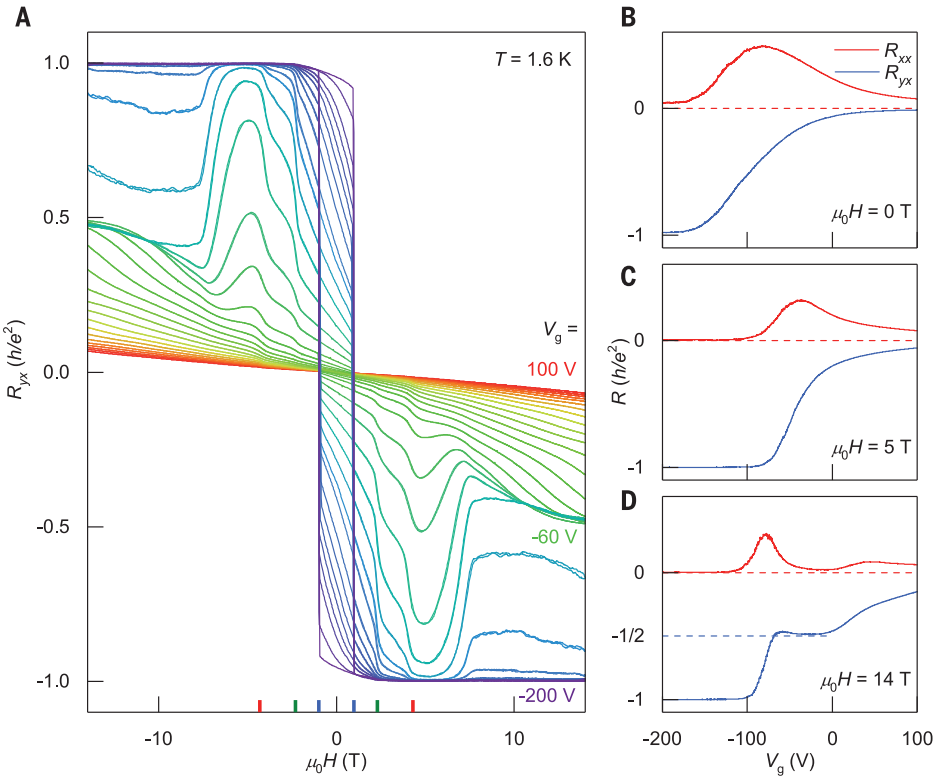

Fig. 3. Gate-tuned QAH effect in a five-layer $MnBi_2Te_4$ flake. (**A**) Magnetic-field–dependent R_{yx}, acquired in sample 5b, under varying gate biases V_g (in 10 V steps). All data were obtained at T = 1.6 K. Curves are antisymmetrized to remove the R_{xx} component. Colored ticks on the horizontal axis mark the location of magnetic transitions. (**B** to **D**) R_{xx} and R_{yx} as functions of V_g under three representative magnetic fields, $\mu_0 H$ = 0, 5, and 14 T. An additional plateau of $R_{yx} = -h/(2e^2)$ emerges at V_g ~ −25 V, accompanied by a vanishing R_{xx} (D). The same plateau is also visible in (A) at $\mu_0 H$ > 10 T during field sweeps under V_g = −60 V. This evidence points to a quantized Hall state with a filling factor ν = −2. All data were obtained in the same sample 5b, but V_g values do not exactly match those in (A) because of hysteresis during gate sweeps.

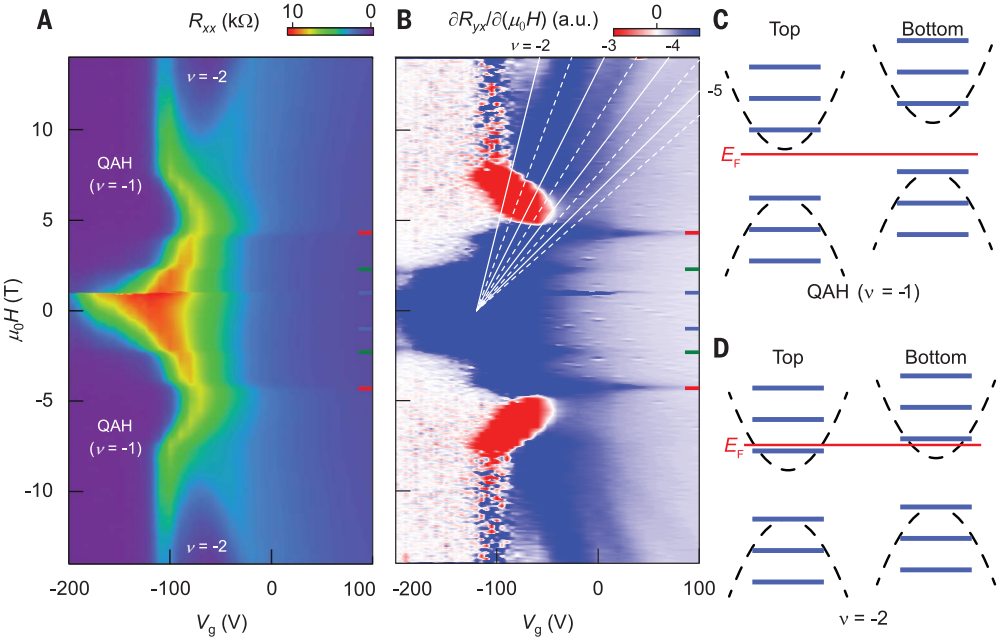

Fig. 4. LLs in a gated five-layer $MnBi_2Te_4$ flake. (**A** and **B**) R_{xx} (A) and $\partial R_{yx}/\partial \mu_0 H$ (B) plotted as functions of V_g and $\mu_0 H$. R_{xx} ($\partial R_{yx}/\partial \mu_0 H$) data taken during magnetic field upsweep have been symmetrized (antisymmetrized) with downsweep data. QAH state with ν = −1 and QH state with ν = −2 appear in regions with vanishing R_{xx} in (A). $\partial R_{yx}/\partial \mu_0 H$ maxima trace out the centers of half-filled LLs that are marked by broken lines in (B). Solid lines indicate fully filled LLs with filling factors ν = −2, −3, −4, and −5. Colored ticks on the right axes mark the magnetic transitions. All data were obtained in sample 5b at T = 1.6 K. a.u., arbitrary units. (**C** and **D**) Schematic band diagrams for the top and bottom surface states of this five-layer sample. Dashed parabolas denote surface bands under zero magnetic field. The bands collapse into LLs (blue horizontal lines) under an external magnetic field. Red horizontal lines represent Fermi level E_F that is tuned by the backgate in our experiment. (C) and (D) display the band configurations of the observed ν = −1 and ν = −2 states, respectively.

manifest as jumps in R_{yx}. Within these magnetic states, the quantized R_{yx} smoothly approaches zero as the backgate dopes electrons into the sample. R_{xx} displays a peak during the process, as is typical for QAH insulator–to–metal transition (*10*, *12*); examples of the transition are shown in Fig. 3, B and C. There is, however, an exception at high magnetic fields: R_{yx} goes through a plateau at $-h/(2e^2)$ during the transition, as shown in Fig. 3D. The same $-h/(2e^2)$ plateau in R_{yx} is also visible at $\mu_0 H > 10$ T during field sweeps under $V_g = -60$ V. The plateau is accompanied by a vanishing R_{xx} (*23*), which signifies the emergence of an additional quantized Hall state apart from the QAH state.

The origin of the additional quantized Hall state becomes clear once we plot R_{xx} and $\partial R_{yx}/\partial \mu_0 H$ as a function of both gate bias, V_g, and magnetic field, $\mu_0 H$ (Fig. 4, A and B; the R_{yx} plot is shown in fig. S8). We observe that $\partial R_{yx}/\partial \mu_0 H$ maxima trace out straight lines that disperse with both V_g and $\mu_0 H$ (Fig. 4B, broken lines), i.e., these states have degeneracies that are proportional to $\mu_0 H$. This behavior is in stark contrast to that of the nondispersive QAH state, but it is characteristic of LLs formed by 2D band electrons; the broken lines traced out by $\partial R_{yx}/\partial \mu_0 H$ maxima mark the center of the half-filled LLs. The slopes of the lines produce the half-integer ratio (1.5:2.5:3.5:4.5), as shown in Fig. 4B. Because the first fully filled LL has a filling factor $\nu = -2$ [R_{yx} quantizes at $-h/(2e^2)$ for the first fully filled LL], the ratio enables us to uniquely determine the filling factor ν of each fully filled state, $\nu = -2$, -3, -4, or -5 (Fig. 4B, indicated by solid lines between the broken lines). When extrapolated to $\mu_0 H = 0$ T, all the lines converge to $V_g = -120$ V, where the backgate starts to fill the surface band with electrons (Fig. 4A). This is unequivocal evidence that the LLs develop concomitantly with the QAH effect. Such coexistence of LLs and QAH is best exemplified by the $R_{yx} = -h/(2e^2)$ quantization at the first fully filled LL: The LL quantization is responsible for only one of the two edge channels, whereas the QAH effect contributes the other edge channel.

All states observed in this work can be understood from a unified view that separates the filling factor into its two constituents, $\nu = \nu_t + \nu_b$, where $\nu_{t(b)} = N_{t(b)} - 1/2$ is the filling factor contributed by the top (bottom) surface of the sample. Here, top and bottom are defined by reference to the substrate underneath the sample; $N_{t(b)}$ is the LL index and $-1/2$ comes from the QAH chiral edge state (*31*, *32*). $(\nu_t, \nu_b) = (-1/2, -1/2)$ describes the QAH state when E_F lies inside of the exchange gap on both surfaces (Fig. 4C). As the sample is gated, ν jumps by -1 ($+1$) each time E_F shifts through each electron (hole) level. Because sample 5b is initially electron doped at $V_g = 0$ V, the $\nu = -2$ state at $V_g = -58$ V will have a large carrier imbalance between the top and bottom surfaces. We determine that the most probable configuration for the $\nu = -2$ state is $(\nu_t, \nu_b) = (-3/2, -1/2)$ as shown in Fig. 4D. Finally, we note that the electrons that form LLs are only a small fraction of the total number of electrons induced by the backgate. Specifically, Hall measurements near zero magnetic field yield a gate efficiency of 5×10^{10} cm^{-2} V^{-1} that agrees reasonably well with the efficiency estimated from the device geometry (fig. S9). The carrier density estimated from the LL degeneracy, however, yields a gate efficiency of only ~10% of this value. The large mismatch has also been observed in gated bismuth chalcogenide TIs (*31*, *32*). Our observation that the $\nu = -2$ state is well quantized—whereas higher LLs appear only as small oscillations (Fig. 4B, marked by broken lines), possibly weakened by a large parallel conduction—points to bulk bands slightly above the surface-band edge as the probable cause of the discrepancy.

Because $MnBi_2Te_4$ is a layered material, the techniques developed for 2D materials can be readily applied to $MnBi_2Te_4$. We anticipate that van der Waals heterostructures integrating $MnBi_2Te_4$ with other magnetic or superconducting 2D materials will provide fertile ground for exploring exotic topological quantum phenomena.

REFERENCES AND NOTES

1. F. D. M. Haldane, *Phys. Rev. Lett.* **61**, 2015–2018 (1988).
2. X.-L. Qi, T. L. Hughes, S.-C. Zhang, *Phys. Rev. B* **78**, 195424 (2008).
3. M. Z. Hasan, C. L. Kane, *Rev. Mod. Phys.* **82**, 3045–3067 (2010).
4. X.-L. Qi, S.-C. Zhang, *Rev. Mod. Phys.* **83**, 1057–1110 (2011).
5. H. Zhang *et al.*, *Nat. Phys.* **5**, 438–442 (2009).
6. Y. L. Chen *et al.*, *Science* **325**, 178–181 (2009).
7. Y. L. Chen *et al.*, *Science* **329**, 659–662 (2010).
8. C.-X. Liu, X.-L. Qi, X. Dai, Z. Fang, S.-C. Zhang, *Phys. Rev. Lett.* **101**, 146802 (2008).
9. R. Yu *et al.*, *Science* **329**, 61–64 (2010).
10. C.-Z. Chang *et al.*, *Science* **340**, 167–170 (2013).
11. Y. Tokura, K. Yasuda, A. Tsukazaki, *Nat. Rev. Phys.* **1**, 126–143 (2019).
12. J. G. Checkelsky *et al.*, *Nat. Phys.* **10**, 731–736 (2014).
13. X. Kou *et al.*, *Phys. Rev. Lett.* **113**, 137201 (2014).
14. A. J. Bestwick *et al.*, *Phys. Rev. Lett.* **114**, 187201 (2015).
15. M. Mogi *et al.*, *Appl. Phys. Lett.* **107**, 182401 (2015).
16. I. Lee *et al.*, *Proc. Natl. Acad. Sci. U.S.A.* **112**, 1316–1321 (2015).
17. M. M. Otrokov *et al.*, *2D Mater.* **4**, 025082 (2017).
18. D. Zhang *et al.*, *Phys. Rev. Lett.* **122**, 206401 (2019).
19. J. Li *et al.*, *Sci. Adv.* **5**, eaaw5685 (2019).
20. M. M. Otrokov *et al.*, arXiv:1809.07389 [cond-mat.mtrl-sci] (19 September 2018).
21. Y. Gong *et al.*, *Chin. Phys. Lett.* **36**, 076801 (2019).
22. M. M. Otrokov *et al.*, *Phys. Rev. Lett.* **122**, 107202 (2019).
23. See supplementary materials.
24. Y. Deng *et al.*, *Nature* **563**, 94–99 (2018).
25. S. H. Lee *et al.*, *Phys. Rev. Research* **1**, 012011 (2019).
26. Y.-J. Hao *et al.*, *Phys. Rev. X* **9**, 041038 (2019).
27. Y. J. Chen *et al.*, *Phys. Rev. X* **9**, 041040 (2019).
28. H. Li *et al.*, *Phys. Rev. X* **9**, 041039 (2019).
29. P. Swatek *et al.*, arXiv:1907.09596 [cond-mat.mtrl-sci] (22 July 2019).
30. J. G. Checkelsky, J. Ye, Y. Onose, Y. Iwasa, Y. Tokura, *Nat. Phys.* **8**, 729–733 (2012).
31. Y. Xu *et al.*, *Nat. Phys.* **10**, 956–963 (2014).
32. R. Yoshimi *et al.*, *Nat. Commun.* **6**, 8530 (2015).
33. Y. Deng *et al.*, Harvard Dataverse (2020); https://doi.org/10.7910/DVN/ZLSDWP.

ACKNOWLEDGMENTS

We thank X. Jin, Y. Wu, C.-Z. Chang, and S. Guo for helpful discussions. Part of the sample fabrication was conducted at the Nanofabrication Laboratory at Fudan University. **Funding:** Y.D., Y.Y., Z.G., J.W., and Y.Z. acknowledge support from the National Key Research Program of China (grant nos. 2016YFA0300703 and 2018YFA0305600), the NSF of China (grant nos. U1732274, 11527805, 11425415, and 11421404), Shanghai Municipal Science and Technology Commission (grant no. 18JC1410300), and the Strategic Priority Research Program of the Chinese Academy of Sciences (grant no. XDB30000000). Y.Y. also acknowledges support from the China Postdoctoral Science Foundation (grant nos. BX20180076 and 2018M641907). J.W. acknowledges additional support from the NSF of China (grant no. 11774065) and the NSF of Shanghai (grant no. 17ZR1442500). M.Z.S. and X.H.C. acknowledge support from the National Natural Science Foundation of China (grant nos. 11888101 and 11534010), the National Key R&D Program of China (grant nos. 2017YFA0303001 and 2016YFA0300201), the Strategic Priority Research Program of the Chinese Academy of Sciences (grant no. XDB25000000), and the Key Research Program of Frontier Sciences of the Chinese Academy of Sciences (grant no. QYZDY-SSW-SLH021). **Author contributions:** Y.Z., X.H.C., J.W., and Z.X. supervised the project. M.Z.S., Z.X., and X.H.C. grew $MnBi_2Te_4$ bulk crystals. M.Z.S., Z.G., Y.Y., and Y.D. characterized bulk crystals. Y.D. and Y.Y. fabricated few-layer devices and performed transport measurements. Y.D., Y.Y., Y.Z., J.W., and X.H.C. analyzed the data. J.W. carried out theoretical calculations. Y.D., Y.Y., J.W., and Y.Z. wrote the manuscript with input from all authors. **Competing interests:** None declared. **Data and materials availability:** The data shown in the paper are available at Harvard Dataverse (*33*).

SUPPLEMENTARY MATERIALS

science.sciencemag.org/content/367/6480/895/suppl/DC1
Materials and Methods
Supplementary Text
Figs. S1 to S12
Table S1
References (*34*–*43*)

27 April 2019; accepted 9 January 2020
Published online 23 January 2020
10.1126/science.aax8156

TOPOLOGICAL MATTER

Intrinsic quantized anomalous Hall effect in a moiré heterostructure

M. Serlin[1]*, C. L. Tschirhart[1]*, H. Polshyn[1]*, Y. Zhang[1], J. Zhu[1], K. Watanabe[2], T. Taniguchi[2], L. Balents[3], A. F. Young[1]†

The quantum anomalous Hall (QAH) effect combines topology and magnetism to produce precisely quantized Hall resistance at zero magnetic field. We report the observation of a QAH effect in twisted bilayer graphene aligned to hexagonal boron nitride. The effect is driven by intrinsic strong interactions, which polarize the electrons into a single spin- and valley-resolved moiré miniband with Chern number $C = 1$. In contrast to magnetically doped systems, the measured transport energy gap is larger than the Curie temperature for magnetic ordering, and quantization to within 0.1% of the von Klitzing constant persists to temperatures of several kelvin at zero magnetic field. Electrical currents as small as 1 nanoampere controllably switch the magnetic order between states of opposite polarization, forming an electrically rewritable magnetic memory.

Two-dimensional insulators can be classified by the topology of their filled energy bands. In the absence of time-reversal symmetry, nontrivial band topology manifests experimentally as a quantized Hall conductivity $\sigma_{xy} = C\frac{e^2}{h}$, where $C \neq 0$ is the total Chern number of the filled bands, e is the electron charge, and h is Plank's constant. Fundamental questions about the nature of topological phase transitions (*1*), as well as possible applications in resistance metrology (*2*) and topological quantum computing (*3*), have motivated considerable efforts to engineer quantum anomalous Hall (QAH) effects showing topologically protected quantized resistance in the absence of an applied magnetic field. To date, QAH effects have been observed only in a narrow class of materials consisting of transition metal–doped $(Bi,Sb)_2Te_3$ (*4*–*10*). In these materials, ordering of the dopant magnetic moments breaks time-reversal symmetry, combining with the strongly spin-orbit coupled electronic structure to produce topologically nontrivial Chern bands (*11*). However, the performance of these materials is limited by the inhomogeneous distribution of the magnetic dopants, which leads to microscopic structural, charge, and magnetic disorder (*12*–*15*). As a result, quantization occurs at temperatures that are approximately one order of magnitude smaller than the magnetic ordering temperature (*4*–*6*).

Moiré graphene heterostructures provide the two essential ingredients needed for engineering intrinsic quantum anomalous Hall effects: topological bands and strong correlations. For both graphene on hexagonal boron nitride (hBN) and twisted multilayer graphene, moiré patterns generically produce bands with a finite Chern number (*16*–*19*), with time-reversal symmetry of the single-particle band structure enforced by the cancellation of Chern numbers in opposite graphene valleys. In certain heterostructures, particularly in twisted bilayer graphene (tBLG) with interlayer twist angle $\theta \approx 1.1°$ and rhombohedral graphene aligned to hBN, the bandwidth of these Chern bands can be made exceptionally small (*17*, *20*–*22*), favoring correlation-driven states that break one or more spin, valley, or lattice symmetries. Experiments have found correlation-driven low temperature phases at integer band fillings when these bands are sufficiently flat (*22*–*26*). Notably, states showing magnetic hysteresis indicative of time-reversal symmetry breaking have recently been reported in both tBLG (*27*) and rhombohedral graphene heterostructures (*28*) at commensurate filling. These systems show large anomalous Hall effects highly suggestive of an incipient Chern insulator at zero magnetic field.

Here, we report the observation of a QAH effect showing robust zero magnetic field quantization in a flat-band ($\theta \approx 1.15 \pm 0.01°$) tBLG sample aligned to hBN. The electronic structure of flat-band tBLG is described by two distinct bands per spin and valley projection isolated from higher-energy dispersive bands by an energy gap. The total capacity of the flat bands is eight electrons per unit cell, spanning $-4 < \nu < 4$, where the band filling factor $\nu = nA_m$, with electron density n and moiré unit cell area $A_m \approx 130\ nm^2$. Figure 1A shows the longitudinal and Hall resistances (R_{xx} and R_{xy}) measured at a magnetic field $B = 150$ mT (*29*) and temperature $T = 1.6$ K as a function of charge density over the entire flat band. The sample is insulating at the overall charge neutral point and shows a weak resistance peak at $\nu = 2$. Additionally, we observe R_{xy} approaching h/e^2 in a narrow range of density near $\nu = 3$, concomitant with a deep minimum in R_{xx} reminiscent of an integer quantum Hall state.

Figure 1B shows the magnetic field dependence of both R_{xx} and R_{xy} at a density of $n = 2.37 \times 10^{12}\ cm^{-2}$ measured at $T = 1.6$ K. The Hall resistivity is hysteretic, with a coercive field of several tens of millitesla, and we observe a well-quantized $R_{xy} = h/e^2$ along with $R_{xx} < 1$ kilohm persisting through $B = 0$, indicative of a QAH state stabilized by spontaneously broken time-reversal symmetry. The switching transitions are marked by discrete Barkhausen jumps in the resistance on the order of h/e^2 in both R_{xx} and R_{xy}, which is typical of magnetic systems consisting of a small number of domains (*15*, *30*). Figure 1C shows the detailed density evolution of the R_{xy} hysteresis near $\nu = 3$. Both the coercive field and zero-field Hall resistance are maximal near $\nu = 3$, although hysteresis can be observed over a much broader range of ν, between 2.84 and 3.68 (fig. S13). Quantized response is only observed for a particular choice of contacts at one end of the device (*29*).

Figure 1D shows a schematic representation of the band structure at full filling ($\nu = 4$) and at $\nu = 3$. In the absence of interaction-driven order, the spin-degenerate bands in each valley have a total Chern number of ±2. The observed QAH state occurs because the exchange energy is minimized when an excess valley- and spin-polarized Chern band (*18*, *19*) is occupied, spontaneously breaking time-reversal symmetry. Magnetic order in two dimensions requires anisotropy. In graphene, the vanishingly small spin-orbit coupling provides negligible anisotropy for the spin system. It is thus likely that the observed magnetism is orbital, with strong, easy-axis anisotropy arising from the two-dimensional nature of the graphene bands (*18*, *19*, *26*, *27*, *31*).

The phenomenology of $\nu = 3$ filling is nonuniversal across tBLG devices: some samples are metallic (*23*, *24*); some show a robust, thermally activated, trivial insulator (*25*, *26*); whereas others show an anomalous Hall effect (*27*). This is consistent with theoretical expectations (*31*) that the phase diagram at integer ν is highly sensitive to details including the interlayer twist angle, both uniform and inhomogeneous strains (*32*), as well as alignment to an hBN encapsulant layer. The prior report of magnetic hysteresis at $\nu = 3$ was indeed associated with close alignment of one of the two hBN layers (*27*). Theoretical analysis has shown (*18*, *19*) that the resultant breaking of the C_2 rotation symmetry of tBLG strongly favors a QAH state at $\nu = 3$.

The device presented here is nominally aligned to one of the hBN layers (fig. S1), and it shows a number of signatures that suggest strong modifications of the band structure relative to unaligned devices. First, our device shows only a weakly resistive feature at $\nu = 2$ but a robust thermally activated insulator at charge neutrality. The activation gap for this

[1]Department of Physics, University of California, Santa Barbara, Santa Barbara, CA 93106, USA. [2]National Institute for Materials Science, 1-1 Namiki, Tsukuba 305-0044, Japan. [3]Kavli Institute for Theoretical Physics, University of California, Santa Barbara, Santa Barbara, CA 93106, USA.
*These authors contributed equally to this work.
†Corresponding author. Email: andrea@physics.ucsb.edu

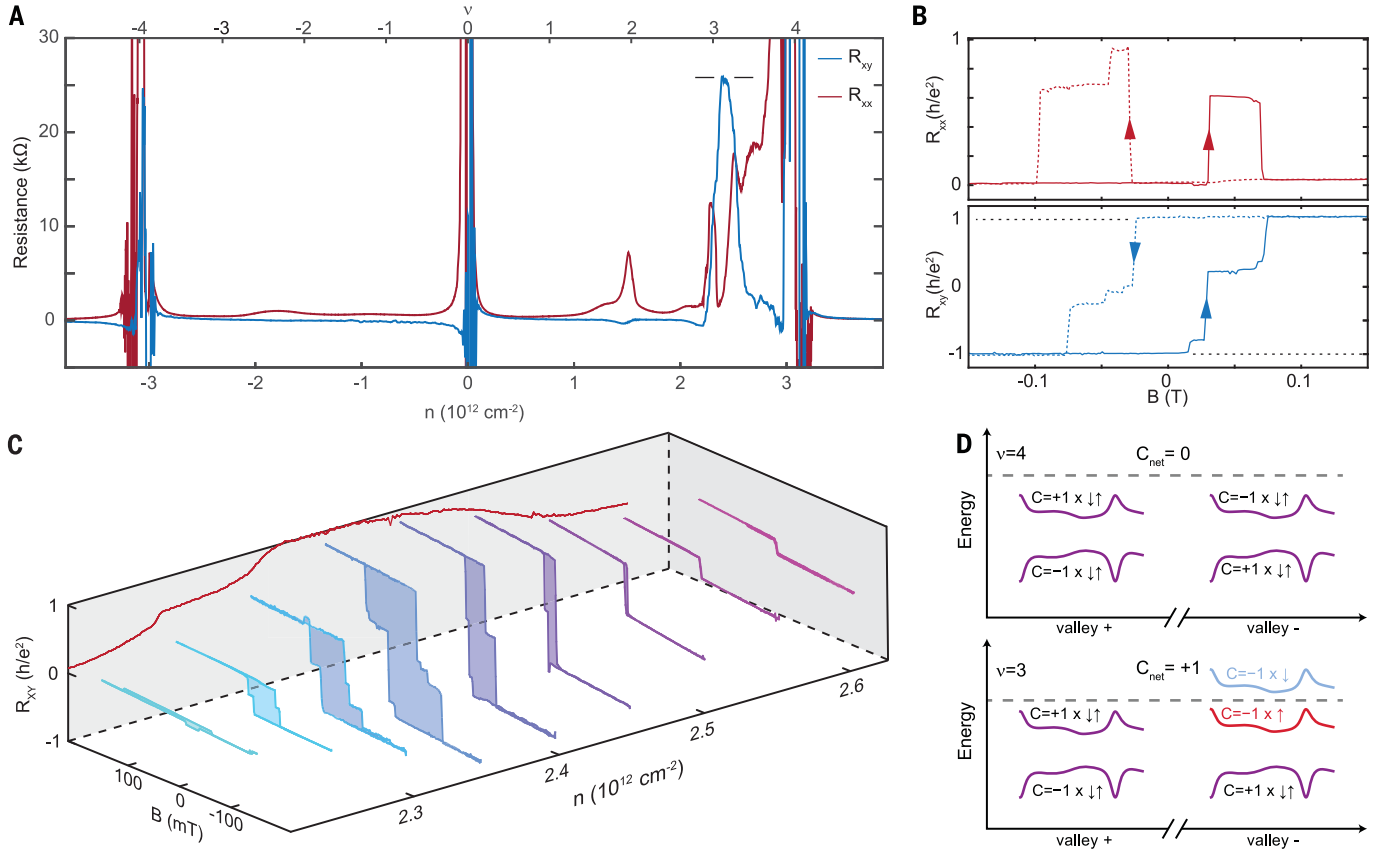

Fig. 1. Quantized anomalous Hall effect in twisted bilayer graphene at 1.6 K. (**A**) Longitudinal resistance R_{xx} and Hall resistance R_{xy} as a function of carrier density n at 150 mT. R_{xy} reaches h/e^2 and R_{xx} approaches zero near $\nu = 3$. Data are corrected for mixing of R_{xx} and R_{xy} components by symmetrizing with respect to magnetic field at $B = \pm 150$ mT (*29*). (**B**) R_{xx} and R_{xy} measured at $n = 2.37 \times 10^{12}$ cm^{-2} as a function of magnetic field B. Data are corrected for mixing using contact symmetrization (*29*). Sweep directions are indicated by arrows. (**C**) R_{xy} as a function of B and n. Hysteresis loop areas are shaded for clarity. The rear wall shows field-training symmetrized values of R_{xy} at $B = 0$. $R_{xy}(0)$ becomes nonzero when ferromagnetism appears, and it reaches a plateau of h/e^2 near a density of $n = 2.37 \times 10^{12}$ cm^{-2}. (**D**) Schematic band structure at full filling of a moiré unit cell ($\nu = 4$) and $\nu = 3$. The net Chern number $C_{net} \neq 0$ at $\nu = 3$.

$\nu = 0$ insulator is larger than even the gaps for the states at $\nu = \pm 4$, which are much smaller than typical (fig. S10) (*29*). Second, the quantum oscillations are highly anomalous, with hole-like quantum oscillations originating at $\nu = 2$, again in contrast to all prior reports (fig. S11) (*23*–*26*). Additional Landau fan features also appear consistent with an hBN alignment of 0.6° (fig. S6); however, twist angle variations within the tBLG preclude unambiguous determination of the hBN-tBLG twist angle. Although no detailed theory for these observations is available, the extreme sensitivity of the detailed structure of the flat bands to model parameters, combined with observations that hBN substrates can produce energy gaps as large as 30 meV in monolayer graphene (*33*), point to the role of the substrate in tipping the balance between competing many-body ground states at $\nu = 3$ in favor of the QAH state. These observations together suggest that hBN-aligned samples constitute a different class of tBLG device with distinct phenomenology.

Figure 2, A and B, shows the temperature dependence of major hysteresis loops in R_{xx} and R_{xy}, respectively. As T increases, we observe both a departure from resistance quantization and a suppression of hysteresis, with the Hall effect showing linear behavior in field by T =12 K. In our measurements, we observe resistance offsets of ~1 kilohm from the ideal quantized value, which vanish when resistance is symmetrized or antisymmetrized with respect to magnetic field (or, for $B \approx 0$, with respect to field training). For quantitative analysis of the T-dependent data, we thus study field-training symmetrized resistances, denoted $\bar{R}_{xy}$ and $\bar{R}_{xx}$. Figure 2C shows $\bar{R}_{xy}(0)$. Finite hysteresis is observed up to temperatures of 8 K (Fig. 2C), which is consistent with the Curie temperature $T_C \approx 7.5$ K determined from an Arrott plot (fig. S12). $\bar{R}_{xy}$ remains quantized up to $T \approx 3$ K, with the average value of $(1.0010 \pm 0.0002) \times \frac{h}{e^2}$ between 2 and 2.7 K.

To quantitatively assess the energy scales associated with the QAH state, we measure the activation energy at low temperature. Figure 2D shows both the measured $\bar{R}_{xx}$ and the deviation from quantization of the Hall resistance, $\delta\bar{R}_{xy} = h/e^2 - \bar{R}_{xy}$, on an Arrhenius plot. We assume that the Hall conductivity σ_{xy} is approximately T-independent and the longitudinal conductivity $\sigma_{xx} \sim e^{-\Delta/(2T)}$, where Δ is the energy cost of creating and separating a particle-antiparticle excitation of the QAH state. Under this assumption, inverting the conductivity tensor gives $\delta R_{xy} \sim e^{-\Delta/(T)}$ and $R_{xx} \sim e^{-\Delta/(2T)}$ (*29*). We find the activation gaps extracted from fitting $\delta\bar{R}_{xy}$ and $\bar{R}_{xx}$ to be $\Delta = 26 \pm 4$ K and $\Delta = 31 \pm 12$ K, respectively, with the large uncertainty in the latter arising from the absence of a single simply activated regime (*29*). The activation energy is thus several times larger than T_C, in contrast to magnetically doped topological insulator films, for which activation gaps are typically between 2% and 10% of T_C (*5*, *6*, *29*).

Ferromagnetic domains in tBLG interact strongly with applied current (*27*). In our device, this allows deterministic electrical control over domain polarization using exceptionally small direct currents. Figure 3A shows R_{xy} at 6.5 K and $B = 0$, measured using a small alternating current excitation of ~100 pA, to which we add a variable direct current bias.

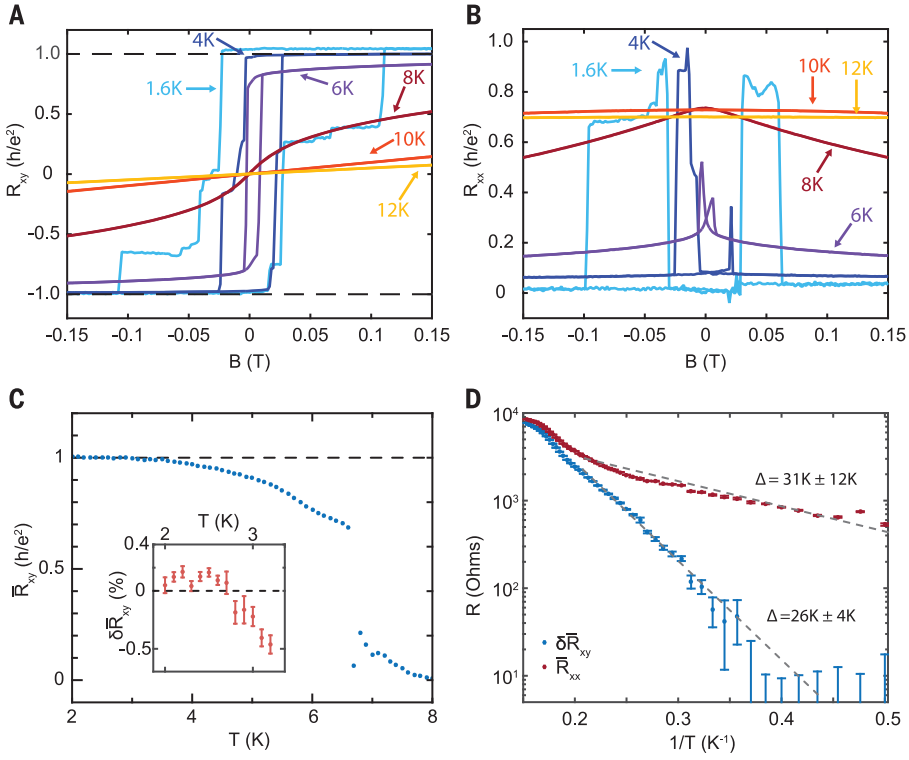

Fig. 2. Temperature dependence of the quantum anomalous Hall effect. (**A**) R_{xy} and (**B**) R_{xx} as a function of B measured at various temperatures for $n = 2.37 \times 10^{12}$ cm^{-2}. R_{xx} and R_{xy} mixing was corrected using contact symmetrization (*29*). (**C**) Temperature dependence of the field-training symmetrized resistance $\bar{R}_{xy}$ at $B = 0$, as described in the main text. The Curie temperature was determined to be $T_C \approx 7.5 \pm 0.5$ K using an Arrott plot analysis (fig. S12). Inset shows detailed low-temperature dependence of the deviation of $\bar{R}_{xy}$ from the quantized value at $B = 0$. Error bars are the standard error derived from 11 consecutive measurements. $\bar{R}_{xy}$ saturates below ≈3 K to a value of $(1.0010 \pm 0.0002) \times \frac{h}{e^2}$, determined by averaging the points between 2 and 2.7 K. (**D**) Arrhenius plots of field-training symmetrized resistances $\bar{R}_{xx}$ and $\delta\bar{R}_{xy} = h/e^2 - \bar{R}_{xy}$ at $B = 0$. Dotted lines denote representative activation fits. Systematic treatment of uncertainty arising from the absence of a single activated regime gives $\Delta = 31 \pm 12$ K and 26 ± 4 K for $\bar{R}_{xx}$ and $\delta\bar{R}_{xy}$, respectively (*29*).

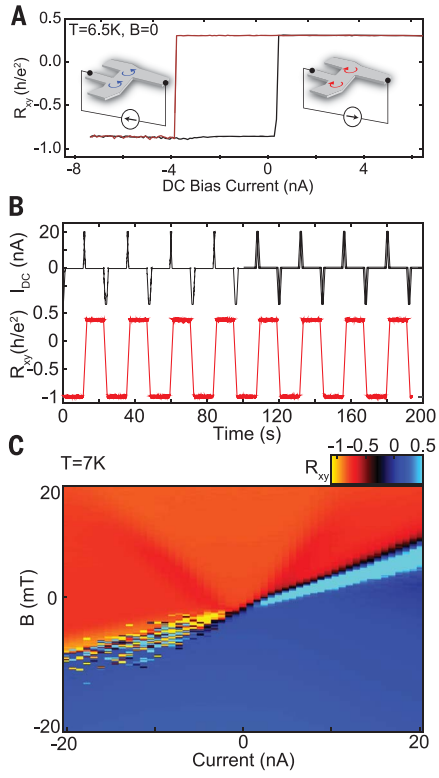

Fig. 3. Current-controlled magnetic switching. (**A**) R_{xy} as a function of applied direct current, showing hysteresis as a function of direct current analogous to response to an applied magnetic field at 6.5 K. Insets show schematic illustrations of current-controlled orbital magnetism. (**B**) Nonvolatile electrical writing and reading of a magnetic bit at $T = 6.5$ K and $B = 0$. A succession of 20-nA current pulses of alternating signs controllably reverses the magnetization, which is read out using the Hall resistance. The magnetization state of the bit is stable for at least 10^3 s (*29*). (**C**) R_{xy} as a function of both direct current bias and magnetic field at 7 K. Opposite directions of direct current preferentially stabilize opposite magnetization states of the bit. Measurements presented in Fig. 3 are neither field nor Onsager symmetrized, which is why there is an offset in R_{xy}.

We find that the applied direct currents drive switching in a manner analogous to that observed in an applied magnetic field, producing hysteretic switching between magnetization states. Direct currents of a few nanoamperes are sufficient to completely reverse the magnetization, which is then indefinitely stable (*29*). Figure 3B shows deterministic writing of a magnetic bit using current pulses, and its nonvolatile readout using the large resulting change in the anomalous Hall resistance. High-fidelity writing is accomplished with 20-nA current pulses, whereas readout requires <100 pA of applied alternating current.

Assuming a uniform current density in our micrometer-sized, two-atom-thick tBLG device results in an estimated current density $J < 10^3$ A·cm^{-2}. Although current-induced switching at smaller direct current densities of $J \approx 10^2$ A·cm^{-2} has been realized in MnSi, readout of the magnetization state in this material has so far only been demonstrated using neutron scattering (*34*). Compared with other systems that allow in situ electrical readout, such as GaMnAs ($J = 3.4 \times 10^5$ A·cm^{-2}) (*35*) and Cr-$(BiSb)_2Te_3$ heterostructures ($J = 8.9 \times 10^4$ A·cm^{-2}) (*36*), the applied current densities are at least one order of magnitude smaller. What is more relevant to device applications is that the absolute magnitude of the current required to switch the magnetization state of the system (~10^{-9} A) in our device is, to our knowledge, considerably smaller than that reported in any other system.

Figure 3C shows the Hall resistance at $T = 7$ K, just below the onset of hysteresis, measured as a function of magnetic field and current. At zero magnetic field, opposite signs of direct current stabilize opposite magnetic polarizations. Furthermore, when a static field is present, direct currents can stabilize configurations disfavored by the applied field. Current breaks time-reversal symmetry, but mirror symmetry across the plane perpendicular to the sample and parallel to the net current flow precludes an injected charge from favoring a particular out-of-plane polarization. We propose (*29*) a simple mechanism for the low-current switching that arises from the interplay of edge-state physics and device asymmetry. In a QAH state, an applied current generates a chemical potential difference between the chiral one-dimensional modes located on opposite sample edges. Owing to the opposite dispersion of a given edge state in opposite magnetic states (which have opposite C), the DC current I changes the energy of the system by $\delta E \sim \pm \frac{8\pi^2}{3} \frac{\hbar^2}{me^3v^3} LI^3$ for a $C = \pm 1$ state, where $\hbar$ is the reduced Planck's constant, m and v are the edge-state effective mass and velocity, e is the elementary charge, and L is the length of the edge state. When the edges have different lengths or velocities, the current favors one of the two domains, with the sign and magnitude of the effect dictated by the

device asymmetry. For a current in the range of 10 to 100 nA, comparable to the switching currents observed at low temperatures, using estimates of m and v based on bulk measurements (*29*) and assuming an edge length difference of ≈1 μm gives δE comparable to the magnetic dipole energy caused by a 1-mT field.

Although this effect should be generic to all QAH systems, it is likely to be dominant at low currents in tBLG because of the weak pinning of magnetic domains and small device dimensions. Crucially, it provides an engineering parameter for electrical control of domain structure that can be deterministically encoded in the device geometry.

REFERENCES AND NOTES

1. F. D. M. Haldane, *Phys. Rev. Lett.* **61**, 2015–2018 (1988).
2. M. Götz *et al.*, *Appl. Phys. Lett.* **112**, 072102 (2018).
3. B. Lian, X.-Q. Sun, A. Vaezi, X.-L. Qi, S.-C. Zhang, *Proc. Natl. Acad. Sci. U.S.A.* **115**, 10938–10942 (2018).
4. C.-Z. Chang *et al.*, *Science* **340**, 167–170 (2013).
5. C.-Z. Chang *et al.*, *Nat. Mater.* **14**, 473–477 (2015).
6. M. Mogi *et al.*, *Appl. Phys. Lett.* **107**, 182401 (2015).
7. X. Kou *et al.*, *Nat. Commun.* **6**, 8474 (2015).
8. X. Kou *et al.*, *Phys. Rev. Lett.* **113**, 137201 (2014).
9. J. Wang, B. Lian, H. Zhang, Y. Xu, S.-C. Zhang, *Phys. Rev. Lett.* **111**, 136801 (2013).
10. J. G. Checkelsky *et al.*, *Nat. Phys.* **10**, 731–736 (2014).
11. R. Yu *et al.*, *Science* **329**, 61–64 (2010).
12. E. O. Lachman *et al.*, *Sci. Adv.* **1**, e1500740 (2015).
13. I. Lee *et al.*, *Proc. Natl. Acad. Sci. U.S.A.* **112**, 1316–1321 (2015).
14. W. Wang *et al.*, *APL Mater.* **3**, 083301 (2015).
15. K. Yasuda *et al.*, *Science* **358**, 1311–1314 (2017).
16. J. C. W. Song, P. Samutpraphoot, L. S. Levitov, *Proc. Natl. Acad. Sci. U.S.A.* **112**, 10879–10883 (2015).
17. Y.-H. Zhang, D. Mao, Y. Cao, P. Jarillo-Herrero, T. Senthil, *Phys. Rev. B* **99**, 075127 (2019).
18. N. Bultinck, S. Chatterjee, M. P. Zaletel, Anomalous Hall ferromagnetism in twisted bilayer graphene. arXiv:1901.08110 [cond-mat.str-el] (23 January 2019).
19. Y.-H. Zhang, D. Mao, T. Senthil, *Phys. Rev. Research* **1**, 033126 (2019).
20. R. Bistritzer, A. H. MacDonald, *Proc. Natl. Acad. Sci. U.S.A.* **108**, 12233–12237 (2011).
21. E. Suárez Morell, J. D. Correa, P. Vargas, M. Pacheco, Z. Barticevic, *Phys. Rev. B* **82**, 121407 (2010).
22. G. Chen *et al.*, *Nat. Phys.* **15**, 237–241 (2019).
23. Y. Cao *et al.*, *Nature* **556**, 80–84 (2018).
24. Y. Cao *et al.*, *Nature* **556**, 43–50 (2018).
25. M. Yankowitz *et al.*, *Science* **363**, 1059–1064 (2019).
26. X. Lu *et al.*, *Nature* **574**, 653–657 (2019).
27. A. L. Sharpe *et al.*, *Science* **365**, 605–608 (2019).
28. G. Chen *et al.*, arXiv:1905.06535 [cond-mat.mes-hall] (16 May 2019).
29. See supplementary materials.
30. M. Liu *et al.*, *Sci. Adv.* **2**, e1600167 (2016).
31. M. Xie, A. H. MacDonald arXiv:1812.04213 [cond-mat.str-el] (11 December 2018).
32. S. Liu, E. Khalaf, J. Y. Lee, A. Vishwanath, arXiv:1905.07409 [cond-mat.str-el] (17 May 2019).
33. B. Hunt *et al.*, *Science* **340**, 1427–1430 (2013).
34. F. Jonietz *et al.*, *Science* **330**, 1648–1651 (2010).
35. M. Jiang *et al.*, *Nat. Commun.* **10**, 2590 (2019).
36. Y. Fan *et al.*, *Nat. Mater.* **13**, 699–704 (2014).
37. M. Serlin *et al.*, Dryad (2019); https://doi.org/10.5061/dryad.ffbg79cqk.

ACKNOWLEDGMENTS

The authors acknowledge discussions with A. Macdonald, Y. Saito, and M. Zaletel. **Funding:** Device fabrication was supported by the Army Research Office under W911NF-17-1-0323. Measurements were supported by the Air Force Office of Scientific Research under FA9550-16-1-0252. C.L.T. acknowledges support from the Hertz Foundation and from the National Science Foundation Graduate Research Fellowship Program under grant 1650114. L.B. was supported by the Department of Energy Office of Sciences Basic Energy Sciences program under award DE-FG02-08ER46524. A.F.Y. acknowledges the support of the David and Lucille Packard Foundation and the Alfred P. Sloan foundation. **Author contributions:** Y.Z. and H.P. fabricated the device. M.S., C.L.T., H.P., J.Z., and A.F.Y. performed the measurements and analyzed the data. T.T. and K.W. provided the hBN crystals. L.B. formulated the theoretical model for the current-induced switching. M.S., C.L.T., H.P., L.B., and A.F.Y. wrote the manuscript. **Competing interests:** The authors declare that they have no competing interests. **Data and materials availability:** All data shown in the main text and supplementary materials are available in the Dryad data repository (*37*).

SUPPLEMENTARY MATERIALS

science.sciencemag.org/content/367/6480/900/suppl/DC1
Materials and Methods
Supplementary Text
Figs. S1 to S17
References (*38*–*47*)

29 June 2019; accepted 6 December 2019
Published online 19 December 2019
10.1126/science.aay5533

NANOMATERIALS

Disassembling 2D van der Waals crystals into macroscopic monolayers and reassembling into artificial lattices

Fang Liu[1], Wenjing Wu[1], Yusong Bai[1], Sang Hoon Chae[2], Qiuyang Li[1], Jue Wang[1], James Hone[2], X.-Y. Zhu[1]*

Two-dimensional materials from layered van der Waals (vdW) crystals hold great promise for electronic, optoelectronic, and quantum devices, but technological implementation will be hampered by the lack of high-throughput techniques for exfoliating single-crystal monolayers with sufficient size and high quality. Here, we report a facile method to disassemble vdW single crystals layer by layer into monolayers with near-unity yield and with dimensions limited only by bulk crystal sizes. The macroscopic monolayers are comparable in quality to microscopic monolayers from conventional Scotch tape exfoliation. The monolayers can be assembled into macroscopic artificial structures, including transition metal dichalcogenide multilayers with broken inversion symmetry and substantially enhanced nonlinear optical response. This approach takes us one step closer to mass production of macroscopic monolayers and bulk-like artificial materials with controllable properties.

Since the first report of monolayer graphene in 2004 (*1*), studies of 2D materials have grown into one of the most active research fields (*2*). Monolayers, and especially their homo- or heterostructures have been excellent subjects for the exploration of new physical phenomena and hold great promise for next-generation devices, particularly quantum devices (*3*–*5*). Many of these new quantum phenomena, such as Moiré excitons in transition metal dichalcogenide (TMDC) heterobilayers and superconductivity in twisted bilayer graphene, rely on monolayers with single-crystal lattices (*3*–*12*). However, despite extensive advances in research, the absence of high-throughput methods to produce high-quality 2D single crystals with macroscopic sizes remains a major challenge for their mass production and potential commercialization. Past attempts at producing 2D monolayers were often limited by problems such as material quality, scalability, and size. Liquid phase exfoliation is scalable but generates small sizes (only a few micrometers) and poor quality (*13*). Chemical vapor deposition (CVD) can grow continuous monolayers on wafer scales, albeit in the polycrystalline form with high defect density, thereby limiting their performance in electronic devices (*14*). Mechanical exfoliation using the famous Scotch tape method (*1*) has produced the highest-quality monolayers thus far; however, the typical lateral dimensions are <100 μm, with very low yield. Larger flakes can be obtained using metals with stronger van der Waals (vdW) adhesion to 2D materials than interlayer vdW force, as demonstrated for TMDCs. Exfoliation of bulk TMDC crystals on gold substrates has been reported to yield monolayers up to the centimeter scale (*15*, *16*), but it is difficult to remove the TMDC monolayers from the gold substrate. Another strategy involves evaporation of metal onto the surface of a bulk TMDC crystal, followed by exfoliation, transferring onto a desired substrate, and chemical etching (*17*, *18*). This method has been demonstrated to yield single-crystal TMDC monolayers up to 500 μm in lateral dimensions (*17*) and transfer CVD films up to wafer scale (*18*). However, direct deposition of metal onto TMDC bulk crystal introduces considerable defects in the TMDC monolayer (*19*).

Here, we demonstrate a nondestructive, high-throughput, and widely applicable technique to disassemble 2D vdW crystals layer by layer into single-crystal monolayers, with near-unity yield. This method works for a range of vdW materials and generates monolayers with macroscopic dimensions limited only by the sizes of the bulk crystals. As schematically shown in Fig. 1A, a critical step is obtaining an atomically flat gold tape, i.e., an ultraflat gold film on a polymer substrate, which is achieved using a template-stripping technique (*20*, *21*). After evaporation of a thin gold film on an ultraflat surface of highly polished silicon wafer, the gold film is stripped off the substrate with thermal release tape and a polyvinylpyrrolidone (PVP) interfacial layer. The exposed gold surface is templated by the flat substrate with roughness on the Å scale (*20*, *21*). The ultraflat gold tape allows intimate and uniform vdW contact between the gold and the 2D vdW crystal surface, exfoliating a complete monolayer that can be transferred onto the desired substrate. After removing the thermal release tape, washing off the PVP layer, and etching the gold with a mild etchant solution (I_2/I^-), a monolayer with macroscopic dimension (typically millimeters to centimeters) is obtained. In addition to increasing the lateral sizes and monolayer yields by two to three orders of magnitude, our gold tape exfoliation turns the stochastic Scotch tape method into a deterministic and quantitative process. Although gold is used in the present study, one can extend the method to other metals provided the etching chemistry does not damage the 2D monolayer of interest.

The strong adhesion of gold to TMDCs can repeatedly generate complete single-crystal monolayers, each adopting the shape of the entire surface of a bulk crystal (Fig. 1B), as illustrated for six WSe_2 monolayers in Fig. 1C. The yield of exfoliation, expressed as the percentage of monolayer area picked up from the contacted bulk crystal surface, is close to unity. This technique can be applied to a broad range of vdW crystals, as we demonstrate here for single-crystal TMDC monolayers (WS_2, MoS_2, WSe_2, $MoSe_2$, and ReS_2) on various substrates such as SiO_2/Si, fused silica, and sapphire. Adhesion of the ultraflat gold to graphene and hexagonal boron nitride (h-BN) is weaker and the monolayers are smaller than those for TMDCs, but still much larger than those obtained by conventional Scotch tape exfoliation. Optical images of the macroscopic TMDC monolayers are shown in fig. S1. Each TMDC sample is dominated by the single-crystal monolayer, sometimes with small regions of multilayers near the edges resulting from the contact of the gold tape with imperfect or nonflat regions on the edges of TMDC bulk crystal.

The quality of the large single-crystal monolayer is comparable to, or slightly better than, that of microscopic single-crystal monolayers produced using the traditional Scotch tape method, as evidenced in the clean surface characterized by atomic force microscopy (AFM) and the crystal quality characterized by photoluminescence (PL) spectroscopy. An AFM image of the TMD monolayer flakes reveals atomic scale flatness, as shown in fig. S2 for an MoS_2 monolayer. PL spectroscopy is particularly sensitive to defects and disorder because increased peak width is evidence of inhomogeneous broadening (disorder) and reduced intensity is indicative of defect-mediated nonradiative recombination. We compare in Fig. 2 the low-temperature PL spectra of the macroscopic TMDC monolayers from our gold tape method and microscopic monolayers from the commonly used Scotch tape method, with all monolayers encapsulated in h-BN to eliminate the effect from substrate defects and inhomogeneity. The $MoSe_2$ and WSe_2 crystals are from flux growth (*22*), MoS_2 from natural crystals (SPI Supplies), and WS_2 from chemical vapor transport growth (HQ Graphene).

[1]Department of Chemistry, Columbia University, New York, NY 10027, USA. [2]Department of Mechanical Engineering, Columbia University, New York, NY 10027, USA.
*Corresponding author. Email: xyzhu@columbia.edu

Note that the highest-quality $MoSe_2$ and WSe_2 crystals from flux growth (*22*) are all of small sizes (~100 μm), and we found that defect density in macroscopic-sized crystals (≥ 1 mm) from flux growth typically is higher than those in the smaller sizes. The PL spectra of MoS_2 and $MoSe_2$ from the two methods are nearly identical. The former is characterized by the dominant A exciton and the latter shows the A exciton and the trion peaks, both nearly independent of the two exfoliation methods. PL image histogram analysis (Fig. 2) shows that the PL intensities from our macroscopic monolayers are consistent with or slightly higher than those from the Scotch tape method. For WS_2 and WSe_2 monolayers, the PL spectra from the two methods are similarly complex because of the presence of dark excitons and many-body states (*23*, *24*); however, the overall PL intensity in our macroscopic monolayers is still comparable to or slightly higher than those from the Scotch tape method. These results confirm the high quality of the macroscopic TMDC monolayers.

Obtaining macroscopic single-crystal monolayers of 2D vdW crystals with high throughput opens the door to a broad range of applications spanning from spectroscopy to scalable devices and to the easy assembly of artificial lattices. For example, the macroscopic size of the TMDC monolayers prepared on transparent substrates allows us to use a conventional ultraviolet-visible spectrometer to easily obtain optical absorption spectra of TMDC monolayers (fig. S3), each featuring the well-known A and B excitons (*25*). Furthermore, the effective disassembly of the bulk crystal into individual single-crystal monolayers with defined crystal orientation allows us to reassemble them into artificial vdW crystals with desired properties. Specifically, we show that the ultraflat gold tape can be used as an effective pickup tool to reassemble higher-order vdW lattices from the macroscopic single crystals. We demonstrate two examples: (i) the reassembly of macroscopic TMDC monolayers into an artificial crystal lattice with AA stacking for greatly enhanced nonlinear optical response and (ii) the formation of a macroscopic heterobilayer from two distinct TMDC monolayers.

The first example targets effective engineering of nonlinear optical properties in an ultrathin material. TMDC monolayers, with intrinsically broken inversion symmetry, are known to have ultrastrong, nonlinear susceptibilities, as reflected in their intense second harmonic generation (SHG) (*26*–*28*). However, TMDC bulk crystals exhibit 2H centrosymmetry; the crystal orientations of neighboring layers are 180° counteraligned with each other in the so-called AB stacking. Because of cancellation between counteraligned layers, the SHG response is smaller in few-layer samples, becoming asymptotically negligible for the bulk crystal (*26*–*28*). Indeed, interference in SHG from individual monolayers in stacked homo- or heterobilayers is very sensitive to the alignment angle between the two layers (*29*). We disassembled the TMDC bulk crystal into individual monolayers and reassembled the even (or odd) monolayers into AA artificial crystals. Figure 3A shows angle-resolved SHG responses from one to five layers of an AA-stacked $MoSe_2$ artificial lattice, with the integrated SHG intensities (I_{SHG}; circles) plotted against the number (n) of the monolayers in Fig. 3B. Similar results for AA-stacked MoS_2 are shown in fig. S4. The dashed line in Fig. 3B corresponds to a fit that takes

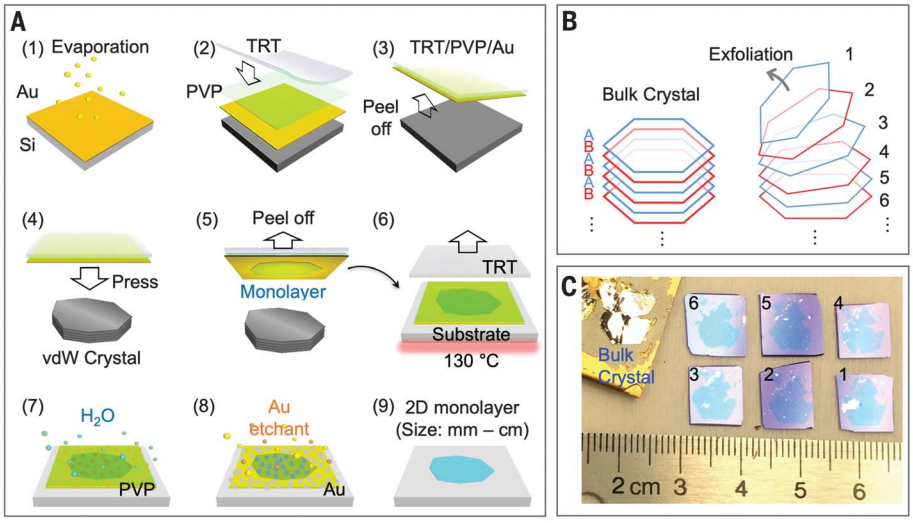

Fig. 1. Schematic illustration of the layer-by-layer exfoliation procedure of bulk vdW single crystals. (**A**) Method: (1) Depositing gold on an ultraflat silicon wafer; (2) spin-coating the surface with a layer of PVP; (3) using thermal release tape (TRT) to pick up the PVP and gold; (4) pressing the ultraflat gold onto the surface of a bulk vdW crystal; (5) peeling off a monolayer and transferring onto a substrate; (6) removing the TRT with heat; (7) dissolving PVP in water; (8) dissolving gold in an I_2/I^- etchant solution; and (9) obtaining the single-crystal monolayer with macroscopic dimensions. (**B**) Schematic of the layer-by-layer exfoliation technique to yield even and odd layers from an AB-stacked vdW crystal. (**C**) Optical images of six monolayer samples (on SiO_2/Si substrate) sequentially exfoliated from a centimeter-size WSe_2 single crystal shown at the upper left corner.

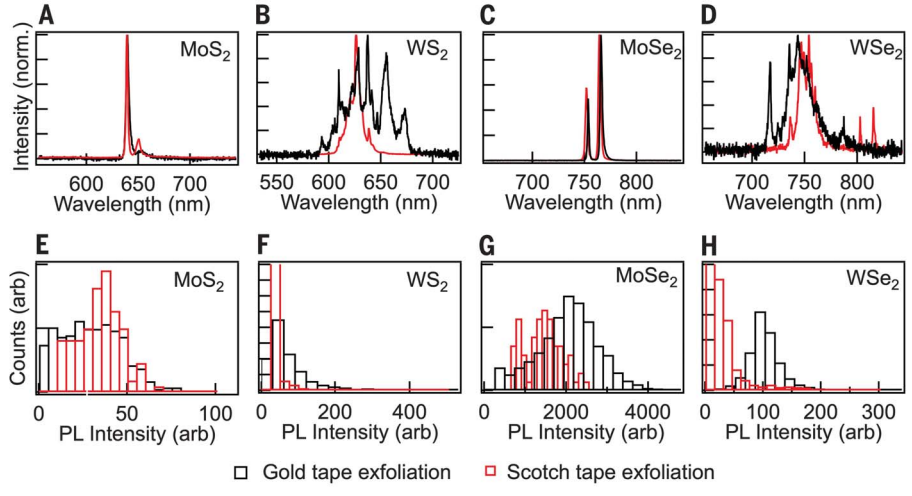

Fig. 2. Comparison of PL spectra and intensity distributions in TMDC monolayers exfoliated using the gold tape and Scotch tape methods. PL spectra (top) and intensity distributions (bottom) for monolayers encapsulated in BN. Black indicates gold tape–exfoliated monolayers; red is traditional Scotch tape–exfoliated monolayers. $MoSe_2$ and WSe_2 monolayers from both methods are exfoliated from the same low–defect-density bulk crystals grown from the flux methods. The MoS_2 and WS_2 monolayers in both methods are exfoliated from the same chemical vapor transport–grown bulk crystals. All PL measurements were at 4 K on monolayer samples with BN encapsulation. arb, arbitrary units.

into account reabsorption and interference of SHG from different layers. At ultrathin thickness, the SHG response is dominated by constructive interference from adjacent layers, close to the ideal limit of a quadratic optical response, $I_{SHG} \propto n^2$ (solid curve in Fig. 3B). The close to perfect coherent enhancement benefits from the negligible phase mismatch over nanometer distances. With increasing thickness of the artificial lattice, the increase of coherent response is expected to continue until ~20 nm, when phase mismatch and reabsorption of SHG light become noticeable, as shown in fig. S5. Although synthesis of 3R phases of TMDC with broken inversion symmetry is possible (*30*), our method is unrestricted by synthesis and can be used to construct any macroscopic vdW multilayer structures with control in interlayer twist angles and chemical identities. As one indication of the consistency of the artificial lattices from our macroscopic monolayers, we measured SHG responses from the $MoSe_2$/WSe_2 at five randomly picked spots (fig. S6). The orientation of the artificial lattice is unchanged from spot to spot within the experimental angular resolution of ±0.5°. The SHG intensity variation is within ±15%, likely because of the small changes in optical alignment as the sample was moved macroscopically under the microscope.

The second example is the creation of heterobilayers with controlled twist angle from two macroscopic single-crystal monolayers. By precisely engineering angular and/or lattice mismatch, vdW bilayers constructed from the same or different single-crystal 2D monolayers have been shown to exhibit a range of quantum phenomena, but all on micrometer-scale samples from the Scotch tape method (*4*–*12*). An intriguing development for their future technological applications is the generation of such bilayer structures at macroscopic dimensions. Using two monolayers of $MoSe_2$ and WSe_2, we fabricated a $MoSe_2$/WSe_2 single-crystal heterobilayer, as shown in the optical image in Fig. 4A, with lateral dimensions of ~4 mm and a twist angle of $\Delta\theta = 3.0 \pm 0.5°$. AFM imaging on part of the macroscopic structure identifies the heterobilayer with a high degree of flatness (fig. S7). The large size of the single-crystal heterobilayer on a dielectric substrate (SiO_2) allows us to map out the band structure with angle-resolved photoemission spectroscopy (ARPES) using a conventional setup with a hemispherical electron energy analyzer without microscopic capabilities. The ARPES spectrum determined in the Γ–K direction is in excellent agreement with theoretical calculations (Fig. 4B) (*31*). Low-temperature PL measurement of the BN-encapsulated heterobilayer stack revealed the dominant radiative recombination from the charge-separated interlayer exciton (Fig. 4C), in excellent agreement with previous reports of interlayer excitons in $MoSe_2$/WSe_2 heterobilayers fabricated from the Scotch tape method (*32*–*34*). Moreover, the intralayer excitons from constituent monolayers in our heterobilayer sample are completely quenched, verifying the high quality of the $MoSe_2$/WSe_2 interface. Note that the detailed peak shape and intensity of interlayer exciton PL vary from location to location on the sample (figs. S8 to S10), which is well known from recent reports on the same system (*8*, *9*), and is likely the result of sensitivity of PL emission to local variation in electrostatic environment and strain (*35*).

To summarize, we show a general method for the facile disassembly of vdW single crystals layer by layer into monolayers with macroscopic dimensions. The quality of the macroscopic single-crystal monolayers is comparable to that of the microscopic dimensions obtained from the state-of-the-art Scotch tape method, as confirmed in AFM imaging and PL characterization. We demonstrate this method for the controlled reassembly of these macroscopic monolayers into artificial lattices, including AA-stacked TMDC multilayers for substantially enhanced nonlinear optical response and heterobilayers for interlayer excitons at macroscopic dimensions. This approach may allow us to extend the exciting discoveries in the so-called "twistronics," i.e., magic angle or Moiré landscapes in 2D bilayers (*4*–*12*), into the multilayer or bulk region. The latter is a formidable challenge for microscopic

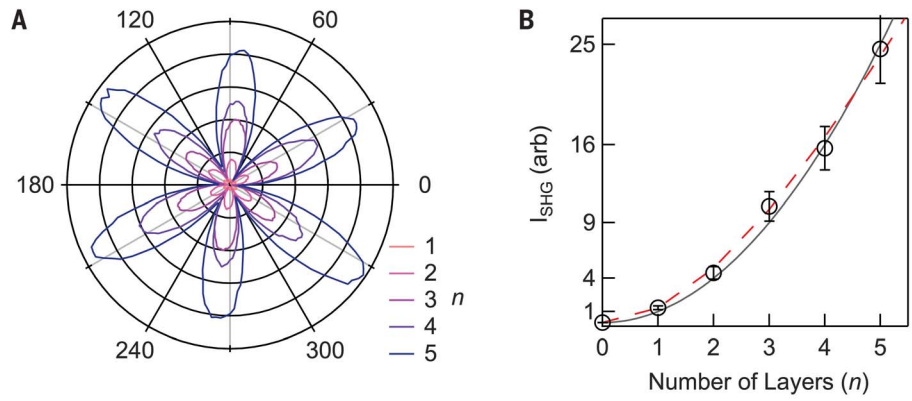

Fig. 3. Artificial AA-stacked TMDC lattices from macroscopic monolayers. (**A**) Angle-resolved SHG intensity of AA-stacked $MoSe_2$ artificial lattices as a function of the rotation angle of crystal with respect to light polarization. (**B**) Integrated SHG intensity (circles) for different number of layers in the AA stacks. The solid line is a quadratic fit, and the red dashed line is a fit that takes into account both coherent interference and reabsorption, as discussed in the supplementary materials. We fabricated each multilayer sample by picking up the monolayers on SiO_2 substrates sequentially with the ultraflat gold tape and measuring the SHG on the tape after each step.

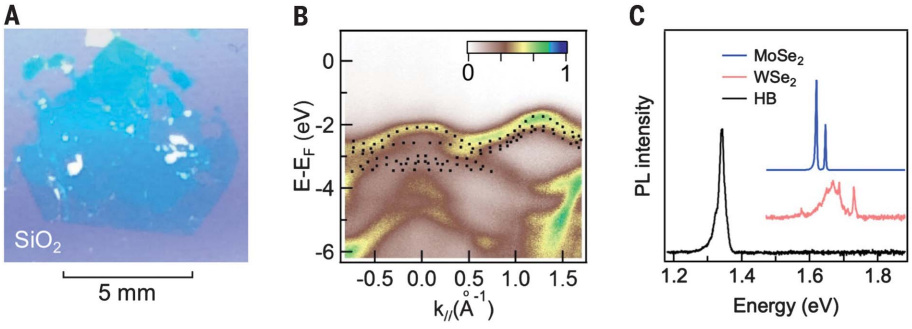

Fig. 4. Macroscopic $MoSe_2$/WSe_2 heterobilayer. (**A**) Optical image of the millimeter-scale $MoSe_2$/WSe_2 heterostructure on SiO_2/Si substrate aligned at $\Delta\theta = 3.0 \pm 0.5°$, as determined in SHG. (**B**) ARPES of the millimeter-scale $MoSe_2$/WSe_2 heterobilayer measured along the Γ–K direction. The dotted curves are theoretical calculations from (*31*). The sample was at 295 K in ARPES measurement. (**C**) Low-temperature (4 K) PL spectra of interlayer exciton in h-BN–encapsulated $MoSe_2$/WSe_2 heterobilayer (HB, black). For comparison, we also show PL spectra from intralayer excitons in h-BN–encapsulated $MoSe_2$ (blue) and WSe_2 (red) monolayers. All monolayers were exfoliated using the gold tape method. For the macroscopic heterobilayer on oxide-terminated silicon in (A) and (B), we used commercial chemical vapor transport–grown $MoSe_2$ and WSe_2 crystals. For the h-BN–encapsulated samples in (C), we used higher-quality, but smaller, flux-grown $MoSe_2$ and WSe_2 crystals.

monolayers from the Scotch tape method, but achievable with our macroscopic monolayers. With techniques for the high-throughput production of macroscopic monolayers, 2D quantum devices on a large scale may become a reality.

REFERENCES AND NOTES

1. K. S. Novoselov *et al*., *Science* **306**, 666–669 (2004).
2. K. S. Novoselov, A. Mishchenko, A. Carvalho, A. H. Castro Neto, *Science* **353**, aac9439 (2016).
3. H. Yu, G.-B. Liu, J. Tang, X. Xu, W. Yao, *Sci. Adv.* **3**, e1701696 (2017).
4. Y. Cao *et al*., *Nature* **556**, 43–50 (2018).
5. Y. Cao *et al*., *Nature* **556**, 80–84 (2018).
6. C. Jin *et al*., *Nature* **567**, 76–80 (2019).
7. E. M. Alexeev *et al*., *Nature* **567**, 81–86 (2019).
8. K. L. Seyler *et al*., *Nature* **567**, 66–70 (2019).
9. K. Tran *et al*., *Nature* **567**, 71–75 (2019).
10. Q. Tong *et al*., *Nat. Phys.* **13**, 356–362 (2017).
11. L. Wang *et al*., Magic continuum in twisted bilayer WSe_2. arXiv:1910.12147 [cond-mat-mes-hall] (26 October 2019).
12. X. Lu *et al*., *Nature* **574**, 653–657 (2019).
13. J. N. Coleman *et al*., *Science* **331**, 568–571 (2011).
14. Z. Cai, B. Liu, X. Zou, H.-M. Cheng, *Chem. Rev.* **118**, 6091–6133 (2018).
15. G. Z. Magda *et al*., *Sci. Rep.* **5**, 14714 (2015).
16. M. Velický *et al*., *ACS Nano* **12**, 10463–10472 (2018).
17. S. B. Desai *et al*., *Adv. Mater.* **28**, 4053–4058 (2016).
18. J. Shim *et al*., *Science* **362**, 665–670 (2018).
19. Y. Liu *et al*., *Nature* **557**, 696–700 (2018).
20. M. Hegner, P. Wagner, G. Semenza, *Surf. Sci.* **291**, 39–46 (1993).
21. N. Vogel, J. Zieleniecki, I. Köper, *Nanoscale* **4**, 3820–3832 (2012).
22. D. Edelberg *et al*., *Nano Lett.* **19**, 4371–4379 (2019).
23. Y. You *et al*., *Nat. Phys.* **11**, 477–481 (2015).
24. G. Plechinger *et al*., *Phys. Status Solidi Rapid Res. Lett.* **9**, 457–461 (2015).
25. Y. Li *et al*., *Phys. Rev. B Condens. Matter Mater. Phys.* **90**, 205422 (2014).
26. Y. Li *et al*., *Nano Lett.* **13**, 3329–3333 (2013).
27. C. Janisch *et al*., *Sci. Rep.* **4**, 5530 (2014).
28. A. Säynätjoki *et al*., *Nat. Commun.* **8**, 893 (2017).
29. W. T. Hsu *et al*., *ACS Nano* **8**, 2951–2958 (2014).
30. J. Shi *et al*., *Adv. Mater.* **29**, 1701486 (2017).
31. R. Gillen, J. Maultzsch, *Phys. Rev. B* **97**, 165306 (2018).
32. P. Rivera *et al*., *Nat. Commun.* **6**, 6242 (2015).
33. P. Rivera *et al*., *Science* **351**, 688–691 (2016).
34. J. Wang *et al*., *Sci. Adv.* **5**, eaax0145 (2019).
35. Y. Bai *et al*., One-dimensional Moiré excitons in transition-metal dichalcogenide heterobilayers. arXiv:1912.06628 [cond-mat-mtrl-sci] (13 December 2019).

ACKNOWLEDGMENTS

Funding: The development of the ultraflat gold tape exfoliation method was supported by the Center for Precision Assembly of Superstratic and Superatomic Solids, a Materials Science and Engineering Research Center (MRSEC), through NSF grant no. DMR-1420634. All TMDC sample preparation, imaging, and spectroscopy experiments were supported by National Science Foundation (NSF) grant no. DMR-1809680. X.-Y.Z. acknowledges support by a Vannevar Bush Faculty Fellowship through Office of Naval Research grant no. N00014-18-1-2080 for the purchase of the laser system used in the ARPES measurements. F.L. acknowledges support by a Department of Energy (DOE) Office of Energy Efficiency and Renewable Energy (EERE) Postdoctoral Research Award under the EERE Solar Energy Technologies Office administered by the Oak Ridge Institute for Science and Education (ORISE). ORISE is managed by Oak Ridge Associated Universities (ORAU) under DOE contract no. DE-SC00014664. All opinions expressed in this paper are the authors' and do not necessarily reflect the policies and views of DOE, ORAU, or ORISE. **Author contributions:** X.-Y.Z. and F.L. conceived this work. F.L. performed all experiments on gold tape exfoliation and characterization. W.W. performed experiments on Scotch tape exfoliation and BN encapsulation. Y.B. and F.L. measured the low-temperature PL. J.H. and S.H.C. conceived the idea of using a PVP protection layer. Q.L. assisted with gold tape exfoliation and SHG measurement. J.W. and Y.B. constructed the low-temperature PL-mapping setup. F.L. and X.-Y.Z. wrote the manuscript with input from all authors. X.-Y.Z. supervised the project. All authors participated in the discussion and interpretation of the results. **Competing interests:** Part of this work is included in a US provisional patent application. **Data and materials availability:** All data needed to evaluate the conclusions in the paper are available in the main text or the supplementary materials.

SUPPLEMENTARY MATERIALS

science.sciencemag.org/content/367/6480/903/suppl/DC1
Materials and Methods
Figs. S1 to S10
References (*36*–*38*)

7 November 2019; accepted 28 January 2020
10.1126/science.aba1416

ATMOSPHERIC METHANE

Old carbon reservoirs were not important in the deglacial methane budget

M. N. Dyonisius[1]*, V. V. Petrenko[1], A. M. Smith[2], Q. Hua[2], B. Yang[2], J. Schmitt[3], J. Beck[3], B. Seth[3], M. Bock[3], B. Hmiel[1], I. Vimont[4]†, J. A. Menking[5], S. A. Shackleton[6]‡, D. Baggenstos[3,6], T. K. Bauska[5,7], R. H. Rhodes[5,8], P. Sperlich[9], R. Beaudette[6], C. Harth[6], M. Kalk[5], E. J. Brook[5], H. Fischer[3], J. P. Severinghaus[6], R. F. Weiss[6]

Permafrost and methane hydrates are large, climate-sensitive old carbon reservoirs that have the potential to emit large quantities of methane, a potent greenhouse gas, as the Earth continues to warm. We present ice core isotopic measurements of methane ($\Delta^{14}C$, $\delta^{13}C$, and δD) from the last deglaciation, which is a partial analog for modern warming. Our results show that methane emissions from old carbon reservoirs in response to deglacial warming were small (<19 teragrams of methane per year, 95% confidence interval) and argue against similar methane emissions in response to future warming. Our results also indicate that methane emissions from biomass burning in the pre-Industrial Holocene were 22 to 56 teragrams of methane per year (95% confidence interval), which is comparable to today.

Methane (CH_4) is an important contributor to the greenhouse effect, with a global warming potential ~28 times higher than that of carbon dioxide (CO_2) on a 100-year time scale (*1*). Natural CH_4 emissions currently account for ~40% of total emissions (*2*) and there are considerable uncertainties in their response to future warming (*3*). Although wetlands are the dominant natural source of CH_4, increased emissions from large, climate-sensitive old carbon reservoirs such as permafrost (*4*) and hydrates under ice sheets (*5*) might become important in the coming century. Marine hydrates may also have the potential to emit a substantial amount of CH_4 into the atmosphere in response to warming (*6*), but the time scale of marine hydrate dissociation is relatively long (on the order of hundreds to thousands of years). Furthermore, there is a growing consensus that CH_4 release to the atmosphere from dissociating marine hydrates will be buffered by efficient CH_4 oxidation in the sediments and water column (*3*, *7*).

The last deglaciation [18 to 8 kilo-annum before present (ka BP)] provides the opportunity for evaluating the long-term sensitivity of these old carbon reservoirs (marine hydrates, permafrost, and hydrates under ice sheets) to a changing climate. There is abundant evidence of the destabilization of marine hydrates (*8*, *9*), land permafrost degradation (*10*), and thermokarst lake (permafrost thaw lake) formation (*11*) during the last deglaciation. However, CH_4 emissions from these old carbon reservoirs into the atmosphere are not well constrained. The paleoatmospheric CH_4 mole fraction and its isotopic composition from trapped air in ice cores provide a historical perspective on how natural CH_4 sources respond to climate change (e.g., *12*, *13*). Measurements of carbon-14 (^{14}C) of CH_4 ($^{14}CH_4$) from ice cores specifically provide an unambiguous top-down constraint on the globally integrated ^{14}C-free CH_4 emissions from all old carbon reservoirs.

^{14}C decays radioactively and is thus strongly depleted in carbon reservoirs that have been isolated from the atmosphere for time periods longer than its half-life of ~5730 years. Because of the low abundance of ^{14}C (on the order of 10^{-12} compared with ^{12}C), measurements of $^{14}CH_4$ in ice cores are challenging, requiring ~1000 kg of ice per sample. We collected ice cores from a well-dated ice ablation site on Taylor Glacier, Antarctica (*14*), which provides easy access to large volumes of old ice at shallow depths. Petrenko *et al.* (*15*) recently presented measurements of paleoatmospheric $^{14}CH_4$ from Taylor Glacier for the Younger Dryas–Preboreal (YD-PB) transition (11.7 to 11.3 ka BP) and concluded that ^{14}C-free CH_4 emissions were small [<7.7% of total CH_4 emissions, 95% confidence interval (CI)]. However, their results only spanned a brief time interval within the deglacial transition. In this study, we present 11 additional measurements of paleoatmospheric $^{14}CH_4$ (Fig. 1A) combined with stable isotope measurements ($\delta^{13}CH_4$ and δD-CH_4) (Fig. 1, C and D) in the 15- to 8-ka BP time interval, providing a more complete picture of the deglacial CH_4 budget.

The Oldest Dryas–Bølling (OD-B) transition (14.6 to 14.45 ka BP) represents the first large and abrupt CH_4 rise during the last deglacial sequence of events (Fig. 1B) at the time when sea level was ~100 m lower than today. This abrupt CH_4 rise was synchronous with the acceleration of Northern Hemisphere (NH) warming (*16*) (Fig. 1E), ice sheet retreat, and rapid sea-level rise (*17*). This climate transition may have also coincided with the first instance of marine hydrate destabilization during the last deglaciation caused by hydrostatic pressure relief from NH ice sheet retreat and incursion of warm intermediate ocean water into shallow, hydrate-bearing Arctic sediments (*8*). During the destabilization of marine hydrate reservoirs, abrupt events such as submarine landslides (*18*) or collapse of marine hydrate pingos (*8*) could result in large and rapid CH_4 expulsions that may have contributed to the rapid atmospheric CH_4 rise (*9*) if they were capable of bypassing oxidation in the water column.

In contrast to old carbon reservoirs, contemporaneous CH_4 sources such as wetlands and biomass burning emit CH_4 with a ^{14}C signature that reflects the contemporaneous $\Delta^{14}CO_2$ at the time (*15*). Our $\Delta^{14}CH_4$ measurements for the OD-B transition are all within 1σ uncertainty of the contemporaneous atmospheric $\Delta^{14}CO_2$ (*19*) (Fig. 1A), indicating a dominant role of contemporaneous CH_4 sources. We used a one-box model (see section 4.2 of the materials and methods) (*20*) to calculate the amount of ^{14}C-free CH_4 emission into the atmosphere (Table 1, fig. S9, and table S10) (*20*). Our box model shows that the total ^{14}C-free CH_4 emissions during the OD-B transition were small [on average, <13 teragrams (Tg) of CH_4 per year, 95% CI upper limit]. Combined with earlier $\Delta^{14}CH_4$ data from the YD-PB transition (*15*), our results argue strongly against the hypothesis regarding old carbon reservoirs being important contributors to the rapid CH_4 increases associated with abrupt warming events (Dansgaard–Oeschger events) (*9*). This conclusion is consistent with previous studies (*13*) showing no major enrichment in the CH_4 deuterium/hydrogen ratio (δD-CH_4) concurrent with the abrupt CH_4 transitions (CH_4 from marine hydrates is relatively enriched in δD). It has been shown that even at a relatively shallow water depth of ~30 m, ~90% of the ^{14}C-free CH_4 released from thawing subsea permafrost was oxidized in the water column (*21*). We hypothesize that during the OD-B transition, relatively rapid sea-level rise associated with meltwater pulse 1-A (*17*), combined with CH_4 oxidation in the water column (*22*), may have prevented CH_4 emissions from disintegrating marine hydrates and sub-sea permafrost from reaching the atmosphere.

Our measurements of $^{14}CH_4$ during the Bølling–Allerød interstadial (14.45 to 13 ka BP) and the early Holocene (10 to 8 ka BP) warm period (Fig. 1A) provide an opportunity to assess

[1]Department of Earth and Environmental Sciences, University of Rochester, Rochester, NY 14627, USA. [2]Australian Nuclear Science and Technology Organisation (ANSTO), Lucas Heights, NSW 2234, Australia. [3]Climate and Environmental Physics, Physics Institute and Oeschger Centre for Climate Change Research, University of Bern, CH-3012 Bern, Switzerland. [4]Institute of Arctic and Alpine Research, University of Colorado Boulder, Boulder, CO 80303, USA. [5]College of Earth, Ocean and Atmospheric Sciences, Oregon State University, Corvallis, OR 97331, USA. [6]Scripps Institution of Oceanography (SIO), University of California, San Diego, La Jolla, CA 92037, USA. [7]British Antarctic Survey High Cross, Cambridge CB3 0ET, UK. [8]Department of Earth Sciences, University of Cambridge, Cambridge CB2 3EQ, UK. [9]National Institute of Water and Atmospheric Research (NIWA), 6021 Wellington, New Zealand.
***Corresponding author. Email: mdyonisi@ur.rochester.edu**
†Present address: Cooperative Institute for Research in Earth Sciences, University of Colorado, Boulder, CO 80309, USA.
‡Present address: Department of Geosciences, Princeton University, Princeton, NJ 08544, USA.

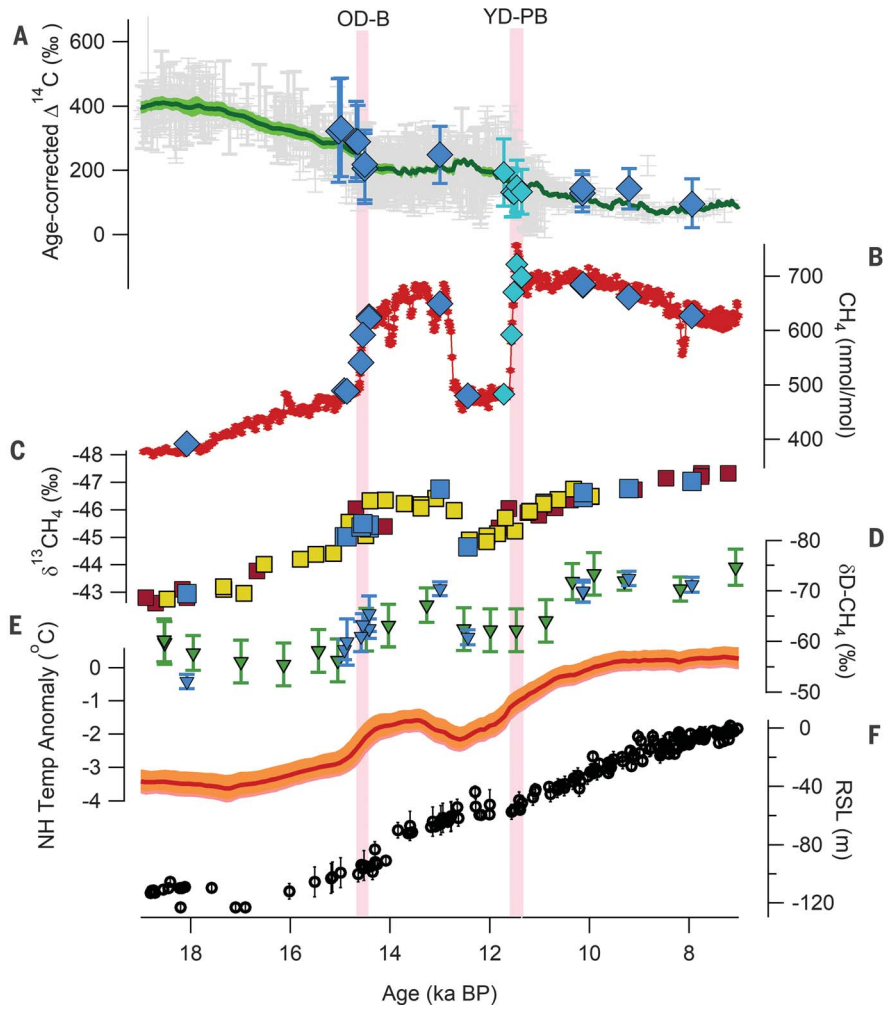

Fig. 1. CH_4 isotopes, mole fraction, NH temperature reconstruction, and relative sea level (RSL) during the last deglaciation. (**A**) $\Delta^{14}CH_4$ from Taylor Glacier (blue diamonds; this study), $\Delta^{14}C$ of contemporaneous CO_2 from IntCal13 [green line (*19*)], IntCal13 raw data [gray crosses (*19*)], and earlier $\Delta^{14}CH_4$ results [light blue diamonds (*15*)]. Two $\Delta^{14}CH_4$ samples from the 2014–2015 field season (at 17.8 and 12.8 ka BP) were rejected because of suspected addition of extraneous ^{14}C [see section 3 of the materials and methods (*20*)]. (**B**) CH_4 mole fraction from discrete WAIS Divide ice core measurements [red dots (*39*)], Taylor Glacier (blue diamonds; this study), and an earlier Taylor Glacier study [light blue diamonds (*15*)]. (**C**) $\delta^{13}CH_4$ from TALDICE (red squares), EDML [yellow squares (*13*)], and Taylor Glacier (blue squares; this study). (**D**) $\delta D\text{-}CH_4$ from EDML [green triangles (*13*)] and Taylor Glacier (blue triangles; this study). (**E**) Composite NH temperature stack (red line) and its 95% CI (shaded orange area) (*16*). (**F**) Global RSL inferred from coral data (*32*). All ice core data are plotted with respect to the WD2014 age scale (*40*); IntCal13, RSL, and NH temperature stacks are plotted on their respective age scales. All error bars represent the 95% CI.

the likelihood of delayed CH_4 emissions from old carbon reservoirs in response to warming. The onset of marine hydrate dissociation might lag the initial warming signal on decadal (*23*), centennial, or even millennial (*18*) time scales. Permafrost degradation could also lag a warming signal on decadal and centennial time scales (*24*) depending on local environmental conditions such as permafrost depth, soil types, and moisture content (*4*). During parts of the early Holocene, Arctic temperatures were likely warmer than today (*25*), providing a good analog for Arctic conditions in the coming decades. Proxy reconstructions of thermokarst lake initiation (*11*) and land permafrost degradation (*10*, *24*) suggested a potential increase of CH_4 emissions from these processes during both the Bølling–Allerød interstadial and the early Holocene warm period. However, our $\Delta^{14}CH_4$ measurements (Fig. 1A and Table 1) show no evidence of delayed ^{14}C-free CH_4 emissions after warming. These results are consistent with present-day observations that carbon from thermokarst lakes and permafrost is predominantly emitted in the form of CO_2 rather than CH_4 (*4*, *26*), and that CH_4 emissions from permafrost systems are dominated by relatively contemporaneous carbon (*26*, *27*).

Because carbon stored in permafrost is not expected to be ^{14}C free (*28*), we also attempted to use our $^{14}CH_4$ results to calculate the possible magnitude of CH_4 emissions from thawing old carbon in permafrost (Section 4.3) (*20*). This calculation assumed that the ^{14}C activity of permafrost CH_4 emissions follows the predepositional age of terrigenous biomarkers released from thawing permafrost (7500 ± 2500 years old relative to our sample age) (*10*). Resulting CH_4 emissions from old permafrost carbon range from 0 to 53 Tg CH_4 per year (table S10) (*20*) throughout the last deglaciation and may have contributed up to 27% of the total CH_4 emissions to the atmosphere (95% CI upper limit) at the end of the OD-B transition (14.42 ka BP). However, we consider this calculation speculative (see section 4.3 of the materials and methods) (*20*).

When the global sea level was lower, exposure of continental shelves may have resulted in higher CH_4 emissions from natural geologic seeps (*29*). A recent study also inferred the existence of CH_4 hydrate deposits underneath ice sheets and suggested that the proglacial meltwater discharge is likely an important source of CH_4 to the atmosphere (*5*). Ice sheet retreat during the last deglaciation may have destabilized the subglacial hydrate deposits, which contain old, ^{14}C-depleted CH_4. However, our data, which span most of the deglacial ice retreat and sea-level rise (Fig. 1F), argue strongly against both hypotheses. The ^{14}C-free CH_4 emissions were small throughout the last deglaciation (Table 1) and appear to be insensitive to both global sea level and ice volume.

Biomass burning is an important component of the global carbon cycle and is tightly coupled with emissions of carbon monoxide (CO), nitrogen oxides (NO_x), nonmethane hydrocarbons, and aerosols that have substantial effects on atmospheric chemistry and radiative energy fluxes. Compared with other proxies of past biomass burning, CH_4 has an advantage because it is a well-mixed gas in the atmosphere and can represent the globally integrated biomass-burning emissions. Bock *et al.* (*13*)

Table 1. CH_4 source strength estimates (95% CI) for the time intervals of our samples. Sample ages were determined by value matching of globally well-mixed gases (CH_4 and $\delta^{18}O$ of atmospheric oxygen) to WD2014 chronology [see section 1 of the materials and methods (*20*)]. The sample ages given in this table represent the "best" (maximum probability) age on the probability distribution (fig. S3) (*20*) with respect to WD2014 chronology (*40*).

Sample name	Sample age (ka BP)	CH_4 mole fraction (nmol/mol)	Age-corrected $\Delta^{14}CH_4$ (‰)	Total source (Tg CH_4/year)	^{14}C-free emissions (Tg CH_4/year)	$CH_{4\ bb}$ emissions (Tg CH_4/year)	$CH_{4\ mic}$ emissions (Tg CH_4/year)
Oldest Dryas 1	14.92	484.5 ± 3.9	317 ± 166	141.3 ± 14.4	0–13	—	
Oldest Dryas 2	14.86	485.9 ± 3.9	327 ± 151	142.3 ± 14.7	0–10	—	
Transition 1	14.58	543.0 ± 3.9	288 ± 128	158.8 ± 17.1	0–11	—	
Transition 2	14.54	584.8 ± 3.9	287 ± 112	164.7 ± 18.8	0–10	—	
Bølling 2	14.42	624.4 ± 3.9	216 ± 109	178.5 ± 19.5	0–17	—	
Bølling 1	14.42	621.1 ± 3.9	204 ± 111	177.9 ± 20.1	0–20	—	
Allerød	13.00	647.2 ± 3.9	246 ± 90	190.2 ± 19.4	0-8	—	
10.2K1	10.13	681.6 ± 3.9	126 ± 58	206.7 ± 20.7	0–11	32–56	131–168
10.2K2	10.13	681.6 ± 3.9	139 ± 57	206.7 ± 20.7	0–8	33–56	132–169
9.2K	9.21	659.7 ± 3.9	141 ± 63	200.4 ± 20.1	0–2	31–53	130–165
8.2K	7.94	623.9 ± 3.9	92 ± 74	187.8 ± 19.3	0–11	27–48	120–156
*Late Holocene**	1.95	—	—	171.0 ± 18.8	0–9*	22–42	123–157

*The ^{14}C-free emissions for this period are extrapolated from the average of ^{14}C-free emissions in the early Holocene (10 to 8 ka BP). This assumption can be justified because a large change in the natural geologic emissions between the early Holocene and 2 ka BP seems unlikely given that the global sea level and ice volume did not change considerably (*36*). We used both the stable isotopes ($\delta^{13}CH_4$, $\delta D\text{-}CH_4$) and CH_4 mole fraction from (*11*) at 2 ka BP to calculate the $CH_{4\ bb}$ and $CH_{4\ mic}$ emissions.

provided the most recent stable isotope–based ($\delta^{13}C$ and δD) study of the glacial–interglacial CH_4 budget, but they were unable to separate the relative contributions from CH_4 sources that are enriched in heavier isotopes (biomass burning and natural geologic emissions). With improved estimates of natural geologic emissions, our results allow for better constraints on the overall CH_4 budget. We used the stable isotope data (Fig. 1, C and D) in a one-box model (see section 5 of the materials and methods) (*20*) to calculate CH_4 emissions from biomass burning ($CH_{4\ bb}$) and microbial sources ($CH_{4\ mic}$, composed of emissions from wetlands, ruminants, and termites) for the Early Holocene (Table 1 and fig. S11) (*20*). We extended our calculation to the late Holocene (~2 ka BP) (Table 1) to directly compare our CH_4 source strength estimates with those of earlier studies (*30*, *31*). This assumption can be justified because a large change in the natural geologic emissions between the early Holocene and 2 ka BP seems unlikely because global sea level and ice volume did not change appreciably after 8 ka BP (*32*). However, we did not perform this calculation for the pre-Holocene samples because estimates of the CH_4 interpolar difference, atmospheric global average CH_4 stable isotope values, and stable isotopic signatures of the sources are more uncertain (Section 5) (*20*).

We calculated relatively high $CH_{4\ bb}$ emissions in the early Holocene (33 to 56 Tg CH_4 per year, 95% CI) at 10 ka BP and a slight decrease of $CH_{4\ bb}$ emissions (22 to 42 Tg CH_4 per year, 95% CI) toward the late Holocene (Table 1). However, the magnitude of the decrease in biomass-burning emissions (~7 Tg CH_4 per year) is small relative to the uncertainties for both the $CH_{4\ bb}$ and $CH_{4\ mic}$ emissions (±11 and ±18 Tg CH_4 per year, respectively, 95% CI uncertainties). Our estimate of 22 to 42 Tg CH_4 per year (95% CI) $CH_{4\ bb}$ emissions for the late Holocene period (~2 ka BP) is within the upper range of estimates from previous ice core studies (*13*, *30*, *31*). Considering the large downward revision of natural geologic emissions inferred from our ^{14}C data, an upward revision in pyrogenic CH_4 emissions is expected to balance the CH_4 stable isotope budget. The increase in $CH_{4\ bb}$ expected from a reduction in natural geologic emissions is partly offset by a −0.5 to −1‰ revision in atmospheric $\delta^{13}CH_4$ values (*12*, *30*, *31*) because the $\delta^{13}CH_4$ values from earlier studies (*30*, *31*) were likely biased because of krypton (Kr) interference (*33*). Our $CH_{4\ bb}$ estimates are also reduced because, unlike previous studies, we accounted for temporal shifts in the isotopic signatures of $CH_{4\ bb}$ and $CH_{4\ mic}$ between the pre-Industrial Holocene and the modern period expected from anthropogenically driven changes in the $\delta^{13}CO_2$ precursor material and land use (see section 5.2 of the materials and methods) (*20*). Our best $CH_{4\ bb}$ estimates for the late Holocene (22 to 42 Tg CH_4 per year, 95% CI) are comparable to the present-day estimates of combined pyrogenic CH_4 emissions from anthropogenic biomass burning and wildfires (*2*). This result is supported by some (*34*, *35*), but not all (*36*), independent paleoproxies of biomass burning.

The last deglaciation serves only as a partial analog to current anthropogenic warming, with the most important differences being the much colder baseline temperature, lower sea level, and the presence of large ice sheets covering a large part of what are currently permafrost regions in the NH. Although Arctic temperatures during the peak early Holocene warmth were likely warmer than today (*25*), they were still lower than the Arctic temperature projections by the end of this century under most warming scenarios (*37*). However, there are also many similarities between the last deglaciation and current anthropogenic warming. Both deglacial and modern warming include strong Arctic amplification, and the magnitude of global warming (~4°C) (*16*) during the last deglaciation was comparable to the expected magnitude of equilibrium global temperature change under mid-range anthropogenic emission scenarios (*37*). Because the relatively large global warming of the last deglaciation (which included periods of large and rapid regional warming in the high latitudes) did not trigger CH_4 emissions from old carbon reservoirs, such CH_4 emissions in response to anthropogenic warming also appear to be unlikely. Our results instead support the hypothesis that natural CH_4 emissions involving contemporaneous carbon from wetlands are likely to increase as warming continues (*38*). We also estimated relatively high $CH_{4\ bb}$ emissions for the pre-Industrial Holocene that were comparable to present-day combined pyrogenic CH_4 emissions from natural and anthropogenic sources. This result suggests either an underestimation of present-day $CH_{4\ bb}$ or a two-way anthropogenic influence on fire activity during the Industrial Revolution: reduction in wildfires from active fire suppression and landscape fragmentation balanced by increased fire emissions from land-use change (deforestation) and traditional biofuel use (burning of plant materials for cooking and heating).

REFERENCES AND NOTES

1. G. Myhre, D. Shindell, in *Climate Change 2013: The Physical Science Basis. Contribution of Working Group I to the Fifth Assessment Report of the Intergovernmental Panel on Climate*

Change, T. F. Stocker *et al*., Eds. (Cambridge Univ. Press, 2013), pp. 659–740.
2. M. Saunois *et al*., *Earth Syst. Sci. Data* **8**, 697 (2016).
3. J. F. Dean *et al*., *Rev. Geophys.* **56**, 207–250 (2018).
4. E. A. G. Schuur *et al*., *Nature* **520**, 171–179 (2015).
5. G. Lamarche-Gagnon *et al*., *Nature* **565**, 73–77 (2019).
6. M. Maslin *et al*., *Philos. Trans. A Math. Phys. Eng. Sci.* **368**, 2369–2393 (2010).
7. C. D. Ruppel, J. D. Kessler, *Rev. Geophys.* **55**, 126–168 (2017).
8. K. Andreassen *et al*., *Science* **356**, 948–953 (2017).
9. J. P. Kennett, K. G. Cannariato, I. L. Hendy, R. J. Behl, in *Methane Hydrates in Quaternary Climate Change: The Clathrate Gun Hypothesis* (American Geophysical Union, 2013).
10. M. Winterfeld *et al*., *Nat. Commun.* **9**, 3666 (2018).
11. K. M. Walter, M. E. Edwards, G. Grosse, S. A. Zimov, F. S. Chapin 3rd, *Science* **318**, 633–636 (2007).
12. J. Beck *et al*., *Biogeosciences* **15**, 7155–7175 (2018).
13. M. Bock *et al*., *Proc. Natl. Acad. Sci. U.S.A.* **114**, E5778–E5786 (2017).
14. D. Baggenstos *et al*., *Clim. Past* **13**, 943–958 (2017).
15. V. V. Petrenko *et al*., *Nature* **548**, 443–446 (2017).
16. J. D. Shakun *et al*., *Nature* **484**, 49–54 (2012).
17. P. Deschamps *et al*., *Nature* **483**, 559–564 (2012).
18. D. Archer, *Biogeosciences* **4**, 993–1057 (2007).
19. P. J. Reimer *et al*., *Radiocarbon* **55**, 1869–1887 (2013).
20. Materials and methods are available as supplementary materials.
21. K. J. Sparrow *et al*., *Sci. Adv.* **4**, eaao4842 (2018).
22. M. Leonte *et al*., *Geochim. Cosmochim. Acta* **204**, 375–387 (2017).
23. C. Stranne, M. O'Regan, M. Jakobsson, *Geophys. Res. Lett.* **43**, 8703–8712 (2016).
24. A. V. Reyes, C. A. Cooke, *Proc. Natl. Acad. Sci. U.S.A.* **108**, 4748–4753 (2011).
25. B. S. Lecavalier *et al*., *Proc. Natl. Acad. Sci. U.S.A.* **114**, 5952–5957 (2017).
26. C. D. Elder *et al*., *Nat. Clim. Chang.* **8**, 166–171 (2018).
27. M. D. A. Cooper *et al*., *Nat. Clim. Chang.* **7**, 507–511 (2017).
28. P. J. Mann *et al*., *Nat. Commun.* **6**, 7856 (2015).
29. B. Luyendyk, J. Kennett, J. F. Clark, *Mar. Pet. Geol.* **22**, 591–596 (2005).
30. D. F. Ferretti *et al*., *Science* **309**, 1714–1717 (2005).
31. C. J. Sapart *et al*., *Nature* **490**, 85–88 (2012).
32. K. Lambeck, H. Rouby, A. Purcell, Y. Sun, M. Sambridge, *Proc. Natl. Acad. Sci. U.S.A.* **111**, 15296–15303 (2014).
33. J. Schmitt *et al*., *Atmos. Meas. Tech.* **6**, 1425–1445 (2013).
34. M. R. Nicewonger, M. Aydin, M. J. Prather, E. S. Saltzman, *Proc. Natl. Acad. Sci. U.S.A.* **115**, 12413–12418 (2018).
35. Z. Wang, J. Chappellaz, K. Park, J. E. Mak, *Science* **330**, 1663–1666 (2010).
36. A.-L. Daniau *et al*., *Global Biogeochem. Cycles* **26**, n/a (2012).
37. M. Collins, R. Knutti, in *Climate Change 2013: The Physical Science Basis. Contribution of Working Group I to the Fifth Assessment Report of the Intergovernmental Panel on Climate Change*, T. F. Stocker *et al*., Eds. (Cambridge Univ. Press, 2013), pp. 1029–1136.
38. P. U. Clark *et al*., *Abrupt Climate Change: A Report by the US Climate Change Science Program and the Subcommittee on Global Change Research* (U.S. Geological Survey, 2008).
39. WAIS Divide Project Members, *Nature* **520**, 661–665 (2015).
40. M. Sigl *et al*., *Clim. Past* **12**, 769–786 (2016).

ACKNOWLEDGMENTS

We thank M. Jayred and J. Jetson for ice drilling; camp managers K. Schroeder and C. Llewelyn and field team members A. Palardy and J. Ward for assistance; the U.S. Antarctic Program for logistical support; M. Sigl and F. Adolphi for assistance with age-scale transfer between IntCal13 and WD2014; H. Schaefer for suggestions regarding the isotope box model; G. Mollenhauer for discussions regarding the ^{14}C-age of terrigenous biomarkers; and P. F. Place Jr., M. Diaz, and M. Paccico for help with field gear preparations. **Funding:** This work was supported by NSF awards PLR-1245659 (V.V.P.), PLR-1245821 (E.J.B), and PLR-1246148 (J.P.S.); the Packard Fellowship for Science and Engineering (V.V.P.); the European Research Council (ERC) under the European Union's Seventh Framework Programme FP7/2007-2013 ERC Grant 226172 [ERC Advanced Grant Modern Approaches to Temperature Reconstructions in Polar Ice Cores (MATRICs); H.F.]; the Swiss National Science Foundation 200020_172506 (H.F.); Australian Government for the Centre for Accelerator Science at ANSTO through the National Collaborative Research Infrastructure Strategy (A.M.S, Q.H., B.Y.); and the National Institute of Water and Atmospheric Research through the Greenhouse Gases, Emissions and Carbon Cycle Science Program (P.S.). **Author contributions:** V.V.P., E.J.B., and J.P.S. designed the study. M.N.D., V.V.P., and B.H. conducted field logistical preparations. M.N.D., V.V.P., J.A.M., S.A.S., B.H., I.V., D.B., T.K.B., P.S., E.J.B., J.P.S., and R.H.R. conducted the field sampling and reconnaissance. M.N.D. extracted CH_4 and CO from air samples. Q.H. and B.Y. graphitized the ^{14}C samples. A.M.S. conducted the ^{14}C measurements. J.B. and B.S. made the CH_4 stable isotopes measurements (δ^{13}C and δD-CH_4) under the supervision of J.S., M.B., and H.F. D.B. and J.P.S. made the Xe/Kr, Kr/N_2, and Xe/N_2 measurements. R.B. made the $\delta^{15}N_2$, $\delta^{18}O_{atm}$, $^{40}Ar/^{36}Ar$, O_2/N_2, and Ar/N_2 measurements. C.H. made the CH_4 mole fraction and halogenated trace gas measurements under the supervision of R.F.W. M.K. made the CH_4 mole fraction and total air content measurements on the ice samples under the supervision of E.J.B. I.V. made the δ^{13}CO measurement for the CO dilution gas. S.A.S and M.N.D. developed the age scale for the samples. M.N.D. and V.V.P. analyzed the results and wrote the manuscript with input from all authors. **Competing interests:** The authors declare no competing interests. **Data and materials availability:** Data from this work are available through the USAP Data Center: https://gcmd.nasa.gov/search/Metadata.do?entry=USAP-1245659.

SUPPLEMENTARY MATERIALS

science.sciencemag.org/content/367/6480/907/suppl/DC1
Materials and Methods
Supplementary Text
Figs. S1 to S12
Tables S1 to S11
References (*41*–*97*)

19 February 2019; accepted 6 January 2020
10.1126/science.aax0504

ANIMAL COGNITION

Bumble bees display cross-modal object recognition between visual and tactile senses

Cwyn Solvi[1,2]*, Selene Gutierrez Al-Khudhairy[1]†, Lars Chittka[1]

Many animals can associate object shapes with incentives. However, such behavior is possible without storing images of shapes in memory that are accessible to more than one sensory modality. One way to explore whether there are modality-independent internal representations of object shapes is to investigate cross-modal recognition—experiencing an object in one sensory modality and later recognizing it in another. We show that bumble bees trained to discriminate two differently shaped objects (cubes and spheres) using only touch (in darkness) or vision (in light, but barred from touching the objects) could subsequently discriminate those same objects using only the other sensory information. Our experiments demonstrate that bumble bees possess the ability to integrate sensory information in a way that requires modality-independent internal representations.

Humans can easily recognize, through touch alone, objects they have previously only seen (*1*). This is demonstrated when we search and find objects on a high shelf or inside a cluttered bag. The ability to recognize objects across different senses increases the flexibility of any object-recognition system because the amount of noise and available information within different senses can vary dramatically across situations.

Cross-modal recognition requires the combination of information from multiple sensory modalities—for example, vision and touch. In humans, visual and tactile abilities are closely linked from birth, but their combination seems incomplete and limited at birth and develops to maturity over many years (*2*). Cross-modal object recognition has been shown across vision and touch in humans (*3*), apes (*4*), monkeys (*5*), and rats (*6*); across vision and hearing in dolphins (*7*); and across vision and electric sense in fish (*8*).

The ability to recognize objects across modalities entails some type of internal representation of an object's shape or its characteristic features (*7*, *9*, *10*). In humans, cross-modal recognition seems to require mental imagery (*11*), an internal representation that occurs in the absence of sensory stimulation in a given sensory modality and that functions as a weak form of perception (*12*–*14*). Theoretical analyses and empirical evidence support the idea that mental imagery involves an internal representation that is not only available to awareness but is a basic building block and integral part of consciousness (*14*–*17*).

The ability to recognize objects across modalities is beneficial and adaptive, allowing for enhanced perceptual monitoring of an animal's environment, flexible recognition of objects between senses, and richer representations of objects across multiple senses. Cross-modal recognition indicates that an animal possesses coherent "mental images" of objects. Whether the small brains of invertebrates perceive the world by storing internal representations of objects is unknown.

Because bumble bees naturally forage in the light but will also forage in the dark in laboratory conditions (*18*), they constitute an ideal system to examine whether an invertebrate is capable of cross-modal recognition across vision and touch. To do this, we trained 44 bumble bees in a dark room (a windowless room with lights turned off and vents, door edges, and all light diodes covered completely) (supplementary materials) to find 50% sucrose solution in one of two differently shaped objects (cube or sphere; 33 training trials) (Fig. 1A). To ensure that bumble bees could learn to discriminate objects in the dark without any visual information in our paradigm, we examined the behavior of 21 of the trained bumble bees in a nonreinforced test in the same dark setup as that in training. During the test, bumble bees spent more time in contact with the previously rewarding object [generalized linear mixed-effect model (GLMM): 95% confidence interval (CI) = 2.60 (1.95 to 3.25), n = 21 bees, $P = 4.51 \times 10^{-15}$] (Fig. 1C). To assess bumble bees' ability for tactile-to-visual cross-modal recognition, we tested the other 23 trained bees in a lighted arena where they were unable to touch the objects (Fig. 1B). In the cross-modal test situation, bumble bees spent more time in contact with the previously rewarding object [GLMM: 95% CI = 1.41 (1.06 to 1.75), n = 23 bees, $P = 9.81 \times 10^{-16}$] (Fig. 1D).

We then evaluated whether bumble bees were capable of visual-to-tactile cross-modal recognition. To do this, we trained 43 bumble bees first to discriminate cubes and spheres in a lighted arena where they could not touch the objects (Fig. 1B). Subsequently, to ensure that our setup was conducive to visual discrimination learning, the behavior of 22 of the trained bumble bees was tested in the same setup as in training but unreinforced (no reinforcements were present). Bumble bees spent more time in contact with the previously rewarding objects [GLMM: 95% CI = 2.00 (1.61 to 2.40), n = 22 bees, $P = 1.36 \times 10^{-23}$] (Fig. 1E). To test bumble bees' ability for visual-to-tactile cross-modal recognition, the behavior of the other 21 trained bees was examined in a dark arena (Fig. 1A). In the test, bumble bees again spent more time in contact with the previously rewarding object [GLMM: 95% CI = 1.85 (0.54 to 3.15), n = 21 bees, $P = 5.63 \times 10^{-3}$] (Fig. 1F). These results suggest that after learning to discriminate objects by using only one sensory modality, bumble bees can discriminate these same objects by using a different sensory modality.

This interpretation rests on the assumption that bumble bees could not touch the objects in the lighted situation and could not see the objects in the dark situation. In the lighted situation, bees could only access the holes of the objects (which were all the same dimensions) with their proboscis but could not touch the outsides of the objects. In the dark situation, the measured light levels within the arena were less than 0.01 lux, and the infrared lights were the only source of illumination that was not covered (supplementary materials). Bumble bees were unable to find their way back to the tunnel that led to the hive without following the walls. Furthermore, the proportion of bees' first entries onto Petri dishes during the tests in the dark was no different between the positively reinforced and negatively reinforced objects [GLMM: trained in dark, 95% CI = 0.69 (−0.21 to 1.60), n = 21 bees, P = 0.13; trained in light, 95% CI = −0.44 (−1.30 to 0.42), n = 23 bees, P = 0.31]. As an additional measure, we tested bees' ability to discriminate the two objects in the dark without being able to touch the objects. One group of bees (n = 20 bees) was trained to discriminate the two objects visually in a lighted arena (Fig. 1B), and another group of bees (n = 21 bees) was trained to discriminate the two objects tactilely in the dark (Fig. 1A). Subsequently, during an unreinforced test in the dark and without being able to touch the objects (Fig. 2A), both groups showed no difference in the duration in contact with the two different objects [GLMM: trained in light, 95% CI = −1.81 (−8.98 to 5.35), n = 20 bees, P = 0.62; trained in dark, 95% CI = −0.85 (−1.90 to 0.21), n = 21 bees, P = 0.12] (Fig. 2, B and C).

Perception of objects results from the integration of information from various sensory modalities (*12*, *19*). Two high-order centers in the insect protocerebrum, the mushroom bodies and central complex, have been shown to receive both visual and mechanosensory information (*20*–*22*).

[1]School of Biological and Chemical Sciences, Queen Mary University of London, London E1 4NS, UK. [2]Department of Biological Sciences, Macquarie University, North Ryde, NSW 2109, Australia.
*Corresponding author. Email: cwyn.solvi@mq.edu.au †Present address: Department of Biology, University of York, York, YO10 5DD, UK.

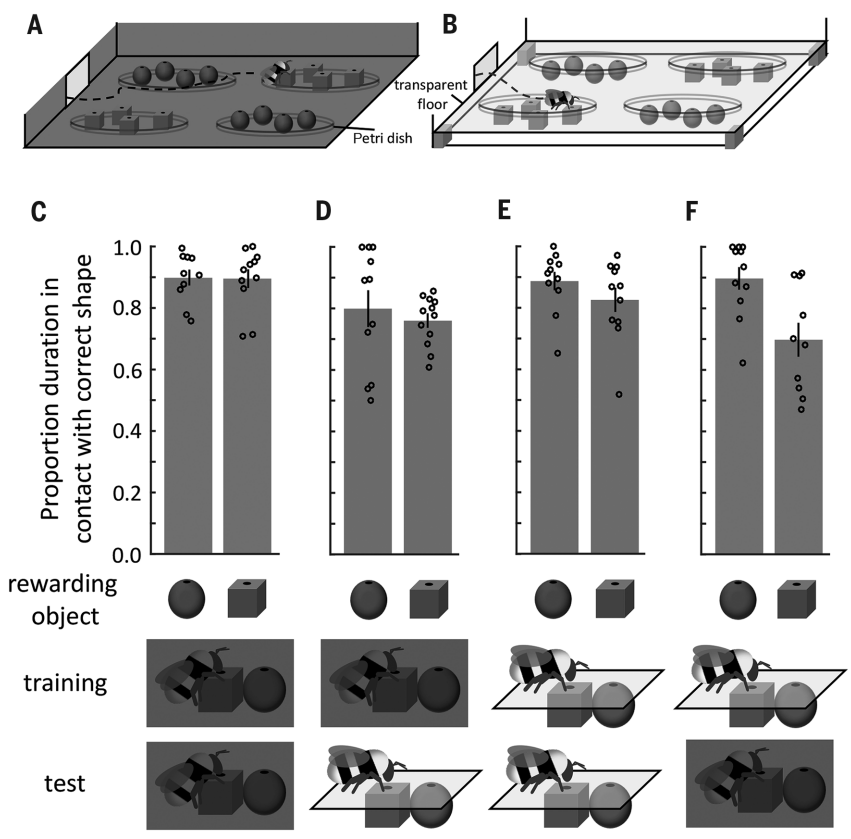

Fig. 1. Cross-modal recognition in bumble bees. (**A** and **B**) Setups for training and testing. Bumble bees were trained to find 50% sucrose solution in one of two differently shaped objects (sphere or cube) in one setup and then tested in the other. (A) In the dark setup, bees entered a dark arena and found two Petri dishes containing four spheres each and two Petri dishes containing four cubes each. (B) In the lighted setup, bees found the same objects, but placed under the Petri dishes so that the bees could see but not touch the objects. Bees accessed the reinforcement solution (rewarding sucrose solution or aversive quinine solution) through small holes in the top of each shape. (**C** and **D**) After being trained in the dark, bumble bees that were tested in the dark [(C) uni-modal] or in the light [(D) cross-modal] spent more time in contact with the previously rewarding object. (**E** and **F**) Similarly, after being trained in the light, bumble bees that were tested in the light [(E) uni-modal] or in the dark [(F) cross-modal] spent more time in contact with the previously rewarding object. Bars indicate mean; vertical lines indicate SEM; open circles indicate individual bees' data points (random *x* axis displacement for individual discernment).

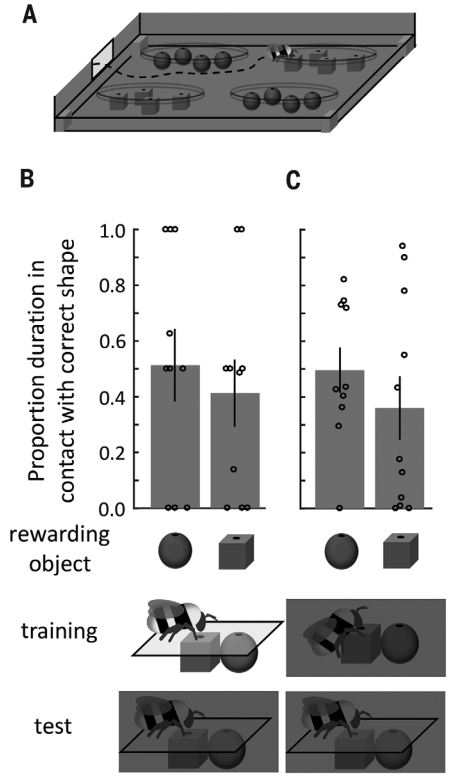

Fig. 2. Bumble bees were unable to see in the dark experimental conditions. (**A**) Setup for testing in control experiments. Bumble bees had no tactile information regarding the objects during these tests in the dark. (**B** and **C**) After being trained in the light (Fig. 1B) or in the dark (Fig. 1A), bumble bees that were tested in the dark, while not being able to touch the objects, had no difference in the amount of time they were in contact with the two different objects. Bars indicate mean; vertical lines indicate SEM; open circles indicate individual bees' data points (random *x* axis displacement for individual discernment).

We thus surmise that these areas are possible candidates for the multisensory integration necessary for the cross-modal object recognition behavior observed here.

Our results indicate more than just direct associations formed between two stimuli across senses, as is the case in simpler forms of cross-modal information transfer (*23*–*26*). Cross-modal object recognition requires that the two different senses provide information about the same object property (such as shape); that the information provided is encoded in such a way that it can be identified as related, even though it is temporally and physically distinct; and that this information is stored in a neuronal representation that is accessible by both senses (*8*).

Whether bumble bees solve the task by storing internal representations of entire object shapes (cube or sphere) or local object features (curved or flat edge) remains unknown. In either case, our experiments show that bumble bees are capable of recognizing objects across modalities, even though the received sensory inputs are temporally and physically distinct. Bumble bees show a kind of information integration that requires a modality-independent internal representation (*7*, *9*, *10*). This suggests that similar to humans and other large-brained animals, insects integrate information from multiple senses into a complete, globally accessible, gestalt perception of the world around them (*12*, *26*, *27*).

REFERENCES AND NOTES

1. M. O. Ernst, M. S. Banks, *Nature* **415**, 429–433 (2002).
2. S. Toprak, N. Navarro-Guerrero, S. Wermter, *Cognit. Comput.* **10**, 408–425 (2018).
3. H. F. Gaydos, *Am. J. Psychol.* **69**, 107–110 (1956).
4. R. K. Davenport, C. M. Rogers, *Science* **168**, 279–280 (1970).
5. A. Cowey, L. Weiskrantz, *Neuropsychologia* **13**, 117–120 (1975).
6. B. D. Winters, J. M. Reid, *J. Neurosci.* **30**, 6253–6261 (2010).
7. L. M. Herman, A. A. Pack, M. Hoffmann-Kuhnt, *J. Comp. Psychol.* **112**, 292–305 (1998).
8. S. Schumacher, T. Burt de Perera, J. Thenert, G. von der Emde, *Proc. Natl. Acad. Sci. U.S.A.* **113**, 7638–7643 (2016).
9. B. E. Stein, M. A. Meredith, *Ann. N. Y. Acad. Sci.* **608**, 51–70 (1990).
10. S. M. Kosslyn, in *Visual Cognition: An Invitation to Cognitive Science* (MIT Press, ed. 2, 1995), vol. 2, pp. 267–296.
11. M. Stoltz-Loike, M. H. Bornstein, *Psychol. Res.* **49**, 63–68 (1987).
12. C. Spence, in *Stevens' Handbook of Experimental Psychology and Cognitive Neuroscience* (American Cancer Society, 2018), pp. 1–56.
13. B. Nanay, *Cortex* **105**, 125–134 (2018).

14. J. Pearson, T. Naselaris, E. A. Holmes, S. M. Kosslyn, *Trends Cogn. Sci.* **19**, 590–602 (2015).
15. D. F. Marks, *Br. J. Psychol.* **90**, 567–585 (1999).
16. D. F. Marks, *Brain Sci.* **9**, 107 (2019).
17. J. S. B. T. Evans, *Thinking and Reasoning (Psychology Revivals): Psychological Approaches* (Psychology Press, 2013).
18. L. Chittka, N. M. Williams, H. Rasmussen, J. D. Thomson, *Proc. Biol. Sci.* **266**, 45–50 (1999).
19. B. De Gelder, P. Bertelson, *Trends Cogn. Sci.* **7**, 460–467 (2003).
20. P. G. Mobbs, The connections and spatial organization of the mushroom bodies, *Philos. Trans. R. Soc. London B Biol. Sci.* **298**, 309–354 (1982).
21. N. J. Strausfeld, *J. Comp. Neurol.* **450**, 4–33 (2002).
22. K. Pfeiffer, U. Homberg, Organization and functional roles of the central complex in the insect brain, *Annu. Rev. Entomol.* **59**, 165–184 (2014).
23. A. L. Yehle, J. P. Ward, *Psychon. Sci.* **16**, 269–270 (1969).
24. J. Guo, A. Guo, *Science* **309**, 307–310 (2005).
25. L. Proops, K. McComb, D. Reby, *Proc. Natl. Acad. Sci. U.S.A.* **106**, 947–951 (2009).
26. L. Mudrik, N. Faivre, C. Koch, *Trends Cogn. Sci.* **18**, 488–496 (2014).
27. O. Deroy *et al*., *Multisens. Res.* **29**, 585–606 (2016).

ACKNOWLEDGMENTS

Funding: This work was supported by European Research Council (ERC) grant SpaceRadarPollinator (grant 339347) and Engineering and Physical Sciences Research Council (EPSRC) grant Brains-on-Board (grant EP/P006094/1) awarded to L.C. **Author contributions:** C.S. conceived and designed the study, with input from L.C.; S.G.A.-K. and C.S. performed experiments and behavioral data analyses; C.S. performed statistical analyses; and C.S. and L.C. wrote the paper. **Competing interests:** None declared. **Data and materials availability:** Data are available in the supplementary materials.

SUPPLEMENTARY MATERIALS

science.sciencemag.org/content/367/6480/910/suppl/DC1
Material and Methods
Supplementary Text
Database S1
Reference (*28*)

View/request a protocol for this paper from *Bio-protocol*.

19 July 2019; accepted 15 January 2020
10.1126/science.aay8064

ENZYME REGULATION

Ancient origins of allosteric activation in a Ser-Thr kinase

Adelajda Hadzipasic[1,2]*, Christopher Wilson[1,2]†‡, Vy Nguyen[1,2]§, Nadja Kern[1,2]¶#, Chansik Kim[1,2], Warintra Pitsawong[1,2], Janice Villali[1,2]**, Yuejiao Zheng[1,2]††, Dorothee Kern[1,2]‡‡

A myriad of cellular events are regulated by allostery; therefore, evolution of this process is of fundamental interest. Here, we use ancestral sequence reconstruction to resurrect ancestors of two colocalizing proteins, Aurora A kinase and its allosteric activator TPX2 (targeting protein for Xklp2), to experimentally characterize the evolutionary path of allosteric activation. Autophosphorylation of the activation loop is the most ancient activation mechanism; it is fully developed in the oldest kinase ancestor and has remained stable over 1 billion years of evolution. As the microtubule-associated protein TPX2 appeared, efficient kinase binding to TPX2 evolved, likely owing to increased fitness by virtue of colocalization. Subsequently, TPX2-mediated allosteric kinase regulation gradually evolved. Surprisingly, evolution of this regulation is encoded in the kinase and did not arise by a dominating mechanism of coevolution.

Allosteric regulation, the process by which a protein's activity can be modulated by binding of an effector molecule distal to the active site, was first formalized more than half a century ago by the groundbreaking work of Monod, Wyman, and Changeux (*1*). Since then, allosteric regulation has been shown to be vital for cellular signaling processes ranging from oxygen transport to synaptic transmission to modulation of catalytic rates of enzymes (*2*–*4*). Given the central role of allosteric control, we wanted to experimentally explore how allosteric regulation developed along evolutionary pathways, a topic that has not been tackled before. We chose to examine the evolution of allosteric regulation for a modern Ser-Thr protein kinase because the vast majority of Ser-Thr kinases are regulated by two distinct allosteric mechanisms—phosphorylation and specific protein-protein interactions (Fig. 1A)—thereby providing signaling diversity. We chose Aurora A, an essential kinase for the cell cycle. Aberrant levels of Aurora A lead to improper centrosome maturation, spindle formation, mitotic entry, and enhanced cancerous growth (*5*–*7*). Binding of TPX2 (targeting protein for Xklp2) to the hydrophobic pocket of Aurora A both targets Aurora A to the spindle microtubules and allosterically activates the kinase (*8*, *9*).

First proposed by Linus Pauling and Emile Zuckerkandl, ancestor sequence reconstruction (ASR) allows for the recreation of ancestral proteins in the laboratory so that inferred pathways of evolution can be studied directly (*10*, *11*). By resurrecting ancestors of both Aurora A kinase and its activator TPX2 along the evolutionary path, we identify activation loop autophosphorylation as the oldest allosteric activation mechanism, followed by TPX2 regulation that evolved in a gradual fashion. The data expose the molecular mechanism of the evolving network in the kinase–allosteric activator pair and aid in defining the allosteric network in the modern kinase.

A Bayesian phylogeny and coestimated alignment of representatives of all known Aurora kinases and the closely related AGC and CAMK Ser-Thr protein kinases were constructed using the program package BAli-Phy (*12*). Interestingly, the resulting Aurora phylogentic tree has the kingdoms Animalia and Plantae adjacent to one another with Fungi more distantly related. This relationship does not match the widely accepted species tree nesting of Animalia and Fungi being more closely related to each other than to Plantae. Our Aurora kinase gene tree topology is not unique and has been observed in other inferred Aurora kinase gene phylogenies (*13*, *14*). Discrepancies between gene trees and species trees are common and can be caused by several factors, including unequal rates of evolution, gene duplication, and loss or horizontal gene transfer (*15*–*17*). Subsequently, the maximum a posteriori (MAP) phylogeny was used as the input for PAML (*18*) to infer the most probable ancestral sequences (Fig. 1B and fig. S1, A to C and E). Similarly, TPX2 homologs from various organisms were used to infer the TPX2 ancestor sequences (Fig. 1B and fig. S1D). A comparison of both trees guided by the phylogeny of the organisms reveals that although Aurora kinases are ubiquitous throughout the eukaryotic kingdom, TPX2 containing the Aurora A binding sequence is only present in certain plants and animal species but not in Protista or Fungi (*19*). This suggests that the appearance of TPX2 postdates that of the Aurora family (Fig. 1B) and indicates that Fungi lost the Aurora binding part of TPX2. The latter point provides a possible explanation of why the Aurora gene tree has Plantae closer to Animalia than Fungi.

We expressed and functionally characterized two Aurora kinase ancestor sequences (Aur_{ANC1} and Aur_{ANC2}) from an evolutionary period before the appearance of a canonical TPX2 motif and two additional ancestor sequences (Aur_{ANC3} and Aur_{ANC4}) with their corresponding TPX2 ancestor sequences ($TPX2_{ANC3}$ and $TPX2_{ANC4}$) (Fig. 1B and fig. S2). Owing to the later appearance of TPX2, we hypothesized that activation-loop autophosphorylation may have evolved first. Enzyme activity for dephosphorylated and phosphorylated Aurora forms was measured by monitoring phosphorylation of a peptide derived from the natural Aurora A kinase substrate Lats2 (large tumor suppressor kinase 2) (*5*) (Fig. 2 and figs. S3 and S4). All four ancestral Aurora kinases had very low activity in their dephosphorylated form. Importantly, all were activated by autophosphorylation of Thr^{288} (T288) to a similar extent (Fig. 2B). Surprisingly, we not only observed that T288 phosphorylation resulted in higher catalytic rates but also observed the evolution of additional regulation through tightening of the substrate Michaelis constant (K_M) upon phosphorylation starting with Aur_{ANC2} (Fig. 2B). The combination of both effects—increase in turnover number (k_{cat}) and decrease in K_M upon phosphorylation—yields an increased catalytic efficiency of more than 50-fold upon activation-loop phosphorylation for all Aurora forms tested (Fig. 2B).

How did the second mode of allosteric modulation by the activator TPX2 evolve? According to the widely held view of coevolution as "reciprocal evolutionary change in interacting species" (*20*), we might expect that only the evolutionarily matching partners display allosteric activation. For allosteric activation by a second protein, two events need to evolve: physical binding and an increase in kinase activity upon activator binding. We found that Aurora ancestors from the era before the appearance of TPX2 (Aur_{ANC1} and Aur_{ANC2}) bind very weakly to TPX2 forms (Fig. 3A and fig. S5), in agreement with our temporal matching of the two evolutionary trees. As soon as TPX2 became available, tight binding to Aurora was established. However, all of the more recently evolved Aurora ancestors (Aur_{ANC3} and Aur_{ANC4}), including human

[1]Department of Biochemistry, Brandeis University, Waltham, MA 02454, USA. [2]Howard Hughes Medical Institute, Brandeis University, Waltham, MA 02454, USA.
*Present address: Biotherapeutic and Medicinal Sciences, Biogen, Cambridge, MA 02142, USA. †Present address: Merkin Institute of Transformative Technologies in Healthcare, Broad Institute of Harvard and MIT, Cambridge, MA 02142, USA. ‡Present address: Department of Chemistry and Chemical Biology, Harvard University, Cambridge, MA 02138, USA. §Present address: Biomolecular Discovery, Relay Therapeutics, Cambridge, MA 02139, USA. ¶Present address: Department of Cellular and Molecular Pharmacology, University of California, San Francisco, Genentech Hall, MC 2200, Room N312E, 600 16th St., San Francisco, CA 94143, USA. #Present address: Howard Hughes Medical Institute, University of California, San Francisco, San Francisco, CA 94143, USA. **Present address: KSQ Therapeutics, 610 N. Main St., Cambridge, MA 02139, USA. ††Present address: Medical Scientist Training Program, Stony Brook University School of Medicine, Stony Brook, NY 11794, USA.
‡‡Corresponding author. Email: dkern@brandeis.edu

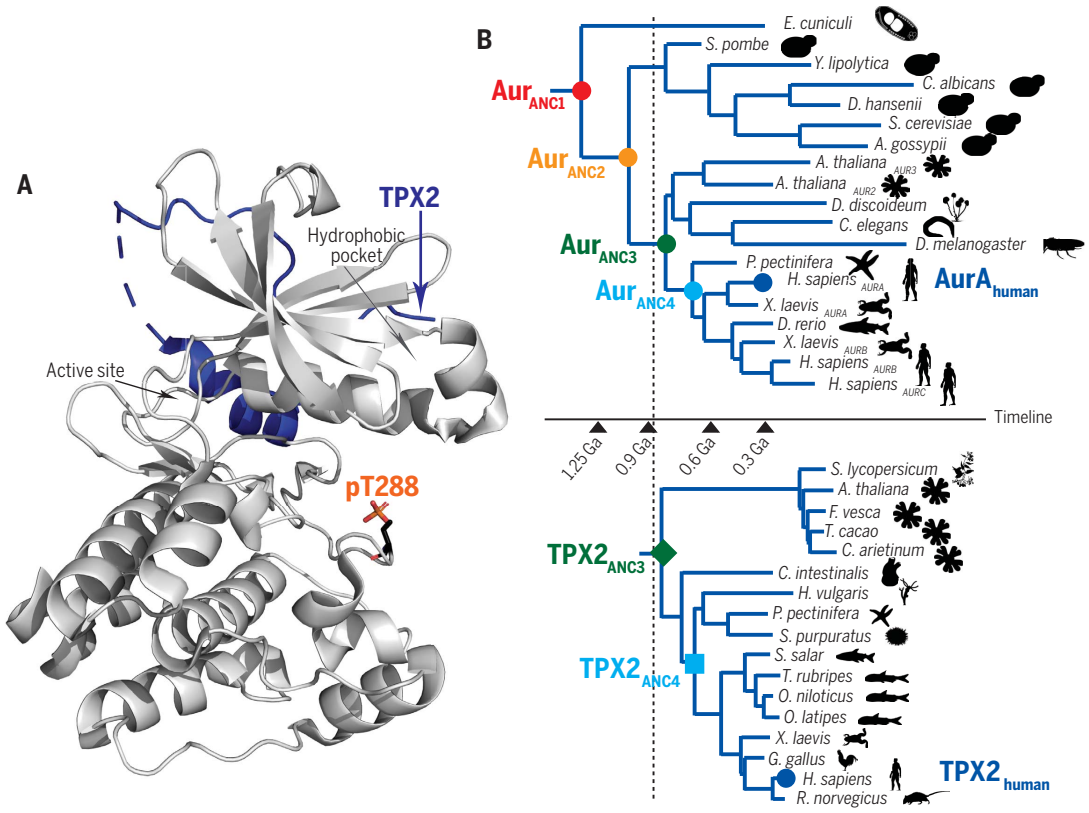

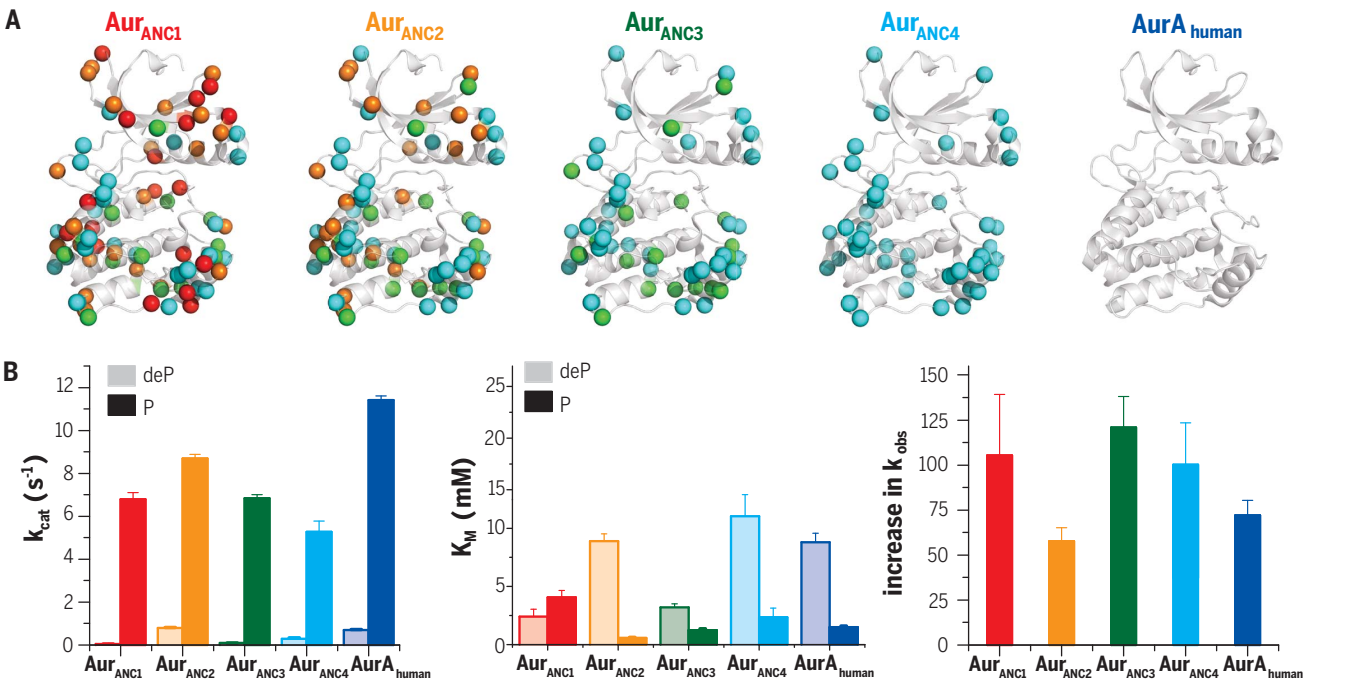

Fig. 1. Strategy to study the ancient origins of allosteric activation. (**A**) X-ray structure of human Aurora A kinase ($AurA_{human}$) bound to TPX2 [Protein Data Bank (PDB) 1OL5] illustrating two distinct $AurA_{human}$ allosteric activation mechanisms: binding of TPX2 to the $AurA_{human}$ hydrophobic pocket and phosphorylation of the activation loop at T288 (pT288). (**B**) Phylogenetic trees for Aurora kinase and TPX2 calculated using BAli-Phy (*12*) are shown together with a rough time estimate, indicating that the older ancestors of Aurora existed before the emergence of TPX2. The same color coding scheme for the species defined here is used throughout the figures. Ga, billion years ago.

Fig. 2. Autophosphorylation is the oldest and uniformly conserved allosteric activation mechanism in all Aurora kinases. (**A**) Additive differences in primary sequence between $AurA_{human}$ and Aur_{ANC4} (82.4% identity), Aur_{ANC3} (80.1% identity), Aur_{ANC2} (72.7% identity), and Aur_{ANC1} (69.5% identity) are shown in cyan, green, orange, and red spheres, respectively. (**B**) Corresponding k_{cat} (left) and K_M (middle) for dephosphorylated (deP, light color) and T288-phosphorylated (P, dark color) Aurora kinases show that phosphorylation increases catalytic efficiency by increasing k_{cat} and decreasing K_M (see also fig. S4). To best illustrate this combined effect, the fold increase in k_{obs} at 1 mM Lats2 upon Aurora's T288 phosphorylation is shown on the right. Phosphorylation of Lats2 peptide was monitored using the ADP-NADH (adenosine diphosphate–reduced nicotinamide adenine dinucleotide) coupled assay with 1 μM dephosphorylated or 0.05 μM phosphorylated Aurora and 5 mM adenosine triphosphate (ATP) and 20 mM $MgCl_2$ at 25°C. Error bars represent the standard error for the estimate of k_{cat} or K_M through the Michaelis-Menten equation and are a measure of the goodness of fit of the data. Error bars for the increase in k_{obs} represent standard error and were calculated using jackknifing and error propagation.

Aurora A ($AurA_{human}$), bind all TPX2 forms with similar affinities and not just their evolutionarily matching TPX2 partners (Fig. 3A and fig. S5). This suggests that efficient TPX2 binding to Aurora was established as soon as TPX2 appeared and remained stable throughout evolution. Indeed, the Aurora-TPX2–interaction surface residues remained extremely conserved starting from their initial appearance in Aur_{ANC3} and $TPX2_{ANC3}$ to the human species (Fig. 3B and fig. S2). We speculate that binding alone added an immediate evolutionary advantage by virtue of colocalization and delivery of the kinase to the spindle microtubules.

Other than this first act of increased fitness resulting from binding, how did allosteric activation by TPX2 evolve? By measuring the changes in kinase activity for Aur_{ANC3}, Aur_{ANC4}, and $AurA_{human}$ in the presence of the matching TPX2 partners $TPX2_{ANC3}$, $TPX2_{ANC4}$, and $TPX2_{human}$, respectively, a gradual increase in allosteric activation is observed (2× → 5× → 10× increase in enzymatic rate in the presence of $TPX2_{ANC3}$, $TPX2_{ANC4}$, and $TPX2_{human}$, respectively) (Fig. 3, C and D). Crucially, this gradual allosteric activation is predominantly encoded in the evolution of the kinase because the "mismatched" TPX2 forms also create this effect. Only a small additional increase in the observed catalytic rate constant at 1 mM substrate (k_{obs}) is measured for $TPX2_{ANC4}$ and $TPX2_{human}$ relative to older $TPX2_{ANC3}$ in activating Aur_{ANC4} and $AurA_{human}$ (Fig. 3, C and D). To test the robustness of the ancestral reconstructions for these key findings, we sampled alternates from the ancestral posterior probability distribution for the key nodes Aur_{ANC2} and Aur_{ANC3} (fig. S6) (*21*). Activity, binding, and allosteric activation by TPX2 for these alternates buttress our conclusions (fig. S7).

Because our data do not support a dominating mechanism of reciprocal change in the

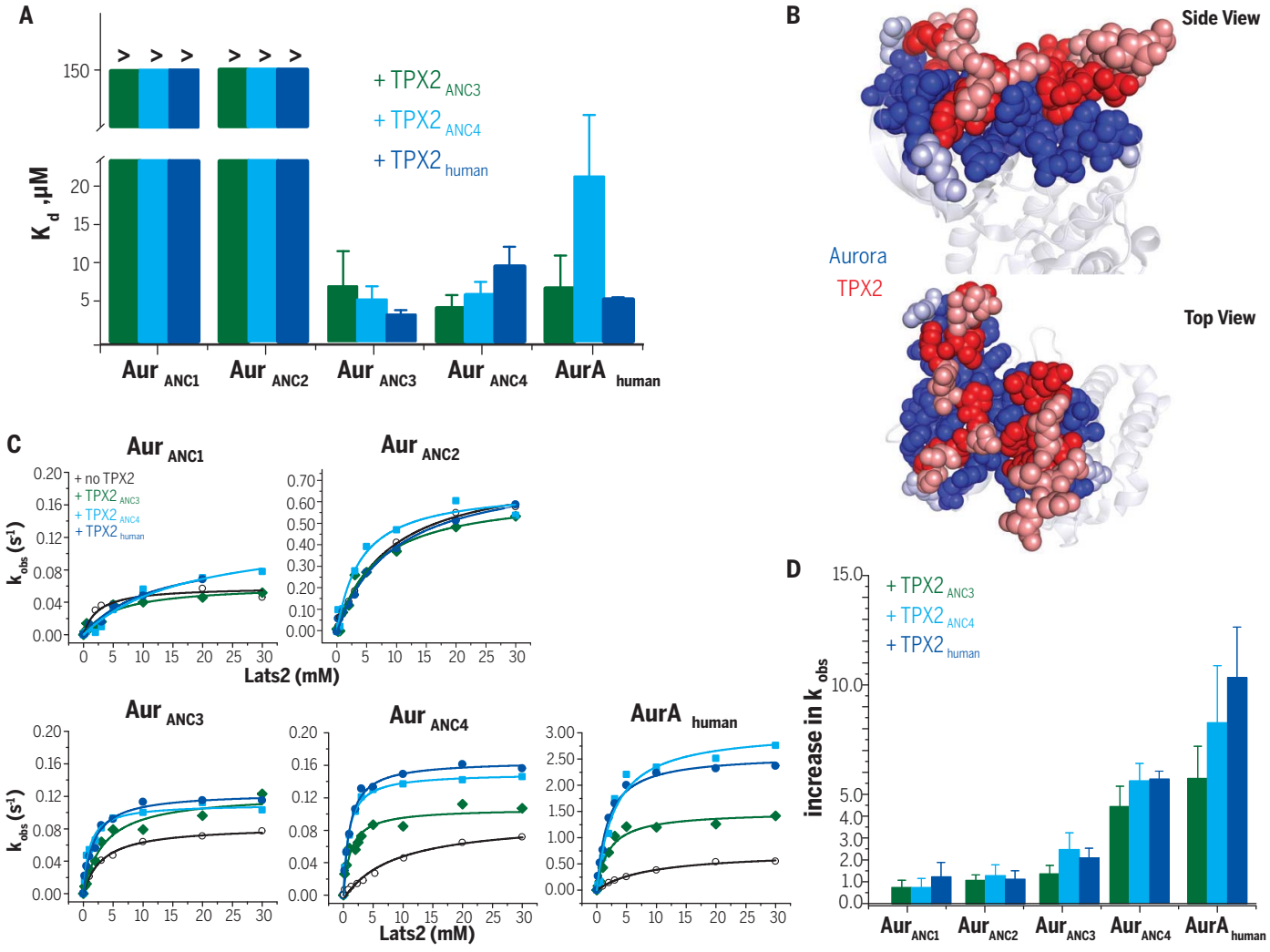

Fig. 3. Allosteric activation through TPX2 binding is a more recent, gradually dialed in, regulatory adaptation for Aurora kinases. (**A**) Dissociation constants (K_d) of ancestral and modern TPX2 constructs binding to all Aurora kinases, as measured by isothermal titration calorimetry (ITC). The ">" above the bars indicates >150 μM. (**B**) Conservation of the Aurora (blue)–TPX2 (red) interface residues. Evolutionarily conserved residues in Aur_{ANC3}, Aur_{ANC4}, and $AurA_{human}$ (dark blue) and in $TPX2_{ANC3}$, $TPX2_{ANC4}$, or $TPX2_{human}$ (dark red) are plotted onto the interface zoom-in of the $AurA_{human}$–TPX2 x-ray structure (PDB 1OL5) highlighting interface residues that are within 5 Å in van der Waal's contacts. (Nonconserved residues are in light blue and light red.) (**C**) Michaelis-Menten plots of ancestral and $AurA_{human}$ in the absence and presence of $TPX2_{ANC3}$, $TPX2_{ANC4}$, or $TPX2_{human}$. In the assays, 100 μM TPX2 (for Aur_{ANC3}, Aur_{ANC4}, or $AurA_{human}$, assuring saturation) and 500 μM TPX2 (for Aur_{ANC1} or Aur_{ANC2}) were used. (**D**) Gradual evolution of allosteric Aurora kinase activation by TPX2 binding illustrated as the fold increase in k_{obs} at 1 mM Lats2. Activity assays were carried out as described above. Error bars in (A) represent the standard error for the estimate of K_d from the isotherms and are a measure of the goodness of fit of the data. Error bars for the increase in k_{obs} in (D) represent standard error and were calculated using jackknifing and error propagation.

coevolution of allosteric activation, we felt the need for additional tests for our new model and turned to Aurora B ($AurB_{human}$), a close, allosterically activated homologous protein to Aurora A. First, $AurB_{human}$'s allosteric activation partner INCENP, which has no similarity to TPX2, can activate Aurora A by the same amount as TPX2, although INCENP binding is weaker (fig. S8). This means that the evolution of specificity between Auroras and their corresponding allosteric partners happened on the level of affinity, and the origin of allosteric activation is indeed encoded in the kinase with almost no reciprocal changes occurring in TPX2 to facilitate increased allosteric activation. Second, coevolution between the kinase and the substrate was ruled out by repeating all activity experiments with a second, generic, synthetic substrate, kemptide. The allosteric activation measured using kemptide is within experimental error of that measured using the natural substrate Lats2 (fig. S9). Third, none of the TPX2 forms allosterically increased the activity of Aurora ancestors from the precanonical-TPX2 era (Aur_{ANC1} and Aur_{ANC2}), even at very high TPX2 concentrations where a substantial fraction of these Aurora ancestors is in the TPX2-bound state (Fig. 3, C and D).

If the evolution of Aurora itself is the origin of allosteric control, can the allosteric network in the kinase be identified? Ancestral resurrection provides a tractable approach to this question, because Aur_{ANC2} lacking allosteric

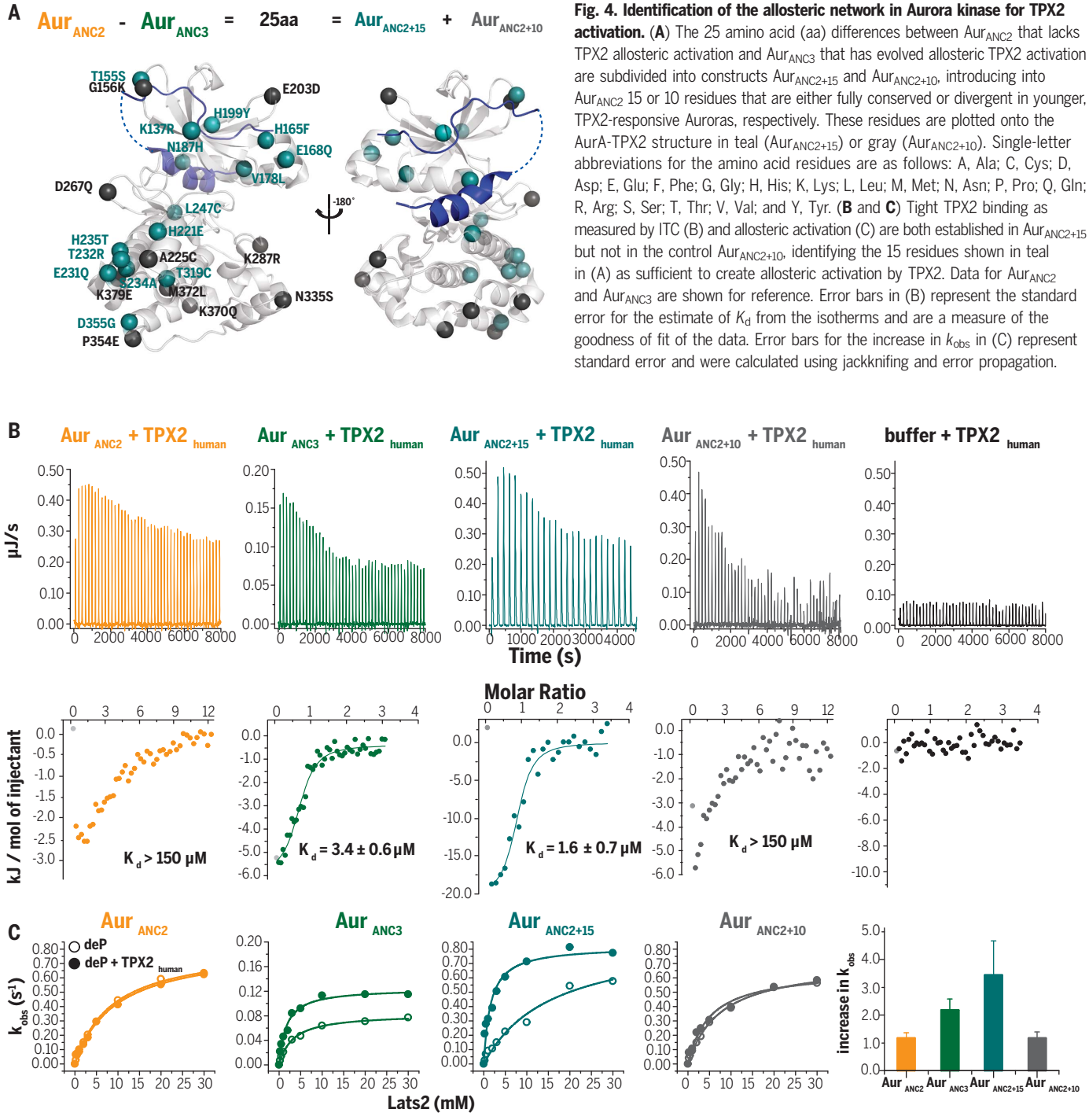

Fig. 4. Identification of the allosteric network in Aurora kinase for TPX2 activation. (**A**) The 25 amino acid (aa) differences between Aur_{ANC2} that lacks TPX2 allosteric activation and Aur_{ANC3} that has evolved allosteric TPX2 activation are subdivided into constructs $Aur_{ANC2+15}$ and $Aur_{ANC2+10}$, introducing into Aur_{ANC2} 15 or 10 residues that are either fully conserved or divergent in younger, TPX2-responsive Auroras, respectively. These residues are plotted onto the AurA-TPX2 structure in teal ($Aur_{ANC2+15}$) or gray ($Aur_{ANC2+10}$). Single-letter abbreviations for the amino acid residues are as follows: A, Ala; C, Cys; D, Asp; E, Glu; F, Phe; G, Gly; H, His; K, Lys; L, Leu; M, Met; N, Asn; P, Pro; Q, Gln; R, Arg; S, Ser; T, Thr; V, Val; and Y, Tyr. (**B** and **C**) Tight TPX2 binding as measured by ITC (B) and allosteric activation (C) are both established in $Aur_{ANC2+15}$ but not in the control $Aur_{ANC2+10}$, identifying the 15 residues shown in teal in (A) as sufficient to create allosteric activation by TPX2. Data for Aur_{ANC2} and Aur_{ANC3} are shown for reference. Error bars in (B) represent the standard error for the estimate of K_d from the isotherms and are a measure of the goodness of fit of the data. Error bars for the increase in k_{obs} in (C) represent standard error and were calculated using jackknifing and error propagation.

activation and Aur_{ANC3} exhibiting allosteric activation differ by only 25 amino acids. Eighteen of those residues are fully conserved in Aur_{ANC3}, Aur_{ANC4}, and $AurA_{human}$ but not in Aur_{ANC1} and Aur_{ANC2}. Three of those 18 residues are not conserved in $AurB_{human}$ (fig. S10A). Therefore, the 15 remaining fully conserved residues were introduced into Aur_{ANC2} ($Aur_{ANC2+15}$) with the goal of creating allosteric regulation (Fig. 4A). As a control, the nonconserved 10 amino acids were introduced into Aur_{ANC2} ($Aur_{ANC2+10}$). Both engineered kinases are fully active enzymes when phosphorylated on the activation loop T288 (fig. S10B). $Aur_{ANC2+15}$ showed full restoration of TPX2 binding as well as allosteric activation, as seen in Aur_{ANC3} (Fig. 4, B and C), suggesting that this network of residues is sufficient to encode for the allosteric response in $AurA_{human}$. Importantly, a further reduction of this network into fewer residues that include only the subset located around the R or C spine did not result in allosteric response (fig. S11), buttressing our model of an extended network in Aurora as the origin of allosteric activation by the partner TPX2. $Aur_{ANC2+10}$ lacks both the ability to bind TPX2 and to be activated by it and is identical to the original Aur_{ANC2} in these properties. We note that these experiments do not show that all 15 residues together are responsible for converting a nonregulated Aurora into an allosterically regulated Aurora but that at least a subset of this combination of those nine and six residues is essential. This allosteric network for activation by TPX2 is different from that responsible for activation through activation-loop T288 phosphorylation and spans the entire kinase from the TPX2-binding site on top of the N lobe to the C lobe (Fig. 4A and fig. S11A).

Exposing the molecular mechanism of evolving two distinct allosteric regulations in one kinase reveals general evolutionary principles as well as new knowledge about the nature of allosteric networks in the modern kinase. Autophosphorylation of the activation loop as the most ancient activation mechanism can be rationalized because the catalytic machinery for kinase activity was already present during early eukaryotic evolution and was exploited for autoregulation. Around 1 billion years ago, with the appearance of the microtubule-associated protein TPX2, Aurora evolved binding to TPX2. This initial binding event may have provided an evolutionary advantage through direct localization of Aurora to the mitotic spindle, and binding remained constant up to modern days. Our data reveal strong coconservation over long evolutionary periods for the protein-protein interaction (Fig. 3B and fig. S2). As the last evolutionary event, successive mutations in the kinase gradually dialed in allosteric activation upon TPX2 binding but with almost no coevolution (Fig. 3), contrary to the notion of reciprocal change for such interactions.

The phenomenon of allosteric coevolution has been of intense interest because it poses a distinct challenge to Darwinian evolution (*22*–*25*). On one hand, it would seem that the two proteins making up the system would have to evolve simultaneously to function correctly, a challenge referred to as the "irreducibly complex system" problem (*22*). This would require both the kinase and its modulator to be "preset" for allosteric control, a statistically unlikely occurrence. On the other hand, if evolutionary complexity could be reduced by a step-wise evolution starting with colocalization of proteins followed by evolving allostery, this would allow for nonspecific surface residue contacts to evolve into productive interactions (*23*), followed by mutations only in the kinase domain to evolve allosteric regulation. This perceptive model of colocalization as the first step toward allostery was logically derived in a thoughtful review by Kuriyan and Eisenberg (*23*).

Colocalization as a catapult toward coevolution in signaling has traditionally been explored in two-component signal transduction systems using directed evolution and computational biology (*26*, *27*). Although very powerful, these techniques lack information on intermediates along the allosteric evolution continuum, starting with the primitive ancestral forms, because they investigate only modern sequences (*28*). More recently, the elegant study by Coyle *et al*. (*29*) on allosteric regulation of mitogen activated protein (MAP) kinase by its effector Fus3 suggested that more primitive protein MAP kinases have a rugged conformational landscape yielding a diverse set of potential allosteric sites that could be explored by the regulator Fus3. Although this proposed evolutionary model is compelling, the study again relied on comparison of only modern-day proteins, therefore not providing direct evidence for evolutionary pathways. Given the generality of autophosphorylation and protein-protein interaction in kinase signaling, resurrecting evolutionary pathways to understand kinase regulation, as established here for Aurora A kinase, promises to illuminate how differential signaling in the protein kinase superfamily evolved, a question highlighted and discussed in a recent review (*30*). Moreover, this new approach led to the identification of a subset of residues that created allosteric activation in Aurora, therefore opening a new potential for characterizing atomistic differences between allosteric regulatory networks in the kinase superfamily that can further be exploited in the design of specific allosteric inhibitors or activators.

REFERENCES AND NOTES

1. J. Monod, J. Wyman, J. P. Changeux, *J. Mol. Biol.* **12**, 88–118 (1965).
2. J. P. Changeux, *Annu. Rev. Biophys.* **41**, 103–133 (2012).
3. R. Nussinov, C. J. Tsai, *Curr. Opin. Struct. Biol.* **30**, 17–24 (2015).
4. P. Tompa, *Chem. Soc. Rev.* **45**, 4252–4284 (2016).
5. S. Toji *et al*., *Genes Cells* **9**, 383–397 (2004).
6. D. M. Glover, M. H. Leibowitz, D. A. McLean, H. Parry, *Cell* **81**, 95–105 (1995).
7. H. Zhou *et al*., *Nat. Genet.* **20**, 189–193 (1998).
8. T. A. Kufer *et al*., *J. Cell Biol.* **158**, 617–623 (2002).
9. A. Zorba *et al*., *eLife* **3**, e02667 (2014).
10. L. Pauling, E. Zuckerkandl, *Acta Chem. Scand.* **17**, S9–S16 (1963).
11. M. J. Harms, J. W. Thornton, *Nat. Rev. Genet.* **14**, 559–571 (2013).
12. B. D. Redelings, M. A. Suchard, *Syst. Biol.* **54**, 401–418 (2005).
13. J. R. Brown, K. K. Koretke, M. L. Birkeland, P. Sanseau, D. R. Patrick, *BMC Evol. Biol.* **4**, 39 (2004).
14. H. Li *et al*., *Eukaryot. Cell* **7**, 894–905 (2008).
15. R. Nichols, *Trends Ecol. Evol.* **16**, 358–364 (2001).
16. P. Pamilo, M. Nei, *Mol. Biol. Evol.* **5**, 568–583 (1988).
17. D. A. Baum, S. D. Smith, *Tree Thinking: An Introduction to Phylogenetic Biology* (Macmillan Learning, 2012).
18. Z. Yang, *Mol. Biol. Evol.* **24**, 1586–1591 (2007).
19. G. Goshima, *PLOS ONE* **6**, e28120 (2011).
20. J. N. Thompson, *The Coevolutionary Process* (Univ. Chicago Press, 1994).
21. E. A. Gaucher, S. Govindarajan, O. K. Ganesh, *Nature* **451**, 704–707 (2008).
22. M. J. Behe, *Darwin's Black Box: The Biochemical Challenge to Evolution* (Free Press, ed. 2, 2006).
23. J. Kuriyan, D. Eisenberg, *Nature* **450**, 983–990 (2007).
24. M. Soskine, D. S. Tawfik, *Nat. Rev. Genet.* **11**, 572–582 (2010).
25. J. D. Bloom, F. H. Arnold, *Proc. Natl. Acad. Sci. U.S.A.* **106** (suppl. 1), 9995–10000 (2009).
26. E. J. Capra, M. T. Laub, *Annu. Rev. Microbiol.* **66**, 325–347 (2012).
27. W. R. Whitaker, S. A. Davis, A. P. Arkin, J. E. Dueber, *Proc. Natl. Acad. Sci. U.S.A.* **109**, 18090–18095 (2012).
28. M. E. Salazar, M. T. Laub, *Curr. Opin. Microbiol.* **24**, 7–14 (2015).
29. S. M. Coyle, J. Flores, W. A. Lim, *Cell* **154**, 875–887 (2013).
30. N. H. Shah, J. Kuriyan, *Nat. Struct. Mol. Biol.* **26**, 25–34 (2019).

ACKNOWLEDGMENTS

We thank D. Theobald for general discussions about evolutionary concepts. **Funding:** This work was supported by the Howard Hughes Medical Institute; U.S. Department of Energy, Office of Basic Energy Sciences, Catalysis Science Program, award DE-FG02-05ER15699; and NIH (GM100966) to D.K. C.W. is the Marion Abbe Fellow of the Damon Runyon Cancer Research Foundation (DRG-2343-18). **Author contributions:** A.H., C.W., and D.K. developed the research plan and experimental strategy. A.H. built TPX2 phylogeny and calculated ancestral sequences with guidance from C.W., adapted the ADP-NADH and high-performance liquid chromatography kinase assays to the Aurora-TPX2 system, and designed mutants and ITC runs. C.W. built the kinase phylogeny and calculated ancestral sequences. A.H., V.N., N.K., J.V., and Y.Z. purified proteins and carried out ITC and kinase assays. W.P. and C.K. performed the same biochemical experiments for the alternate ancestors resurrected from the posteriors. A.H., C.W., V.N., and D.K. wrote the manuscript. All authors contributed to data interpretation and commented on the manuscript. **Competing interests:** D.K. is co-founder of Relay Therapeutics. D.K. and A.H. are the inventors on pending patents applied for by Brandeis University that describe compositions and methods for modulating kinase activity (US20180334510A1 and US20190038582A1), and D.K. is an inventor on pending patents of a Biophysical platform for drug development based on energy landscape (PCT/US2016/15171). The remaining authors declare no competing interests. **Data and materials availability:** All data are available in the main text or the supplementary materials.

SUPPLEMENTARY MATERIALS

science.sciencemag.org/content/367/6480/912/suppl/DC1
Materials and Methods
Figs. S1 to S11
References (*31*–*38*)

View/request a protocol for this paper from *Bio-protocol*.

4 August 2019; resubmitted 9 December 2019
Accepted 15 January 2020
10.1126/science.aay9959

BIOCATALYSIS

Biocatalytic synthesis of planar chiral macrocycles

Christina Gagnon, Éric Godin, Clémentine Minozzi, Johann Sosoe, Corentin Pochet, Shawn K. Collins*

Macrocycles can restrict the rotation of substituents through steric repulsions, locking in conformations that provide or enhance the activities of pharmaceuticals, agrochemicals, aroma chemicals, and materials. In many cases, the arrangement of substituents in the macrocycle imparts an element of planar chirality. The difficulty in predicting when planar chirality will arise, as well as the limited number of synthetic methods to impart selectivity, have led to planar chirality being regarded as an irritant. We report a strategy for enantio- and atroposelective biocatalytic synthesis of planar chiral macrocycles. The macrocycles can be formed with high enantioselectivity from simple building blocks and are decorated with functionality that allows one to further modify the macrocycles with diverse structural features.

Macrocycles are capable of simultaneously displaying extended molecular frameworks while retaining some conformational bias (*1*, *2*). The cyclic skeleton can even impart severe restrictions on bond rotations that can lock functional groups or other molecular fragments in conformations that would be otherwise unfavorable in an acyclic analog (*3*, *4*). Such is the case in planar chiral cyclophanes, a subset of macrocycles for which conformation (or size) limits the rotation of an aromatic unit within the skeleton.

The presence of planar chirality in natural product terpenes as well as macrocyclic peptides is well documented, and atropisomerism has become increasingly apparent in drug discovery (Fig. 1A) (*5*–*7*). As such, methods for forming peptidic cyclophanes have attracted increased attention. However, in most cases, synthetic methods face the steep challenge of having to form the rigidified and often strained macrocycle itself while simultaneously imparting high levels of enantioselection. Consequently, atroposelective macrocyclizations are rare and can be classified into two synthetic strategies (Fig. 1B). Most protocols employ auxiliaries that enforce conformations of the acyclic precursor through noncovalent interactions (*8*, *9*). Much more rare are instances in which catalysis is exploited to induce asymmetry during the formation of the cyclophane (*10*, *11*).

Although macrocyclization has been examined via biocatalysis (*12*–*16*), the preparation of prevalent planar chiral macrocycles has largely been ignored. This is surprising given that biocatalysis has had a profound impact on the synthesis of crucial chiral building blocks such as secondary alcohols and amines (*17*–*21*). In particular, the dynamic kinetic resolution (DKR) developed by Bäckvall and co-workers is a strategy involving transition metal catalysis and biocatalysis working in concert. The process involves a transition metal complex that catalyzes racemization of a substrate (in general, a secondary alcohol or amine) and an enzyme (typically a lipase) that selectively acylates one enantiomer forming an ester or amide (*22*). A subsequent step is then required to access the desired alcohol and amine through deacylation (Fig. 1C). In examining whether an analogous process could be applied to the preparation of planar chiral macrocycles, several differences from the standard DKR are apparent (Fig. 1D). First, in DKR protocols, the acylation is only temporary, as the free alcohol or amine is typically desired. In addition, the acylating agent can be added in excess to improve reaction rates and yields. In a macrocyclization process, the acylation is inherent in the final product and the stoichiometry between alcohol and acylating agent is naturally fixed. Second, in the absence of secondary alcohols, a different racemization process must be used. Despite the challenges, a biocatalytic DKR process to access planar chiral cyclophanes has considerable potential: The thermal stabilities and high enantioselectivities observed with commercially available lipases make them ideal for macrocyclization processes, and the simple building blocks required allow one to rapidly build complexity in a chiral architecture.

A key goal in the development of a chemoenzymatic synthesis of planar chiral macrocycles was to permit synthesis from common and simple building blocks. As such, we envisioned exploiting common diacids or diesters as aliphatic linkers (**A**, Fig. 1D). The chemoenzymatic macrocyclization would take place via sequential acylations using a lipase on an aromatic diol **B** (Fig. 1D) that possessed core functionality amendable to diversification and applicability to drug discovery efforts.

In contrast to the classic DKR process, racemization of intermediate **C** occurs through free rotation of the aromatic ring. Several challenges exist for the chemoenzymatic macrocyclization. The ring-closing event would result in a rigidified macrocycle, and the enzyme must be able to promote such a ring closure. We expected that elevated temperatures could be used to promote macrocyclization, but we were conscious of possibly degrading the enzyme or affecting the conformational stability of the cyclophane (i.e., at what temperature the ansa-bridge would be able to freely rotate and racemize the desired macrocycle). To help favor macrocyclization, longer diesters **A** could be employed, but the aromatic substituents R^1 would have to be bulkier to restrict the rotation of the ansa-bridge. The size of the R^1 substituents is also critical, as they must affect the selectivity of the enzyme but not negatively influence the reactivity.

Given the previous success of the serine hydrolase *Candida antarctica* lipase B (CALB) (*23*, *24*) in DKR of secondary alcohols (*25*, *26*), we used the enzyme in our synthesis of [13]paracyclophanes by macrolactonization of benzylic diols (Fig. 2A). We tested a molecule with an unsubstituted aromatic core (**1a**) and isolated the desired achiral macrocycle **3a** in reasonable yield. Having demonstrated that CALB could promote the macrocyclization, we examined a subsequent cyclization having an aromatic core substituted with OMe (methoxy) groups (**1b**), but the yield of the corresponding [13]paracyclophane **3b** was only 10%. In addition, variable temperature nuclear magnetic resonance (VT NMR) analysis of the benzylic proton signals (highlighted in green, Fig. 2A) showed coalescence of the signals at 50°C. Macrocyclization employing larger bromo substituents (diol **1c**) was even less successful, most likely due to an unfavorable steric clash between the ortho-substituted benzylic diol and the enzyme active site. We redesigned the starting diol with an inserted methylene group next to the aromatic core (**5**, Fig. 2B). With the extended diol, we obtained the desired [14]paracyclophane **6** in good yield and high enantioselectivity. VT NMR analysis of the benzylic proton signals of **6** showed no coalescence of the signals even at 100°C. Although lowering the temperature decreased the yield of **6**, raising the temperature had no beneficial effect on yield and did not promote rotation of the ansa-bridge, which would lower the overall enantiopurity.

Although CALB tends to favor acylation of *R*-centered carbon chiral centers (*27*), it was unknown how the CALB active site, which has naturally evolved to differentiate the geometry of tetrahedral carbons centers, would accommodate the prochiral aromatic plane of the forming macrocycle. To better understand how the active site environment might engage different conformations of the cyclophane substrate, we performed docking with the program Fitted (*28*, *29*) from the Forecaster computational platform (Fig. 2C) (*30*). Lee and co-workers previously reported an x-ray crystal structure of CALB bound to a phosphonate inhibitor (PDB ID 5GV5) (*31*). We replaced the phosphonate inhibitor with each atropisomer of the macrocycle and examined

Département de Chimie, Centre for Green Chemistry and Catalysis, Université de Montréal, CP 6128 Station Downtown, Montréal, Québec H3C 3J7, Canada.
*Corresponding author. Email: shawn.collins@umontreal.ca

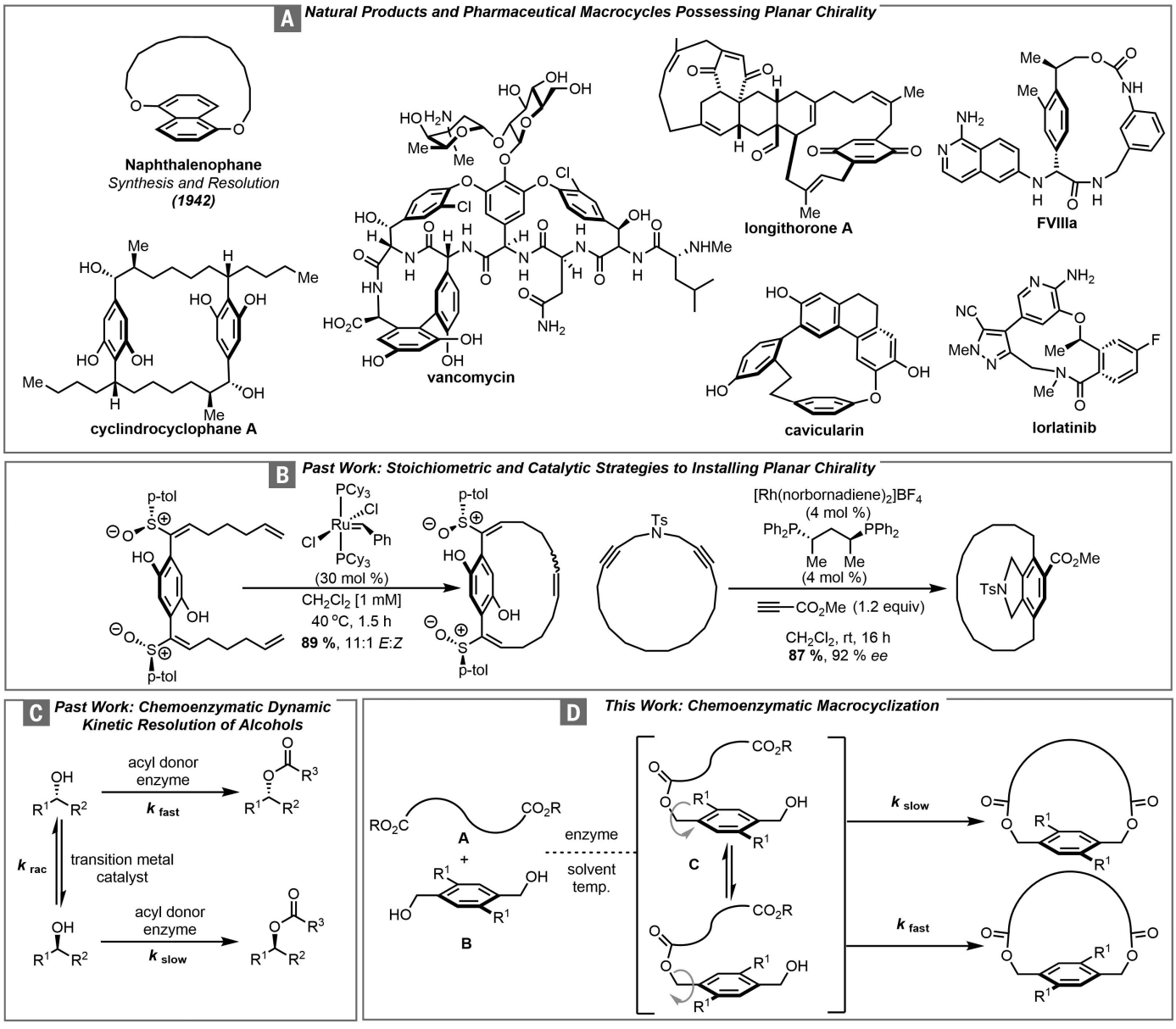

Fig. 1. Planar chirality in macrocycles. (**A**) Examples of planar chiral macrocycles in natural products and pharmaceuticals. (**B**) Methods for installing planar chirality in macrocycles. (**C** and **D**) Notable concepts for a proposed chemoenzymatic synthesis of planar chiral macrocycles. Me, methyl; p-tol, *p*-toluene; Cy, cyclohexyl; Ph, phenyl; Ts, tosyl; R, H, aryl; R^1, alkyl, aryl, halogen; R^2, alkyl, aryl; rt, room temperature; k_{rac}, rate of racemic reaction.

the binding mode suggested by docking (*32*). The major product (–)-**6** is oriented with its carboxyl groups toward the nearby catalytic serine residue (Ser^{105}), with one of the bromine substituents pointing toward the exterior of the active site. The opposite enantiomer is translated by >2.5 Å in the docking model, which suggests that the serine-catalyzed reaction would be geometrically challenging. The projected translation of (+)-**6** results from a clash between a bromine atom and Leu^{140}, precluding binding of the bromine atom into the hydrophobic site delineated by Leu^{140}, Ala^{141}, and Leu^{144}. In a docking of the starting dibromo diol **5**, it fits into the cavity with its alcohol extending toward the catalytically active serine. Indeed, even a monoesterified intermediate orients itself within the active site with its carboxylate toward the serine residue and the bromine substituents in a conformation mirroring that of the desired cyclophane. The biocatalytic synthesis of [14]paracyclophane **6** could be easily reproduced on the gram scale (see supplementary materials), and we proceeded to explore the substrate scope with regard to ring size. Although the dibromo cyclophane **6** could be obtained by using a diacid with a 6-methylene spacer [-$(CH_2)_6$-], reducing the spacer to four or five methylene units did not substantially increase ring strain, and the resulting [12]- and [13]paracyclophanes were obtained in good yields and high enantioselectivities (Fig. 3). This series of macrocycles could be prepared with chlorine or iodine atoms replacing the bromine substituents. The resulting [12]-, [13]-, and [14]paracyclophanes (**10**→**12**) were all isolated with comparable yield and enantiopurity, despite variation in the size of the halogen substituent.

Extending the ansa-bridge by an additional methylene spacer provided a good yield of [15]paracyclophane **9**; however, the product was isolated as a racemic mixture, suggesting that the larger aliphatic ring no longer constrained rotation of the planar cyclophane. The

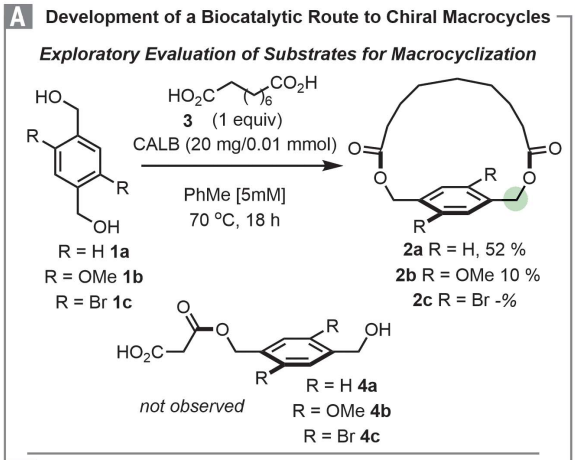

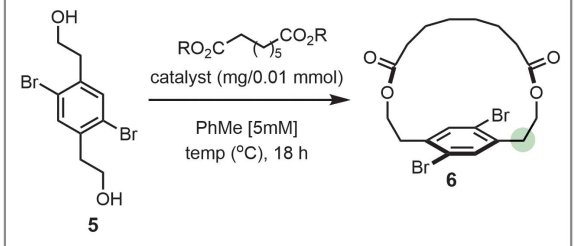

R	Catalyst	Temp (°C)	Yield (%)[a]	ee (%)[b]
H	CALB (20 mg)	50	47	>99
H	CALB (20 mg)	70	80[c,d]	>99
H	CALB (20 mg)	90	69	>99
H	CALB (10 mg)	70	69	>99
H	CALB (40 mg)	70	80	>99
H	CALB (20 mg)	70	77[e]	>99
H	CALB (20 mg)	70	63[f]	>99
H	CALA (20 μL)	70	16	96
C_6F_5	CALB (20 mg)	70	78	>99

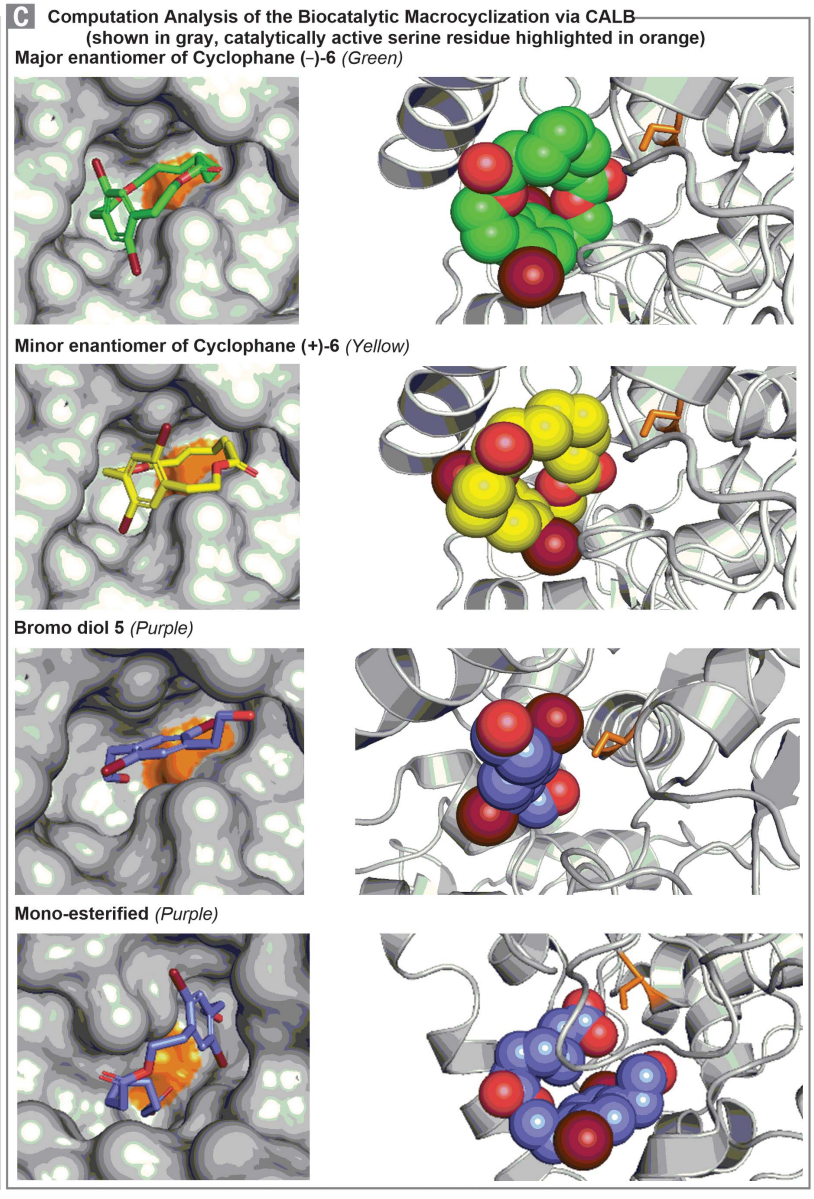

Fig. 2. Biocatalytic synthesis of planar chiral macrocycles employing a lipase CALB. (**A** and **B**) Development of the biocatalytic macrocyclization. Green highlighted areas indicate methylene units monitored by VT NMR. [a]Isolated yields (0.1-mmol scale). [b]Determined by chiral SFC high-performance liquid chromatography analysis. See supplementary materials for details. [c]Extending reaction time to 48 hours: 81% **6**, >99% enantiomeric excess (ee). [d]Using MeCN as solvent: 16% **6**, >99% ee. [e][2.5 mM]. [f][10 mM]. (**C**) Computational docking of products and intermediates to CALB.

larger size of the iodine allowed for the synthesis of the enantioenriched [15]paracyclophane **17**. To investigate whether the active site of the enzyme could tolerate more functionalized ansa-bridges, we prepared two different macrocycles that have rigidified 1,3-diynes in their backbones with phenyl-substituted (**18**) and alkynyl-substituted (**19**) cores, as well as a [14]paracyclophane **20** that has a disulfide bridge, a common motif found in bioactive macrocyclic peptides (*33*). A series of functionalized aromatic diols were also well tolerated in the macrocyclization process. The terphenyl-based macrocycle **21** could be formed via macrocyclization as could similarly substituted *p*-anisoyl and *m*-anisoyl cyclophanes (**22** and **23**, respectively) with high enantioselectivity. We were also able to synthesize [14]paracyclophanes **24** and **25**, which have cores with either phenylalkynyl or hexynyl substituents. Heteroatom-containing functional groups such as the *p*-methylaniline substituents present in macrocycle **26** could also be installed within the chiral macrocyclic frameworks. Finally, C_1-symmetric derivatives were formed in high enantioselectivity. Macrocycle **27** was isolated with one iodide substituent and one alkynyl unit, whereas macrocycle **28** was isolated with one bromide substituent and a C_{sp}^3-hybridized motif (benzyl). Notably, the halogen-containing planar chiral macrocycles can act as a platform for the synthesis of other derivatives through modern cross-coupling techniques (*34*). For example, the macrocycle **29** was prepared having Bpin (pinacolatoboron) functionality via Miyaura borylation. The bromo-substituted cyclophane **6** could be subjected to Heck coupling to form macrocycle **30**. The macrocycle **30** could be formed via the biocatalytic route in high selectivity but lower yield (19%). As such, the ability to exploit the "platform" macrocycles is particularly powerful for accessing other substitution patterns that may not be compatible with the CALB enzyme (*35*–*37*). Other cross-

coupling techniques were also viable for diversification of the macrocycles: Suzuki-coupling formed the terphenyl-based macrocycle **21** from the Br-substituted cyclophane **6**, whereas Sonogashira coupling on the iodo-substituted cyclophane **16** afforded macrocycle **25** in high yield with little loss of enantiopurity, exemplifying the resistance of the macrocycles to cleavage even when heated in basic aqueous conditions. The preparation of a series of functionalized planar chiral macrocycles that have halogen or borylated substituents opens avenues for diversification outside the boundaries of what may be tolerated by the enzyme active site. The challenge in the preparation of planar chiral

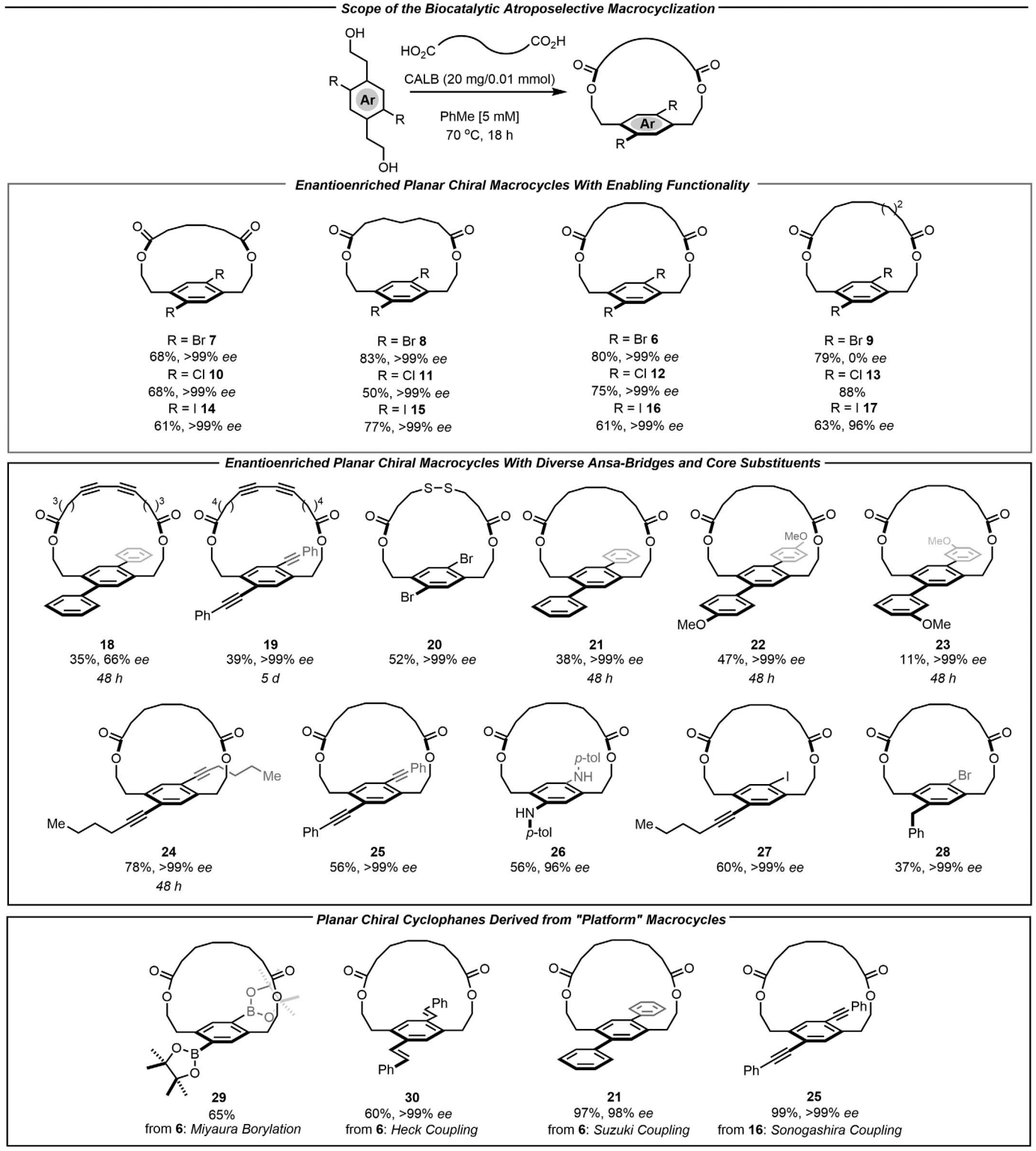

Fig. 3. Scope of the biocatalytic macrocyclization to afford planar chiral cyclophanes. All macrocyclizations were performed under standard conditions. Variations in reaction time are indicated when necessary. Detailed reaction conditions for the derivatizations of **6** are presented in the supplementary materials.

macrocycles in drug discovery is now well recognized. With the pervasive awareness of environmental issues, it would seem apt that biocatalysis provides an innovative solution.

REFERENCES AND NOTES

1. J. C. Roxburgh, *Tetrahedron* **51**, 9767–9822 (1995).
2. H. Matsuda, S. Watanabe, K. Yamamoto, *Chem. Biodivers.* **1**, 1985–1991 (2004).
3. E. Marsault, M. L. Peterson, *J. Med. Chem.* **54**, 1961–2004 (2011).
4. E. Marsault, M. L. Peterson, *Practical Medicinal Chemistry with Macrocycles: Design, Synthesis, and Case Studies* (Wiley, 2017).
5. S. R. LaPlante, P. J. Edwards, L. D. Fader, A. Jakalian, O. Hucke, *ChemMedChem* **6**, 505–513 (2011).
6. J. Clayden, W. J. Moran, P. J. Edwards, S. R. LaPlante, *Angew. Chem. Int. Ed.* **48**, 6398–6401 (2009).
7. S. R. Laplante *et al*., *J. Med. Chem.* **54**, 7005–7022 (2011).
8. K. Mori, K. Ohmori, K. Suzuki, *Angew. Chem. Int. Ed.* **48**, 5638–5641 (2009).
9. R. Morales, M. Frey, J.-M. Mouesca, *J. Am. Chem. Soc.* **124**, 6714–6722 (2002).
10. T. Araki, K. Noguchi, K. Tanaka, *Angew. Chem. Int. Ed.* **52**, 5617–5621 (2013).
11. K. Tanaka, H. Sagae, K. Toyoda, K. Noguchi, M. Hirano, *J. Am. Chem. Soc.* **129**, 1522–1523 (2007).
12. G. W. Heberlig *et al*., *Org. Biomol. Chem.* **16**, 5771–5779 (2018).
13. H. Ludewig *et al*., *ACS Chem. Biol.* **13**, 801–811 (2018).
14. K. A. Rising *et al*., *ACS Chem. Biol.* **10**, 1729–1736 (2015).
15. C. Zhang, P. Dai, A. M. Spokoyny, B. L. Pentelute, *Org. Lett.* **16**, 3652–3655 (2014).
16. N. Kadi, D. Oves-Costales, F. Barona-Gomez, G. L. Challis, *Nat. Chem. Biol.* **3**, 652–656 (2007).
17. G. Hughes, J. C. Lewis, *Chem. Rev.* **118**, 1–3 (2018).
18. G. Carrea, S. Riva, *Organic Synthesis with Enzymes in Non-Aqueous Media* (Wiley, 2008).
19. A. S. Bommarius, B. R. Riebel, *Biocatalysis* (Wiley, 2004).
20. C. M. Clouthier, J. H. Pelletier, *Chem. Soc. Rev.* **41**, 1585–1605 (2012).
21. V. Gotor, I. Alfonso, E. Garcia-Urdiales, *Asymmetric Organic Synthesis with Enzymes* (Wiley, 2008).
22. O. Verho, J.-E. Bäckvall, *J. Am. Chem. Soc.* **137**, 3996–4009 (2015).
23. C. R. Johnson, H. Sakaguchi, *Synlett* **1992**, 813–816 (1992).
24. C. Ortiz *et al*., *Catal. Sci. Technol.* **9**, 2380–2420 (2019).
25. G. Zhi-wei, T. K. Ngooi, A. Scilimati, G. Fulling, C. J. Sih, *Tetrahedron Lett.* **29**, 5583–5586 (1988).
26. S. K. Karmee *et al*., *Biocatal. Biotransform.* **32**, 125–131 (2014).
27. J. Uppenberg *et al*., *Biochemistry* **34**, 16838–16851 (1995).
28. C. R. Corbeil, P. Englebienne, N. Moitessier, *J. Chem. Inf. Model.* **47**, 435–449 (2007).
29. N. Moitessier *et al*., *Acc. Chem. Res.* **49**, 1646–1657 (2016).
30. E. Therrien *et al*., *J. Chem. Inf. Model.* **52**, 210–224 (2012).
31. A. Park *et al*., *ACS Catal.* **6**, 7458–7465 (2016).
32. C. Li, T. Tan, H. Zhang, W. Feng, *J. Biol. Chem.* **285**, 28434–28441 (2010).
33. B. K. W. Chung, A. K. Yudin, *Org. Biomol. Chem.* **13**, 8768–8779 (2015).
34. For full experimental conditions, see the supplementary materials.
35. H. S. G. Beckmann *et al*., *Nat. Chem.* **5**, 861–867 (2013).
36. A. Grossmann, S. Bartlett, M. Janecek, J. T. Hodgkinson, D. R. Spring, *Angew. Chem. Int. Ed.* **53**, 13093–13097 (2014).
37. F. Nie *et al*., *Angew. Chem. Int. Ed.* **55**, 11139–11143 (2016).

ACKNOWLEDGMENTS

We thank N. Moitessier for help with the Forecaster program. **Funding:** This work was supported by the Natural Sciences and Engineering Research Council of Canada (NSERC, Discovery grant 1043344), American Chemical Society Petroleum Research Fund (ACS PRF 60211-ND1), Université de Montréal, and the Fonds de Recherche Nature et Technologie via the Centre in Green Chemistry and Catalysis (grant FRQNT-2020-RS4-265155-CCVC). **Author contributions:** C.G., E.G., C.M., J.S., and C.P. synthesized precursors and macrocycles. C.G. performed docking experiments. S.K.C. designed and directed the investigations. S.K.C., C.G., J.S., and E.G. wrote the manuscript. **Competing interests:** None declared. **Data and materials availability:** All data needed to evaluate the conclusions in the paper are available in the main text or the supplementary materials.

SUPPLEMENTARY MATERIALS

science.sciencemag.org/content/367/6480/917/suppl/DC1
Materials and Methods
NMR Spectra
References (*38*–*52*)

4 October 2019; accepted 21 January 2020
10.1126/science.aaz7381

Discussion leaders are noted in bold italics.

NEW CONFERENCES

NEW! Biology of Winter

Biological Responses to Winter Climate Change

JUNE 21 – 26, 2020 • WATERVILLE VALLEY, WATERVILLE VALLEY, NH

CHAIRS: Brent Sinclair and Sapna Sharma

VICE CHAIRS: Pamela Templer and Steven Cooke

- **Keynote Session: Overwintering of a Keystone Arctic Species in a Changing Climate** *Peter Groffman,* Brian Barnes
- **Predicting Snow and Ice Distribution and Quality in a Warming World** *Laura Brown,* Gina Henderson, Matti Lepparanta, Xiao Yang
- **Late-Breaking Topics** *Raine Kortet*
- **Species and Ecosystem Vulnerability to Changing Winters** *Christa Mulder,* Juergen Kreyling, David Swanson
- **Consequences of Fluctuating Temperatures During Winter** *Chunsen Ma,* Hugh Henry, Katie Marshall
- **Life Under Snow and Ice** *Janneke Hille Ris Lambers,* Hilary Dugan, Robert McKay
- **Microbes as Drivers of Winter Biological Processes** *Bjorn Robroek,* Hannah Carey, Mats Oquist
- **Large-Scale Integration of Winter Biology Across Space and Time** *Kath Dickinson,* Christian Rixen, Emily Stanley, Lloyd Peck
- **Keynote Session: Winter as a Driver of Macrophysiological Patterns in the Oceans** *Pamela Templer,* Amanda Bates
- **The GRC Power Hour™** *Bailey McMeans, Steven Cooke*

NEW! Cell-Cell Fusion

Diverse Organisms and Common Mechanisms in Cell-Cell Fusion

MAY 31 – JUNE 5, 2020 • STONEHILL COLLEGE, EASTON, MA

CHAIR: Elizabeth Chen

VICE CHAIR: Mark Rose

- **Keynote Session: Organelle Dynamics in Cell Fusion** *Mark Rose,* Jennifer Lippincott-Schwartz
- **Intracellular Membrane Fusion** *Jennifer Lippincott-Schwartz,* Axel Brunger, Katja Faelber, Junjie Hu, Reinhard Jahn, Erdem Karatekin
- **Virus-Cell Fusion** *Benjamin Podbilewicz,* Gregory Melikian, Yorgo Modis, James Munro, Felix Rey
- **Cell-Cell Fusogens** *Joshua Zimmerberg,* Roy Duncan, Thomas Krey, Douglas Millay, Benjamin Podbilewicz, William Snell, Hongmei Wang
- **Other Membrane Proteins in Cell Fusion** *N. Louise Glass,* Leonid Chernomordik, Naokazu Inoue, Andrea Pauli
- **Actin Cytoskeleton in Cell Fusion** *Stefanie Sprunck,* Ori Avinoam, Mary Baylies, Jean-Francois Cote, Daniel Fletcher, Sophie Martin, Guangshuo Ou
- **Membrane Organization and Lipids** *Leonid Chernomordik,* Michael Kozlov, Harvey McMahon, Huanghe Yang, Joshua Zimmerberg
- **Diverse Cell Fusion Systems** *Sophie Martin,* Sigal Ben-Yehuda, Don Fox, N. Louise Glass, Massimo Hilliard, Vicki Losick, Stefanie Sprunck
- **Cell Fusion and Disease** *Harvey McMahon,* Melissa Wong, Chiara Zurzolo
- **The GRC Power Hour™** *Mary Baylies, Mark Rose*

NEW! Computational Materials Science and Engineering

Comparing Theories, Algorithms and Computation Protocols in Materials Science and Engineering

AUGUST 2 – 7, 2020 • GRAND SUMMIT HOTEL AT SUNDAY RIVER, NEWRY, ME

CHAIR: Kenny Lipkowitz

VICE CHAIR: Rampi Ramprasad

- **Synthesis Planning Algorithms** *Gerbrand Ceder,* Elsa A. Olivetti, Connor Coley
- **Machine Learning** *Bryce Meredig,* Subramanian Sankaranarayanan, Klaus-Robert Müller, Rama Vasudevan
- **Coarse Graining** *James Warren,* Nikolas Provatas, Gregory Voth
- **Concurrent and Hierarchical Multiscale Modeling** *Kaushik Dayal,* David McDowell, Martin Steinhauser, Ellad Tadmor
- **Non-Adiabatic Quantum Mechanics** *Claudia Draxl,* André Schleife, Priya Vashishta
- **Autonomous Robotic Systems** *Christoph Kreisbeck,* Andy Cooper, A. Gilad Kusne, Loïc Roch
- **Calculation of Phase Diagrams (CALPHAD)** *Raymundo Arroyave,* Ursula Kattner, Axel van de Walle
- **Materials by Design** *Alejandro Strachan,* Juan de Pablo, James Saal, Cormac Toher
- **Quantum Computing** *Hanhee Paik,* Alan Aspuru-Guzik, Veera Sundararaghavan

NEW! Electrochemical Interfaces in Energy Conversion and Storage

Understanding Electrochemical Interfaces at the Atomic Scale

JUNE 28 – JULY 3, 2020 • THE HONG KONG UNIVERSITY OF SCIENCE AND TECHNOLOGY, HONG KONG, CHINA

CHAIRS: Minhua Shao and Jean Marie Tarascon

VICE CHAIRS: Nenad Markovic and Yi Cui

- **Interface in the Aqueous and Nonaqueous Systems** *Peter Faguy,* Shao-Horn Yang, Ying Shirley Meng
- ***In Situ* Spectroscopic Techniques in Understanding Energy Conversion and Storage** *Shi-Gang Sun,* Clare Grey, Masatoshi Osawa, Bin Ren
- **Supercapacitors** *George Zhao,* Patrice Simon, Bruce Dunn
- ***In Situ* Microscopy Revealing Interfaces** *Xiaoqing Pan,* Haimei Zheng, Hector Abruna, Patrick Unwin
- **Lithium Batteries** *Guohua Chen,* Khalil Amine, Jun Liu
- **Flow Batteries and Fuel Cells** *Plamen Atanassov,* Tianshou Zhao, Yushan Yan, Lin Zhuang
- **Solid Electrolyte Interface** *Feng Pan,* Juergen Janek, Chunsheng Wang
- **Modeling the Interface at Atomic and Molecular Scales** *Venkat Srinivasan,* William Goddard, Perla Balbuena, Karen Chan
- **Early-Career Investigator Presentations** *Qing Chen,* William Chueh, Serhiy Cherevko, Haotian Wang, Alexis Grimaud
- **The GRC Power Hour™**

NEW! Immunometabolism in Health and Disease

Basic and Translational Cellular Metabolism in Immunity

JUNE 21 – 26, 2020 • BRYANT UNIVERSITY, SMITHFIELD, RI

CHAIRS: Michael Fessler and Hongbo Chi

VICE CHAIRS: Jeff Rathmell and Kathryn Moore

- **Repurposing of Bioenergetics in Innate Immunity** *Maxim Artyomov,* Luke O'Neill, Edward Pearce
- **Metabolic Programming of Lymphocyte Function** *Peer Karmaus,* Mark Boothby, Vijay Kuchroo, Erika Pearce, Amy Weinmann
- **Trained Immunity** *Claudia Kemper,* Navdeep Chandel, Mihai Netea
- **Sterols in Immunity** *Ping-Chih Ho,* Steven Bensinger, Alan Tall, Chenqi Xu
- **Immunity and Microbiota as a Driver of Metabolic Disease** *Nancie MacIver,* Gokhan Hotamisligil
- **Immunometabolism of the Tumor Microenvironment** *Brent Hanks,* Juan Cubillos-Ruiz, Ming Li, Weiping Zou
- **Metabolism in Host Defense** *Sebastian Riquelme,* Julie Magarian Blander, Peter Ghazal
- **Cell Fate in Immunometabolism** *Jennifer Martinez,* Douglas Green, Gerald Shadel, Ira Tabas
- **Emerging Opportunities for Intervening upon Immunometabolism in Disease** *Ana Mora,* Laurence Turka, Thomas Wynn
- **The GRC Power Hour™** *Jennifer Martinez*

NEW! Lipidomics

Lipidomics and Decoding Life: From the Technology and Biology Landscapes to Clinical Adaptation

AUGUST 9 – 14, 2020 • GRAND SUMMIT HOTEL AT SUNDAY RIVER, NEWRY, ME

CHAIRS: John Bowden and Kim Ekroos

VICE CHAIRS: Gerhard Liebisch and Xianlin Han

- **Lipidomics in Decoding Biology** *Bill Griffiths,* Vytas Bankaitis, Scott Summers
- **Lipidomics in Human Health and Disease** *Edward Dennis,* Michal Holcapek, Rima Kaddurah-Daouk, Michael Kiebish
- **Harmonization and Standardization in Lipidomics** *Maria Fedorova,* Markus Wenk, Martin Giera, Robert Ahrends
- **Novel Lipidomic Mass Spectrometry Strategies** *Christer Ejsing,* Gunda Koellensperger, Shane Ellis, Christoph Thiele
- **Clinical and Translational Lipidomics** *Anne Bendt,* Michelle Mielke, Daisuke Saigusa
- **Lipidomics Data Dimensions and Biological Interpretation** *Stephen Blanksby,* Erin Baker, Yu Xia, Andrej Shevchenko, Steffany Bennett
- **Resolving Lipid Metabolic Networks** *Gavin Reid,* Nathan Hatcher, Jace Jones, Charles Serhan
- **Role of the Environment on the Lipidome** *Ian Blair,* Ivo Feussner, Ameer Taha, Clementina Mesaros
- **Integration of Lipidomics with Genomics, Proteomics and Metabolomics** *Harald Köfeler,* Peter Meikle, Bjoern Titz
- **The GRC Power Hour™** *Erin Baker*

NEW! Neural Mechanisms of Acoustic Communication

Circuits and Specializations for Behavioral Interactions in Acoustic Communication

JULY 19 – 24, 2020 • JORDAN HOTEL AT SUNDAY RIVER, NEWRY, ME

CHAIRS: Sarah Woolley and Michael Long

VICE CHAIRS: Mala Murthy and Marc Schmidt

- **Quantitative Approaches to Behavioral Analysis** *Jan Clemens,* Catherine Perrodin, Roian Egnor, Coen Elemans
- **Vocal Development** *Jon Sakata,* Michale Fee, Asif Ghazanfar, Ghislaine Dehaene-Lambertz
- **Models of Vocal Learning and Production** *Adrienne Fairhall,* Mimi Kao, Jesse Goldberg, Vincent Gracco
- **Vocal Interactions** *Xiaoqin Wang,* Ofer Tchernichovski, Simone Pika, Yossi Yovel
- **Auditory Specializations for Communication** *Robert Liu,* Ioana Carcea, Sarah Woolley, Todd Roberts
- **Genetics of Communication** *Constance Scharff,* Erich Jarvis, Genevieve Konopka, Hopi Hoekstra
- **Predictive Coding in Vocal Motor Networks** *Nate Sawtell,* Caroline Niziolek, David Schneider, Berthold Hedwig
- **Comparative Anatomy and Function of Communication Circuits** *Darcy Kelley,* Anne Von Philipsborn, Benjamin Judkewitz, Steffen Hage
- **Cortical Mechanisms of Vocal Production** *Daniela Vallentin,* Terra Barnes, Michael Brainard, Edward Chang
- **The GRC Power Hour™** *Genevieve Konopka, Anne Von Philipsborn*

NEW! Radionuclide Theranostics for the Management of Cancer

Molecularly Targeted, Radioactive Cancer Diagnosis and Therapy

JUNE 21 – 26, 2020 • JORDAN HOTEL AT SUNDAY RIVER, NEWRY, ME

CHAIR: Sue O'Dorisio

VICE CHAIR: Alan Harris

- **Targets and Radionuclides** *Steven Lamberts,* Richard Baum, Michael Schultz
- **Radiotherapeutics in Oncologic Diseases** *Richard Baum,* Ken Herrmann, Michael Groaning, Frances Johnson
- **Matching a Malignancy with a Diagnostic Target** *Thomas O'Dorisio,* Andrew Bellizzi, Thomas Hope, Jonathan McConathy, Laura Tang
- **Development of Theranostic Radiopharmaceuticals** *Michael Schultz,* Cathy Cutler, Jason Holland, Suzanne Lapi, Richard Wahl
- **Dosimetry-Guided Therapy with Radionuclides** *Yusuf Menda,* Ulrike Garske-Román, Jonathan Gear, Robert Hobbs
- **Optimizing Therapy** *Kjell Oberg,* Katia Beider, Amir Iravani, Jennifer Chan, Josh Mailman
- **Safety Measures in Administration of Radionuclide Theranostics** *Eric Liu,* John Buatti, Yusuf Menda, Erica Sztangret
- **Design of Theranostic Clinical Trials** *Sandy McEwan,* Emily Bergsland, Ebrihim Delpassand, Philip Harris
- **Keynote Session: Advances in Radionuclide Theranostics** *David Metz,* Anthony Chang, Wouter de Herder, Brian Miller, Aldo Scarpa

NEW! Single-Cell Cancer Biology

Dissecting Evolution and Heterogeneity of Single Cancer Cells

JUNE 7 – 12, 2020 • GRAND SUMMIT HOTEL AT SUNDAY RIVER, NEWRY, ME

CHAIRS: Kai Tan and Nicholas Navin

VICE CHAIRS: Mario Suva and Sohrab Shah

- **Pre-Malignancies and Early-Stage Tumors** *Samuel Aparicio,* Kai Kessenbrock, Xin Lu, Jorge Reis-Filho
- **Solid Tumors** *Devon Lawson,* Samuel Aparicio, Peter Van Loo, Michalina Janiszewska, Sam Behjati
- **Hematological Tumors** *Iannis Aifantis,* Charles Gawad, Catherine Wu, Koichi Takahashi, Adam Mead
- **Epigenomic Heterogeneity** *Catherine Wu,* Nicola Aceto, Celine Vallot, Andrew Adey, Ansuman Satpathy
- **Tumor-Immune Cell Interactions in Tumor Microenvironment** *Mario Suva,* Iannis Aifantis, Itay Tirosh, Zemin Zhang
- **Computational Methods for Single-Cell Analysis** *Sohrab Shah,* Rahul Satija, Nancy Zhang, Ken Chen, Dana Pe'er
- **Current Advances in Single-Cell Technologies** *Klaus Pantel,* Bernd Bodenmiller, Joakim Lundeberg, Dario Bressan
- **Circulating Tumor Cells and Metastasis** *Xin Lu,* Daniel Haber, Klaus Pantel, James Hicks
- **Therapeutic Resistance** *Michalina Janiszewska,* Kornelia Polyak, Maxim Artyomov, Liynat Jerby-Arnon, Devon Lawson

NEW! Single-Cell Genomics

When Stochasticity Meets Precision in a Single Cell

MAY 17 – 22, 2020 • VENTURA BEACH MARRIOTT, VENTURA, CA

CHAIRS: Xiaoliang Sunney Xie and Stephen Quake

VICE CHAIRS: Xiaowei Zhuang and Barbara Treutlein

- **Single-Cell Transcriptomics** *Dana Pe'er,* Rickard Sandberg, Jianbin Wang, Allon Klein
- **Imaging** *Robert Singer,* Long Cai, Alistair Boettiger, Loic Royer, Arjun Raj
- **Genomes** *Ido Amit,* Chenghang Zong, Jan Vijg, Paul Blainey
- **Epigenetics** *Alexander Meissner,* Fuchou Tang, Wolf Reik, William Greenleaf
- **3D Genome Structures and Dynamics** *Amos Tanay,* Peter Fraser, Kikue Tachibana, Richard Cao
- **Technology** *Piero Carninci,* Jonathan Weissman, Emma Lundberg, Nikolai Slavov, Martin Enge
- **Applications to Cancer and Immunology** *Michael Clarke,* Nicholas Navin, Zemin Zhang, Charles Gawad
- **Applications to Neurobiology** *Hongkui Zeng,* Bosiljka Tasic, Joseph Ecker, Michelle Chen
- **Human and Model Organism Cell Atlas** *Michael Levine,* Spyros Darmanis, Aki Minoda, Ge Gao

NEW! Systems Aging

Systemic Processes, Omics Approaches and Biomarkers in Aging

MAY 31 – JUNE 5, 2020 • MOUNT SNOW, WEST DOVER, VT

CHAIR: Vadim Gladyshev

VICE CHAIR: Steve Horvath

- **Delaying and Reversing Aging** *Steve Horvath,* Cynthia Kenyon, Richard Miller
- **Whole Organism Approaches and Rejuvenation** *Felipe Sierra,* David Sinclair, Vittorio Sebastiano
- **Genomics of Aging** *Emma Teeling,* Jan Vijg, Mia Petljak
- **Epigenetic Biomarkers of Aging** *Anne Newman,* Morgan Levine, Ake Lu, Riccardo Marioni, Kenneth Raj
- **Clinical and Molecular Biomarkers of Aging** *Morgan Levine,* Daniel Belsky, Sara Hagg, Anne Newman
- **Artificial Intelligence and Machine Learning** *Kristen Fortney,* Jing-Dong Han, Nicholas Schork, Alex Zhavoronkov
- **Aging as a Systemic Process** *Ned David,* Danica Chen, Jessica Tyler, Meng Wang
- **Comparative Genomics of Aging** *Andrei Seluanov,* João Pedro de Magalhães, Vera Gorbunova, Emma Teeling
- **Fundamental Bases of Aging** *Cynthia Kenyon,* Uri Alon, Daniel Promislow
- **The GRC Power Hour™** *Morgan Levine*

ONGOING CONFERENCES

Aqueous Corrosion

Mechanisms, Tools, Agents and Avoidance of Corrosion

JULY 12 – 17, 2020 • COLBY-SAWYER COLLEGE, NEW LONDON, NH

CHAIR: Jamie Noel

VICE CHAIR: Mary Ryan

- **Corrosion Mechanisms** *Sannakaisa Virtanen,* Edwin Garcia, Jingli Luo
- **Analytical Tools** *Dev Chidambaram,* Masayuki Itagaki, Gareth Hinds
- **Passive Films** *John Scully,* Philippe Marcus, Emeka Oguzie
- **Localized Corrosion** *Gerald Frankel,* Jenifer Locke, Michele Ostraat, Janine Mauzeroll
- **The Role of Hydrogen** *Brendy Rincon Troconis,* Bilge Yildiz, Michael Rohwerder
- **Corrosion in Porous Media** *Francisco Presuel-Moreno,* Claire Corkhill, Ueli Angst
- **Microbiologically Influenced Corrosion** *Jason Lee,* Tingyue Gu
- **Advanced Materials** *Oumaïma Gharbi,* Pin Lu, Rebecca Schaller
- **Pre-Emergent Methods, Mechanisms and Processes in Corrosion Science and Engineering** *Robert Asmussen,* David Shoesmith, Robert Kelly
- **The GRC Power Hour™** *Oumaïma Gharbi, Carol Glover*

Aqueous Corrosion
Design of Modern Prediction Tools and Sustainable Corrosion Protection Strategies
JULY 11 – 12, 2020
CHAIRS: Oumaïma Gharbi and Saba N. Esmaeely

THE GRC POWER HOUR™

The GRC Power Hour™ is transforming the culture of science by raising awareness of the challenges women and underrepresented minorities face in science. The program provides a safe and open forum to discuss these shared challenges. Look for GRC Power Hours™ and the names of the respective organizers throughout these program listings.

> *"GRCs provide a forum for experts from academia and industry to engage in meaningful discussions in a relaxed setting that cannot be matched by any other conference."*
>
> JEFFREY D. RIMER, University of Houston, Crystal Growth and Assembly GRC

Auditory System

Preventing Loss and Recovering Function of the Auditory System

JULY 12 – 17, 2020 • BRYANT UNIVERSITY, SMITHFIELD, RI

CHAIR: Ruth Litovsky

VICE CHAIR: Allison Coffin

- **Keynote Session: Communication, Music and Hearing Loss** *Mario Svirsky,* Darcy Kelley, Gabriel Corfas, Monita Chatterjee
- **Predictable and Surprising Coding of Auditory Information** *Melissa Caras,* Jennifer Bizley, Jerome Bourien, Maria Chait
- **Immune and Nervous System Cross-Talk** *Yehoash Raphael,* Andrew Groves, Keiko Hirose, Jeffrey Holt
- **Cognitive and Attentional Aspects of Hearing** *Blake Butler,* Lori Holt, Matthew McGinley, Jonathan Peelle, Matthew Winn
- **Hearing Without Vision and Vision Without Hearing** *Ingrid Johnsrude,* Ione Fine, Ella Striem-Amit
- **Auditory Experience and Development: Hair Cells, Babies and Brains** *Michael Roberts,* Jason Sanchez, Ana Belen Elgoyhen, Jennifer Stone, Yoko Yazaki-Sugiyama, Aaron Tward
- **Diagnoses and Interventions** *Stefan Heller,* Lisa Cunningham, Stephanie Kuchinsky, Konstantina Stankovic, Karen Steel
- **Auditory Function and Pathways: Connecting the Ear and the Brain** *Cynthia Moss,* Paul Forlano, Nace Golding, Ross Maddox, Antje Ihlefeld
- **Interconnection of Cells and Tissues** *Catherine Weisz,* Karina Cramer, Sean Megason, Michael Hoa, Dáibhid Ó Maoiléidigh
- **The GRC Power Hour™** *Allison Coffin, Jennifer Stone*

Auditory System

Preventing Loss and Recovering Function of the Auditory System

JULY 11 – 12, 2020

CHAIR: Amanda Janesick

Bacterial Cell Surfaces

Altering the Bacterial Cell Envelope: Shaping Fitness in Response to the Host and Environment

JUNE 28 – JULY 3, 2020 • MOUNT SNOW, WEST DOVER, VT

CHAIRS: Stephen Trent and Elizabeth Sockett

VICE CHAIRS: Natividad Ruiz and Jean-Francois Collet

- **Exploring the Bacterial Cell Envelope** *Rut Carballido-Lopez,* Thomas Silhavy, Waldemar Vollmer, Christine Jacobs-Wagner
- **Modifying the Bacterial Cell Surface** *Jean-Francois Collet,* Filippo Mancia, Angelika Grundling, Chris Whitfield, Aimee Shen
- **Cell Division and Morphogenesis** *Simon Foster,* Thomas Bernhardt, Erin Goley, Kumaran Ramamurthi
- **Stress Responses and Signaling Across the Cell Envelope** *Marcin Grabowicz,* Sonja-Verena Albers, Tam Mignot, Alexandre Persat, Anna Konovalova
- **Mechanisms of Surface Recognition** *Daniel Wall,* Andrea Wolf, Serge Mostowy, Andrew Lovering
- **Transport Through the Envelope** *Natividad Ruiz,* Susan Buchanan, Lori Burrows, Seok-Yong Lee, Jorge Galan
- **Type VI and Type VII Secretion** *Edith Houben,* Melanie Blokesch, Mario Feldman, Tracy Palmer
- **The Bacterial Surface and Its Influence on Bacterial Communities** *Lotte Sogaard-Andersen,* Cynthia Whitchurch, Nicole Koropatkin, Peggy Cotter, Urs Jenal
- **Biophysical Methods to Improve Antimicrobial Therapies** *Pamela Brown,* Jie Xiao, Kerwyn Huang, Steven Rutherford
- **The GRC Power Hour™** *Erin Goley, Mario Feldman*

Bacterial Cell Surfaces

A Multidimensional View of the Bacterial Cell Envelope: From Molecular Structures to Intracellular Interactions

JUNE 27 – 28, 2020

CHAIRS: Lizah van der Aart and Liselot Dewachter

Barriers of the CNS

Translating Basic Knowledge About Brain Barriers into Treatments for Neurological Disorders

JUNE 14 – 19, 2020 • COLBY-SAWYER COLLEGE, NEW LONDON, NH

CHAIR: William Elmquist

VICE CHAIR: Matthew Campbell

- **Keynote Session: Novel Strategies to Overcome Multiple Barriers in the CNS** *Matthew Campbell, Lester Drewes,* Michael Hayden, Tetsuya Terasaki
- **Experimental Models of Brain Barriers** *Eric Shusta, Samira Azarin,* Ethan Lippmann, Choi-Fong Cho, Nur Mustafaoglu, Richard Daneman, Clive Svendsen
- **Changes in BBB Structure and Function in Disease** *Reina Bendayan, Francesca Cicchetti,* Richard Keep, Stefan Liebner, Bjoern Bauer
- **Delivery of Macromolecular Therapeutics to the Brain** *Danica Stanimirovic, Robert Thorne,* Dhaval Shah, Joy Zuchero, Joelle Straehla, Priti Kumar, Beverly Davidson
- **Understudied Barriers of the CNS** *Christer Betsholtz, Stina Syvânen,* Johanna Andrae, Matthias Nahrendorf, David Antonetti
- **Methods of Delivery to Overcome Brain Barriers** *Sadhana Jackson, Nathalie Agar,* Kullervo Hynynen, Mark Souweidane, Krystof Bankiewicz, Gerry Grant, Rachael Sirianni
- **Influence of Neuroinflammation on the BBB** *Francesca Bosetti, Chaitali Ghosh,* Joel Pachter, Anika Hartz, David Camarillo
- **CSF and ISF: Fluid Flow and Exchange in the CNS** *Jeffrey Iliff, Richard Keep,* Adam Chodobski, Geir Ringstad, Kristopher Kahle, Nanna MacAulay, Jane Preston
- **Keynote Session: Fluid Flow in the Brain** *Irena Loryan, Steven Proulx,* Britta Engelhardt, Laura Lewis
- **The GRC Power Hour™** *Martha O'Donnell*

Barriers of the CNS

The Physiology of CNS Barriers in Health, Aging and Disease

JUNE 13 – 14, 2020

CHAIRS: Michelle Pizzo and Steffen Storck

Bioanalytical Sensors

Interconnecting Biology and Devices to Analyze Microscopic Cells to the Macroscopic World

JUNE 28 – JULY 3, 2020 • SALVE REGINA UNIVERSITY, NEWPORT, RI

CHAIRS: Susan Daniel and Jean-Francois Masson

VICE CHAIRS: Charles Mace and Chenzhong Li

- **Keynote Session: Biosensors for Small to Large Systems** *Christa Brosseau,* Christy Haynes, Jessica Koehne
- **Molecular Recognition at the Nanoscale** *Ling Chao,* Ryan Bailey, Michael Mayer, Daniel Schwartz
- **Sensing for Neuroscience** *Chenzhong Li,* Susan Lunte, Dan Fu
- **Intracellular Biosensing** *Jason Dwyer,* Julie Biteen, Joshua Edel, Neha Kamat, Nicholas Melosh
- **Wearable and Implantable Sensors: Interfacing Sensors with Living Systems** *Charles Mace,* Sahika Inal, Nanshu Lu
- **Pathogen Detection** *Ariel Furst,* Marta Bally, Jaebum Choo, Jacinta Conrad, Michael Serpe
- **Agriculture and Environment: Sensing in the Digital Agriculture Movement** *Juan Pablo Giraldo,* Liang Dong, Abraham Stroock
- **Human Health: Detection and Diagnostics** *Angela Brown,* Roisin Owens, Wei Peng, Menno Prins, Zachary Schultz
- **Keynote Session: Next Generation Bioanalytical Sensors** *Samuel Hinman, Carine Nemr,* Justin Gooding
- **The GRC Power Hour™** *Rebecca Whelan, Matthew Lockett*

Bioanalytical Sensors

Translational Applications of Sensor Technologies

JUNE 27 – 28, 2020

CHAIRS: Samuel Hinman and Carine Nemr

Biocatalysis

Making Biocatalysis More Predictive: Accelerating Biocatalytic Solutions to Synthetic Challenges

JULY 12 – 17, 2020 • SOUTHERN NEW HAMPSHIRE UNIVERSITY, MANCHESTER, NH

CHAIRS: Gerrit Poelarends and Birgit Kosjek

VICE CHAIRS: Sabine Flitsch and Carlos Martinez

- **Keynote Session: Creating New Activities for Chemical Applications** *Bernhard Hauer,* Donald Hilvert, Jeffrey Moore
- **Expanding the Biocatalytic Toolbox with New Enzymes and New Functions** *Mélanie Hall,* Katherine Ryan, Vincent Eijsink, Brent Dorr, John McIntosh
- **Mechanistic Understanding and Innovative Development Strategies to Enable New Applications** *Wilfred van der Donk,* Steven Boxer, Joelle Pelletier, Hans Renata
- **From Big Data to Enzyme Function via Computational and Bioinformatic Enzyme Design** *Joelle Pelletier,* Rama Ranganathan, Silvia Osuna, Daniela Grabs, Rusty Lewis
- **Genome Editing and Genetic Code Expansion to Create New Functions** *Xue Gao,* Anthony Green, John Glass, Chang Liu
- **Radical Biocatalysis** *Sabine Flitsch,* Todd Hyster, Amie Boal, Mohammad Seyedsayamdost, Shelley Minteer
- **Artificial Metalloenzymes** *Todd Hyster,* Gerard Roelfes, Yi Lu, Thomas Ward
- **Natural Product Biosynthetic Enzymes** *Claudia Schmidt-Dannert,* Wilfred van der Donk, Reshma Shetty, Xiaoguang Lei, Tobias Erb
- **Selected Poster Presentations** *Carlos Martinez*
- **The GRC Power Hour™** *Sabine Flitsch*

Biocatalysis

Biocatalytic Cascades, Pathways and Novel Reactions

JULY 11 – 12, 2020

CHAIRS: Matthew McDonald and Thomas Bayer

Biogenic Hydrocarbons and the Atmosphere

Bridging Ecology, Chemistry and Climate

JUNE 28 – JULY 3, 2020 • FOUR POINTS SHERATON / HOLIDAY INN EXPRESS, VENTURA, CA

CHAIRS: Mark Potosnak and Jaana Back

VICE CHAIRS: Kirsti Ashworth and Zhaozhong Feng

- **Use of High-Resolution Remote Sensing Data for Air Quality Models** *Allison Steiner,* Dylan Millet, Karena McKenna
- **Biogenic Versus Anthropogenic Controls on Urban Aerosols and Ozone** *Neil Donahue,* Hai Guo, Tuukka Petäjä
- **Sources, Trends and Effects of Reactive Nitrogen** *Ronald Cohen,* Nga Lee Ng, Xunhua Zheng
- **BVOCs and Plant Stress** *Riikka Rinnan,* Federico Brilli, Meredith Schuman, Todd Rosenstiel
- **The Sentient Plant** *Ted Turlings,* Cristina Davis
- **Early-Career Investigator Presentations** *Kirsti Ashworth*
- **Wildfire and Biomass Burning Emissions** *Clare Murphy,* Jessica Gilman, Vinayak Sinha, Christine Wiedinmyer
- **Coupling Climate, Dynamic Vegetation and BVOC Emissions** *Nadine Unger,* Sebastiaan Luyssaert
- **Keynote Session: Emerging Sources and Sinks** *Alex Guenther,* Chris Geron, Efstratios Bourtsoukidis
- **The GRC Power Hour™** *Kirsti Ashworth, Zhaozhong Feng*

Biogenic Hydrocarbons and the Atmosphere

Linking Biogenic Hydrocarbons Across Scales and from Present to Future

JUNE 27 – 28, 2020

CHAIRS: Ana Yáñez Serrano and Jianhuai Ye

Bioinspired Materials

Materials that Self-Assemble, Display Autonomy and Manipulate Immunity

JUNE 7 – 12, 2020 • LES DIABLERETS CONFERENCE CENTER, LES DIABLERETS, SWITZERLAND

CHAIR: Daniel Hammer

VICE CHAIRS: Christoph Weder and Molly Stevens

- **Keynote Session: Synthetic Cells** *Eric Dufresne,* Anna Balazs, Stephen Mann
- **New Developments in Protocells** *Abigail Knight,* Rachel O'Reilly, Paolo Arosio, Neha Kamat, Cornelia Palivan, Tetsuya Yomo
- **Novel Membrane Design** *Allie Obermeyer,* Neal Devaraj, Atul Parikh, Jeanne Stachowiak
- **Active Matter and Motility** *Zhibin Guan,* Zvonimir Dogic, Peer Fischer, Masaki Sano, Cecile Sykes, Lauren Zarzar

- **Membraneless Organelles and Protein Coacervation** *Ben Schuster,* Ashutosh Chilkoti, Matthew Good, Kimberly Weirich
- **Functional Bioinspired Assemblies** *Leila Deravi,* Kathryn Uhrich, Nicole Steinmetz, David Gracias, Ullrich Steiner
- **Peptide and Protein Assembly** *Gregory Hudalla,* Timothy Deming, Ehud Gazit
- **Tissues and Organoids** *Cole DeForest,* Matthias Lutolf, David Mooney, Ankur Singh
- **Bioinspired Materials for Immune Engineering** *Ankur Singh,* Jennifer Elisseeff, Jeffrey Hubbell
- **The GRC Power Hour™** *Jennifer Elisseeff, Kathryn Uhrich*

Bioinspired Materials

Harnessing Biological Principles for Better Materials

JUNE 6 – 7, 2020

CHAIRS: Lee Schnaider and George Degen

Biointerface Science

Functional Assemblies and Biomolecular Information Processing

JUNE 14 – 19, 2020 • RENAISSANCE TUSCANY IL CIOCCO, LUCCA (BARGA), ITALY

CHAIR: Jay Groves

VICE CHAIR: Katharina Maniura

- **Keynote Session: Emerging Concepts at the Biointerface** *Khalid Salaita,* Christine Keating
- **Phase Transitions and Molecular Assemblies** *William Huang,* Jeanne Stachowiak, Atul Parikh, Alf Honigmann
- **Mechanobiology at the Cell Surface** *Kabir Biswas,* Matthew Paszek, Khalid Salaita, Virgile Viasnoff
- **Signaling Reactions on the Membrane** *Marcus Taylor,* Petra Schwille, Min Wu, Yan Yu, Orion Weiner
- **Spatial and Geometric Effects at the Interface** *Cheng-Han Yu,* Bianxiao Cui, Dimitrios Stamou, Daniel Fletcher
- **Synthetic Responsive Systems** *Atul Parikh,* Dora Tang, Qiong Yang, Sierin Lim, Jwa-Min Nam
- **Emerging Techniques for Interface Characterization** *Dimitrios Stamou,* Gerhard Schuetz, Adam Smith, Daniel Müller
- **Late-Breaking Topics** *Katharina Maniura*
- **Keynote Session: Functional Assemblies** *Yan Yu,* Patricia Bassereau
- **The GRC Power Hour™** *Sierin Lim*

Biointerface Science

Mechanical and Physicochemical Properties at Biointerface: Effects on Structure and Function in Cells and Tissues

JUNE 13 – 14, 2020

CHAIRS: Fatma Pir Cakmak and Sara Correia Carreira

Biology of Host-Parasite Interactions

The Molecular, Cellular and Biochemical Basis of Parasitism by Eukaryotic Pathogens

JUNE 14 – 19, 2020 • SALVE REGINA UNIVERSITY, NEWPORT, RI

CHAIRS: Kirk Deitsch and Michael Barrett

VICE CHAIRS: Gary Ward and F. Nina Papavasiliou

- **Parasite Motility** *Photini Sinnis,* Freddy Frischknecht, Maryse Lebrune, Eva Gluenz
- **Genome Stability and Genetic Diversity** *Galadriel Hovel-Miner,* Jane Carlton, Richard Davis, Jennifer Guler, Gerald Spaeth
- **Immunology and Immuno-Suppression** *Tracey Lamb,* Eva Frickel, P'ng Lok, Meera G. Nair
- **Parasite Dormancy and Persistence** *William Sullivan,* Jon Boyle, Jean-Claude Dujardin, Annmarie Voorberg-Van der Wel, Alexander Paredez
- **Sexual Differentiation and Quorum Sensing** *Manuel Llinas,* Laura Knoll, Isabel Roditi, Andy Waters
- **Host Cell Responses to Manipulation by Parasites** *Ira Blader,* Gordon Langsley, Melissa Lodoen, Alex Loukas, Staffan Svard
- **Molecular Biology and Gene Expression** *Victoria Jeffers,* Iris Bruchhaus, Mohamed Hakimi, Lyn-Maria Birkholtz
- **Metabolism and Drug Targets** *Sara Lustigman,* Frederick Bringaud, Karl Hoffman, Julio Martin, Maria Mota
- **New Intervention Strategies** *Akhil Vaidya,* Emily Derbyshire, Boris Striepen, Jennifer Zambriski, Joerg Moehrle
- **The GRC Power Hour™** *Veronica Jimenez, Laura Knoll*

Biology of Host-Parasite Interactions

The Molecular and Cellular Biology of Eukaryotic Infectious Organisms

JUNE 13 – 14, 2020

CHAIRS: Xu Zhang and Matthew Gould

Biomineralization

Bridging Scientific Disciplines to Understand Biomineral Formation in Breadth and Depth

AUGUST 9 – 14, 2020 • REY DON JAIME GRAND HOTEL, CASTELLDEFELS, SPAIN

CHAIR: Janet Moradian-Oldak

VICE CHAIR: Nils Kröger

- **Regulation of Morphogenesis** *Nils Kröger,* Assaf Gal, Jaroslaw Tyszka
- **Cellular and Genetic Control of Mineral Deposition** *Tali Mass,* Rivka Elbaum, Sylvie Tambutte, Ron Shahar
- **Macromolecules in Biomineralization** *Elia Beniash,* Michiko Nemoto, Liping Xie
- **Ion Transport, Signaling and Homeostasis** *Marc McKee,* Rodrigo Lacruz, Andre Scheffel, Alejandro Navarro
- **Structure and Biomechanics** *Joanna McKittrick,* Francois Barthelat, Derk Joester
- **Chemical and Computational Models of Nucleation, Phase Transformation and Growth** *Wendy Shaw,* Jim Pfaendtner, Thomas Koop, Fiona Meldrum
- **Biomineralization Principles Translated** *Maisoon Al-Jawad,* Luiz Bertassoni, Elena Sturm (née Rosseeva)
- **Biominerals in Pathology** *Willi Jahnen-Dechent,* Sunita Ho, Peter Vekilov, Eileen Shore
- **Keynote Session: Geochemistry, Proxies and Evolution** *Derk Joester,* Alex Gagnon, Tanya Smith

Biomineralization

A Multifaceted Approach Toward Understanding Biomineral Formation Pathways and Purpose

AUGUST 8 – 9, 2020

CHAIRS: Bernette Oosterlaken and Konrad Hedderick

Bioorganic Chemistry

Enabling Technologies in Chemical Biology

JUNE 14 – 19, 2020 • PROCTOR ACADEMY, ANDOVER, NH

CHAIRS: Jennifer Heemstra and John Tallarico

VICE CHAIRS: Daniel Nomura and Jason Thomas

- **Keynote Session: Enabling Technologies** *Wenjing Wang,* Matthew Francis, Yamuna Krishnan
- **Nucleic Acid Technologies** *Kathryn Mouzakis,* Marino Resendiz, Robert Spitale
- **Biomaterials and Biomimetics** *Olalla Vázquez,* Annelise Barron, M.G. Finn, Ronald Zuckermann
- **Glycobiology in Human Health** *Christina Woo,* Yael David, Daniel Kahne, Lara Mahal, Steven Townsend
- **Epigenetics and Epitranscriptomics** *Alexis Komor,* Thomas Carrell, Chuan He, Ralph Kleiner
- **Microfluidics for High-Throughput Biology** *Daniel Nomura,* Adam Abate, Brian Paegel
- **Computational Chemical Biology** *C. Denise Okafor,* Brian Shoichet
- **Proteomics** *Lars Plate,* Keriann Backus, Vishal Rai, Laura Sanchez
- **Cellular Engineering** *Stephen Fried,* David Savage
- **The GRC Power Hour™** *Louise Charkoudian*

Bioorganic Chemistry

Using Molecular Tools to Understand Biological Complexity

JUNE 13 – 14, 2020

CHAIRS: Natalia Milosevich and Pratik Kumar

Cardiac Regulatory Mechanisms

Applying High Resolution Approaches to Cardiac Disorders to Develop Targeted Therapies

JUNE 21 – 26, 2020 • COLBY-SAWYER COLLEGE, NEW LONDON, NH

CHAIRS: Jil Tardiff and Christoph Maack

VICE CHAIRS: Rong Tian and Benjamin Prosser

- **Cardiac Repair and Regeneration** *Bjorn Knollmann, Jop van Berlo,* Bin Zhou, Jennifer Davis, Mauro Giacca, Wolfram Zimmerman
- **Inflammatory Response in Cardiac Remodeling** *Emilio Hirsch, Jeffery Molkentin,* Matthias Nahrendorf, Daniela Carnevale, Slava Epelman, Daniela Cihakova, Kory Lavine, Pilar Alcaide
- **Excitation-Contraction Coupling and Arrhythmias** *Donald Bers, Steven Houser,* Isabelle Deschenes, Sara Liin, Xander Wehrens, Matthew Daniels
- **Myocellular Structural Dynamics in Health and Disease** *Jolanda van der Velden, Jennifer Van Eyk,* Farah Sheikh, Brett Colson, Maria Kontaridis, Wolfgang Linke
- **Emerging Techniques of Analysis in Cardiac Myocytes and Whole Hearts** *Sarah Franklin, Thomas Thum,* Roger Foo, Federica Accornero, Jan Christoph, Yi Yang
- **Mitochondria and Metabolism: Complex Regulatory Mechanisms** *John Elrod, Elizabeth Murphy,* Brian O'Rourke, Mathias Mericskay, Catalina Vasilescu, Johannas Backs, Yibin Wang
- **Cancer and the Heart** *Sumanth Prabhu,* Aarti Asnani, Javid Moslehi, Rudolf de Boer, Anja Karlstaedt
- **Novel Approaches to Targeted Therapies** *Lucie Carrier, Thomas Vondriska,* Laura Zelarayán-Behrend, Timothy McKinsey, Gabriele Schiattarelli, William Pu
- **Keynote Session: From Primary Mechanism to Targeted Therapies for Cardiomyopathies** *Benjamin Prosser, Rong Tian,* Leslie Leinwand, Thomas Eschenhagen
- **The GRC Power Hour™** *Rong Tian, Jennifer Davis*

Cardiac Regulatory Mechanisms

Unraveling the Complexities of Cardiac Disease by Understanding Basic Mechanisms of Heart Function

JUNE 20 – 21, 2020

CHAIRS: Christopher Johnson and Arica Beisaw

Catalysis

Advancing Sustainable Technologies Through Catalysis

JUNE 28 – JULY 3, 2020 • COLBY-SAWYER COLLEGE, NEW LONDON, NH

CHAIR: Susannah Scott

VICE CHAIR: Javier Guzman

- **Sustainability Metrics for Catalysis** *Cathy Tway,* John Holladay, Peter Walther
- **Catalysis with Alternative Energy Inputs** *Umit Ozkan,* William Schneider, Kyoung-Shin Choi, Suljo Linic
- **Alternative Feedstocks for Manufacturing** *Daniel Resasco,* Karen Wilson, Fabio Ribeiro, Feng Wang
- **Synthesis of Well-Defined Catalysts** *Francisco Zaera,* Charles Sykes, Matteo Cargnello
- **Applications of Data Science in Catalysis** *Vassiliki-Alexandra Glezakou,* Hongliang Xin, Joel Schmidt
- **Dynamic Catalytic Behavior** *Philippe Sautet,* Rebecca Fushimi, Norbert Kruse, Anastassia Alexandrova
- ***Operando* Characterization of Catalysts** *Beata Kilos-Reaume,* Angelika Brückner, Juan Bravo-Suarez, Yong Wang
- **Insights from Mechanistic Investigations** *John Lockemeyer,* Rachel Getman, Justin Notestein
- **Keynote Session: Integration of Experiment, Computation and Theory** *Javier Guzman,* Dion Vlachos
- **The GRC Power Hour™** *Eranda Nikolla, Beata Kilos-Reaume*

Catalysis

Designing Catalysts to Advance Sustainability

JUNE 27 – 28, 2020

CHAIRS: Brandon Bukowski and Sarah Specht

Cell Biology of the Neuron

The Impact of Neuronal Shape, Structure and Size on Neuronal Function in Health and Disease

JUNE 28 – JULY 3, 2020 • WATERVILLE VALLEY, WATERVILLE VALLEY, NH

CHAIRS: Kang Shen and Valeria Cavalli

VICE CHAIRS: Monica Driscoll and Patrik Verstreken

- **Keynote Session: Transport Machinery and Structural Organization in Axons** *Yishi Jin,* Ron Vale, Matthew Rasband
- **Controlling Neuronal Shape, Size and Repair** *Binhai Zheng,* Mike Fainzilber, Oren Schuldiner, Alyson Fournier, Marc Hammarlund
- **Gene Regulation and Phase Transition in Health and Disease** *Pietro De Camilli,* Antonella Riccio, Mingjie Zhang, Don Cleveland
- **Synaptic Transmission** *Patrik Verstreken,* Camin Dean, Matthew Dalva, Ege Kavalali, Matthijs Verhage
- **Mitochondria and Cytoskeleton** *Antonina Roll-Mecak,* Erin Schuman, Richard Youle, Andrew Carter, Lukas Kapitein
- **Membrane Trafficking and Transport** *Thomas Schwarz,* Rejji Kuruvilla, Bettina Winckler, Erika Holzbaur, Giampietro Schiavo
- **Translation and Protein Homeostasis in Health and Disease** *Monica Driscoll,* Anne Bertolotti, Andrew Dillin, Jeffery Twiss
- **Neuron-Glia Interaction and Communication** *Cagla Eroglu,* Nicola Allen, Aiman Saab, Marc Freeman, Michael Granato
- **Keynote Session: New Technologies in Neuronal Cell Biology** *Erik Jorgensen,* Edward Boyden, Xiaowei Zhuang
- **The GRC Power Hour™** *Monica Driscoll, Rejji Kuruvilla*

Cell Biology of the Neuron

Molecular Understanding of the Neuron: Development, Plasticity and Function

JUNE 27 – 28, 2020

CHAIRS: Paul Donlin-Asp and Chinyere Agbaegbu Iweka

Cell Death

Cell Death-Associated Inflammation in Disease

JUNE 14 – 19, 2020 • FOUR POINTS SHERATON / HOLIDAY INN EXPRESS, VENTURA, CA

CHAIR: Francis Chan

VICE CHAIR: Pascal Meier

- **Keynote Session: Perspectives on the Mechanisms and Functions of Cell Death in Physiology** *Pascal Meier,* Marion MacFarlane, Vishva Dixit
- **Fundamental Mechanisms of Cell Death** *Kim Newton,* Ana Garcia-Saez, Douglas Green, Xiaodong Wang
- **Cell Death in Neuroinflammation and Neurological Disorders** *Carla Rothlin,* Junying Yuan, Marc Freeman, Dimitry Ofengeim
- **Cell Death in Immunity** *Hiroyasu Nakano,* Seamus Martin, Domagoj Vucic, Henning Walczak
- **Non-Canonical Cell Death** *Stephen Tait,* John Abrams, Eric Baehrecke, Marcus Conrad, J. Marie Hardwick
- **Immunogenic Cell Death** *Elizabeth Hartland,* Matthew Albert, Julie Magarian Blander, Carla Rothlin, Peter Vandenabeele
- **Harnessing Cell Death Mechanisms in Cancer** *Ana Garcia-Saez,* Anne Hamacher-Brady, Andreas Strasser, Stephen Tait
- **Infectious Diseases and Cell Death** *Julie Magarian Blander,* Elizabeth Hartland, Andrew Oberst, Feng Shao
- **Inflammation and Tissue Homeostasis** *Andrew Oberst,* Kim Newton, Manolis Pasparakis, John Silke
- **The GRC Power Hour™** *Marion MacFarlane*

Cell Death

Mechanisms of Cell Death in Homeostasis and Disease

JUNE 13 – 14, 2020

CHAIRS: Katherine Stewart and Florian Bock

Cell Polarity Signaling

Dynamics of Cell Polarity

MAY 31 – JUNE 5, 2020 • COLBY-SAWYER COLLEGE, NEW LONDON, NH

CHAIR: Jeremy Nance

VICE CHAIR: Yukiko Yamashita

- **Keynote Session: Polarity Within and Across Cells** *Yukiko Yamashita,* Geraldine Seydoux, Denise Montell
- **Dynamics of Cell Polarization** *Danelle Devenport,* Dominique Bergmann, Daniel Lew, Clemens Cabernard, Edwin Munro
- **Polarity Transitions During Development** *Sander van den Heuvel,* Jessica Feldman, Jean-Léone Maître, Ulrich Tepass
- **Polarity and Morphogenesis: Eggs and Embryos** *Jessica Feldman,* Sally Horne-Badovinac, John Wallingford, Yu-Chiun Wang
- **Cell Polarization and the Cytoskeleton** *William Bement,* Julie Canman, Gregg Gundersen, Stephanie Gupton, Terry Lechler
- **Polarity Transitions During Disease** *Terry Lechler,* Gillian Griffiths, Carole Parent, Erik Sahai
- **Polarity and Morphogenesis: Tissues and Organs** *Sally Horne-Badovinac,* Michel Bagnat, Danelle Devenport, Shigeo Hayashi, Jeff Rasmussen
- **Tissue Homeostasis: Wound Healing and Organs** *Carole Parent,* William Bement, Anne Classen, Jody Rosenblatt
- **Asymmetric Division and Stem Cells** *Dominique Bergmann,* Xin Chen, Ahna Skop, Renata Basto, Sander van den Heuvel
- **The GRC Power Hour™** *Danelle Devenport, Ahna Skop*

Cell Polarity Signaling

Cell Polarity Across Developmental Time and Space

MAY 30 – 31, 2020

CHAIRS: Andrew Tilston-Lunel and Melissa Pickett

Cellular and Molecular Fungal Biology

Understanding Fungal Function and Diversity: Complex Communities, Pathogenicity and Bioresources

JUNE 21 – 26, 2020 • HOLDERNESS SCHOOL, HOLDERNESS, NH

CHAIRS: Jason Stajich and Alexandra Brand

VICE CHAIRS: Nick Talbot and Anna Selmecki

- **Fungal Hijacking and Host Manipulation** *David Hughes,* Charissa de Bekker, Carolyn Elya, Matthew Kasson, Pietro Spanu
- **Cellular Organization and Molecular Biology** *James Kronstad,* Amy Gladfelter, Harold Corby Kistler, Joshua Nosanchuk, Duncan Wilson, Erfei Bi, Gero Steinberg
- **Fungal Mutualism and Symbiotic Interactions** *Christine Voisey,* Gregory Bonito, Jana U'Ren, Cameron Currie, Anna Rosling

- **Genomic Perspectives on Fungal Evolution** *Christina Cuomo,* David Hibbett, Antonis Rokas, Daniel Berry, Bridget Barker, Iuliana Ene, Daniel Croll, Annegret Kohler
- **Fungi in the Microbiome and Complex Communities** *Anthony Amend,* Nina Gunde-Cimerman, Iliyan Iliev, Teresa Pawlowska
- **Fungal Virulence and Drug Resistance** *Elaine Bignell,* Tamara Doering, Antonio Di Pietro, Jeniel Nett, Johanna Rhodes, Nicole Ludwig, Carol Munro
- **Fungi as Bioresources** *Nancy Keller,* Phillip Wiemann, Patrik Inderbitzin, Jason Slot
- **Sensing, Signaling and Development** *Alexander Idnurm,* Yi Liu, Janet Quinn, Neil Brown, Michael Freitag, Daniel Kornitzer, Julia Schumacher, Lauren Ryder
- **Late-Breaking Topics** *Anna Selmecki, Nick Talbot*
- **The GRC Power Hour™** *Elaine Bignell, Christina Cuomo*

Cellular and Molecular Fungal Biology

Fungal Diversity, Genetics and Pathogenicity

JUNE 20 – 21, 2020

CHAIRS: Elisa Vesely and Nicholas Raffa

Centromere Biology

Evolution, Structure, Regulation and Function of Centromeres in Health and Disease

JULY 26 – 31, 2020 • MOUNT SNOW, WEST DOVER, VT

CHAIR: Sylvia Erhardt

VICE CHAIR: Iain Cheeseman

- **Keynote Session: Centromeres: From Evolution to Human Health** *Iain Cheeseman,* Harmit Malik, Genevieve Almouzni
- **Biophysical Properties of Centromeres** *Stephen Harrison,* David Barford, Michael Lampson, Ekaterina Grishchuk, Andrea Musacchio
- **Centromere Dysfunction: Chromosome Segregation Defects and Disease** *Ben Black,* Don Cleveland, Beth Sullivan, Daniele Fachinetti, Hironori Funabiki
- **Centromeres in Meiosis and Stem Cell Division** *Arshad Desai,* Elaine Dunleavy, Julia Cooper, Yukiko Yamashita
- **Centromere Genomics, Evolution and Variability** *Steven Henikoff,* Ines Drinnenberg, Luca Comai, Karen Miga
- **Epigenetic Regulation of Centromere Identity** *Patrick Heun,* Daniel Foltz, Yael Nechemia-Arbely, Fangpu Han, Barbara Mellone
- **Transcripts and Transcription Control of Centromere Function** *Claire Francastel,* Rachel O'Neill, Michael Blower, Dawn Carone, Robin Allshire
- **Building Blocks Around and Above the Centromere** *Ann Ehrenhofer-Murray,* Sue Biggins, Tatsuo Fukagawa, Jennifer Deluca, Hitoshi Kurumizaka
- **New Concepts of Centromere Function and Regulation** *Lars Jansen,* Gary Karpen, William Earnshaw, Aaron Straight
- **The GRC Power Hour™** *Elaine Dunleavy, Rachel O'Neill*

Centromere Biology

Regulating Centromere Function Through Structure

JULY 25 – 26, 2020

CHAIRS: Samuel Corless and Maiko Kitaoka

Chemistry and Biology of Tetrapyrroles

The Roles of Tetrapyrroles in Catalysis, Regulation, Metabolism and Disease

JULY 19 – 24, 2020 • SALVE REGINA UNIVERSITY, NEWPORT, RI

CHAIR: Emma Raven

VICE CHAIR: Amy Medlock

- **Structural Approaches to the Study of Tetrapyrroles** *Syun-Ru Yeh,* Wyatt Yue, Allen Orville, Hitomi Sawai
- **Trafficking, Signalling and Regulation by Heme** *Ann English,* Emily Weinert, Hiroaki Kitagishi, Andrew Hudson, Dennis Stuehr
- **The Biogenesis and Functions of Bilins** *J. Clark Lagarias,* Beronda Montgomery, Tammi Richardson, William Lanzilotta
- **Tetrapyrroles in Human Health and Disease** *Peter Meissner,* Makiko Yasuda, Barden Chan, Levi Wood, Diane Ward
- **The Biology of Tetrapyrroles: Catalysis and Mechanism** *Elizabeth Boon,* Elisa Tomat, Brian Crane, Micah Nelp
- **B_{12}: Biosynthesis, Transport, Pharmacology and Mechanistic Enzymology** *Stephen Ragsdale,* Dorota Gryko, Alison Smith, Ritimukta Sarangi, Tessa Young
- **Regulation and Biosynthesis of Chlorophyll Pigments** *Jennifer Bridwell-Rabb,* Min Chen, Jean Alric, Neil Hunter
- **Microbial Tetrapyrrole Metabolism** *Mark Shepherd,* Celia Goulding, Stefan Hofbauer, Juliette Lecomte, Michael Niederweis
- **Keynote Session: Tetrapyrrole Regulation and Homeostasis** *Samuel Beale,* Angela Wilks, Mark O'Brian
- **The GRC Power Hour™** *Amy Medlock*

Chemotactic Cytokines

Orchestrating Cell Migration and Location in Health and Disease

JUNE 14 – 19, 2020 • LES DIABLERETS CONFERENCE CENTER, LES DIABLERETS, SWITZERLAND

CHAIR: Marcus Thelen

VICE CHAIR: Ronen Alon

- **Keynote Session: Chemokines in Rare Diseases** *Gerry Graham,* Philip Murphy, Sergio Lira
- **Signal Transduction in Cell Migration and Biased/ G-Protein Independent Signaling** *Tracy Handel,* Mario Mellado, Silvano Sozzani, Michel Bouvier, Mette Rosenkilde
- **State-of-the-Art Methods to Explore the Chemokine System in Cell Migration** *Bernhard Moser,* Matthias Mehling, Tal Arnon, Carole Parent
- **Chemokine Patterns and Atypical Chemokine Receptors** *Daniel Legler,* Michael Sixt, Burkhard Ludewig, Ralf Stumm, Antal Rot
- **Alternate Signaling by Chemokine Receptors** *Philip Murphy,* Erez Raz, Barbara Moepps, Daniel Legler
- **Chemokines in Cancer Immunity and Metastasis** *Sergio Lira,* Andrew Luster, Joanna Groom, Adit Ben-Baruch, Ann Richmond
- **Chemokine and Chemokine Receptor Structure and *In Silico* Modeling** *Mette Rosenkilde,* Thomas Schall, Brian Volkman, Tracy Handel
- **Chemokines in Immune Pathologies** *Andrew Luster,* Gerry Graham, Sussan Nourshargh, Christoph Scheiermann, Mariagrazia Uguccioni
- **Keynote Session: Chemokines in Immune Responses** *Ronen Alon,* Eugene Butcher, Ziv Shulman, Reinhold Förster
- **The GRC Power Hour™** *Ann Richmond*

Chemotactic Cytokines

Chemokine Structure, Function and Receptor Interactions in Homeostasis and Disease

JUNE 13 – 14, 2020

CHAIRS: Acacia Dishman and Gillian Wilson

Chromatin Structure and Function

Chromatin Modifications, RNA and Metabolism

MAY 31 – JUNE 5, 2020 • REY DON JAIME GRAND HOTEL, CASTELLDEFELS, SPAIN

CHAIR: Asifa Akhtar

VICE CHAIR: Geeta Narlikar

- **Remodeling Chromatin Structure** *Ali Shilatifard,* Carl Wu, Karolin Luger, Craig Peterson, Shiv Grewal
- **Chromatin Assembly, Replication and Repair** *Peter Becker,* Thomas Jenuwein, Robert Kingston, Danny Reinberg, Caroline Dean, Steven Jacobsen
- **Histone and RNA Modifications** *Wendy Bickmore,* Jeannie Lee, Claire Rougeulle, Tony Kouzarides, William Greenleaf
- **Chromosomes and Genome Architecture** *Karolin Luger,* Edith Heard, Wendy Bickmore, Peter Fraser, Ting (C-ting) Wu, Peter Becker
- **Chromatin, Metabolism and Physiology** *Robert Kingston,* Paolo Sassone-Corsi, Raul Mostoslavsky, Shelley Berger, Andreas Ladurner
- **Reprogramming and Regeneration** *Joanna Wysocka,* Anne Ferguson-Smith, Yi Zhang, Bradley Cairns, Amanda Fisher, Alexander Meissner
- **Chromatin and Disease Mechanisms** *Karen Adelman,* Sharon Dent, Ali Shilatifard, Joanna Wysocka, Cigall Kadoch
- **Chromatin Biophysics** *Geeta Narlikar,* Xavier Darzacq, Ibrahim Cisse, Michael Rosen, Leonid Mirny, Zhucheng Chen
- **Transcription and Post-Transcriptional Events** *Ibrahim Cisse,* Karen Adelman, Hiroshi Kimura, Dirk Schubeler, Jerry Workman
- **The GRC Power Hour™** *Anne Ferguson-Smith, Claire Rougeulle*

Chromatin Structure and Function

Micro to Macro Chromatin Structure in Epigenetics and Disease

MAY 30 – 31, 2020

CHAIRS: Robert Porter and Jumana AlHaj Abed

Climate Engineering

Processes and Impacts of Radiation Management Approaches to Climate Change

JUNE 28 – JULY 3, 2020 • GRAND SUMMIT HOTEL AT SUNDAY RIVER, NEWRY, ME

CHAIRS: Douglas MacMartin and Trude Storelvmo

VICE CHAIRS: Simone Tilmes and Ulrike Lohmann

- **Keynote Session: Climate Engineering Scenarios** *Mark Lawrence,* Thomas Stocker, Piers Forster
- **Stratospheric Processes** *Valentina Aquila,* Jadwiga Richter, Alan Robock, Karen Rosenlof
- **Alternative Methods** *Ulrike Niemeier,* Kate Ricke, Sonia Seneviratne
- **Cloud-Mediated Processes** *Thomas Leisner,* Daniel Rosenfeld, Robert Wood, Helene Muri
- **Combining and Comparing Different Methods** *Olivier Boucher,* Daniele Visioni, Blaz Gasparini
- **Climate Response and Impacts** *Daniel Schrag,* Isla Simpson, Peter Irvine, Jonathan Proctor
- **Developing World Impacts** *Michael Taylor,* Govindasamy Bala, Ines Camilloni
- **Engineering and Risk Management** *Thomas Ackerman,* David Keith, Ben Kravitz, Wake Smith
- **Transdisciplinary Research for Radiation Management** *James Hurrell,* Chris Field
- **The GRC Power Hour™** *Ulrike Lohmann, Simone Tilmes*

Climate Engineering

Physical Processes and Societal Impacts of Radiation Management Approaches to Climate Change

JUNE 27 – 28, 2020

CHAIRS: Katherine Dagon and Daniele Visioni

Colloidal Semiconductor Nanocrystals

Nanocrystal Chemistry, Physics and Applications

JULY 5 – 10, 2020 • LES DIABLERETS CONFERENCE CENTER, LES DIABLERETS, SWITZERLAND

CHAIRS: Maksym Kovalenko and Matt Law

VICE CHAIRS: Gordana Dukovic and Efrat Lifshitz

- **Synthesis Science** *Brandi Cossairt,* Uri Banin, Elena Shevchenko
- **Bioapplications** *Carlos Toro,* Allison Dennis, Wolfgang Parak, Teresa Pellegrino, Inge Herrmann
- **Assemblies and Collective Phenomena** *Dmitri Talapin,* Nuri Yazdani, Sara Bals, Christopher Murray, Christophe Delerue
- **Charge, Energy and Heat Transport** *Mikhail Zamkov,* Lea Nienhaus, Maria Ibáñez, Cherie Kagan, Marcus Scheele
- **Photophysics** *Vanessa Wood,* Victor Klimov, Patanjali Kambhampati, Zeger Hens, Daniel Gamelin
- **Towards Quantum Light Sources** *Matthew Sheldon,* Peter Sercel, Brahim Lounis, Yoshihiko Kanemitsu, Moungi Bawendi
- **Photochemistry and Energy Conversion** *Raffaella Buonsanti,* Emily Weiss, Jillian Dempsey, Susanna Thon, Vivian Ferry
- **Optoelectronics** *Maria Antonietta Loi,* Hilmi Volkan Demir, Eunjoo Jang, Sohee Jeong, Sergio Brovelli
- **Nanocrystals for the Infrared** *Javier Vela,* Wolfgang Heiss, Philippe Guyot-Sionnest, Gerasimos Konstantatos, Emmanuel Lhuillier
- **The GRC Power Hour™** *Gordana Dukovic, Efrat Lifshitz*

Colloidal Semiconductor Nanocrystals

Light-Matter Interactions in Semiconductor Nanomaterials

JULY 4 – 5, 2020

CHAIRS: Tyler Milstein and Xing Yee Gan

Computational Chemistry

Multiscale Modeling of Complex Systems: Methods and Applications

JULY 19 – 24, 2020 • REY DON JAIME GRAND HOTEL, CASTELLDEFELS, SPAIN

CHAIRS: Adrian Roitberg and Zoe Cournia

VICE CHAIRS: Natalie Fey and Frank Neese

- **Linking Molecular Structure and Dynamics to Function** *Andrea Cavalli,* Syma Khalid, Marco De Vivo, Adrian Mulholland, Darrin York
- **Methods and Applications in Free Energy Calculations** *Chris Chipot,* William Jorgensen, Lee Woodcock, Hugo Gutierrez-De-Teran, Xinjun Hou
- **From Quantum Dynamics to Multiscale Modeling of Materials and Interfaces** *Spiridoula Matsika,* Gerald Tanoury, Sotiris Xantheas, Ana Nicoleta Bondar
- **Modeling Nucleic Acids** *Modesto Orozco,* Thomas Cheatham, Pablo Dans
- **Modeling Functional Materials** *Fernanda Duarte Gonzalez,* Seonah Kim, Edward Sherer
- **Using Machine Learning for Molecular Design** *Natalie Fey,* Frank Noe, Gianni De Fabritiis, Olexandr Isayev, Tatjana Braun
- **Integrating Big Data in Drug Discovery Applications: From Allostery to Biologics Design** *Kenneth Merz,* Ivet Bahar, Rebecca Wade, Chris de Graaf, Masha Niv
- **Multiscale Modeling for Computer-Aided Drug Design** *Simone Fulle,* Ronald Knegtel, Silvia Lovera, Jeremy Smith
- **Modeling Long-Scale Conformational Dynamics** *Lee Woodcock,* Cecilia Clementi, Karissa Sanbonmatsu
- **The GRC Power Hour™** *Zoe Cournia, Syma Khalid*

Computational Chemistry

How Computational Method Development Translates into Application

JULY 18 – 19, 2020

CHAIRS: Anna Kamenik and Taylor Quinn

Correlated Electron Systems

Topology and Correlations: Long-Range Entanglement in Many-Body Systems

JUNE 28 – JULY 3, 2020 • MOUNT HOLYOKE COLLEGE, SOUTH HADLEY, MA

CHAIRS: Nandini Trivedi and James Analytis

VICE CHAIRS: Senthil Todadri and Suchitra Sebastian

- **Strange Metals and Fundamental Bounds on Transport** *Louis Taillefer,* Erez Berg, Ian Hayes, Dan Shahar
- **Hydrodynamics and Unconventional Transport in Ultra-Pure Systems** *Andrew Mackenzie,* Julia Link, Shahal Ilani, Dmitri Basov, Veronika Sunko
- **Quantum Spin Liquids: Topological Order** *Hae-Young Kee,* Xie Chen, Ciaran Hickey, Kate Ross
- **Quantum Spin Liquids: Kitaev Systems** *Natalia Perkins,* Johannes Knolle, Alex Frano, Stephen Wilson, Minoru Yamashita
- **Fractionalization and Anomalous Quantum Hall** *Ashvin Vishwanath,* Mitali Banerjee, Gael Grissonnanche, Yuji Matsuda
- **Magic Angles and Correlations in Moire Materials** *Senthil Todadri,* Pablo Jarillo-Herrero, Cory Dean, Ali Yazdani, Mohit Randeria
- **Moire Magnetism and Superconductivity** *ChunNing Lau,* Liang Fu, David Goldhaber-Gordon, Feng Wang
- **Non-Equilibrium Dynamics in Correlated Materials** *Joerg Schmalian,* Michel Devoret, Ehud Altman, Vedika Khemani, Dragan Mihailovic
- **Late-Breaking Topics** *Subir Sachdev,* Harold Hwang, Nicholas Butch
- **The GRC Power Hour™** *Suchitra Sebastian*

Correlated Electron Systems

Emergent Electronic Order, Fractionalization and Long-Range Entanglement in Quantum Materials

JUNE 27 – 28, 2020

CHAIRS: Ali Husain and Debanjan Chowdhury

Crystal Engineering

Inspired Design, Assembly and Properties of Molecular Materials

JUNE 21 – 26, 2020 • GRAND SUMMIT HOTEL AT SUNDAY RIVER, NEWRY, ME

CHAIR: Jennifer Swift

VICE CHAIR: Andy Cooper

- **Order, Disorder and Defects** *Aurora Cruz-Cabeza,* Lynne Taylor, Karena Chapman
- **Crystal Assembly** *Michael Mcbride,* Matteo Salvalaglio, Katharina Edkins, Jeffrey Rimer, Ying Diao
- **Polymorphs and Mixtures** *Yu-Sheng Chen,* Steven Halaby, Robert Schurko, Karah Knope
- **Crystals Under Pressure** *Bruno Hancock,* Iain Oswald, Jack Clegg, Calvin Sun, Daniel Hooks
- **Crystal Reactivity** *Pance Naumov,* Kana Sureshan, Jason Benedict
- **Pharmaceuticals and Cocrystals** *Rositza Petrova,* Nair Rodriguez, Doris Braun, Franziska Emmerling, Michael Bellucci
- **Big Data and Informatics** *Graeme Day,* Ian Bruno, Christer Aakeroy
- **Porosity and Open Framework Materials** *Brian Smith,* Rahul Banerjee, Kim Jelfs, Craig Brown, Katherine Mirica
- **Engineering on Different Length Scales** *Kristin Hutchins,* Chenfeng Ke, Benjamin Palmer
- **The GRC Power Hour™**

Crystal Engineering

Engineering Crystals in the Fourth Dimension: Monitoring of Structural Changes in Crystals

JUNE 20 – 21, 2020

CHAIRS: Ivana Brekalo and Ren Wiscons

Cyclic Nucleotide Phosphodiesterases

Probing and Targeting PDEs: From Local Control of Signaling Nanodomains to Functional Impact

JUNE 28 – JULY 3, 2020 • LES DIABLERETS CONFERENCE CENTER, LES DIABLERETS, SWITZERLAND

CHAIRS: Jos Prickaerts and Jin Zhang

VICE CHAIRS: Viacheslav Nikolaev and Michy Kelly

- **Cyclic Nucleotide Signaling Pathways: From Receptors to Targets** *Miles Houslay,* Carmen Dessauer, Martin Lohse, Susan Taylor, Martina Schmidt
- **Spatiotemporal Regulation of Cyclic Nucleotide Signaling** *Viacheslav Nikolaev,* Manuela Zaccolo, John Scott, Aldebaran Hofer, Mark Gomelsky
- **Structural, Molecular and Systems Dissection of PDE Signaling** *Nikolai Artemyev,* Colleen Clancy, Rick Cote, Friederike Cuello
- **Cyclic Nucleotide Signaling in Cardiovascular Systems** *Rodolphe Fischmeister,* Christina Kruuse, Yang Xiang, Xiaodong Cheng, Chen Yan, David Kass
- **Novel and Atypical Signaling** *Manuela Zaccolo,* Roland Seifert, Dagmar Wachten, David Baker
- **Selective PDE Targeting of Central Nervous System Functions** *Michy Kelly,* Achim Schmidtko, Dorit Ron, Pierre Vincent, Jan Kehler
- **PDEs in Vascular and Metabolic Processes** *Enno Klussmann,* Donald Maurice, Mary Anna Venneri, Anders Tengholm, Alexander Pfeifer
- **PDE Mediated Signaling in Immunological and Inflammatory Processes** *Joseph Beavo,* Haibin Luo, Gretchen Snyder, Stefan Brocke, Kjetil Tasken, Ralf Hoffmann
- **Therapeutic Considerations and Path to the Clinic** *Gretchen Snyder,* Coleen Atkins, Harald Schmidt
- **The GRC Power Hour™** *Michy Kelly, Viacheslav Nikolaev*

Cyclic Nucleotide Phosphodiesterases

Mapping of PDE Pathways and the Translation into Functional Impact

JUNE 27 – 28, 2020

CHAIRS: Melissa Schepers and Amy Tibbo

Cytoskeletal Motors

Molecular Machines: From Biophysics to Physiology to Disease

JULY 12 – 17, 2020 • MOUNT SNOW, WEST DOVER, VT

CHAIR: Steven Rosenfeld

VICE CHAIR: Margaret Titus

- **Keynote Session: Motors Working in a Context** *Margaret Titus,* Vladimir Gelfand, Kathleen Trybus
- **Motors in Cardiovascular Disease** *David Warshaw,* Anne Houdusse, James Spudich, Theresia Kraft, Sanford Bernstein
- **Structure and Regulation** *Carolyn Moores,* Ahmet Yildiz, Anthony Roberts, Hernando Sosa, Stefan Raunser
- **Motors in Cell Motility and Transport** *James Sellers,* David Warshaw, Richard Cheney, Samara Reck-Peterson, Matthew Lang
- **Modeling and Analysis of Molecular Motor Systems** *Erkan Tuzel,* David Odde, Tamara Bidone, Michael Murrell, Michael Diehl
- **Motor Generated Forces in Cell Function** *Sarah Heissler,* Michael Ostap, Ewa Paluch, Andre Levchenko, Dylan Burnette
- **Tracks and Filaments** *Antonina Roll-Mecak,* Anna Kashina, Enrique De La Cruz, Jennifer Ross, Casper Hoogenraad
- **Motors in Cancer, Psychiatric, Metabolic and Infectious Diseases** *Lee Sweeney,* Anne Bresnick, Jonathan Kirk, Dominique Soldati-Favre, Michael Way, Courtney Miller
- **Motors in Mitosis** *Jason Stumpff,* Ekaterina Grishchuk, William Bement, Tarun Kapoor, Sophie Dumont
- **The GRC Power Hour™** *Carolyn Moores*

Cytoskeletal Motors

Molecular Machines: From Biophysics to Physiology to Disease

JULY 11 – 12, 2020

CHAIRS: Ashley Arthur and Donte Stevens

Deep Carbon Science

Exploring Fluxes, Forms and Origins of Deep Carbon in Earth and Other Terrestrial Planets

JUNE 28 – JULY 3, 2020 • BATES COLLEGE, LEWISTON, ME

CHAIRS: Edward Young and Kai-Uwe Hinrichs

VICE CHAIRS: Tamsin Mather and Doug LaRowe

- **Origins of Carbon in the Solar System** *Mary Voytek,* Bernard Marty, Siyi Xu
- **Earth's Deep Carbon Cycle** *Michael Walter,* Andrea Giuliani, Graham Pearson, Jonathan Tucker, Katherine Armstrong
- **Extreme Physics, Chemistry and Biology of Carbon** *Jie Li,* Razvan Caracas, Susannah Dorfman, Jung-Fu Lin
- **New Tracers of the Provenance of Hydrocarbons** *Scott Wankel,* Thomas Giunta, Max Lloyd, Jeffrey Marlow, Jill McDermott
- **Serpentinization and Deep Life** *Matthew Schrenk,* Susan Lang, Florence Schubotz, Alexis Templeton
- **Life at Its Limits** *Doug LaRowe,* Jennifer Macalady, Brandy Toner, Elizabeth Trembath-Reichert, Fengping Wang
- **Connections Between Deep Carbon and Atmospheres** *Tamsin Mather,* Peter Barry, Francis Macdonald, Sabin Zahirovic
- **The Fate of Carbon During Subduction** *Terry Plank,* Maarten de Moor, Megan Duncan, Matthieu Galvez, Craig Manning
- **Late-Breaking Topics** *Rachel Harris*
- **The GRC Power Hour™** *Jennifer Macalady*

Deep Carbon Science

Carbon at the Intersection of the Biosphere and Geosphere

JUNE 27 – 28, 2020

CHAIRS: Jonathan Tucker and Rachel Harris

Defects in Semiconductors

Defect Formation, Characterization, Control and Utilization

AUGUST 16 – 21, 2020 • COLBY-SAWYER COLLEGE, NEW LONDON, NH

CHAIR: Jeffrey McCallum

VICE CHAIR: Kai-Mei Fu

- **Developments in Defect Spectroscopy and Metrology** *Lasse Vines,* Darshana Wickramaratne, Jean-Philippe Tetienne
- **Color Centers in Wide Band-Gap Semiconductors and 2D Materials for Quantum Applications** *Marina Radulaski,* Chitraleema Chakraborty, Cyrus Dreyer
- **Characteristics of Defects in 2D Materials and Oxide Semiconductors** *Joel Varley,* John Lyons, Matt McCluskey, Prineha Narang
- **Spin Centers: Spectroscopy and Applications** *Takeshi Ohshima,* Stefania Castelletto, Sophia Economou, Alexander Weber-Bargioni
- **Defects in Nitride Semiconductors** *Mary Ellen Zvanut,* Ramon Collazo, Annemarie Exarhos
- **Defects in Photovoltaic Materials and Devices, Identification and Control** *Gudrun Kissinger,* Clas Persson, Hele Savin, Vladan Stevanovic
- **Defect Characterization and Control** *Elif Ertekin,* Jinwoo Hwang, Anyao Liu, Atsushi Oshiyama
- **High Resolution Imaging and Characterization of Defects** *Paul Koenraad,* Joe Salfi, Lorenzo Rigutti
- **Keynote Session: Toward Single Defect Imaging in Layered and 3D Materials** *Kai-Mei Fu,* Jianwei Miao
- **The GRC Power Hour™** *Hongling Lu, Kai-Mei Fu*

Defects in Semiconductors

Defect Formation, Characterization, Control and Utilization

AUGUST 15 – 16, 2020

CHAIRS: Philip Weiser and Hongling Lu

Diffraction Methods in Structural Biology

Steering Methods Toward Overcoming the Most Difficult Challenges in Structural Biology

JULY 26 – 31, 2020 • BATES COLLEGE, LEWISTON, ME

CHAIR: James Holton

VICE CHAIR: Janet Newman

- **Structural Biology with a Trillion Dollars** *Eleanor Dodson,* Tom Blundell, Chao Zhang
- **Optimal Data Collection Limited by Time, Equipment and Sample Quality** *Ana Gonzalez,* Elspeth Garman, Arwen Pearson, Sarah Perry, Kunio Hirata
- **Growing and Blotting: Best Sample Prep Given Uncooperative Molecules** *Alex McPherson,* Sarah Bowman, Anchi Cheng
- **Processing Algorithms for Difficult Data** *Kay Diederichs,* Jennifer Wierman, Thomas White, Nicholas Sauter, Dominika Borek, Wolfgang Kabsch
- **Massive Radiations: Electrons, Neutrons and Helium** *Garib Murshudov,* Gloria Borgstahl, Wah Chiu, James Fitzpatrick
- **Interpreting Low-Resolution Maps** *Paul Emsley,* Tristan Croll, Airlie McCoy, Jane Richardson, Isabel Uson
- **Divining Ligands with Confidence** *Bernhard Rupp,* Tom Peat, Frank Von Delft
- **Selected Poster Presentations** *Edward Snell*
- **The R-Factor Gap: Disorder, Dynamics and Function** *Helen Ginn,* Rozaliya Barabash, Andrea Thorn
- **The GRC Power Hour™** *Eleanor Dodson*

Diffraction Methods in Structural Biology

Data-Rich Experiments in Serial Crystallography, Time-Resolved Studies and MicroED

JULY 25 – 26, 2020

CHAIRS: Jennifer Wierman and James Parkhurst

DNA Topoisomerases in Biology and Medicine

Topoisomerase Mechanism, Function and Inhibition: From Single-Molecule Analyses to Clinical Trials

AUGUST 9 – 14, 2020 • BRYANT UNIVERSITY, SMITHFIELD, RI

CHAIRS: Lynn Zechiedrich and Keir Neuman

VICE CHAIRS: Yuk-Ching Tse-Dinh and Dagmar Klostermeier

- **Keynote Session: Molecular Mechanisms to Clinical Trials** *Valakunja Nagaraja,* Sue Jinks-Robertson, Yves Pommier
- **Topoisomerases as Targets for Antimicrobial Agents** *Marc Drolet,* Alexandra Aubry, Pan Chan, Neil Osheroff
- **Processing of Topoisomerase Adducts** *Hanna Klein,* Heidrun Interthal, Robert Van Waardenburg
- **Interplay Between Genome Topology and Topoisomerase Interactions** *David Levens,* Konstantin Severinov, Laura Baranello, Erez Aiden
- **Modeling DNA Topoisomerases and Topology** *Sarah Harris,* Mariel Vasquez, Davide Marenduzz
- **Topoisomerases and DNA Topology in Cancer Chemotherapy** *Scott Kaufmann,* Mary-Ann Bjornsti, Junjie Chen, Karen Vasquez
- **DNA Topology and Topoisomerases at the Single Molecule Level** *Alice Pyne,* Zev Bryant, Michelle Wang
- **Topoisomerases as Cellular Poisons and Essential Enzymes** *Shunichi Takeda,* Nayun Kim, Yuh-Hwa Wang, Anna Bizard
- **Topoisomerase Structure and Function** *Valerie Lamour,* Nei-Li Chan, James Berger
- **The GRC Power Hour™** *Yuk-Ching Tse-Dinh*

DNA Topoisomerases in Biology and Medicine

Enzymology, Cellular Functions, Roles in Diseases and Therapeutic Targeting

AUGUST 8 – 9, 2020

CHAIRS: Amanda Riccio and Thomas Germe

Drug Carriers in Medicine and Biology

Enabling New Therapies Through Drug Carrier Design

AUGUST 2 – 7, 2020 • MOUNT SNOW, WEST DOVER, VT

CHAIRS: Suzie Pun and Samir Mitragotri

VICE CHAIRS: Kathryn Whitehead and Vadim Dudkin

- **Keynote Session: Drug Carriers Revolutionizing Therapeutic Approaches** *Vladimir Muzykantov, Dennis Lee,* Laura Sepp-Lorenzino, David Mooney, Jennifer West
- **New Materials for Drug Delivery** *Ester Kwon,* Kristy Ainslie, Jianjun Cheng, Jean-Christophe Leroux, Paul Wender
- **Advances Toward Translation** *Elizabeth Nance,* Hongming Chen, Jinming Gao, Anna Schwendeman
- **Drug Carriers in Oncology** *Rizia Bardhan,* Natalie Artzi, Michael Kavanaugh, Tatiana Novobrantseva, Anand Subramony
- **Cell-Mediated Drug Delivery** *Aaron Anselmo,* Thomas Andresen, Elena Batrakova, Zhen Gu
- **Intracellular Delivery of Biologics** *Michael Mitchell,* Roger Adami, Julie Champion, Craig Duvall, Jonathan Gilbert
- **Selected Poster Presentations** *Kathryn Whitehead, Vadim Dudkin*
- **Biological Carriers** *Olivia Merkel,* Laura Ensign, Don Hilvert, David Schaffer, Nicole Steinmetz
- **Overcoming Barriers to Oral Drug Delivery** *Omid Veiseh,* Maria Jose Alonso, Giovanni Traverso, Sujatha Sonti
- **The GRC Power Hour™** *Kristy Ainslie*

Drug Carriers in Medicine and Biology

Exploring Size-Based Delivery Strategies for Biologics and Novel Drug Cargos

AUGUST 1 – 2, 2020

CHAIRS: Anusha Pusuluri and Nicholas Lamson

Drug Metabolism

Drug Discovery to Precision Therapeutics: Novel Mechanisms, Models and Technologies

JULY 12 – 17, 2020 • HOLDERNESS SCHOOL, HOLDERNESS, NH

CHAIR: J. Steven Leeder

VICE CHAIR: Jane Kenny

- **Keynote Session: Integration of Drug Metabolism Science and Big Data to Inform Precision Medicine** *Jane Kenny,* Sir Munir Pirmohamed
- **Drug Metabolism by the Intestinal Microbiome** *Andrew Goodman,* Peter Turnbaugh, Nichole Klatt, Matthew Redinbo, Michael Zimmerman
- **Drugs of the Future: Probing the ADME Properties of Novel Therapeutics** *Sara Humphreys,* Gaurav Bhardwaj, Diane Ramsden, Larry Snyder
- **Drug Transporters: Advancing Drug Development and Precision Therapeutics** *Kim Brouwer,* Bruno Hagenbuch, Kaspar Locher, Pallabi Mitra, Gauri Rao
- **New Techniques in Drug Metabolism Methodology** *Katherine Elvira,* Yingying Guo-Avrutin, Cristina Shen, Boyang Zhang
- **Prediction of Drug Metabolism *In Vivo* from *In Vitro* Studies** *R. Scott Obach,* Leslie Benet, Murat Cirit, Charity Nofziger, Kazuo Takayama
- **Selected Poster Presentations** *Patrick Murphy*
- **Mechanisms of Drug Metabolism** *Emily Scott,* Richard Auchus, Xinxin Ding, Ruili Huang, Eric Johnson

"GRCs maintain the optimal balance of allowing researchers to openly and extensively discuss emergent and unpublished work while providing ample opportunities for social activities to help forge meaningful professional relationships."

JASON TORRES, Wellcome Centre for Human Genetics, Human Genetics and Genomics GRC

- **Harnessing Technology to Advance Individualized Therapeutics** *Namandje Bumpus,* Netz Arroyo, Catherine Fenselau, David Rodriguez
- **The GRC Power Hour™** *Klarissa Jackson, Francesca Toselli*

Drug Metabolism
Translational Models and Technologies to Predict Drug Disposition and Response
JULY 11 – 12, 2020
CHAIR: Chelsea Hosey-Cojocari

Drug Resistance
Strategies to Disrupt Drug Resistance in Infectious Disease, Cancer and Agriculture
JUNE 28 – JULY 3, 2020 • BRYANT UNIVERSITY, SMITHFIELD, RI
CHAIRS: Lizbeth Hedstrom and Daruka Mahadevan
VICE CHAIRS: Aaron Goldman and Alexis Kaushansky

- **Keynote Session: Protecting New Drugs and Pesticides Against Resistance** *Alexis Kaushansky,* Seva Rostovtsev, Sumathi Nambiar
- **Resistance Mechanisms** *Pradipsinh Rathod,* Houra Merrikh, Susan Rosenberg, Sophie Helaine
- **Systems and Modeling Strategies to Address Resistance** *Alita Miller,* Funda Meric-Bernstam, Pamela Yeh, Nitin Baliga
- **Combating Resistance with Novel Targets** *Mithila Jugulam,* Emily Derbyshire, Franck Dayan, Eachan Johnson, Mark Rolfe
- **Durable Drug Design** *Timothy Wencewicz,* Andrew Hopkins, David Epstein
- **Eco-Evolutionary Strategies to Address Resistance** *Andriy Marusyk,* Eugene Shakhnovich, Jacob Scott
- **Threats and Responses** *Funda Meric-Bernstam,* Pradipsinh Rathod, Sarat Chandarlapaty
- **Microbiome and Resistance** *Bree Aldridge,* Yoshitomo Kikuchi, Neha Garg, Peter Belenky, Christopher Ford
- **Keynote Session: Emerging Strategies to Combat Resistance** *Aaron Goldman,* Paul Turner, James Welsh, Richard Alm
- **The GRC Power Hour™** *Priscilla Yang, Celia Schiffer*

Drug Resistance
Mechanisms and Approaches to Overcoming Drug Resistance in Cancer, Infectious Disease and Agriculture
JUNE 27 – 28, 2020
CHAIR: Michael Lombardo

Drug Safety
Advances in Machine Learning, Models and Clinical Considerations for Drug Safety
JUNE 14 – 19, 2020 • STONEHILL COLLEGE, EASTON, MA
CHAIR: Myrtle Davis
VICE CHAIR: Mark Fielden

- **Keynote Session: Modeling Complex Biological Systems** *David Watson,* Dennis Discher
- **Emerging Applications of Big Data and Machine Learning in Safety Assessment** *Donald Mager, James Stevens,* K. Melissa Hallow, Lazlo Urban
- **Leveraging Human Genetics and Big Data to Inform Drug Safety** *Blanca Rodriguez,* Danish Saleheen, Lucas Ward, Hao Zhu
- **Biomarker Science in Drug Discovery and Development** *Vishal Vaidya,* Guru Aithal, Holly Soares, Benjamin Humphreys
- **Microphysiological Models: Advances in Modeling Complex *In Vivo* Functions and Organ Responses** *Anthony Bahinski, Kyle Kolaja,* Mark Donowitz, Hunter Rogers, Girija Goyal
- **New Paradigms in Translational Safety Science** *Leigh Ann Burns Naas, Ruth Roberts,* Lolke Dehaan, Ekaterina Malievskaia, Michael Morton, Eric Sobie
- **Novel Therapeutic Modalities: Challenges and Opportunities in Nonclinical Safety Assessment Strategies** *Wendy Freebern, Jeff Willy,* James Bradner, Kathy Meyer, Padma Narayanan
- **Full Utilization of the Clinical Experience in the Nonclinical Space** *Michelle Berny-Lang, Lori Minasian,* Bonnie Ky, Christine Miaskowski, Yinghong (Mimi) Wang
- **Keynote Session: Advancing Drug Safety Through Innovation** *Mark Fielden,* Manasi Nandi
- **The GRC Power Hour™** *Michelle Berny-Lang, Leigh Ann Burns Naas*

Drug Safety
Emerging Technologies and Strategies for Drug Safety Evaluation
JUNE 13 – 14, 2020
CHAIRS: Lauren Lewis and Molly Morgan

Electron Donor-Acceptor Interactions
Electron and Energy Transfer Processes: New Perspectives and Emerging Directions
AUGUST 2 – 7, 2020 • SALVE REGINA UNIVERSITY, NEWPORT, RI
CHAIRS: Felix Castellano and Claudia Turro
VICE CHAIRS: Lin Chen and Ferdinand Grozema

- **Bio-Inspired Charge Transfer Chemistry** *Jessica White,* Leif Hammarström, Hannah Shafaat, Harry Gray
- **Spin Control of Electron Transfer Processes** *Malcolm Forbes,* Martin Kirk, Natia Frank, Stephen Holmes, Danna Freedman
- **Photoredox Driven Chemical Transformations** *James McCusker,* Corey Stephenson, Carsten Milsmann, Oliver Reiser
- **Photonic Materials** *Lea Nienhaus,* Dan Congreve, Xiaosong Li, Nobuhiro Yanai, Justin Caram
- **Molecular Charge Transfer** *Elena Galoppini,* Mark Thompson, Gerald Meyer, Karen Mulfort
- **Catalysis Towards Sustainable Fuels** *Etsuko Fujita,* Clifford Kubiak, Jenny Yang, Elena Jakubikova, Alexander Miller
- **Charge Transport in Complex Architectures and Interfaces** *Prashant Kamat,* Cody Schlenker, Gemma Solomon
- **Energy Transfer, Fusion and Fission** *David Shultz,* Amanda Morris, Justin Johnson, Oliver Wenger, Ken Hanson
- **Keynote Session: Coherence in Charge Transfer Processes** *Niels Damrauer,* Gregory Scholes, Jeffrey Rack, Michael Wasielewski
- **The GRC Power Hour™** *Amanda Morris, Jessica White*

Electron Donor-Acceptor Interactions
Fundamentals of Donor-Acceptor Chemistry and Its Applications: From Materials to Biomolecules
AUGUST 1 – 2, 2020
CHAIRS: Alexandria Bredar and Jacob Spies

Electronic Processes in Organic Materials
From Bioelectronics and Optoelectronics to Emerging Light-Induced Quantum Phenomena
JUNE 28 – JULY 3, 2020 • RENAISSANCE TUSCANY IL CIOCCO, LUCCA (BARGA), ITALY
CHAIRS: Carlos Silva and Ana Claudia Arias
VICE CHAIRS: Garry Rumbles and Gitti Frey

- **Keynote Session: Fundamental Processes in Organic Optoelectronics** *Karl Leo,* Richard Friend, Jenny Nelson, C. Daniel Frisbie
- **Emerging Applications in Bioelectronics** *Francesca Santoro,* Luisa Torsi, Jonathan Rivnay, Eleni Stavrinidou
- **Polymeric Materials for Bioelectronics** *Paul Meredith,* Alberto Salleo, Marco Rolandi
- **Hybrid Metal-Halide Perovskites** *Juan-Pablo Correa-Baena,* Cherie Kagan, Maria Antonietta Loi, Xiaoyang Zhu
- **Organic Photodetectors and Photovoltaics** *Ulrich Lemmer,* Thuc-Quyen Nguyen, Seunghyup Yoo
- **Chemical and Electrochemical Doping** *Seth Marder,* Lay-Lay Chua, Jian Pei, Erin Ratcliff
- **Strong Light-Matter Coupling and Quantum Phenomena** *Joel Yuen-Zhou,* Stéphane Kéna-Cohen, David Lidzey
- **Molecular Photophysics** *Eric Bittner,* Libai Huang, Jenny Clark, Andrew Marcus
- **Design of High-Performance Polymeric Materials** *Iain McCulloch,* Martin Heeney, Henry Yan

Electronic Processes in Organic Materials
From Material Design to Device Operation for Organic and Hybrid Electronics
JUNE 27 – 28, 2020
CHAIRS: Peter Budden and Jovana Milic

Endothelial Cell Phenotypes in Health and Disease
Understanding Endothelial Cell Diversity: Regulation and Regenerative Potential
JUNE 28 – JULY 3, 2020 • REY DON JAIME GRAND HOTEL, CASTELLDEFELS, SPAIN
CHAIR: Karen Hirschi
VICE CHAIR: Christiana Ruhrberg

- **Endothelial Cell Heterogeneity** *Rong Wang,* Ralf Adams, Christer Betsholtz, Mariona Graupera
- **Molecular Regulation of Endothelial Phenotypes** *Karina Yaniv,* Victoria Bautch, Natasha Harvey, Mark Kahn, Kristy Red-Horse, Martin Schwartz

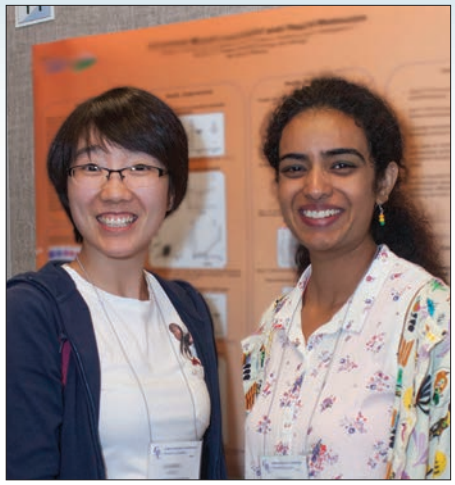

- **Congenital Defects and Clinical Therapy** *Gou Young Koh,* Jason Fish, Pia Ostergaard, Susan Quaggin, Miikka Vikkula
- **Harnessing the Regenerative Potential of Endothelium** *Joyce Bischoff,* Ebba Brakenhielm, Luisa Iruela-Arispe, Yoshiaki Kubota, Shahin Rafii
- **Aging Endothelium and Impact on Disease Progression** *Eli Keshet,* Elisabetta Dejana, Anne Eichmann, Jaime Grutzendler
- **Hematovascular Interactions in Development and Disease** *Christiana Ruhrberg,* Taija Makinen, Stefania Nicoli, Kenneth Walsh
- **Advances in Vascular Imaging and Bioengineering** *Mary Dickinson,* Rui Benedito, Roger Kamm, Friedemann Kiefer, Julien Vermot
- **Endothelial Cell Metabolism** *Timothy Hla,* Zoltan Arany, Massimiliano Mazzone, Michael Potente, Michael Simons
- **Emerging Approaches to Understanding Endothelial Cell Diversity** *Hellmut Augustin,* Kari Alitalo, Holger Gerhardt, Clint Miller, Bin Zhou
- **The GRC Power Hour™** *Luisa Iruela-Arispe*

Endothelial Cell Phenotypes in Health and Disease
Understanding Endothelial Cell Diversity: Regulation and Regenerative Potential
JUNE 27 – 28, 2020
CHAIRS: Nicholas Chavkin and Rosa Maria Correra

Energetic Materials
The Confluence of Science-Based and Machine Learning Approaches in Energetic Materials Research
MAY 31 – JUNE 5, 2020 • GRAND SUMMIT HOTEL AT SUNDAY RIVER, NEWRY, ME
CHAIR: Joseph Zaug
VICE CHAIR: Lori Groven

- **From Atomic- to Micro-Scale Phenomena: Beginning at Ignition** *Katharine Tibbetts,* Rebecca Lindsey, Lee Perry, Joseph Olles
- **Meso-Scale Phenomena Illuminated by Science- and Machine-Based Learning** *Santanu Chaudhuri,* Cole Yarrington, Paul Lafourcade, Oishik Sen
- **Materials Synthesis: Organic, Inorganic and *In Silico*** *Brian Barnes,* Koji Tsuda, Bartosz Grzybowski, Anshumali Shrivastava
- **Machine-Based Learning: Algorithms in Support of Chemical Prescriptions** *Qian Yang,* Olexandr Isayev, Connor Coley, Virginia Manner
- **Advanced Manufacturing: Optimizing Performance by Design** *Jena McCollum,* Joost van Lingen, Yoav Eichen
- **Thermodynamics and Kinetics: Tailoring the Power of Energetic Materials** *Matthew Kroonblawd,* Sorin Bastea, Elaine Oran, Deanna Lacoste
- **Thermal-Mechanical Dynamics: Learning from Emergent Response** *Jesus Mares,* Gary Seidel, Marisol Koslowski
- **Intelligently Designed Propellants** *Andrew Demko,* Devon Swanson, Ralf Kaiser, Joseph Kalman
- **Fireball Dynamics** *Michael Soo,* Mark Phillips, Jennifer Gottfried, Christopher Goldenstein
- **The GRC Power Hour™** *Deanna Lacoste*

Energetic Materials
Physiochemical Processes in Reacting Energetic Materials from the Nano to Macro Scale
MAY 30 – 31, 2020
CHAIRS: William Bassett and Matthew Kroonblawd

Environmental Endocrine Disruptors

Integration of Human, Environmental and Model System Data

MAY 31 – JUNE 5, 2020 • JORDAN HOTEL AT SUNDAY RIVER, NEWRY, ME

CHAIRS: Susan Nagel and Jodi Flaws

VICE CHAIRS: Juliette Legler and Angel Nadal

- **Keynote Session: Environmental Endocrine Disrupting Chemicals** *Gail Prins, Angel Nadal,* Linda Birnbaum, Shanna Swan
- **Evidence for and Mechanisms of EDC-Induced Reproductive Toxicity** *Vasantha Padmanabhan, Bernard Robaire,* Gail Prins, Pauliina Damdimopoulou, Aileen Keating, Laura Vandenberg
- **Environmental Endocrine Disruptors in the Marine and Terrestrial Environment** *Juliette Legler, Ramji Bhandari,* Ben Parrott, Turk Rhen, Heather Leslie
- **Social, Cultural and Political Determinants of Evaluating Risks from EDCs** *Ana Soto, Linda Birnbaum,* Kevin Elliott, Julia Brody, Veena Singla, Kris Thayer, Ami Zota
- **Emerging Exposures, Nonclassical Environmental Endocrine Disruptors and Safer Alternatives** *Genoa Warner, Laura Vandenberg,* Terry Collins, Sofie Christiansen, Bernard Robaire
- **Short and Long-Term Consequences of Developmental Exposure to EDCs** *Heather Patisaul, Terry Collins,* Marisa Bartolomei, Ramji Bhandari, Paola Palanza, Almudena Veiga Lopez
- **Impacts on the Brain and Behavior** *Andrea Gore, R. Thomas Zoeller,* Heather Patisaul, Sakina Mhaouty-Kodja, Ramendra Saha
- **EDC Effects in the Context of Human Exposure** *Shanna Swan, Leonardo Trasande,* Rita Strakovsky, Jennifer Adibi, Riana Bornman, Cynthia Curl
- **Effects of Environmental Endocrine Disruptors on Energy Balance and Cellular Metabolism** *Daniel Zalko, Kylie Rock,* Nikki Posnack, Lindsey Trevino, R. Thomas Zoeller
- **The GRC Power Hour™** *Laura Vandenberg, Heather Patisaul*

Environmental Endocrine Disruptors

Harnessing Interdisciplinary Evidence for Endocrine Disruption to Improve Public Health

MAY 30 – 31, 2020

CHAIRS: Kylie Rock and Genoa Warner

Environmental Sciences: Water

Innovative Science for the Grand Challenges in Aquatic Environmental Sciences

JUNE 28 – JULY 3, 2020 • HOLDERNESS SCHOOL, HOLDERNESS, NH

CHAIR: Heileen Hsu-Kim

VICE CHAIR: Thomas Hofstetter

- **Biodegradable Polymers and Plastic Contamination** *Ann-Christine Albertsson,* Marc Hillmyer, Richard Gross
- **New Materials and the Water Energy Nexus** *Marta Hatzell,* Christopher Gorski, T. Alan Hatton, Wendy Queen
- **Environmental Metabolomics** *David Wishart,* Pieter Dorrestein, Michael Zimmermann
- **The Continuing Threat of Halogenated Contaminants** *Elizabeth Edwards,* Norbert Heeb, Frank Löffler, Carla Ng
- **The Increasing Complexity of Chemical Pollution** *Beate Escher,* Emma Schymanski, Natalia Garcia-Reyero
- **Environmental Biogeochemistry and Anthropogenic Impacts** *Desiree Plata,* Christopher Reddy, Ulf Skyllberg, Lenny Winkel
- **Molecular Views on Contaminant Redox Reactions and Interfacial Processes** *Thomas Borch,* Juan Liu, Huichun Zhang
- **Water Treatment from Biomolecule Transformation to Microbial Ecology Monitoring** *Torsten Schmidt,* Michael Dodd, Peiying Hong, Krista Wigginton
- **Aquatic Sciences at the Science-Policy Interface** *Rainer Lohmann,* Laurel Schaider

Environmental Sciences: Water

Water Quality, Technology and Distribution from Glacial Sources to Contaminated Runoff

JUNE 27 – 28, 2020

CHAIRS: Imari Walker Karega and Adam Simpson

Enzymes, Coenzymes and Metabolic Pathways

Enzyme Mechanisms with Applications to Metabolism, Epitranscriptomics and Drug Discovery

JULY 26 – 31, 2020 • WATERVILLE VALLEY, WATERVILLE VALLEY, NH

CHAIRS: Andrew Murkin and Lynn Abell

VICE CHAIRS: Satish Nair and Luiz Pedro Carvalho

- **Enzyme Mechanisms** *Katherine Hicks,* Squire Booker, Emily Parker, Manal Swairjo, Timothy Wencewicz
- **Inhibitor Design** *Victoria Korboukh,* Argyrides Argyrou, Elham Behshad, Andrew Bennet, Caren Freel Meyers
- **Conformational Effects on Catalysis and Inhibition** *Patrick Frantom,* James Fraser, Randy Kipp, John Richard
- **Enzyme Kinetics in Complex Systems** *Erin Artin,* Swati Nagar, Matthew Robers, Peter Tonge
- **Enzymes Involved in Post-Translational Modifications** *Walter Fast,* Sonja Lorenz, Minkui Luo, Paul Thompson
- **Enzymes Involved in Innate Immunity** *Heather Hundley,* Peter Beal, James Cole, Yorgo Modis
- **Enzyme Evolution and Engineering** *Nicholas Silvaggi,* Donald Hilvert, Dan Tawfik, Michael Toney
- **Methodological Advances for Studying Enzymes** *Audrey Lamb,* David Dulin, Gabriel Lander, Denis Rousseau
- **Keynote Session: Perspectives on Modulation of Enzyme Activity** *Catherine Drennan,* Carol Fierke, Paul Fitzpatrick
- **The GRC Power Hour™** *Lynn Abell*

Enzymes, Coenzymes and Metabolic Pathways

The Enzymology of Human Health, Biotechnology and the Environment

JULY 25 – 26, 2020

CHAIR: Tyler Stack

Epithelial Stem Cells and Niches

Tissue Stem Cell Regulation by Autonomous and Non-Autonomous Mechanisms

JULY 12 – 17, 2020 • VENTURA BEACH MARRIOTT, VENTURA, CA

CHAIRS: Michael Shen and Valerie Horsley

VICE CHAIRS: Ophir Klein and Kim Jensen

- **Generation of Tissue Architecture** *Sarah Millar,* Danelle Devenport, Nan Tang, Kim Jensen
- **Mechanisms of Stem Cell Maintenance** *Jianwen Que,* Nick Barker, Sarah Millar, Emi Nishimura, Ophir Klein
- **Immune Regulation and Aging** *Arial Zeng,* Nancy Manley, Will Wood, Valerie Horsley
- **Bioengineering and Systems Approaches to Studying Stem Cell Function** *Rongwen Xi,* Boris Hinz, Sara Wickstrom
- **Regulation of Stem Cell Differentiation** *Jane Visvader,* Ya-chieh Hsu, Jianwen Que, Rongwen Xi
- **Stem Cells and Cancer** *Philip Beachy,* Arial Zeng, Wei-Qiang Gao, Michael Shen
- **Niche Regulation of Tissue Homeostasis** *Nancy Manley,* Ting Chen, Cheng-Ming Chuong, Sarah Knox
- **Niche Dysregulation in Cancer** *Sarah Knox,* Carla Kim, Traci Lyons, Claire Magnon
- **Keynote Session: Stem Cells, Niches and Cancer** *Carla Kim,* Philip Beachy, Jane Visvader
- **The GRC Power Hour™** *Danelle Devenport, Sarah Knox*

Epithelial Stem Cells and Niches

Epithelium Dynamics During Development, Regeneration, Disease and Aging

JULY 11 – 12, 2020

CHAIRS: Francesco Cambuli and David Castillo-Azofeifa

Extracellular Vesicles

Understanding Extracellular Vesicle Biogenesis and Composition for Detection and Treatment of Diseases

JULY 26 – 31, 2020 • GRAND SUMMIT HOTEL AT SUNDAY RIVER, NEWRY, ME

CHAIRS: Paul Robbins and Kenneth Witwer

VICE CHAIRS: Esther Nolte and Edit Buzas

- **Keynote Session: Physiologic and Pathologic Roles of EVs** *Giovanni Camussi,* Clotilde Théry, David Lyden
- **Biogenesis and Composition of EVs** *Esther Nolte,* Deborah Goberdhan, Stanley Lemon, Cryslin D'Souza-Schorey, Anthony Ferrante
- **New Technologies for Quantitating and Analyzing EVs** *Adrian Morelli,* Louise Laurent, Shannon Stott, Juan Falcon-Perez
- **Role of Endogenous EVs in Driving Disease Pathology** *David Lyden,* Andrew Hill, Lucia Languino, Dolores Di Vizio, Jacky Goetz
- **EVs as Delivery Vehicles for Drugs and RNAs** *Andrew Hill,* Pieter Vader, Charles Lai
- **Novel Therapeutic Applications of EVs** *Jacqueline Bromberg,* Adrian Morelli, Bharat Ramratnam, Joy Wolfram
- **EVs in Host-Pathogen Interactions** *Edit Buzas,* Ana Torrecilhas, Arne Weiberg, Jeff Schorey
- **Stem Cell EVs for Regenerative Medicine** *Anastasia Khvorova,* Susmita Sahoo, Sai Kiang Lim, Benedetta Bussolati, Ewa Zuba-Surma
- **Current Clinical Trials with EVs** *Sai Kiang Lim,* Giovanni Camussi, Eva Rohde
- **The GRC Power Hour™** *Edit Buzas, Dana Larocca*

Extracellular Vesicles

The Dichotomy of EVs: From Biomarkers and Purveyors of Disease to Potential Therapeutic Agents

JULY 25 – 26, 2020

CHAIRS: Kilean Lucas and Kyle Mentkowski

Flow and Transport in Permeable Media

Interactions Between Fluids, Elements, Materials, Energy and Life in Porous and Fractured Media

JULY 19 – 24, 2020 • LES DIABLERETS CONFERENCE CENTER, LES DIABLERETS, SWITZERLAND

CHAIR: Tanguy Le Borgne

VICE CHAIR: Marc Hesse

- **Mixing Dynamics, Chaotic Flows and Viscoelastic Turbulence** *Marco Dentz,* Daniel Lester, Andrew Clarke
- **Multi-Phase Flows and Wettability** *Steffen Berg,* Ryan Armstrong, Chris MacMinn, Alex Hansen
- **CO_2 Sequestration** *Martin Blunt,* Sam Krevor, Benedicte Menez
- **Micro-Scale Fluid Dynamics and Biophysics** *Dani Or,* Yohan Davit, François Gallaire
- **Innovative Sensors and Data Assimilation Strategies for Monitoring Subsurface Processes** *Niklas Linde,* Haruko Wainwright, Lee Slater
- **Biogeochemical Processes and Reactive Transport** *Ilenia Battiato,* Kate Maher, James Kirchner
- **Soil Processes from Micro to Continental Scales** *Insa Neuweiler,* John Selker, Claire Chenu
- **Fractures, Hydromechanics and Seismicity** *Ruben Juanes,* Marie Violay, Robert Viesca, Francois Renard
- **Coupled Flow and Transport in Ice and Planetary Systems** *Jerome Neufeld,* Klara Kalousova, Kenneth Golden
- **The GRC Power Hour™**

Flow and Transport in Permeable Media

Active and Passive Transport Processes in Biological and Geophysical Flows

JULY 18 – 19, 2020

CHAIRS: Amir Pahlavan and Rebecca Liyanage

Forensic Analysis of Human DNA

Leveraging Human Diversity, Data Science and Marker Discovery to Shape Future Forensic Applications

JUNE 21 – 26, 2020 • MOUNT SNOW, WEST DOVER, VT

CHAIRS: Sarah Seashols Williams and Steven Lee

VICE CHAIRS: Katherine Gettings and Titia Sijen

- **Keynote Session: Forensic Applications of New Genetic and Biomedical Technologies** *Pamela King,* Christopher Mason
- **Forensic Genetic Genealogy: Inferring Identity with Long-Range Familial Searches** *Thomas Callaghan, Erin Murphy,* Debbie Kennett, Gabrielle Samuel, Fred Bieber
- **Haploid and Alternate Autosomal Forensic Markers** *Manfred Kayser, Rebecca Just,* Walther Parson, Arwin Ralf, Daniele Podini
- **Activity Level Research and Impact on Forensic Reporting** *Duncan Taylor, Laurence Devesse,* Lydie Samie-Foucart, Roland van Oorschot, Mechthild Prinz
- **Tissue Source Attribution: Epigenetic, microRNA and mRNA Approaches to Attribution** *Robin Cotton,* Cordula Haas, Hwan Lee, Jack Ballantyne
- **Age, Ancestry and Appearance Prediction** *Denise Syndercombe Court, Lutz Roewer,* Susan Walsh, Ana Freire-Aradas, Runa Daniel
- **Proteomic, Methylomic and Microbiomics** *Sally Harbison, Glendon Parker,* Zachary Goecker, Athina Vidaki
- **Bioinformatics and Data Science** *Christopher Phillips,* Noah Rosenberg, Ellen Greytak, Rolf Ypma
- **Addressing Human Factors and Confirmation Bias in Forensic DNA Analysis** *Charlotte Word, Tiffany Layne,* Melissa Taylor, David Kaye, Paul Speaker
- **The GRC Power Hour™** *Katherine Gettings*

Forensic Analysis of Human DNA

New Methods for Human Identification and Investigative Intelligence

JUNE 20 – 21, 2020

CHAIRS: Tiffany Layne and Laurence Devesse

Fragile X and Autism-Related Disorders

Novel Technologies to Advance Discovery of Disease Mechanisms and Therapeutics for Fragile X and Autism

MAY 31 – JUNE 5, 2020 • RENAISSANCE TUSCANY IL CIOCCO, LUCCA (BARGA), ITALY

CHAIR: Mustafa Sahin

VICE CHAIR: Kimberly Huber

- **Keynote Session: From Genes to Drugs in Neurodevelopmental Disorders** *Kimberly Huber,* Evdokia Anagnostou, Peter Kind, Tracy King
- **Genetic Heterogeneity** *Louis Reichardt,* Catalina Betancur, Sebastien Jacquemont
- **Convergence of Molecular Mechanisms** *Jennifer Darnell,* Barbara Bardoni, Joel Richter, Helen Bateup
- **Human Cellular Models** *Alice Luo Clayton,* Xinyu Zhao, Robin Kleiman
- **Circuit Biology in Animal Models** *Laura Mamounas,* Andreas Frick, Peter Tsai, Zhaolan (Joe) Zhou
- **Human Physiology and Biomarkers** *Michael Tranfaglia,* Shafali Jeste, Charles Nelson, Lauren Ethridge
- **Interface with the Environment** *Thomas Frazier,* Mark Zylka
- **Novel Model Systems and Platforms** *Emily Osterweil,* Michela Fagiolini, Omar Khwaja, Ricardo Dolmetsch, David Hampson
- **Innovative Approaches to Clinical Outcome Measures and Trial Design** *Elizabeth Berry-Kravis,* Randi Hagerman, Ernest Pedapati, Michelle Krishnan
- **The GRC Power Hour™** *Elizabeth Berry-Kravis, Emily Osterweil*

Fragile X and Autism-Related Disorders

Lessons from Differences and Similarities in FXS and Other ASDs

MAY 30 – 31, 2020

CHAIRS: Sophie Thomson and Elizabeth McCullagh

Fuel Cells

Integrating Theory, Synthesis, Characterization and Validation for the Advancement of Fuel Cell Research

JULY 26 – 31, 2020 • BRYANT UNIVERSITY, SMITHFIELD, RI

CHAIRS: Marc Secanell and Shanna Knights

VICE CHAIRS: Iryna Zenyuk and Vojislav Stamenkovic

- **A Global Perspective on Fuel Cell Development** *Jonathan Sharman,* David Hart, Rod Borup, Siyu Ye
- **Novel Oxygen Reduction Reaction Catalysts** *Plamen Atanassov,* Frederic Maillard, Lior Elbaz, Arunima Singh
- **Characterizing Catalyst Activity** *Yu Morimoto,* Anthony Kucernak, Karen Swider-Lyons, Kateryna Artyushkova
- **Designing Better Solid Electrolytes** *Steven Holdcroft,* Wen Liu, Yushan Yan, Stephen Paddison
- **Novel Membrane Fabrication Approaches** *Göran Lindbergh,* Marcelo Lozada-Hidalgo, Simon Thiele
- **Understanding Material-Structure-Performance Interactions in Fuel Cell Electrodes** *Kensaku Kodama,* Adam Weber, Paulo Ferreira, Jeff Gostick
- **Technologies for a Hydrogen Economy** *Huyen Dinh,* Thomas Jaramillo, Nemanja Danilovic, Lauren Greenlee
- **Advances in Reactant Transport and Cell Durability** *Aimy Bazylak,* Marc-Olivier Coppens, Hubert Gasteiger, Felix Buchi
- **Advances in Polymer Electrolyte Fuel Cell Design** *Thomas Zawodzinski,* Shimshon Gottesfeld
- **The GRC Power Hour™** *Aimy Bazylak, Shanna Knights*

Fuel Cells

Experimental and Theoretical Characterization of Fuel Cell Materials and Electrodes

JULY 25 – 26, 2020

CHAIRS: Sadia Kabir and Mayank Sabharwal

Genomic Instability

Genomic Integrity, DNA Repair and Human Diseases

AUGUST 2 – 7, 2020 • THE HONG KONG UNIVERSITY OF SCIENCE AND TECHNOLOGY, HONG KONG, CHINA

CHAIRS: Lee Zou and Michael Huen

VICE CHAIRS: Agata Smogorzewska and Kyungjae Myung

- **Keynote Session: New Frontiers in the DNA Damage Response** *Michael Huen,* Roger Greenberg, Andre Nussenzweig
- **Repair of Chromosome Breaks** *Gary Chan,* Maria Jasin, Stephen Kowalczykowski, Tanya Paull, Patrick Sung
- **DNA Replication and Replication Stress** *Yuanliang Zhai,* Dana Branzei, Anindya Dutta, Bik Tye, Xiaolan Zhao
- **Transcription, R-Loops and DNA Repair** *Jason Wong,* Andres Aguilera, Li Lan, Gaelle Legube

- **Chromatin Dynamics and Epigenetic Regulation of DNA Repair** *Xingzhi Xu,* Jessica Downs, Qing Li, Kyle Miller, Jun Huang
- **Genomic Instability and DNA Repair During the Cell Cycle** *Randy Poon,* Larraine Symington, Stephen West, Hongtao Yu, Zhenkun Lou
- **DNA Repair Defects and Cancer Therapy** *Karen Wing Yee Yuen,* Junjie Chen, Binghui Shen, Xiaochun Yu, Robert Weiss
- **Emerging DNA Repair Pathways** *Dongyi Xu,* Niels Mailand, Kyungjae Myung, Evi Soutoglou, J. Ross Chapman
- **DNA Repair Defects and Diseases** *Kyoo-young Lee,* Ketan Patel, Yosef Shiloh, Agata Smogorzewska, Shan Zha
- **The GRC Power Hour™** *Larraine Symington, Tanya Paull*

Genomic Instability

Influence of Chromosome Architecture and Cell Cycle on Repair and Maintenance of the Genome

AUGUST 1 – 2, 2020

CHAIRS: Travis White and Ka Man Wong

Geochemistry of Mineral Deposits

Geochemical Frontiers, Critical Processes and Value Creation

MAY 24 – 29, 2020 • REY DON JAIME GRAND HOTEL, CASTELLDEFELS, SPAIN

CHAIRS: Sarah Gleeson and David Braxton

VICE CHAIR: Isabelle Chambefort

- **Big Data and Mineral Deposits** *John Vann,* Shaunna Morrison
- **Geochemistry and Fundamental Mineral-System-Forming Processes** *John Dilles,* Kate Kiseeva, Madeleine Humphreys, Constantino Mpodozis, Nicholas Hayward
- **Next Generation Models** *Koen Torremans,* Stefan Luth, Juan Carlos Afonso
- **Geochemical Processes Leading to Superior-Grade Development** *Pilar Lecumberri-Sanchez,* Brian Tattich, Iain Pitcairn, Amy Gartman
- **Mining Frontiers** *Melissa Anderson,* Abigail Calzada, John Jamieson
- **Geochemistry for Discovery** *Christian Ihlenfeld,* Nathan Reid, Michael Whitbread, Cari Deyell-Wurst
- **Biological Processes, Geochemistry and Ore Deposits** *Isabelle Chambefort,* Gordon Southam, Donato Giovannelli
- **Geochemistry in Value Realization and Stewardship** *Kathy Ehrig,* Mei-Fu Zhou, Angela Escolme, Sasha Wilson, Evelyn Mervine
- **Geochemical Frontiers** *Anthony Williams-Jones,* John Thompson
- **The GRC Power Hour™** *Sarah Gleeson*

Geochemistry of Mineral Deposits

Geochemical Frontiers, Critical Processes and Value Creation

MAY 23 – 24, 2020

CHAIRS: Philip Rieger and Irene del Real Contreras

Granular Matter

Particulate Systems Across Scales: From Colloidal Science to Geophysical Flows

JUNE 21 – 26, 2020 • STONEHILL COLLEGE, EASTON, MA

CHAIRS: Xiang Cheng and Nathalie Vriend

VICE CHAIRS: Kimberly Hill-Malvick and Joshua Dijksman

- **Keynote Session: Granular Matter in Industrial Processes** *Paul Mort,* Jeremy Lechman, Massih Pasha
- **Jamming and Glass Transition** *Eric Corwin,* Sidney Nagel, Xiaoming Mao, Rajesh Ganapathy
- **Active Suspensions** *Daphne Klotsa,* John Brady, David Saintillan
- **Dynamics and Structures of Granular Flows** *JC Tsai,* Nathan Keim, Kerstin Nordstrom, Shmuel Rubinstein
- **Impact and Cratering** *German Varas,* Hiroaki Katsuragi, Devaraj Van Der Meer
- **Discrete and Continuum Mechanics** *Douglas Durian,* Karen Daniels, Ken Kamrin, Prabhu Nott
- **Granular Geotechnical Engineering** *Elisabeth Bowman,* Catherine O'Sullivan, Kenichi Soga
- **Geophysical Granular Flows** *Jin Sun,* Emily Brodsky, Chris Johnson, Anne Mangeney
- **Selected Poster Presentations** *Matthias Schröter,* Olivier Pouliquen
- **The GRC Power Hour™** *Jennifer Rieser, Kimberly Hill-Malvick*

Granular Matter

Particulate Systems Across Scales: From Colloidal Science to Geophysical Flows

JUNE 20 – 21, 2020

CHAIRS: Jennifer Rieser and Ishan Srivastava

Green Chemistry

Chemical Sciences Driving Sustainability

JULY 26 – 31, 2020 • REY DON JAIME GRAND HOTEL, CASTELLDEFELS, SPAIN

CHAIRS: Walter Leitner and Emilio Bunel

VICE CHAIRS: Audrey Moores and Jinlong Gong

- **Keynote Session: A Systems Approach to Green Chemistry** *Steve Howdle, Paul Anastas,* Peter Seeberger, Elsje Alessandra Quadrelli
- **Molecular Principles and Synthetic Applications** *Carmen Claver, Laszlo Mika,* Paul Chirik, Aiwen Lei, Timo Repo, Mimi Hii
- **Advanced Materials** *Buxing Han,* Seth Darling, Eva Hevia, Bruno Chaudret
- **Chemical Value Chains Based on Biomass and CO_2** *Yonas Chebude, David Contreras,* Regina Palkovits, Mahdi Abu-Omar, Francois Jerome, Thomas Schaub
- **Valorization of Waste Material** *Heriberto Cabezas,* Hassan Bazzi, Adam Best, Jean-Paul Lange
- **Harvesting Renewable Energy with Green Chemistry** *Marcella Bonchio, John Hansen,* Yogesh Surendranath, Greta Patzke, Gonzalo Prieto, Luca Gonsalvi
- **Designing Greener Products** *Julie Zimmerman,* Jakub Kostal, Silvia Vignolini, Christoph Guertler
- **Environmentally Benign Synthesis, Processes and Products** *Martina Peters, Audrey Moores, Jinlong Gong,* Jason Tedrow, Daniel Garcia Rivera
- **Keynote Session: From Mechanistic Understanding to Industrial Processes** *Philip Jessop, R. Tom Baker,* Avelino Corma
- **The GRC Power Hour™** *Karen Goldberg*

Green Chemistry

Mapping Green Paths to Critical Elements, Molecules and Materials

JULY 25 – 26, 2020

CHAIRS: Ana Patricia Pacheco and Amit Kumar

Hemostasis

Structure, Biochemistry and Physiology of Hemostasis

AUGUST 2 – 7, 2020 • WATERVILLE VALLEY, WATERVILLE VALLEY, NH

CHAIRS: Sidney Whiteheart and Alan Mast

VICE CHAIR: Gow Arepally

- **Coagulation: Signaling and Structure** *Sriram Krishnaswamy,* JoAnn Trejo, Jonas Emsley, Colin Kretz
- **Coagulation and Platelets in Inflammation** *Edward Conway,* A. Koneti Rao, Anthony Washington, Justin Hamilton, Eric Boilard, Zhenyu Li
- **Maintaining Hemostatic Balance** *Sanjana Dayal,* Marie-Christine Bouton, Jill Johnsen, Martha Sola-Visner
- **Clots and DVT Structure** *Heyu Ni,* Jose Diaz, Alisa Wolberg, Abhishek Jain, Nicola Mutch, Brian Storrie
- **Lessons of Molecular Hemostasis from Organisms that Feed on Blood** *Mettine Bos,* Brendan McMorran, Ivo Francischetti, Diana Imhof
- **Coagulation and Platelets in Chronic Diseases** *Ulhas Naik,* Gustaf Edgren, Sidney Strickland, Anna Falanga, John Hwa, Aaron Petrey
- **Late-Breaking Topics** *Gow Arepally*
- **Bleeding and Clotting Control** *William Hobbs,* Bjorn Dajlback, Weikai Li, Walter Kahr, Jing Yang, Christopher Ng
- **Keynote Session: Von Willebrand Factor and Kindlins in Bleeding Disorders** *Gary Gilbert,* Edward Plow, Robert Montgomery
- **The GRC Power Hour™**

Hemostasis

Regulation and Molecular Dynamics of Hemostasis and Thrombosis

AUGUST 1 – 2, 2020

CHAIRS: Amy Siebert-McKenzie and Xu Han

"The conference location stimulated interaction among progressive scientists. The poster sessions allowed for in-depth one-on-one discussions and an opportunity to receive valuable feedback from scientists of different backgrounds."

ERNEST PHILLIPS, Florida State University, Chromosome Dynamics GRC

Heterocyclic Compounds

Design, Synthesis and Application of Biologically Active Heterocycles

JUNE 21 – 26, 2020 • SALVE REGINA UNIVERSITY, NEWPORT, RI

CHAIR: R. Jason Herr

VICE CHAIR: Catharine Larsen

- **Strategic Approaches to the Preparation of Heterocyclic Natural Products** *Wei Li,* Ang Li, Margaret Brimble
- **Novel Approaches to Heterocyclic Compound Construction** *Sudeshna Roy,* Lee Silverberg, Larry Yet, Shanina Johnson
- **Design and Synthesis of Biologically Active Heterocycles** *Carmela Molinaro,* Brian Aquila, Stephen Greszler, Donn Wishka
- **Paradigm Shifting Synthesis Technologies** *Kevin Frankowski,* James Beck, Oliver Kappe, Kevin Moeller
- **Catalytic Methods for Heterocyclic Compound Preparation and Functionalization** *Eric Voight,* Todd Hyster, Tanja Gulder, Helene Lebel
- **Advanced Reaction Strategies for Heterocyclic Compound Design** *Jeffrey Gustafson,* Tomas Smejkal, Thomas Stevenson
- **Total Synthesis of Complex Heterocycles** *Matthew Cook,* Victor Snieckus, Tomas Hudlicky
- **Route Optimization of Heterocyclic Compounds of Pharmaceutical Relevance** *David Lathbury,* Aaron Sather, David Ennis, Austin Smith, Maryll Geherty
- **Keynote Session: Construction of Complex Molecular Architectures** *Daniel Elbaum,* Peter Wipf, Barry Trost
- **The GRC Power Hour™** *Catharine Larsen*

Human Genetic Variation and Disease

Deciphering Genetic Complexity: Risk Assessment and Treatment Opportunities

MAY 31 – JUNE 5, 2020 • SOUTHERN NEW HAMPSHIRE UNIVERSITY, MANCHESTER, NH

CHAIRS: Yana Bromberg and Olivier Lichtarge

VICE CHAIRS: Hannah Carter and Kai Tan

- **Keynote Session: Genome Perturbations in Health and Disease** *Graham McVicker,* Vivian Cheung, Douglas Fowler
- **Genetic Underpinnings of Early Onset Complex Diseases** *Laura Conlin,* Elizabeth Bhoj, Wendy Chung, Martin Kircher, Jinchuan Xing
- **Human Variation and Aging** *Zhao Zhang,* Marylyn Ritchie, Janet Thornton
- **Mutational Determinants of Cardiovascular and Metabolic Health** *Gary Hon,* Neil Chi, Dmitry Korkin, Sean Mooney, Nicola Mulder
- **Genetic Changes in Neurodegeneration** *Lucia Peixoto,* Iuliana Ionita-Laza, Predrag Radivojac
- **Cancer Genomics** *Michael Lawrence,* Rachel Karchin, Anna Panchenko, Mona Singh, Itai Yanai
- **Genetics of Gastrointestinal Health** *Chengsheng Zhu,* Steven Brant, Ramnik Xavier
- **Immune Modulation by Genome Variants** *Benjamin Greenbaum,* Adam Godzik, Dennis Ko, Marianne Rooman, Rob Russell
- **Learning from Hidden, Missing and Engineered Genomic Data** *Valerie Arboleda,* Steven Brenner, Yves Moreau
- **The GRC Power Hour™** *Yana Bromberg, Olivier Lichtarge*

Human Genetic Variation and Disease GRS

Interpretations of Genetic Variation and Their Application in Treatment and Diagnosis of Disease

MAY 30 – 31, 2020

CHAIRS: Anh-Thu Lam and Timothy Bergquist

Image Science

Emerging Imaging Techniques at the Intersection of Physics and Data Science

JUNE 7 – 12, 2020 • STONEHILL COLLEGE, EASTON, MA

CHAIR: Rafael Piestun

VICE CHAIR: Jannick Rolland

- **Information Extraction via Computational Imaging** *Richard Paxman,* Laura Waller, Sjoerd Stallinga
- **Quantum Imaging** *George Barbastathis,* Dan Oron, Nick Vamivakas
- **Artificial Intelligence in Image Science** *Gordon Wetzstein,* George Barbastathis, Aydogan Ozcan
- **Inverse Problems** *Laura Waller,* Demetri Psaltis, Mini Das
- **Multimodal and Biomedical Imaging** *Kyle Myers,* Sophie Brasselet, David Sampson, Amy Oldenburg
- **Imaging in Emerging Consumer Applications** *Kaan Aksit,* Chris Dainty, Zeb Barber
- **Astronomical Imaging from Light-Years Away** *Thomas Bifano,* Jeff Kuhn
- **Eyes and Vision** *Kristina Irsch,* Hakan Úrey, Brian Wandell
- **Early-Career Investigator Presentations** *Joyce Farrel,* Roarke Horstmeyer, Kristina Irsch

Image Science GRS

Image Acquisition, Processing and Visualization

JUNE 6 – 7, 2020

CHAIRS: Raman Saggu and Dennis Gardner

Immunochemistry and Immunobiology

Immune System in Health, Disease and Therapy

JUNE 7 – 12, 2020 • REY DON JAIME GRAND HOTEL, CASTELLDEFELS, SPAIN

CHAIR: Facundo Batista

VICE CHAIR: Alexander Rudensky

- **Keynote Session: Immune Responses** *Alexander Rudensky,* Gillian Griffiths, Akiko Iwasaki, Jason Cyster
- **Immune Cells Trafficking and Activation** *Matteo Iannacone, Morgan Huse,* Ronald Germain, Michael Sixt, Gabriel Victora, Carola Vinuesa
- **Gene Programming of Immune Cells** *Carola Vinuesa, Sebastian Amigorena,* Thomas Boehm, Laura Mackay, Nir Yosef, Gioacchino Natoli
- **Immunoregulation** *Laura Mackay, Gioacchino Natoli,* Sebastian Amigorena, Ken Murphy, Federica Sallusto, Jamie Spangler
- **Immune Responses to Vaccine and Infection** *Federica Sallusto, Jason Cyster,* Shane Crotty, Matteo Iannacone, Marc Jenkins, Antonio Lanzavecchia
- **Immunity at Mucosal Sites** *Shannon Turley, Janelle Ayres,* Greg Barton, Douglas Kwon, Diane Mathis, Gitta Stockinger
- **Sensors, Microbes and Inflammation** *Diane Mathis, Ruslan Medzhitov,* Sun Hur, Leo James, Caetano Reis e Sousa, Carla Rothlin
- **Integrative Immunology** *Carla Rothlin, Leo James,* Janelle Ayres, Burkhard Becher, Ruslan Medzhitov, Andrea Schietinger
- **Tumor Immunity** *Caetano Reis e Sousa, Jamie Spangler,* Ana Domingos, Morgan Huse, Shannon Turley, John Wherry

Immunochemistry and Immunobiology GRS

Immunoengineering: Fundamental and Applied Approaches to Modulate the Immune System

JUNE 6 – 7, 2020

CHAIRS: Asheley Chapman and Veronica Davé

In Vivo Magnetic Resonance

Identifying the Next 20 Years of Need in In Vivo MR

JULY 19 – 24, 2020 • PROCTOR ACADEMY, ANDOVER, NH

CHAIR: Jeff Dunn

VICE CHAIR: Kim Butts Pauly

- **Keynote Session: Opportunities for Breakthroughs in New Research Areas** *Joseph Ackerman,* Michael Smith, Charles Springer
- **Engineering the Future of Magnetic Resonance Technology** *Lawrence Wald,* Clarissa Cooley, Jan Korvink, Christoph Juchem
- **Multimodal MRI: Combining Technologies with MRI** *Sharmila Majumdar,* Blaise Frederick, Vesna Sossi
- **Embracing Machine Learning and Graphics for MR Processing and Visualization** *Daniel Sodickson, Karin Shmueli,* Brian Hargreaves, Valentina Pedoia
- **Microimaging: Pushing the Limits with High Field** *Stephen Blackband,* Samuel Grant, Klaus Scheffler
- **Novel Biomedical Targets for the Application of Magnetic Resonance** *Elaine Bearer,* Helene Benveniste, Youssef Zaim Wadghiri, Catherine Lebel
- **Magnetic Resonance Applications Beyond Homo Sapiens** *Joel Garbow,* Stephen Altobelli, Sarah Pownder
- **Methods and Sequences for Acquiring Magnetic Resonance Data** *Jurgen Hennig,* Moritz Zaiss, Claudia Prieto, Jan-Bernd Hovener
- **MRI for Space Research and Medicine** *Cornelia Laule,* Gordon Sarty, Rachael Seidler
- **The GRC Power Hour™** *Kim Butts Pauly, Melissa Haskell*

In Vivo Magnetic Resonance GRS

Identifying the Next 20 Years of Need in In Vivo MR

JULY 18 – 19, 2020

CHAIRS: Manushka Vaidya and Melissa Haskell

Industrial Ecology

The Impact of Data Science Advances on Industrial Ecology and Sustainability Systems Science

JUNE 14 – 19, 2020 • GRAND SUMMIT HOTEL AT SUNDAY RIVER, NEWRY, ME

CHAIR: Anu Ramaswami

VICE CHAIR: Ming Xu

- **Keynote Session: Data Innovations, Industrial Ecology and a Sustainable Society** *Arpad Horvath,* Stefanie Hellweg, Tasso Azevedo
- **Integrative Data Frameworks Linking Industrial Ecology with Multiple Sustainability Outcomes** *Reid Lifset,* Mikhail Chester, Stefan Pauliuk, Dana Boyer, Julian Marshall
- **Key Provisioning Systems: Energy** *Amy Landis,* Clinton Andrews, Marta Gonzalez, Inês Azevedo
- **Core IE Methods: Input Output Analysis and Material Flow Accounts** *Tomer Fishman,* Bing Zhu, Arnold Tukker, Edgar Hertwich, Richard Wood
- **Key Provisioning Systems: Mobility** *Shoshanna Saxe,* Yang Jiang, Hua Cai
- **Core IE Methods: Advances in Life Cycle Assessment** *Valerie Thomas,* Yuan Yao, Ramzy Kahhat, Shweta Singh
- **Key Provisioning Systems: Water and Food Systems** *Callie Babbitt,* Timothy Smith, Junming Zhu
- **Smart Cities, Sustainability and Well-Being** *Yuliya Kalmykova,* Luis Bettencourt, Lucy Hutyra
- **The Science of Co-Production** *Christopher Kennedy,* Maria Lemos, Beatriz Cárdenas
- **The GRC Power Hour™** *Callie Babbitt, Ming Xu*

Industrial Ecology GRS

The Impact of Data Science Advances on Industrial Ecology and Sustainability Systems Science

JUNE 13 – 14, 2020

CHAIRS: Joe Bozeman III and Alexandra Lavers Westin

Inorganic Chemistry

Using the Versatility of Inorganic Elements to Address Grand Challenges in Health, Energy and the Environment

MAY 31 – JUNE 5, 2020 • SALVE REGINA UNIVERSITY, NEWPORT, RI

CHAIR: Amy Prieto

VICE CHAIR: Jacqueline Veauthier

- **Harnessing Reactivity** *James Mayer,* George Stanley, Fabian Dielmann
- **The Heavy Elements** *Justin Walensky,* Suzanne Bart, Eric Schelter, Stosh Kozimor
- **Interfacing Metals and Biology** *Elisa Tomat,* Marcetta Darensbourg
- **Modes of Bonding** *Tracy Lohr,* Francois Gabbai, Laurel Schafer
- **Spanning Molecules to Solids** *Natalia Shustova,* Raffaella Buonsanti, Bart Bartlett
- **Condensed Matter and Its Applications** *Evgeny Dikarev,* Lisa McElwee-White, Susan Kauzlarich
- **Physical Inorganic Chemistry** *Suzanne Bart,* Ping Yang, Jakoah Brgoch
- **Energy Production and Storage** *Bart Bartlett,* James Mayer, Marinella Mazzanti
- **Inorganic Chemistry as a Driver of Innovation** *Jacqueline Veauthier,* Polly Arnold, T. Don Tilley
- **The GRC Power Hour™** *Jacqueline Veauthier*

Inorganic Chemistry GRS

Applications of Inorganic Molecules and Materials in Magnetism, Catalysis and Energy Storage

MAY 30 – 31, 2020

CHAIRS: Avery Baumann and Trevor Latendresse

Intermediate Filaments

Linking Cells, the Cytoskeleton and the Nucleus in Mechanobiology, Aging and Disease

JUNE 7 – 12, 2020 • MOUNT SNOW, WEST DOVER, VT

CHAIRS: Jan Lammerding and Roy Quinlan

VICE CHAIRS: Elly Hol and Howard Worman

- **Visualizing Filament Organization and Dynamics at the Nanoscale** *Milos Pekny,* Birgit Lane, Ohad Medalia, Jennifer Lippincott-Schwartz
- **Functional Insights into the Structure and Biophysics of Intermediate Filaments** *Pierre Coulombe,* Roy Beck-Barkai, Sarah Koester, Duane Harland
- **Technologies and Therapeutic Targets for Dynamic Structures** *Sandrine Etienne-Manneville,* Gaudenz Danuser, Ming Guo, Pierre Thibault
- **Connecting the Nucleus, Cytoskeleton and Extracellular Environment** *Gregg Gundersen,* Catherine Shanahan, Daniel Starr, Kathleen Green
- **Integration of Muscle Mechanobiology by Intermediate Filaments in Health and Disease** *Dennis Discher,* Shenhav Cohen, Brian Glancy, Benjamin Prosser
- **Linking Intermediate Filaments to Neurodegenerative Diseases** *Ronald Liem,* Pascale Bomont, Jean-Pierre Julien, Sanjay Kumar
- **Progenitors, Senescence and Cancer** *Dennis Roop,* Ganna Bilousova, Elaine Fuchs, Andy Xiang
- **Mechanistic Insights into Intermediate Filament Diseases** *Cecilia Sahlgren,* Nicole Schwarz, Kurt Zatloukal, Dolores Perez-Sala
- **Emerging Therapeutic Approaches for Intermediate Filament-Based Diseases** *Gisele Bonne,* Stephen Young, Leslie Gordon, Lori Wallrath
- **The GRC Power Hour™** *Sarah Koester, Karen Ridge*

Intermediate Filaments

Bridging the Gap Between Molecules and Tissue: How Intermediate Filaments Affect Our Health

JUNE 6 – 7, 2020

CHAIR: Rebecca de Leeuw

Intrinsically Disordered Proteins

The Functional Role of Disorder in Biological Systems

JUNE 21 – 26, 2020 • LES DIABLERETS CONFERENCE CENTER, LES DIABLERETS, SWITZERLAND

CHAIRS: Elizabeth Rhoades and Philipp Selenko

VICE CHAIRS: Birthe Kragelund and Tanja Mittag

- **Keynote Session: Ensembles and Allostery** *Birthe Kragelund,* Vincent Hilser, Sheena Radford
- **Liquid-Liquid Phase Separation: Cell Biology** *Vincent Hilser,* Ibrahim Cisse, Lucas Pelkmans, Lucia Strader, Cesar Cuevas-Velazquez
- **IDPs in Health and Disease** *Michal Sharon,* Lucia Chemes, Toby Gibson, Amayra Hernández-Vega, Liesbeth Veenhoff
- **Biomaterials and Assemblies** *Martin Blackledge,* Sara Cuylen-Haering, Meytal Landau, Ali Miserez, Katharina Ribbeck, Andrea Sinz
- **Unique Aspects of Structure-Function Relationships** *Jane Clarke,* Katherine Aurelia Ball, Samrat Mukhopadhyay, Andrea Soranno, Zachary Wood
- **Evolution and Proteomics** *Keith Dunker,* Allan Drummond, Debora Marks, Paula Picotti, Agnes Toth-Petroczy
- **Networks and Signalling** *Peter Wright,* Hagen Hofmann, Jennifer Hurley, Kresten Lindorff-Larsen, Carrie Partch
- **Liquid-Liquid Phase Separation: Biophysics and Biochemistry** *Rohit Pappu,* Cliff Brangwynne, Michael Feig, Frank Julicher
- **Keynote Session: Dynamic Ensembles and Functional Interactions** *Tanja Mittag,* Martin Blackledge, Jane Dyson
- **The GRC Power Hour™** *Sheena Radford, Lucia Strader*

Intrinsically Disordered Proteins

How Life Harnesses Disorder: Emergent Functions of IDPs in Cells, Materials and Medicine

JUNE 20 – 21, 2020

CHAIRS: Alexander Chin and Megan Cohan

Ion Channels

Molecular Mechanisms of Electrical Signaling in Health and Disease

JULY 12 – 17, 2020 • MOUNT HOLYOKE COLLEGE, SOUTH HADLEY, MA

CHAIR: Brad Rothberg

VICE CHAIRS: Teresa Giraldez and Baron Chanda

- **Keynote Session: Ion Signaling in Metabolism and Excitability** *Show-Ling Shyng,* Nancy Carrasco, Rod MacKinnon
- **Anions, Eggs and Fluids** *Michael Pusch,* Anne Carlson, Merritt Maduke, Zhaozhu Qiu, William Skach
- **Glutamate Receptors, Synapses and Memory** *Vasanthi Jayaraman,* Hiro Furukawa, Gabriela Popescu, Lonnie Wollmuth, Ingo Greger
- **Nav and Kv Channels in Pain and Cognition** *William Kobertz,* Frank Bosmans, Chris Ahern, Geoffrey Pitt
- **Calcium Channels in Muscle, Nerve and Immune Cell Function** *Henry Colecraft,* Donald Gill, Ute Hellmich, Amy Lee
- **Ion Channels that Control Your Heart** *David Jones,* Peter Larsson, Jianmin Cui, Jana Kusch, Gail Robertson
- **Channel Pharmacology and Therapeutics** *Geoffrey Abbott,* Stephen Tucker, Markus Rapedius, Paul Slesinger, Michaela Jansen
- **Electrical Signaling and Transport in Prokaryotes** *Crina Nimigean,* Gurol Suel, Inga Hänelt, Joao Morais-Cabral, Rachelle Gaudet
- **Channels in Sensory Biology** *Vera Moiseenkova-Bell,* Ellen Lumpkin, Andrew Ward, Miriam Goodman, Martin Chalfie
- **The GRC Power Hour™** *Sudha Chakrapani, Lucie Delemotte*

Ion Channels

Molecular Mechanisms of Electrical Signaling in Health and Disease

JULY 11 – 12, 2020

CHAIRS: Alexandria Miller and Valeria Kalienkova

Ionic Liquids

Linking Ionic Liquid Structure, Reactions and Applications Across Temperatures

AUGUST 9 – 14, 2020 • JORDAN HOTEL AT SUNDAY RIVER, NEWRY, ME

CHAIR: Paul Trulove

VICE CHAIR: Jared Anderson

- **Keynote Session: The Future of Ionic Liquids** *Robert Mantz,* Charles Hussey, Mark Shiflett
- **Ionic Liquids Beyond the Boundaries** *Sheng Dai,* Frank Endres, Claudio Margulis, James Davis
- **Natural and Synthetic Polymers** *Paula Berton,* Stephen Paddison, Nolene Byrne, David Durkin
- **Biology and Ionic Liquids** *Hugh De Long,* Rajesh Naik, Mara Freire, Gloria Elliott
- **Energy Applications of Ionic Liquids** *Wesley Henderson,* Debbie Silvester, Patrick Howlett, Donald Sadoway
- **Ionic Liquids and Deep Eutectic Solvents** *Burcu Gurkan,* Isabel Marrucho, Karen Edler
- **Structure-Property Relationships in Ionic Liquids** *Luke Haverhals,* Rosa M. Espinosa-Marzal, Ralf Ludwig, Jesse McDaniel, Susan Perkin
- **Ionic Liquids in Future Sustainable Technologies** *Elizabeth Biddinger,* Joan Brennecke, Edward Maginn
- **Late-Breaking Topics** *Eric Fox*
- **The GRC Power Hour™** *Burcu Gurkan, Jared Anderson*

Ionic Liquids

Linking Ionic Liquid Structure, Reactions and Applications Across Temperatures

AUGUST 8 – 9, 2020

CHAIRS: Emmanuel Varona-Torres and Hemant Choudhary

Lignin

Realizing Lignin's Potential in Biorefining by Bridging Plant Biology, Chemistry and Engineering

JULY 19 – 24, 2020 • STONEHILL COLLEGE, EASTON, MA

CHAIRS: Yuriy Román and Katalin Barta

VICE CHAIRS: Laura Bartley and Jeremy Luterbacher

- **Keynote Session: Converging Disciplines for the Sustainable Valorization of Lignin** *Jeremy Luterbacher,* Lacey Samuels, Bert Weckhuysen
- **Methods to Tailor Lignin Biosynthesis *In Planta*** *Claire Halpin,* Aymerick Eudes, Laura Bartley, Taku Demura, Shinya Kajita
- **Designing Enzymatic Systems for Lignin Depolymerization** *Rebecca Smith,* Takashi Watanabe, Steven Singer
- **Catalytic Lignin Depolymerization and Upgrading** *Seema Singh,* Yanqin Wang, Guangbin Dong, Roberto Rinaldi, Chen Zhao, Emiel Hensen
- **Convergent Microbial Lignin Conversion Strategies** *Timothy Donohue,* Tim Bugg, Lindsay Eltis
- **Lignin from an Industrial Perspective** *Jean-Pierre Lindner,* Annelie Jongerius, Michael Rushton, Karolien Vanbroekhoven, Raymond Buser, Ian Klein, Sander van den Bosch, Christian Dahlstrand
- **Tools and Methods for the Analysis, Visualization and Structural Elucidation of Lignin** *Yuki Tobimatsu,* Ohkamae Park, Susannah Scott
- **Tailoring Chemical Routes for the Synthesis of Direct and Functional Replacement Products from Lignin** *Pieter Bruijnincx,* Martin Lawoko, Mojgan Nejad, Chris Saffron, Ning Yan

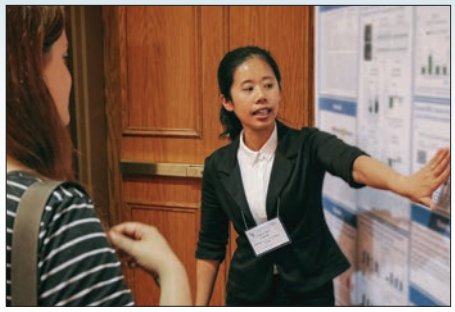

- **Incorporating Process Engineering in the Lignin Upgrading Workflow** *Sankar Nair,* Christos Maravelias, Junyong Zhu
- **The GRC Power Hour™** *Claudia Crestini, Rebecca Smith*

Lipoprotein Metabolism

New Lipid and Lipoprotein Genes, Pathways and Therapies

JUNE 7 – 12, 2020 • WATERVILLE VALLEY, WATERVILLE VALLEY, NH

CHAIRS: M. Mahmood Hussain and Kiran Musunuru

VICE CHAIRS: Marlys Koschinsky and Daisy Sahoo

- **Genetics of Lipids and Cardiovascular Disease** *Marlys Koschinsky,* Sekar Kathiresan
- **The Lipoprotein Lipase Pathway** *Ira Goldberg,* Anne Beigneux, Karin Bornfeldt, Sander Kersten, Xiao Wang
- **Therapeutic Approaches to Modulate Plasma Lipids and Lipoproteins** *Mary Sorci-Thomas,* Bruce Given, Viktoria Gusarova, Richard Lee
- **Noncoding RNAs in Lipoprotein Metabolism** *Katey Rayner,* Kathryn Moore, Muredach Reilly, Tamer Sallam, Yajaira Suarez
- **Lipid Metabolism in Adipose Tissue** *Loredana Quadro,* Robert Farese, Susan Fried, Sujith Rajan, Judith Storch
- **The Post-Genomic Era in Lipoprotein Metabolism** *Masahiro Koseki,* Robert Bauer, Mary Haas, Elizabeth Tarling, Noam Zelcer
- **Permanent Modification of Lipid Levels** *Daisy Sahoo,* Alexandra Chadwick, Steven Farber, Klaus Ley
- **Lipoproteins** *Gissette Reyes-Soffer,* Ashira Blazer, Edward Fisher, Roop Mallik, Nathalie Pamir, Lloyd Ruddock, Shadab Siddiqi
- **Cutting-Edge Technologies for Lipid and Lipoprotein Research** *Qing Miao,* Stephen Duncan, Chiara Giannarelli, Alan Remaley
- **The GRC Power Hour™** *Marlys Koschinsky, Daisy Sahoo*

Lipoprotein Metabolism

Molecular Mechanisms of Lipid Metabolism in Health and Disease

JUNE 6 – 7, 2020

CHAIRS: Aspen Gutgsell and Paul "Li-Hao" Huang

Liquid Biopsy for Cancer

Advancing to Clinical Applications for Precision Medicine in Liquid Biopsy Research

JUNE 21 – 26, 2020 • MOUNT HOLYOKE COLLEGE, SOUTH HADLEY, MA

CHAIRS: Klaus Pantel and Shana Kelley

VICE CHAIRS: Min Yu and Rosandra Kaplan

- **Grand Challenges in Liquid Biopsy Research** *Min Yu,* Howard Scher
- **The Biology Behind Liquid Biopsy Biomarkers** *Rosandra Kaplan,* John Condeelis, Jacky Goetz, Jean Paul Thiery
- **Genotypic CTC and ctDNA Analysis** *Daniel De Carvalho,* Wai Kei Jacky Lam, Ralph Graeser, Jacqui Shaw, Brian Dougherty
- **Phenotypic and Functional Analysis of CTCs** *Jacky Goetz,* Nicola Aceto, Matt Trau, Catherine Alix-Panabieres
- **Early-Career Investigator Presentations** *Amy Herr*
- **Liquid Biopsy and Clinical Utility** *Daniel Chiu,* Andrew Armstrong, Harriet Wikman, Alison Allan, Ellen Heitzer
- **High Performance Analytical Technologies for Liquid Biopsy** *Shannon Stott,* Amy Herr, Daniel Chiu, Vanessa Jonsson
- **Extracellular Vesicles** *Catherine Alix-Panabieres,* David Lyden, Shannon Stott, Yong Zeng
- **New Liquid Biopsy Biomarkers** *Alison Allan,* Daniel De Carvalho, Michael Sixt, Ryan Sullivan
- **The GRC Power Hour™** *Shana Kelley, Min Yu*

Liquid Biopsy for Cancer

Emerging Liquid Biopsy Technologies for Early Detection, Disease Profiling and Monitoring of Cancer

JUNE 20 – 21, 2020

CHAIRS: Fredrik Thege and Nykia Walker

Lysosomes and Endocytosis

Physiological Adaptations of the Endo-Lysosomal System

JUNE 21 – 26, 2020 • PROCTOR ACADEMY, ANDOVER, NH

CHAIR: Christopher Burd

VICE CHAIR: Phyllis Hanson

- **The Endo-Lysosomal System and Disease** *Scott Emr, Leon Murphy,* Rushika Perera, Marco Sardiello, Miguel Seabra
- **Lysosomes and the Control of Cellular Metabolism** *Robert Piper, Suzanne Pfeffer,* Michael Overholtzer, Haoxing Xu, Roberto Zoncu, Andrea Ballabio
- **Entering Cells** *Frances Brodsky, Lauren Jackson,* Gunther Hollopeter, Jennifer Stow, Min Wu
- **Inter-Organelle and Inter-Cellular Communication** *Sandra Schmid, Philip Stahl,* Erik Jorgensen, Avital Rodal, Guillaume van Niel, Lois Weisman, Meng Wang
- **Roles of the Endosomal Network in Organismal Physiology** *Tomas Kirchhausen, Margaret Robinson,* Peter Cullen, Max Gutierrez, Joseph Mindell, Francesca Peri
- **The Lysosome, Autophagy and Cellular Catabolism** *Markus Babst, James Hurley,* Florian Froehlich, Thomas Melia, Anne Simonsen
- **Late-Breaking Topics** *Alexander Sorkin,* Michael Bassik, Yamuna Krishnan
- **Sorting and Trafficking in the Endosomal Network** *Elizabeth Conibear, Manoj Puthenveedu,* Juan Bonifacino, Harald Stenmark, Michael Marks, Andreas Mayer
- **Keynote Session: Lysosome-Like Organelles** *Fred Maxfield,* Graca Raposo
- **The GRC Power Hour™** *Phyllis Hanson*

Lysosomes and Endocytosis

Life Cycle, Functions and Environment of the Endolysosomal System in Health and Disease

JUNE 20 – 21, 2020

CHAIRS: Roya Dayam and Roni Levin Konigsberg

Mammalian Reproduction

Reproduction from Bench to Bedside: From Regulatory Mechanisms to Practical Applications

AUGUST 9 – 14, 2020 • MOUNT HOLYOKE COLLEGE, SOUTH HADLEY, MA

CHAIRS: Margaret Petroff and Kyle Orwig

VICE CHAIRS: Richard Freiman and Joan Jorgensen

- **Building Blocks for Reproduction: Eggs, Sperm and Uterus** *Julie Kim,* Thomas Spencer, Francesca Duncan, Stefan Schlatt
- **Molecular and Genetic Control of Reproduction** *Sue Hammoud,* Nehemiah Alvarez, Chen Chen, Sarah England
- **Reproduction in the Age of Omics** *John Schimenti,* Pat Lonergan, Roser Vento-Tormo, Miles Wilkinson
- **Immune Function in Reproductive Biology** *Tony De Falco,* Janette Dufour, Maria Battistone, Dorothy Sojka, Tippi MacKenzie
- **Developmental Biology and Sex Determination** *Lane Christenson,* Diana Laird, Fei Zhao, Anthony Perry
- **Applied Reproduction** *Miguel Brieno-Enriquez,* Ans Van Pelt, Sherman Silber, James Turner, Sean Limesand
- **Next Generation Technologies in Reproduction** *Monica Laronda,* Jon Oatley, Ariella Shikanov, Helen Jones
- **Stem Cells in Reproductive Processes** *Robin Hobbs,* Ina Dobrinski, Katsuhiko Hayashi, James Pru
- **Keynote Session: Determinants of Reproductive Outcomes and Disease** *Richard Freiman, Joan Jorgensen,* Mary Ann Handel, Asgi Fazleabas
- **The GRC Power Hour™** *Mellissa Mann, Francesca Soncin*

Mammalian Reproduction

Safeguarding Fertility for the Present and Future

AUGUST 8 – 9, 2020

CHAIRS: Margeaux Wetendorf and Klementina Fon Tacer

Mammary Gland Biology

Normal Breast Biology and Its Relationship to Breast Cancer Initiation and Progression

JUNE 7 – 12, 2020 • RENAISSANCE TUSCANY IL CIOCCO, LUCCA (BARGA), ITALY

CHAIRS: Maria Vivanco and Beatrice Howard

VICE CHAIRS: Russell Hovey and Senthil Muthuswamy

- **Keynote Session: Breast Stem Cell Biology** *Barry Gusterson,* Connie Eaves
- **Normal Breast Biology: Progenitor and Stem Cells** *Cathrin Brisken,* Marja Mikkola, Pamela Cowin, Lone Rønnov-Jessen
- **Abnormal Breast Biology: Precancerous Lesions (DCIS)** *Fariba Behbod,* Louise Jones, Jelle Wesseling
- **Heterogeneity in Breast Cancer** *Walid Khaled,* Rama Khokha, Joan Brugge, Helen Piwnica-Worms
- **Molecular Alterations During Pregnancy and Lactation** *Russell Hovey,* Catharina Svanborg, Kai Kessenbrock
- **Residual Disease and Metastasis** *Eva Gonzalez-Suarez,* Marianna Rapsomaniki, Bob van de Water, Douglas Hanahan
- **Hormone Receptor Signaling** *Senthil Muthuswamy,* Linda Lindström, Leonie Young
- **Novel Approaches to Study Mammary Development and Disease** *Marisa Luisa Faraldo,* Michael Lewis, Joaquin Arribas, Thea Tlsty
- **Keynote Session: Breast Stem Cell Biology and Translational Breast Cancer Research** *Matthew Smalley,* Geoffrey Lindeman
- **The GRC Power Hour™** *Leonie Young, Walid Khaled*

Mammary Gland Biology

Tracing the Cellular Processes Driving Mammary Gland Development and Breast Cancer

JUNE 6 – 7, 2020

CHAIRS: Veronica Richina and Karsten Bach

Marine Microbes

The Interconnected Microbial Ocean

MAY 24 – 29, 2020 • LES DIABLERETS CONFERENCE CENTER, LES DIABLERETS, SWITZERLAND

CHAIR: Corina Brussaard

VICE CHAIRS: Lasse Riemann and Ramunas Stepanauskas

- **Pathogenic Microbe Interactions and Their Influence on Biogeochemical Cycling** *Curtis Suttle,* Steven Wilhelm, Rui Zhang
- **Single Celled Microbes Versus Assembled Microbial Communities** *Martin Ackermann,* Roman Stocker, Knut Drescher, Nicole Dubilier
- **Evolution of Marine Microbes** *Alexandra Worden, Rogier Braakman,* Anja Spang, Kasper Kjeldsen, Gabrielle Rocap
- **Microbial Predator-Prey Interchange in Relation to Marine Ecological Theories** *Thomas Kiorboe,* Susanne Wilken, Selina Våge, Chih-hao (Zac) Hsieh
- **Synergistic Microbe-Microbe and Microbe-Host Connections and Communication** *Madeleine van Oppen, Hanna Farnelid,* Nicole Webster, Jonathan Zehr, Kim Ritchie
- **The Complex Marine Microbiomes Captured in Networks and Ecosystem Models** *Naomi Levine,* Christian Mueller, Victoria Coles, Marina Levy
- **Environmental Shaping of Microbial Communities and *Vice Versa*** *Xosé Anxelu Morán, Laura Alonso-Saez,* Daniele Bianchi, Ed Hall, Clara Ruiz-González
- **Living at the Ocean's Boundaries** *Victoria Orphan,* Filip Meysman, Heide Schulz-Vogt, Julie Huber
- **A Changing Ocean: Challenges to Overcome for Microbial Functional Success** *Oded Beja, Charmaine Yung,* Stephen Giovannoni, Osvaldo Ulloa, Katherine Mackey
- **The GRC Power Hour™** *Anja Spang, Julie Huber*

Marine Microbes

Integrative Microbial Oceanography

MAY 23 – 24, 2020

CHAIRS: B. B. Cael and Deepa Rao

Mechanical Systems in the Quantum Regime

Quantum Phononics for Fundamental Measurements and Quantum Technology

JUNE 21 – 26, 2020 • VENTURA BEACH MARRIOTT, VENTURA, CA

CHAIRS: Cindy Regal and Klemens Hammerer

VICE CHAIRS: Thomas Purdy and Amir Safavi-Naeini

- **Surface Acoustic Waves and Brillouin Optomechanics** *Amir Safavi-Naeini,* Konrad Lehnert, Audrey Bienfait, Peter Rakich
- **Gravitational Wave Detectors** *Thomas Purdy,* Nergis Mavalvala, Yanbei Chen, David McClelland, Karsten Danzmann
- **Nonreciprocity and Chirality in Optomechanics** *Ewold Verhagen,* Aash Clerk, Haitan Xu, Etienne Brasselet
- **Levitated Mechanical Systems** *Tongcang Li,* Markus Aspelmeyer, Benjamin Stickler, Hendrik Ulbricht, Jack Harris
- **Fundamental Physics Searches with Mechanical Sensors** *Yiwen Chu,* Swati Singh, Holger Mueller, Jacob Taylor
- **Heralding Single Phonons and Quantum Tests** *Aash Clerk,* Simon Groeblacher, Magdalena Zych, Christophe Galland, Eugene Polzik
- **Quantum Electromechanics and Magnetomechanics** *Eva Weig,* John Teufel, Silvia Viola Kusminskiy, Adrian Bachtold
- **Spin Coupling to Nanomechanics** *Donghun Lee,* Ania Bleszynski-Jayich, Christian Degen, Raffi Budakian, Philipp Treutlein
- **Late-Breaking Topics** *John Teufel*
- **The GRC Power Hour™** *Eva Weig, Jack Harris*

Mechanical Systems in the Quantum Regime

Optomechanical Systems Enabling Novel Quantum-Enhanced Technologies and Tests of Fundamental Physics

JUNE 20 – 21, 2020

CHAIRS: Charles Brown and Martin Koppenhoefer

Mechanisms of Epilepsy and Neuronal Synchronization

Molecular and Network Complexity in the Epileptic Brain

AUGUST 16 – 21, 2020 • REY DON JAIME GRAND HOTEL, CASTELLDEFELS, SPAIN

CHAIRS: Jeffrey Noebels and Chris Dulla

VICE CHAIRS: Helen Scharfman and Viji Santhakumar

- **Complexity in Epilepsy** *Gemma Carvill,* Danielle Bassett, Liset Menendez de la Prida
- **Local and Long-Range Circuitry** *Esther Krook-Magnuson,* Yoav Adam, Peyman Golshani
- **Cell Type-Specific Contributions to Seizures** *Ivan Soltesz,* Gordon Fishell, Mauro Costa-Mattioli
- **Synaptic and Network Homeostasis** *Istvan Mody,* Seth Grant, Eve Marder, Upi Bhalla, Joseph Raimondo
- **Glial Signaling and Epileptogenesis** *Amy Brewster,* Ukpong Eyo, Philip Haydon
- **Developmental Circuit Refinement** *Heinz Beck,* Arnold Kriegstein, Annapurna Poduri, Beatriz Rico
- **New Gene Targets and Therapies** *Dimitri Kullmann,* Amy Brooks-Kayal, Harald Sontheimer, Stephen Traynelis
- **Oscillations, Rhythms and Network Dynamics** *Jennifer Gelinas,* Christophe Bernard, Vikaas Sohal, Rafael Yuste, Laura Ewell
- **Epigenetic and Metabolic Targets in Epileptic Brain** *Jeannie Chin,* David Henshall, Katja Kobow, Farah Lubin

Mechanisms of Epilepsy and Neuronal Synchronization

Approaching Complexity in Neuroscience and Epilepsy

AUGUST 15 – 16, 2020

CHAIRS: Melanie McNally and Wesley Clawson

Medicinal Chemistry

Enabling Targeted Therapies for Unmet Medical Needs

AUGUST 9 – 14, 2020 • COLBY-SAWYER COLLEGE, NEW LONDON, NH

CHAIR: Janeta Popovici-Muller

VICE CHAIR: Cynthia Parrish

- **How Cryo-EM Structures Are Enabling Drug Discovery** *John Van Drie,* Andrew Marks, Jue Chen, Seungil Han
- **Recent Advances in Rare Disease Drug Discovery** *Darby Schmidt,* Sue Stokes, David Piotrowski, Susan Ashwell, Kevin Hunt
- **Emerging Technologies: From *In Silico* to Implementation** *Alessandro Boezio,* Patrick Walters, Eric Martin, Timothy Cernak
- **Novel Pain and Addiction Therapeutics to Combat the Opioid Crisis** *Lewis Pennington,* Kurt Rasmussen, Brian Aquila, Steven McKerrall, Miles Congreve
- **Modern Screening Approaches for the Identification of High Value Leads** *Alex Cortez,* Brian Shoichet, Jorge Esquivias, Linghong Xie
- **Novel Strategies Targeting Immunotherapies** *Pamela Haile,* David Moffatt, Mark Schnute, Alan Corin, David Harrison
- **Driving Pharmacology Through Tissue and Target Access** *Emily Peterson,* Simon Peace, Thomas Durand-Reville, Thomas Chappie
- **Late-Breaking Topics: First Disclosures of Clinical Candidates** *Erin DiMauro,* Mark Ledeboer, Alicia Regueiro-Ren, Dustin Mergott, Zenon Konteatis
- **Keynote Session: From Targeted Small Molecules to Targeted Cell Therapies** *Cynthia Parrish,* Julian Adams
- **The GRC Power Hour™** *Jennifer Riggs, H. Rachel Lagiakos*

Medicinal Chemistry

Key Concepts and Strategies in Small Molecule Drug Discovery

AUGUST 8 – 9, 2020

CHAIR: Thomas Simpson

Meiosis

Diverse and Conserved Molecular Mechanisms Preventing Aneuploidy During Gamete Production

JUNE 7 – 12, 2020 • COLBY-SAWYER COLLEGE, NEW LONDON, NH

CHAIR: Paula Cohen

VICE CHAIR: Jeff Sekelsky

- **Physical Properties and Organization of the Synaptonemal Complex** *Scott Hawley,* Needhi Bhalla, Sean Burgess, Monica Colaiacovo
- **Conservation and Diversity of Meiotic Events Across Evolution: Implications for Human Meiotic Errors** *Patricia Hunt,* Beth Dumont, Fernando Manuel de Villena, Karen Schindler, Sarah Zanders, Jacob Mueller, Eva Hoffmann
- **Placement and Induction of Double Strand Breaks** *Peter Schlögelhofer,* Scott Keeney, Bernard de Massy
- **DSB Processing and Pathway Choice** *James Haber,* Douglas Bishop, Raphael Mercier, Francesca Cole, Gregory Copenhaver, Diana Libuda, Maria Jasin, Liangran Zhang
- **Spindle Assembly, Chromosome Segregation and Checkpoint Control** *John Schimenti,* Ewelina Bolcun-Filas, Sadie Wignall
- **Crossover Designation, Maturation and Homeostasis** *Jeff Sekelsky,* Nancy Kleckner, Anne Villeneuve, Michael Lichten, Ian Henderson
- **Chromosome Dynamics, Cohesion and Pairing** *Denise Zickler,* Kikue Tachibana
- **Chromatin Organization, Gene Expression and Epigenetic Control of Meiosis** *James Turner,* Kevin Corbett, Andreas Hochwagen, Matthew Neale, Elcin Unal
- **Post-Translational Modifications as Essential Regulators of Meiotic Progression** *Nancy Hollingsworth,* Valentin Boerner, Gloria Brar, Neil Hunter
- **The GRC Power Hour™** *Francesca Cole, Douglas Bishop*

Meiosis
Molecular Mechanisms and Regulation of Sexual Reproduction
JUNE 6 – 7, 2020
CHAIRS: Maria Bravo Nunez and Katherine Billmyre

Membrane Transport Proteins

Biomedical Transporters: Physiology, Dysfunction and Targets of Pharmacotherapy

JUNE 14 – 19, 2020 • REY DON JAIME GRAND HOTEL, CASTELLDEFELS, SPAIN

CHAIR: Aurelio Galli

VICE CHAIRS: Renae Ryan and Susan Ingram

- **Channelopathies and Transportopathies** *Renae Ryan,* Hanne Poulsen, Al George, Jeffrey Rothstein, Virginia Nunes
- **Targeting Transporters for Pharmacotherapies** *Erin Calipari, Sandra Hewett,* Nancy Carrasco, Robert Vandenberg, Manuel Palacin, Amy Newman
- **Transporter Function and Dysfunction in Metabolism, Diabetes and Obesity** *Habibeh Khoshbouei,* Zachary Freyberg, Sophie Hambleton, Amira Klip, Michael Koettgen
- **Invertebrates as Animal Models to Study Transporter Functions** *Randy Blakely, Freja Herborg,* Susan Amara, Lucia Carvelli, Laura Bianchi, David Krantz
- **Na,K-ATPase and Related Pumps** *Imogen Coe,* Matthias Hediger, Jonathan Javitch, Poul Nissen, Daniela Pietrobon
- **Neurological and Neuropsychiatric Disorders: Transporters at Play** *Rajini Rao,* Antonello Bonci, Heinrich Matthies, Haley Melikian, Gaia Novarino, Harald Sitte
- **New Strategies, Ideas and Techniques to Study Membrane Protein Structure-Function and Trafficking** *Ulrik Gether,* Sergio Grinstein, Olga Boudker, Parastoo Hashemi, Eduardo Perozo
- **Peptides, Hormones and Neurotransmitter Release: The Importance of Transporters in the Gut and Brain** *Michael Freissmuth, Susan Ingram,* Eric Gouaux, Naoki Yamanaka, Robert Edwards
- **Detailing Mechanisms of Importers and Exporters** *Roxanne Vaughan,* Isabelle Baconguis, Hassane Mchaourab, Christine Ziegler
- **The GRC Power Hour™** *Imogen Coe, Renae Ryan*

Membrane Transport Proteins
The Structure-Function Relationship of Transporters in Health and Disease
JUNE 13 – 14, 2020
CHAIRS: Susanna Concilio and Eric Figueroa

Membranes: Materials and Processes

Convergence in Membrane Research Across Disciplines and Scales

AUGUST 2 – 7, 2020 • COLBY-SAWYER COLLEGE, NEW LONDON, NH

CHAIRS: Isabel Escobar and William Phillip

VICE CHAIRS: J.R. Johnson and Lucy Camacho

- **Keynote Session: Interfacial Engineering of Membranes for Environmental Applications** *Audie Thompson, Steven Weinman,* Dibakar Bhattacharyya, Lidietta Giorno
- **Rational Design of Membrane Materials** *Christopher Arges, Hee Jeung Oh, Jamie Hestekin,* Moises Carreon, Qilin Li, Zachary Smith
- **Process Optimization and Intensification** *Ngai Yin Yip, William Tarpeh,* Uwe Beuscher, Kathy Lee
- **Membrane Manufacturing** *Tequila Harris, Ramy Swaidan,* Maria Coleman, Marcus Worsley, Glenn Fredrickson
- **Real-Time Process Control/Membrane Fouling** *Johannes Vrouwenvelder, Katherine Zodrow,* Daniel Miller, Jessica Schiffman
- **Composite Membrane Structures** *Laura Biedermann, Marta Hatzell,* Nicholas Kotov, Andrea Schaefer, Sibudjing Kawi
- **Reactive, Emerging and Hybrid Membrane Processes** *Lauren Greenlee, Kerri Hickenbottom,* Seth Darling, Suzana Nunes
- **Industrial Separations Needs** *TorOve Leiknes, Hannah Murnen,* Christina Carbrello, Chunqing Liu, Stephen Ritchie
- **Keynote Session: From Lab-Scale Discoveries to Industrial Gas Separation Processes** *Ayse Asatekin, Robert Schucker,* William Koros, Matthias Wessling
- **The GRC Power Hour™** *Christina Carbrello, Jamie Hestekin*

Membranes: Materials and Processes
Connecting Pathways Between Molecular Design and Module Commercialization in Membrane Science
AUGUST 1 – 2, 2020
CHAIRS: John Lawrence III and Gabrielle Levato

Metallocofactors

Bioinorganic Active Sites that Drive Challenging Chemical Conversions

JUNE 7 – 12, 2020 • SALVE REGINA UNIVERSITY, NEWPORT, RI

CHAIR: Serena DeBeer

VICE CHAIR: Kyle Lancaster

- **Keynote Session: Frontiers of Metallocofactor Design** *Kelly Chacon,* Andrew Borovik, Yi Lu
- **Hydrogenase: From Models to Enzymes** *Kara Bren,* Alison Parkin, Hannah Shafaat, Ulf-Peter Apfel, Jason Shearer
- **Recent Advances in Nitrogenase Research** *Oliver Einsle,* Shelley Minteer, Simone Raugei, Kylie Vincent
- **Iron-Sulfur Biosynthesis and Reactivity** *Joan Broderick,* Sean Elliott, Daniel Suess, Seigo Shima
- **CO and CO_2 Conversion by Enzymes and Models** *Louise Berben,* Abhishek Dey, Holger Dobbek, Christine Thomas
- **Lanthanide Metallobiochemistry** *Eric Schelter,* Lena Daumann, Norma Cecilia Martinez-Gomez, Joseph Cotruvo, Jr.
- **Protein Engineering** *Lisa Olshansky,* Akira Onoda, Ross Anderson, Julie Renner
- **Water Oxidation in Enzymes and Models** *Theodor Agapie,* Yulia Pushkar, Nicholas Cox, Julio Lloret Fillol, Greta Patzke
- **Keynote Session: C-H Activation by Copper** *William Tolman,* Amy Rosenzweig, Paul Walton
- **The GRC Power Hour™** *Lisa Olshansky, Paul Walton*

Metals in Medicine

Advancing the Use of Metal-Based Compounds and Nanotheranostics for Personalized Medicine

JUNE 28 – JULY 3, 2020 • PROCTOR ACADEMY, ANDOVER, NH

CHAIRS: Edith (Phoebe) Glazer and Angela Casini

VICE CHAIRS: Carolyn Anderson and Anne-Kathrin Duhme-Klair

- **Keynote Session: Supramolecular Metal-Based Molecules for Biomedical Applications** *Michael Hannon,* Makoto Fujita, Xiaoyuan (Shawn) Chen, Wenbin Lin
- **Clinical Advances for Metals in Medicine** *Walter Berger,* Thomas Meade, Sherri McFarland, Paul Donnelly, Anton Simeonov
- **Catalysis in Cells** *Luca Salassa,* James Cowan, José Luis Mascareñas, Sanjana Gopalakrishnan
- **Novel Metallomics Methods and Tools** *Ana Maria Costa Ferreira,* Hongzhe Sun, Nigel Robinson, Sarah Michel, Alessandra Magistrato
- **Late-Breaking Topics** *Carolyn Anderson, Anne-Kathrin Duhme-Klair,* Eszter Boros, Camilla Abbehausen, Orazio Vittorio
- **Novel Chelation Strategies and Applications for Radionuclides and Contrast Agents** *Eric Gale,* Katherine Vallis, Peter Caravan, Jason Lewis, Rebecca Abergel
- **Essential Metals in Disease Mechanisms** *Katherine Franz,* Donita Brady, Martin Burke
- **Stimuli-Responsive Materials for Therapy and Imaging** *Zijian Guo,* Rachela Popovtzer, Zhuang Liu, Anna Samia
- **Targeted Metal-Based Therapeutics** *Thomas Meade,* Maria Contel, Seth Cohen
- **The GRC Power Hour™** *Maria Contel*

Microbial Stress Response

Bacterial Mechanisms for Sensing, Responding and Adapting to Stress

JULY 19 – 24, 2020 • MOUNT HOLYOKE COLLEGE, SOUTH HADLEY, MA

CHAIRS: Michael Laub and Jade Wang

VICE CHAIRS: Amy Schmid and Peter Chien

- **Regulatory Systems for Stress** *Amy Gehring,* Mark Buttner, Sean Crosson, Susan Gottesman, Gisela Storz
- **Cell Envelope Stress** *Eduardo Groisman,* Jean-Francois Collet, Petra Levin, Natividad Ruiz, Allison Williams
- **Replication Stress** *William Navarre,* Susan Rosenberg, Lyle Simmons, Jan-Willem Veening
- **Temperature, Oxidative and Metal Stress** *Joan Slonczewski,* Frederic Barras, Carol Gross, John Helmann, Arash Komeili
- **Stress of Phage and Mobile Genetic Elements** *Lyle Simmons,* Alan Grossman, Kim Seed
- **Stress of Other Cells** *Petra Levin,* Marie Elliot, Daniel Wall, Chris Waters
- **Stress of Being in a Host** *Marie Elliot,* Seemay Chou, Sophie Helaine, William Navarre
- **Proteotoxic and Translational Stress** *Amy Schmid,* Pierre Genevaux, Daniel Kearns
- **Energy and Metabolic Stress** *Peter Chien,* Lars Dietrich, Caroline Harwood, Norma Cecilia Martinez-Gomez

Microbial Stress Response
Microbial Sensing, Signaling and Survival in Stress
JULY 18 – 19, 2020
CHAIRS: Mona Orr and Jan-Ulrik Dahl

Microbial Toxins and Pathogenicity

Mechanisms of Action, Detection and Evasion of Microbial Toxins

JULY 12 – 17, 2020 • WATERVILLE VALLEY, WATERVILLE VALLEY, NH

CHAIR: Heran Darwin

VICE CHAIR: Mary O'Riordan

- **Keynote Session: Virulence Regulation During Infections** *Andrew Darwin,* Britney Hardy, Andrew Perault, Virginia Miller
- **Bacterial Toxins: Structure, Function and Outcome** *Victor Torres,* Borden Lacy, Jeongmin Song, Isaac Chiu, Andreas Peschel, John Mekalanos
- **Bacteria-on-Bacteria Warfare: Toxins and Phages** *Peggy Cotter,* Marek Basler, Alecia Septer, Christopher Hayes
- **Subverting Host Functions with Bacterial Toxins and Effectors** *Eric Skaar,* Olivier Neyrolles, Sophie Helaine, ZhaoQing Luo, Jim Cassat, Ralph Isberg
- **Regulation of Genes and Proteins in Pathogens** *Raphael Valdivia,* Petra Dersch, Aimee Shen, Joshua Woodward
- **Intracellular Problems and Solutions** *Joanne Engel,* Marcia Goldberg, Rebecca Lamason, Isabelle Derré, Renee Tsolis, Sarah Stanley
- **Evolution of Virulence Factors** *Manuela Raffatellu,* Tamara O'Connor, Ankur Dalia, Matthew Waldor
- **Detection and Response to Bacterial Infections** *Russell Vance,* Anna Tischler, Katrin Mayer-Barber, Sebastian Winter, Ivan Dikic, Edward Miao
- **Keynote Session: Innate Sensing of Pathogens** *Kim Orth,* Feng Shao
- **The GRC Power Hour™** *Drusilla Burns*

Microbial Toxins and Pathogenicity
Intercellular Interactions and Pathologic Outcomes
JULY 11 – 12, 2020
CHAIRS: Britney Hardy and Andrew Perault

Microbiology of the Built Environment

Microbes at the Interface of Water, Air and Human Health in Built Environments

JUNE 7 – 12, 2020 • PROCTOR ACADEMY, ANDOVER, NH

CHAIR: Kyle Bibby

VICE CHAIR: Amy Pruden

- **Linking Building Microbiomes and Health** *Karen Dannemiller,* Laura-Isobel McCall, Chuck Gerba
- **Drinking Water Microbiome** *Amy Pruden,* Frederik Hammes, Ameet Pinto
- **Extreme and Confined Environments** *Kevin Sato,* Cheryl Nickerson, Charlie Ott
- **Antibiotic Resistance** *Erica Hartmann,* Kerry Hamilton, Tao Yan
- **Microbiology of Sewage Collection Systems** *Jordan Peccia,* Lydia Bourouiba, Amy Mathers
- **Microbiology of the Built Environment in the Developing World** *Krista Wigginton,* Joe Brown, Kara Nelson, Amy Pickering
- **Microbiologically-Informed Green Engineering Design** *Mark Hernandez,* Tim Julian, William Rhoads
- **Standardizing Built Environment Microbiological Methods** *Rachel Adams,* Scott Kelley, Lynn Schriml
- **Biofilms** *Kerry Kinney,* Andrew Jackson, Robert McLean
- **The GRC Power Hour™** *Karen Dannemiller, Erica Hartmann*

Mitochondria and Chloroplasts

Semi-Autonomous Organelles: From Fundamental Processes to Translation in Agriculture and Medicine

JULY 19 – 24, 2020 • MOUNT SNOW, WEST DOVER, VT

CHAIR: Zach Adam

VICE CHAIR: Antoni Barrientos

- **Evolution and Dynamics of Organelle Genomes** *Andreas Weber,* Dan Mishmar
- **Organelle Gene Expression** *Zofia Chrzanowska-Lightowlers,* Alice Barkan, Brendan Battersby, Flavia Fontanesi
- **Protein Import, Sorting and Assembly** *Agnieszka Chacinska,* Hsou-Min Li, Peter Rehling, Masato Nakai, Danja Schunemann
- **Organelle Dynamics: Division, Differentiation and Contacts** *Liza Pon,* Yoshiki Nishimura, Maya Schuldiner, Samantha Lewis
- **Structure and Function of Organelle Complexes** *Martin Ott,* Amandine Marechal, Oliver Daumke, Karen Davies
- **Organelle Metabolism** *Sabeeha Merchant,* A. Harvey Millar, Veronica Maurino, Ken Nakamura
- **Signaling and Stress Response** *Asa Starnd,* Valentina Perissi, Jaakko Kangasjärvi
- **Proteostasis, Mitophagy and Chlorophagy** *Klaas Van Wijk,* Thomas Becker, Paul Jarvis, Hagai Abeliovich, Steven Glynn
- **Organelle Biology Translated into Medicine and Agriculture** *Richard Hartley,* Stephen Long, Giovanni Manfredi, Ralph Bock
- **The GRC Power Hour™** *Liza Pon, Maya Schuldiner*

Mitochondria and Chloroplasts

Semi-Autonomous Organelles: From Fundamental Processes to Translation in Agriculture and Medicine

JULY 18 – 19, 2020

CHAIRS: Florian Schober and Laura Klasek

Molecular and Cellular Neurobiology

Emerging Technologies to Study Nervous System Development, Function and Neurological Disease

JULY 5 – 10, 2020 • THE HONG KONG UNIVERSITY OF SCIENCE AND TECHNOLOGY, HONG KONG, CHINA

CHAIR: Aaron Gitler

VICE CHAIR: Mingjie Zhang

- **Keynote Session: Mechanisms of Neurological Disease** *Katja Brose,* Carla Shatz, Li-Huei Tsai, Hailan Hu
- **Development of the Nervous System** *Kang Shen,* Daniel Colón-Ramos, Melissa Rolls, Hongyan Wang, Gordon Fishell, Xuecai Ge, Shen-Ju Chou, Carina Hanashima, Yukiko Gotoh
- **Synapses and Synaptic Function** *Xiang Yu,* Thomas Sudhof, Camin Dean, Lu Chen, Peter Scheiffele
- **Neural Circuits and Behavior** *Shernaz Bamji,* Yang Dan, Nirao Shah, Anna Beyeler, Yi Zuo, Steven Flavell, Juan Song, Ishmail Abdus-Saboor, Shan Meltzer, Ai Nakashima
- **Brain Imaging and Connectomics** *Yimin Zou,* Tianyi Mao, Na Ji
- **Genetics and Epigenetics of the Nervous System** *Louis Reichardt,* Daniel Geschwind, Nancy Bonini, Jie Shen, Coleen Murphy, Nancy Ip, Theodore Price
- **Sensory Systems** *John Ngai,* Amita Sehgal, Sandeep Robert Datta, Craig Montell, Alexander Chesler, Fengwei Yu
- **Mechanisms of Neurodegeneration and Regeneration** *Leonard Petrucelli,* Don Cleveland, James Shorter, Michael Ward, Eric Huang, Jun Ding, Zhigang He, Frank Bradke, Claire Le Pichon
- **Keynote Session: Advanced Technologies for Neuroscience Research** *Yi Sun,* Feng Zhang, Alice Ting, Ryohei Yasuda
- **The GRC Power Hour™** *Shernaz Bamji, Aaron Gitler*

Molecular and Cellular Neurobiology

Integration of Neural Mechanisms in Health and Disease

JULY 4 – 5, 2020

CHAIRS: Nicole Leung and Zacharie Taoufiq

Molecular Basis of Microbial One-Carbon Metabolism

Enzymes and Metabolisms Driving the Global Carbon Cycle

AUGUST 9 – 14, 2020 • WATERVILLE VALLEY, WATERVILLE VALLEY, NH

CHAIR: Seigo Shima

VICE CHAIR: Christopher Marx

- **Keynote Session: Methane and the Carbon Cycle** *F. Robert Tabita,* Stephen Lippard, William Metcalf
- **Biochemistry and Physiology of Aerobic Methylotrophy** *Yasuyoshi Sakai,* Amy Rosenzweig, Marina Kalyuzhnaya, Arren Bar-Even
- **Chemoautotrophy and Electron Donors** *Amelia-Elena Rotaru,* Takuro Nunoura, Miriam Agler-Rosenbaum, Chris Greening
- **From C_1 to C_2: Acetogens, Reactions and Applications** *Mirko Basen,* Volker Mueller, Byung-Kwan Cho, Stephen Ragsdale, Hannah Shafaat, Michael Koepke
- **Ecology and Evolution of C_1 Metabolism** *Kathleen Scott,* Mandy Joye
- **CO_2 Fixation and Photorespiration** *Tobias Erb,* Elke Dittmann, Elizaveta Bonch-Osmolovskaya, Manajit Hayer-Hartl, Cheryl Kerfeld
- **Key Enzymes of Anaerobic C_1 Metabolism** *Silvan Scheller,* Gerrit Schut, Florin Musat, Rafael Laso-Pérez
- **Physiology and Structural Biology** *Diana Sousa,* Masaru Nobu, Norma Cecilia Martinez-Gomez, Cornelia Welte, Bonnie Murphy
- **Syntrophy and Eukaryogenesis** *Colleen Cavanaugh,* Nicolai Müller, Anja Spang, Hiroyuki Imachi
- **The GRC Power Hour™** *Cornelia Welte*

Molecular Basis of Microbial One-Carbon Metabolism

Microbial One-Carbon Conversion from the Microscale to the Global Scale

AUGUST 8 – 9, 2020

CHAIRS: Marie Schölmerich and Kristen Farley

Molecular Interactions and Dynamics

Dynamics and Spectroscopy of Chemical Systems

JUNE 28 – JULY 3, 2020 • STONEHILL COLLEGE, EASTON, MA

CHAIR: Hua Guo

VICE CHAIR: Ricardo Metz

- **Cold and Ultracold Collisions and Reactions** *Svetlana Kotochigova,* Kang-Kuen Ni, Nandini Mukherjee, Balakrishnan Naduvalath
- **Molecular Interactions and Collisions in the Gas Phase** *Jun Li,* Arthur Suits, Uwe Manthe, Roland Wester, Richard Dawes
- **Kinetics of Combustion, Atmospheric and Interstellar Reactions** *David Osborn,* Marsha Lester, Stephen Klippenstein, Albert Viggiano
- **Molecular Interactions and Dynamics at Interfaces** *Jörg Meyer,* Rainer Beck, Bin Jiang, Timothy Minton, Gilbert Nathanson
- **Impact of Machine Learning** *Philipp Marquetand,* Roman Krems, Francesco Paesani, David Wilkins
- **Photochemistry and Nonadiabatic Dynamics** *Michael Schuurman,* David Yarkony, Joseph Subotnik, Benjamin Levine, Kaijun Yuan
- **Ultrafast Processes** *Oriol Vendrell,* Marcos Dantus, Luis Banares, Irene Burghardt
- **Molecular Interactions and Dynamics in Complex Systems** *Jian Liu,* Wei Kong, Vicki Grassian, Caroline Jarrold, Richard Loomis
- **Keynote Session: Spectroscopy and Dynamics** *Ricardo Metz,* George Schatz, Daniel Neumark, Robert Field
- **The GRC Power Hour™** *Vicki Grassian, Caroline Jarrold*

Molecular Interactions and Dynamics

Reactions, Collisions and Energy Transfer on Short to Long Timescales

JUNE 27 – 28, 2020

CHAIR: Matthew Bain

> ***"This was by far the best conference I have ever attended. I met many amazing scientists and made lasting professional and personal connections."***
>
> SYLVIA HANNA, Northwestern University, Nanoporous Materials and Their Applications GRC

Molecular Structure Elucidation

Recent Advances in Analytical Technologies to Expedite the Development of New Modalities

AUGUST 2 – 7, 2020 • JORDAN HOTEL AT SUNDAY RIVER, NEWRY, ME

CHAIRS: Mohammad Alsayah and R. Graham Cooks

VICE CHAIRS: Yongchao Su and Gaurav Chopra

- **Keynote Session: Discovery and Development of New Drug Modalities** *Roy Helmy,* Wayne Fairbrother, David Brayden
- **Analytical Characterization of New Modalities** *Cinzia Stella, Amin Famili,* Wendy Sandoval, Rainer Fischer, Martin Gilar
- **High Throughput Experimentation, Computational Chemistry and Machine Learning** *Gaurav Chopra,* Joshua Schrier, Spencer Dreher
- **Advances in Spectroscopic Techniques** *Shengli Ma, Yongchao Su,* Mei Hong, Krishna Mallela, Jean-Francois Masson, Zheng Ouyang
- **Emerging Techniques in Separation Science** *Samuel Yang,* Robert Kennedy, Peter Shoenmakers, Kevin Schug
- **Advancing Pharmaceutical Discovery and Development Through Molecular Structure Elucidation** *Naijun Wu, Jason Cheung,* Peter Yehl, Allen Templeton
- **The Dark Metabolome and Lipidome** *Christina Ferreira, Filippos Michopoulos,* Stephen Blanksby, Peter Nemes, Xin Yan
- **Proteins in Unusual States** *David Russell, Vicki Wysocki,* Jennifer Brodbelt, David Clemmer, Arthur Laganowsky
- **Efficient Development of Novel Analytical Technologies via Collaborations Between Academia and the Pharmaceutical Industry** *Christopher Welch, Archana Kumar,* Rebecca Whelan, Paul Bohn, Yong Liu

Multiferroic and Magnetoelectric Materials

Science and Technology of Spin-Charge Coupling in Materials

AUGUST 2 – 7, 2020 • BATES COLLEGE, LEWISTON, ME

CHAIRS: Ramamoorthy Ramesh and Venkatraman Gopalan

VICE CHAIR: Tsuyoshi Kimura

- **User Facilities for Materials Synthesis and Probes of Fundamental Phenomena** *Padraic Shafer,* John Freeland, Di-Jing Huang, David Tennant, Aaron Lindenberg, Gerrit Vander Laan
- **Theoretical Frameworks, Machine Learning Approaches** *Jorge Iniguez,* Alexander Balatsky, Long-Qing Chen, Geoffroy Hautier, Javier Junquera, Daniel Khomskii
- **Multiferroic Crystal Synthesis** *Tsuyoshi Kimura,* Vivien Zapf, Ram Seshadri, Anatoly Zvezdin, Yasunori Furukawa
- **Thin Films, Heterostructures and Nanostructures** *Taewon Noh,* YinHao Chu, Valanoor Nagarajan, Chan-Ho Yang, Pu Yu, Patrycja Paruch
- **Applications of Multiferroics and Magnetoelectrics** *Cheng Song,* Geoffrey Beach, Nian Sun, Cewen Nan, Lane Martin, Neil Mathur
- **Picoscale Metrology** *Xiaoqing Pan,* Manfred Fiebig, David A. Muller, Jan Seidel, Jan Musfeldt
- **Quantum Materials, 2-Dimensional Multiferroics** *Silvia Picozzi,* Taro Nakajima, Xiaodong Xu, Arzhang Ardavan, Zhiqiang Mao
- **Symmetry, Topology, Non-Reciprocal and Emergent Phenomena: Real Space and Reciprocal-Space** *Venkatraman Gopalan,* Jirka Hlinka, Yoshinori Onose, Shinichiro Seki, Sang-Wook Cheong, Vincent Garcia
- **Keynote Session: Fundamental and Applied Science of Multiferroics** *Ramamoorthy Ramesh,* Nicola Spaldin, Ian Young, Darrell Schlom
- **The GRC Power Hour™** *Patrycja Paruch, Nicola Spaldin*

Multiferroic and Magnetoelectric Materials

Multiferroic Coupling Effects and Dynamics of Domains and Domain Walls at the Nanoscale

AUGUST 1 – 2, 2020

CHAIRS: Mads Weber and Johanna Nordlander

Multiphoton Processes

Study of Dynamics by Light-Matter Interaction: From Atoms to Complex Systems

JUNE 14 – 19, 2020 • BRYANT UNIVERSITY, SMITHFIELD, RI

CHAIR: Caterina Vozzi

VICE CHAIRS: Nirit Dudovich and Daniel Rolles

- **Keynote Session: Multiphoton Science** *Marc Vrakking,* Donna Strickland
- **Chirality** *Markus Ilchen,* Margaret Murnane, Valerie Blanchet, Olga Smirnova
- **Electronic and Nuclear Dynamics in Complex Systems** *Adam Kirrander,* Matthias Kling, Zhi Heng Loh
- **Solid-State Dynamics** *Hadas Soifer,* Ursula Keller, Ralph Ernstorfer, Rupert Huber
- **Nonlinear XUV and X-Ray Science** *Kevin Prince,* James Cryan, Tommaso Mazza
- **Multidimensional Imaging of Chemical Dynamics** *Jochen Küpper,* Stefanie Gräfe, Itzik Ben-Itzhak, Till Jahnke
- **Dynamics at Conical Intersections** *Heide Ibrahim,* Mizuho Fushitani, Michael Schuurman
- **Attosecond Dynamics** *Jonathan Marangos,* Paul Corkum, Francesca Calegari, Andrew Brown
- **Emerging Techniques** *Emma Springate,* Fabien Quere, Jochen Mikosch
- **The GRC Power Hour™** *Valerie Blanchet, Nirit Dudovich*

Multiphoton Processes

Study of Dynamics by Light-Matter Interaction: From Atoms to Complex Systems

JUNE 13 – 14, 2020

CHAIRS: Ruaridh Forbes and Omer Kneller

Multiscale Plant Vascular Biology

Assessing Plant Vascular Function Through Optical Approaches

JUNE 7 – 12, 2020 • JORDAN HOTEL AT SUNDAY RIVER, NEWRY, ME

CHAIRS: Brent Helliker and Jeannine Cavender-Bares

VICE CHAIRS: Anna Sala and Rachel Spicer

- **Keynote Session: Viewing Plant Vascular Function Across Scales** *Noel Holbrook,* John Sperry, Abigail Swann
- **Plant-Atmosphere Connections from Landscapes to Whole Earth** *Alexandra Konings,* Kyla Dahlin, Alexander Damm, Susan Ustin
- **Water Movement Through Leaves to Ecosystems** *Sybil Gotsch,* Abraham Stroock, Andrew Leakey
- **3D Elucidation of Leaf Structure and Function** *Lawren Sack,* Margaret Barbour, Craig Brodersen, Christine Scoffoni
- **Vascular Transport from Whole Plants to Ecosystems** *Sally Thompson,* Kim O'Keefe, Anna Trugman
- **Xylem Structure-Function Relationships** *Francesca Secchi,* Jochen Schenk, Maciej Zwieniecki
- **Phloem Structure-Function Relationships** *Jozica Gricar,* Jessica Savage, Sanna Sevanto
- **Stomatal and Aquaporin Mediated Water Flux** *Tom Buckley,* Tim Brodribb, David Granot, Menachem Moshelion
- **Evolution of Plant Vascular Systems** *Adam Roddy,* Charles Boyce, Monica Carvalho
- **The GRC Power Hour™** *Katherine McCulloh*

Multiscale Plant Vascular Biology

Challenges for Plant Vascular Function in the Anthropocene

JUNE 6 – 7, 2020

CHAIRS: Gerard Sapes and William Hammond

Musculoskeletal Biology and Bioengineering

New Approaches to Accelerate Discovery in the Musculoskeletal System

AUGUST 9 – 14, 2020 • PROCTOR ACADEMY, ANDOVER, NH

CHAIR: Tamara Alliston

VICE CHAIR: Louis Defrate

- **Keynote Session: Advancing Musculoskeletal Discovery and Health with New Biological and Bioengineering Approaches** *Constance Chu,* Paula Hammond, Linda Sandell
- **Biology and Bioengineering of Aging in the Musculoskeletal System** *Samuel Ward,* Thomas Rando, Adetola Adesida, Sarah Dallas, Kharma Foucher
- **Musculoskeletal Pain: Causes and Cures** *Anne-Marie Malfait,* Tony Yaksh, Gregory Hicks, A. Vania Apkarian
- **Spatial Context in the Musculoskeletal System** *Catherine Kuo,* Ralph Müller, Lin Han, Stefano Di Talia, Alessandra Sacco
- **Immunology in Musculoskeletal Health and Disease** *Laura McCabe,* Hiroshi Takayanagi, Danièle Noël, Dana Graves
- **Tracking Musculoskeletal Histories over Time** *Ivo Kalajzic,* Terence Capellini, Qing-Jun Meng, George Muschler
- **Multiscale Metabolism in Musculoskeletal Tissue Crosstalk** *Peter Croucher,* Tri Phan, Graham Williams, Ronald June, Nancy Lane
- **Multiscale Musculoskeletal Mechanobiology** *Pen-Hsiu Chao,* Melissa Knothe Tate, Alayna Loiselle, Elise Morgan, Belinda Beck
- **Synthetic Musculoskeletal Biology and Biomaterials** *Alan Grodzinsky,* Robert Bowles, Blanka Sharma, Johnna Temenoff
- **The GRC Power Hour™** *Jennifer Westendorf, Carolyn Chlebek*

Musculoskeletal Biology and Bioengineering

Multi-Scale Approaches to Understanding Musculoskeletal Tissues

AUGUST 8 – 9, 2020

CHAIRS: Sun Peck and Stefaan Verbruggen

Mutagenesis

Fundamental Mechanisms of Genomic Change and Adaptation

JUNE 14 – 19, 2020 • JORDAN HOTEL AT SUNDAY RIVER, NEWRY, ME

CHAIR: Julian Sale

VICE CHAIR: Houra Merrikh

- **Keynote Session: Fundamental Mechanisms of Mutagenesis** *Daniel Jarosz,* Reuben Harris, Sue Jinks-Robertson
- **DNA Damage Tolerance at the Replication Fork** *Sarah Lambert,* Helle Ulrich, Susan Lovett, Wei Yang, Dana Branzei
- **Visualizing Mutagenic Mechanisms** *Wei Yang,* Joseph Loparo, Antoine Van Oijen, David Rueda
- **Mutagenesis Arising from Replication Errors** *Susan Lovett,* Thomas Kunkel, Roger Woodgate, David Pellman
- **RNA-Dependent Mutagenesis** *Thomas Kunkel,* Karlene Cimprich, Andres Aguilera, Hannah Klein
- **Repeat and Barrier-Induced Mutagenesis** *Hannah Klein,* Marcel Tijsterman, Catherine Freudenreich, Sarah Lambert, Sergei Mirkin
- **Understanding Mutation Signatures in Cancer and Aging** *Ketan Patel,* Nuria Lopez-Bigas, Ruben van Boxtel
- **Environmental and Endogenous Mutagenesis** *Reuben Harris,* Shana Sturla, Ivan Matic, Ketan Patel, Bjoern Schwer
- **Evolvability and Adaptation** *Houra Merrikh,* Lilach Hadany, Melissa Gymrek, Daniel Jarosz
- **The GRC Power Hour™** *Hannah Klein, Susan Lovett*

Mutagenesis

Mechanisms of Mutagenesis and Their Clinical Implications

JUNE 13 – 14, 2020

CHAIRS: Claudia Aloisi and Nicole Stantial

Myelin

Translational Science of Myelin: From Glial Biology to Repair

MAY 17 – 22, 2020 • RENAISSANCE TUSCANY IL CIOCCO, LUCCA (BARGA), ITALY

CHAIRS: Catherine Lubetzki and Kelly Monk

VICE CHAIRS: Terri Wood and Jonah Chan

- **Remyelination in Multiple Sclerosis** *Anne Baron-Van Evercooren, Jonah Chan,* Christine Stadelmann-Nessler, Lou Brundin, Benedetta Bodini, Robin Franklin
- **Cell-Cell Interactions in Myelination** *Charles ffrench-Constant, Terri Wood,* Elior Peles, Eva-Maria Krämer-Albers, Jun Hee Kim, Keiichiro Susuki, Nathalie Sol-Foulon, Stephen Fancy, Sophie Belin
- **Oligodendroglial Heterogeneity** *Wendy Macklin, Bernard Zalc,* Ragnhildur Karadottir, Goncalo Castelo-Branco, Patrizia Casaccia, Vahbiz Jokhi
- **Novel Imaging Tools: From Cells to Human Tissue** *Jennifer Orthmann-Murphy, Bruno Stankoff,* Jaime Grutzendler, Emmanuel Beaurepaire, Dies Meijer, Martina Absinta, Heidi Johansen-Berg, Peter Stys, Ethan Hughes
- **Multiple Sclerosis: A Therapeutic Perspective** *Marco Salvetti, Frauke Zipp,* Mariapia Sormani, Jeremy Chataway, Ari Green, Gianvito Martino, Meredith Hartley
- **Development of Myelinating Glia** *Leda Dimou, Ben Emery,* Hyun Kyoung Lee, Bruce Appel, Brad Zuchero, Jayshree Samanta, Fiona Doetsch, Ueli Suter, Ruth Stassart
- **Schwann Cell Development and Repair** *Laura Feltri, James Salzer,* Piotr Topilko, Claire Jacob, Alison Lloyd, Peter Arthur-Farraj, Lydia Daboussi
- **Innate Immune Cells in Myelin Damage and Repair** *Roberta Magliozzi, William Talbot,* Marco Prinz, Veronique Miron, Sebastian Werneburg, Inge Huitinga, Hans Lassmann, Robert Hill
- **Adaptive Myelination and Remyelination** *Maria Cecilia Angulo, Tobias Merson,* Maarten Kole, Dwight Bergles, Letizia Leocani
- **The GRC Power Hour™** *Jennifer Orthmann-Murphy, Violetta Zujovic*

Myelin

Dynamics of Myelin Formation, Function and Repair

MAY 16 – 17, 2020

CHAIRS: Meng-meng Fu and Jenea Bin

Nanoscale Science and Engineering for Agriculture and Food Systems

Convergence of Nanotechnology with Food and Agriculture

JUNE 21 – 26, 2020 • SOUTHERN NEW HAMPSHIRE UNIVERSITY, MANCHESTER, NH

CHAIRS: Antje Baeumner and Julie Goddard

VICE CHAIRS: Carmen Gomes and Melanie Kah

- **Convergence of Nanotechnology with Food and Agriculture** *Jason White,* Sharon Walker, Fabio Pulizzi
- **Advances in Nanomaterials** *Margaret Frey,* Brenda Hutton-Prager, Khara Grieger, Tony McNally
- **Translation of Nano-Based Science for Application in Food and Agriculture** *Nick Dokoozlian, Timothy Duncan,* Kevin Nichols, Lynn Frewer
- **Nanobiosensor Approaches to Improving Human and Animal Health** *Man Bock Gu,* Jason Dwyer, Jenny Emneus, Sundaram Gunasekaran
- **Environmental Nanotechnology** *Gregory Lowry,* Leonardo Fraceto, Rebecca Klaper
- **Big Data in Food and Agricultural Nanotechnology: IoT and Predictive Modelling** *Arturo Keller,* Amalia Turner, Riccardo Accolla, Abigail Horn
- **Nanodelivery Approaches to Improving Human and Animal Health** *Cristina Sabliov,* Debora Rodrigues, Ja-an Ho
- **Nanotechnology's Impact on Food Safety** *Richard Canady,* Evangelyn C. Alocilja, Eric McLamore
- **Nanotechnology's Role in Agriculture** *David Britt,* Michael Adams
- **The GRC Power Hour™** *Carmen Gomes, Melanie Kah*

Nanoscale Science and Engineering for Agriculture and Food Systems

Convergence of Nanotechnology with Food and Agriculture

JUNE 20 – 21, 2020

CHAIRS: Ying Wang and Daniel White

Nasopharyngeal Carcinoma

New Targets in Nasopharyngeal Carcinoma: Viral Latency, Genome Discoveries and Tumor Microenvironment

JUNE 14 – 19, 2020 • THE HONG KONG UNIVERSITY OF SCIENCE AND TECHNOLOGY, HONG KONG, CHINA

CHAIRS: Kwok Wai Lo and Quynh-Thu Le

VICE CHAIRS: Mu Sheng Zeng and Alan Chiang

- **Keynote Session: Viruses and Tumor Development** *Lawrence Young,* Joan Steitz, Ian Frazer
- **EBV as a Target for Therapy and Vaccination** *George Tsao,* Paul Lieberman, Wei Bu, Ka-Leung Wong, Ming-Han Tsai, A. Dimitrios Colevas
- **Preclinical Models for NPC and EBV Infection** *Pierre Busson,* Christian Münz, Anna Chi-Man Tsang, Robert West
- **Translating NPC Genomics to the Clinics: Therapeutic and Biomarker Perspectives** *Maria Lung, Allen Chan,* Jin-Xin Bei, Vivian Lui, Ming-Yuan Chen, Benjamin Pinsky, Scott Bratman
- **Prevention and Screening for NPC** *Wei-Hua Jia,* Dennis Lo, Miao Xu, Allan Hildesheim
- **Tumor Microenvironment of NPC** *Chwee Ming Lim,* Rajiv Khanna, Qian Zhong, Fuchou Tang, Jaap Middeldorp
- **Advances in NPC Imaging, Pathology, Treatment Planning and Clinical management** *Anne Lee,* Nasir M. Rajpoot, Jun Ma, Matt Lechner
- **Immunotherapy in NPC: Non-Cell-Based and Cell-Based** *Brigette Ma, Rajiv Khanna,* Edwin Hui, Graham Taylor, Han Chong Toh, Bilal Omer, Christian Hinrichs
- **Keynote Session: Future Perspectives in NPC Research and Treatment** *Fei-Fei Liu,* Robert Schreiber, Garry Nolan
- **The GRC Power Hour™** *Fei-Fei Liu, Brigette Ma*

Natural Products and Bioactive Compounds

The Function of Natural Products at the Interface of Chemistry and Biology

AUGUST 2 – 7, 2020 • PROCTOR ACADEMY, ANDOVER, NH

CHAIR: Amber Onorato

VICE CHAIR: Philip Kym

- **Keynote Session: Biomimetic Inspired Synthesis of Natural Products** *Michael Schmidt,* Hosea Nelson, Richmond Sarpong, Dirk Trauner
- **Innovative Chemical and Biological Technology** *Elizabeth Swift,* Lisa Marcaurelle, Francis Gosselin, Michael Vannieuwenhze, Derek Tan
- **Chemical Biology of Natural Products and Bioactive Compounds** *Ryan Rafferty,* Amanda Garner, Gavin Williams, Janet Smith
- **Novel Synthetic Strategies and Methodology** *Rodrigo Andrade,* Timothy Newhouse, Mark Rizzacasa, Tehshik Yoon, Uttam Tambar
- **Unique Methods for the Discovery of Natural Products** *John D'Angelo,* Ikuro Abe, Jeffrey Bode, Tadeusz Molinski
- **Medicinal Chemistry of Natural Products and Bioactive Compounds** *Carlos Zepeda,* Gunda Georg, Michael Acker, Jamie McCabe Dunn, David Myles
- **Discovery and Biological Activity of Natural Products** *Jeremy Cody,* Cassandra Quave, Chambers Hughes, Jon Thorson
- **Chemical Modifications and Biological Activity of Natural Products** *Tricia May-Dracka,* David Perrin, Daniel Appella, Paul Hergenrother, Gregory Dudley
- **Keynote Session: Pioneering Synthetic Efforts** *Jonathan Scheerer,* David Williams, Yoshito Kishi
- **The GRC Power Hour™** *Jamie McCabe Dunn*

Natural Products and Bioactive Compounds

Biological and Synthetic Approaches of Natural Product Chemistry

AUGUST 1 – 2, 2020

CHAIRS: Bernhard Kepplinger and Gina Morgan

Neural Development

Building the Nervous System: Insights from Development, Evolution and Disease

AUGUST 9 – 14, 2020 • SALVE REGINA UNIVERSITY, NEWPORT, RI

CHAIR: Claude Desplan

VICE CHAIR: Debby Silver

- **Keynote Session: Neurogenesis Across Development and Evolution** *Flora Vaccarino,* Magdalena Goetz, Fiona Doetsch, Catarina Homem
- **Neural Cell Fate Specification** *Fiona Doetsch,* Alessandra Pierani, Laure Bally-Cuif, Shubha Tole, Yukkiko Gotoh, Bassem Hassan
- **The Generation of Neural Diversity** *Yukkiko Gotoh,* Barbara Treutlein, Stavros Lomvradas, Denis Jabaudon
- **Neural Lineages: From Genomics to Imaging** *Barbara Treutlein,* James Gagnon, Ben Simons, Zhirong Bao, Simon Hippenmeyer, Rick Livesey
- **Evolution of Brain Development** *James Gagnon,* Alejandro Sanchez Alvarado, Colette Dehay, Maria Tosches, Victor Borrell
- **Axon Generation and Degeneration** *Maria Tosches,* Jessica Treisman, Samantha Butler, Stephanie Gupton, Dietmar Schmucker, Rosalind Segal
- **Function of Glial in Development** *Samantha Butler,* Vilaiwan Fernandes, Dong Yan, Maxwell Heiman, Cody Smith
- **Development of Neural Circuitry** *Cody Smith,* Oliver Hobert, Richard Mann, Claire Wyart, Niels Ringstad, Genevieve Konopka
- **Keynote Session: Human Development and Disease** *Genevieve Konopka,* Silvia Cappello, Flora Vaccarino, Arturo Alvarez-Buylla
- **The GRC Power Hour™** *Shubha Tole*

Neural Development

Building the Nervous System: Cell Diversity, Circuit Assembly and Disease

AUGUST 8 – 9, 2020

CHAIRS: Daniel Pederick and Stephanie Redmond

Neurobiology of Brain Disorders

Fundamental Mechanisms Leading to Novel Therapeutics and Biomarkers for Neurodegenerative Disease

AUGUST 2 – 7, 2020 • REY DON JAIME GRAND HOTEL, CASTELLDEFELS, SPAIN

CHAIRS: Leonard Petrucelli and Alison Goate

VICE CHAIRS: Karen Duff and Chris Shaw

- **Keynote Session: Development of ASOs as an FDA Approved Treatment for Neurodegenerative Disease** *Bart De Strooper,* Don Cleveland
- **Genetic and Genomic Approaches to Neurodegenerative Disease** *Carlos Cruchaga,* Julie Williams, Rosa Rademakers, Peter Heutink, Hemali Phatnani
- **Epigenetics of Neurodegenerative Disease** *Bess Frost,* Manolis Kellis, Jonathan Mill, Leslie Thompson, Anne Schaefer
- **Frontotemporal Dementia and ALS: Mechanisms** *Benjamin Wolozin,* Dorothee Dormann, Jeffrey Rothstein, Aaron Gitler, Ludo Van Den Bosch
- **Parkinson's Disease: Mechanisms** *Mark Cookson,* Valina Dawson, Towfique Raj, Patrik Verstreken, Dario Alessi
- **Alzheimer's Disease: Mechanisms** *Soyon Hong,* Beth Stevens, Christian Haass, Guojun Bu, Tara Spires-Jones
- **Tauopathies: Mechanisms, Biomarkers and Novel Therapeutics** *Karen Duff,* David Holtzman, Li Gan, Bess Frost, Anthony Fitzpatrick
- **Biomarkers: Diagnoses and Theranostics** *Chris Shaw,* Anne Fagan, Magdalini Polymenidou, Bradley Boeve, Donna Wilcock
- **Therapeutics Approaches** *Donna Wilcock,* Eric McDade, Chris Henderson, Carole Ho, Beverly Davidson
- **The GRC Power Hour™** *Karen Duff, Leonard Petrucelli*

Neurobiology of Brain Disorders

Neurodegenerative Disease: From Molecular Mechanisms to Potential Therapies

AUGUST 1 – 2, 2020

CHAIRS: Judith Houtman and Brian Lananna

Neurobiology of Cognition

Neural Circuits, Dynamics and Computations of Cognition and Behavior

JULY 26 – 31, 2020 • JORDAN HOTEL AT SUNDAY RIVER, NEWRY, ME

CHAIRS: David Freedman and Sabine Kastner

VICE CHAIRS: Joni Wallis and Aaron Batista

- **Keynote Session: Attention and Working Memory** *Elisabeth Murray,* Robert Desimone, Kia Nobre
- **Subcortical Contributions to Cognition** *Helen Barbas,* Farran Briggs, Michael Halassa, Richard Krauzlis, Melanie Wilke
- **Cognitive Computation and Artificial Intelligence** *Xiao-Jing Wang,* Tatiana Engel, Daniel Yamins, Joshua Tenenbaum
- **New Approaches for Probing Circuits of Cognition** *Christopher Harvey,* Denise Cai, Jessica Cardin, John Maunsell, Jude Mitchell
- **Electrophysiology of Human Cognition** *Rony Paz,* Anne-Lise Giraud, Randolph Helfrich, Robert Knight
- **Neural Mechanisms of Memory** *Tatiana Pasternak,* Christos Constantinidis, Earl Miller, Nicole Rust, Anna Schapiro
- **Motor Cognition** *Charles Schroeder,* Michele Basso, Mark Churchland, Karel Svoboda
- **Neural Encoding: Convergence and Controversy** *Stephanie Palmer,* Brent Doiron, Ila Fiete, Stefano Fusi, Jennifer Groh
- **Cognitive Maps** *Talia Konkle,* Danielle Bassett, Elizabeth Buffalo, Sylvia Wirth
- **The GRC Power Hour™** *Sabine Kastner, Joni Wallis*

Neurobiology of Cognition

Multidisciplinary Approaches to Understanding the Neural Circuits of Cognition

JULY 25 – 26, 2020

CHAIRS: Raman Saggu and Sebastien Tremblay

Neurobiology of Drug Addiction

Addiction Research: From Molecules to Circuits to Treatment

AUGUST 16 – 21, 2020 • GRAND SUMMIT HOTEL AT SUNDAY RIVER, NEWRY, ME

CHAIRS: Yavin Shaham and Marina Wolf

VICE CHAIRS: Marina Picciotto and Serge Ahmed

- **Keynote Session: Advances in Epigenetic and Circuit Mechanisms of Drug Addiction: Implications to Treatment** *Pier Vincenzo Piazza,* Eric Nestler, Nora Volkow
- **Cellular and Circuit Mechanisms of Opioid Addiction and Pain** *Cecilia Flores,* Brigitte Kieffer, Laura Bohn, Stefan Schulz, Nurulain Zaveri, Gregory Scherrer
- **Learning Mechanisms of Drug Addiction** *Karen Ersche,* Rita Fuchs, Geoffrey Schoenbaum, Regina Carelli, Stephanie Groman
- **Synaptic Mechanisms of Drug Addiction** *Paul Kenny,* Yan Dong, Huib Mansvelder, Kasia Radwanska, Vincent Pascoli, Carrie Ferrario, Meaghan Creed
- **Addiction Theories** *Rita Goldstein,* David Epstein, Jane Taylor, Hanna Pickard, Lee Hogarth
- **Animal Models of Drug Addiction and Relapse** *Gavan McNally,* Olivier George, Michael Nader, Chris Pierce, Marco Venniro, Nathan Marchant, Morgan James, Erin Calipari
- **Translational Research in Drug Addiction** *Markus Heilig,* Aldo Badiani, Sandra Comer, Courtney Miller, Matt Banks, Hedy Kober
- **Circuitry of Drug Addiction** *Marisela Morales,* John Mantsch, Sara Jones, Kate Wassum, Nii Addy, Drew Kiraly, Kathryn Reissner
- **New Imaging Methods to Visualize the Effect of Addictive Drugs on the Brain** *Veronica Alvarez,* Byungkook Lim, Lin Tian, Ream Al-Hasani, Seksiri Arttamangkul
- **The GRC Power Hour™** *Rajita Sinha, Dorit Ron*

Neurobiology of Drug Addiction

Mechanisms Underlying Development and Persistence of Drug Addiction

AUGUST 15 – 16, 2020

CHAIRS: Sam Golden and Megan Fox

Neuroplasticity of Sensory Systems

Neuroplasticity of Attention, Prediction and Learning

JUNE 21 – 26, 2020 • THE HONG KONG UNIVERSITY OF SCIENCE AND TECHNOLOGY, HONG KONG, CHINA

CHAIRS: Anna Wang Roe and Jan Schnupp

VICE CHAIRS: Xiongjie Yu and Chun-Yue Geoffrey Lau

- **Neuroplasticity in Development** *Stephen David,* Patrick Kanold, Jianhua Cang
- **Synaptic and Circuitry Mechanisms of Sensory Plasticity** *Kexin Yuan,* Xiao-Ming Li, Liping Wang, Kun Li
- **Adaptation and Predictive Coding** *Xiongjie Yu,* Israel Nelken, Yumei Gong
- **Neuroprostheses and Neuroplasticity** *Patrick Kanold,* Stephen David, Nicole Rosskothen-Kuhl
- **Neuroplasticity in Attention** *Ranulfo Romo,* Xiaoke Chen, Mitchell Sutter, Qiaojie Xiong
- **Neuroplasticity in Learning and Memory** *Yi Rao,* Tianming Gao, Jufang He, Bruno Averbeck, Zhai Yuying
- **Cross-Modal Plasticity** *Tianming Gao,* Yale Cohen, Josef Rauschecker, Aihua Chen, Lizabeth Marie Romanski
- **Language and Social Behavior** *Lizabeth Marie Romanski,* Robert Liu, Luis Lemus, Nai Ding, Lixia Gao, Xiaoqin Wang
- **Cutting-Edge Technology in Neuroscience** *Xiaoqin Wang,* Xu Zhang, Yi Rao, Guohua Xu
- **The GRC Power Hour™** *Lixia Gao*

Noble Metal Nanoparticles

Harnessing Designer Metal Nanostructures for Diverse Applications

JUNE 14 – 19, 2020 • MOUNT HOLYOKE COLLEGE, SOUTH HADLEY, MA

CHAIR: Sara Skrabalak

VICE CHAIR: Gregory Hartland

- **Keynote Session: Metal Nanoparticle Design** *Teri Odom,* Younan Xia
- **Characterization and Theory** *Christy Haynes,* Kenneth Knappenberger, David Masiello, Jennifer Dionne, Utkur Mirsiadov
- **Synthesis** *Pedro Camargo,* Ki Tae Nam, Svetlana Neretina, Richard Tilley
- **Nanostructures for Diagnosis and Delivery** *Catherine Murphy,* Belinda Heyne, Shana Kelley, Somin Lee, Xiaohu Xia
- **The Nanoparticle Surface** *Amanda Haes,* Jill Millstone, Kristen Fichthorn, Ayman Karim
- **Designer Catalysts** *Xingchen Ye,* Graeme Henkelman, Michelle Personick, Anatoly Frenkel, Peng Chen
- **Plasmonics for Energy Conversion** *Marina Leite,* Tamar Seideman, Matthew Sheldon, Christy Landes
- **Assembly, Self-Organization and Reconfiguration of Nanoparticles** *Matthew Jones,* Robert Macfarlane, Michael Engel, Vivian Ferry, Xing Yi Ling
- **Selected Poster Presentations** *Gregory Hartland,* Luis Liz-Marzan
- **The GRC Power Hour™** *Amanda Haes*

Noble Metal Nanoparticles

Structure-Function Relationships of Noble Metal Nanomaterials from Design Principles to Diverse Applications

JUNE 13 – 14, 2020

CHAIRS: Melissa King and Stephen Lee

Notch Signaling in Development, Regeneration and Disease

Mechanisms of Notch Signaling in Health and Disease

JULY 19 – 24, 2020 • BATES COLLEGE, LEWISTON, ME

CHAIRS: Ivan Maillard and Freddy Radtke

VICE CHAIRS: Jon Aster and Kim Dale

- **Keynote Session: Setting Notch in Context** *Jon Aster, Kim Dale,* Nancy Speck, Kun-Liang Guan
- **Structure and Mechanisms of Notch Activation** *Rhett Kovall, Susan Lea,* Stephen Blacklow, Robert Haltiwanger, Penny Handford, Guanghui Yang
- **Notch and Development** *Sarah Bray,* Nadean Brown, Ryoichiro Kageyama, Francois Schweisguth
- **Transcription, Epigenetics and Notch** *Rachael Kuintzle,* Sarah Bray, Robert Faryabi, Vivian Li, Norbert Perrimon
- **Notch, Cancer and Therapeutics** *Lucio Miele,* Adolfo Ferrando, Birgit Knoechel, Rajwinder Lehal
- **Notch and Liver Disease** *Anna Bigas,* Emma Andersson, Stacey Huppert, Hamed Jafar-Nejad, Utpal Pajvani, Christian Siebel, David Piccoli
- **Late-Breaking Topics** *Raphael Kopan,* Nathalie Labrecque, Daniel Lafkas, Kevin Wei
- **Signaling Interactions and Modulations** *Daniel Lafkas,* Wendy Gordon, Vincent Luca, John Ngo, David Sprinzak
- **Blood and Vessels** *Irwin Bernstein,* Ralf Adams, Anna Bigas, Julia Mack
- **The GRC Power Hour™** *Emma Andersson*

Notch Signaling in Development, Regeneration and Disease

Mechanisms of Notch Signaling in Health and Disease

JULY 18 – 19, 2020

CHAIRS: Rachael Kuintzle and David Sloas

NOX Family NADPH Oxidases

NOX Enzymes in Cellular Communication and Metabolism in Health and Disease

MAY 31 – JUNE 5, 2020 • WATERVILLE VALLEY, WATERVILLE VALLEY, NH

CHAIR: Albert Van Der Vliet

VICE CHAIR: Marie Jose Stasia

- **Keynote Session: The NOX Family in the World of Redox Biology** *William Nauseef,* Karl-Heinz Krause, Rafael Radi
- **NOX Structure and Functional Regulation** *Susan Smith,* Francesca Magnani, David Thomas, Sumin Kang, Agnes Görlach
- **Novel Tools to Assess NOX Activity and Function** *Louise Hecker,* Hadley Sikes, Christopher Bonham, Thomas Michel
- **Peroxidases, Thiol Proteins and Ion Channels as NOX Targets** *Franck Fieschi,* Miklós Geiszt, Cristina Furdui, Ivan Bogeski
- **NOX in Immunology and Microbiome Regulation** *Mary Dinauer,* Ulla Knaus, Anna Martner, Balazs Rada
- **NOX in Cellular Metabolism and Metabolic Disease** *Ajay Shah,* Francis Miller, Roberto Di Maio, Edward Chouchani, Thomas Jensen
- **Subcellular Actions of NOX** *Francisco R. Laurindo,* Vikas Anathy, Veronique Witko-Sarsat, Dongmin Kang
- **NOX in Cell Differentiation and Stem Cell Function: Implications for Disease Pathology** *Kathy Griendling,* Gareth Thomas, A. Brent Carter, Katrin Schröder, Lucia Lopes
- **NOX in Translation: Implications for Clinical Application** *Patrick Pagano,* Rhian Touyz, Victor Thannickal
- **The GRC Power Hour™** *Susan Smith*

NOX Family NADPH Oxidases

The Role of NOX-Dependent Oxidant Signaling in Health and Disease: Towards Therapeutic Targets

MAY 30 – 31, 2020

CHAIRS: Dina Vara and Carmen Veith

Ocean Global Change Biology

Integrating Environmental, Organismal and Community Complexity into Ocean Global Change Research

JULY 19 – 24, 2020 • WATERVILLE VALLEY, WATERVILLE VALLEY, NH

CHAIR: Sinead Collins

VICE CHAIR: Mary Sewell

- **Modeling Different Timescales in Ocean Change Biology** *Andy Ridgwell,* Patricia Sanchez-Baracaldo, Ben Ward
- **Horizon-Scanning in Ocean Global Change Biology** *Francis Chan,* Victoria Coles, David Hutchins, Andreas Osclies
- **Understanding the Role of Environmental Fluctuations in Shaping Organismal Responses** *Luis-Miguel Chevin,* Juan Diego Gaitan-Espitia, David Vasseur, Joanna Bernhardt
- **Epigenetics and Transgenerational Plasticity** *Naomi Levine,* Melanie Heckwolf, Frank Johannes, Katie Lotterhos
- **Organismal Interactions in Changing Oceans** *Paul Renaud,* Corina Brussaard, Fernando Lima
- **Tropicalization** *Chris Harley,* Jason Hall-Spencer, Adriana Verges
- **Biological Variation and Responses to Changing Environments** *C. Elisa Schaum,* Amanda Bates, Colin Kremer, Tatiana Rynearson
- **Life Histories and Ocean Change** *Mary Sewell,* Catriona Clemmesen, Jonathan Havenhand, Anke Kremp
- **Incorporating Conservation and Mitigation Goals into Fundamental Research** *Gretchen Hofmann,* Trisha Atwood, Philip Boyd
- **The GRC Power Hour™**

Ocean Global Change Biology

Eco-Evolutionary Dynamics in a Changing Ocean

JULY 18 – 19, 2020

CHAIRS: Hanny Rivera and Mark Bitter

Ocean Mixing

The Impact of Ocean Mixing on the Earth, Ocean and Atmosphere Systems, Climate and Society

JUNE 14 – 19, 2020 • SOUTHERN NEW HAMPSHIRE UNIVERSITY, MANCHESTER, NH

CHAIRS: Jonathan Nash and Kurt Polzin

VICE CHAIRS: Sonya Legg and Alberto Naveira Garabato

- **The Evolving Perspective of Ocean Mixing: Certainties, Uncertainties and Impacts** *Sjoerd Groeskamp,* Angelique Melet, Eric D'Asaro
- **Physics Near the Ice-Ocean Interface: Mixing in Ice-Influenced Oceans** *Mary-Louise Timmermans,* Jennifer MacKinnon, Thomas Rippeth, Bishakhdatta Gayen
- **Physics Near the Ice-Ocean Interface: Mixing Beneath Ice Shelves, in Fjords and Near Sea Ice** *Andrew Wells,* Satoshi Kimura, Claudia Cenedese
- **Mixing in the Interior: Internal Waves and the Next Generation of Parameterizations** *Cynthia Bluteau,* Alexis Kaminski, Clement Vic, Friederike Pollmann
- **Upper-Ocean Mixing and Impacts on Biogeochemistry** *Daniele Iudicone,* Amala Mahadevan, Amelie Meyer
- **Mesoscale and Submesoscale Processes: Eddies, Eddy-Wave Interactions and Nonlinear Coupling** *Leah Johnson,* Emily Shroyer, Amit Tandon, Hideharu Sasaki
- **Mixing and Its Role in Climate Dynamics** *Sonya Legg,* David Marshall, Andreas Schmittner
- **Mixing at the Bottom** *Ruth Musgrave,* Ryan Holmes, Jacob Wenegrat
- **Pathways to Reducing Uncertainty** *Alberto Naveira Garabato,* Tom Farrar, Matthew Alford
- **The GRC Power Hour™** *Sally Warner*

Ocean Mixing

Relevant Processes and Their Impact on Ocean Dynamics, Biogeochemistry and the Climate System

JUNE 13 – 14, 2020

CHAIRS: Marion Alberty and Sjoerd Groeskamp

Optics and Photonics in Medicine and Biology

Biophotonics Spanning the Biology-Medicine Continuum

JULY 12 – 17, 2020 • BATES COLLEGE, LEWISTON, ME

CHAIRS: Kristen Maitland and David Sampson

VICE CHAIRS: E. Duco Jansen and Snow Tseng

- **Bridging Electron and Light Microscopy** *Mark Ellisman,* Winfried Denk, Judith Klumperman, Aubrey Weigel
- **Neuroscience and the Brain** *David Boas,* John Rogers, Anna Devor, Jana Kainerstorfer, Daniel Cote
- **Engineering Contrast** *Kevin Francis,* Robert Campbell, Cristina Zavaleta, Summer Gibbs
- **Label-Free Imaging** *Stephani Otte,* Irene Georgakoudi, YongKeun Park, Shalin Mehta, Daniel Razansky
- **Endoscopy** *Matthew Brenner,* Caroline Boudoux, Eman Namati, Kev Dhaliwal
- **Imaging in the Circulatory System** *Charles Lin,* Clemens Alt, Sarah Bohndiek, Darren Roblyer, Eva Sevick-Muraca
- **Noninvasive Probing of the Eye** *Ralf Brinkmann,* Kirill Larin, Yali Jia, Gereon Huttmann
- **Margin Assessment and Surgical Guidance** *Brian Pogue,* Jonathan Liu, Christopher Contag, Laura Marcu
- **Photo-Activation and Inactivation** *Tayyaba Hasan,* Vanderlei Bagnato, Kaushal Rege
- **The GRC Power Hour™** *Caroline Boudoux, Irene Georgakoudi*

Optics and Photonics in Medicine and Biology

The Role of Machine Learning in the Future of Biophotonics

JULY 11 – 12, 2020

CHAIRS: Danielle Harper and Madeleine Durkee

Optogenetic Approaches to Understanding Neural Circuits and Behavior

Linking Brain Circuits to Behavior: Novel Methods and Biological Insights Derived from Optogenetic Approaches

JULY 19 – 24, 2020 • GRAND SUMMIT HOTEL AT SUNDAY RIVER, NEWRY, ME

CHAIR: Bernardo Sabatini

VICE CHAIR: Denise Cai

- **Keynote Session: Optogenetics at the Cutting Edge** *Catherine Dulac,* Edward Boyden, Kay Tye
- **Global Signaling Across Brain States** *Saskia de Vries,* Anne Churchland, Yang Dan, Karl Deisseroth, Kafui Dzirasa
- **Large-Scale Imaging** *Joshua Trachtenberg,* Elizabeth Hillman, Na Ji, Yevgenia Kozorovitskiy
- **Circuitry of Social Interactions** *Gul Dolen,* Catherine Dulac, Dayu Lin, Robert Malenka
- **Novel Methods of Behavioral Analysis** *Anne Churchland,* Sandeep Robert Datta, Mackenzie Mathis, Mala Murthy
- **Reward and Reinforcement** *Mark Andermann,* Veronica Alvarez, Paul Kenny, Zayd Khaliq, Kate Wassum
- **Sensors and Molecules** *Mark Harnett,* Luke Lavis, Michael Lin, Lin Tian
- **Translating Brain Activity to Action** *Mackenzie Mathis,* Gwyneth Card, Gaby Maimon, Adam Hantman, John Tuthill
- **Circuitry of Stress and Pain** *Steve Ramirez,* Michael Bruchas, Thomas Kash, Garret Stuber
- **The GRC Power Hour™** *Denise Cai, Bernardo Sabatini*

Optogenetic Approaches to Understanding Neural Circuits and Behavior

Expanding and Integrating Optogenetic Tools and Techniques

JULY 18 – 19, 2020

CHAIRS: Kevin Monk and Sarah Stern

Organic Geochemistry

The Formation and Fate of Organic Matter: How It Regulated Earth History and Will Shape Its Future

AUGUST 2 – 7, 2020 • HOLDERNESS SCHOOL, HOLDERNESS, NH

CHAIR: Richard Pancost

VICE CHAIR: Anna Martini

- **The Limits of Our Understanding of Organic Matter** *Erdem Idiz,* Sylvie Derenne, Roland Pellenq, Alon Amrani
- **The Evolutionary and Geological History of Biosynthetic and Metabolic Pathways** *Paula Welander,* Jochen Brocks, Betul Kacar, Sarah Hurley, Patrick Shih
- **Interfaces Between Organic and Inorganic Chemistry: Preservation, Destruction and Interactions** *Johan Weijers,* Elizabeth Coward, Christian Maerz, Sander Van Den Boorn
- **Lipid Membranes: From Biophysics to Adaptation to Novel Proxies** *Nicole Bale, Florence Schubotz,* Phil Oger, Guy Schleyer, Laura Villanueva, Jiasong Fang
- **Big Data Approaches to Obtain New Understanding of Geological Systems** *Jeff Sheremata,* Thomas Abraham
- **The Myriad Pools and Archives of OM: Beyond Lipids** *Ryan Pereira,* Asmeret Asefaw Berhe, Peter Hernes, Thomas Blattmann, Anja Engel
- **The Organic Geochemistry of the Arctic** *Bart van Dongen,* Naomi Harada, Birgit Wild, Carolyn Ruppel
- **Measuring and Deciphering Intramolecular Isotopes Across Space and Time** *Kate Freeman,* Alexis Gilbert, Peter Douglas, Barbara Sherwood Lollar, Cajetan Neubauer
- **Late-Breaking Topics** *Julia Krawielicki, Elise Wilkes*
- **The GRC Power Hour™** *Florence Schubotz, Richard Pancost*

Organic Geochemistry
Mechanistic and Experimental Insights on Geochemical Archives
AUGUST 1 – 2, 2020
CHAIRS: Julia Krawielicki and Elise Wilkes

Organic Reactions and Processes

Catalysis, Methods and Strategies Empowering Organic Synthesis

JULY 19 – 24, 2020 • BRYANT UNIVERSITY, SMITHFIELD, RI

CHAIRS: Craig Merlic and Michael Zacuto

VICE CHAIRS: Sriram Naganathan and Jimmie Weaver

- **Stereochemical Control in Organic Synthesis** *Jimmie Weaver,* Varinder Aggarwal, Martin Oestreich
- **Organometallic Catalysis and Mechanisms** *Doug Frantz,* Jonathan Ellman, Elizabeth Jarvo, Peng Liu
- **Synthesis of Complex Bioactive Molecules** *Jennifer Albaneze-Walker,* Matthias Christmann, Dawei Ma
- **Catalysis and Process Chemistry** *David Martin,* Dean Toste, Qi-Lin Zhou
- **New Oxidative Transformations to Generate Molecular Complexity** *Scott Sieburth,* Andrew McNally, Paolo Melchiorre, Laurel Schafer
- **Novel Strategies and Methodologies for Synthesis** *Silas Cook,* Janine Cossy, Nuno Maulide
- **Advances in Alkene and Aromatic Functionalization Reactions** *Graham Murphy,* Ohyun Kwon, Song Lin, Alison Narayan
- **Process Chemistry Research for the Synthesis of Pharmaceuticals** *Jean Suffert,* Mark Lautens
- **Transition Metal Catalyzed Reactions** *Sriram Naganathan,* Naoto Chatani, Barry Trost
- **The GRC Power Hour™**

Organometallic Chemistry

Transition Metal and Main Group Synthesis and Catalysis for a Sustainable Future

JULY 12 – 17, 2020 • SALVE REGINA UNIVERSITY, NEWPORT, RI

CHAIR: Mitch Smith

VICE CHAIR: Heather Spinney

- **Bioorganometallic Chemistry** *Paula Diaconescu,* Hannah Shafaat, Joan Broderick
- **Late and Heavy Metal Chemistry** *Selvan Demir,* Aaron Tondreau, Vincent Lavallo, Jennifer Schomaker
- **Harnessing Photons and Electrons** *John Gordon,* Louise Berben, Yogesh Surendranath, Daniel Nocera
- **Synthesis and Catalysis with More Abundant Metals** *Aaron Sadow,* Kyle Lancaster, Alex Carpenter, Corinna Schindler
- **Early-Career Investigator Presentations** *Thomas Cundari,* Neil Tomson, Hosea Nelson, Jenny Yang
- **Main Group Chemistry** *Jenny Yang,* Holger Braunschweig, Steve Westcott, Christopher Cummins
- **Organometallic Chemistry at Surfaces** *Odile Eisenstein,* John Roberts, Matthew Conley, Christophe Copere
- **Bond Activation and Functionalization** *Yogesh Surendranath,* Robert Phipps, Matthew Sigman
- **Ligands and Metals** *Heather Spinney,* Paul Chirik, R. Tom Baker
- **The GRC Power Hour™** *Jenny Yang, Mitch Smith*

Organometallic Chemistry
Improvements in Synthesis, Reactivity and Sustainability Through Organometallic Chemistry
JULY 11 – 12, 2020
CHAIRS: Natalia Loewen and Eric Cueny

Oscillations and Dynamic Instabilities in Chemical Systems

Nonequilibrium to Induce and Maintain Spatio-Temporal Patterns

JULY 12 – 17, 2020 • STONEHILL COLLEGE, EASTON, MA

CHAIR: Satoshi Nakata

VICE CHAIR: Marcus Hauser

- **Spatio-Temporal Pattern Based on Reaction-Diffusion Systems** *Tomohiko Yamaguchi,* Annette Taylor, Alberto Munuzuri
- **Self-Organized Active Matter** *Kouichi Asakura,* Raymond Kapral, Wei Wang, Masaharu Nagayama
- **Oscillations and Patterns in Electrochemistry and Catalysis** *Marcus Hauser,* Istvan Kiss, Ronald Imbihl
- **Spatio-Temporal Collective Behaviors** *Hiroyuki Kitahata,* Veronique Pimienta, Jeremie Palacci, Nobuhiko Suematsu, Hiraku Nishimori
- **Molecular Design of Self-Organized Structures** *John Pojman,* Anna Balazs, Andreas Walther
- **Biological Oscillations and Patterns** *Takashi Amemiya, Yutaka Sumino,* Geneviève Dupont, Takashi Miura
- **Emergence Under Nonequilibrium Conditions** *Toshiyuki Nakagaki,* Castern Beta, Agota Toth
- **Nonlinear Dynamics: Synchronization, Bifurcation and Chaos** *Dezso Horvath,* Irving Epstein, Jerzy Gorecki, Sumana Dutta
- **Pattern Formation Coupled with Mass Transfer and Flow** *Kenneth Showalter,* Anne De Wit, Oliver Steinbock
- **The GRC Power Hour™** *Veronique Pimienta, Sumana Dutta*

Oscillations and Dynamic Instabilities in Chemical Systems
Examining Science and Technology from a Nonlinear Chemistry Standpoint
JULY 11 – 12, 2020
CHAIRS: Domenico Bullara and Pamela Knoll

Personalized Medicine

Precision Oncology Highlighting Molecular Diagnostics and Experimental Therapeutics

JULY 19 – 24, 2020 • THE HONG KONG UNIVERSITY OF SCIENCE AND TECHNOLOGY, HONG KONG, CHINA

CHAIRS: Steven Rosen and Hsing-Jien Kung

VICE CHAIRS: Dean Ho and Pui-Yan Kwok

- **Population Science** *Rick Kittles,* Susan Neuhausen, Yu-Chuan Li, Stephen Gruber
- **Advanced Diagnostics** *Anna Wu,* Sandy Cheng-Yu Chen, Wen Li
- **Metabolism** *David Ann,* Whei-Mei Teresa Fan, Mala Shanmugam, Qunying Lei, Zhimin Lu
- **Long Non-Coding RNA and Epigenomics** *Colin Collins,* Wenching Wang, Li-Jung Juan
- **Integrated Omics Applications** *Jonathan Keats,* Arul Chinnaiyan, Jianjun Liu, Nagarajan Vaidehi, Chiou-Hwa Cathy Yuh
- **Biomedical Engineering** *John Williams,* Chih-Ming Ho, Chih-Hwa Chen
- **Targeted Therapeutics** *Yen Yun,* Owen O'Connor, Dan Robinson, Hongwu Chen
- **Immuno-Therapeutics** *Christiane Querfeld,* Jedd Wolchok
- **Cellular Therapeutics** *Larry Kwak,* Michael Caligiuri
- **The GRC Power Hour™** *Karen Popkin*

Personalized Medicine
Precision Oncology Highlighting Molecular Diagnostics and Experimental Therapeutics
JULY 18 – 19, 2020
CHAIRS: Chia-Lin Chen and Emine Gunes

Phosphorylation and G-Protein Mediated Signaling Networks

Molecular Mechanisms of Signal Integration in Cellular and Organismal Regulation

JUNE 14 – 19, 2020 • WATERVILLE VALLEY, WATERVILLE VALLEY, NH

CHAIR: Rebecca Berdeaux

VICE CHAIR: Alan Smrcka

- **Keynote Session: Regulation of Protein Kinase Signaling** *Anton Bennett,* Alexandra Newton, Yonghao Yu, Robert Screaton
- **Membrane Proximal G Protein Signaling** *Alan Smrcka,* Heidi Hamm, Angeline Lyon, Nevin Lambert, Ku-Lung Hsu
- **Cyclic Nucleotide Regulated Signaling** *Carmen Dessauer,* Susan Taylor, Xiaodong Cheng, Lonny Levin
- **G Protein and Kinase Signaling in Physiological Control** *Henrik Dohlman,* Melanie Cobb, Joan Heller Brown, Greg Tall, Carmen Dessauer, Kirill Martemyanov
- **Physiological and Chemical Regulation of G Protein Activity** *Kirill Martemyanov,* Roger Sunahara, Evi Kostenis, Kendall Blumer
- **GPCR-Activated Signaling in Control of Cell Proliferation and Cancer** *Melanie Cobb,* J. Silvio Gutkind, Michelle Kimple, Kun-Liang Guan, Antonio Amelio
- **Signaling Beyond the Plasma Membrane** *John Scott,* Carol Williams, Jeff Frost, Alan Jones, Roshanak Irannejad
- **Integration of Phosphorylation and G Protein Mediated Signaling** *Joan Heller Brown,* Anton Bennett, John Scott, Jurgen Wess
- **Keynote Session: Structural Aspects of G Protein Signaling** *Roger Sunahara,* John Tesmer, Stephen Sprang, Arun Shukla
- **The GRC Power Hour™** *Carol Williams, Angeline Lyon*

Phosphorylation and G-Protein Mediated Signaling Networks
Mechanisms in G-Protein and Kinase-Mediated Signaling
JUNE 13 – 14, 2020
CHAIR: Ankita Jaykumar

Photonuclear Reactions

Frontiers in Nuclear and Hadronic Physics

AUGUST 9 – 14, 2020 • HOLDERNESS SCHOOL, HOLDERNESS, NH

CHAIR: Huey-Wen Lin

VICE CHAIRS: Douglas Higinbotham and Marc Vanderhaeghen

- **New Results in Precision Hadron Structure with Electromagnetic Probes** *Aldo Antognini,* Sylvester Joosten, Amar Vutha
- **Femtography of Hadrons** *Barbara Pasquini,* Christine Aidala, Zhongbo Kang, Andreas Metz, Julie Roche, Jianhui Zhang, Caroline Riedl
- **Electrons for Neutrinos** *Or Hen,* Afroditi Papadopoulou, Noemi Rocco, Sam Zeller, Adi Ashkenazi
- **Hadrons in the Nuclear Medium** *Eliezer Piasetzky,* Gerald Miller, Efrain Segarra, Holly Szumila-Vance, Ronen Weiss, Igor Korover
- **Low Energy Precision Physics and Applications** *Concettina Sfienti,* Chiara Mazzocchi
- **Hadron Spectroscopy** *Ulrike Thoma,* Lothar Tiator, Annika Thiel
- **From QCD to Gravitational Waves** *Jocelyn Read,* Kenta Kiuchi, Jeremy Holt
- **Nuclear Physics and Quantum Information Science** *Ian Cloet,* Matthew Dietrich, Christine Muschik
- **Physics with an Electron Ion Collider** *Abhay Deshpande,* Xiaoxuan Chu, Barak Schmookler, Matthew Sievert, Elena Long
- **The GRC Power Hour™** *Huey-Wen Lin*

Photosensory Receptors and Signal Transduction

Mechanisms, Applications and Effects of Natural and Engineered Photoreceptors

JUNE 28 – JULY 3, 2020 • VENTURA BEACH MARRIOTT, VENTURA, CA

CHAIR: John Kennis

VICE CHAIR: Brian Crane

- **Light Perception and Behavioral Responses** *Stuart Peirson,* Richard Cerione, Keita Sato
- **Flavin-Based Photoreceptors** *Tilman Kottke,* John Christie, Joshua Goings, Brian Zoltowski
- **Microbial Light Responses** *Annegret Wilde,* Reinhard Fischer, Conrad Mullineaux, Laura Gomez-Consarnau
- **Opsins, Retinal-Binding Proteins and Ion Channels** *Hideki Kandori,* Mitsumasa Koyanagi, Valerie Panneels, Igor Schapiro

- **Optogenetics and Synthetic Biology** *Matias Zurbriggen,* Valentina Emiliani, Viviana Gradinaru, Jared Toettcher
- **Signal Integration in Plant Photobiology** *Eirini Kaiserli,* Hongtao Liu, Ullas Pedmale
- **Advanced Techniques and Multicolor Photoreception** *Xiaojing Yang,* Mei Li
- **Bilin-Based Photoreceptors** *Emina Stojkovic,* Delmar Larsen, Richard Vierstra
- **Circadian Rhythms** *Deborah Bell-Pedersen,* Amita Sehgal, Luis Larrondo
- **The GRC Power Hour™** *Emina Stojkovic*

Photosensory Receptors and Signal Transduction
Molecular Basis, Engineering and Application of Photoreceptor Proteins
JUNE 27 – 28, 2020
CHAIRS: Yusaku Hontani and Maria Agustina Dominguez Martin

Plant and Microbial Cytoskeleton

Cytoskeletal Diversification Across the Domains of Life

AUGUST 16 – 21, 2020 • PROCTOR ACADEMY, ANDOVER, NH
CHAIRS: Erin Goley and Geoffrey Wasteneys
VICE CHAIRS: Sophie Martin and Alexander Paredez

- **Keynote Session: Evolution of the Cytoskeleton** *Magdalena Bezanilla,* Marko Kaksonen, Joe Pogliano
- **Cell Division** *Christopher de Graffenried,* Carolyn Rasmussen, Alexandre Bisson-Filho, Simonetta Piatti, David Twell
- **Interactions with Membranes** *Anthony Vecchiarelli,* Sue Jaspersen, Aoife Heaslip, Snezhka Oliferenko
- **Wall Polymer Placement and Cell Morphogenesis** *Sabine Mueller,* Nina Salama, Nicolas Minc, Chris Ambrose
- **Selected Poster Presentations** *Prachee Avasthi*
- **Cell Polarity and Polar Growth** *Daniel Lew,* Shanjin Huang, Liedewij Laan, Luis Vidali, Michelle Facette
- **Cell Motility and Dynamics** *Lillian Fritz-Laylin,* Kent Hill, Tam Mignot, Freddy Frischknecht
- **Regulating Cytoskeletal Dynamics** *Kathryn Ayscough,* David Kovar, Ram Dixit, Alphee Michelot, Hiroyasu Motose
- **Keynote Session: Host-Microbe Interactions** *Sophie Martin, Alexander Paredez,* Dominique Soldati-Favre, Chris Staiger
- **The GRC Power Hour™** *Erin Goley, Geoffrey Wasteneys*

Plant and Microbial Cytoskeleton
An Evolving Cytoskeleton: Diverging Mechanisms and Converging Patterns
AUGUST 15 – 16, 2020
CHAIRS: Laryssa Halat and Pusparanee Hakim

Plant Molecular Biology

Spatial and Temporal Dynamics in Plant Biology

JUNE 14 – 19, 2020 • HOLDERNESS SCHOOL, HOLDERNESS, NH
CHAIR: C. Robertson McClung
VICE CHAIR: Rebecca Mosher

- **Keynote Session: Symbioses** *Cara Haney,* Giles Oldroyd, Maria Harrison
- **Development in Space** *Madelaine Bartlett,* Zach Lippman, Miltos Tsiantis, Minako Ueda
- **Biotic Interactions** *Hua Lu,* Hailing Jin, Ken Shirazu
- **RNA: Roles Beyond the Message** *Aman Husbands,* Blake Meyers, Xiaofeng Cao
- **Nutrient Regulation and Transport** *Terri Long,* Rodrigo Gutierrez, David Mendoza Cozatl
- **Development in Time** *Stacey Harmer,* Mark Estelle, Hong Gil Nam
- **Modeling and Gene Regulatory Networks** *Gabriel Krouk,* Martin Howard, Amy Marshall-Colon
- **Environmental Sensing** *Ullas Pedmale,* Dawn Nagel, Richard Vierstra, Julia Bailey-Serres
- **Keynote Session: Gene and Genome Evolution** *Benjamin Blackman,* Jennifer Wisecaver, Pamela Soltis
- **The GRC Power Hour™** *Stacey Harmer*

Plant Molecular Biology
Emerging Approaches for Understanding and Engineering Plants
JUNE 13 – 14, 2020
CHAIRS: Jennifer Brophy and Signe Lolle

Plasma Processing Science

Plasmas and Their Interactions with Matter

JULY 26 – 31, 2020 • PROCTOR ACADEMY, ANDOVER, NH
CHAIR: Anthony Murphy
VICE CHAIR: Lorenzo Mangolini

- **Plasmas for the Environment** *Sylvain Coulombe,* Mariadriana Creatore, Tomohiro Nozaki
- **Plasmas and Catalysts** *Maria Carreon,* William Schneider, Jingguang Chen, Volker Hessel
- **Linking Plasma Processing and Fusion Plasmas** *Yevgeny Raitses,* Michael Keidar, David Ruzic
- **Plasma Surface Modification and Deposition** *Michael Gordon,* Sumit Agarwal, Lenka Zajickova
- **Complex Chemical Synthesis Using Plasmas** *Elodie Fourre,* Julia Bandow, Felipe Iza
- **Plasma Interactions with Biological Materials** *Gregory Fridman,* Antoine Rousseau, Katia Bazaka, Nevena Puac
- **Measuring the Interplay Between Plasmas and Matter** *Richard Engeln,* Ana Sobota, Jochen Schein
- **The Plasma-Liquid Interface** *Peter Bruggeman,* Dingxin Liu, Fumiyoshi Tochikubo, Ester Marotta
- **Plasma Synthesis of Novel Materials** *Elijah Thimsen,* R. Mohan Sankaran, Makoto Kambara, Rebecca Anthony
- **The GRC Power Hour™**

Plasma Processing Science
Multiphase and Multiscale Plasma-Material Interactions
JULY 25 – 26, 2020
CHAIRS: Judith Golda and Marien Simeni Simeni

Plasmonics and Nanophotonics

Nanoscale Light-Matter Interactions for Sustainability

JULY 12 – 17, 2020 • GRAND SUMMIT HOTEL AT SUNDAY RIVER, NEWRY, ME
CHAIR: Jennifer Dionne
VICE CHAIR: Javier Aizpurua

- **Keynote Session: Dynamic Light-Matter Interactions** *Nader Engheta,* Mark Brongersma, Peter Nordlander, Teri Odom
- **Photochemistry and Catalysis** *Renee Frontiera,* Peng Chen, Prashant Jain, Yousoo Kim, Christy Landes
- **Sustainable Energy and the Environment** *Harry Atwater,* Shanhui Fan, Vivian Ferry, Matthew Sheldon
- **Nanophotonics for Biology and Medicine** *Laura Fabris,* Rizia Bardhan, Gennady Shvets
- **Metasurfaces and Metamaterials** *Jon Schuller,* Andrea Alu, Jason Valentine
- **Active Nanophotonics and Molecular-Scale Optoelectronics** *Carsten Rockstuhl, Josh Caldwell,* Jeremy Baumberg, Christian Nijhuis, Uriel Levy, Maiken Mikkelsen, Anatoly Zayats
- **Quantum and Nonlinear Nanophotonics** *Aitzol Garcia-Etxarri,* Yuri Kivshar, Prineha Narang, Timur Shegai, Francisco Garcia-Vidal
- **Novel Syntheses and Spectroscopies** *Javier Garcia de Abajo,* Bin Ren, Mathieu Kociak
- **Keynote Session: Technology Translation** *Albert Polman,* Naomi Halas, Vladimir Shalaev, Luat Vuong
- **The GRC Power Hour™** *Teri Odom, Luat Vuong*

Plasmonics and Nanophotonics
Engineering Nanoscale Light-Matter Interactions for Energy, Communication and Biomedical Applications
JULY 11 – 12, 2020
CHAIRS: Loza Tadesse and Pavlos Pachidis

Polymer Physics

The Intersection of Polymer Physics with Soft Matter

JULY 26 – 31, 2020 • MOUNT HOLYOKE COLLEGE, SOUTH HADLEY, MA
CHAIR: Sanat Kumar
VICE CHAIR: Rachel Segalman

- **Block Copolymer Quasicrystals** *Thomas Epps, Richard Register,* Frank Bates, Sharon Glotzer
- **Nanocomposites** *Jacques Jestin, Arthi Jayaraman,* Daeyeon Lee, Pinar Akcora, Zihong Nie, Marc Couty
- **Multiscale Modeling and Big Data** *Debra Audus, Jean Yves Delannoy,* Kurt Kremer, Alexander Hexemer
- **Coacervates and Origins of Life** *Eric Dufresne, Matthew Tirrell,* Cliff Brangwynne, Jodie Lutkenhaus, Allie Obermeyer, Jonathan Whitmer
- **Networks** *Peter Olmsted, Lynn Walker,* Costantino Creton, Bradley Olsen
- **Reconfigurable Polymers and Sustainability** *Kathryn Beers, Karen Winey,* Brett Helms, Megan Robertson, Meredith Silberstein
- **Polymer Membranes** *Miguel Modestino, Chinedum Osuji,* Benny Freeman, Ayse Asatekin, William Mickols
- **Rheological Behavior** *Ralph Colby, Ryan Hayward,* Dimitris Vlassopoulos, Vivek Sharma, Evelyne van Ruymbeke, Hiroshi Watanabe
- **Charged Polymer** *Nitash Balsara, Venkat Ganesan,* Timothy Lodge, Murugappan Muthukumar

Polymer Physics
Leveraging Fundamentals to Enhance Polymer Applications
JULY 25 – 26, 2020
CHAIRS: Whitney Loo and Konane Bay

Post-Transcriptional Gene Regulation

Coordination and Integration of RNA Processing from Transcription to Translation

JULY 12 – 17, 2020 • JORDAN HOTEL AT SUNDAY RIVER, NEWRY, ME
CHAIRS: Tom Cooper and Kristen Lynch
VICE CHAIRS: Karla Neugebauer and Nicholas Conrad

- **Keynote Session: Emerging Concepts in RNA Biology** *Joan Steitz,* Christine Mayr, Mitch Guttman, Benjamin Blencowe, Roy Parker
- **3' Processing** *Chris Burge,* Eric Wagner, Bin Tian, Yongsheng Shi
- **Integration of RNA Biogenesis** *Nicholas Conrad,* David Bentley, Matthew Simon, Tracy Johnson
- **RNA Structure and Modifications** *Wendy Gilbert,* Kevin Weeks, Richard Gregory, Kathy Fange Liu, Rui Zhao
- **RNA Localization and Assembly** *Douglas Black,* Kimberly Mowry, Robin Stanley, Lingling Chen, Beatriz Fontoura
- **Role of Post-Transcriptional Regulation from Genotype to Phenotype** *Brenton Graveley,* Xinshu Xiao, Juan Valcarcel, Alain Laederach, Angela Brooks, Auinash Kalsotra, William Fairbrother
- **RNP Function and Disease Implications** *Manuel Ares,* Eric Wang, Sara Cherry, Kathryn Hamilton, Peter Sarnow, Adrian Krainer
- **Translation Regulation** *Rachel Green,* Susan Ackerman, Davide Ruggero, Gloria Brar, Joel Neilson, Jeff Coller
- **RNA Decay** *Melissa Moore,* Lynne Maquat, Olivia Rissland, Robert Hogg, Heidi Cook-Anderson, Torben Jensen
- **The GRC Power Hour™** *Kristen Lynch, Karla Neugebauer*

Post-Transcriptional Gene Regulation
Emerging Roles of RNA in Gene Regulation
JULY 11 – 12, 2020
CHAIRS: Nicole Martinez and Ana Fiszbein

Protein Processing, Trafficking and Secretion

Tracking the Fate of Proteins and Lipids in the Secretory Pathway: From Cell Biology to Human Disease

JULY 19 – 24, 2020 • COLBY-SAWYER COLLEGE, NEW LONDON, NH
CHAIR: Alan Attie
VICE CHAIR: Julia von Blume

- **Protein Folding in the Secretory Pathway** *Peter Arvan,* Judith Frydman, Papa Feroz, Clare Futter, Julie Hollien
- **Proteolysis in the Secretory Pathway** *Michael Ailion,* Thomas Delong, Annik Prat, Regina Fluhrer, Stefan Lichtenthaler
- **Regulation of Insulin Secretion: Nutrient Sensing, Ion Channels and Vesicle Trafficking** *Regina Fluhrer,* Matthew Merrins, Debbie Thurmond, Patrick MacDonald, Melkam Kebede
- **Protein Aggregation and Autophagy** *Iris Lindberg,* Gentry Patrick, Carmine Settembre, Luigi Puglielli, Thomas Melia
- **Cancer and Neurological Diseases** *Carmine Settembre,* Robert Day, Anjon Audhya
- **Visualizing the Secretory Pathway** *Anjon Audhya,* Lingjun Li, Michele Solimena, Amelia Linnemann, Joerg Bewersdorf
- **Lipid Transport Through the Secretory Pathway** *Thomas Melia,* Anant Menon, Russell Debose-Boyd, Ody Sibon, Elina Ikonen
- **Glycosylation and Phosphorylation in the Secretory Pathway** *Melkam Kebede,* Hudson Freeze, Kelly Ten Hagen, Michael Boyce
- **Exosomes** *Julia von Blume,* Carole Parent, Philipp Scherer, Wei Guo
- **The GRC Power Hour™** *Julia von Blume, Iris Lindberg*

Protein Processing, Trafficking and Secretion
Insights into the Molecular Mechanisms of Protein Trafficking
JULY 18 – 19, 2020
CHAIRS: James Checco and Julie Cruanes

Proteoglycans

Frontiers in Basic and Translational Proteoglycan Research to Improve Human Health

JULY 12 – 17, 2020 • PROCTOR ACADEMY, ANDOVER, NH

CHAIRS: Liliana Schaefer and Charles Frevert

VICE CHAIR: Catherine Merry

- **Keynote Session: Recent Progress in Proteoglycan Biology** *Renato Iozzo, Marian Young,* Rudolf Jaenisch
- **Proteoglycan-Mediated Tissue Homeostasis** *Suneel Apte, Thomas Wight,* Nicola Allen, Fransiska Malfait, Josephina Meester
- **Proteoglycan Homeostasis** *Billy Hudson, Nikos Karamanos,* Eri Arikawa-Hirasawa, Anthony Day, Johan van der Vlag
- **Proteoglycans and GAGs in Immuno-Oncology** *Karin Forsberg-Nilsson, Stephen Hewitt,* Fotis Asimakopoulos, Mattias Belting, Wantong Yao, Paul Timpson
- **Role of Proteoglycans in Development and Regenerative Medicine** *Hideto Watanabe, Vincent Hascall,* Jorge Filmus, Alyssa Panitch
- **Proteoglycan Signaling** *John Couchman, Jeffrey Esko,* Herbert Geller, Nunzio Bottini, Aaron Petrey
- **New Technologies to Define the Role of PGs and GAGs in Health and Disease** *Robert Linhardt, Brooke Farrugia,* Adam Hall, Juergen Seibel, Sylvie Ricard-Blum
- **Development of New Drugs Targeting Proteoglycans** *Jin-Ping Li, Ralph Sanderson,* Mitchell Ho, Rashmin Savani
- **Matrix-Targeted Glycan Therapeutics in Clinical Trials** *Glenn Prestwich, Alberto Passi,* Denis Barritault, Thomas Kennedy, Mats Wahlgren, John Paderi
- **The GRC Power Hour™** *Catherine Merry*

Proteoglycans

Integrated Proteoglycan Research to Improve Human Health

JULY 11 – 12, 2020

CHAIRS: Marissa Maciej-Hulme and Ryan Weiss

Proteolytic Enzymes and Their Inhibitors

The Regulation of Proteolysis in Health, Disease and Treatment

MAY 24 – 29, 2020 • RENAISSANCE TUSCANY IL CIOCCO, LUCCA (BARGA), ITALY

CHAIR: James Huntington

VICE CHAIR: Jeanne Hardy

- **Cancer** *Klaudia Brix,* Christopher Scott, Boris Turk
- **Blood Coagulation** *Hans Brandstetter,* Jim Crawley, Ruby Law, Thomas Renné, Galia Blum
- **Immunity and Inflammation** *James Whisstock,* Piet Gros, Christopher Overall, Christoph Reinhardt
- **Pathogens** *Jan Potempa,* Charles Craik, Joanna Koziel
- **Intracellular Proteolysis** *Paula Da Fonseca,* Charaf Benarafa, Andreas Martin, Kim Newton, Guy Salvesen
- **Proteolysis in and on Cell Membranes** *Manu Platt,* Joanne Lemieux, Christoph Becker-Pauly, Rui Zhou, Regina Fluhrer
- **New Tools for Probing Protease Action *In Situ*** *Marcin Drag,* Laura Edgington-Mitchell, Paulina Kasperkiewicz, Matthew Bogyo
- **Therapeutic Targeting of Proteolytic Activities** *Jeanne Hardy,* Dennis Wolan, Celia Schiffer, Henry Maun, Grant Blouse
- **Late-Breaking Topics** *Joanne Lemieux*
- **The GRC Power Hour™** *Galia Blum*

Proteolytic Enzymes and Their Inhibitors

The Regulation of Proteolysis in Health, Disease and Treatment

MAY 23 – 24, 2020

CHAIRS: Paulina Kasperkiewicz and Amy Weeks

Quantum Science

Many-Body Quantum Systems: From Quantum Computing and Simulation to Metrology and Communication

JULY 26 – 31, 2020 • STONEHILL COLLEGE, EASTON, MA

CHAIRS: Markus Greiner and Eugene Demler

VICE CHAIRS: Susanne Yelin and Jonathan Simon

- **Quantum Simulation** *Ana Maria Rey,* Monika Aidelsburger, Tilman Esslinger, Fabian Grusdt
- **Progress in Quantum Computing and Algorithms** *Mikhail Lukin,* Ignacio Cirac, Andrew Houck, Eliot Kapit
- **Non-Equilibrium Quantum Matter** *Monika Aidelsburger,* Richard Averitt, Waseem Bakr, Julian Léonard, Ana Maria Rey
- **From Quantum Simulation to Quantum Computing** *Ignacio Cirac,* Rainer Blatt, Mikhail Lukin, Dries Sels
- **Quantum Metrology and Sensing** *Tilman Esslinger,* Ania Bleszynski-Jayich, Nergis Mavalvala, Holger Mueller, Vladan Vuletic
- **Late-Breaking Topics** *Andrew Houck*
- **Quantum Information and Condensed Matter** *Andrea Cavalleri,* Logan Clark, Amir Yacoby, Andrea Young
- **Light-Matter Interactions and Many-Body Quantum Optics** *Peter Zoller,* Andrea Cavalleri, Atac Imamoglu, Angel Rubio, Ephraim Shahmoon
- **Connections Between Quantum Science and Other Fields** *Vladan Vuletic,* Eun-Ah Kim, Xiao-Liang Qi, Peter Zoller
- **The GRC Power Hour™**

Quantum Science

Quantum Matter for Communications, Fundamental Investigations, Simulation and Computation

JULY 25 – 26, 2020

CHAIRS: Julia Cline and Kristine Rezai

Research at High Pressure

Exploring High Pressure Science at the Extremes Through Experiment and Computation

JULY 19 – 24, 2020 • HOLDERNESS SCHOOL, HOLDERNESS, NH

CHAIR: Sakura Pascarelli

VICE CHAIR: Chris Pickard

- **Challenges to Our Understanding of Dense Matter** *Russell Hemley,* Jon Eggert, Ion Errea
- **Scientific Opportunities Opened by New Experimental Approaches** *Angelika Rosa,* Norman Yao, Thomas Meier, Siegfried Glenzer, Stewart McWilliams
- **Emergent Phenomena at High Densities** *Gilbert Lonzarich,* Audrey Grockowiak, Sergiy Medvediev
- **Hydrogen Under Extreme Experimental Pressure** *Serge Desgreniers,* Xiao-Di Liu, Alexander Drozdov, Ho-Kwang Mao, Paul Loubeyre, Vladimir Fortov, Marcus Knudson, Gilbert Collins
- **Beyond Earth: Pressure as an Experimental Probe** *Lars Stixrude,* Federica Coppari, Stephanie Brygoo
- **The Limits of Computation and the Role of Data Driven Approaches** *Mao-Sheng Miao,* Eva Zurek, Clemens Prescher, Qiang Zhu, Philip Avraam
- **New Functional Materials by Design** *Yanming Ma,* Lilia Boeri, Maddury Somayazulu
- **Earth: From Crust to Inner Core** *Simon Redfern,* Natalia Solomatova, Miki Nakajima, Masayuki Nishi
- **Keynote Session: Extremely Dense Matter** *Chris Pickard,* Burkhard Militzer
- **The GRC Power Hour™** *Larissa Huston, Xiaolei Feng*

Research at High Pressure

Exploring High Pressure Science at the Extremes Through Experiment and Computation

JULY 18 – 19, 2020

CHAIR: Dean Smith

Rock Deformation

Combining Laboratory Measurements with Observational Constraints to Understand Tectonic Processes

AUGUST 9 – 14, 2020 • BATES COLLEGE, LEWISTON, ME

CHAIR: Daniel Faulkner

VICE CHAIR: Heather Savage

- **Lithospheric Rheology from Small-Scale Experiments** *Brian Evans,* David Kohlstedt, Philip England
- **Fundamental Frictional Processes** *Marie Violay,* Izabela Szlufarska, Kathryn Hayward, David Goldsby
- **Earthquake Mechanics** *Roland Burgmann,* Nadia Lapusta, Gregory McLaskey
- **Fault Slip in Nature** *Alex Copley,* Marion Thomas, Steven Smith, Rachel Abercrombie
- **Early-Career Investigator Presentations** *Heather Savage*
- **Lower Crustal Dynamics** *Virginia Toy,* William Shinevar, Luca Menegon, Andrew Freed
- **Mantle Rheology** *Benjamin Holtzman,* Sylvie Demouchy, David Dobson
- **Shallow Subduction Processes** *Greg Hirth,* Laura Wallace, Rob Skarbek, Demian Saffer
- **Deeper Subduction Processes** *Nadege Hilairet,* Geoff Abers, Greg Hirth
- **The GRC Power Hour™**

Rock Deformation

Integrating Rock Deformation Studies with Geophysics, Field Geology and Modeling

AUGUST 8 – 9, 2020

CHAIRS: Taka Kanaya and Carolyn Tewksbury-Christle

Salt and Water Stress in Plants

Mechanisms of Abiotic Stress Resilience and Applications for Agriculture

MAY 31 – JUNE 5, 2020 • LES DIABLERETS CONFERENCE CENTER, LES DIABLERETS, SWITZERLAND

CHAIRS: Jose Dinneny and Christa Testerink

VICE CHAIRS: Thomas Juenger and Amelia Henry

- **Keynote Session: The Role of Metabolites and Ions in Plant Stress Responses** *Julia Bailey-Serres,* Katayoon Dehesh, David Salt
- **Signaling from the Outside to the Inside of the Cell** *Katayoon Dehesh,* Takashi Hashimoto, Jürgen Kleine-Vehn, Staffan Persson, Liwen Jiang, Zhen-Ming Pei
- **Synthetic and Systems Biology Approaches to Water Stress** *Magdalena Julkowska,* Siobhan Brady, Sean Cutler, David Des Marais
- **Photosynthesis, Climate Change and Agriculture** *Amelia Henry,* Moises Exposito-Alonso, Andrew Leakey, Marjorie Lundgren
- **Adaptation to Water Stress and Salinity** *David Salt,* Maheshi Dassanayake, Jill Farrant, Rashmi Sasidharan
- **Root-Soil Interface and Transport of Ions and Water in Plants** *Caitlin Byrt,* Malcolm Bennett, Niko Geldner, Matthew Gilliham, Jennifer Pett-Ridge
- **Tissue Hydraulics** *Yann Boursiac,* Noel Holbrook, Guillaume Lobet, Diana Santelia
- **Genomic Approaches to Understanding Stress Acclimation** *Robert VanBuren,* Malia Gehan, Sonia Negrao, Melvin Oliver

- **Interfaces Between Water, Biotic Stress and Other Environmental Factors** *Sheng Yang He,* Andrea Carminati, Kenichi Tsuda, Cyril Zipfel
- **The GRC Power Hour™** *Julia Bailey-Serres, Thomas Juenger*

Salt and Water Stress in Plants

Multi-Disciplinary Approaches to Understand Plant Stress Tolerance Mechanisms

MAY 30 – 31, 2020

CHAIRS: Stephanie Klein and Abdeljalil Elhabti

Scientific Methods in Cultural Heritage Research

Integrating Multidisciplinary Approaches for Deeper Characterization, Interpretation and Preservation of Heritage

JULY 12 – 17, 2020 • LES DIABLERETS CONFERENCE CENTER, LES DIABLERETS, SWITZERLAND

CHAIRS: Julie Arslanoglu and Loïc Bertrand

VICE CHAIRS: Admir Masic and Costanza Miliani

- **Keynote Session: Insights and Visions Connecting Cultural Heritage Research** *Katrien Keune,* Hartwig Fischer, Livio de Luca
- **Artistic and Conservation Practice-Driven Material Study** *Marika Spring,* Siyakha Mguni, Maartje Stols-Witlox
- **Botanical and Zoological Materials** *Joanne Dyer,* Jean-Denis Vigne, Gabriela Siracusano, Else Marie Friis
- **Study of Ancient and Historical Biological Materials** *Marta Maier,* Caroline Tokarski, Ludovic Orlando
- **Heritage Material Systems from Nanometric to Macroscopic Scales** *Dominique Derome,* Letizia Monico, Lara Maldanis, Patrick Dietemann
- **Safer Experimental Conditions for Heritage Studies** *Marta Castillejo,* Maria João Melo, Samuel Webb, Alexander Immel
- **Engineering and Materials Sciences in Cultural Heritage Research** *Demetrios Anglos,* Clément Sanchez, Daniel Asmar, Joris Sprakel
- **Novel Materials Inspired by Ancient Materials and Practices** *Lukasz Bratasz,* Marie Jackson, Roberto Giustetto, Romain Bordes
- **Keynote Session: Future Frontiers for Heritage Research by Strengthening Collaboration Between the Humanities and Science** *Barbara Berrie,* Johanna Tummers
- **The GRC Power Hour™** *Carolyn Carta, Marcie Wiggins*

Scientific Methods in Cultural Heritage Research

The Art of Method in Heritage Science: Innovative Model Systems and New Chemical Probing Techniques

JULY 11 – 12, 2020

CHAIRS: Victor Gonzalez and Carolyn Carta

Signal Transduction by Engineered Extracellular Matrices

Microenvironmental Regulation of Stem and Somatic Cells in Organismal Development and Regenerative Medicine

JULY 19 – 24, 2020 • SOUTHERN NEW HAMPSHIRE UNIVERSITY, MANCHESTER, NH

CHAIRS: David Schaffer and Matthias Lutolf

VICE CHAIRS: Shelly Peyton and Sanjay Kumar

- **Keynote Session: Exploring and Manipulating the Cell-Matrix Interface in Health and Disease** *Adam Engler,* Stefano Piccolo, Valerie Weaver
- **Organoids** *Alex Hughes,* Jianping Fu, Nuria Montserrat
- **Organs-on-a-Chip** *Peter Loskill,* Nancy Allbritton, Roger Kamm
- **Advanced Engineered ECMs** *Shyni Varghese,* Jason Burdick, Cole DeForest, Sarah Heilshorn
- **Single Cell Biology and Development** *Karthik Shekhar,* Siddharth Dey, Gay Crooks
- **ECM Mechanobiology** *Catherine Kuo,* Ovijit Chaudhuri, Xavier Trepat
- **ECM and Stem Cell Fate Regulation** *Kris Kilian,* Penney Gilbert, Samira Musah, Muhammad Zaman
- **Bioinspired Fabrication** *Fabien Guillemot,* Jordan Miller, Kelly Stevens, Akhilesh Gaharwar
- **Engineering and Application of Immune-Modulatory Materials** *David Wilson,* Takahsi Kishimoto, Ankur Singh
- **The GRC Power Hour™** *Sarah Heilshorn*

Signal Transduction by Engineered Extracellular Matrices

Nano to Macroscale Engineering in Biology and Regenerative Medicine

JULY 18 – 19, 2020

CHAIRS: Claudia Loebel and Woojin Han

Signaling by Adhesion Receptors

Adhesion Across Scales: From Molecules to Morphogenesis

JUNE 28 – JULY 3, 2020 • SOUTHERN NEW HAMPSHIRE UNIVERSITY, MANCHESTER, NH

CHAIR: Ann Miller

VICE CHAIR: Patrick Derksen

- **Keynote Session: Adhesion Across Scales: From Molecules to Morphogenesis** *Ann Miller,* Johanna Ivaska, Bob Goldstein
- **Mechanotransduction by Adhesion Receptors** *Karin Wang,* Carl-Philipp Heisenberg, Erin Cram, Clare Waterman
- **Maintaining Adhesion in Dynamic Environments** *Kathleen Green,* Carien Niessen, Yusuke Toyama, Jennifer Zallen
- **Engineering Adhesion** *Margaret Gardel,* Christopher Chen, Michael Murrell, Otger Campas
- **Adhesive Control of Cell Division** *Martijn Gloerich,* Cara Gottardi, Yohanns Bellaïche, Sarah Woolner
- **Advances in Adhesion Signaling** *Alpha Yap,* Rafael Garcia-Mata, Tony Koleske, Jessica Treisman
- **Adhesion Signaling and Cell Migration** *Brent Hoffmann,* Danijela Matic Vignjevic, Maddy Parsons, Sally Horne-Badovinac
- **Adhesion, Morphogenesis and Tissue Remodeling** *Mark Peifer,* Scott Holley, Danelle Devenport, Adam Martin
- **Adhesion and Disease** *Andrea McClatchey,* Laura Machesky, Asma Nusrat, Patrick Derksen
- **The GRC Power Hour™** *Petra Gross, Carien Niessen*

Signaling by Adhesion Receptors

Examining the Basic Biomechanics and Biomedical Aspects of Cell Adhesion Signaling

JUNE 27 – 28, 2020

CHAIRS: Kate Cavanaugh and Fiona Passanha

Single Molecule Approaches to Biology

Uncovering Physical Principles of Life with Single Molecule Approaches

JULY 5 – 10, 2020 • REY DON JAIME GRAND HOTEL, CASTELLDEFELS, SPAIN

CHAIRS: Erwin Peterman and Olga Dudko

VICE CHAIRS: Samuel Hess and Suliana Manley

- **Keynote Session: Probing the Non-Equilibrium Nature of Life** *Carlos Bustamante,* Hermann Gaub, Christopher Jarzynski
- **Diffusion as Transport Mechanism in the Cell** *Samuel Hess,* Julie Biteen, Maria Garcia-Parajo, David Holcman, Cornelis Murre
- **Beating the Diffusion Speed Limit: Biological Motors** *Stefan Diez,* Carlos Bustamante, Cees Dekker, Lukas Kapitein
- **Navigating Energy and Fitness Landscapes** *Chirlmin Joo,* Thomas Perkins, Michael Woodside, Irene Chen
- **The Dynamic Nature of Cellular Structures** *Gijs Wuite,* Ariel Amir, Patricia Bassereau, Daniel Needleman
- **Biology in Bits: Information Approaches** *Suliana Manley,* Felix Ritort, Yoav Shechtman, Gasper Tkacik
- **Crossing the Phase Boundary** *Stephanie Weber,* Ibrahim Cisse, Gary Karpen, Yaojun Zhang
- **Searching for Principles in Biological Complexity** *Nynke Dekker,* Toshio Ando, Taekjip Ha, Zan Luthey-Schulten, Antoine Van Oijen
- **Keynote Session: From Single Molecules to Unifying Principles of Life** *Taekjip Ha,* Stefan Grill, Petra Schwille
- **The GRC Power Hour™** *Julie Biteen, Antoine Van Oijen*

Single Molecule Approaches to Biology

Single Molecule Perspectives for a Deeper Understanding of Biology

JULY 4 – 5, 2020

CHAIRS: Lukas Milles and Carleen Kluger

Solid State Chemistry

Functional Inorganic Materials: Exploratory Synthesis, Advanced Characterization and Computational Methods

JULY 26 – 31, 2020 • COLBY-SAWYER COLLEGE, NEW LONDON, NH

CHAIR: Shiv Halasyamani

VICE CHAIR: Arthur Mar

- **Layered Materials and Composites** *Arthur Mar,* Veronica Augustyn, Andrew Grosvenor
- **Energy Materials** *Linda Nazar,* Jakoah Brgoch, Taylor Sparks, Serena Corr, Jack Vaughey
- **Advanced Characterization Techniques** *Katharine Page,* John Evans, Joke Hadermann
- **Synthesis of Functional Materials** *Simon Clarke,* Michael Hayward, Daniel Shoemaker, Mario Bieringer, Bayrammurad Saparov
- **Computational Methods** *James Rondinelli,* Nicole Benedek, Elsa A. Olivetti
- **Non-Oxide Materials: Thermoelectrics, Intermetallics and Clusters** *Julia Chan,* Paul Canfield, Kanishka Biswas, Oliver Janka, Stefanie Dehnen
- **Solid State Inorganic Materials Chemistry Research in Industrial Laboratories** *Kenneth Poeppelmeier,* Chris Sheets, Erin Sorensen
- **Non-Oxide Materials: Superconductors, Hydrides and Magnetocalorics** *Danna Freedman,* Weiwei Xie, Ulrich Häussermann, Bettina Lotsch, Yurij Mozharivskyj
- **Modulated Structures** *Daniel Fredrickson,* Sven Lidin
- **The GRC Power Hour™** *Nicole Benedek, Danna Freedman*

Solid State Chemistry

Functional Inorganic Materials: Exploratory Synthesis, Advanced Characterization and Computational Methods

JULY 25 – 26, 2020

CHAIRS: Christopher Perez and Rebecca Smaha

Solid State Studies in Ceramics

Multiphysical, Coupled Phenomena in Ceramics at the Atomistic and Nanometer Scales

AUGUST 2 – 7, 2020 • MOUNT HOLYOKE COLLEGE, SOUTH HADLEY, MA

CHAIR: Ivar Reimanis

VICE CHAIRS: Wayne Kaplan and Edwin Garcia

- **Processing Complex Structures** *John Blendell,* Lisa Rueschhoff, Julia Greer
- **Exceptional Responses in Structural Ceramics** *Leslie Lamberson,* Jessica Krogstad, Frank Zok, Kevin Hemker
- **Thermal-Mechanical Behavior in Extreme Environments** *William Fahrenholtz,* Alexandra Navrotsky, Elizabeth Opila
- **Interfaces and Grain Boundaries** *Amanda Krause,* Hans-Joachim Kleebe, Monika Backhaus-Ricoult, Roger de Souza
- ***In Situ* Observations** *Klaus van Benthem,* Shen Dillon, Yuichi Ikuhara
- **Ceramics for Energy Applications** *Sandrine Ricote,* Jennifer Rupp, Christina Scheu, Elizabeth Dickey
- **Perovskites for Solar Cells** *Catherine Bishop,* Annamaria Petrozza, Nitin Padture
- **Coupled Phenomena in Perovskites** *Michael J. Hoffmann,* Veronica Augustyn, Nicole Benedek, Bryan Huey
- **Keynote Session: Nucleation and Growth in Glass Ceramics** *Wolfgang Rheinheimer,* Edgar Dutra Zanotto
- **The GRC Power Hour™** *Kristen Brosnan*

Solid State Studies in Ceramics

Fundamental Phenomena in Ceramics from the Atomistic Level to the Microstructure

AUGUST 1 – 2, 2020

CHAIRS: Hadas Sternlicht and Jasmin Koldehoff

Stereochemistry

Different Forms of Stereochemistry: From Catalysis and Synthesis to Macromolecules and the Natural World

JULY 26 – 31, 2020 • SALVE REGINA UNIVERSITY, NEWPORT, RI

CHAIRS: Varinder Aggarwal and Eric Ashley

VICE CHAIRS: Eric Jacobsen and Tamas Benkovics

- **Keynote Session: Synthesis and Translation to Medicine** *Eric Jacobsen,* Paul Wender, Phil Baran
- **Stereochemistry of Radicals and Peptides** *Alastair Lennox,* Michelle Chang, Song Lin, Ivan Huc, Alison Narayan
- **Functionalization of Multiple Bonds** *Santanu Mukherjee,* Tomislav Rovis, Keary Engle, Ryan Shenvi
- **Transition Metals in Asymmetric Catalysis** *Robert Paton,* Matthew Gaunt, Franziska Schoenebeck, Kyle Mack, Gregory Fu
- **Functionalization of Strong Bonds** *Shauna Paradine,* Corinna Schindler, Bill Morandi, Abigail Doyle
- **Discovery and Synthesis of Medicinal Molecules** *Juana Du,* Robert Singer, Michael Corbett, Andrew Neel, Cameron Cowden
- **Natural Product Synthesis and Manipulation** *Alison Wendlandt,* Sarah Reisman, Daniele Leonori, Richmond Sarpong
- **Asymmetric Catalysis and Mechanism** *Nicholas Race,* James Morken, Guy Lloyd-Jones, Keiji Maruoka
- **Keynote Session: *De Novo* Generation of Chirality** *Tamas Benkovics,* Michael Mcbride, Donna Blackmond
- **The GRC Power Hour™** *Shauna Paradine, Alison Wendlandt*

Streptococcal Biology

Evolving Genomes, Behavior and Pathogenic Mechanisms of Streptococci and Enterococci

AUGUST 16 – 21, 2020 • JORDAN HOTEL AT SUNDAY RIVER, NEWRY, ME

CHAIRS: Kelly Doran and Shiranee Sriskandan
VICE CHAIRS: Michael Federle and Jan-Willem Veening

- **Keynote Session: Insights into Pathogen and Host Biology** *Brady Spencer, Joseph Merriman,* Michael Gilmore, Victor Nizet
- **Evolution of Genomes, from Genomics to Function** *Andrew Camilli,* Bill Hanage, Mark Davies, Willem van Schaik
- **Regulation and Virulence Mechanisms** *Elaine Tuomanen,* Michael Wessels, Melanie Hamon, Jose Lemos
- **Host-Pathogen Interactions and the Fight for Survival** *Lakshmi Rajagopal,* Mattias Collin, David Aronoff, Eric Schmidt, Annelies Zinkernagel
- **At the Surface of the Bacterial-Host Encounter** *Shaynoor Dramsi,* Paul Sullam, Nina van Sorge, Angela Nobbs
- **Interactions Within the Microbial Community** *Kimberly Kline,* Mohammad Seyedsayamdost, Amanda Lewis, Joseph Zackular, Katherine Lemon
- **Phage and Mobile Genetic Elements** *Breck Duerkop,* Angela Brueggemann, Kelli Palmer
- **Evolving Therapeutic Approaches and Methodologies** *Jan-Willem Veening,* Annaliesa Anderson, Joshua Osowicki
- **Early-Career Investigator Presentations** *Michael Federle*
- **The GRC Power Hour™** *Elaine Tuomanen*

Streptococcal Biology

Physiology, Host-Interactions and Vaccine Development in Streptococcal Pathogenesis

AUGUST 15 – 16, 2020

CHAIRS: Brady Spencer and Joseph Merriman

Structural Nanomaterials

Design, Microstructure and Mechanical Behavior of Structural Nanomaterials

JULY 26 – 31, 2020 • THE HONG KONG UNIVERSITY OF SCIENCE AND TECHNOLOGY, HONG KONG, CHINA

CHAIRS: Qing Ping Sun and Andrea Hodge
VICE CHAIRS: Lei Lu and Xun-Li Wang

- **Keynote Session: Materials Design at the Nanoscale** *Ruth Schwaiger,* Christopher Schuh, Diana Farkas
- **Homogeneous and Heterogeneous Nanoscale Microstructures** *Lei Lu,* Koichi Tsuchiya, Thomas Waitz, Wendy Gu
- **Advanced Characterization Techniques** *Aslan Ahadi,* Xian (Sherry) Chen, Jason Trelewicz, Erica Lilleodden
- **Mechanics at the Nanoscale** *I-Chung Cheng,* Megan Cordill, Corinne Packard, Daniel Kiener
- **Atomistic and Nanoscale Simulations** *Paulo Branicio,* Mark Asta, David Srolovitz
- **Advances in Hierarchical Materials Design** *Yang Lu,* Mingxin Huang, Lorenzo Valdevit, Christoph Eberl
- **Synthesis of New Nanostructures and Alloys** *Wenjing Ye,* Yuri Estrin, Jian Lu
- **Heretical Material Design and Properties** *Timothy Rupert,* Ralph Spolenak, Qiming Wang, Alfonso Ngan
- **Non-Equilibrium Structures** *Xun-Li Wang,* Yilong Han, Si Lan

Synaptic Transmission

Context-Specific Synaptic Function

JUNE 21 – 26, 2020 • RENAISSANCE TUSCANY IL CIOCCO, LUCCA (BARGA), ITALY

CHAIR: Alison Barth
VICE CHAIRS: Daniel Choquet and Graeme Davis

- **Keynote Session: Synaptic Plasticity: The Brain's Response to Experience** *Massimo Scanziani,* Robert Malenka
- **Presynaptic Regulation of Synaptic Function** *Pablo Castillo,* Jeremy Dittman, Annette Dolphin, Timothy Ryan, Matthijs Verhage
- **Imaging Fine-Scale Synaptic Structure** *Daniel Choquet,* Kristen Harris, Na Ji, Valentin Nagerl, Antoine Triller
- **Synaptic Transmission in the Living Brain** *Linda Overstreet-Wadiche,* Marlene Bartos, James Poulet, Massimo Scanziani
- **Synaptic Pathologies Across the Lifespan** *Graeme Davis,* Paola Arlotta, Laurent Groc, Gaia Novarino, Morgan Sheng
- **Trisynaptic Interactions** *Helene Marie,* Kevin Bender, Stephanie Cragg, Michael Higley, Beth Stevens, Thomas Nevian
- **Synaptic Computation and Network Design** *Srikanth Ramaswamy,* Yevgenia Kozorovitskiy, Timothy Lillicrap, Andreas Tolias, Wei Wei
- **Target-Specific Synaptic Function** *Mario Penzo,* Anirvan Ghosh, Peter Jonas, Jeff Magee, Zoltan Nusser, Xiang Yu
- **Keynote Session: Synaptic and Circuitry Mechanisms of Psychiatric Disorders** *Anirvan Ghosh,* Guoping Feng
- **The GRC Power Hour™** *Alison Barth*

Synaptic Transmission

Synaptic Function: From Molecules to Networks

JUNE 20 – 21, 2020

CHAIRS: Hannah Monday and Simon Chamberland

Systems Chemistry

Life-Like and Emergent Behavior in Complex Molecules and Ensembles

JUNE 28 – JULY 3, 2020 • JORDAN HOTEL AT SUNDAY RIVER, NEWRY, ME

CHAIRS: Sijbren Otto and Rein Ulijn
VICE CHAIRS: Rebecca Schulman and Rafal Klajn

- **From Self-Assembly to Life Through Modelling and Experiment** *Rebecca Schulman,* Egbert Meijer, Monica Olvera de la Cruz, Ramanarayanan Krishnamurthy
- **Fueled Reaction Networks and Metabolic Materials** *Sergey Semenov,* Kenneth Showalter, Agota Toth, Wilhelm Huck
- **Origins and Synthesis of Life** *Ramanarayanan Krishnamurthy,* David Lynn, Gonen Ashkenasy, Eörs Szathmáry, Oliver Trapp, Joseph Moran
- **Navigating Shallow Energy Landscapes in Supramolecular Systems** *Julia Ortony,* Rachel O'Reilly, Matthew Rosseinsky, Tell Tuttle, Jonathan Nitschke, Sarah Perry, Akif Tezcan
- **Emergent Catalysis, Machines and Motility** *Ivan Korendovych,* Beatriu Escuder, Steve Granick, Daniela Wilson, Nathalie Katsonis
- **Active and Adaptive Materials Through Molecular Self-Assembly** *Rienk Eelkema,* Job Boekhoven, Andreas Walther, Adam Braunschweig, Ronit Freeman
- **Active and Adaptive Materials Based on Nanoparticles or Colloids** *Rafal Klajn,* Daniela Kraft, Robert Macfarlane, Willem Noorduin, Alfredo Alexander-Katz
- **Systems Chemistry in Flow** *Peter Korevaar,* Roy Bar-Ziv, Lee Cronin, Andrew Griffiths
- **Biological Systems Chemistry** *Ayala Lampel,* Tom de Greef, Henry Hess, Cecilia Leal, Ilja Voets, Steven Benner
- **The GRC Power Hour™** *Ayala Lampel, Julia Ortony*

Systems Chemistry

Fundamental Principles and Emergent Behavior Within Networks of Molecules

JUNE 27 – 28, 2020

CHAIRS: Ivana Maric and Ignacio Colomer

Thiol-Based Redox Regulation and Signaling

Challenges and Opportunities in Sulfur Biochemistry

JULY 12 – 17, 2020 • REY DON JAIME GRAND HOTEL, CASTELLDEFELS, SPAIN

CHAIR: Kate Carroll
VICE CHAIR: Joris Messens

- **Keynote Session: Reactive Nitrogen Species as Signaling Molecules and Therapeutics** *Helmut Sies,* Rafael Radi, Jonathan Stamler, Stuart Lipton
- **Quantitative Measures of Redox Signaling** *Ursula Jakob, Jing Yang,* Che Pillay, Philipp Niethammer, Benjamin Neel, F. Peter Guengerich, Sandra Anjo, Jin Wang
- **Redox Metabolism in Health and Disease** *Cristina Furdui, Roberto Sitia,* Arne Holmgren, Luke Lairson, Maria Hatzoglou, Donald Becker, Dean Jones
- **Mechanisms of H_2O_2 Signaling: Direct Oxidation** *Leslie Poole, Albert Van Der Vliet,* Fernando Antunes, Vsevolod Belousov, Philip Eaton, Derek Pratt, Luis Delgado, Katrin Schröder, Brooke Christian, Chu Wang
- **Mechanisms of H_2O_2 Signaling: One- and Two-Component Relays** *Elena Hidalgo, Christine Winterbourn,* Tobias Dick, Sun Jin Moon, Franz-Josef Meyer-Almes, Carola Neumann, Ana Denicola
- **Reactive Sulfur Species in Metabolism and Signaling** *Peter Nagy, Ming Xian,* Ruma Banerjee, Michael Pluth, Milos Filipovic, Beatriz Alvarez, Luying Xun, Willem Koppenol, John Wallace
- **Advances in Redox Medicine** *Yimon Aye, Michael Murphy,* Bruce Freeman, Yvonne Janssen-Heininger, Michael McManus, Carmen Wong, Pietro Ghezzi
- **Methionine Oxidation and Selenoproteins** *Vadim Gladyshev, Elias Arner,* Mark Anderson, Sina Ghaemmaghami, Robert Hondal, Bruno Manta, Benjamin Tu, Yaoyang Zhang, Eranthie Weerapana
- **Glutathione in Regulation and Detoxification** *Haike Antelmann, Thomas Michel,* Young-Hoon Ahn, Neal Zondlo, Francisco Schopfer, Bindu Paul, Michel Toledano
- **The GRC Power Hour™** *Carola Neumann, Yimon Aye*

Thiol-Based Redox Regulation and Signaling

Redox Signaling Factors: From the Molecular Mechanisms to the Physiological Consequences

JULY 11 – 12, 2020

CHAIRS: Brandan Pedre Perez and Evanna Mills

Three Dimensional Electron Microscopy

Visualizing Biological Complexity Across Scales in 3DEM

JUNE 21 – 26, 2020 • REY DON JAIME GRAND HOTEL, CASTELLDEFELS, SPAIN

CHAIR: Sharon Wolf
VICE CHAIR: Daniela Nicastro

- **Keynote Session: The Future Impact of 3DEM on Structural Biology Research: Nobel Perspectives** *Eva Nogales,* Jacques Dubochet, Joachim Frank, Richard Henderson
- **Sample Preparation and Workflows** *Mario Borgnia,* Juergen Plitzko, Xinzheng Zhang, Chi-Min Ho, Roman Koning, Hongwei Wang
- **Hybrid and Correlative Methods** *Tamir Gonen,* Lena Kourkoutis, Harald Hess, Lia Addadi
- **Innovations in Algorithms and Software** *Michael Cianfrocco,* Joseph Davis, Dimitry Tegunov, Pilar Cossio, Steven Ludtke, Jose Carazo
- **Selected Poster Presentations: Breakthrough Methods and Workflows** *Daniela Nicastro*
- **Cellular and Molecular Tomography** *Julia Mahamid,* Alex de Marco, Beata Turonova, Thomas Sharp, Yongning He, Stefan Raunser
- **Hardware and Instrument Developments** *Benjamin Bammes,* Peiyi Wang, Sara Campbell, David Bhella
- **CryoEM in Drug Discovery** *Alexey Amunts,* Shee-Mei Lok, Melinda Diver, Christian Wiesmann, Marissa Matsumoto, Patrick Sexton
- **Selected Poster Presentations: Solving Challenging Structures** *Nadav Elad*
- **The GRC Power Hour™** *Daniela Nicastro*

Three Dimensional Electron Microscopy

Visualizing Biological Complexity Across Scales in 3DEM

JUNE 20 – 21, 2020

CHAIRS: Cameron Varano and Colin Palmer

Transglutaminases in Human Disease Processes

Known and Emerging Transglutaminase-Related Diseases and New Methods for Detection and Treatment

JUNE 14 – 19, 2020 • MOUNT SNOW, WEST DOVER, VT

CHAIR: Jeffrey Keillor
VICE CHAIR: Kiyotaka Hitomi

- **Keynote Session: Clinical Relevance of Tissue Transglutaminase Druggability** *Elisabetta Verderio,* Richard Cerione, Richard Eckert
- **Emerging Research Tools** *Reik Loeser,* Diana Imhof, William Katt, Thung Lai, Lakshmi Santhanam
- **Emerging Diseases** *Laszlo Fesus,* Mari Kaartinen, Zhao-Qing Luo, Ian Maze
- **Cardiovascular Diseases** *Lakshmi Santhanam,* Martin Griffin, In-Gyu Kim, Nicola Mutch, Michal Neeman
- **Neurological Diseases** *Manuela Basso,* Manuela D'Eletto, Gail Johnson, Xianhua Piao
- **Cancer and Signalling Disorders** *Daniela Matei,* Nicoletta Bianchi, Salvatore Condello, Soo-Youl Kim, Nicholas Peake
- **Celiac Disease and Inflammation** *Mauro Piacentini,* Ludvig Sollid, Valeria Villella, Yang Xia
- **Fibrosis and Remodelling** *Patricia Sime,* Timothy Johnson, James Luyendyk, Hideki Tatsukawa, Elisabetta Verderio
- **Keynote Session: Activation and Inactivation of Tissue Transglutaminase** *Anne-Marie Van Dam,* Chaitan Khosla
- **The GRC Power Hour™**

Transglutaminases in Human Disease Processes

Pathology, Mechanism and Intervention of Transglutaminases

JUNE 13 – 14, 2020

CHAIRS: Nicole McNeil and Estéfano Pinilla Pérez

Tribology

Understanding Sliding Interfaces to Master Tribological Systems Across Length Scales

JUNE 21 – 26, 2020 • BATES COLLEGE, LEWISTON, ME

CHAIR: Julien Fontaine

VICE CHAIR: Judith Harrison

- **Understanding the Sliding Interface** *Tobin Filleter,* Jean Denape, Nicolas Fillot
- **Adhesive Phenomena in Tribology** *Kathryn Wahl,* Tevis Jacobs, Ramin Aghababaei
- **Analytical Tribology: Probing the Sliding Surfaces** *Angela Pitenis,* Antonella Rossi, Tomoko Hirayama
- **Lamellar Solid Lubricants** *Thomas Scharf,* Clotilde Minfray, John Curry
- **Tribologically-Induced Surface Changes** *Brian Borovsky,* Nuria Espallargas, Christian Greiner
- **Wear of Materials** *Richard Chromik,* Ken'Ichi Hiratsuka, Alfons Fischer
- **Tribology at the Extreme** *Arup Gangopadhyay,* Pantcho Stoyanov, Satish Achanta, Joichi Sugimura
- **Soft Tribology** *David Burris,* Sissi de Beer
- **Keynote Session: Tribology for Health** *Judith Harrison,* Robert Carpick

Tribology

Understanding Sliding Interfaces to Master Tribological Systems Across Length Scales

JUNE 20 – 21, 2020

CHAIRS: Maelani Negrito and Yijue Diao

Two Dimensional Electronics Beyond Graphene

Emerging Complex Phenomena and Computing Applications

JUNE 7 – 12, 2020 • SOUTHERN NEW HAMPSHIRE UNIVERSITY, MANCHESTER, NH

CHAIRS: Xiaodong Xu and Deji Akinwande

VICE CHAIRS: Jie Shan and Frank Koppens

- **Synthesis and Characterization** *Anna Isaeva,* James Hone, Jiwoong Park
- **Collective Optical Excitation** *Tony Heinz,* Hui Deng, Kin Fai Mak, Marco Polini
- **Device Applications** *Huili Xing,* Iuliana Radu, Peide Ye
- **Magnets and Heterostructures** *Roland Kawakami,* Alberto Morpurgo, Daniel Ralph, Emanuel TuTuc
- **Quantum and Nonlinear Optical Effects** *Hongkun Park,* Atac Imamoglu, Shiwei Wu
- **Complex Phenomena** *Feng Wang,* Kenneth Burch, David Cobden, Yuanbo Zhang
- **Modeling Grand Challenges** *Liang Fu,* Vladimir Falko, Allan Macdonald
- **Tunable Correlated States in Twisted 2D Materials** *Philip Kim,* Pablo Jarillo-Herrero, Ali Yazdani, Andrea Young
- **Emerging Phenomena** *David Tomanek,* Andres Castellanos-Gomez, Hyeon-Jin Shin
- **The GRC Power Hour™** *Huili Xing*

Two Dimensional Electronics Beyond Graphene

Fundamentals and Applications of Emerging 2D Crystals

JUNE 6 – 7, 2020

CHAIRS: Zhong Lin and Dmitry Ovchinnikov

Unifying Ecology Across Scales

Integrating Theory and Empiricism in Ecology and Evolution Through Energetics, Elements and Information

JULY 26 – 31, 2020 • SOUTHERN NEW HAMPSHIRE UNIVERSITY, MANCHESTER, NH

CHAIR: Angelica Gonzalez

VICE CHAIR: John DeLong

- **Keynote Session: Integration and Synthesis in Ecology and Evolution Through Fundamental Principles** *Helmut Hillebrand,* Pablo Marquet, Elizabeth Borer
- **Causal Links Between Temperature, Metabolism and Stoichiometry Through Biological Scaling** *Frieda Taub,* Andrew Kerkhoff, Elena Litchman, Guy Woodward, Joey Bernhardt, Marika Schulhof, Giulia Ghedini
- **Variation in Biological Scaling and the Four Dimensions of Life** *John Damuth,* James Brown, Craig White, Ian Hatton
- **Integrating Ecological Theories to Explain Ecological Patterns Across Spatial Scales** *Jonathan Chase,* Annette Ostling, Craig McClain, Thomas Lewinsohn, Erica Newman, Andrew Rominger, Daniel Wieczynski

> ***"There is a high level of interaction between the GRC/GRS participants that leads to great discussions, ideas and collaborations."***
>
> SUSANA KIMURA, University of Calgary, Water Disinfection, Byproducts and Health GRC

- **Structure of Multitrophic Species Interactions and the Function of Ecosystems** *Owen Petchey,* Priyanga Amarasekare, Jes Hines, Matias Arim
- **Wrapped Hierarchies and Disease Ecology: The Interplay of Ecological and Evolutionary Theories** *Ryan Hechinger,* Mercedes Pascual, Cynthia Downs, Dedmer Van de Waal, Clay Cressler, Rachel Paseka, Ann Tate
- **Synergies Between Paleoecological and Neoecological Perspectives** *Jessica Blois,* Felisa Smith, Jacquelyn Gill, Rebecca Rowe
- **Evolutionary Underpinnings of Ecological Physiology** *James Gillooly,* Art Woods, Sonya Auer, Joel Kingsolver, Matt Barbour, Seth Rudman, Lynn Govaert
- **Keynote Session: Challenges and Opportunities for an Integrative Ecology** *John DeLong,* Jonathan Chase, James Gillooly

Unifying Ecology Across Scales

Investigating Sources of Constraint and Flexibility in Ecological Systems Across Scales

JULY 25 – 26, 2020

CHAIRS: Joey Bernhardt and Daniel Wieczynski

Venom Evolution, Function and Biomedical Applications

Bridging Gaps in Venom Research: From Ecology and Evolution to Socio-Economic Impacts

AUGUST 9 – 14, 2020 • MOUNT SNOW, WEST DOVER, VT

CHAIRS: Ashlee Rowe and Glenn King

VICE CHAIRS: Stephen Mackessy and Irina Vetter

- **Keynote Session: Functional Ecology and Biodiversity of Venom** *Yehu Moran,* Maria Modica
- **Ecological and Evolutionary Processes Shaping Venoms: Connecting Basic Research with Downstream Applications** *Ricardo Rodriguez de la Vega,* Darin Rokyta, Joachim Surm
- **Emerging Models in Venom Research** *Andrew Walker,* Mandë Holford, Björn von Reumont
- **Advances in Technological and Methodological Approaches** *Beatrix Ueberheide,* Greg Neely, Eivind Undheim
- **Toxin Structure and Function** *Sebastien Dutertre,* R. Manjunatha Kini, Paul Alewood, Ana Maria Moura Silva
- **Characterizing Toxin-Target Interactions** *Micaiah Ward,* Jian Payandeh, Evelyne Deplazes, Ray Norton
- **Antivenom: Advances in Development and Production** *Nicholas Casewell,* Andreas Laustsen, Leslie Boyer, Julian White
- **Biomedical and Pesticidal Applications of Venom** *Baldomero Olivera,* Maria Ikonomopoulou, Volker Herzig, Thomas Reiner, Helena Safavi-Hemami
- **Keynote Session: Socio-Economic and Human Health Impacts of Venom** *Irina Vetter,* José María Gutiérrez
- **The GRC Power Hour™** *Nancy Gray, Micaiah Ward*

Venom Evolution, Function and Biomedical Applications

Bridging Gaps in Venom Research: From Ecology and Evolution to Socio-Economic Impacts

AUGUST 8 – 9, 2020

CHAIRS: Aida Verdes and Micaiah Ward

Vibrational Spectroscopy

Unraveling Molecular Heterogeneity with Vibrational Spectroscopy

AUGUST 2 – 7, 2020 • BRYANT UNIVERSITY, SMITHFIELD, RI

CHAIRS: Lauren Webb and Aaron Massari

VICE CHAIRS: Judy Kim and Poul Petersen

- **Complex Charged Liquids** *Amber Krummel,* Heather Allen, Steven Corcelli, Franz Geiger
- **Biological Complexity at Surfaces** *Elsa Yan,* Vicki Grassian, Jennifer Lee, Lu Wang, Wei Zhuang
- **Biological Complexity in Solution** *Scott Brewer,* Carlos Baiz, Steven Boxer, Casey Londergan
- **Environmental Applications of Vibrational Spectroscopy** *Amanda Mifflin,* Mark Johnson, Cristina Puzzarini, Jana Roithova, Ruth Signorell
- **New Approaches to Obtain Vibrational Information** *Melanie Reber,* Adam Dunkelberger, Hui Li
- **Heterogeneous Catalytic Systems** *Jahan Dawlaty,* Alexander Cowan, Renee Frontiera, Wei-Tao Liu, Sandra Luber
- **Vibrations on the Nanoscale** *Joanna Atkin, Wei Xiong,* George Schatz, Katarzyna Marzec, Wei Min
- **Probing Vibrations at Charged Interfaces** *John Asbury, Carol Hirschmugl,* Marie-Pierre Gaigeot, Julianne Gibbs, Sylvie Roke, Andrei Tokmakoff
- **Vibrational Spectroscopy Without Photons** *Thomas Allison, Aaron Rury,* Katharina Franke, Jordan Hachtel
- **The GRC Power Hour™** *Elsa Yan, Lauren Webb*

Vibrational Spectroscopy

Interrogating Chemical Structures, Functions and Dynamics Using Molecular Vibrations

AUGUST 1 – 2, 2020

CHAIRS: Kajari Bera and Mark Babin

Visual System Development

Building and Rebuilding the Visual System: From Genes to Cells to Circuits

AUGUST 16 – 21, 2020 • WATERVILLE VALLEY, WATERVILLE VALLEY, NH

CHAIR: Seth Blackshaw

VICE CHAIR: Valerie Wallace

- **Keynote Session: Frontiers in Visual Systems Development and Disease** *Nadean Brown, Brian Link,* Thomas Reh, Masayo Takahashi
- **From Retinal Patterning to Cell Fate Specification** *Kristen Kwan,* Susan da Silva, Vilaiwan Fernandes, Justin Kumar, Simon Sprecher, Jin Woo Kim
- **Emerging Approaches for Studying Visual Development** *Michael Dyer,* Brian Clark, Joshua Sanes
- **Building and Repairing Retinal Circuitry** *Jeremy Kay,* Peter Robin Hiesinger, Iris Salecker, Melanie Samuel, Chi-hon Lee
- **Non-Neuronal Cells and Tissues** *Ruth Ashery-Padan,* Ruby Shalom-Feuerstein, Monica Vetter, Sumiko Watanabe, Cagla Eroglu
- **Central Visual Development and Sensory Integration** *Claude Desplan,* Xin Duan, Samer Hattar, Takao Hensch, Hongkui Zeng
- **Development and Dysfunction of the Primate Retina** *Robert Johnston,* Rod Bremner, Anna La Torre, Xiaoqun Wang
- **Cellular Regeneration and Stem Cells** *Michel Cayouette,* Katia Del Rio-Tsonis, David Gamm, Mike Karl, Jeff Mumm, Carol Schuurmans
- **Emerging Model Systems** *Tiffany Cook,* Joseph Corbo, Kristen Koenig, Zuzana Musilova
- **The GRC Power Hour™** *Monica Vetter*

Visual System Development

Establishing a Visual System: From Retinal Cell Fate to Higher Order Connectivity and Processing

AUGUST 15 – 16, 2020

CHAIRS: Rebecca James and Cameron Prigge

Water and Aqueous Solutions

Water on Multiple Length Scales from the Molecular Level to the Global Hydrosphere

JULY 26 – 31, 2020 • HOLDERNESS SCHOOL, HOLDERNESS, NH

CHAIR: Mary Jane Shultz

VICE CHAIR: Susan Rempe

- **Keynote Session: Molecular-Scale Water Clusters** *Michael Duncan,* Mark Johnson, Anne McCoy
- **Nonlinear Probes of the Surface from THz to Vibrational** *Hilton Barbosa de Aguiar,* Mischa Bonn, Tahei Tahara, Marie-Pierre Gaigeot
- **Nonlinear Spectra: Electronic and Polarization** *Heather Allen,* Richard Saykally, Francesco Paesani
- **Confined Water** *Qiang Cui,* Larry Anovitz, Anastasia Ilgen, Tod Pascal
- **Neutron Probes and Biological Water** *Douglas Tobias,* Heloisa Bordallo, Ken Dill
- **Water Mediated Aggregation** *Lorena Tribe,* Dor Ben-Amotz, Steve Seibner, Nonne Prisle
- **Hydrated Electrons in Water** *Revati Kumar,* Petr Slavicek, Ruth Signorell
- **Atmospheric Water** *Dennis Hore,* Ken-ichiro Murata, Bertrand Chazallon, Teresa Head-Gordon
- **Keynote Session: Water from the Subsurface to the Stratosphere** *Veronica Vaida,* Antonio Mannino
- **The GRC Power Hour™** *Nancy Levinger, Pavel Jungwirth*

Water and Aqueous Solutions

Water on Multiple Length Scales from the Molecular Level to the Global Hydrosphere

JULY 25 – 26, 2020

CHAIRS: Clara-Magdalena Saak and Elise Duboue-Dijon

SPECIAL JOB FOCUS:

Biology

Issue date: March 20
Book ad by March 5

Ads accepted until March 13 if space allows

Deliver your message to a global audience of targeted, qualified scientists.

129,566
subscribers in print every week

57,905
yearly unique active job seekers searching for biology jobs

37,720
yearly applications submitted for biology positions

What makes *Science* the best choice for recruiting?

- Read and respected by 400,000 readers around the globe
- Your ad dollars support AAAS and its programs, which strengthens the global scientific community.

Why choose this job focus for your advertisement?

- Relevant ads lead off the career section with a special biology banner
- Bonus distribution:
  Experimental Biology, April 4–7, San Diego, CA.

Expand your exposure by posting your print ad online:

- Link on the job board homepage to a landing page for biology jobs
- Additional marketing driving relevant job seekers to the job board.

To book your ad, contact:
advertise@sciencecareers.org

The Americas
202 326 6577
Europe
+44 (0) 1223 326527
Japan
+81 3 6459 4174
China/Korea/Singapore/Taiwan
+86 131 4114 0012

Produced by the *Science*/AAAS Custom Publishing Office.

Science Careers
AAAS
SCIENCECAREERS.ORG

FOR RECRUITMENT IN SCIENCE, THERE'S ONLY ONE *SCIENCE*.

By **Gursel Alici**

Stepping down to step forward

It was nearly 20 years ago, but I remember the day clearly. I sat down and wrote a letter resigning from my faculty position in Turkey. "I have been subjected to injustices," I wrote in Turkish. "I want to resign from my duty as of 17 September 2001." I had spent the preceding 5 years fighting for the pay raise that I was owed when I was promoted to associate professor. University administrators argued that I hadn't completed my military service, and the dispute eventually went to court. I was fed up, so my wife and I decided to make a new beginning—on the other side of the world.

After completing my Ph.D. in the United Kingdom, I had returned to my home country—Turkey—to fulfill the conditions of a scholarship that I received to study abroad. As the first person in my family to attend a university, I was looking forward to serving as an educator and academic leader in the place where I was raised; I wanted to make a difference. Within a few months, I was appointed to a tenure-track faculty position, and I began to teach courses and ramp up my research lab.

My career seemed to be sailing along until the salary dispute. I no longer felt valued by my university, which made it hard to stay motivated. But I carried on with my research, at one point attending a conference in Colombia. There I met a professor from an Australian university who shared many of my research interests, and we stayed in touch.

"I'm glad that I took a risk to rebuild my career from scratch in another country."

Over the next few years, we swapped occasional emails. Then one day, he wrote to offer me a postdoc position in his lab. The rank was well below my position; at that point, I was 6 months away from being eligible to apply for a promotion to full professor. But the position in Australia offered me a chance to get out of my work situation in Turkey, which was making me profoundly unhappy, so I took it seriously.

My wife liked the idea of moving to Australia. We had one small child at the time—with plans to have another—and she thought we'd have better opportunities to raise our family there. So, with her encouragement, I took a leave of absence from my faculty position to do a reconnaissance trip to Australia. Before I left, I typed out a resignation letter, signed a printed copy, and gave it to my wife for safekeeping.

After a month, it was clear to me that we'd enjoy living in Australia and that it was the right career move for me. My wife agreed. So she put my letter in the mail; our decision was final.

When I look back now, I realize what a daring decision that was—for both of us. My wife couldn't speak a word of English and, as a trained lawyer, couldn't practice her profession in Australia, which has a very different legal system. It was hard for us to say goodbye to our relatives in Turkey. Our finances also tightened. The cross-continent move was expensive, and my postdoc salary was our only source of income in Australia.

But we never looked back with regret. My wife quickly became proficient in English and eventually went back to school part-time to study accounting. And I've been much happier professionally. I left my legal disputes behind and got a chance to work with supportive colleagues on a research project that I was excited about. My postdoc adviser also entrusted me with co-supervising some of his Ph.D. students, which made me feel as though my expertise was valued.

When I quit my faculty position in Turkey, I was hopeful that I could work my way back up the academic ladder. And, indeed, that's what happened: After 2.5 years, I secured a tenure-track job at another university in Australia, which is where I am now.

I hope that others can gain inspiration from my nontraditional career path. It was devastating when my professional life appeared to crumble. But that challenge set me on a new path, one that has led to a productive and enjoyable career. I'm glad I took a risk to rebuild my career from scratch in another country—and that my wife was excited to make a change along with me. As Franklin D. Roosevelt once said, "A smooth sea never made a skilled sailor." ■

Gursel Alici is a professor at the University of Wollongong in Australia. Send your career story to SciCareerEditor@aaas.org.

ILLUSTRATION: ROBERT NEUBECKER